frontiers | Research Topics

Insights in general cardiovascular medicine 2022

Edited by
Junjie Xiao, Pietro Enea Lazzerini
and Maurizio Acampa

Published in
Frontiers in Cardiovascular Medicine

ISSN 1664-8714
ISBN 978-2-8325-3319-2
DOI 10.3389/978-2-8325-3319-2

About Frontiers

Frontiers is more than just an open access publisher of scholarly articles: it is a pioneering approach to the world of academia, radically improving the way scholarly research is managed. The grand vision of Frontiers is a world where all people have an equal opportunity to seek, share and generate knowledge. Frontiers provides immediate and permanent online open access to all its publications, but this alone is not enough to realize our grand goals.

Frontiers journal series

The Frontiers journal series is a multi-tier and interdisciplinary set of open-access, online journals, promising a paradigm shift from the current review, selection and dissemination processes in academic publishing. All Frontiers journals are driven by researchers for researchers; therefore, they constitute a service to the scholarly community. At the same time, the *Frontiers journal series* operates on a revolutionary invention, the tiered publishing system, initially addressing specific communities of scholars, and gradually climbing up to broader public understanding, thus serving the interests of the lay society, too.

Dedication to quality

Each Frontiers article is a landmark of the highest quality, thanks to genuinely collaborative interactions between authors and review editors, who include some of the world's best academicians. Research must be certified by peers before entering a stream of knowledge that may eventually reach the public - and shape society; therefore, Frontiers only applies the most rigorous and unbiased reviews. Frontiers revolutionizes research publishing by freely delivering the most outstanding research, evaluated with no bias from both the academic and social point of view. By applying the most advanced information technologies, Frontiers is catapulting scholarly publishing into a new generation.

What are Frontiers Research Topics?

Frontiers Research Topics are very popular trademarks of the *Frontiers journals series*: they are collections of at least ten articles, all centered on a particular subject. With their unique mix of varied contributions from Original Research to Review Articles, Frontiers Research Topics unify the most influential researchers, the latest key findings and historical advances in a hot research area.

Find out more on how to host your own Frontiers Research Topic or contribute to one as an author by contacting the Frontiers editorial office: frontiersin.org/about/contact

Insights in general cardiovascular medicine: 2022

Topic editors

Junjie Xiao — Shanghai University, China

Pietro Enea Lazzerini — University of Siena, Italy

Maurizio Acampa — Siena University Hospital, Italy

Citation

Xiao, J., Lazzerini, P. E., Acampa, M., eds. (2023). *Insights in general cardiovascular medicine: 2022*. Lausanne: Frontiers Media SA. doi: 10.3389/978-2-8325-3319-2

Table of contents

frontiers | Frontiers in Cardiovascular Medicine

TYPE Editorial
PUBLISHED 09 August 2023
DOI 10.3389/fcvm.2023.1259212

OPEN ACCESS

EDITED AND REVIEWED BY
Hendrik Tevaearai Stahel,
University Hospital of Bern, Switzerland

*CORRESPONDENCE
Maurizio Acampa
M.Acampa@ao-siena.toscana.it

RECEIVED 15 July 2023
ACCEPTED 31 July 2023
PUBLISHED 09 August 2023

CITATION
Acampa M, Accioli R, Salvini V, Xiao J and Lazzerini PE (2023) Editorial: Insights in general cardiovascular medicine: 2022.
Front. Cardiovasc. Med. 10:1259212.
doi: 10.3389/fcvm.2023.1259212

Editorial: Insights in general cardiovascular medicine: 2022

Maurizio Acampa[1]*, Riccardo Accioli[2], Viola Salvini[2], Junjie Xiao[3] and Pietro Enea Lazzerini[2]

[1]Stroke Unit, Department of Emergency-Urgency and Transplants, Azienda Ospedaliera Universitaria Senese, "Santa Maria alle Scotte" General-Hospital, Siena, Italy, [2]Department of Medical Sciences, Surgery and Neurosciences, University of Siena, Siena, Italy, [3]Institute of Cardiovascular Sciences, Shanghai Engineering Research Center of Organ Repair, School of Life Science, Shanghai University, Shanghai, China

KEYWORDS

heart failure, atrial cardiopathy, coronary artery disease, syncope, pulmonary hypertension

Editorial on the Research Topic
Insights in General Cardiovascular Medicine: 2022

In this Research Topic, an international selection of high-quality papers by our editorial board members contributed to highlight the latest advancements in research across the field of cardiovascular medicine. Specifically, these papers offer new insights into various conditions, including heart failure (HF), atrial cardiopathy, coronary artery disease (CAD), pulmonary hypertension, and syncope.

Heart failure

Several contributions focused on chronic HF and explored the potential risk factors that can impact clinical outcomes and mortality. Sleep apnea (SA) (including both obstructive and central SA) represents one of these factors, associated with a poor prognosis in patients with HF (1). In particular, in their retrospective observational study, Naito et al. demonstrated that in patients with HF, SA, which was not effectively suppressed by continuous positive airway pressure (CPAP), was associated with worse prognosis as compared to those with suppressed SA by CPAP. Another interesting risk factor is represented by the epigenetics, that can influence myocardial structure modifications during HF natural history (2). In this view, Han et al. provided evidence on the role of methyltransferase-like 5 (METTL5) whose loss in the animal model could promote pressure overload-induced cardiomyocyte hypertrophy and adverse remodelling. In their work, authors demonstrated how a missing m6A catalysation of 18S rRNA about the METTL5 would reduce the efficiency of mRNA translation of SUZ12, a core component of PRC2 complex, strong inhibitor of cardiac hypertrophy–related genes in hypertrophy hearts (3). One of this gene is GATA4. According to the study by Yan et al., GATA4 protein directly binds the promotor site of Cardiac ISL1-Interacting Protein (CIP), responsible to the production of CIP protein, that inhibits cardiac remodelling and protects the heart from HF after cardiac hypertrophy through IGF, mTORC2 and TGFβ signalling pathways, which regulate cardiac hypertrophy–related genes expression. A deeper understanding of cardiac remodelling is crucial in identifying potential molecular targets for pharmacotherapies. Furthermore, it is equally intriguing to anticipate the risk of mortality and re-hospitalization in patients with HF (4). Zhao et al. developed machine

learning-based models specifically designed for patients with mild-reduced ejection fraction (HFmrEF), which demonstrated superior performance compared to traditional models in predicting mortality and rehospitalization. From the perspective of heart failure, an intriguing aspect is heart failure with preserved ejection fraction, where diastolic dysfunction of the left ventricle (LVDD) assumes a significant role. In septic patients LVDD is common and associated with high mortality. The endothelial dysfunction, characteristic of sepsis, results in increased vascular permeability, potentially causing pulmonary edema. Unfortunately, the quantification of acute pulmonary edema in septic patients using the lung ultrasound score (LUSS) is frequently challenging or unreliable. Indeed, Kahl et al. in a prospective cohort study observed that in 54 patients with sepsis, LVDD was not significantly associated with LUSS, even in the presence of severe pulmonary edema. Heart failure is also burdened by an important arrhythmic risk. Ventricular tachycardia, which occurs primarily in the context of structurally abnormal hearts, can result in severe hemodynamic compromise. Ventricular tachycardia ablation (VTA) is often a challenge. This procedure can be performed safely in selected high-risk patients using veno-arterial extracorporeal membrane oxygenation (VA-ECMO) support. In this regard, Sabbag et al. evaluated how early decanullation from VA-ECMO is associated with a higher survival at one year after VTA than in those in which it is not performed. Therefore, this procedure should be considered and performed immediately upon completion of VTA in most cases.

Atrial cardiopathy

Within this Research Topic, several intriguing articles delve into the role of atrial cardiopathy as a significant substrate for promoting cardiac arrhythmias, including atrial fibrillation, as well as the pro-thrombotic state, which can occur independently of atrial fibrillation (5). In their review article, Donniacuo et al. provided valuable insights into the pathogenesis of COVID-19-related atrial fibrillation events, specifically addressing the cardiovascular safety profile of drugs used for the treatment of COVID-19. The authors highlighted multiple putative mechanisms, such as a reduced availability of angiotensin-converting enzyme 2, binding of viral spike protein to CD147 or sialic acid, enhancement of inflammatory signalling culminating in cytokine storm, endothelial damage, and increased adrenergic drive. Atrial cardiopathy, along with the intricate interplay of multiple mechanisms, may also contribute to the pathogenesis of many ischemic strokes of undetermined causes (6), especially embolic strokes of undetermined source (ESUS), where inflammation can promote both atrial fibrillation events and a prothrombotic state (7). In line with this perspective, the study conducted by Acampa et al. demonstrated that the presence of atrial cardiopathy, as assessed through electrocardiographic and echocardiographic markers, could serve as the underlying pathogenic mechanism in a subgroup of ESUS patients. Notably, this subgroup exhibits more severe neurological deficits and presents a clinical pattern resembling cardioembolic strokes attributed to atrial fibrillation. As regards the complications of stroke, spasticity stands out as one of them. In a randomized double-blind, placebo-controlled crossover study, Rosa et al. investigated the impact of nabiximols, a cannabinoid-derived drug, on post-stroke spasticity. The study findings indicate that nabixomols effectively alleviate spasticity without causing significant changes in blood pressure, heart rate, or cardiovascular complications in patients who in patients who have experienced a cerebrovascular accident. However, additional research is needed to explore other potential cardiovascular benefits of cannabinoids, such as their potential role in delaying the progression of atherosclerosis and inflammation.

Coronary artery disease

The risk of mortality due to cardiac infarction can be enhanced in presence of complication related to the natural history of the disease, such as infections (8) in hospitalized patient and cardiac autonomic imbalance. Considering these concerns, prevention has become one of the top priorities in healthcare, to better improve the prognosis in patient with acute coronary syndrome (ACS). Given that, Liu et al. developed a 24-point risk score to use in ST-segment elevation myocardial infarction (STEMI), including seven variables such as age, Killip classification, insulin use, white blood cell count, serum albumin, diuretic use, and transfemoral approach. The score not only established a simple bedside tool to estimate the risk of developing infection for patient with STEMI but also demonstrated good performance for in-hospital all-cause death, and major adverse cardiovascular events (MACE) among these patients and even in the non-ST-elevation acute coronary syndrome (NSTE-ACS) treated with PCI. On the other hand, Duan et al. evaluated a possible extension of post-discharge GRACE score, considering in addition cardiac autonomic nerve imbalance, measured through the value of 24 h deceleration capacity (DC), a feasible and non-invasive indicator that captures autonomic activity-related modulations of heart rate. Combination of DC and the post-discharge GRACE score significantly enhanced the discriminatory ability and accuracy in the prediction of poor long-term follow-up prognosis. As regards the mortality induced by acute myocardial infarction, it is necessary to consider ischemia reperfusion injury (IRI), a possible cause of secondary myocardial damage. Evaluating the possible therapeutic strategies able to attenuate the IRI, Wei et al. analysed the protective role of Danlou tablet (Dan), a Chinese herbal compound. This study provided for the first time evidence that Dan could attenuate cardiomyocyte apoptosis and ischemia-reperfusion injury, by experiments conducted *in vivo*, using an acute IRI model in mice, and *in vitro*, through oxygen-glucose deprivation-reperfusion (OGD/R)-induced apoptosis in primary neonatal rat cardiomyocytes (NRCMs). Mechanistically, Dan could activate proliferator-activated receptor gamma (PPAR-γ) in both models, while inhibition of PPAR-γ could attenuate the protective effect of Dan. These data provide a new potential strategy for the precise treatment of ischemic heart diseases complications. Left

ventricular (LV) remodelling is one of the possible functional complications following a STEMI. Pharmacological interventions, able to prevent LV remodelling following a STEMI, improve the outcome of this condition. Egea Iborra et al. evaluated the possible effects of paroxetine, a GRK2 inhibitor also known as beta-adrenergic receptor kinasi 1. Among the drugs used for neuronormal antagonism (beta-blockers,angiotensin converting enzyme inhibitors, mineralcorticoid receptor antagonists, angiotensin receptor blockers), capable of preventing LV remodelling, only beta-blockers act directly on GRK2 as paroxetine. For this reason, paroxetine, sharing the same molecular target with beta-blockers, could be used when these are contraindicated (for example in subjects with hypotension) or poorly tolerated.

Pulmonary hypertension

Another topic of particular interest in the management of cardiovascular patient is pulmonary hypertension, which is often a consequence of heart disease. In this context, given the high impact of this condition on cardiovascular health, Miao et al. presented a more in-depth insight about the complex molecular mechanisms of chronic thromboembolic pulmonary hypertension, highlighting the role of specific mRNAs, miRNAs, and circRNAs and inflammatory cells recruitment in the progression of the disease. Instead, Rodrigues et al. evaluated the impact of a blunted cardiac autonomic modulation and a pro-inflammatory profile on pulmonary artery pressure (PAPs) in systemic sclerosis patients, suggesting a relationship among cardiac autonomic control, inflammatory status, and cardiopulmonary mechanics.

Syncope

A common challenge in cardiovascular medicine involves the impact of syncope in childhood, which exhibits a high prevalence and multiple etiologies (9). To distinguish syncope due to an excess in vasovagal reflex [vasovagal (VVS) syncope] and syncope due to a conversion disorder [psychogenic (PPS)] poses a significant difficulty, as these two forms share several clinical manifestations, including repeated episodes of transient loss of consciousness and falls usually without convulsions. On this argument, Li et al. designed a study to evaluate a clinical manifestation-based scoring, consisting of 4 variables, aiming to aid in the initial differential diagnosis between PPS and VVS. On a different note, to gain a better understanding of the pathophysiology of VVS, Wang et al. investigated the profile of plasma human growth cytokines. Their findings revealed that elevated plasma concentrations of HGF and IGFBP-1, and decreased EGF were typical in pediatric VVS.

In conclusion, the remarkable contributions within this Research Topic have greatly advanced our comprehension of various aspects within cardiovascular medicine. These studies have illuminated intricate physiological and pathogenic mechanisms, which bear significant clinical implications for patient management. Moreover, they have provided valuable insights and recommendations that pave the way for further exploration in this rapidly evolving field.

Author contributions

MA: Conceptualization, Supervision, Writing – original draft, Writing – review & editing. RA: Writing – original draft, Writing – review & editing. VS: Writing – original draft, Writing – review & editing. JX: Conceptualization, Writing – original draft, Writing – review & editing. PL: Conceptualization, Writing – original draft, Writing – review & editing.

Conflict of interest

The authors declare that the research was conducted in the absence of any commercial or financial relationships that could be construed as a potential conflict of interest.

The author(s) declared that they were an editorial board member of Frontiers, at the time of submission. This had no impact on the peer review process and the final decision.

Publisher's note

References

1. Naito R, Kasai T, Narui K, Momomura SI. Association between frequency of central respiratory events and clinical outcomes in heart failure patients with sleep apnea. *J Clin Med*. (2022) 11(9):2403. doi: 10.3390/jcm11092403

2. Shi Y, Zhang H, Huang S, Yin L, Wang F, Luo P, et al. Epigenetic regulation in cardiovascular disease: mechanisms and advances in clinical trials. *Signal Transduct Target Ther*. (2022) 7(1):200. doi: https://doi.org/10.1038/s41392-022-01055-2

3. Wang Z, Zhang XJ, Ji YX, Zhang P, Deng KQ, Gong J, et al. The long noncoding RNA chaer defines an epigenetic checkpoint in cardiac hypertrophy. *Nat Med*. (2016) 22:1131–9. doi: 10.1038/nm.4179

4. Gheorghiade M, Vaduganathan M, Fonarow GC, Bonow RO. Rehospitalization for heart failure: problems and perspectives. *J Am Coll Cardiol*. (2013) 61 (4):391–403. doi: 10.1016/j.jacc.2012.09.038

5. Shen M, Arora R, Jalife J. Atrial myopathy. *J Am Coll Cardiol Basic Trans Science*. (2019) 4(5):640–54. doi: https://doi.org/10.1016/j.jacbts.2019.05.005

6. Acampa M, Lazzerini PE, Martini G. Atrial cardiopathy and sympatho-vagal imbalance in cryptogenic stroke: pathogenic mechanisms and effects on electrocardiographic markers. *Front Neurol*. (2018) 9:469. doi: 10.3389/fneur.2018.00469

7. Acampa M, Lazzerini PE, Guideri F, Tassi R, Lo Monaco A, Martini G. Inflammation and atrial electrical remodelling in patients with embolic strokes of undetermined source. Heart. *Lung and Circulation*. (2019) 28:917–22. doi: 10.1016/j.hlc.2018.04.294

8. Putot A, Chague F, Manckoundia P, Cottin Y, Zeller M. Post-Infectious myocardial infarction: new insights for improved screening. *J Clin Med*. (2019) 8:827. doi: 10.3390/jcm8060827

9. Ikiz MA, Cetin II, Ekici F, Güven A, Değerliyurt A, Köse G. Pediatric syncope: is detailed medical history the key point for differential diagnosis? *Pediatr Emerg Care*. (2014) 30(5):331–4. doi: 10.1097/PEC.0000000000000123

frontiers in Cardiovascular Medicine

ORIGINAL RESEARCH
published: 27 January 2022
doi: 10.3389/fcvm.2022.839183

Differential Diagnosis Between Psychogenic Pseudosyncope and Vasovagal Syncope in Children: A Quantitative Scoring Model Based on Clinical Manifestations

Changjian Li[1,2†], Yong Zhang[2†], Ying Liao[1†], Lu Han[3†], Qingyou Zhang[1], Jia Fu[2], Dan Zhou[2], Shuai Long[3], Hong Tian[3], Hongfang Jin[1*] and Junbao Du[1,4*]*

[1] Department of Pediatrics, Peking University First Hospital, Beijing, China, [2] Department of Cardiology, Wuhan Children's Hospital (Wuhan Maternal and Child Healthcare Hospital), Tongji Medical College, Huazhong University of Science and Technology, Wuhan, China, [3] Cardiovascular Center, Children's Hospital, Fudan University, Shanghai, China, [4] Key Laboratory of Molecular Cardiovascular Sciences, The Ministry of China, Beijing, China

OPEN ACCESS

Edited by:
Jiu-Chang Zhong,
Capital Medical University, China

Reviewed by:
Runmei Zou,
Central South University, China
Jie Tian,
Children's Hospital of Chongqing Medical University, China
Yu-Ming Kang,
Xi'an Jiaotong University, China

***Correspondence:**
Junbao Du
junbaodu1@126.com
Hong Tian
hong916a@189.cn
Hongfang Jin
jinhongfang51@126.com

[†] These authors have contributed equally to this work and share first authorship

Specialty section:
This article was submitted to General Cardiovascular Medicine, a section of the journal Frontiers in Cardiovascular Medicine

Received: 19 December 2021
Accepted: 05 January 2022
Published: 27 January 2022

Citation:
Li C, Zhang Y, Liao Y, Han L, Zhang Q, Fu J, Zhou D, Long S, Tian H, Jin H and Du J (2022) Differential Diagnosis Between Psychogenic Pseudosyncope and Vasovagal Syncope in Children: A Quantitative Scoring Model Based on Clinical Manifestations. Front. Cardiovasc. Med. 9:839183. doi: 10.3389/fcvm.2022.839183

The study was designed to explore a clinical manifestation-based quantitative scoring model to assist the differentiation between psychogenic pseudosyncope (PPS) and vasovagal syncope (VVS) in children. In this retrospective case-control study, the training set included 233 pediatric patients aged 5–17 years (183 children with VVS and 50 with PPS) and the validation set consisted of another 138 patients aged 5–15 years (100 children with VVS and 38 with PPS). In the training set study, the demographic characteristics and clinical presentation of patients were compared between PPS and VVS. The independent variables were analyzed by binary logistic regression, and the score for each variable was given according to the approximate values of odds ratio (OR) to develop a scoring model for distinguishing PPS and VVS. The cut-off scores and area under the curve (AUC) for differentiating PPS and VVS cases were calculated using receiver operating characteristic (ROC) curve. Then, the ability of the scoring model to differentiate PPS from VVS was validated by the true clinical diagnosis of PPS and VVS in the validation set. In the training set, there were 7 variables with significant differences between the PPS and VVS groups, including duration of loss of consciousness (DLOC) ($p < 0.01$), daily frequency of attacks ($p < 0.01$), BMI ($p < 0.01$), 24-h average HR ($p < 0.01$), upright posture ($p < 0.01$), family history of syncope ($p < 0.05$) and precursors ($p < 0.01$). The binary regression analysis showed that upright posture, DLOC, daily frequency of attacks, and BMI were independent variables to distinguish between PPS and VVS. Based on the OR values of each independent variable, a score of 5 as the cut-off point for differentiating PPS from VVS yielded the sensitivity and specificity of 92.0% and 90.7%, respectively, and the AUC value was 0.965 (95% confidence interval: 0.945–0.986, $p < 0.01$). The sensitivity, specificity, and accuracy of this scoring model in the external validation set to distinguish PPS from VVS were 73.7%, 93.0%, and 87.7%, respectively. Therefore, the clinical manifestation-based scoring model is a simple and efficient measure to distinguish between PPS and VVS.

Keywords: psychogenic pseudosyncope, vasovagal syncope, differential diagnosis, scoring model, binary logistic regression

INTRODUCTION

Syncope is the inability to maintain an autonomous body position due to recoverable whole-brain hypoperfusion and manifests as a transient loss of consciousness (TLOC) (1). It is typically characterized by spontaneous and complete recovery of TLOC within a short period of time (2, 3). Vasovagal syncope (VVS) accounts for about 60–70% of syncope in children and adolescents (4). Psychogenic pseudosyncope (PPS) is the other entity of TLOC without virtual cerebral hypoperfusion or impaired physiological function (5–7). It is considered a conversion disorder in nature (8). The prevalence of PPS varies from 0 to 12%, with an average incidence rate of 4% (9–11). PPS and VVS share several similarities in clinical manifestations, such as recurrent episodes of TLOC and falls usually without convulsions. Since children with PPS have no convulsion-like symptoms, their attacks are sometimes considered as syncope in the preliminary evaluation in many cases. In a study including both adults and children as study subjects, even up to 50% of PPS cases were misdiagnosed as VVS at the beginning (9). In addition, the manifestation of some children with PPS may be taken as malingering attacks and the actual diagnosis is ignored due to the uneven understanding of PPS among medical institutions at all levels (12). Therefore, increasing reports suggested that the incidence of PPS in children may be underestimated (13–15). Furthermore, although PPS and VVS are similar in clinical manifestations, the management strategies and prognosis of PPS are completely different from those of VVS. The above facts suggest the absolute necessity of distinguishing PPS from VVS.

At present, there has not been any acknowledged clinical manifestation-based systematic procedure to differentiate PPS and VVS in children. Head-up tilt test (HUTT) has been performed to clarify the cause of syncope and is one of the auxiliary examinations to distinguish between VVS and PPS (16, 17). However, under many circumstances, the response of patients to HUTT alone is not sufficient enough to confirm the diagnosis of VVS as its sensitivity in the diagnosis is low (18). Therefore, several guidelines emphasized that it is important to explain the results of HUTT together with the clinical manifestations and make careful differentiation (19, 20). In addition, there are some limitations of the HUTT use. For example, the basic HUTT sometimes takes 45 min (min), and the drug-provocated HUTT is extended by another 20 min under certain circumstances (19). Furthermore, during HUTT, patients may sometimes present as cardiac arrest (21). Even after careful evaluation, the HUTT for pediatric patients may be suspended just because the child cannot cooperate very well and it is not being widely used in grassroots hospitals or even in some general hospitals (17, 22). Therefore, a simple, efficient, and rapid measure for the differentiation between PPS and VVS based on clinical manifestations is urgently needed.

Previous studies have shown that the episodes of unconsciousness in children with PPS usually last for a longer time (from 5 to 20 min or longer) and occur more frequently than those in children with VVS (11). Other clinical characteristics indicating the diagnosis of PPS include closing eyes without being pale look, no sweating during the attack, and seldom physical injury (20, 23). However, how to quantify these various clinical features and use them to discriminate between PPS and VVS is an urgent issue in clinical practice. In a previous study, the authors described a model composing of the posture during an episode, loss of consciousness (LOC) duration, and electrocardiogram-derived QT dispersion (24). However, the result of QT dispersion cannot be determined in a very quick and convenient way in grassroots hospitals.

Therefore, the present study was undertaken to develop a new scoring model to differentiate between PPS and VVS using recognized clinical features to help pediatricians, especially those working in grassroots hospitals, to differentiate pediatric PPS from VVS in a simple and rapid way.

METHODS

Subjects

Totally, 233 children hospitalized in the Department of Pediatrics, Peking University First Hospital, China, from January 2012 to June 2021 were included in the training set. Of whom, 183 children (71 males and 112 females) had VVS with a median age of 11.0 (9.0, 13.0) years, and 50 children (22 males and 28 females) had PPS with a median age of 12.0 (9.0, 13.0) years. An additional 138 children treated at the Cardiovascular Center, Children's Hospital, Fudan University, China, from January 2009 to June 2021 were included in the external validation set, of whom 100 children (47 males and 53 females) had VVS with a median age of 10.0 (8.0, 12.0) years and 38 children (24 males and 14 females) had PPS with a median age of 11.0 (9.0, 13.0) years.

The diagnostic criteria of VVS are: (1) occurring primarily in older children and adolescents; (2) often accompanied by precipitating factors such as long periods of uprightness, mental tension, and sultry environment; (3) a clear history or aura of syncope; (4) a positive HUTT test; and (5) exclusion of other diseases such as cardiogenic, cerebrovascular or metabolic diseases (19, 20). The diagnostic criteria for PPS are based on the Diagnostic and Statistical Manual of Mental Disorders, Fifth Edition (DSM-V) (25).

The inclusion criteria of the study subjects: (1) those diagnosed as VVS or PPS; (2) patients under the age of 18 years old; (3) patients with normal routine biochemistry and 24-h Holter recordings results; (4) the data of the first confirmed hospitalization were included in the study for those with multiple hospitalizations; and (5) the children did not receive medication within 2 weeks.

Exclusion criteria of research subjects: (1) syncope caused by cardiogenic, cerebrovascular, and other diseases; (2) patients with non-sinus rhythm in electrocardiogram (ECG); (3) patients with incomplete medical records, and loss of data; (4) the children without HUTT examination; (5) patients diagnosed as PPS with VVS.

This study was approved by the Ethics Committee of Peking University First Hospital (2021–424) and Children's Hospital of Fudan University (2021–476), and the informed consent was permitted to be waived.

Data Collection

We collected the demographic data of all the participants based on the medical records during their hospitalizations, including sex, age, and body mass index (BMI). The clinical manifestations as triggers or predisposing factors (e.g., upright posture, emotional stress, and stuffy environment), precursors, duration of loss of consciousness (DLOC), the daily frequency of attacks (the highest number of LOC episodes within 1 day, at least once) in the present history and the family history of syncope were collected. The upright posture means that the attacks happen when the patient is at an orthostatic posture, including standing for a long time and/or just standing up suddenly. Other kinds of situations were non-upright posture, for example, postures except orthostatism or walking, and/or exercising in the upright position. DLOC referred to the maximum recorded duration of the real or apparent LOC reported by the witness according to the medical records. We defined a child with a history of syncope in the family within two generations as having a positive family history. Besides, the baseline data of resting HR, resting systolic blood pressure (SBP), and resting diastolic blood pressure (DBP) as well as the 24-h average HR in Holter monitoring records of the patients were also recorded. The above data were obtained from the Medical Recording Management Digital System (Kaihua, Beijing, China). The medical history and laboratory findings of all the patients were reviewed in detail and recorded by a specialized investigator. The records were carefully proofread by another investigator independently.

Methodology of HUTT and Dynamic Electrocardiogram

Children fasted for at least 4 h before the testing, stopped any vasoactive medication for at least five half-lives, and avoided the drink that could affect autonomic nervous system function (e.g., coffee). The test was performed in the morning, and the environment was kept quiet and dimly-lit at a suitable room temperature. Children first laid on the tilt table (SHUT-100A, Standard, Jiangsu and ST-711, Juchi, Beijing, China) for 10–30 min. During HUTT, HR, BP and ECG were recorded continuously with an ECG monitor (General Electric, New York, USA) and Finapres Medical System (FinometerPRO, FMS, The Netherlands). After the stabilization of HR and BP, the table was tilted upward at 60° and HR, BP, and ECG were continuously monitored till the positive response appeared, or otherwise till the whole test duration (45 min) if no positive response was observed. Positive response criteria of HUTT are listed below: (1) significant blood pressure drop (i.e., SBP $\leq$80 mmHg, DBP $\leq$50 mmHg, or $\geq$25% decrease in mean BP); (2) bradycardia (i.e., HR <75 bpm for children at 4–6 years of age, <65 bpm for children at 6–8 years of age, and <60 bpm for children at 8 years of age and older); (3) the presence of sinus arrest, premature junctional contractions; or (4) transient second-degree or higher atrioventricular block or cardiac arrest $\geq$3 s (19, 26, 27).

A 24-h ECG was recorded with an ECG recorder (Mortara Instrument, Milwaukee, Wisconsin, USA) and coffee, tea, or other drugs and strenuous exercise were avoided during the 24-h ECG. The 24-h ECG results were automatically analyzed by Mortara software (Mortara H-Scribe 7.0, Milwaukee, Wisconsin, USA) to obtain the 24-h average HR after automatic analysis.

Statistical Analysis

All statistical analyses were performed using SPSS version 25.0 (IBM, New York, USA). The normality test of continuous variables was performed using the Shapiro–Wilk test. For data where both groups obeyed a normal distribution, the measured data were expressed as ($x \pm$ s) and the t-test was used to compare between the two groups. Non-normally distributed data were described as median (25th percentile, 75th percentile) and the differences between groups were compared using the Mann-Whitney U test. The categorical variables were described by frequency and constituent ratio, and comparisons between groups were made using chi-square tests.

To establish a scoring system for differential diagnosis, variables with a statistical difference of $p < 0.05$ in the univariate analysis of the comparison between the PPS and VVS groups were included in a binary logistic regression, and for clinical application, continuous variables were transformed into dichotomous variables using cut-off values extracted from receiver operating characteristic (ROC) curves. Each variable derived from the regression was given a score according to the approximate odds ratio (OR) values, and the total score of a patient was calculated by adding up the scores of all identified variables, forming a scoring model. The Hosmer-Lemeshow test was used to assess the goodness of fit of the discriminant model. The ROC curve was performed to assess the power of the above scoring model in the differential diagnosis and determine the optimal cut-off score based on the maximum Youden index. Finally, the sensitivity, specificity, and accuracy of the scoring model were evaluated in the differentiation between PPS and VVS in an external verification study. A p-value < 0.05 was considered significant.

RESULTS

Demographic Features

In the training set, 183 and 50 children were included in the VVS and PPS groups, respectively. The two groups did not show any statistically significant difference in sex, age, resting HR, resting SBP, and resting DBP ($p > 0.05$). Children in the PPS group had a much higher BMI (21.0 kg/m^2 vs. 17.7 kg/m^2) and 24-h average HR (84.0 bpm vs. 81.0 bpm) than those in VVS group, and the differences were statistically significant ($p < 0.01$, **Table 1**).

Comparisons of Clinical Features Between PPS and VVS Groups

There was no statistical difference in emotional stress ($p = 0.097$) and stuffy environment ($p = 0.096$) before syncopal episode between the two groups; while, the significant differences were found in other manifestations, including DLOC ($p < 0.01$), daily frequency of attacks ($p < 0.01$), upright posture ($p < 0.01$), precursors ($p < 0.01$), and family history of syncope ($p < 0.05$, **Table 2**).

TABLE 1 | Comparison of the demographic characteristics between the VVS and PPS groups in training set.

Groups	VVS	PPS	t/Z/x^2	*p*-value
Patients (n)	183	50		
Age (y)	11.0 (9.0, 13.0)	12.0 (9.0, 13.0)	−0.489	0.625
Sex (M/F)	71/112 (38.8%/61.2%)	22/28 (44.0%/56.0%)	0.443	0.506
BMI (kg/m^2)	17.7 (16.1, 20.0)	21.0 (17.0, 24.0)	−4.102	<0.01
Resting HR (bpm)	76.0 (68.0, 85.0)	79.5 (73.0, 86.3)	−1.839	0.066
Resting SBP (mmHg)	106.0 (98.0, 112.0)	108.0 (100.0, 116.3)	−1.578	0.115
Resting DBP (mmHg)	62.8 ± 7.2	64.9 ± 9.0	−1.733	0.085
24-h average HR (bpm)	81.0 (75.0, 89.0)	84.0 (79.0, 93.0)	−2.900	<0.01

VVS, vasovagal syncope; PPS, psychogenic pseudosyncope; M/F, Male/Female; BMI, body mass index; HR, heart rate; bpm, beat per minute; SBP, systolic blood pressure; DBP, diastolic blood pressure.

TABLE 2 | Clinical features of patients diagnosed with VVS and PPS groups in training set.

Groups	VVS	PPS	Z/x^2	*p*-value
Patients (n)	183	50		
DLOC (min)	2.0 (1.0, 4.0)	20.0 (5.8, 60.0)	−7.205	<0.01
Daily frequency of attacks (times)	1 (1, 1)	1 (1, 3)	−7.763	<0.01
Upright posture (Yes/No)	165/18 (90.2%/9.8%)	13/37 (26.0%/74.0%)	89.655	<0.01
Stuffy environment (Yes/No)	37/146 (20.2%/79.8%)	5/45 (10.0%/90.0%)	2.775	0.096
Emotional stress (Yes/No)	26/157 (14.2%/85.8%)	12/38 (24.0%/76.0%)	2.759	0.097
FH of syncope (Yes/No)	34/149 (18.6%/81.4%)	2/48 (4.0%/96.0%)	6.390	0.011
Precursors (Yes/No)	132/51 (72.1%/27.9%)	22/28 (44.0%/56.0%)	13.868	<0.01

VVS, vasovagal syncope; PPS, psychogenic pseudosyncope; DLOC, duration of loss of consciousness; min, minute; FH, family history.

TABLE 3 | The cut-off value for diclassification the continuous variables in training set.

Test result variable (s)	Cut-off value	AUC (95% CI)	*p*-value	Sensitivity	Specificity
DLOC	≥9 min	0.824 (0.749, 0.900)	<0.01	0.740	0.863
Daily frequency of attacks	≥1.5 times[a]	0.705 (0.611, 0.800)	<0.01	0.440	0.962
BMI	≥20.5 kg/m^2	0.689 (0.601, 0.778)	<0.01	0.580	0.792
24-h average HR	≥93 bpm	0.634 (0.549, 0.719)	<0.01	0.300	0.913

AUC, Area under curve; CI, Confidence Interval; DLOC, duration of loss of consciousness; min, minute; BMI, body mass index; DBP, diastolic blood pressure; HR, heart rate; bpm, beat per minute. [a]The cutoff value of daily frequency of attacks was defined as ≥twice because the actual number of syncope is an integer in clinical practice.

TABLE 4 | Coefficients of binary logistic regression in training set.

Variable (s)	Cut-off value	*p*-value	Odds ratio (95% CI)	Points
Upright posture	Yes/No	<0.01	24.390 (7.179, 82.861)	4
DLOC	9 min	<0.01	22.694 (6.257, 82.317)	4
Daily frequency of attacks	Twice	<0.01	49.476 (10.286, 238.407)	8
BMI	20.5 kg/m^2	<0.01	5.974 (1.898, 18.801)	1

CI, Confidence Interval; DLOC, duration of loss of consciousness; min, minute; BMI, body mass index.

The Cut-Off Value for Binary Classification of the Continuous Variables

Among the 7 variables showing statistical differences ($p < 0.05$) in comparison between PPS and VVS groups, including upright posture, DLOC, daily frequency of attacks, BMI, precursors, family history of syncope and 24-h average HR, there were 4 continuous variables (DLOC, daily frequency of attack, BMI and 24-h average HR) which were converted into dichotomous variables, respectively, for the ease of clinical application. The cut-off value, *p*-value, sensitivity

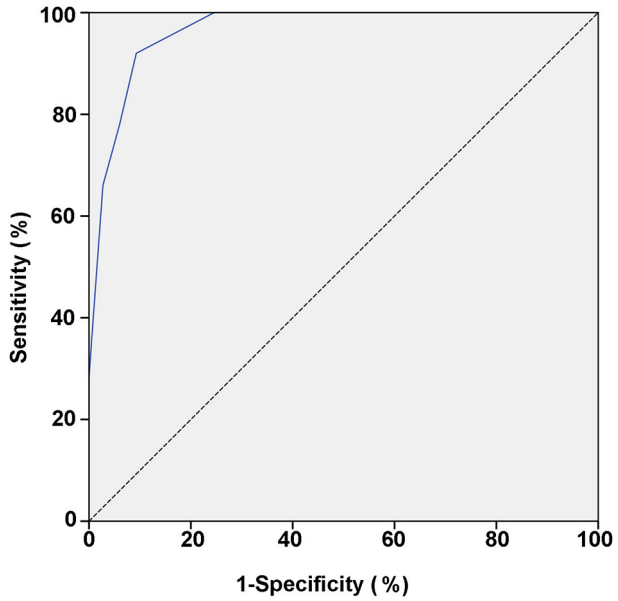

FIGURE 1 | ROC curve of the scoring model between VVS and PPS groups. The vertical and horizontal axes of the curve represent predictive sensitivity and positivity (1-specificity), respectively. The 45° slash indicates that the sensitivity is equal to the false positive rate, indicating no predictive value. The blue curve represents the ROC curve of the scoring model for the predictive value of the PPS. The AUC represents the predicted value for different cut-off values and it has a value of 0.965 (95% CI: 0.945–0.986; $p < 0.01$). ROC, receiver operating characteristic; PPS, psychogenic pseudosyncope; VVS, vasovagal syncope; AUC, area under the curve; CI, confidence interval.

and specificity of these continuous variables were shown in **Table 3**.

Building a Scoring Model to Identify PPS and VVS

Totally seven dichotomous variables were selected as independent variables for further logistic regression analysis using the backward conditional method, including upright posture (Yes/No), DLOC (≥9 min/<9 min), daily frequency of attacks (≥twice/<twice), BMI (≥20.5 kg/m^2/<20.5 kg/m^2), precursors (Yes/No), family history of syncope (Yes/No) and 24-h average HR (≥93.0 bpm/<93.0 bpm). Finally, four variables (upright posture, DLOC, daily frequency of attacks, and BMI) were determined as the independent variables to distinguish PPS from VVS. The statistical data of Hosmer-Lemeshow in each step did not show any significance ($p > 0.05$), suggesting that the goodness of fit was satisfactory.

According to the OR value of each independent variable, the score was assigned for each variable as follows (**Table 4**). (1) Upright posture: if there was no static upright posture as a predisposing factor before the TLOC event, four points were assigned, and otherwise, 0 point was assigned; (2) DLOC: if DLOC was ≥9 min, four points were assigned, and otherwise, 0 point was assigned; (3) daily frequency of attack: if daily frequency of attacks was ≥twice, 8 points were assigned, and otherwise, 0 point was assigned; and (4) BMI: if BMI was ≥20.5 kg/m^2, 1 point was assigned, and otherwise, 0 point was assigned. The total score for the four variables was calculated for each patient in the PPS and VVS groups, respectively.

TABLE 5 | Predictive values of scoring model in external validation set.

Score (point)	Clinical diagnosis		Total
	PPS	VVS	
≥5	28	7	35
<5	10	93	103
Total	38	100	138

VVS, vasovagal syncope; PPS, psychogenic pseudosyncope.

The power for differential diagnosis of the total score based on this model was assessed by the ROC curve. As a result, the area under the curve of the ROC was 0.965 (95% confidence interval: 0.945–0.986, $p < 0.01$). When the total score ≥5 points was used as the cut-off value for initial differentiation between pediatric PPS and VVS, its sensitivity was 92.0% and specificity was 90.7% for the diagnosis of PPS (**Table 4**; **Figure 1**).

External Validation

To verify the efficiency of the scoring model, total scores of the patients with a definite clinical diagnosis of PPS or VVS in the validation set were calculated. Patients with total scores ≥5 points or <5 points were suspected to be PPS or VVS, respectively, according to the scoring model (**Table 5**). The suspected diagnosis based on the scoring model was then compared with the patient's true definitive clinical diagnosis, and the sensitivity, specificity, and accuracy of the scoring model in distinguishing between PPS and VVS were calculated to be 73.7%, 93.0%, and 87.7%, respectively.

DISCUSSION

PPS and VVS share many similar clinical characteristics, but they are completely different diseases. This study showed that there were significant differences between the two diseases in DLOC, daily frequency of attacks, upright posture, family history of syncope, precursors, BMI, and 24-h average HR. The scoring model for the preliminary discrimination between PPS and VVS by four variables (daily frequency of attacks, upright posture, DLOC, and BMI) was established through binary logistic regression. By assigning scores for the four variables according to the OR values, we determined the final model with a maximum total score of 17 points. When the total score of the child was ≥5 points, the sensitivity and specificity for the possible differentiation of PPS from VVS were 92.0% and 90.7%, respectively.

In this study, the daily frequency of attacks ≥twice had the highest weight (eight points) in indicating the diagnosis of PPS, followed by DLOC ≥9 min (four points) and onset without predisposing upright posture (four points). In other words, children with PPS were more likely to experience more than one

event within 1 day and have a longer duration of each episode. The median of DLOC in the PPS group reached 20 min in this study. The difference in frequency and DLOC between PPS and VVS are closely related to their distinct pathogenesis. A PPS-like event can occur anytime and anywhere with or without psychological triggers, which may vary from person to person and the duration may also differ in length without the challenge of cerebral ischemia. As for VVS, the syncopal events often occur under specific inducement and the events are usually not that frequent (28). Although VVS is sometimes characterized by cluster attacks, the recurrences usually occur a few days later after the first episode (29). Regarding the posture as a predisposing factor of attacks, children in the VVS group were more likely to have an event while standing upright than those in the PPS group (90.2 vs. 26.0%, $p < 0.01$). VVS is an important form of acute orthostatic intolerance. When standing, the peripheral blood volume in the abdomen and lower limbs increases due to the gravity; therefore, when paradoxical vagal activation occurs in children with VVS during the adaptation to upright posture, a decrease in blood return volume causes a sharp drop in cardiac output, leading to syncope (28). In contrast, the mechanism for PPS attack is not directly related to the posture, and children with PPS may faint at any posture. Finally, BMI $\geq$20.5 kg/m^2 was assigned as 1 point to cue the diagnosis of PPS. Some scholars found that children with VVS had a lower BMI than healthy controls (30). This may be due to the fact that children with low BMI have relatively lower blood volume, which may deteriorate orthostatic intolerance (31). However, the relationship between BMI and PPS is not clear. Collectively, the four variables derived from the binary logistic regression equation can reflect the distinct characteristics between pediatric PPS and VVS.

In the external validation, the sensitivity of the scoring model is not as high as that of the training set in our study. The reason may be the fact that BMI and clinical characteristics of children in different regions may not be that identical. In addition, the DLOC is difficult to be reported exactly because the duration is often estimated by the witness. Therefore, the large sample sizes and multicenter studies are still necessary to improve the efficiency of the discriminant model.

In the previous clinical differential diagnosis between PPS and VVS, no clinical manifestations are specific and the weight of each feature is not clear. Therefore, pediatricians can only analyze the clinical data and make judgment according to their own experiences. HUTT is an important examination to identify the causes of syncope, but as mentioned above, its value in distinguishing between PPS and VVS is limited (32).

In this present study, several features with the most distinguishing significance were analyzed, and these variables were quantified according to the weight assignment. By this scoring model, a rapid preliminary judgment between PPS and VVS can be made just through a simple inquiry of medical history and basic measurement of height and weight, which is highly practical and easy to be popularized. Of course, in the diagnostic procedure of TLOC, it is also necessary to identify other causes except for PPS and VVS. Nevertheless, the significance of this study is that, contrary to the relatively complex diagnostic procedure at present, doctors at different levels can obtain a preliminary judgment and make a more targeted investigation plan for children suffering from TLOC with the help of our scoring model. If the total score indicates PPS, the patient should be recommended to see the psychiatric specialists for further evaluation while screening for other physical diseases, to manage the patient in a more efficient and comprehensive way. While, if the total score suggests VVS, the patient should be recommended to have HUTT, etc. Therefore, the results of this study will be helpful to suggest reasonable referrals and optimize the differential diagnostic process in clinical practice. Furthermore, compared with the previous study (24), this scoring model, for the first time, used the clinical manifestations only instead of doing a variety of laboratory investigations at the initial diagnostic step, and the newly developed scoring model yielded relatively high sensitivity and specificity for differentiating PPS from VVS.

Our study also had some limitations. Children with VVS were unable to accurately describe the frequency and duration of syncope, and the information of syncopal attack was sometimes described by their family members or bystanders. In the training set, we included children aged 5–17 years, and in the validation set, we recruited the subjects aged 5–15 years, although the diagnostic criteria were kept the same. The study was a retrospective study, in which only hospitalized children were included. Therefore, prospective, multicenter and large sample-sized studies are still necessary to optimize this model. Nevertheless, in the present study, we developed a useful, easy-to-operate, and very inexpensive clinical characteristics-based scoring model for pediatricians to make a quick and initial differentiation between PPS and VVS in children.

CONCLUSION

This study developed a clinical manifestation-based scoring model to differentiate PPS from VVS, assisting in making a quick initial differential diagnosis. Further multicenter studies are still needed to improve the ability to differentially diagnose pediatric TLOC cases.

DATA AVAILABILITY STATEMENT

The raw data supporting the conclusions of this article will be made available by the authors, without undue reservation.

ETHICS STATEMENT

The studies involving human participants were reviewed and approved by the Ethics Committee of Peking University First Hospital and Children's Hospital of Fudan University. Written informed consent for participation was not provided by the participants' legal guardians/next of kin because the required informed consent was permitted to be waived by the Ethics Committee of Peking University First Hospital and Children's Hospital of Fudan University.

AUTHOR CONTRIBUTIONS

YZ, HJ, JD, and HT presented thesis ideas and contributed to discussion. CL, YL, JD, HJ, and QZ assisted in collecting and analyzing data. HT, LH, and SL provided external validation data and performed analysis. JF and DZ contributed to discussion. CL, YL, and LH wrote the original manuscript. JD, YZ, HJ, and HT critically reviewed and proofread the manuscript. All authors have read and agreed to submit the manuscript.

FUNDING

This study was supported by Peking University Clinical Scientist Program (BJMU2019LCKXJ001) and the Fundamental Research Funds for the Central Universities.

REFERENCES

1. Sheldon RS, Grubb BP, Olshansky B, Shen WK, Calkins H, Brignole M, et al. 2015 heart rhythm society expert consensus statement on the diagnosis and treatment of postural tachycardia syndrome, inappropriate sinus tachycardia, and vasovagal syncope. *Heart Rhythm.* (2015) 12:e41–63. doi: 10.1016/j.hrthm.2015.03.029
2. Moya A, Sutton R, Ammirati F, Blanc JJ, Brignole M, Dahm JB, et al. Guidelines for the diagnosis and management of syncope (version 2009). *Eur Heart J.* (2009) 30:2631–71. doi: 10.1093/eurheartj/ehp298
3. Kenny RA, Brignole M, Dan GA, De Haro JC, Savelieva I. Syncope unit: rationale and requirement—the European Heart Rhythm Association position statement endorsed by the Heart Rhythm Society. *Europace.* (2015) 17:1325–40. doi: 10.1093/europace/euv115
4. Jin H. Du J. Pediatric syncope: where are we now? *Chin Med J (Engl).* (2014) 127:3681–3. doi: 10.3760/cma.j.issn.0366-6999.20132944
5. Heyer GL. Youth with psychogenic non-syncopal collapse have more somatic and psychiatric symptoms and lower perceptions of peer relationships than youth with syncope. *Pediatr Neurol.* (2018) 79:34–9. doi: 10.1016/j.pediatrneurol.2017.11.009
6. Heyer GL, Pabst LM, Kaucic BN, Coley TA. Early outcomes in youth with psychogenic nonsyncopal collapse. *Neurology.* (2018) 91:e850–8. doi: 10.1212/WNL.0000000000006098
7. Saal DP, Overdijk MJ, Thijs RD, van Vliet IM, van Dijk JG. Long-term follow-up of psychogenic pseudosyncope. *Tijdschr Psychiatr.* (2018) 60:297–305. doi: 10.1212/WNL.0000000000003361
8. Heyer GL, Albert DV, Weber A, Gedela S, Vidaurre J. Comparison of semiologies between tilt-induced psychogenic nonsyncopal collapse and psychogenic nonepileptic seizures. *Epilepsy Behav.* (2016) 62:171–5. doi: 10.1016/j.yebeh.2016.06.027
9. Walsh KE, Baneck T, Page RL, Brignole M, Hamdan MH. Psychogenic pseudosyncope: not always a diagnosis of exclusion. *Pacing Clin Electrophysiol.* (2018) 41:480–6. doi: 10.1111/pace.13316
10. Robinson JA, Shivapour JK, Snyder CS. Tilt table testing to diagnose pseudosyncope in the pediatric population. *Congenit Heart Dis.* (2017) 12:411–6. doi: 10.1111/chd.12458
11. Iglesias JF, Graf D, Forclaz A, Schlaepfer J, Fromer M, Pruvot E. Stepwise evaluation of unexplained syncope in a large ambulatory population. *Pacing Clin Electrophysiol.* (2009) 32(Suppl. 1):S202–6. doi: 10.1111/j.1540-8159.2008.02291.x
12. Heyer GL, Harvey RA, Islam MP. Comparison of specific fainting characteristics between youth with tilt-induced psychogenic nonsyncopal collapse versus reflex syncope. *Am J Cardiol.* (2017) 119:1116–20. doi: 10.1016/j.amjcard.2016.12.018
13. Raj V, Rowe AA, Fleisch SB, Paranjape SY, Arain AM, Nicolson SE. Psychogenic pseudosyncope: diagnosis and management. *Auton Neurosci.* (2014) 184:66–72. doi: 10.1016/j.autneu.2014.05.003
14. Benbadis SR, Chichkova R. Psychogenic pseudosyncope: an underestimated and provable diagnosis. *Epilepsy Behav.* (2006) 9:106–10. doi: 10.1016/j.yebeh.2006.02.011
15. Alciati A, Shiffer D, Dipaola F, Barbic F, Furlan R. Psychogenic pseudosyncope: clinical features, diagnosis and management. *J Atr Fibrillation.* (2020) 13:2399. doi: 10.4022/jafib.2399
16. Kenny RA, Ingram A, Bayliss J, Sutton R. Head-up tilt: a useful test for investigating unexplained syncope. *Lancet.* (1986) 1:1352–5. doi: 10.1016/S0140-6736(86)91665-X
17. Shen WK, Sheldon RS, Benditt DG, Cohen MI, Forman DE, Goldberger ZD, et al. 2017 ACC/AHA/HRS guideline for the evaluation and management of patients with syncope: a report of the American College of Cardiology/American Heart Association Task Force on Clinical Practice Guidelines and the Heart Rhythm Society. *Heart Rhythm.* (2017) 14:e155–217. doi: 10.1016/j.hrthm.2017.03.004
18. Lai WT, Chen MR, Lin SM, Hwang HK. Application of head-up tilt table testing in children. *J Formos Med Assoc.* (2010) 109:641–6. doi: 10.1016/S0929-6646(10)60104-0
19. Wang C, Du J, Y Li, Y Liao, Tian H, Huang M, et al. 2018 Chinese Pediatric Cardiology Society (CPCS) guideline for diagnosis and treatment of syncope in children and adolescents. *Sci Bull.* (2018) 63:1558–64. doi: 10.1016/j.scib.2018.09.019
20. Brignole M, Moya A, de Lange FJ, Deharo JC, Elliott PM, Fanciulli A, et al. 2018 ESC Guidelines for the diagnosis and management of syncope. *Eur Heart J.* (2018) 39:1883–948. doi: 10.1093/eurheartj/ehy037
21. Anderson JB, Willis M, Lancaster H, Leonard K. Thomas C. The evaluation and management of pediatric syncope. *Pediatr Neurol.* (2016) 55:6–13. doi: 10.1016/j.pediatrneurol.2015.10.018
22. Seifer CM, Kenny RA. Head-up tilt testing in children. *Eur Heart J.* (2001) 22:1968–71. doi: 10.1053/euhj.2001.2907
23. Tannemaat MR, Thijs RD, van Dijk JG. Managing psychogenic pseudosyncope: facts and experiences. *Cardiol J.* (2014) 21:658–64. doi: 10.5603/CJ.a2014.0070
24. Zhang Z, Jiang X, Han L, Chen S, Tao L, Tao C, et al. Differential diagnostic models between vasovagal syncope and psychogenic pseudosyncope in children. *Front Neurol.* (2020) 10:1392. doi: 10.3389/fneur.2019.01392
25. Francesmonneris A, Pincus H, First M. Diagnostic and statistical manual of mental disorders: DSM-V[M]. Washington, DC: *American Psychiatric Association*. (2013). pp. 318–9.
26. Subspecialty Group of Cardiology, The Society of Pediatrics, Chinese Medical Association, Editorial Board, Chinese Journal of Pediatrics. Guidelines for diagnosis of syncope in children. *Zhonghua er ke za zhi, Chin J Pediatr.* (2009) 47:99–101. doi: 10.3760/cma.j.issn.0578-1310.2009.02.006
27. Lin J, Wang Y, Ochs T, Tang C, Du J, Jin H. Tilt angles and positive response of head-up tilt test in children with orthostatic intolerance. *Cardiol Young.* (2015) 25:76–80. doi: 10.1017/S1047951113001601
28. Tannemaat MR, van Niekerk J, Reijntjes RH, Thijs RD, Sutton R, van Dijk JG. The semiology of tilt-induced psychogenic pseudosyncope. *Neurology.* (2013) 81:752–8. doi: 10.1212/WNL.0b013e3182a1aa88
29. Blad H, Lamberts RJ, van Dijk GJ, Thijs RD. Tilt-induced vasovagal syncope and psychogenic pseudosyncope: overlapping clinical entities. *Neurology.* (2015) 85:2006–10. doi: 10.1212/WNL.0000000000002184
30. Tao CY, Chen S, Li XY, Tang CS, Du JB, Jin HF. Body mass index is a promising predictor of response to oral rehydration saline in children with vasovagal syncope. *Chin Med J (Engl).* (2020) 134:463–8. doi: 10.1097/CM9.0000000000001168
31. Ghristou GA, Kiortsis DN. The effects of body weight status on orthostatic intolerance and predisposition to noncardiac syncope. *Obes Rev.* (2017) 18:370–9. doi: 10.1111/obr.12501

32. Forleo C, Guida P, Iacoviello M, Resta M, Monitillo F, Sorrentino S, et al. Head-up tilt testing for diagnosing vasovagal syncope: a meta-analysis. *Int J Cardiol.* (2013) 168:27–35. doi: 10.1016/j.ijcard.2012.09.023

Conflict of Interest: The authors declare that the research was conducted in the absence of any commercial or financial relationships that could be construed as a potential conflict of interest.

Publisher's Note: All claims expressed in this article are solely those of the authors and do not necessarily represent those of their affiliated organizations, or those of the publisher, the editors and the reviewers. Any product that may be evaluated in this article, or claim that may be made by its manufacturer, is not guaranteed or endorsed by the publisher.

frontiers in Cardiovascular Medicine

ORIGINAL RESEARCH
published: 28 February 2022
doi: 10.3389/fcvm.2022.852775

Loss of m^{6}A Methyltransferase METTL5 Promotes Cardiac Hypertrophy Through Epitranscriptomic Control of SUZ12 Expression

Yanchuang Han[1,2†], Tailai Du[1,2†], Siyao Guo[1†], Lu Wang[1], Gang Dai[2], Tianxin Long[1,2], Ting Xu[1,2], Xiaodong Zhuang[1,2], Chen Liu[1,2], Shujuan Li[1,2], Dihua Zhang[3], Xinxue Liao[1,2], Yugang Dong[1,2], Kathy O. Lui[4], Xu Tan[5], Shuibin Lin[1], Yili Chen[1,2] and Zhan-Peng Huang[1,2*]*

[1] Department of Cardiology, Center for Translational Medicine, Institute of Precision Medicine, The First Affiliated Hospital, Sun Yat-sen University, Guangzhou, China, [2] NHC Key Laboratory of Assisted Circulation, Sun Yat-sen University, Guangzhou, China, [3] Department of Nephrology, The First Affiliated Hospital, Sun Yat-sen University, Guangzhou, China, [4] Department of Chemical Pathology, Li Ka Shing Institute of Health Sciences, The Chinese University of Hong Kong, Prince of Wales Hospital, Shatin, Hong Kong SAR, China, [5] School of Pharmaceutical Sciences, Center for Infectious Disease Research, School of Medicine, Tsinghua University, Tsinghua-Peking Center for Life Sciences, Beijing, China

Enhancement of protein synthesis from mRNA translation is one of the key steps supporting cardiomyocyte hypertrophy during cardiac remodeling. The methyltransferase-like5 (METTL5), which catalyzes m^{6}A modification of 18S rRNA at position A_{1832}, has been shown to regulate the efficiency of mRNA translation during the differentiation of ES cells and the growth of cancer cells. It remains unknown whether and how METTL5 regulates cardiac hypertrophy. In this study, we have generated a mouse model, METTL5-cKO, with cardiac-specific depletion of METTL5 *in vivo*. Loss function of METTL5 promotes pressure overload-induced cardiomyocyte hypertrophy and adverse remodeling. The regulatory function of METTL5 in hypertrophic growth of cardiomyocytes was further confirmed with both gain- and loss-of-function approaches in primary cardiomyocytes. Mechanically, METTL5 can modulate the mRNA translation of SUZ12, a core component of PRC2 complex, and further regulate the transcriptomic shift during cardiac hypertrophy. Altogether, our study may uncover an important translational regulator of cardiac hypertrophy through m6A modification.

Keywords: cardiac hypertrophy, METTL5, RNA modification, translational regulation, SUZ12

OPEN ACCESS

Edited by:
Jin Li,
Shanghai University, China

Reviewed by:
Dongchao Lu,
Hannover Medical School, Germany
Zhi Xin Shan,
Guangdong Provincial People's Hospital, China

***Correspondence:**
Zhan-Peng Huang
huangzhp27@mail.sysu.edu.cn
Yili Chen
chenyil7@mail.sysu.edu.cn

†These authors have contributed equally to this work

Specialty section:
This article was submitted to General Cardiovascular Medicine, a section of the journal Frontiers in Cardiovascular Medicine

Received: *11 January 2022*
Accepted: *02 February 2022*
Published: *28 February 2022*

Citation:
Han Y, Du T, Guo S, Wang L, Dai G, Long T, Xu T, Zhuang X, Liu C, Li S, Zhang D, Liao X, Dong Y, Lui KO, Tan X, Lin S, Chen Y and Huang Z-P (2022) Loss of m^{6}A Methyltransferase METTL5 Promotes Cardiac Hypertrophy Through Epitranscriptomic Control of SUZ12 Expression. Front. Cardiovasc. Med. 9:852775. doi: 10.3389/fcvm.2022.852775

INTRODUCTION

The cardiac plasticity refers to the capability of the heart to remodel in response to environmental demands. One of the cardiac responses to mechanical or pathological stress is cardiac hypertrophy (1). Hypertrophic growth of cardiomyocytes, in which the size and contractile force of cardiomyocytes increase significantly, is one of the major cellular changes in response to stress. It has been well-studied that hypertrophic growth involves control of cardiomyocyte gene expression at multiple molecular levels (2, 3). Multiple signal transduction pathways, such as PI3K/AKT (4)

and MAPK (5), and transcriptional factors, such as MEF2 (6), NFAT (7), and GATA4 (8), have been demonstrated to control the shift of transcriptome toward hypertrophy. Enhanced protein synthesis and sarcomere assembly are main features of hypertrophic growth of cardiomyocytes. The observation that transcriptome data deviate from mass spectrum data (9) indicates that translational control is a key step of regulating this cellular process. Recently, our study suggests that the increased quantity of ribosomes is one of the main contributors of enhanced protein synthesis in cardiomyocyte hypertrophy (10). However, how cardiac hypertrophy is controlled at the step of translation remains largely unknown.

Methylation is one of the well-known modifications in ribonucleic acid, including m^6A, m^5C, m^1A, m^7G, and m^6Am (11). These modified nucleic acids widely exist in ribosomal RNAs, transfer RNAs, messenger RNAs and even some non-coding RNAs (12). Enzymes responsible for the dynamics of these RNA modifications have also been explored. For example, the METTL3/METTL14/WTAP protein complex is responsible for adding a methyl group to the targeted adenosine in RNAs (13, 14), whereas demethylases, such as FTO (15) and ALKBH5 (16), erase the existing m^6A modification from RNA molecules. In addition, multiple proteins, including YTHDC1, YTHDC2, YTHDF1, YTHDF2, and YTHDF3, have been identified as "readers," which recognize and bind to m6A-modifed RNAs, and promote different processes, such as mRNA export from nucleus, mRNA degradation and mRNA translation (17). Two m^6A RNA modification readers, YTHDF1 and YTHDF3, have been shown to promote the translational efficiency of their target mRNAs by interacting with ribosome 40S and 60S subunits and translation initiation factor complex 3 (18, 19). These studies indicate m^6A methylation could play an important role in regulating gene expression at the step of translation. Indeed, alteration of m^6A methylation leads to the change of protein abundance in an mRNA-level-independent manner during heart failure (20). The importance of translational control in cardiac remodeling and cardiomyocyte hypertrophy indicates m^6A RNA methylation dynamics is critical to the pathogenesis of cardiac disease. Supportively, recent work has demonstrated that manipulation of cardiac m^6A modification level by either depleting m^6A "writer" METTL3 (21) or overexpressing "eraser" FTO (22) regulates cardiac disease progression in different pathological conditions.

METTL5 is a methyltransferase containing a typical SAM-binding motif and a conserved m^6A-catalyzing NPPF motif (23). Recent studies have demonstrated that METTL5 forms a complex with TRMT112 and catalyzes methylation of 18S rRNA m^6A_{1832} (23–25). METTL5 has been shown to regulate the differentiation of embryonic stem (ES) cells (24, 26) and the growth of cancer cells (27). Furthermore, mechanistic studies link the function of METTL5 to the regulation of mRNA translation by possibly fine-tuning the interaction between ribosome decoding center and translating mRNA through methylation of 18S rRNA (27). However, the functional role of METTL5 in cardiac physiology and pathology has not yet been studied. In this study, we take advantage of a genetic model, in which the function of METTL5 is abolished in a cardiomyocyte-specific manner, to study its function in the heart. We show that METTL5 promotes stress-induced cardiac hypertrophy mainly via regulating the translation of SUZ12 mRNA. Altogether, our study may uncover an important translational mechanism for maintaining the homeostats of heart cells via epitranscriptomic regulation.

RESULTS

The Expression Profile of METTL5 and Its Physiological Function in the Heart

Thus far, little is known about how N^6-methyladenosine (m^6A) modification of 18S rRNA at position A_{1832}, which has been widely reported to be mediated by methyltransferase METTL5 (23–27), regulates cardiac physiology and/or pathology. To understand its function in the heart, we first examined its expression levels in different organs. Multiple mouse organs, including the heart, liver, lung, spleen, kidney, eye, brain and skeletal (Sk.) muscle, were collected from the neonatal (1 week) and adult (4.5 months) stages. METTL5 was detected as ubiquitously expressed in all tissues examined (**Figure 1A**). We then asked whether the expression level of METTL5 alters under pathological conditions. As a result, the expression level of METTL5 was reduced in Calcineurin transgenic (CnA-Tg) hearts but remained unaltered in transverse aortic binding (TAC)-induced cardiac hypertrophy (**Figure 1B**). In addition, the expression level of METTL5 in human samples collected from patients with heart failure was also tested (**Supplementary Table 1**). The mRNA and protein levels of METTL5 tended to decrease in the human failing hearts, respectively (**Figures 1C,D**).

METTL5 knockout (KO) mice were reported viable recently by our group and others (24, 26). Cardiac histological and transcriptomic analyses of 1-month-old METTL5-KO mice and their control littermates showed no obvious cardiac abnormality (**Supplementary Figures 1, 2** and **Supplementary Table 2**), indicating that METTL5 is dispensable for heart development. To specifically study the function of METTL5 in cardiomyocytes *in vivo*, Myh6-Cre was crossed with $METTL5^{fl/fl}$, in which exons 2, 3 and 4 are floxed, to generate the cardiac-specific METTL5 depleted (METTL5-cKO) mice (**Figure 1E**). The 3 months old METTL5-cKO mouse hearts showed no obvious abnormality by echocardiography and histological examination (**Supplementary Figure 3** and **Supplementary Table 3**). Similarly, transcriptomic analyses only detected 28 genes with significant difference in METTL5-cKO hearts (**Supplementary Table 4**). Of note, the floxed exons 2–4 of METTL5 were almost undetectable in METTL5-cKO hearts, indicating that METTL5 was predominately expressed in cardiomyocytes (**Figure 1F**).

Cardiac-Specific Ablation of METTL5 Promotes Stress-Induced Cardiac Remodeling

In order to understand the function of METTL5 in cardiac remodeling, METTL5-cKO mice and control littermates were subjected to TAC surgery, which induced pressure overload in the left ventricle. As expected, echocardiographic examination

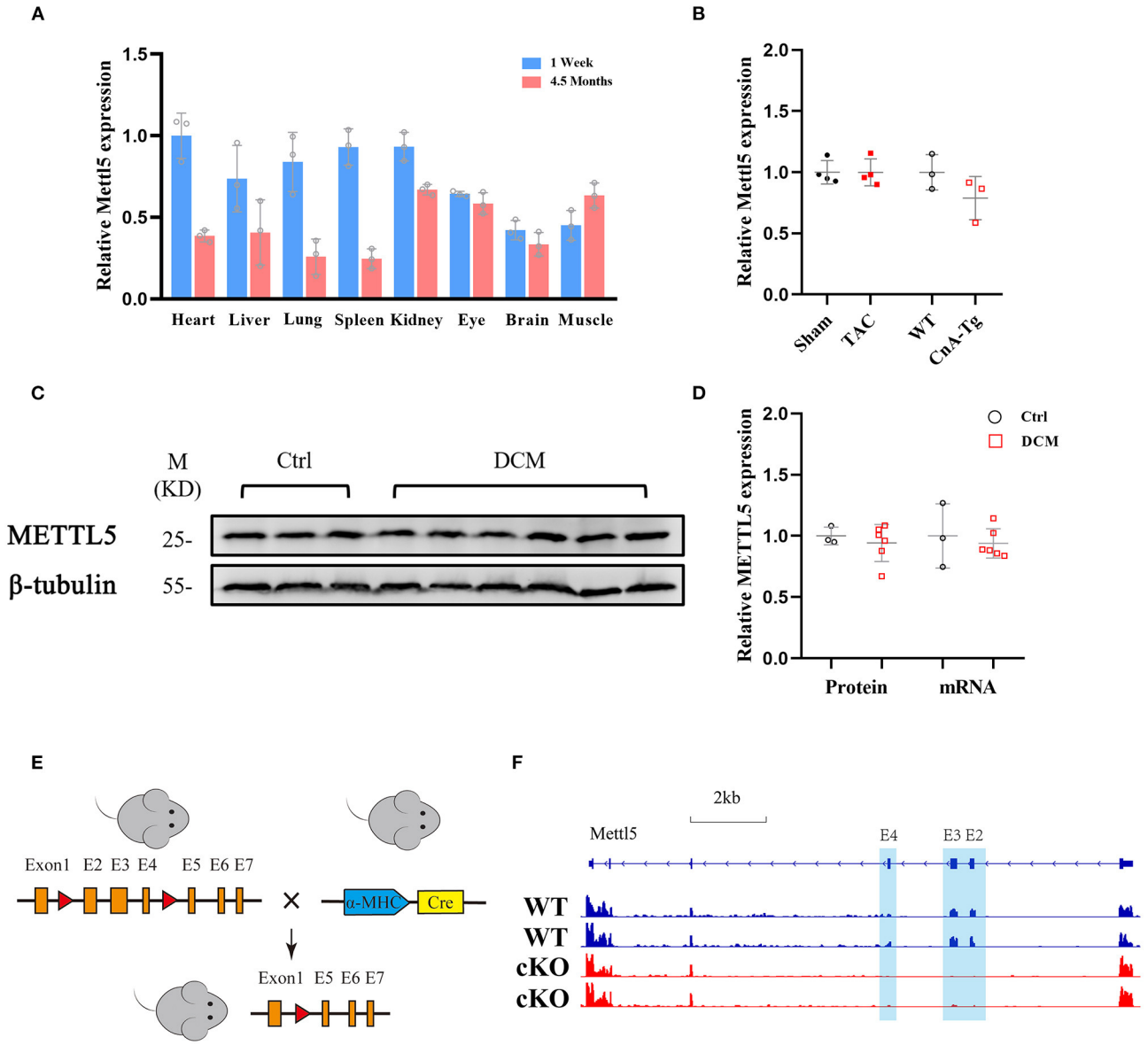

FIGURE 1 | METTL5 expression profile and the generation of METTL5-cKO mouse. **(A)** Relative gene expression of METTL5 in different organs from 1 week and 4.5 months old mice by RT-PCR. $n = 3$ mice in each group. **(B)** Relative gene expression of METTL5 in TAC vs. Sham ($n = 3$ mice in each group) and CnA-Tg vs. WT ($n = 4$ mice in each group) mouse hearts by RT-PCR. **(C)** The protein level of METTL5 in control patient hearts ($n = 3$) and dilated cardiomyopathy (DCM) patient hearts ($n = 6$) by western blotting. β-tubulin srerves as a control. **(D)** Quantification of western blotting in panel C and the relative expression of METTL5 in control patient hearts ($n = 3$) and DCM patient hearts ($n = 6$) by RT-PCR. **(E)** Schematic of generation of METTL5 cardiomyocyte-specific knockout (METTL5-cKO) mouse. **(F)** The genomic view of reads in RNA-seq for METTL5 in the IGV browser.

showed significant increase in left ventricular posterior wall thickness (LVPW) without obvious chamber dilation and decrease in cardiac function in control mice at 4 weeks post-TAC (**Figures 2A,B** and **Table 1**). In contrast, loss of METTL5 promoted TAC-induced cardiac remodeling with progression to heart failure in the METTL5-cKO group, which was associated with significantly increased left ventricular internal dimension (LVID) and dramatic reduced fraction shortening (FS) (**Figures 2B,C** and **Table 1**). Hearts were collected at 4 weeks post-TAC after echocardiographic examination. The ratio of ventricular weight vs. body weight (Vw vs. Bw) and gross morphology consistently demonstrated the enlargement of METTL5-cKO hearts in the TAC group compared to that of the control hearts (**Figures 2D,E**). In addition, histological examination showed the obvious chamber dilation of METTL5-cKO TAC hearts (**Figure 2F**). Adverse cardiac remodeling and heart failure are often associated with increased cardiac fibrosis. Indeed, Sirius red/Fast green staining showed significantly

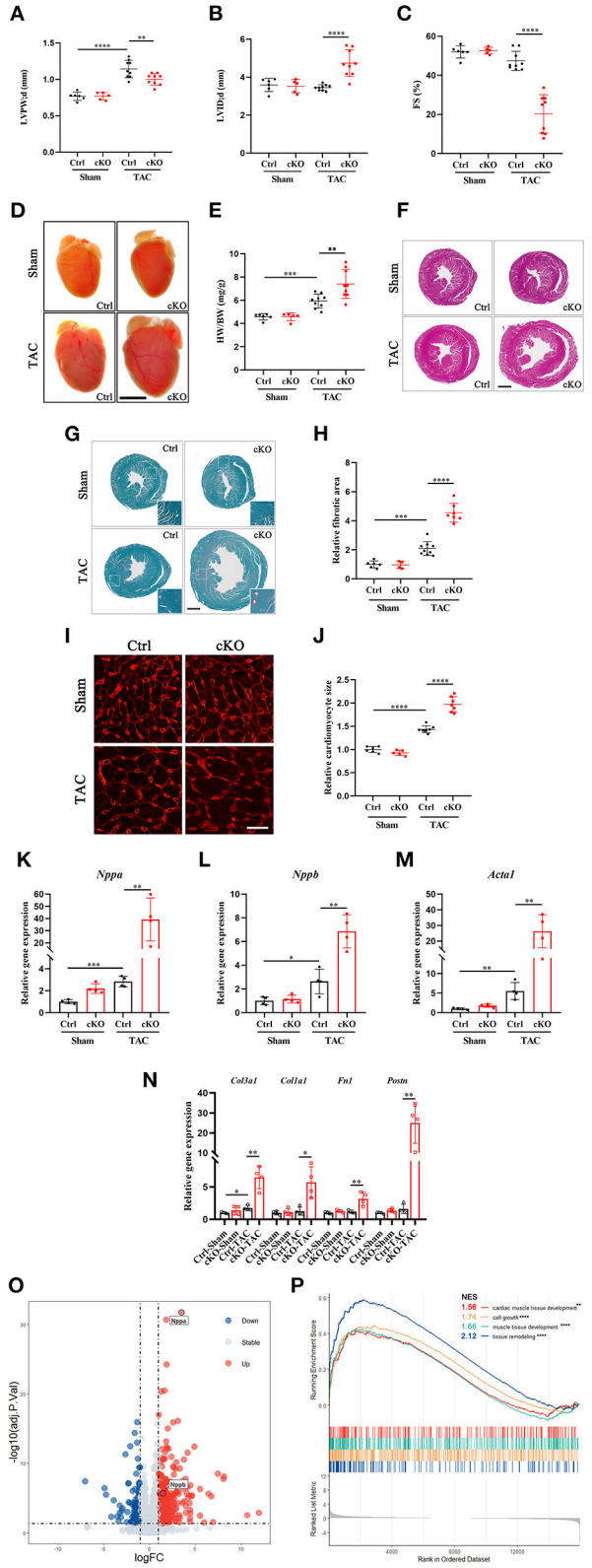

FIGURE 2 | Cardiac-specific knockout of METTL5 *in vivo* promotes TAC-induced cardiac remodeling. **(A–C)** Left ventricular posterior wall thickness at end-diastole (LVPW;d), Left ventricular internal dimension at end-diastole (LVID;d), and Fractional shortening (FS) of TAC or sham operated METTL5-cKO and control mice at 4 weeks after surgery. *N* number ($n > 4$) for each group is indicated by the number of dots. **(D)** Representative images of gross morphology of METTL5-cKO and control hearts 4 weeks after TAC or sham operation. Scale bar = 5 mm. **(E)**. Quantification of heart weight to body weight ratio (HW/BW) of METTL5-cKO and control mice 4 weeks after TAC or sham operation. *N* number ($n > 4$) for each group is indicated by the number of dots. **(F)** Representative images of H&E staining of METTL5-cKO and control hearts 4 weeks after TAC or sham operation. Scale bar = 1 mm. **(G)** Representative images of Fast green and Sirius red staining of METTL5-cKO and control hearts 4 weeks after TAC or sham operation. Scale bar = 1 mm. **(H)** The fibrotic area of images from Fast green and Sirius red staining is quantified. *N* number ($n > 3$) for each group is indicated by the number of dots. **(I)** Heart cross sections were stained with wheat germ agglutinin (WGA). Scale bar = 25 μm. **(J)** Cardiomyocyte cross-sectional area was quantified. More than 500 cardiomyocytes from five hearts are quantified for each group. **(K–M)** Relative gene expression of hypertrophy marker genes by RT-PCR. $n = 4$ mice in each group. N. Relative gene expression of fibrosis related genes by RT-PCR. $n = 4$ mice in each group. **(O)** Volcano plot of differentially expressed genes in METTL5-cKO and control hearts 4 weeks after TAC operation. **(P)** GSEA analysis of differentially expressed genes in METTL5-cKO and control hearts 4 weeks after TAC operation. (The unpaired *T*-test was used for 2-group comparisons. $^{*}P < 0.05$, $^{**}P < 0.01$, $^{***}P < 0.001$, $^{****}P < 0.0001$).

increased fibrosis in TAC control hearts, which was further increased in METTL5-cKO TAC hearts (**Figures 2G,H**). In line with the further progression of cardiac remodeling in METTL5-cKO TAC group, Wheat Germ Agglutinin (WGA) staining indicated further hypertrophic growth of cardiomyocytes, which was evident by the cross area of cardiomyocytes, in METTL5-cKO TAC hearts compared to that of the control TAC hearts (**Figures 2I,J**).

Gene expression was detected to confirm the above observation. The expression levels of fetal genes, including Nppa, Nppb, and Acta1, which are often elevated in cardiac hypertrophy, were further increased in METTL5-cKO TAC hearts (**Figures 2K–M**). Similarly, the expression levels of genes related to fibrosis, such as Col1a1, Col3a1, Fn1, and Postn, were dramatically increased in METTL5-cKO group under stress (**Figure 2N**). RNA sequencing were further performed to monitor the globe shift of transcriptome. A total of 392 upregulated genes, including Nppa and Nppb, and 146 downregulated genes ($|\text{Log}_2 \text{ fold change}| > 1$; $p < 0.05$) were detected (**Figure 2O** and **Supplementary Table 5**). GSEA analysis showed the activities of several cardiac hypertrophy-related KEGG pathways, such as cardiac muscle tissue development, cell growth, muscle tissue development and tissue remodeling, were enhanced (**Figure 2P**). Together, these data consistently demonstrated that the loss of METTL5 promoted cardiac remodeling induced by pressure overload.

METTL5 Mediates Hypertrophic Growth of Cardiomyocytes

Our data indicated that METTL5 was dominantly expressed in cardiomyocytes. We therefore suggested that METTL5 could

TABLE 1 | Echocardiography examination of METTl5-cKO mice and their control littermates with transverse aortic constriction (TAC) or sham operation at 4 weeks after surgery.

	Ctrl; Sham ($N = 6$)	METTL5-cKO; Sham ($N = 5$)	Ctrl; TAC ($N = 9$)	METTL5-cKO; TAC ($N = 9$)
IVS;d (mm)	0.732 ± 0.053	0.752 ± 0.022	1.145 ± 0.085**	1.004 ± 0.079##
IVS;s (mm)	1.362 ± 0.033	1.415 ± 0.148	1.789 ± 0.145**	1.345 ± 0.191##
LVID;d (mm)	3.590 ± 0.345	3.526 ± 0.353	3.452 ± 0.152	4.741 ± 0.706##
LVID;s (mm)	1.728 ± 0.233	1.672 ± 0.203	1.816 ± 0.199	3.834 ± 1.009##
LVPW;d (mm)	0.768 ± 0.056	0.769 ± 0.051	1.143 ± 0.120**	1.002 ± 0.078##
LVPW;s (mm)	1.413 ± 0.059	1.416 ± 0.117	1.733 ± 0.124**	1.346 ± 0.218##
EF (%)	83.83 ± 2.96	84.51 ± 1.61	79.53 ± 4.60	40.40 ± 17.75##
FS (%)	52.01 ± 3.16	52.64 ± 1.71	47.43 ± 4.90	20.30 ± 9.83##
LV Mass (mg)	91.01 ± 17.39	89.93 ± 16.93	156.84 ± 24.75**	212.53 ± 46.00##
LV Mass (Corrected, mg)	72.81 ± 13.91	71.94 ± 13.55	125.47 ± 19.80**	170.02 ± 36.80##
LV Vol;d (uL)	54.73 ± 11.90	52.42 ± 12.24	49.35 ± 5.25	107.42 ± 36.59##
LV Vol;s (uL)	8.99 ± 2.78	8.22 ± 2.45	10.14 ± 2.81	69.25 ± 41.25##
Heart Rate (BPM)	663 ± 42	674 ± 15	696 ± 17	671 ± 45

$^{**}P_{Ctrl;Shamvs.Ctrl;TAC} < 0.01$; $^{\#\#}P_{Ctrl;TACvs.CIP-OE;TAC} < 0.01$.

regulate hypertrophic growth of cardiomyocytes in a cell-autonomous manner. The expression of METTL5 was knocked down in isolated neonatal rat ventricular cardiomyocytes (NRVM) (**Figure 3A**). Quantification of cell size indicated that loss-of-function of METTL5 promoted phenylephrine (PE)-induced hypertrophic growth of cardiomyocytes (**Figures 3B,C**). To confirm this observation, the detection of gene expression showed that knockdown of METTL5 further promoted the expression of hypertrophic marker genes, including Nppa, Nppb, and Acta1, in PE-treated NRVMs (**Figures 3D–F**). The enhanced levels of phosphorylation of ERK1/2 and S6 ribosomal protein are often connected to cardiac hypertrophy. Western blotting showed that the expression levels of both phosphorylated proteins were further elevated in the PE-treated METTL5 knockdown NRVMs (**Figures 3G–J**). On the contrary, we asked whether forced expression of METTL5 in NRVMs showed the opposite effect on hypertrophy. Indeed, forced expression of METTL5 with adenovirus repressed PE-induced hypertrophic growth in NRVMs as evident by the smaller cell size of Ad-METTL5-treated NRVMs (**Figures 3K,L** and **Supplementary Figure 4**). In addition, forced expression of METTL5 dramatically inhibited the induced expression of Nppa, Nppb, and Acta1 by PE treatment (**Figures 3M–O**). Collectively, these data demonstrated that METTL5 regulated the hypertrophic growth of cardiomyocytes.

SUZ12 Is a Key Regulator of METTL5-Medited Cardiac Phenotype

To explore the molecular mechanism downstream of METTL5 in cardiomyocytes, transcriptomic shift caused by gain- and loss-of-function of METTL5 in NRVMs were monitored by RNA sequencing followed by a series of analyses (**Figure 4A**). A total of 316 and 981 dysregulated genes ($|\text{Log}_2$ fold change$|>1$; $p < 0.05$) were detected in si-METTL5 and Ad-METTL5 treated NRVMs under the stimulation of PE, respectively (**Figure 4B** and **Supplementary Tables 6, 7**). Analyses indicated that 52 dysregulated genes, including Nppa, Nppb, and Acta1, were overlapped but showed an opposite expression trend of dysregulation between Ad-METTL5 and si-METTL5 treated NRVMs (**Figures 4C,D**). Multiple key pathways of cardiac hypertrophy, such as Adrenegic signaling and MAPK signaling, were significantly altered in the KEGG analyses, that showed an opposite direction of alteration in si-METTL5 treated NRVMs vs. Ad-METTL5 treated NRVMs (**Figure 4E**). We further asked whether these dysregulated genes were controlled by one or more upstream regulators. Dysregulated genes from both datasets were subjected to upstream factor analysis with two independent algorithms, X2K (28) and Lisa (29). Excitingly, SUZ12, a core component of PRC2 complex, was the top hit of the list from both analyses (**Figure 4F** and **Supplementary Figure 5**). Given that PRC2 complex has been recently reported to participate in regulating cardiac hypertrophy (30, 31), our data could suggest that SUZ12 was a key upstream regulator mediating the METTL5-related cardiac phenotype observed above.

METTL5 Translationally Regulates the Expression of SUZ12

Next, we asked how METTL5 regulated the SUZ12-mediated signaling in cardiac hypertrophy. First, we carefully checked the transcript level of SUZ12 from transcriptome analyses of Ad-METTL5 and si-METTL5 treated NRVMs. To our surprise, no significant alteration of SUZ12 expression is found (**Figures 5A,B**). METTL5 is known to regulate mRNA translation via modifying nucleotide (m^6A) in 18s rRNA (24, 27). Recently, METTL5-mediated translational control of differentiation regulator FBXW7 has been reported to play a key role in ES cell differentiation (32). Therefore, we suspected that METTL5 regulated the translational efficiency of SUZ12 mRNA in cardiac hypertrophy. Protein and mRNA expression of SUZ12 were detected in si-METTL5 treated NRVMs with PE induction. As a result, protein expression of SUZ12 was significantly decreased with no alteration of mRNA expression

(**Figures 5C,D**), indicating that the translational efficiency of SUZ12 mRNA was repressed when expression of METTL5 was reduced (**Figure 5E**). On the contrary, gain-of-function of METTL5 promoted the translational efficiency of the SUZ12 mRNA, evidenced with the increased SUZ12 protein level without change in its mRNA expression level (**Figures 5F–H**). To validate the role of SUZ12 in METTL5-mediated inhibition of cardiac hypertrophy, we performed a rescue experiment by knocking down SUZ12 (**Figure 5I**). The expression of hypertrophic marker genes Nppa and Nppb, which was repressed by the overexpression of METTL5, was partially rescued by the SUZ12 knockdown (**Figure 5J**). Furthermore, the partial rescue effect in cardiac hypertrophy was also observed in the treatment of SUZ12/PRC2 inhibitors, EED226 and Boc-NH-C4-acid, during METTL5 overexpression (**Figure 5K**). Our data indicated that SUZ12 is an important regulator mediating the inhibitory function of METTL5 in cardiac hypertrophy. Mef2a and Mef2d are two major Mef2 family members expressed in the heart and key transcriptional factors for activating hypertrophy-related downstream genes (33, 34). Furthermore, PRC2 complex has been reported to regulate the expression of Mef2 family members (30). Therefore, we detected the expression of Mef2a and Mef2d in NRVMs with PE induction. As indicated, the expression levels of both Mef2a and Mef2d were significantly downregulated in NRVMs with forced expression of METTL5; while that of Mef2d was significantly increased after si-METTL5 treatment (**Figure 5L**). Taken together, our results suggested that the SUZ12(PRC2)-Mef2d axis could be critical in the regulation of cardiac hypertrophy by METTL5 mainly through modulating the translational efficiency of SUZ12 mRNA.

DISCUSSION

Nowadays, heart failure is still a deadly disease without effective cure. The complexity of the gene regulatory network underlying the disease development and the lack of fully understood molecular mechanism prevent us from developing novel and effective therapies targeting heart failure. Transcriptional and translational regulation are two critical control steps in the central dogma. Huge amount of efforts have been spent on investigating the transcriptomic shift in the failing heart, giving important insights into key signaling pathways and transcriptional factors in regulating the disease progression. Moreover, the recent findings of m^6A RNA modification connect the alteration of mRNA translational efficiency to heart failure, indicating the importance of translational control underlying the pathogenesis. However, little is known about how the key step of translation is regulated in the failing heart. In this study, we showed that METTL5 participated in the translational regulation of cardiac remodeling. Forced expression of METTL5 in cardiomyocytes repressed cardiac hypertrophy via modulating the translation of SUZ12 mRNA. In the future, investigation with a model using cardiac-specific overexpression of METTL5 *in vivo* should be carried out to test the therapeutic potential of controlling mRNA translation via METTL5 in delaying cardiac hypertrophy and the progression of heart failure.

METTL5 was ubiquitously detected in mouse organs, which was consistent with the expression data from Genotype-Tissue Expression Project (GTEx) in human. However, it was surprising to find that METTL5 was predominantly expressed in cardiomyocytes. This may suggest that METTL5 could mainly regulate the physiology and/or pathology of the heart. Although the decreased faction of polysome in the METTL5 loss-of-function system has been observed in several reports (24, 27), which indicates the translational efficiency of global mRNAs is affected; however, it seems that it is not entirely true when individual mRNA is evaluated. Ignatova et al. showed that only ∼500 transcripts with altered ribosome occupancy without concordant changes in mRNA levels in METTL5-KO ES cells (24), and a portion of these transcripts was even increased in translational efficiency. Therefore, the affected gene target(s) responsible for the observed phenotype could be context-dependent. For example, the decreased translational efficiency of FBXW7 affected by the loss of METTL5 has been reported to be mainly responsible for promoting mouse ES cell differentiation (32). In this study, our data indicated that the enhanced cardiac hypertrophy was mainly mediated by the decreased translation of SUZ12 mRNA in METTL5-depleted cardiomyocytes. More tissues or cell types are warrant to be investigated for the loss-of-function of METTL5 to gain more information of its function of translational regulation in the future.

In summary, our study uncovered that METTL5 was a key regulator of cardiac hypertrophy, highlighting the importance of regulation at the step of mRNA translation during the development of heart disease. The SUZ12-controlled PRC2-mef2d axis was identified in this study as the main signaling cascade mediating the function of METTL5 in cardiac remodeling (**Figure 6**). In the future, further investigation should be carried out to dissect the detail mechanism to explain how translational regulation and epigenetic regulation are coupled in the gene regulatory network during the development of cardiac hypertrophy and heart failure.

MATERIALS AND METHODS

Human Samples

Left ventricular (LV) tissues were collected from patients with dilated cardiomyopathy (DCM) during heart transplantation performed in the First Affiliated Hospital, Sun Yat-sen University. In brief, diseased hearts were removed at the time of transplantation and LV tissue was subsequently dissected and snap-frozen. We used LV samples from not implanted healthy hearts to serve as controls (**Supplementary Table 1**). All the procedures followed the protocol approved by the First Affiliated Hospital, Sun Yat-sen University, Guangzhou, China. All procedures conformed to the 1964 Helsinki declaration and its later amendments or comparable ethical standards.

Animal Studies

All experiments involving animals in this study were reviewed and approved by the Medical Ethics Committee of The First Affiliated Hospital, SunYet-sen University. Mice were housed under a 12 h light/dark cycle under pathogen-free conditions and

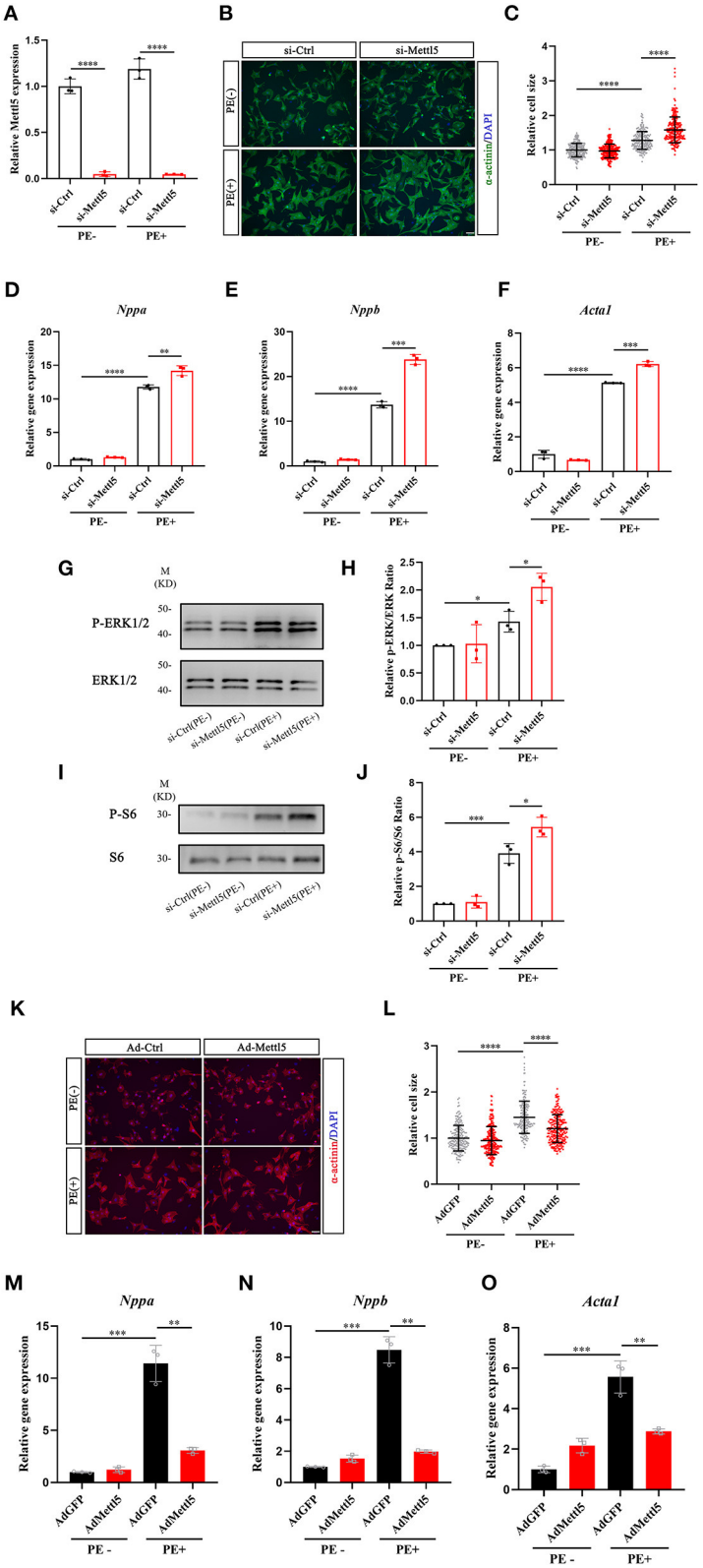

FIGURE 3 | METTL5 promotes hypertrophic growth of cardiomyocytes *in vitro.* **(A)** qRT-PCR detecting the knockdown of METTL5 in neonatal rat ventricular cardiomyocytes (NRVMs) with siRNA. $n = 3$ in each group. **(B)** Representative images of immunostaining of NRVMs transfected with si-METTL5 or control siRNA

(Continued)

FIGURE 3 | (si-Ctrl) with or without PE treatment. α-actinin labels cardiomyocytes. DAPI marks nuclei. Scale bar = 50 μm. **(C)** Quantification of the size of cardiomyocytes in panel B. More than 200 cells are measured in each group. **(D–F)** Relative gene expression of hypertrophy markers in NRVMs transfected with si-METTL5 or si-Ctrl with or without PE treatment. $n = 3$ in each group. **(G,H)** Detection of the expression of phosphorylated and total ERK in NRVMs transfected with si-METTL5 or si-Ctrl with or without PE treatment by western blotting. Protein level is quantified and the ratio of phospho-ERK to total ERK is presented. $n = 3$ in each group. **(I,J)** Detection of the expression of phosphorylated and total S6 in NRVMs transfected with si-METTL5 or si-Ctrl with or without PE treatment by western blotting. Protein level is quantified and the ratio of phospho-S6 to total S6 is presented. $n = 3$ in each group. **(K)** Representative images of immunostaining of NRVMs transduced with Ad-METTL5 or control virus (Ad-GFP) with or without PE treatment. α-actinin labels cardiomyocytes. DAPI marks nuclei. Scale bar = 50 μm. **(L)** Quantification of the size of cardiomyocytes in **(K)** More than 200 cells are measured in each group. **(M–O)** Relative gene expression of hypertrophy markers in NRVMs transduced with Ad-METTL5 or Ad-GFP with or without PE treatment. $n = 3$ in each group. The unpaired *T*-test was used for 2-group comparisons. $^{*}P < 0.05$, $^{**}P < 0.01$, $^{***}P < 0.001$, $^{****}P < 0.0001$.

with free access to standard mouse chow and tap water. This study conformed to the Guide for the Care and Use of Laboratory Animals published by the US National Institutes of Health (8th Edition, National Research Council, 2011). The METTL5-flox allele mice containing a floxed exon 2–4 of METTL5, which was engineered by CRISPR-mediated homologous recombination, was bred with αMHC-Cre mice (35) to generate cardiomyocyte-specific METTL5 knockout mice. Transverse aortic constriction (TAC) surgery was performed as previously described (36). 2–4% Isoflurane (in oxygen) was used for anesthetization and heating pad was used to maintain the mouse body temperature during the transverse aortic constriction surgery. Anesthesia of the mouse was performed with a nose cone delivering 2–4% Isoflurane in oxygen via small animal ventilator. The setting of ventilator was 110–120 breaths per min with a tidal volume of 0.1 mL under constant monitoring of the inspiratory pressure. At the end of the experiments, mice were killed with the intraperitoneal injection of an overdose of sodium pentobarbital (200 mg/kg).

Echocardiography Examination

Echocardiographic measurements of mice were performed using a Visual Sonics Vevo 2,100 Imaging System (Visual Sonics, Toronto, Canada) with an 18–38 MHz MicroScan transducer (model MS400). Heart rate and left ventricular (LV) dimensions, including diastolic and systolic wall thicknesses and LV end-diastolic and end-systolic chamber dimensions were measured from two dimensional (2D) short axis under M-mode tracings at the level of the papillary muscle. LV mass and functional parameters such as percentage of fractional shortening (FS%) and ejection fraction (EF%) were calculated using the above primary measurements and accompanying software.

Histology and Immunostaining

Mouse heart tissues were dissected out, rinsed with PBS, and fixed in 4% paraformaldehyde (pH 8.0) overnight. After dehydration through a series of ethanol baths, samples were embedded in paraffin wax according to standard laboratory procedures. Five micrometer sections were stained with H&E for routine histological examination with light microscope.

For Sirius red/Fast green staining, sections were fixed with pre-warmed Bouin's solution at 55°C for 1 h and then washed in running water. Sections were stained in 0.1% fast green solution for 10 min, then washed with 1% acetic acid for 2 min. After rinsing in tap water, sections were stained in 0.1% Sirius resolution for 30 min. After staining, sections were dehydrated and cleared with xylene. The images were examined with light scope and quantified with Image-Pro Plus software.

To quantify the cross-sectional area of cardiomyocytes, heart sections were deparaffined and stained with Wheat Germ Agglutinin (Alexa Fluor 594 Conjugate WGA; 1:200, Invitrogen) for labeling the cardiomyocyte membrane. Stained sections were examined with a fluorescence microscope (Zeiss; Imager.Z2), and the cross-sectional area of cardiomyocytes in the papillary muscles was quantified with ImageJ software.

qRT-PCR and Western Blot Analysis

Total RNAs were isolated using Trizol Reagent from cells and tissue samples. For qRT-PCR, 2.0 μg RNA samples were used for cDNA synthesis. In each analysis, 0.1 μL cDNA pool was used for qPCR. The relative expression of interested genes was normalized to the expression of GAPDH, β-actin or 18S. Primers for qRT-PCR were listed in **Supplementary Table 8**.

For western blotting analyses, tissue samples and cells were lysed in radioimmunoprecipitation assay (RIPA) buffer containing 1 mM PMSF and then denatured at 98°C for 10 min. Samples were subsequently analyzed by SDS-PAGE and transferred to 0.45 μm PVDF membranes. Blocking and blotting with primary antibodies were performed in Tris-buffered saline with Tween-20 (TBST), supplemented with 5 and 3% Bovine Serum Albumin (BSA), respectively. The antibodies used in this study included the following: ant-METTL5 (Proteintech; 16791-1-AP), anti-FLAG M2 (Sigma-Aldrich; F1804), anti-GAPDH (Cell Signaling Technology; cat #2118), anti-β-tubulin (Sigma-Aldrich; T0198), anti-phospho-Erk1/2 (Cell Signaling Technology; cat #4370), anti-total-Erk1/2 (Cell Signaling Technology; cat #4695), anti-phospho-S6 (Cell Signaling Technology; cat #4858), anti-total-S6 (Cell Signaling Technology; cat #2217), anti-SUZ12(Cell Signaling Technology; cat #3737). The membrane was incubated overnight at 4°C with the primary antibodies and washed three times with TBST buffer before adding horseradish peroxidase (HRP)-conjugated secondary antibodies. Specific protein bands were visualized using the Immobilon Western chemiluminescent HRP substrate (Millipore; WBKLS0500) by ImageQuant LAS4000 Mini (GE Healthcare).

METTL5 Expression Vector and Adenoviral Construction

The human METTL5 coding sequence was cloned into the adenoviral empty vector harboring the murine

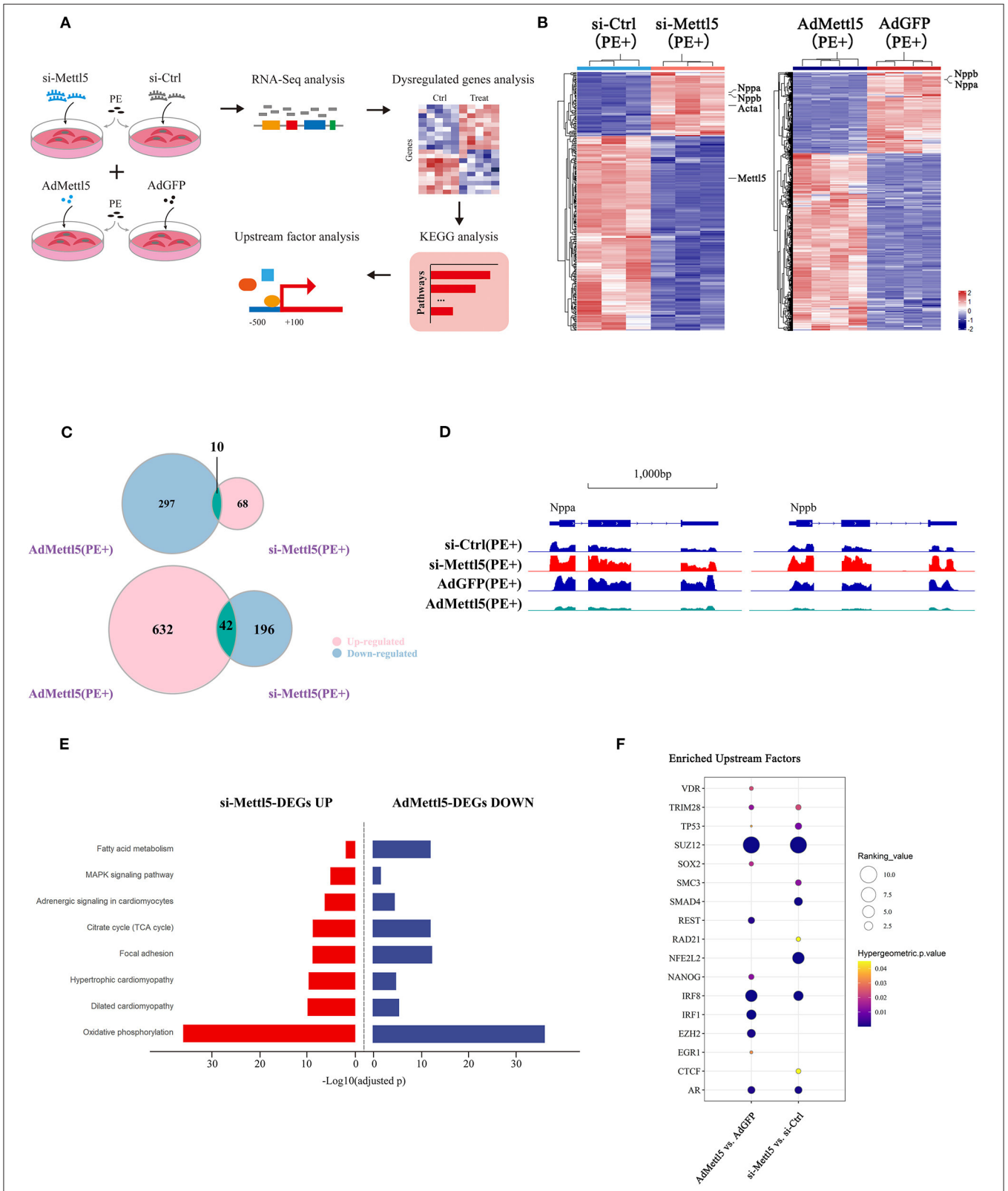

FIGURE 4 | Transcriptome analyses reveal SUZ12 as a key mediator of METTL5-regulated cardiac phenotype. **(A)** Schematic showing the experimental design and workflow of transcriptome analyses of siRNA and adenovirus-treated NRVMs under the stimulation of PE. **(B)** Hierarchical clustering of differentially expressed genes

(Continued)

FIGURE 4 | in groups of si-METTL5 vs. si-Ctrl and AdMETTL5 vs. AdGFP under the stimulation of PE. (|Log2FoldChange|>1, adjusted *P*-value < 0.05). **(C)** Venn diagram showing the overlap of upregulated- and downregulated-genes in groups of si-METTL5 vs. si-Ctrl and AdMETTL5 vs. AdGFP under the stimulation of PE, respectively. (|Log2FoldChange|>1, adjusted *P*-value < 0.05). **(D)** The genomic view of reads in RNA-seq for hypertrophic marker gene Nppa, Nppb in the IGV browser. **(E)** KEGG pathway enrichment analysis of dysregulated genes in groups of si-METTL5 vs. si-Ctrl and AdMETTL5 vs. AdGFP under the stimulation of PE (adjusted *P*-value < 0.05). **(F)** Upstream factor analysis by X2K of the top 500 dysregulated genes (|Log2FoldChange|>1, adjusted *P*-value < 0.05; ranking by adjusted *P*-value) in groups of si-METTL5 vs. si-Ctrl and AdMETTL5 vs. AdGFP under the stimulation of PE. The upstream factors were selected by Hypergeometric *p*-value < 0.05. The algorithm of independent hypothesis weighting (IHW) in DEseq2 was used for calculating the adjusted *P*-value of the RNA-seq data.

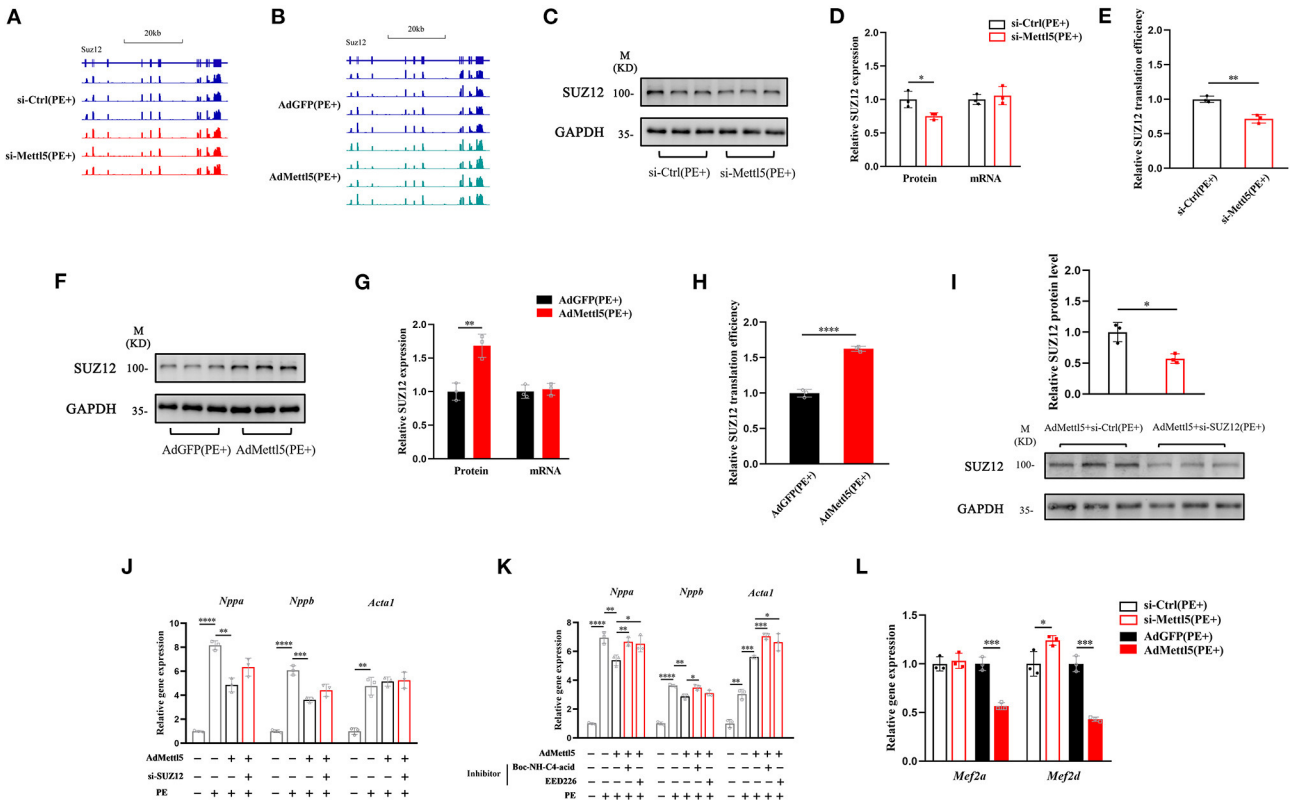

FIGURE 5 | METTL5 regulates the translation efficiency of SUZ12. **(A,B)** The genomic view of SUZ12 mRNA reads of RNA-seq of si-METTL5 vs. si-Ctrl and AdMETTL5 vs. AdGFP under the stimulation of PE in the IGV browser. **(C)** Detection of the expression of SUZ12 in si-METTL5 and si-Ctrl treated NRVCs under the stimulation of PE. GAPDH serves as control. **(D)** Quantification of SUZ12 protein level and qRT-PCR detection of the relative gene expression of SUZ12 in si-METTL5 and si-Ctrl treated NRVCs under the stimulation of PE. **(E)** The translation efficiency (TE) is presented by calculating the ratio between transcript level and protein level. $n = 3$ for each group. **(F)** Detection of the expression of SUZ12 in Ad-METTL5 and Ad-Ctrl treated NRVCs under the stimulation of PE. GAPDH serves as control. **(G)** Quantification of SUZ12 protein level and qRT-PCR detection of the relative gene expression of SUZ12 in Ad-METTL5 and Ad-Ctrl treated NRVCs under the stimulation of PE. **(H)** The translation efficiency (TE) is presented by calculating the ratio between transcript level and protein level. $n = 3$ for each group. **(I)** Detection and quantification of the knockdown of SUZ12 in Ad-METTL5 treated NRVCs under the stimulation of PE. GAPDH serves as control. $n = 3$ for each group. **(J,K)** Relative gene expression of hypertrophy markers in NRVMs treated with (H) si-SUZ12 or (I) SUZ12 inhibitors under Ad-METTL5 or Ad-GFP transfection with or without PE treatment. $n = 3$ in each group. **(L)** Relative gene expression of Mef2a and Mef2d in METTL5 knockdown and overexpression NRVCs and control cells under the stimulation of PE by RT-PCR. $n = 3$ in each group. The unpaired *T*-test was used for 2-group comparisons. $^*P < 0.05$, $^{**}P < 0.01$, $^{***}P < 0.001$, $^{****}P < 0.0001$.

cytomegalovirus (mCMV). The shuttle vector and an adenoviral backbone plasmid, pAd-ΔE1E3, was then transfected in 293AD cells with PEI (1 mg/mL) to produce packed adenovirus. Subsequently, 293AD cells were transduced with adenovirus for viral amplification. Adenovirus was collected, purified and concentrated by gradient centrifugation with the ViraTrap Adenovirus Purification Miniprep Kit, according to the manufacturer's instructions (Biomiga; V1160).

Cardiomyocyte Culture

Neonatal rat ventricular cardiomyocytes (NRVCs) were prepared as previously described (37). Briefly, NRVCs were isolated from 1- or 2-day-old neonatal Sprague-Dawley rat hearts by repeated enzymatic dissociation. All isolated cells were pre-plated for 1 h to remove fibroblasts. Non-adherent cells were then plated on 0.5% gelatin-coated plates and cultured in DMEM high-glucose medium (Gibco) containing 10% fetal bovine serum, sodium pyruvate (1×), GlutaMAX (1×) and antibiotics. Cardiomyocytes

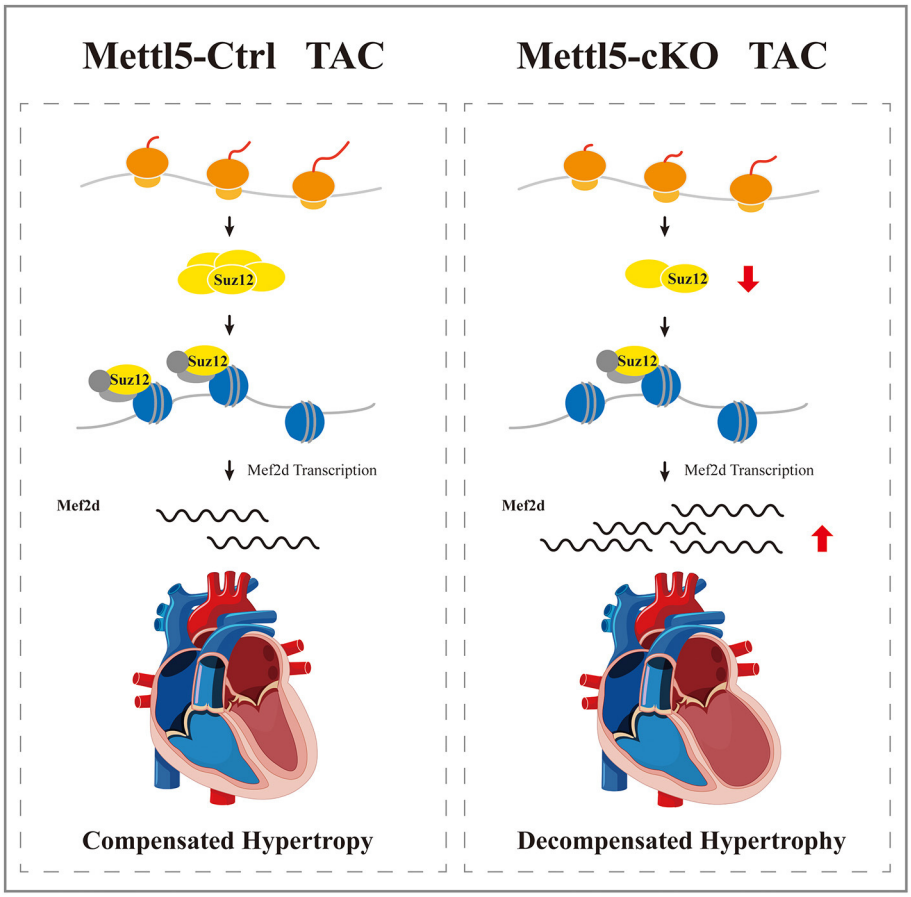

FIGURE 6 | A proposed working model of METTL5 in cardiac remodeling.

were changed into serum-free medium after plating for 18 h and transduced with adenovirus for 24 h prior to hypertrophic agent PE (20 μM) treatment. Suz12/PRC2 inhibitors, EED226 (20 μM, HY-101117, MCE), and Boc-NH-C4-acid (50 μM, HY-W014099, MCE) were used in the PE treatment in the rescue experiments. The inhibitors were dissolved in DMSO and manipulated according to the manufacturer's instructions. For the treatment of siRNA, 50 nM siRNA targeting METTL5 or SUZ12 transcript and control siRNA (from GenePharma) was transfected into cardiomyocytes by using Lipofectamine RNAiMAX transfection reagent. 6 h later, media with transfection reagent were removed and cardiomyocytes were then treated with the hypertrophic agent PE (20 μM) by changing the PE-contained serum-free medium. Cells were harvested 24 h after PE treatment for RNA isolation or 48 h after PE treatment for immunochemistry and total proteins or 0.5 h for detection of phosphorylated protein.

Immunofluorescence Staining

Cardiomyocytes were washed with PBS three times and fixed with 4% PFA for 15 min. After washing with PBS, cells were then blocked with 3% BSA in PBS containing 0.1% TritonX-100 for 1 h, followed by incubation with anti-sarcomeric a-actinin (1:200; Abcam; ab9465) in blocking buffer for 2 h at room temperature. After three times wash with PBS, cells were incubated with anti-mouse secondary antibodies conjugated with Alexa 488 (1:1,000; Thermo Fisher Scientific; A-11029) or Alexa 594 (1:1,000; Thermo Fisher Scientific; A-11032), together with the nuclear stain DAPI (0.1 mg/mL; Sigma; D9542) in PBS for 1 h. Images ware captured using a fluorescence microscope (Olympus; IX71). The surface area of cardiomyocytes was quantified with ImageJ software.

RNA-Seq Data Analysis

Raw reads were aligned to the rat or mouse genome (Rattus_norvegicus.Rnor_6.0; Mus_musculus.GRCm38) using HISAT2 (38). We generated read counts using StringTie (v2.1.4) with default options (39). Differentially expressed gene was calculated using DESeq2 (40). To view the distribution of reads, the bam files were converted to bigwig format using deepTools (v.3.3.1) (41) and visualized with the Integrative Genomics Viewer (IGV).

The raw data of RNA-seq in this study were deposited in Gene Expression Omnibus (GEO) database of the National Center for Biotechnology Information (NCBI) (Accession: GSE186615).

Upstream Factor Analysis

The dysregulated genes in si-METTL5 (vs. si-Ctrl) and AdMETTL5 (vs. AdGFP) were analyzed with the parameter of |Log2FoldChange|>1 and adjusted *P*-value < 0.05. Two independent algorithms, X2K (7, https://maayanlab.cloud/X2K/) and Lisa (8, http://lisa.cistrome.org/), were used for upstream factor analysis, and top 500 dysregulated genes (ranking by adjusted *P*-value) were selected and subjected to analysis according to the instructions.

Statistics

Values are reported as mean ± SD unless indicated otherwise. For multiple group comparisons, a *post-hoc* Tukey's test was performed when ANOVA reached significance. In addition, the unpaired *T*-test was used for two-group comparisons. *P*-values < 0.05 were considered statistically significant.

DATA AVAILABILITY STATEMENT

The datasets presented in this study can be found in online repositories. The names of the repository/repositories and accession number(s) can be found in the article/**Supplementary Material**.

ETHICS STATEMENT

The studies involving human participants were reviewed and approved by the Medical Ethics Committee of The First Affiliated Hospital, SunYet-sen University. The patients/participants provided their written informed consent to participate in this study. The animal study was reviewed and approved by the Medical Ethics Committee of The First Affiliated Hospital, SunYet-sen University. Written informed consent was obtained from the owners for the participation of their animals in this study.

AUTHOR CONTRIBUTIONS

Z-PH conceived the project, designed and analyzed the experiments, and wrote the manuscript. YH, TD, and SG performed most of the experiments. XZ, YC, CL, SLi, XL, and YD contributed to human sample acquisition and western blotting analysis. LW, TL, TX, and GD generated METTL5-cKO mice, performed transverse aortic constriction surgery, and collected mouse heart samples. YH and TD contributed to the echocardiographic data acquisition and analysis. TD contributed to bioinformatic analyses of RNA-seq data. KL, DZ, XT, and SLin supervised the data analyses and reviewed the manuscript.

FUNDING

This work was supported by the National Natural Science Foundation of China (81873463 to Z-PH, 81970429 to DZ, and 81900350 to SLi), the Guangdong Basic and Applied Basic Research Foundation (2019B151502003 to Z-PH, 2019A1515011956 to DZ, and 2018A030313448 and 2021A1515010433 to YC), and the donation for scientific research from the Terry Fox Foundation to Z-PH.

ACKNOWLEDGMENTS

We thank members of the Huang laboratory for advice and support.

SUPPLEMENTARY MATERIAL

The Supplementary Material for this article can be found online at: https://www.frontiersin.org/articles/10.3389/fcvm.2022.852775/full#supplementary-material

REFERENCES

1. Hill JA, Olson EN. Cardiac plasticity. *N Engl J Med*. (2008) 358:1370–80. doi: 10.1056/NEJMra072139
2. Heineke J, Molkentin JD. Regulation of cardiac hypertrophy by intracellular signaling pathways. *Nat Rev Mol Cell Biol*. (2006) 7:589–600. doi: 10.1038/nrm1983
3. Jaalouk DE, Lammerding J. Mechanotransduction gone awry. *Nat Rev Mol Cell Biol*. (2009) 10:63–73. doi: 10.1038/nrm2597
4. Schluter KD, Goldberg Y, Taimor G, Schafer M, Piper HM. Role of phosphatidylinositol 3-kinase activation in the hypertrophic growth of adult ventricular cardiomyocytes. *Cardiovasc Res*. (1998) 40:174–81. doi: 10.1016/S0008-6363(98)00171-0
5. Rolfe M, McLeod LE, Pratt PF, Proud CG. Activation of protein synthesis in cardiomyocytes by the hypertrophic agent phenylephrine requires the activation of erk and involves phosphorylation of tuberous sclerosis complex 2 (tsc2). *Biochem J*. (2005) 388:973–84. doi: 10.1042/BJ20041888
6. Passier R, Zeng H, Frey N, Naya FJ, Nicol RL, McKinsey TA, et al. Cam kinase signaling induces cardiac hypertrophy and activates the mef2 transcription factor *in vivo*. *J Clin Invest*. (2000) 105:1395–406. doi: 10.1172/JCI8551
7. van Rooij E, Doevendans PA, de Theije CC, Babiker FA, Molkentin JD, de Windt LJ. Requirement of nuclear factor of activated t-cells in calcineurin-mediated cardiomyocyte hypertrophy. *J Biol Chem*. (2002) 277:48617–26. doi: 10.1074/jbc.M206532200
8. Molkentin JD, Lin Q, Duncan SA, Olson EN. Requirement of the transcription factor gata4 for heart tube formation and ventral morphogenesis. *Genes Dev*. (1997) 11:1061–72. doi: 10.1101/gad.11.8.1061
9. Vogel C, Marcotte EM. Insights into the regulation of protein abundance from proteomic and transcriptomic analyses. *Nat Rev Genet*. (2012) 13:227–32. doi: 10.1038/nrg3185
10. Yan Y, Tang R, Li B, Cheng L, Ye S, Yang T, et al. The cardiac translational landscape reveals that micropeptides are new players involved in cardiomyocyte hypertrophy. *Mol Ther Am J Soc Genome Therapy*. (2021) 29:2253–67. doi: 10.1016/j.ymthe.2021.03.004
11. Zhang Z, Park E, Lin L, Xing Y. A panoramic view of RNA modifications: exploring new frontiers. *Genome Biol*. (2018) 19:11. doi: 10.1186/s13059-018-1394-4
12. Oerum S, Meynier V, Catala M, Tisne C. A comprehensive review of m6a/m6am RNA methyltransferase structures. *Nucleic Acids Res*. (2021) 49:7239–55. doi: 10.1093/nar/gkab378
13. Geula S, Moshitch-Moshkovitz S, Dominissini D, Mansour AA, Kol N, Salmon-Divon M, et al. Stem cells. M6a mRNA methylation facilitates

resolution of naive pluripotency toward differentiation. *Science*. (2015) 347:1002–6. doi: 10.1126/science.1261417
14. Wang P, Doxtader KA, Nam Y. Structural basis for cooperative function of METTL3 and METTL14 methyltransferases. *Mol Cell*. (2016) 63:306–17. doi: 10.1016/j.molcel.2016.05.041
15. Jia G, Fu Y, Zhao X, Dai Q, Zheng G, Yang Y, et al. N6-methyladenosine in nuclear RNA is a major substrate of the obesity-associated fto. *Nat Chem Biol*. (2011) 7:885–7. doi: 10.1038/nchembio.687
16. Zheng G, Dahl JA, Niu Y, Fedorcsak P, Huang CM, Li CJ, et al. Alkbh5 is a mammalian RNA demethylase that impacts RNA metabolism and mouse fertility. *Mol Cell*. (2013) 49:18–29. doi: 10.1016/j.molcel.2012.10.015
17. Kumari R, Ranjan P, Suleiman ZG, Goswami SK, Li J, Prasad R, et al. MRNA modifications in cardiovascular biology and disease: with a focus on m6a modification. *Cardiovasc Res*. (2021). doi: 10.1093/cvr/cvab160. [Epub ahead of print].
18. Wang X, Zhao BS, Roundtree IA, Lu Z, Han D, Ma H, et al. N(6)-methyladenosine modulates messenger RNA translation efficiency. *Cell*. (2015) 161:1388–99. doi: 10.1016/j.cell.2015.05.014
19. Shi H, Wang X, Lu Z, Zhao BS, Ma H, Hsu PJ, et al. Ythdf3 facilitates translation and decay of n(6)-methyladenosine-modified RNA. *Cell Res*. (2017) 27:315–28. doi: 10.1038/cr.2017.15
20. Berulava T, Buchholz E, Elerdashvili V, Pena T, Islam MR, Lbik D, et al. Changes in m6a RNA methylation contribute to heart failure progression by modulating translation. *Eur Heart Fail J*. (2020) 22:54–66. doi: 10.1002/ejhf.1672
21. Dorn LE, Lasman L, Chen J, Xu X, Hund TJ, Medvedovic M, et al. The n(6)-methyladenosine mRNA methylase mettl3 controls cardiac homeostasis and hypertrophy. *Circulation*. (2019) 139:533–45. doi: 10.1161/CIRCULATIONAHA.118.036146
22. Mathiyalagan P, Adamiak M, Mayourian J, Sassi Y, Liang Y, Agarwal N, et al. Fto-dependent n(6)-methyladenosine regulates cardiac function during remodeling and repair. *Circulation*. (2019) 139:518–32. doi: 10.1161/CIRCULATIONAHA.118.033794
23. Leismann J, Spagnuolo M, Pradhan M, Wacheul L, Vu MA, Musheev M, et al. The 18s ribosomal RNA m(6) a methyltransferase METTL5 is required for normal walking behavior in drosophila. *EMBO Rep*. (2020) 21:e49443. doi: 10.15252/embr.201949443
24. Ignatova VV, Stolz P, Kaiser S, Gustafsson TH, Lastres PR, Sanz-Moreno A, et al. The rRNA m(6)a methyltransferase METTL5 is involved in pluripotency and developmental programs. *Genes Dev*. (2020) 34:715–29. doi: 10.1101/gad.333369.119
25. van Tran N, Ernst FGM, Hawley BR, Zorbas C, Ulryck N, Hackert P, et al. The human 18s rRNA m6a methyltransferase METTL5 is stabilized by trmt112. *Nucleic Acids Res*. (2019) 47:7719–33. doi: 10.1093/nar/gkz619
26. Wang L, Liang Y, Lin R, Xiong Q, Yu P, Ma J, et al. METTL5 mediated 18s rRNA n6-methyladenosine (m6a) modification controls stem cell fate determination and neural function. *Genes Dis*. (2022) 9:268–74. doi: 10.1016/j.gendis.2020.07.004
27. Rong B, Zhang Q, Wan J, Xing S, Dai R, Li Y, et al. Ribosome 18s m(6)a methyltransferase mettl5 promotes translation initiation and breast cancer cell growth. *Cell Rep*. (2020) 33:108544. doi: 10.1016/j.celrep.2020.108544
28. Clarke DJB, Kuleshov MV, Schilder BM, Torre D, Duffy ME, Keenan AB, et al. Expression2kinases (x2k) web: linking expression signatures to upstream cell signaling networks. *Nucleic Acids Res*. (2018) 46:W171–79 doi: 10.1093/nar/gky458
29. Qin Q, Fan J, Zheng R, Wan C, Mei S, Wu Q, et al. Lisa: inferring transcriptional regulators through integrative modeling of public chromatin accessibility and chip-seq data. *Genome Biol*. (2020) 21:32. doi: 10.1186/s13059-020-1934-6
30. Yu J, Yang Y, Xu Z, Lan C, Chen C, Li C, et al. Long non-coding RNA ahit protects against cardiac hypertrophy through suz12 (suppressor of zeste 12 protein homolog)-mediated downregulation of mef2a (myocyte enhancer factor 2a). *Circ Heart Fail*. (2020) 13:e006525. doi: 10.1161/CIRCHEARTFAILURE.119.006525
31. Wang Z, Zhang XJ, Ji YX, Zhang P, Deng KQ, Gong J, et al. The long non-coding RNA chaer defines an epigenetic checkpoint in cardiac hypertrophy. *Nat Med*. (2016) 22:1131–39. doi: 10.1038/nm.4179
32. Xing M, Liu Q, Mao C, Zeng H, Zhang X, Zhao S, et al. The 18s rRNA m(6) a methyltransferase mettl5 promotes mouse embryonic stem cell differentiation. *EMBO Rep*. (2020) 21:e49863. doi: 10.15252/embr.201949863
33. Kim Y, Phan D, van Rooij E, Wang DZ, McAnally J, Qi X, et al. The mef2d transcription factor mediates stress-dependent cardiac remodeling in mice. *J Clin Invest*. (2008) 118:124–32. doi: 10.1172/JCI33255
34. Naya FJ, Black BL, Wu H, Bassel-Duby R, Richardson JA, Hill JA, et al. Mitochondrial deficiency and cardiac sudden death in mice lacking the mef2a transcription factor. *Nat Med*. (2002) 8:1303–09. doi: 10.1038/nm789
35. Oka T, Maillet M, Watt AJ, Schwartz RJ, Aronow BJ, Duncan SA, et al. Cardiac-specific deletion of gata4 reveals its requirement for hypertrophy, compensation, and myocyte viability. *Circ Res*. (2006) 98:837–45. doi: 10.1161/01.RES.0000215985.18538.c4
36. Huang ZP, Kataoka M, Chen J, Wu G, Ding J, Nie M, et al. Cardiomyocyte-enriched protein cip protects against pathophysiological stresses and regulates cardiac homeostasis. *J Clin Invest*. (2015) 125:4122–34. doi: 10.1172/JCI82423
37. Huang ZP, Young Seok H, Zhou B, Chen J, Chen JF, Tao Y, et al. Cip, a cardiac isl1-interacting protein, represses cardiomyocyte hypertrophy. *Circ Res*. (2012) 110:818–30. doi: 10.1161/CIRCRESAHA.111.259663
38. Kim D, Paggi JM, Park C, Bennett C, Salzberg SL. Graph-based genome alignment and genotyping with hisat2 and hisat-genotype. *Nat Biotechnol*. (2019) 37:907–15. doi: 10.1038/s41587-019-0201-4
39. Pertea M, Kim D, Pertea GM, Leek JT, Salzberg SL. Transcript-level expression analysis of RNA-seq experiments with hisat, stringtie, and ballgown. *Nat Protoc*. (2016) 11:1650–67. doi: 10.1038/nprot.2016.095
40. Love MI, Huber W, Anders S. Moderated estimation of fold change and dispersion for RNA-seq data with deseq2. *Gen Biol*. (2014) 15:550. doi: 10.1186/s13059-014-0550-8
41. Ramirez F, Dundar F, Diehl S, Gruning BA, Manke T. Deeptools: a flexible platform for exploring deep-sequencing data. *Nucleic Acids Res*. (2014) 42:W187–91. doi: 10.1093/nar/gku365

Conflict of Interest: The authors declare that the research was conducted in the absence of any commercial or financial relationships that could be construed as a potential conflict of interest.

Publisher's Note: All claims expressed in this article are solely those of the authors and do not necessarily represent those of their affiliated organizations, or those of the publisher, the editors and the reviewers. Any product that may be evaluated in this article, or claim that may be made by its manufacturer, is not guaranteed or endorsed by the publisher.

frontiers in Cardiovascular Medicine

ORIGINAL RESEARCH
published: 17 March 2022
doi: 10.3389/fcvm.2022.857049

Cardiac ISL1-Interacting Protein, a Cardioprotective Factor, Inhibits the Transition From Cardiac Hypertrophy to Heart Failure

Youchen Yan[1,2†], Tianxin Long[1,2†], Qiao Su[3†], Yi Wang[4], Ken Chen[5,6], Tiqun Yang[1,2], Guangyin Zhao[3], Qing Ma[4], Xiaoyun Hu[4], Chen Liu[1,2], Xinxue Liao[1,2], Wang Min[1], Shujuan Li[1,2], Dihua Zhang[7], Yuedong Yang[5,6], William T. Pu[4], Yugang Dong[1,2], Da-Zhi Wang[4], Yili Chen[1,2]* and Zhan-Peng Huang[1,2,8]**

[1] Department of Cardiology, Center for Translational Medicine, Institute of Precision Medicine, The First Affiliated Hospital, Sun Yat-sen University, Guangzhou, China, [2] NHC Key Laboratory of Assisted Circulation, Sun Yat-sen University, Guangzhou, China, [3] Laboratory Animal Center, The First Affiliated Hospital, Sun Yat-sen University, Guangzhou, China, [4] Department of Cardiology, Boston Children's Hospital, Harvard Medical School, Boston, MA, United States, [5] School of Data and Computer Science, Sun Yat-sen University, Guangzhou, China, [6] Key Laboratory of Machine Intelligence and Advanced Computing, Ministry of Education, Sun Yat-sen University, Guangzhou, China, [7] Department of Nephrology, The First Affiliated Hospital, Sun Yat-sen University, Guangzhou, China, [8] National-Guangdong Joint Engineering Laboratory for Diagnosis and Treatment of Vascular Diseases, Guangzhou, China

OPEN ACCESS

Edited by:
Qingchun Zeng,
Southern Medical University, China

Reviewed by:
Zhi Xin Shan,
Guangdong Provincial People's Hospital, China
Luis Alberto Gonano,
Universidad Nacional de La Plata, Argentina

***Correspondence:**
Da-Zhi Wang
dwang@enders.tch.harvard.edu
Yili Chen
chenyil7@mail.sysu.edu.cn
Zhan-Peng Huang
huangzhp27@mail.sysu.edu.cn

[†] These authors have contributed equally to this work

Specialty section:
This article was submitted to General Cardiovascular Medicine, a section of the journal Frontiers in Cardiovascular Medicine

Received: 18 January 2022
Accepted: 17 February 2022
Published: 17 March 2022

Citation:
Yan Y, Long T, Su Q, Wang Y, Chen K, Yang T, Zhao G, Ma Q, Hu X, Liu C, Liao X, Min W, Li S, Zhang D, Yang Y, Pu WT, Dong Y, Wang D-Z, Chen Y and Huang Z-P (2022) Cardiac ISL1-Interacting Protein, a Cardioprotective Factor, Inhibits the Transition From Cardiac Hypertrophy to Heart Failure. Front. Cardiovasc. Med. 9:857049. doi: 10.3389/fcvm.2022.857049

Heart failure is characterized by the inability of the heart to pump effectively and generate proper blood circulation to meet the body's needs; it is a devastating condition that affects more than 100 million people globally. In spite of this, little is known about the mechanisms regulating the transition from cardiac hypertrophy to heart failure. Previously, we identified a cardiomyocyte-enriched gene, CIP, which regulates cardiac homeostasis under pathological stimulation. Here, we show that the cardiac transcriptional factor GATA4 binds the promotor of CIP gene and regulates its expression. We further determined that both CIP mRNA and protein decrease in diseased human hearts. In a mouse model, induced cardiac-specific overexpression of CIP after the establishment of cardiac hypertrophy protects the heart by inhibiting disease progression toward heart failure. Transcriptome analyses revealed that the IGF, mTORC2 and TGFβ signaling pathways mediate the inhibitory function of CIP on pathologic cardiac remodeling. Our study demonstrates GATA4 as an upstream regulator of CIP gene expression in cardiomyocytes, as well as the clinical significance of CIP expression in human heart disease. More importantly, our investigation suggests CIP is a key regulator of the transition from cardiac hypertrophy to heart failure. The ability of CIP to intervene in the onset of heart failure suggests a novel therapeutic avenue of investigation for the prevention of heart disease progression.

Keywords: heart failure, cardiac hypertrophy, CIP, gene regulation, cardiac remodeling

INTRODUCTION

Heart failure (HF), characterized by insufficient cardiac output to meet the body's needs, is generally believed to be a clinical consequence of cardiac remodeling. Pressure overload of the left ventricle induced by various clinical conditions, such as hypertension and aortic stenosis, triggers pathological cardiac remodeling (1). Indeed, clinical data revealed that hypertension is a major

risk factor for the development of HF (2). Pathological changes of cardiac cells, including hypertrophic growth of cardiomyocytes, necrosis and apoptosis of cardiomyocytes, and activation of cardiac fibroblasts, are closely linked to cardiac remodeling (3, 4). A complex gene regulatory network is thought to control these cellular processes (5). Since the recognition that cardiac remodeling is a key process leading to the development of HF, the slowing or reversing of remodeling has become a goal of HF therapy (1). Therefore, fully understanding the underlying molecular mechanism of cardiac remodeling is a prerequisite for developing new HF therapies. Although several important signaling pathways, such as IGF (6, 7), TGF-beta (8, 9), Mitogen-activated protein kinases (10, 11), Calmodulin-Calcineurin signaling (12, 13), have been identified and well-studied in cardiac hypertrophy, a comprehensive understanding of the molecular mechanisms responsible for progression toward HF remains elusive.

Recently, we identified a striated muscle-enriched protein, CIP (14). CIP is predominately expressed in cardiomyocytes in the heart. Loss-of-function of CIP promotes pressure overload-induced cardiac remodeling and leads to premature HF *in vivo* through modulation of the FOXO1 signaling pathway (15). Human genetic studies revealed that mutation of the CIP gene is associated with human dilated cardiomyopathy (16). Interestingly, our recent study demonstrated the expression of CIP in skeletal muscle plays an important role in regulating nucleus positioning in multinucleated muscle fibers (17). Although overexpression of CIP inhibits hypertrophic growth of cardiomyocytes (14), whether CIP is able to inhibit or even reverse cardiac remodeling after disease status has been established remains unanswered. In this study, we show how CIP expression is regulated in cardiomyocytes and diseased human hearts. Furthermore, we demonstrate that CIP inhibits cardiac remodeling and protects the heart from HF after cardiac hypertrophy has been established, providing evidence of a role for CIP in cardiac hypertrophy and HF treatment.

RESULTS

Cardiac Transcription Factor GATA4 Binds to the Promotor of Cardiac ISL1-Interacting Protein and Regulates Its Expression

Cardiac ISL1-interacting Protein (CIP) (14) or Muscle-enriched A-type Lamin-Interacting Protein (MLIP) (18) has been previously identified as a striated muscle-enriched gene. In the heart, CIP is dominantly expressed in cardiomyocyte cells. However, transcriptional factor(s) that control the expression of CIP in cardiomyocytes have not yet been investigated. Genome-wide binding sites for multiple cardiac transcriptional factors, including GATA4, Tbx5, Nkx2-5, Mef2A, and SRF, have been carefully investigated (19). Binding sites for GATA4, Tbx5, and Nkx2-5 were detected in the promotor region of CIP (**Figure 1A**). Knock-down of GATA4 alone or both GATA4 and mef2a decreased the expression of CIP in cardiac cells (**Supplementary Figure 1**), indicating GATA4 is a key transcriptional factor for the expression of CIP. To determine whether CIP is directly regulated by GATA4, we generated luciferase reporters controlled by a series of CIP promotor sequence variants, each of which contains the GATA4-binding sequences detected by previous CHIP-seq assay (19). In transient cell-based luciferase assays, all CIP-Luc reporter variants were responsive to GATA4 transactivation. The 554bp CIP-Luc reporter construct, containing a proximal GATA4 binding sequence, was the most responsive one in the assay, indicating a functional GATA4 enhancer located in this binding sequence (**Figure 1B**). Four putative GATA4 binding motifs, which are evolutionarily conserved, were found in 554 bp CIP promotor fragment (**Figure 1C**). To determine which of the binding motifs were functional, we generated three mutant variants of the 554 bp CIP-Luc reporter that contained mutant versions of motifs 1 and 2, motif 3, and motif 4, respectively. The results of the luciferase assay revealed that mutations in motif 3 and motif 4, but not motif 1 and 2, decreased the responsivity of 554 bp CIP-Luc reporter to GATA4 transactivation (**Figure 1D**), suggesting motif 3 and motif 4 are functional GATA4 binding motifs in CIP promotor. Therefore, our data demonstrated that GATA4 is a key transcriptional factor regulating the expression of CIP in cardiomyocytes.

Decreased Expression of Cardiac ISL1-Interacting Protein Correlated With Dysregulated Oxidative Phosphorylation Pathway Activity in Diseased Human Hearts

In order to further investigate the relevance of CIP in human cardiac diseases, we collected a total of 194 RNA-seq datasets based on analyses of human heart tissue from the NCBI public database, including 53 non-failing heart samples (NF), 28 hypertrophic cardiomyopathy samples (HCM), 40 ischemic cardiomyopathy samples (ICM), and 73 dilated cardiomyopathy samples (DCM). After normalizing the data from different batches, we found that expression of CIP was significantly decreased in all groups of diseased hearts, while cardiac disease markers, NPPA and NPPB, were significantly upregulated (**Figure 2A**). Furthermore, the downregulation of CIP in human DCM hearts was further confirmed by Western blotting analysis (**Figure 2B**). Next, we examined the data to detect genes co-expressed with CIP to define a potential CIP-based gene regulation network. Human genes were divided into multiple modules based on the Spearman correlation coefficient score of genes, then the module containing CIP was further subjected to KEGG pathway analysis. Pathways related to "Parkinson disease," "oxidative phosphorylation," "Huntington disease," and "metabolic pathways" were on the top of the list (**Figure 2C**). Given that we focused on cardiac disease in this study, our data suggest that CIP was involved in the regulation of OXPHOS pathway. OXPHOS-related genes with the strongest correlation coefficient, including ATP5PF, SDHB, SDHA, etc., are illustrated in a Circos plot (**Figure 2D**). Together, our data from this genome-wide analyses of human diseased hearts suggest CIP

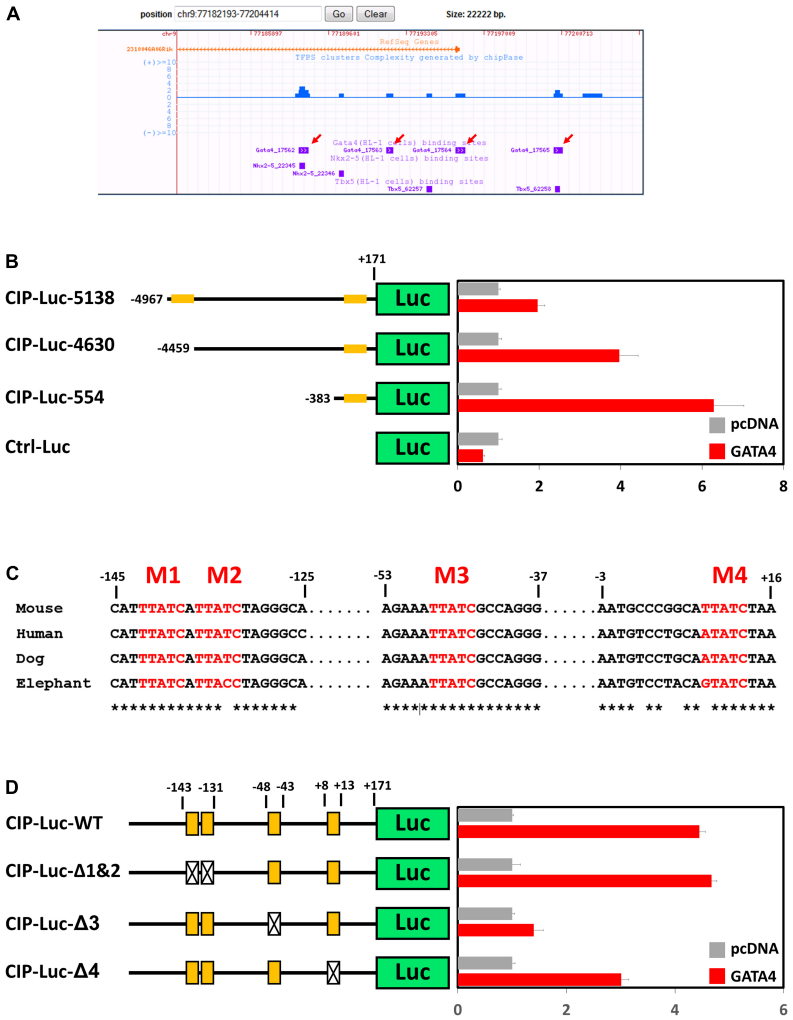

FIGURE 1 | GATA4 regulates the expression of cardiac ISL1-interacting protein (CIP). **(A)** Distribution of reported binding sequences for cardiac transcriptional factors around the transcriptional starting site of CIP gene in a genome browser. Red arrows indicate GATA4 binding sequences. **(B)** Luciferase reporter assay of reporters with full length or truncated CIP promotors with or without GATA4 activation. Orange bars indicate potential GATA4 binding sites. **(C)** Conservation of potential GATA4 binding motifs in mammalian, which are shown in red letters. Asterisks indicate the conserved nucleotides. **(D)** Luciferase reporter assay of reporters with full wildtype or mutant CIP promotors with or without GATA4 activation. Orange boxes indicate potential GATA4 binding motifs. Boxes with cross indicate mutant motifs.

plays an important role in human heart disease by regulating oxidative phosphorylation in cardiomyocyte.

Cardiac Overexpression of Cardiac ISL1-Interacting Protein Protects the Heart From Disease Progression to Heart Failure

In a previous study, we reported that overexpression of CIP in the heart before cardiac stress inhibited the stress-induced cardiac mal-remodeling (15). In order to test the therapeutic potential of CIP in interfering the progression of adverse cardiac remodeling, we performed transverse aortic constriction (TAC) surgery, which induced ventricular pressure overload, on an inducible cardiac-specific CIP overexpressing mouse model (Rosa26-CIP-flox; Myh6-MerCreMer, and CIP-OE mice). Mice were administrated Tamoxifen to induce the cardiac-specific overexpression of CIP 2 weeks after TAC surgery (**Supplementary Figure 2**). The establishment of cardiac remodeling was confirmed at 2 weeks after TAC as indicated by the echocardiography examination of the left ventricular posterior wall (LVPW; **Figures 3A,B** and **Table 1**). Cardiac parameters were measured at 2 and 8 weeks post-surgery by echocardiography (**Table 1**). Compared to the sham-operated group, the ventricular wall became thicker and the ventricular chamber was dilated in control mice when the stress was prolonged (**Figures 3A,C**). As expected, their cardiac function reflected by fraction shortening (FS) decreased significantly, indicating disease progression to heart failure (**Figures 3A,D**). In contrast, overexpression of CIP in the heart during stress significantly repressed the thickening of the ventricular wall and chamber dilation. More importantly, cardiac function was

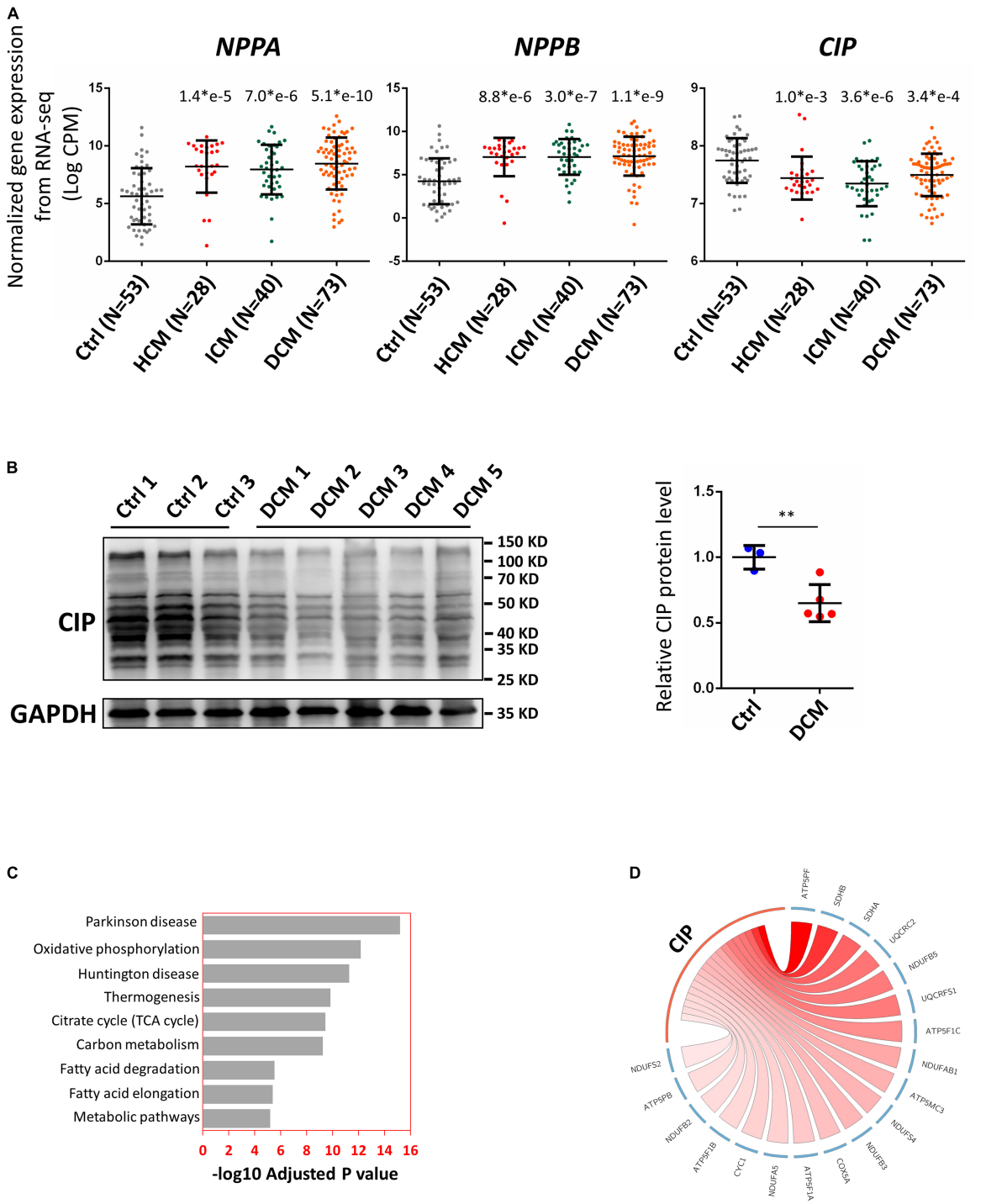

FIGURE 2 | Cardiac ISL1-interacting protein expression is down-regulated in diseased human hearts. **(A)** Relative gene expression indicated by log counts per million (CPM) from disease human heart RNA-seq data. *N* number for each group is show. The significance between each category of heart disease and control was tested with 1-way ANOVA with *post hoc* Tukey's test and shown. **(B)** Western blotting detecting the expression of CIP in human hearts with dilated cardiomyopathy (DCM) and controls. GAPDH served as loading control. The significance between groups was tested with 1-way ANOVA with *post hoc* Tukey's test. $^{**}P < 0.01$. **(C)** The ranking of enriched KEGG pathways in the gene set having strong expression correlation coefficient with CIP, which is determined by Spearman correlation coefficient (SCC). SCC between CIP and individual genes genome-wide from 194 human hearts was calculated. Pathways were ranked by the adjusted *P* value. **(D)** The expression of CIP has strong expression correlation coefficient with oxidative phosphorylation (OXPHOS) related genes in human heart ($p = 6.77 \times e10^{-13}$). OXPHOS genes with SCC > 0.4 are shown in Circos plot. The color of line linked between CIP and each gene indicates the expression correlation coefficient. A darker line suggests a stronger expression correlation coefficient.

TABLE 1 | Echocardiography examination of cardiac ISL1-interacting protein (CIP)-OE mice and their control littermates with transverse aortic constriction (TAC) or sham operation at different time points after surgery.

	Ctrl; Sham (*N* = 6)		CIP-OE; Sham (*N* = 6)		Ctrl; TAC (*N* = 9)		CIP-OE; TAC (*N* = 14)	
	2 weeks	8 weeks	2 weeks	8 weeks	2 weeks	8 weeks	2 weeks	8 weeks
IVS;d (mm)	0.770 ± 0.065	0.811 ± 0.075	0.784 ± 0.042	0.807 ± 0.057	1.014 ± 0.090**	1.305 ± 0.031**	1.063 ± 0.089	1.188 ± 0.148#
IVS;s (mm)	1.421 ± 0.102	1.499 ± 0.096	1.448 ± 0.135	1.494 ± 0.174	1.647 ± 0.136**	1.742 ± 0.158**	1.679 ± 0.130	1.825 ± 0.140
LVID;d (mm)	3.387 ± 0.284	3.332 ± 0.144	3.350 ± 0.250	3.383 ± 0.182	3.361 ± 0.407	3.740 ± 0.441*	3.198 ± 0.214	3.386 ± 0.268#
LVID;s (mm)	1.632 ± 0.213	1.600 ± 0.129	1.595 ± 0.115	1.623 ± 0.074	1.696 ± 0.296	2.509 ± 0.706**	1.550 ± 0.197	1.766 ± 0.306##
LVPW;d (mm)	0.775 ± 0.021	0.793 ± 0.088	0.793 ± 0.032	0.788 ± 0.033	1.036 ± 0.092**	1.366 ± 0.118**	1.021 ± 0.070	1.133 ± 0.072##
LVPW;s (mm)	1.513 ± 0.130	1.494 ± 0.210	1.503 ± 0.071	1.609 ± 0.182	1.739 ± 0.164*	1.803 ± 0.272*	1.734 ± 0.191	1.829 ± 0.181
EF (%)	83.94 ± 2.75	84.07 ± 2.52	84.30 ± 2.68	83.91 ± 2.91	81.99 ± 3.69	62.21 ± 16.10**	83.76 ± 3.49	80.08 ± 6.47##
FS (%)	51.93 ± 3.04	52.02 ± 2.88	52.31 ± 3.12	51.91 ± 3.46	49.79 ± 3.74	33.86 ± 10.38**	51.64 ± 3.92	48.11 ± 5.97##
LV Mass (mg)	85.89 ± 13.71	87.95 ± 11.87	86.49 ± 9.48	89.49 ± 11.42	128.89 ± 32.07**	224.51 ± 45.51**	121.01 ± 13.79	155.39 ± 20.19##
LV Mass (Corrected, mg)	68.71 ± 10.97	70.36 ± 9.50	69.19 ± 7.59	71.59 ± 9.13	103.11 ± 25.66**	179.61 ± 36.41**	96.81 ± 11.03	124.31 ± 16.15##
LV Vol;d (μL)	47.44 ± 9.92	45.29 ± 4.72	46.12 ± 8.31	47.03 ± 5.87	47.09 ± 13.32	60.78 ± 18.05	41.17 ± 6.64	47.41 ± 8.87#
LV Vol;s (μL)	7.75 ± 2.79	7.24 ± 1.52	7.17 ± 1.30	7.46 ± 0.85	8.77 ± 3.86	25.30 ± 20.09*	6.79 ± 2.30	9.75 ± 4.48#
Heart Rate (BPM)	705 ± 17	687 ± 21	711 ± 48	731 ± 16	663 ± 58	655 ± 84	726 ± 32	698 ± 63

*$P_{Ctrl;Sham\ (same\ timepoint)\ vs.\ Ctrl;TAC\ (same\ timepoint)} < 0.05$; **$P_{Ctrl;Sham\ (same\ timepoint)\ vs.\ Ctrl;TAC\ (same\ timepoint)} < 0.01$; #$P_{Ctrl;TAC\ (same\ timepoint)\ vs.\ CIP-OE;\ TAC\ (same\ timepoint)} < 0.05$; ##$P_{Ctrl;TAC\ (same\ timepoint)\ vs.\ CIP-OE;\ TAC\ (same\ timepoint)} < 0.01$.

preserved by CIP overexpression during the prolonged stress (**Figures 3A–D**).

Mice were sacrificed at 8 weeks post-surgery for cardiac tissue collection. Consistent with echocardiographic data, significant adverse cardiac remodeling was induced by pressure overload in control mice, which was indicated by the ratio of ventricular weigh vs. body weight (Vw vs. Bw) and histological examination (**Figures 4A,B**). Overexpression of CIP in the heart resulted in a smaller heart under pressure overload. Consistently, cardiomyocyte size, indicated by its cross area determined by Wheat Germ Agglutinin (WGA) staining, was significantly larger in the control group after TAC but became smaller when CIP was overexpressed (**Figure 4C**). Heart failure is often accompanied with increased cardiac fibrosis. Sirius red/Fast green staining showed less cardiac fibrosis in CIP-OE hearts under cardiac stress compared to the control group (**Figure 4D**). We further examined the molecular markers for cardiac disease and fibrosis, including NPPA, NPPB, ACTA1, and FBN1. The induction of these marker gene expression by cardiac stress was significantly repressed by the CIP overexpression (**Figure 4E**). Together, all these data demonstrated that cardiac overexpression of CIP after the pathological remodeling has been initiated is able to inhibit disease progression and protect the heart from failure.

The Protective Function of Cardiac ISL1-Interacting Protein Is Mediated by IGF and mTORC2 Signaling Pathways

In order to investigate the potential mechanism of the protective effect of CIP in cardiac remodeling, we carried out unbiased transcriptome profiling with hearts of CIP-OE mice at 8 weeks post-surgery by performing RNA-seq. In total, 444 genes, including CIP, were significantly up-regulated, while 792 gene were significantly down-regulated in CIP-OE hearts (fold change > 1.5, $p < 0.05$; **Figure 5A**). A hierarchical clustering heatmap revealed that the dysregulation of these genes was induced by TAC surgery in the control group but rescued by the overexpression of CIP in stressed hearts (**Figure 5B**). In order to further characterize this subset of genes, 1,236 dysregulated genes were subjected to GO term analysis. Consistent with what we had found in human diseased hearts, genes related to "Mitochondrion" and "Oxidative phosphorylation" were enriched in the down-regulated genes (**Figure 5C**). To gain more information of the gene regulation network, we further searched for upstream regulators of these dysregulated genes using Ingenuity Pathway Analysis (IPA). Several regulators, including IGF1R (p = 7.27e-8; **Figure 5D**), Rictor (a core component of mTORC2, p = 6.25e-14; **Figure 5D**) and TGFB1 (p = 4.76e-7; **Supplementary Figure 3**), were showed in the top list. It is worth noting that the IGF1R was reported to modulate the activity of FoxO1 through regulating AKT, which is consistent with our previous report that CIP regulated pathological cardiac remodeling through the FoxO1/CnA signaling cascade (15). Dysregulation of downstream targets for IGF1R from IPA analysis, including TGFB1, BAX, CEBRA, CEBRB, COX6A2, COX8B, DES, NDUFA1, and NDUFB9, as well as several downstream targets for Rictor and TGFB1 were further confirmed by qRT-PCR (**Figure 5E**). All these data suggested that the inhibitory function of CIP on the progression of adverse cardiac remodeling was mediated, at least in part, by IGF and mTORC2 signaling pathways.

DISCUSSION

Although it has been recognized for a long time that the progression from cardiac hypertrophy to heart failure is detrimental, how this transition process is regulated remains

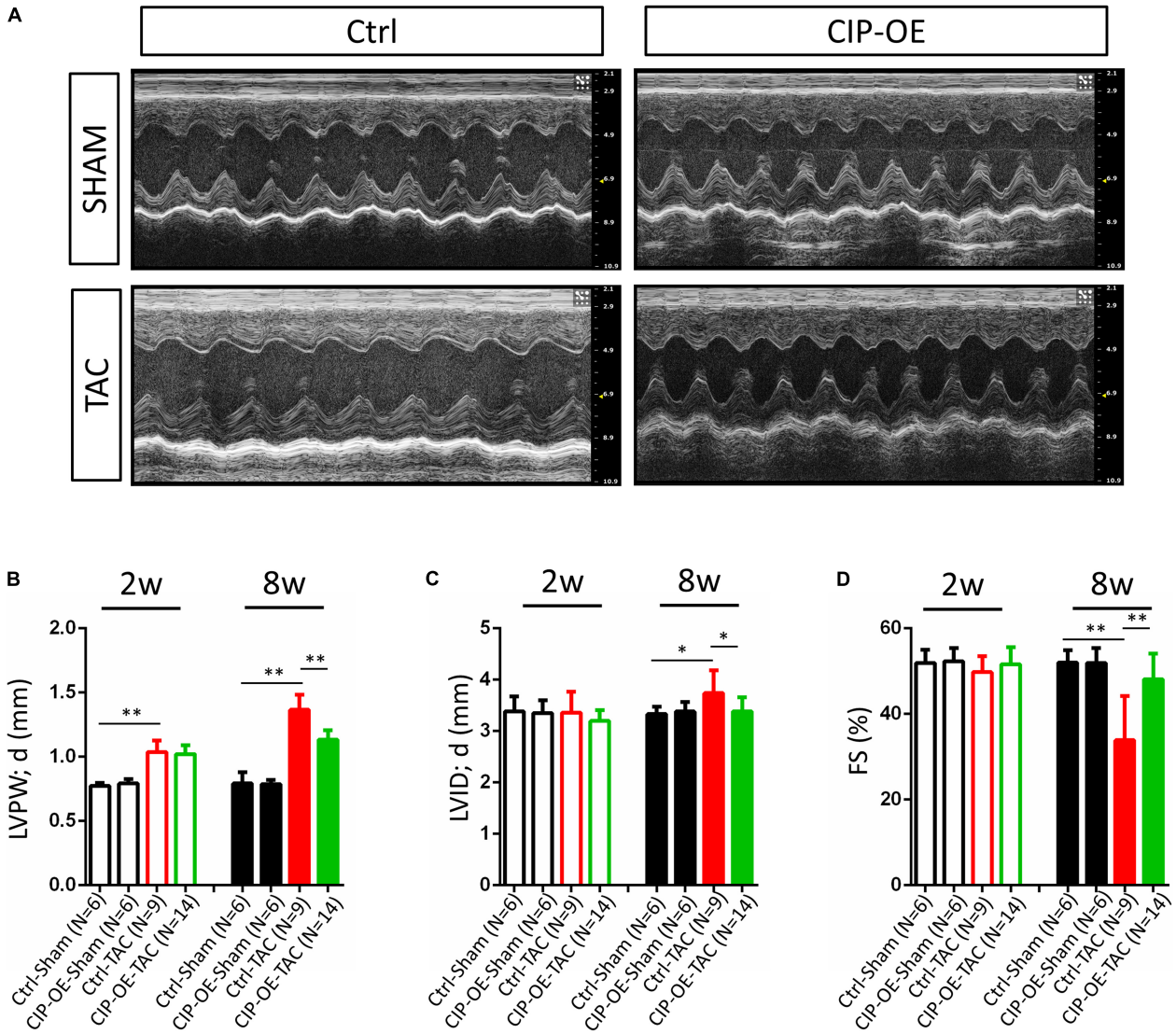

FIGURE 3 | Cardiac-overexpression of CIP preserves cardiac function during the disease progression toward heart failure. **(A)** Representative echocardiographic images from indicated group at 8 weeks after operation. **(B)** Left ventricular posterior wall thickness at end-diastole (LVPW;d), **(C)** Left ventricular internal dimension at end-diastole (LVID;d) and **(D)** Fractional shortening (FS) of CIP-OE mice and their control littermates with TAC or Sham operation determined by echocardiography at 2 weeks (2w) and 8 weeks (8w) after operation. *N* number for each group is show. The significance between groups was tested with 1-way ANOVA with *post hoc* Tukey's test. $^{*}P < 0.05$; $^{**}P < 0.01$.

largely unknown. Exploring a new regulator and associated molecular mechanisms connected to this disease progression will promote the development of new therapeutic approaches for heart failure. We have previously identified a striated muscle-enriched expressed gene, CIP, and showed it participated in the modulation of cardiac disease (14, 15). More and more genetic evidences indicate that CIP is a critical gene associated with human muscular diseases, both cardiac and skeletal ones. An exonic mutation of CIP gene was reported to associate with human dilated cardiomyopathy (16). Recently, loss-of-function of CIP induced by DNA mutations was demonstrated to cause myopathy with hyperCKemia in human (20, 21). CIP is specifically expressed in cardiomyocyte in the heart, but the regulatory mechanism of CIP's expression remains unclear. Here, we reported that GATA4, a key cardiac transcriptional factor, binds to the promotor of CIP and regulates its expression. Interestingly, GATA4 was shown to be upregulated in human failing hearts (22), and its expression decreases in response to the treatment of left ventricular assist device (LVAD) in heart failure (23), indicating other regulatory factors exist for CIP expression control. Significantly, CIP was shown to be down-regulated in various human heart diseases at both the mRNA and protein levels, indicating CIP plays an important regulatory role in the pathogenesis of human heart diseases and could be a target for reversing the adverse effects of the remodeling process and remodeling itself, thereby preventing heart failure.

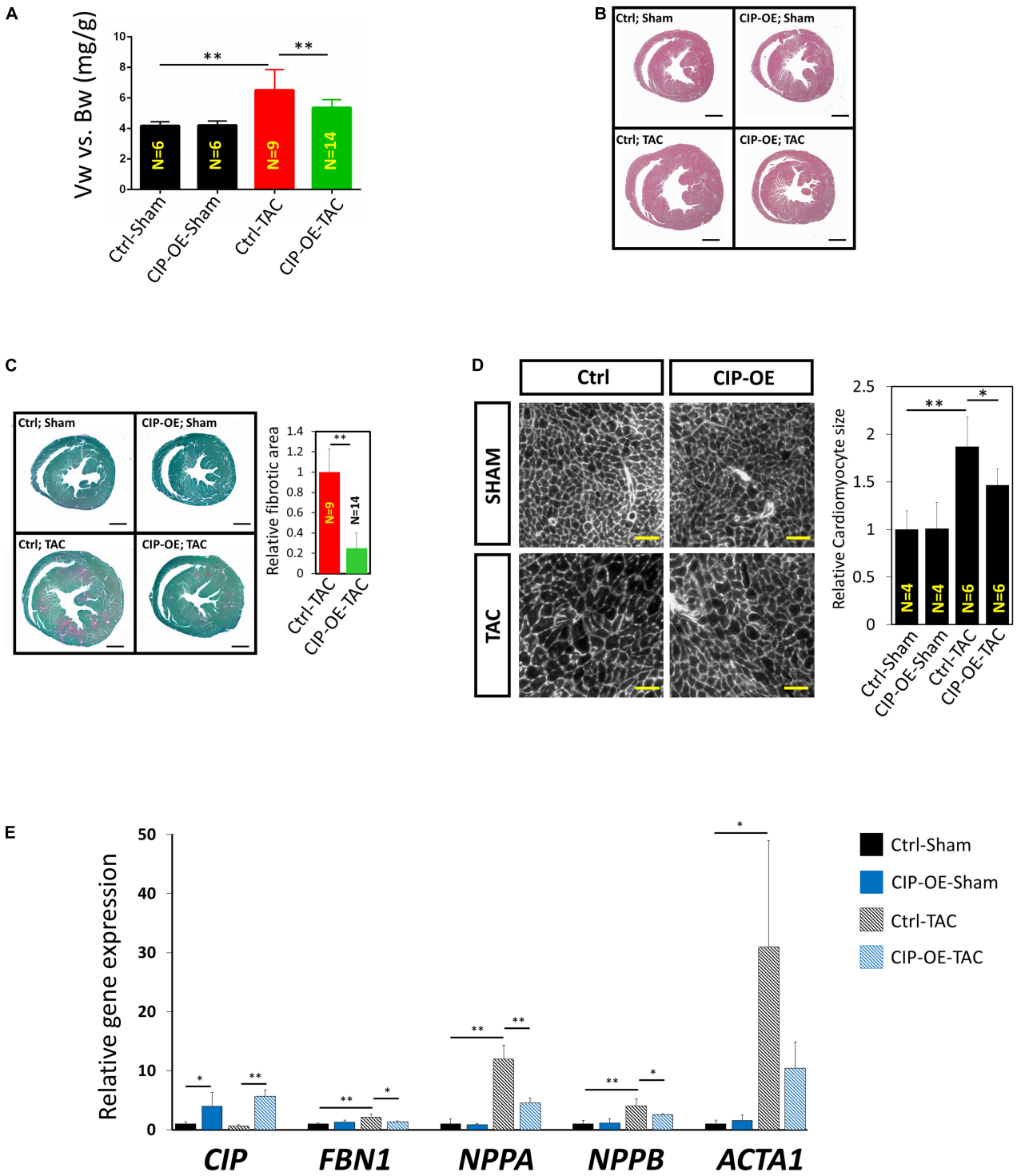

FIGURE 4 | Cardiac ISL1-interacting protein inhibits cardiac remodeling in the transition from cardiac hypertrophy to failure. **(A)** The ratio of ventricle weight vs. body weight of CIP-OE mice and their control littermates at 8 weeks after TAC or sham operation. *N* number of each group is shown. **(B)** Haematoxylin Eosin (H&E) staining of hearts from CIP-OE mice and their control littermates at 8 weeks after TAC or sham operation. Bars = 1 mm. **(C)** Fast green and Sirius red staining of hearts from CIP-OE mice and their control littermates at 8 weeks after TAC or sham operation. The fibrotic area was quantified. Bars = 1 mm. **(D)** Wheat germ agglutinin staining detecting the cross area of cardiomyocytes in TAC- or sham-operated CIP-OE hearts and littermate controls. The size of cardiomyocyte was quantified. Bars = 40 μm. **(E)** qRT-PCR detection of expression of cardiac fibrosis and heart disease marker genes in TAC- or sham-operated CIP-OE hearts and littermate controls. $N = 4$ for each group. The significance between groups was tested with 1-way ANOVA with *post hoc* Tukey's test. $^{*}P < 0.05$; $^{**}P < 0.01$.

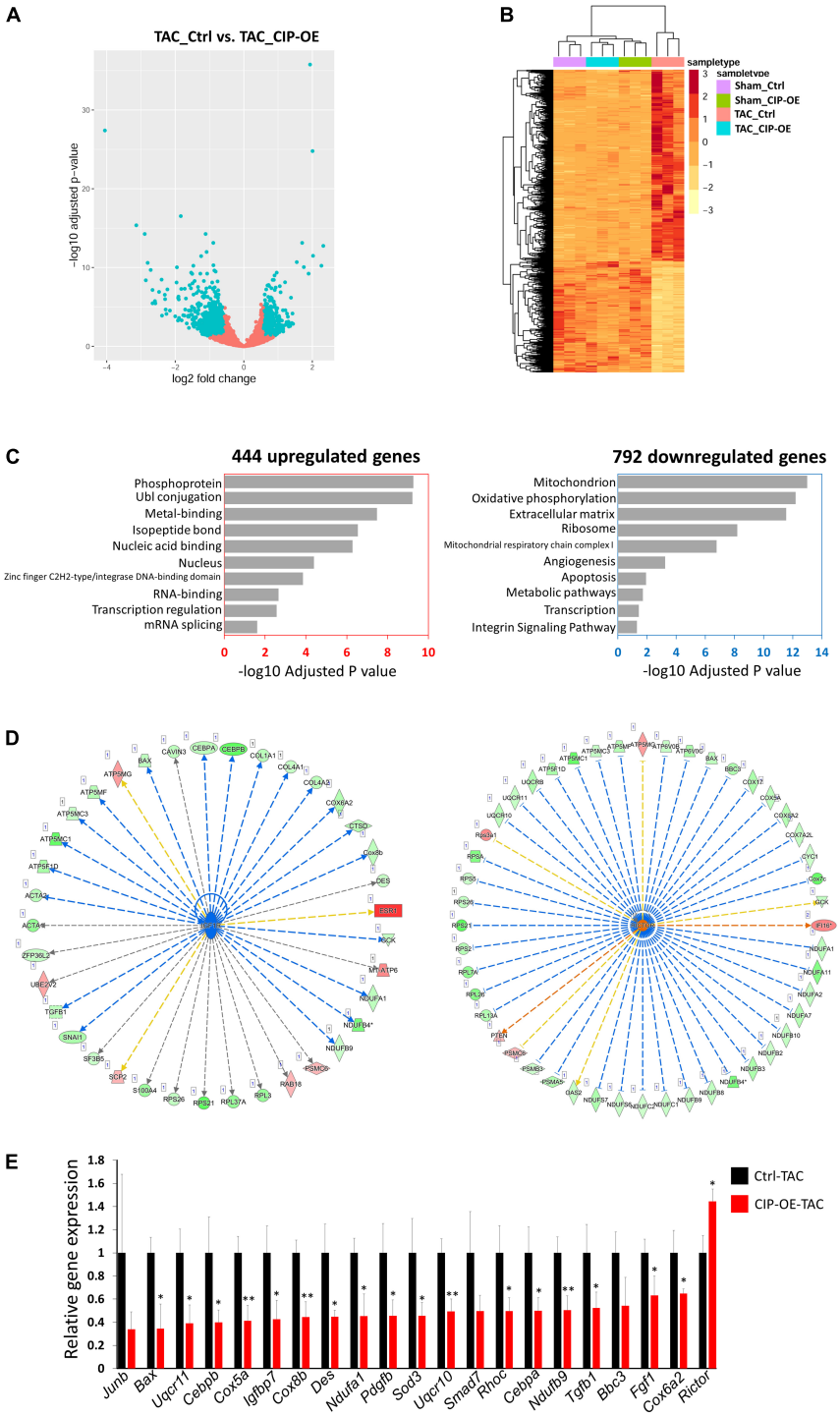

FIGURE 5 | IGF1R and mTORC2 signaling pathways mediates the function of CIP in cardiac protection. **(A)** A volcano plot of all detected genes in RNA-seq. Each dot represent one gene and the blue dots indicate dys-regulated genes in TAC-CIP-OE hearts comparing to TAC-Ctrl hearts. **(B)** A hierarchical clustering heatmap of 1,236 dys-regulated genes in all groups. **(C)** Gene ontology analysis of 444 up-regulated ($p < 0.05$) and 792 down-regulated ($p < 0.05$) genes in TAC-CIP-OE hearts. The GO terms are ranked by the adjusted *P* values. **(D)** Ingenuity Pathway Analysis (IPA) of upstream regulators of dys-regulated genes in CIP-OE heart after 8 weeks of TAC operation. Genes in green indicate their expression in CIP-OE heart is down-regulated. Genes in red indicate their expression in CIP-OE heart is up-regulated. Blue lines indicate that the dysregulation of upstream regulator lead to the down-regulation of the downstream genes, which is consistent with reported data; Red lines indicate that the dysregulation of upstream regulator lead to the up-regulation of the downstream genes, which is consistent with reported data. Yellow lines indicate that the gene regulation is inconsistent with reported data. Gray lines indicate the unknown gene regulation; **(E)** qRT-PCR validation of dys-regulated genes downstream of IGF1R, Rictor or TGF1B. *N* = 3 for each group. The significance between groups was tested with 1-way ANOVA with *post hoc* Tukey's test. $^{*}P < 0.05$; $^{**}P < 0.01$.

The molecular mechanism of CIP's function in protecting the heart was further explored in this study. Several key upstream regulators, including IGF1R, Rictor and TGFB1, were identified. Previously, we showed that CIP regulates the activity of a key cardiac remodeling regulator, Calcineurin, through FoxO1 (15). Here, we found that CIP regulated the activity of IGF1R, an upstream regulator of FoxO1 (24, 25) and played an important role in cardiac hypertrophy (26). Rictor, a core component in mTORC2 (27), displayed increased expression levels in CIP-overexpressing hearts, indicating activation of mTORC2. Indeed, activation of mTORC2 shows a cardioprotective effect in stressed hearts (28). TGFB1, which showed decreased expression in stressed CIP-overexpressing hearts, seems to be another key factor mediating CIP's function. Although TGFB1 has been widely demonstrated to regulate cardiac fibrosis in heart disease (29, 30), it was also shown to regulate the hypertrophic growth of cardiomyocytes through TAK1 (9). Interestingly, TGFB1 stimulates mitochondrial oxidative phosphorylation in non-cardiomyocytes (31). Consistently, the decreased expression of TGFB1 is coincident with the pattern of down-regulation of "oxidative phosphorylation" genes in the heart when CIP was overexpressed in our study. Indeed, we showed that CIP has a strong expression correlation coefficient with "oxidative phosphorylation" genes in human cardiac samples. In addition, our recent study indicated that CIP modulates oxidative stress by regulating CnA-NFAT-Nox4 signaling cascade in dystrophic cardiomyopathy (32). Further study is required to further dissect how CIP regulates this gene network before it can be pursued as a therapeutic approach for heart failure.

Previously, we demonstrated that CIP functions as a stress sensor and inhibited pathological hypertrophy from base line (15). This observation is a good sign that CIP has the potential for clinical application; however, we often face patients who have already developed severe cardiac sequelae in the hospital. To explore the potential of CIP in this situation, we induced cardiac-specific overexpression of CIP after a disease model of cardiac hypertrophy was established. Our data demonstrated that CIP significantly delayed disease progression and pathological cardiac remodeling, as well as protecting the heart from heart failure during prolonged stress; however, the overexpression could not reverse the hypertrophy. The results suggests that the CIP protein has great therapeutic potential in the treatment of cardiac disease progression toward heart failure. In the future, cardiac CIP overexpression mediated by adeno-associated virus (AAV), which has been well established for transgene expression in the heart and proposed for clinical study (33, 34), should be tested to further support this potential.

MATERIALS AND METHODS

Human Samples

Left ventricular (LV) tissues were collected from patients with end-stage heart failure during heart transplantation performed in the First Affiliated Hospital, Sun Yat-sen University. In brief, diseased hearts were removed at the time of transplantation and LV tissue was subsequently dissected and snap-frozen. We used LV samples from not implanted healthy hearts to serve as controls (**Supplementary Table 1**). All the procedures followed the protocol approved by the First Affiliated Hospital, Sun Yat-sen University, Guangzhou, China.

Mice

Cardiac ISL1-interacting Protein-KI-flox mice were generated in a previous study (15). CIP-KI-flox mice, which have a Rosa-CIP allele (the stop codon is present and floxed) were bred with aMHC–Mer–Cre–Mer mice to obtain CIP-OE (CIP-KI-flox; aMHC–Mer–Cre–Mer) mice. Tamoxifen was administrated through intraperitoneal injection to activate the expression of Cre recombinase and the excision of the stop codon for the ectopic expression of CIP transgene in the heart in CIP-OE mice. CIP-KI-flox littermates were used as controls.

Measurement of Cardiac Function by Echocardiography

Echocardiographic measurements were performed on mice using a Visual Sonics Vevo® 2100 Imaging System (Visual Sonics, Toronto, ON, Canada) with a 40 MHz MicroScan transducer (model MS-550D). Mice were anesthetized with isoflurane (2.5% isoflurane for induction and 0.1% for maintenance). Heart rate and LV dimensions, including diastolic and systolic wall thicknesses, LV end-diastolic and end-systolic chamber dimensions were measured from 2-D short-axis under M-mode tracings at the level of the papillary muscle. LV mass and functional parameters such as percentage of fractional shortening (FS%) and ejection fraction (EF%) were calculated using the above primary measurements and accompanying software.

Transverse Aortic Constriction Operation

Mice were anesthetized with isoflurane (3–4% isoflurane for induction, 1–2% isoflurane for maintenance). The chest was shaved and cleaned with alcohol. A suture was placed around the front upper incisors and pulled taut so that the neck was slightly extended. The tongue was retracted and held with forceps, and a 20-G catheter was inserted into the trachea. The catheter was then attached to the mouse ventilator via a Y-shaped connector. Ventilation was performed with a tidal volume of 220–240 μl for a 25–30 g mouse and a respiratory rate of 130–140 breaths per min. 100% oxygen was provided to the inflow of the ventilator. The chest was opened through a left 2nd intercostal thoracotomy. The 26-G needle without its sharp tip was put on the ascending aorta. They were tightly ligated together using 7-0 Nylon suture (Ethicon, Edinburgh, Scotland) at the position between brachiocephalic artery and left common carotid artery, and the 26-G needle was removed immediately after ligation. In the sham operation, no ligation was performed. Isoflurane was stopped, and the lungs were slightly overinflated to assist in removal of air in the pleural cavity. Dissected intercostal space and chest skin were closed using 6-0 silk suture (Ethicon,

Edinburgh, Scotland). All manipulations were performed by an operator without knowledge of genotype.

Haematoxylin and Eosin Staining and Fast Green/Sirius Red Collagen Staining

Mouse heart tissues were dissected from the animals, rinsed with PBS and fixed in 4% paraformaldehyde (pH 8.0) overnight. After dehydration through a series of ethanol baths, samples were embedded in paraffin wax according to standard laboratory procedures. Sections of 5 μm were stained with haematoxylin and eosin (H&E) for routine histological examination with light microscope. For Sirius red/fast green collagen staining sections were fixed with pre-warmed Bouins' solution, 55°C for 1 h then washed in running water. Sections were stained in 0.1% fast green solution for 10 mins then washed with 1% Acetic acid for 2 mins. After rinsing in tape water, sections were stained in 0.1% Sirius resolution for 30 mins. After staining, sections were dehydrated and cleared with Xylene. The images were examined with light scope and quantified with ImageJ software.

Quantitative RT-PCR and Western Blot Analysis

Total RNAs were isolated using Trizol Reagent (Life Technologies, Carlsbad, CA, United States) from cells and tissue samples. For Quantitative RT-PCR, 2.0 μg RNA samples were reverse-transcribed to cDNA by using random hexamers and MMLV reverse transcriptase (Life Technologies) in 20 μl reaction system. In each analysis, 0.1 μl cDNA pool was used for quantitative PCR. The relative expression of interested genes is normalized to the expression of ACTB or PRKG1. Primers used in this study were listed (**Supplementary Table 2**). For Western blot analyses, tissue homogenate were cleared by 10,000 × *g* centrifugation for 10 min. Samples were subsequently analyzed by SDS/PAGE and transferred to PVDF membranes that were incubated with 5% non-fat dry milk in TBST and Anti-CIP (1:2,000, 21st Century Biochemical, Marlboro, MA, United States) or Anti-GAPDH (1:5,000, Proteintech, Rosemont, IL, United States) overnight at 4°C and then washed three times with TBST buffer before adding IgG secondary antibody. Specific protein bands were visualized through chemiluminescent detection.

Constructs, Cell Culture, and Luciferase Reporter Assays

HEK293T cells were cultured in DMEM supplemented with 10% FBS in a 5% CO^2 atmosphere at 37°C. Wildtype, mutant or truncated CIP promoter sequences were cloned into multiple cloning sites of the pGL3-Basic vector (Promega, Madison, WI, United States) to generate CIP-Luc reporters used in this study. The indicated combinations of CIP-Luc reporter, pRL Renilla reporter (internal control) and GATA4 construct were transfected into HEK293T cells with PEI reagents. Forty Eight hours after transfection, cell extracts were prepared and luciferase activity was determined. For dual-luciferase assay, normalized firefly luciferase expression from triplicate samples in 12-well plates relative to renilla luciferase expression was calculated.

Mouse Heart RNA-Seq Data Analyses

Total RNAs from mouse heart were used to perform RNA-seq in BGI Genomics (Wuhan, China). RNA-seq reads were mapped to mouse genome mm10 by STAR and reads counts were calculated with FeatureCounts. Expression analysis was run in RStudio. DESeq2 was employed to perform statistical analysis of differential gene expression. An adjusted *P* value of 0.05 were used as cutoff to identify differentially regulated genes. Volcano plot were performed with the ggplot2 library. Hierarchical clustering heatmap was made with the pheatmap library. The raw data of RNA-seq in this study were deposited in Gene Expression Omnibus (GEO) database of the National Center for Biotechnology Information (NCBI) (Accession: GSE194149).

Human Heart RNA-Seq Data Collection and Analyses

Human diseased heart RNA-seq data, including GSE57344, GSE71613, GSE116250, GSE46224, GSE108157, GSE55296, GSE120836, and GSE130036, were downloaded from NCBI database. Gene-level quantification were calculated by featureCounts-v1.6.3. To perform strand-specific reads counting, the strand type (non-strand, stranded, reversely stranded) of each sample was inferred from sorted bam file using infer_expriment.py (3.0.0). Then we provided featureCounts with strand type information to calculate read counts of every gene in each sample and merged the quantification results together to make an expression matrix for differential gene expression analysis. Differential gene expression analysis was performed using DESeq2-1.24.0. The design matrix in DESeq2 model was written as "∼series + gender + phenotype" to adjust the differences between data series and gender. Only differential expressed genes with FDR < 0.05 and log2FoldChange > 0.25 identified by DESeq2 were kept. Then, we applied the classic weighted correlation network analysis (WGCNA) algorithm for co-expression analysis. The R implementation of WGCNA (version: 1.68) was used in our study.

Statistics

Values are reported as means ± SEM unless indicated otherwise. Statistical significance was determined with ANOVA. For multiple group comparisons, a *post hoc* Tukey's test was performed when ANOVA reached significance. Values of $P < 0.05$ were considered statistically significant.

DATA AVAILABILITY STATEMENT

The datasets presented in this study can be found in online repositories. The names of the repository/repositories and accession number(s) can be found below: GEO, GSE194149.

ETHICS STATEMENT

The studies involving human participants and animal study were reviewed and approved by the Medical Ethics Committee of the First Affiliated Hospital, Sun Yat-sen University. The

patients/participants provided their written informed consent to participate in this study. Written informed consent was obtained from the owners for the participation of their animals in this study.

AUTHOR CONTRIBUTIONS

Z-PH and D-ZW conceived the project, designed and analyzed the experiments, and wrote the manuscript. YoY, TL, TY, and XH performed molecular biology experiments. CL, XL, SL, YC, and YD contributed to the human sample acquisition and western blotting analysis. QS, QM, and GZ generated CIP-OE mice, performed transverse aortic constriction surgery, and collected mouse heart samples. QS and GZ contributed to the echocardiographic data acquisition and analysis. TY, DZ, and XH contributed to the histological and immunofluorescent data acquisition and analysis. YW, KC, and YuY contributed to bioinformatic analyses of RNA-seq data. WM and WP supervised the CIP-KO mice generation and surgery and reviewed the manuscript. All authors contributed to the article and approved the submitted version.

FUNDING

This work was supported by the National Natural Science Foundation of China (81873463 to Z-PH, 81970429 to DZ, and 81900350 to SL), the Guangdong Basic and Applied Basic Research Foundation (2019B151502003 to Z-PH, 2019A1515011956 to DZ, and 2018A030313448 and 2021A1515010433 to YC), and the NIH (HL085635, HL116919, and HL125925 to D-ZW) and Muscular Dystrophy Association (294854 to D-ZW).

ACKNOWLEDGMENTS

We thank members of the Huang and Wang laboratories for advice and support.

SUPPLEMENTARY MATERIAL

The Supplementary Material for this article can be found online at: https://www.frontiersin.org/articles/10.3389/fcvm.2022.857049/full#supplementary-material

REFERENCES

1. Cohn JN, Ferrari R, Sharpe N. Cardiac remodeling–concepts and clinical implications: a consensus paper from an international forum on cardiac remodeling. Behalf of an international forum on cardiac remodeling. *J Am Coll Cardiol.* (2000) 35:569–82. doi: 10.1016/s0735-1097(99)00630-0
2. Messerli FH, Rimoldi SF, Bangalore S. The transition from hypertension to heart failure: contemporary update. *JACC Heart Fail.* (2017) 5:543–51. doi: 10.1016/j.jchf.2017.04.012
3. Hill JA, Olson EN. Cardiac plasticity. *N Engl J Med.* (2008) 358:1370–80.
4. Ahmad F, Seidman JG, Seidman CE. The genetic basis for cardiac remodeling. *Annu Rev Genomics Hum Genet.* (2005) 6:185–216. doi: 10.1146/annurev.genom.6.080604.162132
5. Frey N, Olson EN. Cardiac hypertrophy: the good, the bad, and the ugly. *Annu Rev Physiol.* (2003) 65:45–79. doi: 10.1146/annurev.physiol.65.092101.142243
6. Welch S, Plank D, Witt S, Glascock B, Schaefer E, Chimenti S, et al. Cardiac-specific IGF-1 expression attenuates dilated cardiomyopathy in tropomodulin-overexpressing transgenic mice. *Circ Res.* (2002) 90:641–8. doi: 10.1161/01.res.0000013780.77774.75
7. Ren J, Samson WK, Sowers JR. Insulin-like growth factor I as a cardiac hormone: physiological and pathophysiological implications in heart disease. *J Mol Cell Cardiol.* (1999) 31:2049–61. doi: 10.1006/jmcc.1999.1036
8. Schultz Jel J, Witt SA, Glascock BJ, Nieman ML, Reiser PJ, Nix SL, et al. TGF-beta1 mediates the hypertrophic cardiomyocyte growth induced by angiotensin II. *J Clin Invest.* (2002) 109:787–96. doi: 10.1172/JCI14190
9. Koitabashi N, Danner T, Zaiman AL, Pinto YM, Rowell J, Mankowski J, et al. Pivotal role of cardiomyocyte TGf-beta signaling in the murine pathological response to sustained pressure overload. *J Clin Invest.* (2011) 121:2301–12. doi: 10.1172/JCI44824
10. Heineke J, Molkentin JD. Regulation of cardiac hypertrophy by intracellular signalling pathways. *Nat Rev Mol Cell Biol.* (2006) 7:589–600. doi: 10.1038/nrm1983
11. Wang Y. Mitogen-activated protein kinases in heart development and diseases. *Circulation.* (2007) 116:1413–23. doi: 10.1161/CIRCULATIONAHA.106.679589
12. Frey N, McKinsey TA, Olson EN. Decoding calcium signals involved in cardiac growth and function. *Nat Med.* (2000) 6:1221–7. doi: 10.1038/81321
13. Molkentin JD, Lu JR, Antos CL, Markham B, Richardson J, Robbins J, et al. A calcineurin-dependent transcriptional pathway for cardiac hypertrophy. *Cell.* (1998) 93:215–28. doi: 10.1016/s0092-8674(00)81573-1
14. Huang ZP, Young Seok H, Zhou B, Chen J, Chen JF, Tao Y, et al. CIP, a cardiac Isl1-interacting protein, represses cardiomyocyte hypertrophy. *Circ Res.* (2012) 110:818–30. doi: 10.1161/CIRCRESAHA.111.259663
15. Huang ZP, Kataoka M, Chen J, Wu G, Ding J, Nie M, et al. Cardiomyocyte-enriched protein CIP protects against pathophysiological stresses and regulates cardiac homeostasis. *J Clin Invest.* (2015) 125:4122–34. doi: 10.1172/jci82423
16. Esslinger U, Garnier S, Korniat A, Proust C, Kararigas G, Muller-Nurasyid M, et al. Exome-wide association study reveals novel susceptibility genes to sporadic dilated cardiomyopathy. *PLoS One.* (2017) 12:e0172995. doi: 10.1371/journal.pone.0172995
17. Liu J, Huang ZP, Nie M, Wang G, Silva WJ, Yang Q, et al. Regulation of myonuclear positioning and muscle function by the skeletal muscle-specific CIP protein. *Proc Natl Acad Sci USA.* (2020) 117:19254–65. doi: 10.1073/pnas.1922911117
18. Ahmady E, Deeke SA, Rabaa S, Kouri L, Kenney L, Stewart AF, et al. Identification of a novel muscle A-type lamin-interacting protein (MLIP). *J Biol Chem.* (2011) 286:19702–13. doi: 10.1074/jbc.M110.165548
19. He A, Kong SW, Ma Q, Pu WT. Co-occupancy by multiple cardiac transcription factors identifies transcriptional enhancers active in heart. *Proc Natl Acad Sci USA.* (2011) 108:5632–7. doi: 10.1073/pnas.1016959108
20. Lopes Abath Neto O, Medne L, Donkervoort S, Rodriguez-Garcia ME, Bolduc V, Hu Y, et al. MLIP causes recessive myopathy with rhabdomyolysis, myalgia and baseline elevated serum creatine kinase. *Brain.* (2021) 144:2722–31. doi: 10.1093/brain/awab275
21. Salzer-Sheelo L, Fellner A, Orenstein N, Bazak L, Lev-El Halabi N, Daue M, et al. Biallelic truncating variants in the muscular A-type lamin-interacting protein (MLIP) gene cause myopathy with hyperckemia. *Eur J Neurol.* (2021).
22. Cortes R, Rivera M, Rosello-Lleti E, Martinez-Dolz L, Almenar L, Azorin I, et al. Differences in MEF2 and NFAT transcriptional pathways according to human heart failure aetiology. *PLoS One.* (2012) 7:e30915. doi: 10.1371/journal.pone.0030915
23. Hall JL, Grindle S, Han X, Fermin D, Park S, Chen Y, et al. Genomic profiling of the human heart before and after mechanical support with a ventricular assist device reveals alterations in vascular signaling networks. *Physiol Genomics.* (2004) 17:283–91. doi: 10.1152/physiolgenomics.00004.2004

24. Nakae J, Barr V, Accili D. Differential regulation of gene expression by insulin and IGF-1 receptors correlates with phosphorylation of a single amino acid residue in the forkhead transcription factor FKHR. *EMBO J.* (2000) 19:989–96. doi: 10.1093/emboj/19.5.989
25. Liu TJ, Lai HC, Ting CT, Wang PH. Bidirectional regulation of upstream IGF-I/insulin receptor signaling and downstream FOXO1 in cardiomyocytes. *J Endocrinol.* (2007) 192:149–58. doi: 10.1677/joe.1.07020
26. Anversa P, Kajstura J, Cheng W, Reiss K, Cigola E, Olivetti G. Insulin-like growth factor-1 and myocyte growth: the danger of a dogma part II. Induced myocardial growth: pathologic hypertrophy. *Cardiovas Res.* (1996) 32:484–95.
27. Sarbassov DD, Ali SM, Kim DH, Guertin DA, Latek RR, Erdjument-Bromage H, et al. Rictor, a novel binding partner of mTOR, defines a rapamycin-insensitive and raptor-independent pathway that regulates the cytoskeleton. *Curr Biol.* (2004) 14:1296–302. doi: 10.1016/j.cub.2004.06.054
28. Yano T, Ferlito M, Aponte A, Kuno A, Miura T, Murphy E, et al. Pivotal role of mTORC2 and involvement of ribosomal protein S6 in cardioprotective signaling. *Circ Res.* (2014) 114:1268–80. doi: 10.1161/CIRCRESAHA.114.303562
29. Euler-Taimor G, Heger J. The complex pattern of smad signaling in the cardiovascular system. *Cardiovasc Res.* (2006) 69:15–25. doi: 10.1016/j.cardiores.2005.07.007
30. Kuwahara F, Kai H, Tokuda K, Kai M, Takeshita A, Egashira K, et al. Transforming growth factor-beta function blocking prevents myocardial fibrosis and diastolic dysfunction in pressure-overloaded rats. *Circulation.* (2002) 106:130–5. doi: 10.1161/01.cir.0000020689.12472.e0
31. Abe Y, Sakairi T, Beeson C, Kopp JB. TGF-beta1 stimulates mitochondrial oxidative phosphorylation and generation of reactive oxygen species in cultured mouse podocytes, mediated in part by the mtor pathway. *Am J Physiol Renal Physiol.* (2013) 305:F1477–90. doi: 10.1152/ajprenal.00182.2013
32. He X, Liu J, Gu F, Chen J, Lu YW, Ding J, et al. Cardiac CIP protein regulates dystrophic cardiomyopathy. *Mol Ther.* (2022) 30:898–914. doi: 10.1016/j.ymthe.2021.08.022
33. Wasala NB, Yue Y, Lostal W, Wasala LP, Niranjan N, Hajjar RJ, et al. Single SERCA2a therapy ameliorated dilated cardiomyopathy for 18 months in a mouse model of duchenne muscular dystrophy. *Mol Ther.* (2020) 28:845–54. doi: 10.1016/j.ymthe.2019.12.011
34. Zsebo K, Yaroshinsky A, Rudy JJ, Wagner K, Greenberg B, Jessup M, et al. Long-term effects of AAV1/SERCA2a gene transfer in patients with severe heart failure: analysis of recurrent cardiovascular events and mortality. *Circ Res.* (2014) 114:101–8. doi: 10.1161/CIRCRESAHA.113.302421

Conflict of Interest: The authors declare that the research was conducted in the absence of any commercial or financial relationships that could be construed as a potential conflict of interest.

Publisher's Note: All claims expressed in this article are solely those of the authors and do not necessarily represent those of their affiliated organizations, or those of the publisher, the editors and the reviewers. Any product that may be evaluated in this article, or claim that may be made by its manufacturer, is not guaranteed or endorsed by the publisher.

frontiers in Cardiovascular Medicine

ORIGINAL RESEARCH
published: 25 March 2022
doi: 10.3389/fcvm.2022.858909

PPARγ Mediates the Cardioprotective Roles of Danlou Tablet After Acute Myocardial Ischemia-Reperfusion Injury

Meng Wei[1,2], *Mengying Guo*[1,2], *Xinxiu Meng*[1,2], *Lin Li*[1,2], *Hongyun Wang*[1,2*], *Mingxue Zhang*[3*] and *Yihua Bei*[1,2*]

[1] Cardiac Regeneration and Ageing Lab, Institute of Geriatrics (Shanghai University), Affiliated Nantong Hospital of Shanghai University (The Sixth People's Hospital of Nantong), School of Medicine, Shanghai University, Nantong, China, [2] Shanghai Engineering Research Center of Organ Repair, School of Life Science, Shanghai University, Shanghai, China, [3] Affiliated Hospital of Liaoning University of Traditional Chinese Medicine, Shenyang, China

Ischemic heart disease is one of the biggest threats to human life in the world. Reperfusion therapy is an effective strategy to reduce infarct size and ischemic injury. However, reperfusion process may cause secondary myocardial injury which is defined as ischemia-reperfusion injury (IRI). Exploring potential therapeutic strategy to attenuate IRI is extremely important. Danlou tablet (Dan), a Chinese herbal compound consisting of ten herbs, has been identified to be protective for the heart. However, the mechanism of Dan-induced cardioprotection after acute reperfusion was unelucidated. In this study, to investigate the role and mechanism of Dan in myocardial IRI, we performed acute IRI modeling in mice and oxygen-glucose deprivation–reperfusion (OGD/R)-induced apoptosis in primary neonatal rat cardiomyocytes (NRCMs). We found that Dan had protective effect against acute IRI in mice, as evidenced by reduced infarct size, TUNEL-positive cardiomyocytes (CMs), and Bax/Bcl2 ratio and cleaved-caspase 3/caspase 3 ratio *in vivo*. Meanwhile, Dan inhibited OGD/R-induced apoptosis of NRCMs *in vitro*. Mechanistically, Dan could activate proliferator-activated receptor gamma (PPARγ) in both IRI hearts and OGD/R-stressed NRCMs, while inhibition of PPARγ attenuated the protective effect of Dan against IRI *in vivo* and OGD/R-induced CM apoptosis *in vitro*. These data reveal that Dan attenuates acute myocardial IRI and CM apoptosis through activating PPARγ. Our findings may extend the knowledge of Chinese medicine and provide potential strategy for the precise treatment of ischemic heart diseases.

Keywords: Danlou tablet, PPARγ, ischemia-reperfusion injury, cardiomyocyte, apoptosis

OPEN ACCESS

Edited by:
Zhanpeng Huang,
The First Affiliated Hospital of Sun Yat-sen University, China

Reviewed by:
Zhi Xin Shan,
Guangdong Provincial People's Hospital, China
Mingming Zhang,
Tangdu Hospital, China

***Correspondence:**
Hongyun Wang
hongyun19@shu.edu.cn
Mingxue Zhang
zhmx6228@163.com
Yihua Bei
beiyh36@shu.edu.cn

Specialty section:
This article was submitted to General Cardiovascular Medicine, a section of the journal Frontiers in Cardiovascular Medicine

Received: *20 January 2022*
Accepted: *28 February 2022*
Published: *25 March 2022*

Citation:
Wei M, Guo M, Meng X, Li L, Wang H, Zhang M and Bei Y (2022) PPARγ Mediates the Cardioprotective Roles of Danlou Tablet After Acute Myocardial Ischemia-Reperfusion Injury. Front. Cardiovasc. Med. 9:858909. doi: 10.3389/fcvm.2022.858909

INTRODUCTION

Cardiovascular disease (CVD), especially ischemic heart disease, is one of the biggest killers to human life worldwide (1, 2). Percutaneous coronary intervention (PCI)–reperfusion therapy is an effective strategy to rescue ischemic injury and to reduce the risk of death (3, 4). Nevertheless, reperfusion can cause secondary myocardial injury in the patients undergoing PCI therapy (5). This sudden myocardial reperfusion after ischemia can induce a series of pathological processes, such as oxidative stress, Ca^{2+} overload, altered mitochondrial function, DNA strand breaks, and cell damages, which is termed as ischemia-reperfusion injury (IRI) (6–8). Prolonged myocardial IRI may further develop cardiac remodeling and even heart failure, which severely influences clinical prognosis (9).

Ischemia-reperfusion injury-induced cardiomyocyte (CM) apoptosis has been attracting an increasing attention in the past years, and exploring potential therapeutic medicine to rescue IRI is extremely important. To date, several potential molecules or targets are identified effective to attenuate IRI. For example, exendin-4, a glucagon-like protein-1 receptor agonist, was found to protect myocardium against IRI in rats (10). Noncoding RNAs, microRNA (miR)-486, was reported to be downregulated upon IRI, while increasing miR-486 can relieve IRI and myocardial apoptosis (11). Long noncoding RNA (lncRNA) CPhar was identified to be induced by exercise training, whose upregulation can protect against IRI (12). Recently, it was reported that inhibition of acid sensing ion channel 1a can recover cardiac function after IRI (13). Absolutely, increasing studies have been performed to explore an appropriate method to protect the heart against IRI. However, the potential role and biological mechanism of Chinese traditional medicine is poorly explored in IRI therapy.

Danlou tablet (Dan), a Chinese proprietary medicine, has been used for angina pectoris treatment (14). From 2012, scientists and doctors tried to investigate the protective roles of Dan in heart. It was found that Dan can improve cardiac function in swine with coronary disease (15). Later, Dan was identified effective to attenuate arrhythmia in rats (16), peri-procedural myocardial injury (17), and atherosclerosis (18), etc. In addition, Dan can attenuate hypoxia-induced dyslipidemia (19) and reduce inflammation induced by high fat *in vivo* (20). Increasing evidence has demonstrated that Dan plays protective roles in coronary heart diseases. Interestingly, it was reported that Dan may protect myocardium against IRI *in vivo* (21). However, the functional role and molecular mechanism of Dan in CMs upon IRI was largely not elucidated.

To investigate the mechanism of Dan attenuating acute IRI, we built *in vivo* and *in vitro* models using mice and primary neonatal rat CMs (NRCMs), respectively. For exploring the downstream target and pathway of Dan, pharmacological inhibition strategy was used in this study. To reveal the mechanism of Dan in IRI may extend the knowledge of Chinese medicine and provide new strategy for precise treatment of ischemic heart diseases.

MATERIALS AND METHODS

Animals and IRI Modeling

Male C57BL/6J mice (8 weeks old) were purchased from Charles River (Beijing, China) and were housed in a specific pathogen-free atmosphere. To investigate the effect of Danlou tablet in IRI, Dan was dissolved with saline (70 mg/ml, ultrasonic for 1 h) and was administrated to mice by gavage at a dose of 700 mg/kg/d for 2 consecutive weeks before acute IRI modeling. The control mice were administrated with equal volume of saline. Then, myocardial IRI was induced by ligating the left anterior descending artery for 30 min followed by reperfusion for 24 h according to the previous study (22). To study whether peroxisome proliferator-activated receptor gamma (PPARγ) mediated the function of Dan in IRI, mice were intraperitoneally injected with PPARγ inhibitor T0070907 (Selleck, S2871) at a dose of 1 mg/kg/d in the presence of Dan treatment. All animal experiments were approved by the Ethics Committee of Shanghai University and performed in accordance with the guidelines.

2,3,5-Triphenyl Tetrazolium Chloride (TTC) Staining

To evaluate the effect of Dan on the infarct size after acute IRI, TTC staining was performed after 24 h of reperfusion. Briefly, 1 ml of Evans blue (1% in phosphate-buffered saline) was injected into the left ventricle, and the heart was sliced to 1-mm-thick tissue sections and stained with TTC. The homogeneity of modeling was assessed by calculating the ratio of area at risk to left ventricle weight (AAR/LV), and the infarct size of heart was assessed by the ratio of infarct size/area at risk (INF/AAR).

Primary NRCM Isolation and Treatment

Left ventricles were freshly harvested from neonatal Sprague-Dawley rats (1–3 days old) and minced into 1-mm^2 small pieces on ice. Primary NRCMs were digested using Collagenase II (Gibco, 17101015) and Pancreatin from porcine pancreas (Sigma, P3292) and isolated using Percoll (GE healthcare, 17-0891-01) centrifugation (23). NRCMs were cultured in Dulbecco's modified Eagle's medium (DMEM) supplemented with 5% fetal bovine serum and 10% horse serum for further experiments. To explore the effect of Dan on CM apoptosis, NRCMs were treated with 50 μg/ml of Dan for 48 h followed by oxygen-glucose deprivation–reperfusion (OGD/R) modeling. To inhibit the activity of PPARγ in NRCMs, two PPARγ inhibitors GW9662 (10 μm, Selleck, S2915) and T0070907 (1 μm, Selleck, S2871) were used to treat NRCMs for 24 h *in vitro*, respectively.

Oxygen-Glucose Deprivation–Reperfusion

To induce OGD/R model, NRCMs were cultured in serum-free and glucose-deprived DMEM medium under oxygen deprivation atmosphere at 37°C for 8 h. Then, the cells were cultured with NRCM culture medium under normal oxygen condition for 12 h. The OGD/R-driven cells were divided into negative control

group (vehicle), Dan group (Dan), GW9662 (or T0070907) group, and Dan+GW9662 (or T0070907) group. The control group was not undergoing OGD/R.

TUNEL Staining

To reveal CM apoptosis *in vivo* and *in vitro*, TdT-mediated dUTP nick end labeling (TUNEL) staining complemented with α-actinin immunostaining was performed. Briefly, to assess CM apoptosis in mice, heart tissues were harvested after acute IRI for 24 h and embedded into optimal cutting temperature compound (OCT) for subsequent frozen section. The 10-μm-thick heart sections or primary cultured NRCMs were fixed by 4% paraformaldehyde and stained with TUNEL FITC Apoptosis Detection Kit according to the manufacturer's instructions (Vazyme, China). Immunostaining for α-actinin (Sigma, A7811) was performed to label CMs. Finally, sections were incubated with Hoechst for 20 min at room temperature before fluorescence imaging. The percentage of TUNEL-positive CMs was calculated to determine apoptosis in mice hearts upon IRI or in NRCMs upon OGD/R modeling.

Western Blot

NRCMs or heart tissues were homogenized in RIPA lysis buffer complemented with 1% PMSF for 30 min at 4°C and subsequently centrifuged at 12,000 g for 20 min. Then, protein supernatants were obtained and added with loading buffer to boil for 10 min. A total of 10 to 30 μg proteins were used to perform western blot as previously reported (24). Primary antibodies for Bax (Abclonal, A0207), Bcl-2 (Abclonal, A2845), caspase 3 (Cell Signaling, 9662), and PPARγ (Abclonal, A0270) were used, respectively. GAPDH or β-actin was used as an internal control.

Reverse Transcription Quantitative PCR

Total RNA was isolated from mouse heart tissues or NRCMs using TRIzol RNAiso Plus Kit (TaKaRa) and then reverse-transcribed to cDNA using RevertAid First Strand cDNA Synthesis Kit (Thermo K1622). The mRNA levels were analyzed by quantitative PCR (qPCR) using TaKaRa SYBR Premix Ex Taq™ (Tli RNaseH Plus, Japan) on Roche LightCycler480 PCR System. The primers used were as follows: mmu-PPARγ (5′-3′ forward and reverse) CGAGAAGGAGAAGCTGTTG and TCAGCGGGAAGGACTTTA; rno-PPARγ (5′-3′ forward and reverse) GGGAGTTCCTCAAAAGCC and TTCACGTTCAGCAAGCC; 18s (5′-3′forward and reverse) TCAAGAACGAAAGTCGGAGG and GGACATCTAAGGGCATCAC. The 18s was used as internal controls.

Statistical Analysis

All data in this study were analyzed using SPSS software version 20.0 or GraphPad Prism 8.0 software and were reported as mean ± standard deviation (SD). Student's *t*-test (two-sided) was used for two independent group comparisons. One-way ANOVA followed by Bonferroni or Dunnett's T3 test was used for comparisons among 3 groups. Two-way ANOVA followed by Tukey's correction was performed for more than 3 group comparisons. A $p<0.05$ was considered statistically significant.

RESULTS

Dan Protects Against Acute Myocardial IRI *in vivo*

To investigate the potential role of Dan on the heart, mice were undergoing IRI modeling for 24 h followed by TTC staining to evaluate the infarct size. There is no significant difference in AAR/LV ratio between IRI and Dan/IRI group, which demonstrates that a stable IRI modeling was constructed in this study. Interestingly, administration of Dan significantly reduced INF/AAR ratio after acute IRI (**Figure 1A**), which indicates that Dan protected mice against IRI-induced myocardial injury. To evaluate whether Dan is associated with IRI-induced CM apoptosis, TUNEL staining and apoptotic proteins were assessed in heart tissues. TUNEL/α-actinin staining showed that Dan significantly reduced IRI-induced CM apoptosis (**Figure 1B**). Consistent with TUNEL data, western blot experiments showed that IRI increased pro-apoptotic markers Bax/Bcl2 ratio and cleaved-caspase 3/caspase 3 ratio, while Dan attenuated their increase induced by IRI (**Figures 1C,D**). These data provided *in vivo* evidence that Dan exerts a protective effect against acute myocardial IRI and CM apoptosis.

Dan Attenuates OGD/R-Induced CM Apoptosis

To further evaluate the effects of Dan on CM apoptosis *in vitro*, primary NRCMs were isolated and used to mimic IRI *in vitro*. During myocardial ischemia stress, hypoxia stress is usually accompanied with an alteration of glucose metabolism in the myocardium. Thus, we used the deprivation and reperfusion of both oxygen and glucose in cultured CMs *in vitro* in order to better mimic myocardial I/R injury *in vivo* in our study. TUNEL staining and pro-apoptotic protein markers were performed to assess the efficiency of OGD/R modeling. Notably, OGD/R caused significant increase in TUNEL-positive CMs (**Figure 2A**), and increased Bax/Bcl2 ratio and cleaved-caspase 3/caspase 3 ratio (**Figure 2B**). These data demonstrated that we successfully constructed OGD/R-induced CM apoptosis model *in vitro*. Then, we treated NRCMs with Dan for 48 h to investigate the functional role of Dan on OGD/R-induced CM apoptosis. Under basal condition, treatment with Dan did not influence CM apoptosis, while it attenuated ODG/R-induced increase in TUNEL-positive CMs (**Figure 2C**). Western blot showed that Dan treatment did not influence the Bax/Bcl2 ratio or caspase 3 cleavage at baseline, but reduced the Bax/Bcl2 ratio and cleaved-caspase 3/caspase 3 ratio in CMs upon OGD/R stress (**Figure 2D**). All these data indicate that treatment with Dan can effectively protect CMs against OGD/R-induced apoptosis.

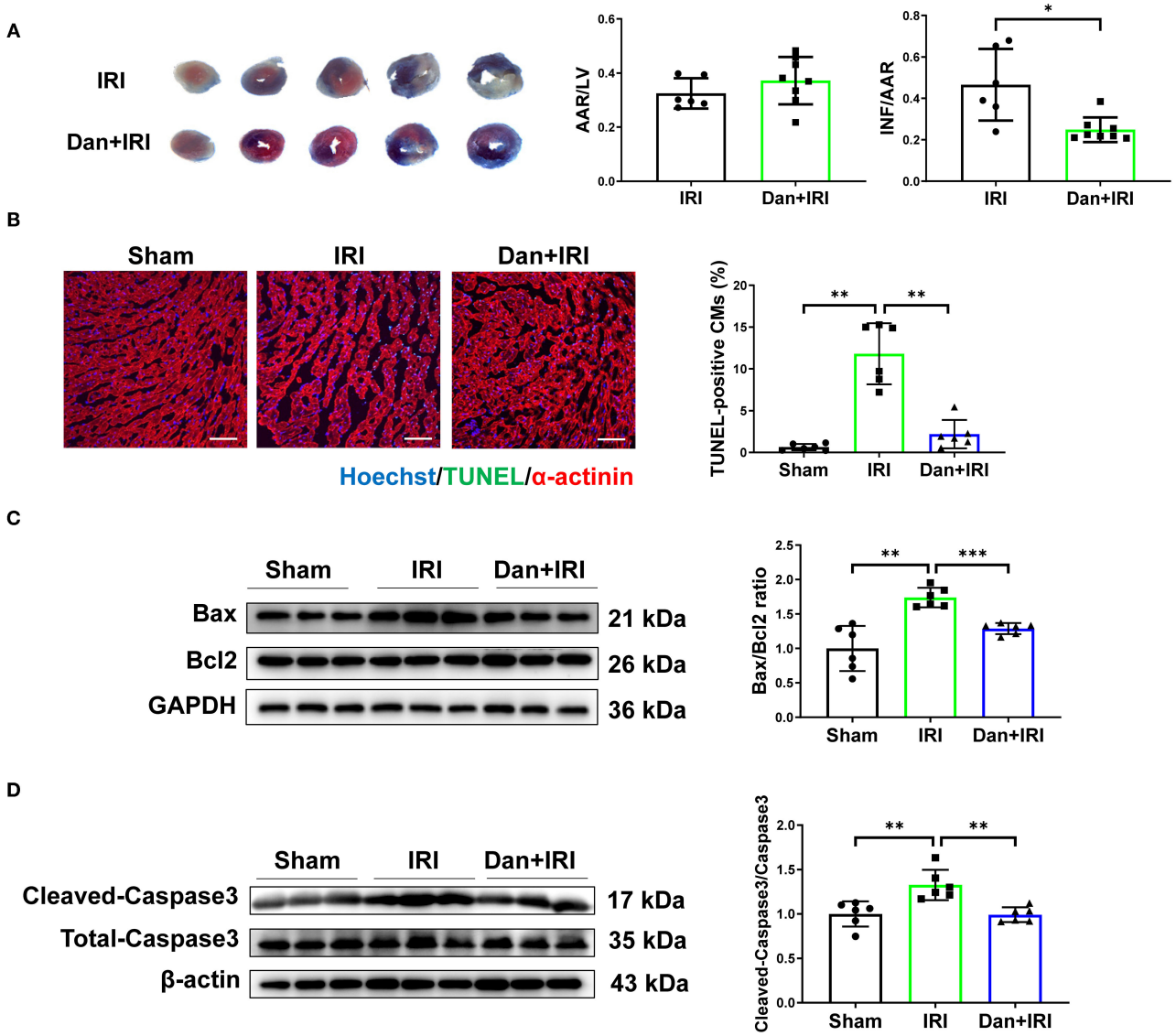

FIGURE 1 | Dan protects mice against acute myocardial ischemia-reperfusion injury *in vivo*. **(A)** Adult male mice were administrated by gavage with 700 mg/kg/d of Dan or equal volume of saline for 2 consecutive weeks followed by acute IRI modeling. TTC staining was performed at 24 h after IRI. The ratio of AAR/LV was determined for the homogeneity of modeling, and the ratio of infarct area/area at risk (INF/AAR) was determined for the infarct size ($n = 6$ vs. 8). **(B)** Representative images and quantification results of TUNEL/α-actinin staining were shown for myocardial apoptosis of mice ($n = 6$). Scale bar = 100 μm. **(C,D)** Western blot analysis for apoptotic-associated proteins in heart tissues, including Bax and Bcl2 **(C)** and cleaved-caspase 3 and total caspase 3 **(D)** ($n = 6$). $^{*}p < 0.05$; $^{**}p < 0.01$; $^{***}p < 0.001$.

Dan Prevents CM Apoptosis Through Activating PPARγ

Multiple evidence showed that PPARγ was involved in IRI not only in myocardium (25) but also in liver (26). Reduced PPARγ expression or activity is associated with aggravated IRI. To assess whether PPARγ is involved in the cardioprotective roles of Dan after IRI, we first examined PPARγ expression level in heart tissues. We observed that IRI significantly downregulated PPARγ in the heart, while Dan reversed IRI-induced PPARγ reduction at both mRNA and protein level (**Figures 3A,B**). To further investigate whether PPARγ is involved in Dan-induced cardioprotection, we also assessed PPARγ expression in OGD/R-induced CM apoptosis model and performed functional rescue experiments *in vitro*. Our data showed that Dan treatment caused an increase in PPARγ mRNA and protein levels in NRCMs after OGD/R modeling (**Figures 3C,D**). To block the activity of PPARγ, we chose two PPARγ inhibitors (GW9662 and T0070907) to observe the change of CM apoptosis in OGD/R model. In OGD/R-induced CM apoptosis model, Dan treatment reduced TUNEL-positive CMs, while Dan co-treatment with

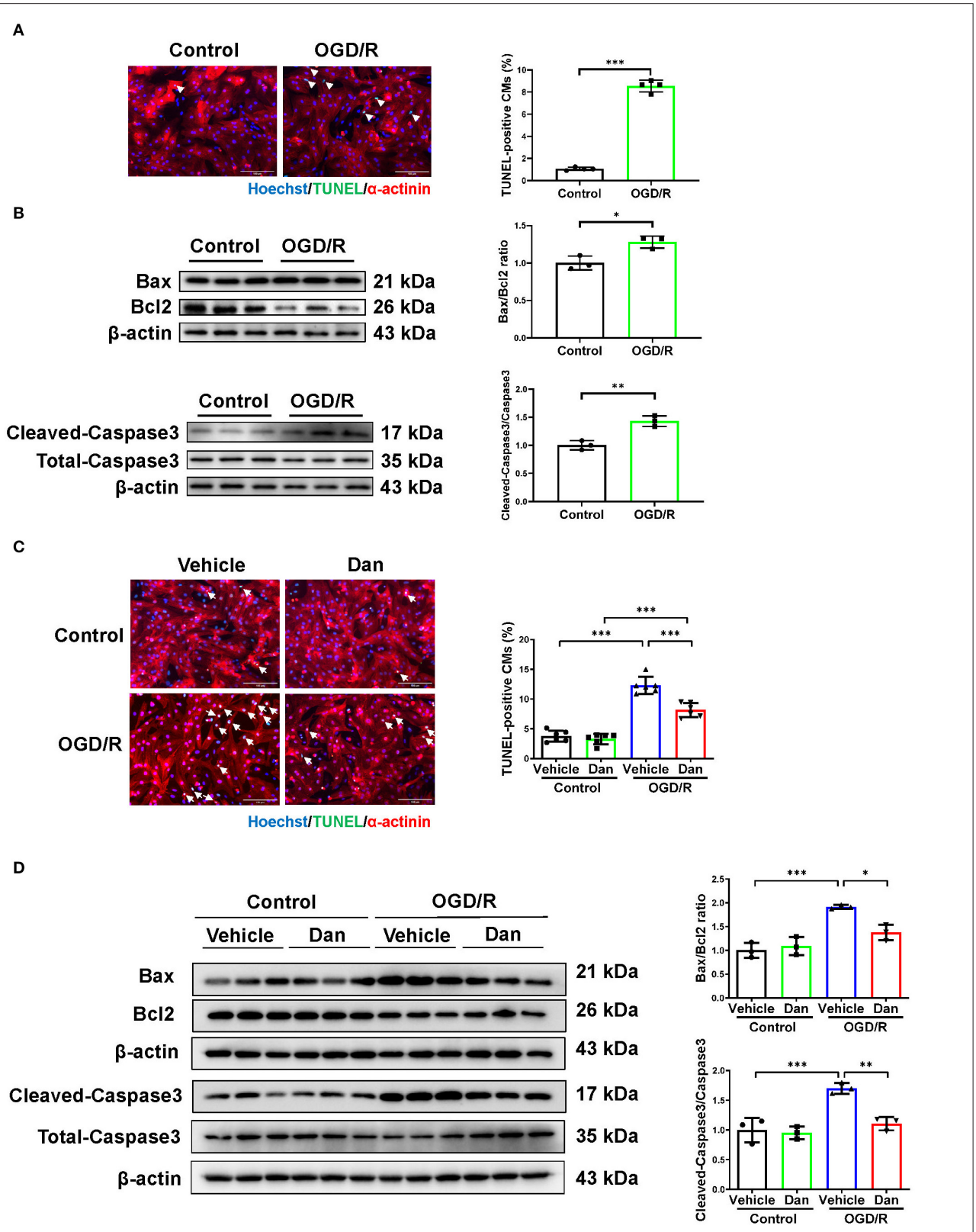

FIGURE 2 | Dan attenuates oxygen-glucose deprivation–reperfusion-induced CM apoptosis *in vitro*. **(A)** Primary NRCMs were submitted to oxygen-glucose deprivation–reperfusion (OGD/R) modeling to induce apoptosis. TUNEL/α-actinin staining was performed to assess CM apoptosis ($n = 4$). Scale bar = 100 μm. **(B)** Western blot analysis for apoptotic-associated proteins in OGD/R-induced apoptosis of NRCMs ($n = 3$). **(C)** TUNEL/α-actinin staining for OGD/R-induced apoptosis of NRCMs in the presence or absence of Dan treatment ($n = 6$). Scale bar = 100 μm. **(D)** Western blot analysis for apoptotic-associated proteins in OGD/R-induced apoptosis of NRCMs in the presence or absence of Dan treatment ($n = 3$). *$p < 0.05$; **$p < 0.01$; ***$p < 0.001$.

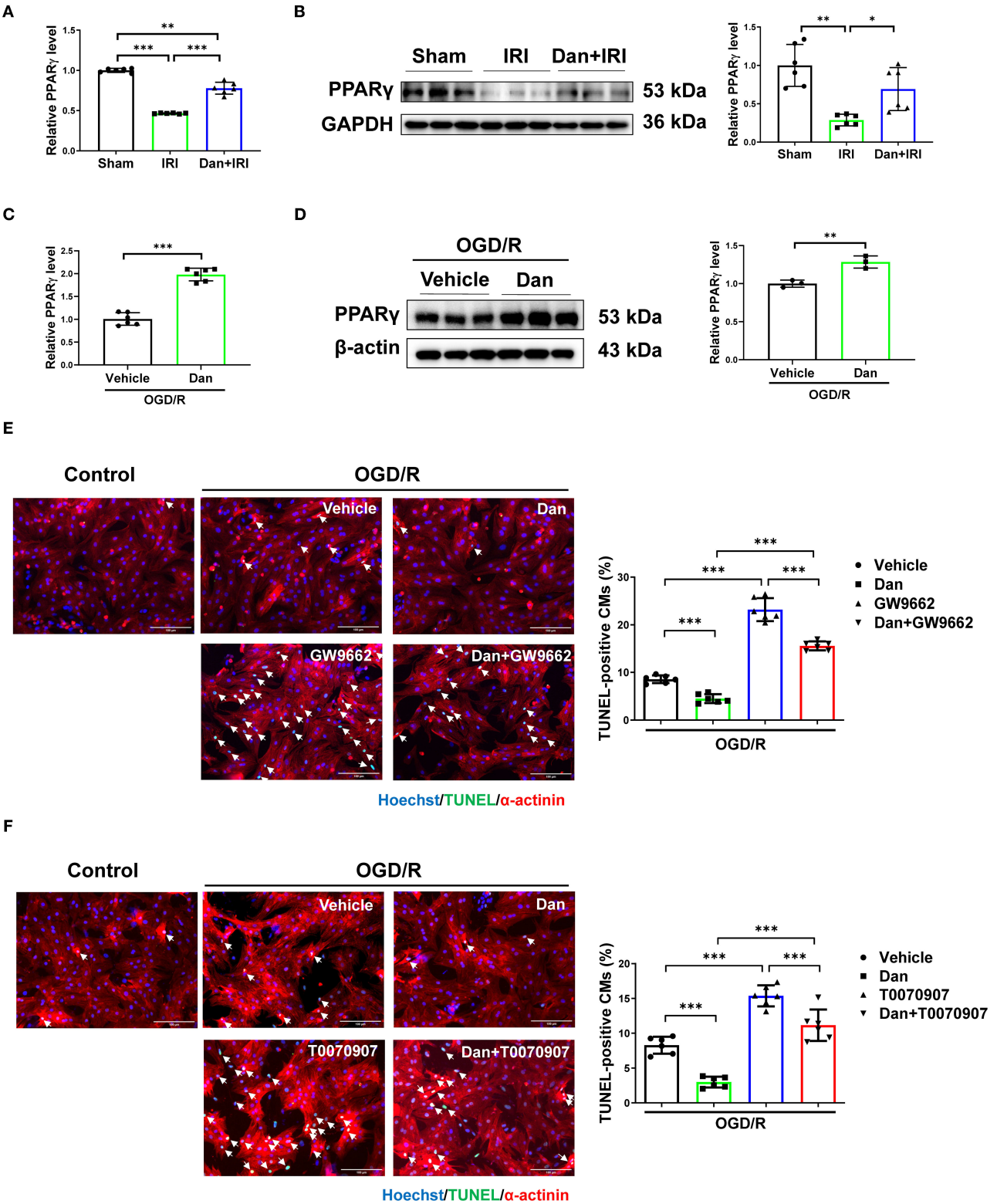

FIGURE 3 | Dan prevents CM apoptosis through activating PPARγ *in vitro*. **(A,B)** RT-qPCR [**(A)**, $n = 6$] and western blot [**(B)**, $n = 6$] for PPARγ in mice heart tissues of myocardial ischemia-reperfusion injury (IRI) in the presence or absence of Dan treatment. **(C,D)** RT-qPCR [**(C)**, $n = 6$] and western blot [**(D)**, $n = 3$] for PPARγ in oxygen-glucose deprivation–reperfusion (OGD/R)-induced apoptosis of NRCMs in the presence or absence of Dan treatment. **(E,F)** TUNEL/α-actinin staining for OGD/R-induced apoptosis of NRCMs treated with PPARγ inhibitors, GW9662 **(E)** or T0070907 **(F)**, in the presence or absence of Dan treatment ($n = 6$). Scale bar = 100 μm. $^{*}p < 0.05$; $^{**}p < 0.01$; $^{***}p < 0.001$.

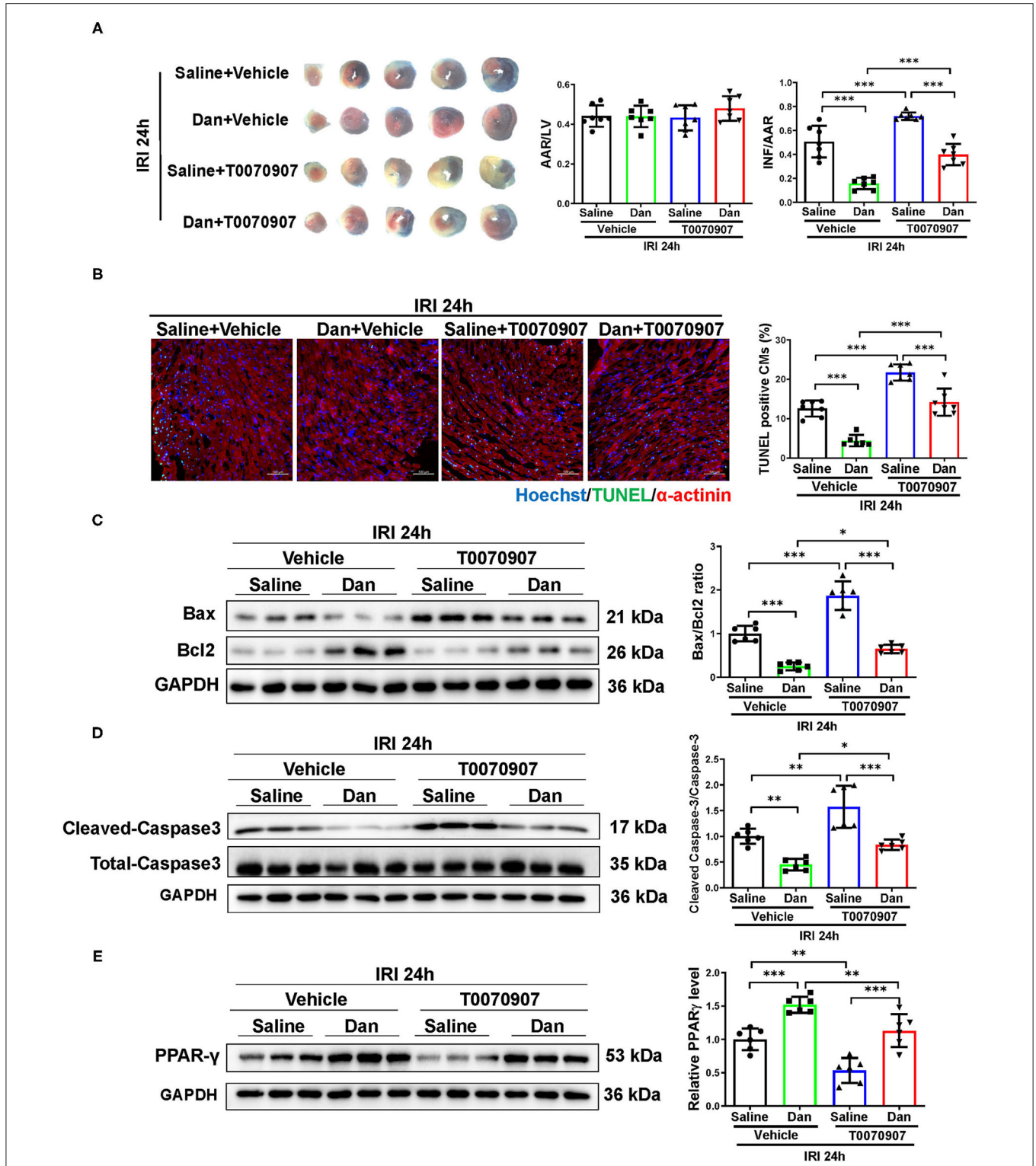

FIGURE 4 | Inhibition of PPARγ attenuates Dan-induced cardioprotection in acute myocardial ischemia-reperfusion injury *in vivo*. **(A)** Adult male mice were intraperitoneally injected with T0070907 (1 mg/kg/day) or vehicle controls and administrated by gavage with 700 mg/kg/d of Dan for 2 consecutive weeks followed by myocardial ischemia-reperfusion injury (IRI) modeling for 24 h. TTC staining was performed at 24 h after IRI. The ratio of AAR/LV was determined for the homogeneity of modeling, and the ratio of infarct area/area at risk (INF/AAR) was determined for the infarct size ($n = 7$). **(B)** Representative images and quantification results of TUNEL/α-actinin staining were shown for myocardial apoptosis of mice ($n = 6$–7). Scale bar = 100 μm. **(C,D)** Western blot analysis for apoptotic-associated proteins in heart tissues, including Bax and Bcl2 **(C)** and cleaved-caspase 3 and total caspase 3 **(D)** ($n = 6$). **(E)** Western blot for PPARγ in mice IRI heart tissues administrated with T0070907 or vehicle in the presence or absence of Dan treatment ($n = 6$). $^{*}p < 0.05$; $^{**}p < 0.01$; $^{***}p < 0.001$.

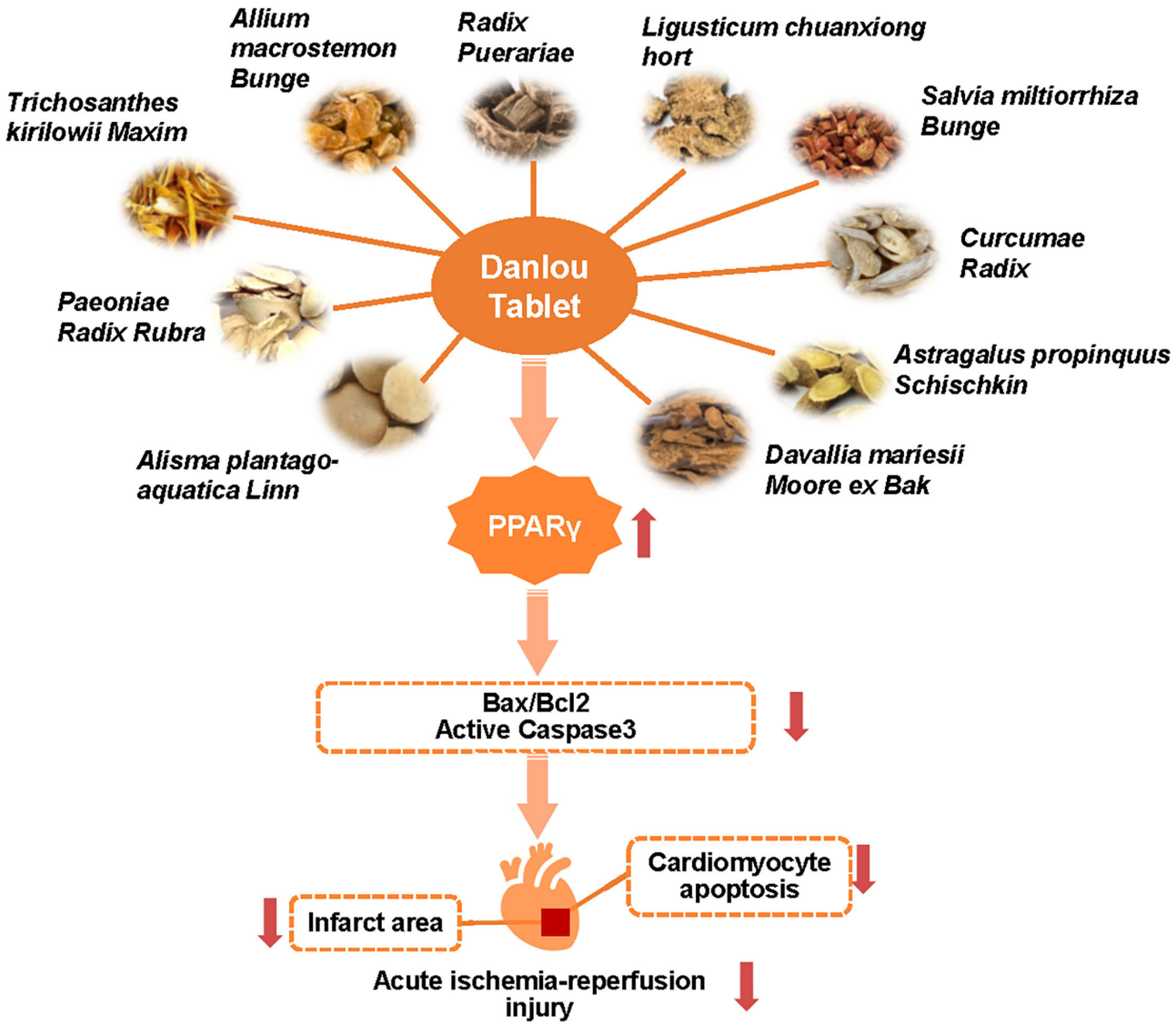

FIGURE 5 | Danlou tablet protects against acute myocardial ischemia-reperfusion injury and reduces CM apoptosis through activating PPARγ.

GW9662 reversed this change in NRCMs (**Figure 3E**). In addition, the protective effect of Dan against OGD/R-induced CM apoptosis was also abolished by Dan co-treatment with T0070907 (**Figure 3F**). These data indicate that PPARγ activation is necessary to mediate the protective effect of Dan against OGD/R-induced CM apoptosis.

Dan Prevents Acute Myocardial IRI Through Activating PPARγ *in vivo*

To further investigate whether PPARγ mediates the cardioprotective effects of Dan *in vivo*, we performed functional rescue experiments using PPARγ inhibitor T0070907 in Dan-treated IRI mice. Mice were randomly arranged into four groups, which include vehicle+IRI, Dan+IRI, T0070907+IRI, and Dan+T0070907+IRI. TTC staining was performed to evaluate the infarct size after acute IRI modeling for 24 h. As shown in **Figure 4A**, Dan effectively reduced the INF/AAR ratio compared to vehicle-treated IRI group. Interestingly, co-treatment with Dan and T0070907 attenuated the protective effect of Dan in reducing the infarct size in IRI mice (**Figure 4A**). Next, we also performed apoptotic analysis *via* TUNEL staining and western blot. Compared to Dan-treated IRI group, co-treatment with Dan and T0070907 caused increased TUNEL-positive CMs (**Figure 4B**), as well as increased Bax/Bcl2 ratio and cleaved-caspase 3/caspase 3 ratio (**Figures 4C,D**). Consistent with these results, Dan treatment was able to increase PPARγ protein level in heart tissues, while PPARγ inhibitor T0070907 attenuated Dan-induced PPARγ expression (**Figure 4E**). These

data demonstrate that PPARγ activation is also necessary to mediate the protective effect of Dan against acute IRI and myocardial apoptosis *in vivo*.

DISCUSSION

In this study, we explored the potential role of Dan in acute cardiac IRI and myocardial apoptosis and further investigated the mechanism of Dan-induced cardioprotection. Our findings reveal that Dan protects against acute cardiac IRI and myocardial apoptosis, while PPARγ inhibition prior to IRI attenuates Dan-induced cardioprotection *in vivo* and *in vitro*, which demonstrates that Dan prevents acute myocardial IRI through activating PPARγ (**Figure 5**). We revealed the mechanisms of Dan-induced cardioprotective role in IRI, which may extend our knowledge of Dan in reducing IRI and provide a potential strategy for IRI treatment.

Dan is a complex with ten kinds of ingredients, which includes *Allium macrostemon Bunge*, *Radix Puerariae*, *Salvia miltiorrhiza Bunge,* and *Paeoniae Radix Rubra*, etc. Increasing evidence has shown that Dan plays important roles in improving coronary heart diseases (27), such as atherosclerosis (18) and myocardial injury (17). However, the mechanisms of Dan-induced cardioprotection need to be illustrated. To date, some studies showed that Dan can attenuate oxidative redox state and inflammatory reaction to regulate cardiac homeostasis. For example, a recent study reported that Dan significantly improved chronic stable angina through reducing circulating inflammatory factors (interleukin-6/IL-6, interleukin-10/IL-10, and tumor necrosis factor-α/TNF-α, etc.) and regulating gut microbiota (28). Another study showed that Dan treatment inhibited inflammation in high-fat diet-induced atherosclerosis *via* suppressing nuclear factor kappa-B (NF-κB) signaling pathway (20). Furthermore, administration of Dan reduced infarct area through inducing endothelial and inducible nitric oxide synthase production in rat model (29). Of interest, the involvement of PPARγ in Dan-induced cardioprotection has not been investigated in the past years.

In this study, we first demonstrated that Dan had protective effect against acute cardiac IRI. We provided direct evidence that Dan could attenuate CM apoptosis both *in vivo* and *in vitro*. We further revealed that Dan treatment can activate PPARγ in the IRI hearts and OGD/R-stressed CMs. Using PPARγ inhibitors *in vivo* and *in vitro*, we demonstrated that PPARγ inhibition attenuated the protective effect of Dan in acute cardiac IRI and CM apoptosis, which indicates that PPARγ was involved in the cardioprotection of Dan upon IRI. These data suggest that Dan may be a potential activator of PPARγ, whose usage may deserve further investigations in other PPARγ-associated diseases.

Peroxisome proliferator-activated receptor gamma, an important transcription factor, is involved in multiple physiological and pathological processes such as cell differentiation, glucose–lipid metabolism, and endothelial function (30). Increasing evidence has revealed the effect of PPARγ in CVDs. For example, PPARγ was found to be involved in doxorubicin (Dox)-induced acute cardiac injury in mice, whose inactivity blocked miR-128-3p inhibition-triggered protection upon Dox injury (31). Inhibiting PPARγ by GW9662 can abolish piperine-induced cardioprotection in cardiac fibrosis model (32). Furthermore, PPARγ has been proved to be beneficial for the heart, whose activation or upregulation can attenuate diabetic cardiomyopathy (33), atherosclerosis (34), hypertension (35), and heart failure (33, 36). It is widely accepted that aerobic exercise is protective for the heart (37, 38). Of note, PPARγ is also involved in exercise-induced cardioprotection (39). Therefore, PPARγ is considered as a therapeutic target in CVDs such as atherosclerosis and heart failure, and its activators have been tried to be used as potential strategy for CVD treatment. For example, rosiglitazone (RGZ) has been widely used in type 2 diabetes therapy (30). However, whether and how PPARγ activation can be applicated to treat cardiovascular-related diseases need more clinical trials.

In conclusion, our findings reveal that Dan can protect myocardial tissue against acute IRI *via* activating PPARγ *in vivo* and *in vitro* and demonstrate that Dan is a potential activator of PPARγ in reducing myocardial apoptosis. This study may extend our knowledge of Chinese medicine and provide new strategy for the precise treatment of ischemic heart diseases.

DATA AVAILABILITY STATEMENT

The raw data supporting the conclusions of this article will be made available by the authors, without undue reservation.

ETHICS STATEMENT

The animal study was reviewed and approved by the Ethics Committee of Shanghai University.

AUTHOR CONTRIBUTIONS

MW, MG, XM, and LL performed the experiments and analyzed the data. MZ provided technical assistance. YB and HW designed the study and drafted the manuscript. All authors read and approved the final manuscript.

FUNDING

This work was supported by the grants from National Key Research and Development Program of China (2017YFC1700401 to MZ and YB), National Natural Science Foundation of China (81970335 and 82170285 to YB, 82000253 to HW), Shanghai Rising-Star Program (19QA1403900 to YB), Shanghai Committee of Science and Technology (21SQBS00100 to YB), and Chenguang Program of Shanghai Education Development Foundation and Shanghai Municipal Education Commission (20CG46 to HW).

REFERENCES

1. WHO. *The Top 10 Causes of Death.* (2020). Available online at: https://www.who.int/news-room/fact-sheets/detail/the-top-10-causes-of-death (accessed December 9, 2020)
2. Wang H, Xie Y, Guan L, Elkin K, Xiao J. Targets identified from exercised heart: killing multiple birds with one stone. *NPJ Regen Med.* (2021) 6:23. doi: 10.1038/s41536-021-00128-0
3. Bates ER. Reperfusion therapy reduces the risk of myocardial rupture complicating ST-elevation myocardial infarction. *J Am Heart Assoc.* (2014) 3:e001368. doi: 10.1161/JAHA.114.001368
4. Lindblom RPF, Tovedal T, Norlin B, Hillered L, Englund E, Thelin S. Mechanical Reperfusion Following Prolonged Global Cerebral Ischemia Attenuates Brain Injury. *J Cardiovasc Transl Res.* (2021) 14:338–47. doi: 10.1007/s12265-020-10058-9
5. Rentrop KP, Feit F. Reperfusion therapy for acute myocardial infarction: Concepts and controversies from inception to acceptance. *Am Heart J.* (2015) 170:971–80. doi: 10.1016/j.ahj.2015.08.005
6. Qin Z, Gao L, Lin G, Zhu H, Chen Y, Zhong F, et al. The nuclear receptor co-repressor 1 is a novel cardioprotective factor against acute myocardial ischemia-reperfusion injury. *J Mol Cell Cardiol.* (2022) 166:50–62. doi: 10.1016/j.yjmcc.2022.01.006
7. Xiao H, Zhang M, Wu H, Wu J, Hu X, Pei X, et al. CIRKIL Exacerbates Cardiac Ischemia/Reperfusion Injury by Interacting With Ku70. *Circ Res.* (2022) 130:e3–e17. doi: 10.1161/CIRCRESAHA.121.318992
8. Gong Y, Lin J, Ma Z, Yu M, Wang M, Lai D, et al. Mitochondria-associated membrane-modulated Ca(2+) transfer: a potential treatment target in cardiac ischemia reperfusion injury and heart failure. *Life Sci.* (2021) 278:119511. doi: 10.1016/j.lfs.2021.119511
9. Hinkel R, Ramanujam D, Kaczmarek V, Howe A, Klett K, Beck C, et al. AntimiR-21 Prevents Myocardial Dysfunction in a Pig Model of Ischemia/Reperfusion Injury. *J Am Coll Cardiol.* (2020) 75:1788–800. doi: 10.1016/j.jacc.2020.02.041
10. Eid RA, Bin-Meferij MM, El-Kott AF, Eleawa SM, Zaki MSA, Al-Shraim M, et al. Exendin-4 Protects Against Myocardial Ischemia-Reperfusion Injury by Upregulation of SIRT1 and SIRT3 and Activation of AMPK. *J Cardiovasc Transl Res.* (2021) 14:619–35. doi: 10.1007/s12265-020-09984-5
11. Bei Y, Lu D, Bar C, Chatterjee S, Costa A, Riedel I, et al. miR-486 attenuates cardiac ischemia/reperfusion injury and mediates the beneficial effect of exercise for myocardial protection. *Mol Ther.* (2022). doi: 10.1016/j.ymthe.2022.01.031
12. Gao R, Wang L, Bei Y, Wu X, Wang J, Zhou Q, et al. Long Noncoding RNA Cardiac Physiological Hypertrophy-Associated Regulator Induces Cardiac Physiological Hypertrophy and Promotes Functional Recovery After Myocardial Ischemia-Reperfusion Injury. *Circulation.* (2021) 144:303–17. doi: 10.1161/CIRCULATIONAHA.120.050446
13. Redd MA, Scheuer SE, Saez NJ, Yoshikawa Y, Chiu HS, Gao L, et al. Therapeutic Inhibition of Acid Sensing Ion Channel 1a Recovers Heart Function After Ischemia-Reperfusion Injury. *Circulation.* (2021) 144:947–60. doi: 10.1161/CIRCULATIONAHA.121.054360
14. Yang G, He H, Li H, Shen Z, Zhou S, Lu B, et al. Effects of Danlou tablet for the treatment of stable angina pectoris: A study protocol of a randomized, double-blind, and placebo-controlled clinical trial. *Medicine (Baltimore).* (2020) 99:e23416. doi: 10.1097/MD.0000000000023416
15. Liu JX, Lin CR, Ren JX, Li L, Hou JC, Li D, et al. Protective effect of formula of removing both phlegm and blood stasis on myocardial tissues of Chinese mini-swine with coronary heart disease of phlegm-stasis cementation syndrome. *Zhongguo Zhong Yao Za Zhi.* (2014) 39:726–31. doi: 10.4268/cjcmm20140434
16. Guo LL, Wang J, Lin F, He YX. Effect of danlou tablet on arrhythmia model rats induced by transient myocardial ischemia/ reperfusion. *Zhongguo Zhong Xi Yi Jie He Za Zhi.* (2014) 34:1125–9. doi: 10.7661/CJIM.2014.09.1125
17. Wang L, Mao S, Qi JY, Ren Y, Guo XF, Chen KJ, et al. Effect of Danlou Tablet () on peri-procedural myocardial injury among patients undergoing percutaneous coronary intervention for non-ST elevation acute coronary syndrome: a study protocol of a multicenter, randomized, controlled trial. *Chin J Integr Med.* (2015) 21:662–6. doi: 10.1007/s11655-015-2284-1
18. Miao J, Zhou XB, Mao W, Chen J, Xu XM. Effects of Xuefu Zhuyu Granule and Danlou Tablet on Anti-atherosclerosis Rats and Potential Mechanisms. *Zhongguo Zhong Xi Yi Jie He Za Zhi.* (2016) 36:80–4. doi: 10.7661/CJIM.2016.01.0080
19. Tang JJ, Li GX, Liu ZG, Yi R, Yu D, Zhang YB, et al. Danlou Tablet () Improves Chronic Intermittent Hypoxia-induced Dyslipidemia and Arteriosclerosis by HIF-1 alpha-Angptl4 mRNA Signaling Pathway. *Chin J Integr Med.* (2020). doi: 10.1007/s11655-020-3255-8
20. Gao S, Xue X, Yin J, Gao L, Li Z, Li L, et al. Danlou tablet inhibits the inflammatory reaction of high-fat diet-induced atherosclerosis in ApoE knockout mice with myocardial ischemia via the NF-kappaB signaling pathway. *J Ethnopharmacol.* (2020) 263:113158. doi: 10.1016/j.jep.2020.113158
21. Qi JY, Wang L, Gu DS, Guo LH, Zhu W, Zhang MZ. Protective Effects of Danlou Tablet () against Murine Myocardial Ischemia and Reperfusion Injury In Vivo. *Chin J Integr Med.* (2018) 24:613–20. doi: 10.1007/s11655-016-2448-7
22. Bei Y, Pan LL, Zhou Q, Zhao C, Xie Y, Wu C, et al. Cathelicidin-related antimicrobial peptide protects against myocardial ischemia/reperfusion injury. *BMC Med.* (2019) 17:42. doi: 10.1186/s12916-019-1268-y
23. Liu X, Xiao J, Zhu H, Wei X, Platt C, Damilano F, et al. miR-222 is necessary for exercise-induced cardiac growth and protects against pathological cardiac remodeling. *Cell Metab.* (2015) 21:584–95. doi: 10.1016/j.cmet.2015.02.014
24. Wang H, Shen X, Tian G, Shi X, Huang W, Wu Y, et al. AMPKalpha2 deficiency exacerbates long-term PM25 exposure-induced lung injury and cardiac dysfunction. *Free Radic Biol Med.* (2018) 121:202–14. doi: 10.1016/j.freeradbiomed.2018.05.008
25. Huang R, Zhang C, Wang X, Hu H. PPARgamma in Ischemia-Reperfusion Injury: Overview of the Biology and Therapy. *Front Pharmacol.* (2021) 12:600618. doi: 10.3389/fphar.2021.600618
26. Linares I, Farrokhi K, Echeverri J, Kaths JM, Kollmann D, Hamar M, et al. PPAR-gamma activation is associated with reduced liver ischemia-reperfusion injury and altered tissue-resident macrophages polarization in a mouse model. *PLoS ONE.* (2018) 13:e0195212. doi: 10.1371/journal.pone.0195212
27. Li Z, Yang L, Liu Y, Xu H, Wang S, Liu Y, et al. Anti-inflammatory and antioxidative effects of Dan-Lou tablets in the treatment of coronary heart disease revealed by metabolomics integrated with molecular mechanism studies. *J Ethnopharmacol.* (2019) 240:111911. doi: 10.1016/j.jep.2019.111911
28. Zhao X, Chen Y, Li L, Zhai J, Yu B, Wang H, et al. Effect of DLT-SML on Chronic Stable Angina Through Ameliorating Inflammation, Correcting Dyslipidemia, and Regulating Gut Microbiota. *J Cardiovasc Pharmacol.* (2021) 77:458–69. doi: 10.1097/FJC.0000000000000970
29. Dai X, Chen R, Chen T, Yan H, Wang Y, Zhou K, et al. Danlou Fang reduces microvascular obstruction through the endothelial/inducible nitric oxide synthase pathway in a rat model. *J Tradit Chin Med.* (2021) 41:246–53. doi: 10.19852/j.cnki.jtcm.20201019.001
30. Wang S, Dougherty EJ, Danner RL. PPARgamma signaling and emerging opportunities for improved therapeutics. *Pharmacol Res.* (2016) 111:76–85. doi: 10.1016/j.phrs.2016.02.028
31. Zhang WB, Zheng YF, Wu YG. Inhibition of miR-128-3p Attenuated Doxorubicin-Triggered Acute Cardiac Injury in Mice by the Regulation of PPAR-gamma. *PPAR Res.* (2021) 2021:7595374. doi: 10.1155/2021/7595374
32. Ma ZG, Yuan YP, Zhang X, Xu SC, Wang SS, Tang QZ. Piperine Attenuates Pathological Cardiac Fibrosis Via PPAR-gamma/AKT Pathways. *EBioMedicine.* (2017) 18:179–87. doi: 10.1016/j.ebiom.2017.03.021
33. Montaigne D, Butruille L, Staels B. PPAR control of metabolism and cardiovascular functions. *Nat Rev Cardiol.* (2021) 18:809–823. doi: 10.1038/s41569-021-00569-6
34. Xiong W, Zhao X, Villacorta L, Rom O, Garcia-Barrio MT, Guo Y, et al. Brown Adipocyte-Specific PPARgamma (Peroxisome Proliferator-Activated Receptor gamma) Deletion Impairs Perivascular Adipose Tissue Development and Enhances Atherosclerosis in Mice. *Arterioscler Thromb Vasc Biol.* (2018) 38:1738–47. doi: 10.1161/ATVBAHA.118.311367

35. Stump M, Mukohda M, Hu C, Sigmund CD. PPARgamma Regulation in Hypertension and Metabolic Syndrome. *Curr Hypertens Rep.* (2015) 17:89. doi: 10.1007/s11906-015-0601-x
36. Legchenko E, Chouvarine P, Borchert P, Fernandez-Gonzalez A, Snay E, Meier M, et al. PPARgamma agonist pioglitazone reverses pulmonary hypertension and prevents right heart failure via fatty acid oxidation. *Sci Transl Med.* (2018) 10:eaao0303. doi: 10.1126/scitranslmed.aao0303
37. Wang R, Tian H, Guo D, Tian Q, Yao T, Kong X. Impacts of exercise intervention on various diseases in rats. *J Sport Health Sci.* (2020) 9:211–27. doi: 10.1016/j.jshs.2019.09.008
38. Wang L, Wang J, Cretoiu D, Li G, Xiao J. Exercise-mediated regulation of autophagy in the cardiovascular system. *J Sport Health Sci.* (2020) 9:203–10. doi: 10.1016/j.jshs.2019.10.001
39. Bastien M, Poirier P, Brassard P, Arsenault BJ, Bertrand OF, Despres JP, et al. Effect of PPARgamma agonist on aerobic exercise capacity in relation to body fat distribution in men with type 2 diabetes mellitus and coronary artery disease: a 1-yr randomized study. *Am J Physiol Endocrinol Metab.* (2019) 317:E65–73. doi: 10.1152/ajpendo.00505.2018

Conflict of Interest: The authors declare that the research was conducted in the absence of any commercial or financial relationships that could be construed as a potential conflict of interest.

Publisher's Note: All claims expressed in this article are solely those of the authors and do not necessarily represent those of their affiliated organizations, or those of the publisher, the editors and the reviewers. Any product that may be evaluated in this article, or claim that may be made by its manufacturer, is not guaranteed or endorsed by the publisher.

frontiers | Frontiers in Cardiovascular Medicine

ORIGINAL RESEARCH
published: 15 April 2022
doi: 10.3389/fcvm.2022.845307

Risk Estimation for Infection in Patients With ST-Segment Elevation Myocardial Infarction Undergoing Percutaneous Coronary Intervention: Development and Validation of a Predictive Score

Yuanhui Liu[1,2†], Litao Wang[1,3†], Pengyuan Chen[4], Yining Dai[1,2], Yaowang Lin[5], Wei Chen[6], Zhengrong Xu[7], Lihuan Zeng[1,2], Hualin Fan[1,2], Ling Xue[1,2], Simin Liu[8], Jiyan Chen[1,2], Ning Tan[1,2,9], Pengcheng He[1,2,9]* and Chongyang Duan[10]**

[1] Department of Cardiology, Guangdong Cardiovascular Institute, Guangdong Provincial People's Hospital, Guangdong Academy of Medical Sciences, Guangzhou, China, [2] Guangdong Provincial Key Laboratory of Coronary Heart Disease Prevention, Guangdong Provincial People's Hospital, Guangdong Academy of Medical Sciences, Guangzhou, China, [3] Department of Cardiology, Shanghai Institute of Cardiovascular Diseases, Zhongshan Hospital, Fudan University, Shanghai, China, [4] Department of Cardiology, The Second People's Hospital of Nanhai District, Guangdong General Hospital's Nanhai Hospital, Foshan, China, [5] Department of Cardiology, Second Clinical Medical College of Jinan University, Shenzhen People's Hospital, First Affiliated Hospital of South University of Science and Technology, Shenzhen, China, [6] Clinical College of Fujian Provincial Hospital, Fujian Provincial Hospital, Fujian Provincial Key Laboratory of Cardiovascular Disease, Fujian Provincial Center for Geriatrics, Fujian Medical University, Fujian Cardiovascular Institute, Fuzhou, China, [7] Department of Cardiology, People's Hospital of Baoan Shenzhen, Shenzhen, China, [8] Center for Global Cardiometabolic Health, Department of Epidemiology, Medicine, and Surgery, Brown University, Providence, RI, United States, [9] The Second School of Clinical Medicine, Southern Medical University, Guangzhou, China, [10] Department of Biostatistics, School of Public Health, Southern Medical University, Guangzhou, China

Background: Infection during hospitalization is a serious complication among patients who suffered from acute myocardial infarction (AMI) undergoing percutaneous coronary intervention (PCI); however, there are no suitable and accurate means to assess risk. This study aimed to develop and validate a simple scoring system to predict post-AMI infection in such patients.

Methods: All patients with ST-segment elevation myocardial infarction (STEMI) undergoing PCI consecutively enrolled from January 2010 to May 2016 were served as derivation cohort, and those from June 2016 to May 2018 as validation cohort, respectively. The primary endpoint was post-AMI infection during hospitalization, and all-cause death and major adverse cardiovascular events (MACE) were considered as secondary endpoints. The simplified risk model was established using logistic regression. The area under the receiver operating curve and calibration of predicted and observed infection risk were calculated.

Results: A 24-point risk score was developed, with infection risk ranging from 0.7 to 99.6% for patients with the lowest and highest score. Seven variables including age, Killip classification, insulin use, white blood cell count, serum albumin, diuretic

OPEN ACCESS

Edited by:
Manuel Martínez-Sellés,
Hospital General Universitario Gregorio Marañón, Spain

Reviewed by:
Minzhou Zhang,
Guangdong Provincial Hospital of Traditional Chinese Medicine, China
Bin Liang,
Capital Medical University, China
Qiang Su,
Guilin Medical University, China

***Correspondence:**
Ning Tan
gdtanning@126.com
Pengcheng He
gdhpc100@126.com
Chongyang Duan
donyduang@126.com

[†] These authors have contributed equally to this work

Specialty section:
This article was submitted to General Cardiovascular Medicine, a section of the journal Frontiers in Cardiovascular Medicine

Received: 29 December 2021
Accepted: 16 March 2022
Published: 15 April 2022

Citation:
Liu Y, Wang L, Chen P, Dai Y, Lin Y, Chen W, Xu Z, Zeng L, Fan H, Xue L, Liu S, Chen J, Tan N, He P and Duan C (2022) Risk Estimation for Infection in Patients With ST-Segment Elevation Myocardial Infarction Undergoing Percutaneous Coronary Intervention: Development and Validation of a Predictive Score. Front. Cardiovasc. Med. 9:845307. doi: 10.3389/fcvm.2022.845307

use, and transfemoral approach were included. This model achieved the same high discrimination in the development and validation cohort (C-statistic:0.851) and revealed adequate calibration in both datasets. The incidences of post-AMI infection increased steadily across risk score groups in both development (1.3, 5.1, 26.3, and 69.1%; $P < 0.001$) and validation (1.8, 5.9, 27.2, and 79.2%; $P < 0.001$) cohort. Moreover, the risk score demonstrated good performance for infection, in-hospital all-cause death, and MACE among these patients, as well as in patients with the non-ST-elevation acute coronary syndrome.

Conclusion: This present risk score established a simple bedside tool to estimate the risk of developing infection and other in-hospital outcomes in patients with STEMI undergoing PCI. Clinicians can use this risk score to evaluate the infection risk and subsequently make evidence-based decisions.

Keywords: risk score, infection, ST-elevation myocardial infarction, percutaneous coronary intervention, observational study

INTRODUCTION

Infection during hospitalization is a severe complication among patients with acute myocardial infarction (AMI) (1, 2), which increases mortality risk, prolongs hospital stay, and drives up costs (3, 4). Considering these growing concerns, infection prevention is one of the highest priorities for healthcare payers and providers. Since a substantial proportion of infection is considered preventable, it is urgent to accurately and efficiently identify the risk of infection in patients with AMI and to develop an intervention for infection prevention.

Several mortality risk scores have been proposed for patients with ST-segment elevation myocardial infarction (STEMI) to date (5, 6), however, few of them have been validated for the post-AMI infection prediction. Although some other risk scores were developed to predict infection after cardiac surgery (7, 8), no study has established a simplified scoring model yet to estimate an individual patient's risk of infection in patients with STEMI after cardiac catheterization. Therefore, we aimed to develop and validate a simple-to-use risk model to identify patients with STEMI at risk of post-AMI infection.

MATERIALS AND METHODS

Study Population

The patient population used to develop this risk score (development cohort) consisted of the eligible patients enrolled in Guangdong Provincial People's Hospital between January 2010 and May 2016. All patients with STEMI underwent PCI *via* radial, femoral, or both approaches, while patients with both accesses were classified as those with femoral assess, and patients with implantation of intra-aortic balloon pump (IABP) were also included. According to the same criteria, the population used for the validation (validation cohort) included those enrolled between June 2016 and May 2018, with complete data compared to the development cohort. Additionally, the patients screened in accordance with the criteria in other research centers were included for external validation. To widen the extent of application, this risk model was also validated among patients with the non-ST-elevation acute coronary syndrome (NSTE-ACS) treated with PCI in our recent publication (9).

Other details of the patients, study design, treatment and procedure, and outcome definitions have been addressed in our previously published protocol (10). Clinical data including patient demographics, laboratory tests, procedural details, medical treatments, and clinical outcomes were collected from the medical records. Vital variables (such as clinical events) were double-checked, and inconsistent data were verified by a third researcher. All clinical adverse events were evaluated by an independent clinical events committee blinded to the research.

Study Endpoints

The primary endpoint was the occurrence of a P-AMI infection during hospitalization, which was defined as the infection requiring antibiotics (reflecting the clinical influence of infection compatible with the necessity for additional treatment) (11). Besides, the infection was determined using ICD-10-CM codes. The types of infections included pulmonary infection, urinary infection, or other infections including abdominal sepsis, primary bacteremia, and unidentified primary infection site based on the clinical records. Other details were reported in the published protocol (10). The secondary endpoints were in-hospital all-cause death, and major adverse cardiovascular events (MACE) including stroke, all-cause death, target vessel revascularization, and recurrent myocardial infarction.

Sample Size

As for sample size determination, the concept of events per variable (EPV) of 10 or greater was applied as previously reported (12). Considering that no more than 8 factors were included in the development model, at least 80 infections were required. Our

development dataset comprised 296 infections, and the value of events per variable was 42.3 (296/7).

Statistical Analysis

Categorical variables were expressed as number (percentage) and continuous variables were expressed as mean ± SD, as appropriate. We chose a backward stepwise logistic regression model to develop the risk score. All listed candidate predictors (**Supplementary Table 1**) were included to develop the risk score, while variables with ≥ 10% missing values were excluded. And for those with incomplete data, we assumed that patients with the missing data ≤ 5% occurred at random depending on the clinical variables and used multiple imputations. Besides, a bootstrap method was applied to pick out the best subset of risk factors.

The predictive accuracy was evaluated using both discriminations evaluated by the C-statistic, and calibration assessed by the Hosmer-Lemeshow χ^2 statistic and calibration plot. We performed the external and subgroup validation (older, sex, anemia, diabetes, and chronic kidney disease in the development and validation cohorts) to further measure the risk score's stability. Additionally, we compared the discrimination of the present model with other risk scores previously reported using the area under the receiver operating characteristic (13–15). To assess the utility of the risk score, we conducted the decision curve analysis. A higher net benefit across the whole range of clinically applicable and acceptable probability thresholds indicated better clinical values (16). Other detailed information of the statistical analysis has been previously published (10).

All analyses were performed with SAS (version 9.4, SAS Institute, 210 Cary, NC, United States) and all figures were plotted with R (version 3.6.2, R Foundation for Statistical Computing, Vienna, Austria).

RESULTS

Characteristic of the Development Cohort

A total of 1,842 patients with STEMI who underwent PCI (mean age, 61.54 years; 17.5% female) were finally included in the development cohort (**Figure 1**). Among them, 217 patients (11.8%) experienced post-AMI infection during hospitalization. The in-hospital all-cause death was 17.5%, compared to 1.9% for patients without infections. Patients with post-AMI infection were more likely to be older, and have diabetes, chronic obstructive pulmonary disease (COPD), higher white blood cell (WBC) counts, and diuretics or insulin use. Moreover, these patients had lower levels of serum albumin, hemoglobin, estimated glomerular filtration rate, and left ventricular ejection fraction (**Table 1**).

Variable Identification and Risk Score Development

Among all 72 variables recorded according to the clinical data, 56 candidates were enrolled for the risk model development, while 16 variables were excluded for ≥ 10% missing values (**Supplementary Table 1**). After multivariate

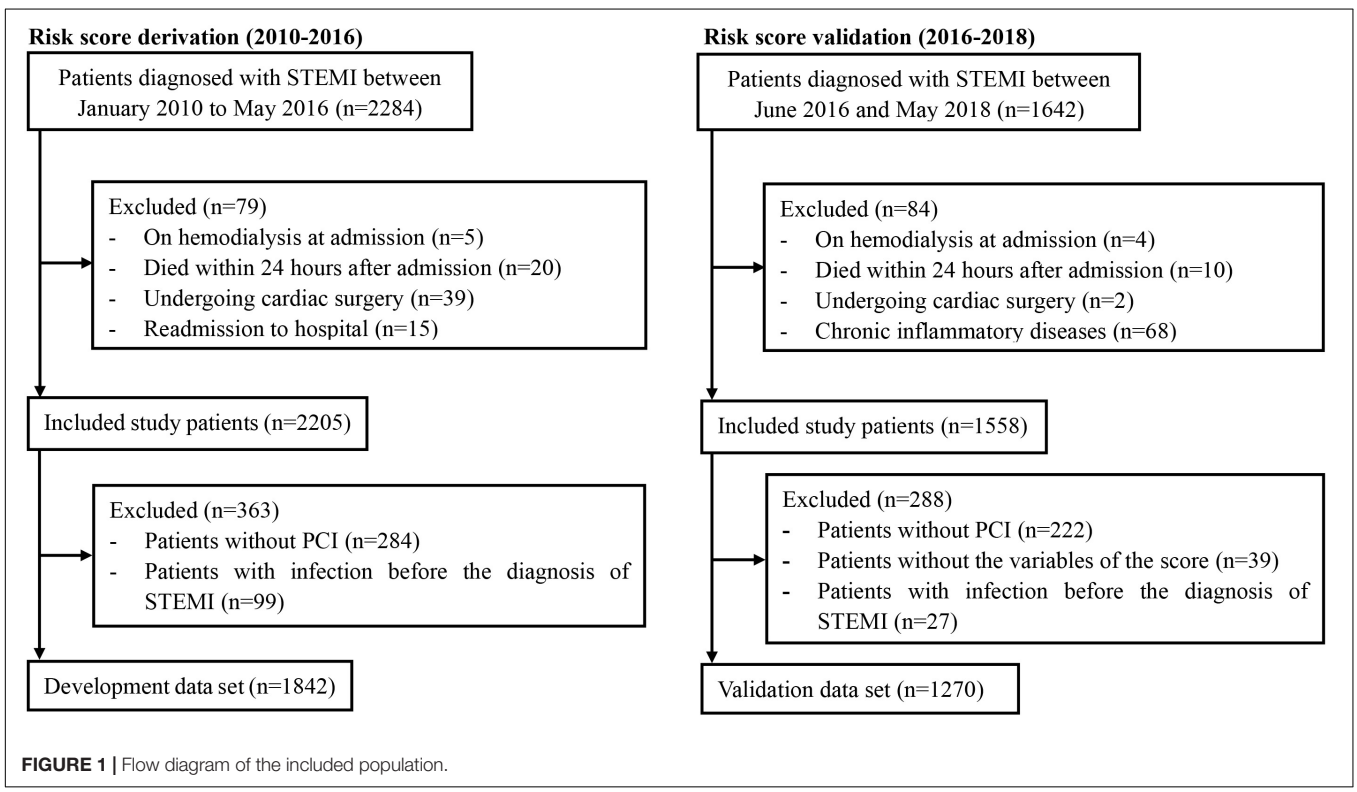

FIGURE 1 | Flow diagram of the included population.

TABLE 1 | Baseline characteristics of included patients in the development cohort and validation cohort.

Variables	Development cohort		*P*-value	Validation cohort		*P*-value
	Infection (*n* = 217)	No infection (*n* = 1,625)		Infection (*n* = 142)	No infection (*n* = 1,128)	
Age, (years)	67.74 ± 11.94	60.71 ± 12.12	<0.001	67.96 ± 11.85	61.22 ± 11.91	<0.001
Age > 75 year, n (%)	135 (62.2%)	635 (39.1%)	<0.001	90 (63.4%)	453 (40.2%)	<0.001
Male, n (%)	177 (81.6%)	1,342 (82.6%)	0.711	110 (77.5%)	926 (82.1%)	0.180
Systolic blood pressure, (mmHg)	114.83 ± 23.90	122.90 ± 21.61	<0.001	114.58 ± 19.92	123.84 ± 20.68	<0.001
Diastolic blood pressure, (mmHg)	69.26 ± 13.27	74.11 ± 13.06	<0.001	71.29 ± 15.50	74.93 ± 13.06	0.008
Heart rate (bpm)	86.24 ± 21.23	78.85 ± 14.84	<0.001	86.75 ± 17.49	77.53 ± 13.66	<0.001
Killip class, n (%)						
I	82 (37.8%)	1263 (77.7%)	<0.001	58 (40.8%)	840 (74.5%)	<0.001
II	74 (34.1%)	283 (17.4%)		33 (23.2%)	240 (21.3%)	
III	29 (13.4%)	46 (2.8%)		31 (21.8%)	32 (2.8%)	
IV	32 (14.7%)	33 (2.0%)		20 (14.1%)	16 (1.4%)	
Medical history, n (%)						
Hypertension	124 (57.1%)	811 (49.9%)	0.045	82 (57.7%)	559 (49.6%)	0.066
Diabetes	70 (32.3%)	396 (24.4%)	0.012	47 (33.1%)	336 (29.8%)	0.418
Current smoker	80 (36.9%)	741 (45.6%)	0.015	40 (28.2%)	439 (39.0%)	0.012
Prior myocardial infraction	12 (5.5%)	76 (4.7%)	0.580	64 (45.1%)	690 (61.2%)	<0.001
Prior coronary artery bypass graft	1 (0.5%)	2 (0.1%)	0.246	0 (0.0%)	1 (0.1%)	0.723
COPD	10 (4.6%)	25 (1.5%)	0.002	2 (1.4%)	18 (1.6%)	0.866
Atrial fibrillation	13 (6.0%)	40 (2.5%)	0.003	12 (8.5%)	31 (2.7%)	<0.001
Prior stroke	28 (12.9%)	83 (5.1%)	<0.001	19 (13.4%)	63 (5.6%)	<0.001
Laboratory characteristics						
eGFR, (mL/min/1.73 m^2)	63.42 ± 31.73	88.76 ± 30.48	<0.001	59.76 ± 28.04	82.01 ± 26.81	<0.001
Creatine kinase MB, (U/L) (IQR)	25.4 (12.3–64.3)	39.2 (14.1–84.4)	0.005	26.7 (10.5–124.63)	39.35 (13.25–276.03)	0.004
Serum creatinine, (mg/dL)	1.62 ± 1.40	1.06 ± 0.69	<0.001	1.70 ± 1.77	1.14 ± 0.82	<0.001
Serum albumin, (g/L)	31.29 ± 4.31	33.86 ± 3.94	<0.001	33.13 ± 3.90	36.59 ± 3.95	<0.001
Random blood glucose, (mmol/L) (IQR)	7.28 (6.17–9.28)	8.32 (6.98–11.25)	<0.001	7.15 (5.97–9.69)	8.48 (7.02–11.39)	<0.001
White blood cell count, (10^9/L)	14.17 ± 4.49	11.55 ± 3.58	<0.001	14.13 ± 5.17	10.56 ± 3.58	<0.001
Hemoglobin, (g/L)	130.91 ± 21.08	134.95 ± 22.84	0.014	124.75 ± 22.62	133.31 ± 17.66	<0.001
Triglycerides, (mmol/L)	1.46 ± 1.00	1.59 ± 1.18	0.077	1.46 ± 0.72	1.73 ± 1.03	<0.001
Total cholesterol, (mmol/L)	4.58 ± 1.28	4.94 ± 1.20	<0.001	4.73 ± 1.61	4.83 ± 1.26	0.449
Total bilirubin, (mmol/L)	20.69 ± 11.99	17.70 ± 7.18	<0.001	18.55 ± 8.80	14.99 ± 7.11	<0.001
Low-density lipoprotein, (mmol/L)	2.85 ± 1.06	3.17 ± 1.04	<0.001	3.18 ± 1.21	3.24 ± 0.97	0.535
High-density lipoprotein, (mmol/L)	0.96 ± 0.28	0.97 ± 0.25	0.344	1.00 ± 0.27	1.00 ± 0.30	0.982
LVEF, (%)	47.01 ± 12.87	53.37 ± 10.47	<0.001	42.40 ± 11.18	52.58 ± 11.21	<0.001
Medication during hospitalization, n (%)						
Glycoprotein IIb/IIIa inhibitors	152 (70.0%)	1,115 (68.6%)	0.669	85 (59.9%)	516 (45.7%)	0.001
Statins	212 (97.7%)	1,606 (98.8%)	0.166	125 (88.0%)	1,101 (97.6%)	<0.001
Acetylsalicylic acid	214 (98.6%)	1,604 (98.7%)	0.912	139 (97.9%)	1,112 (98.6%)	0.521
Clopidogrel	213 (98.2%)	1,607 (98.9%)	0.349	127 (90.1%)	1,043 (92.5%)	0.299
Warfarin	3 (1.4%)	16 (1.0%)	0.586	3 (2.1%)	18 (1.6%)	0.649
ACEI	154 (71.0%)	1,339 (82.4%)	<0.001	81 (57.0%)	742 (65.8%)	0.040
Calcium channel blockers	34 (15.7%)	138 (8.5%)	<0.001	14 (9.9%)	108 (9.6%)	0.914
Angiotensin receptor blockers	44 (20.3%)	226 (13.9%)	0.013	26 (18.3%)	189 (16.8%)	0.642
β-blockers	163 (75.1%)	1,410 (86.8%)	<0.001	95 (66.9%)	925 (82.0%)	<0.001
Insulin therapy	64 (29.5%)	188 (11.6%)	<0.001	37 (26.1%)	154 (13.7%)	<0.001
Metformin	6 (2.8%)	71 (4.4%)	0.267	5 (3.6%)	76 (6.8%)	0.147
Proton pump inhibitor	163 (75.1%)	1,075 (66.2%)	0.008	108 (76.1%)	855 (75.8%)	0.946
Diuretics	122 (56.2%)	331 (20.4%)	<0.001	66 (46.5%)	212 (18.8%)	<0.001

(Continued)

TABLE 1 | (Continued)

Variables	Development cohort		*P*-value	Validation cohort		*P*-value
	Infection (n = 217)	No infection (n = 1,625)		Infection (n = 142)	No infection (n = 1,128)	
Procedural characteristics						
Radial access, n (%)	135 (62.2%)	1,426 (87.8%)	<0.001	90 (63.4%)	995 (88.2%)	<0.001
Femoral access, n (%)	82 (37.8%)	199 (12.2%)		52 (36.6%)	133 (11.8%)	
Multi-lesion, n (%)	172 (79.3%)	1095 (67.4%)	<0.001	115 (81.0%)	864 (76.6%)	0.241
Contrast volume, (mL) (IQR)	100 (100–150)	100 (100–150)	0.490	100 (82.5–150)	100 (90–132.5)	0.125
Number of stents, (n) (IQR)	1 (1–2)	1 (1–2)	0.204	1 (1–2)	1 (1–2)	0.855
Total length of stent, (mm) (IQR)	30 (18–50)	30 (21–46)	0.649	36 (23.75–58.5)	33 (22–54)	0.333
In-hospital stay, (d) (IQR)	6 (5–8)	12 (8–19)	<0.001	5 (4–7)	11 (8–14.25)	<0.001

Values are mean ± SD, n (%) or median (interquartile range). ACEI, angiotensin-converting enzyme inhibitors; COPD, chronic obstructive pulmonary disease; eGFR, estimated glomerular filtration rate; IQR, interquartile range; LVEF, left ventricular ejection fraction.

logistic regression analysis, the following seven variables were ultimately included: age, Killip classification, WBC count, serum albumin, insulin use, diuretic use, and transfemoral approach (**Table 2** and **Supplementary Figures 1, 2**). Subsequently, the risk score, named post-AMI infection score (PAMIIS), was developed attributing corresponding points to each variable (**Figure 2**), and achieved predicted probabilities for infection development ranging from 0.7 to 99.6%, with a score range between 0 and 24 points (**Supplementary Table 2** and **Supplementary Figure 3**).

Risk Score Internal Validation

This risk score showed good discriminative power (C-statistic:0.851, 95% confidence interval [CI]:0.824–0.877), with good calibration ability in line with the Hosmer-Lemeshow test ($\chi^2 = 10.07$; $P = 0.345$) (**Figure 2**), while the internal validation with bootstrapping also yielded a similar result (C-statistic:0.851, bias-corrected 95% CI:0.831–0.871). More notably, the calibration plots of predicted vs. observed incidences of post-AMI infection across risk scores confirmed an excellent calibration (**Figure 3**).

Risk Score External Validation

For external validation, 1,270 patients with STEMI undergoing PCI were enrolled, and 142 patients (11.2%) experienced post-AMI infection, with a similar infection rate compared to the development cohort (11.2% vs. 11.8%; $P = 0.607$) (**Table 1**). Multiple differences in baseline characteristics were observed between the validation and development cohorts (**Supplementary Table 3**). The validation dataset exhibited semblable distribution of factors (excluding serum albumin, and WBC count) incorporated in the current risk model, and mean risk scores in comparison with the development dataset.

In the validation cohort, this model had similarly good discriminative power and calibration as the development cohort (C-statistic: 0.851, 95% CI:0.818–0.884; Hosmer-Lemeshow test $\chi^2 = 5.974$, $P = 0.650$), respectively (**Figure 2**). The observed incidences of post-AMI infection were highly consistent with the predicted ones (**Figure 3**).

Furthermore, after validation in the population from other two centers, in which 1,002 patients with STEMI undergoing PCI were included (**Supplementary Figure 4**) and 75 (7.5%) experienced post-AMI infection, this model remained a prominent predictor of infection (C-statistic:0.770, 95% CI:0.710–0.831; Hosmer-Lemeshow test $\chi^2 = 15.412$, $P = 0.118$) (**Supplementary Figure 5**).

Risk Score Validation in Other Patients

To extend the utility, we further validated the risk score among patients with NSTE-ACS after PCI. A total of 4,745 patients (mean age, 63.70 years, 24.4% female, mean risk score 3.03 ± 2.15) were included (**Supplementary Figure 6**), and 118 (2.49%) experienced infection. The incidence of all-cause death and MACE were 0.30 and 0.80%, respectively. The comparison of baseline data was summarized between patients with or without infection in **Supplementary Table 4**. This risk model demonstrated analogously favorable discriminative ability in patients with NSTE-ACS (C-statistic:0.800, 95% CI:0.754–0.845), but the predicted risk was higher than the observed one in these relatively low-risk patients (**Supplementary Figures 7, 8**). After times 0.684 to the predicted risk, the observed incidences of post-AMI infection were highly consistent with the predicted ones with Hosmer-Lemeshow test χ^2 value of 5.596 ($P = 0.588$, **Supplementary Figure 7**).

Risk Score Predictive Values for Other In-Hospital Outcomes

Furthermore, this risk score exhibited good predictive values for in-hospital all-cause death and MACE in both cohorts. Similar results were observed among patients with NSTE-ACS (**Supplementary Figure 9**).

Subgroup Analysis and Comparison With Other Risk Scores

As for IABP, there were 196 patients with implantation of IABP in the development cohort. To evaluate the potential influence of IABP on the risk score, we performed the subgroup of IABP analysis. And the result showed that

TABLE 2 | Univariate and multivariable logistic regression analysis of risk factors that were selected to develop the risk model for predicting post-AMI infection in the development cohort.

	Univariate analysis			Multivariable analysis			Multivariable analysis combined result based on 10 imputed data		
Variables	**OR**	**95% CI**	***P*-value**	**OR**	**95% CI**	***P*-value**	**OR**	**95% CI**	***P*-value**
Age	1.05	1.04–1.07	<0.001	1.04	1.02–1.06	<0.001	1.04	1.02–1.05	<0.001
Killip classification									
I (reference)									
II	4.03	2.87–5.66	<0.001	2.05	1.39–3.01	<0.001	2.09	1.43–3.07	<0.001
III	9.71	5.80–16.26	<0.001	3.04	1.63–5.67	<0.001	2.77	1.51–5.08	0.001
IV	14.94	8.75–25.50	<0.001	5.38	2.83–10.26	<0.001	4.66	2.50–8.70	<0.001
White blood cell count	1.18	1.14–1.220	<0.001	1.16	1.12–1.21	<0.001	1.16	1.12–1.21	<0.001
Serum albumin	0.86	0.83–0.894	<0.001	0.92	0.88–0.95	<0.001	0.92	0.88–0.96	<0.001
Transfemoral approach	4.35	3.19–5.947	<0.001	2.58	1.78–3.76	<0.001	2.39	1.65–3.45	<0.001
Diuretics use	5.02	3.74–6.74	<0.001	2.35	1.65–3.34	<0.001	2.52	1.78–3.55	<0.001
Insulin use	3.20	2.30–4.44	<0.001	1.99	1.34–2.96	0.001	2.13	1.44–3.15	<0.001

CI, confidence interval; OR, odds ratio.

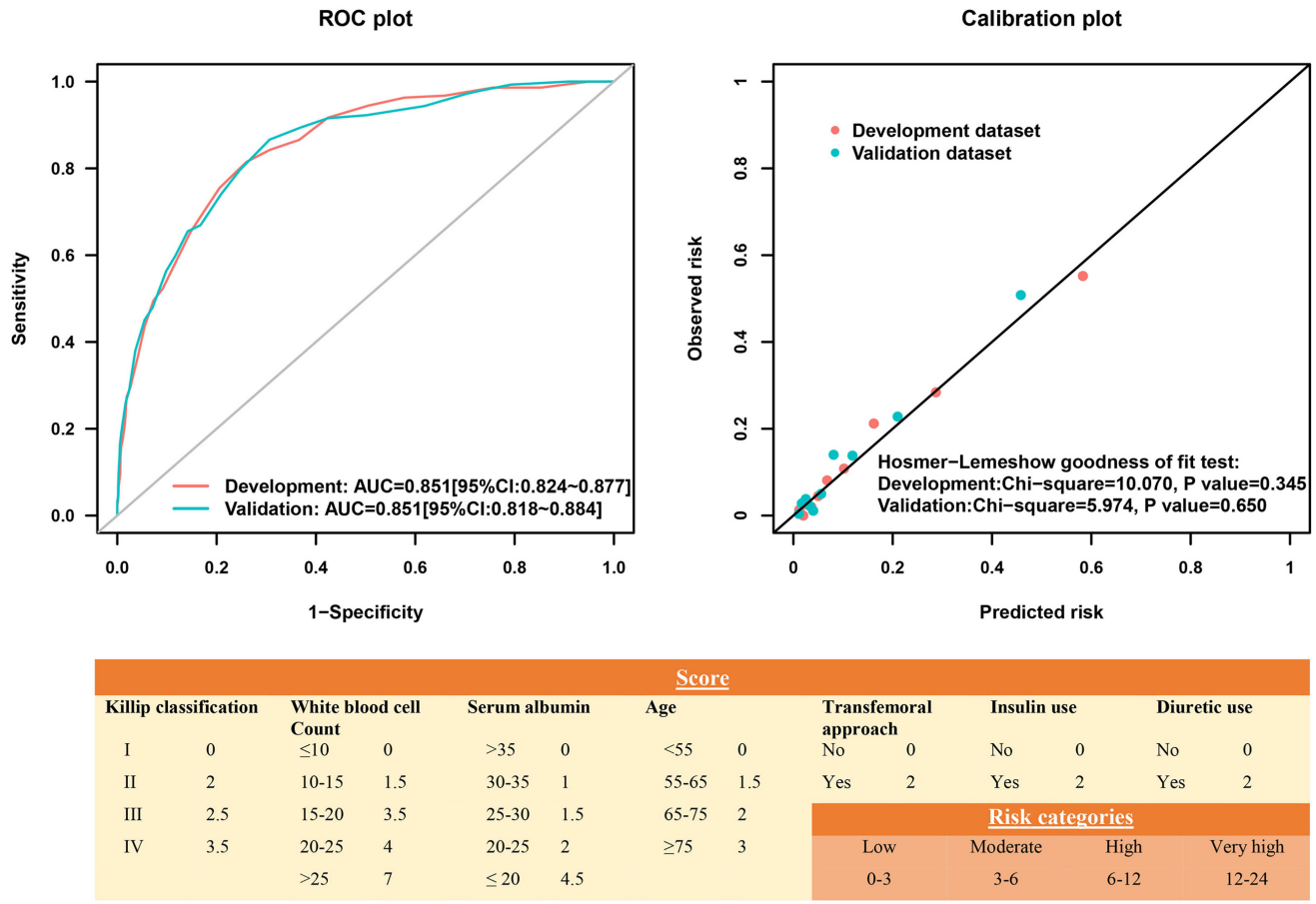

Score												
Killip classification		**White blood cell Count**		**Serum albumin**		**Age**		**Transfemoral approach**		**Insulin use**		**Diuretic use**	
I	0	≤10	0	>35	0	<55	0	No	0	No	0	No	0
II	2	10-15	1.5	30-35	1	55-65	1.5	Yes	2	Yes	2	Yes	2
III	2.5	15-20	3.5	25-30	1.5	65-75	2						
IV	3.5	20-25	4	20-25	2	≥75	3						
		>25	7	≤ 20	4.5								

Risk categories			
Low	Moderate	High	Very high
0-3	3-6	6-12	12-24

FIGURE 2 | Receiver operating characteristic curve and calibration plot of the risk score for post-acute myocardial infarction (AMI) infection.

the present risk score showed a similar predictive effect on infection between patients with (AUC:0.816, 95% CI:0.779–0.854) and without (AUC:0.789, 95% CI:0.724–0.854) use of IABP (**Supplementary Table 5**). Besides, subgroup analyses including age, gender, anemia, diabetes, and chronic kidney disease proved consistent predictive values for P-AMI infection in

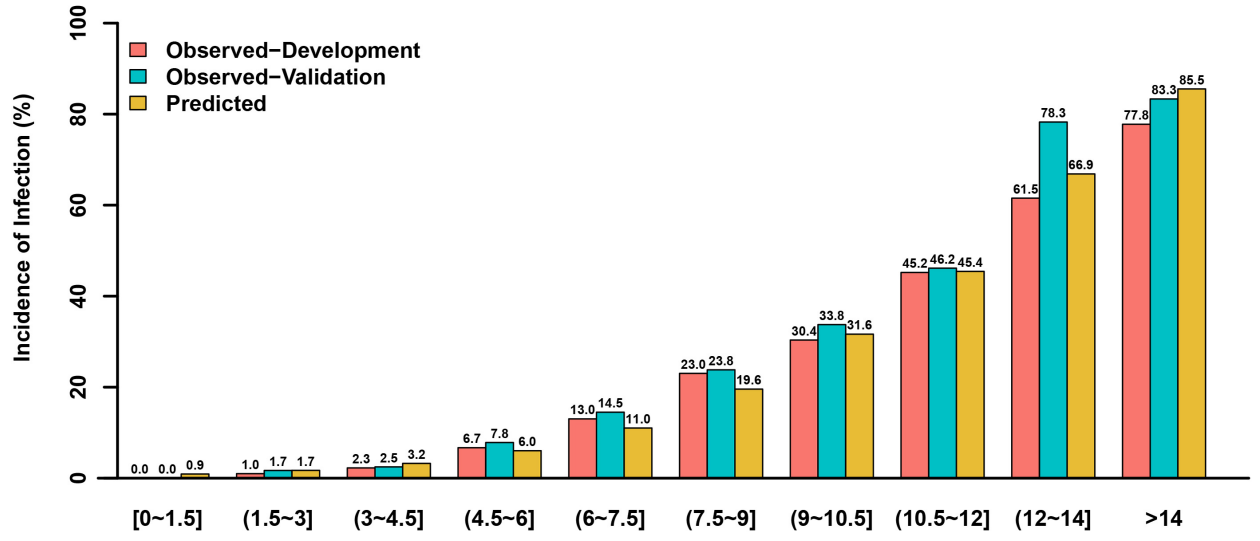

FIGURE 3 | The observed and predicted incidences of post-AMI infection in the development and validation cohorts based on different risk scores.

both datasets (**Supplementary Table 5**), with the best calibration in the aforementioned subgroups (calibration slope nearly 1) (**Supplementary Figure 10**).

Additionally, compared to previously established risk scores [age, estimated glomerular filtration rate, and ejection fraction (AGEF); age, creatinine, and ejection fraction (ACEF); and Canada Acute Coronary Syndrome (CACS) risk score], the present risk score, PAMIIS, achieved better discriminative power (**Supplementary Figure 11**).

Clinical Use

The optimal cut-off identifying post-AMI infection was a score of 6.5 (sensitivity 81.5%; specificity 74.0%). As shown in **Supplementary Figures 12, 13**, increased risk of infection was obtained across risk score groups. Compared to those with a low-risk score, high-risk patients also presented elevated MACE and all-cause death in the development, validation, and NSTE-ACS cohorts ($P < 0.001$). Based on the types of infection, the incidences of pulmonary and urinary infection performed as the upward trend across groups in both datasets (**Supplementary Figure 14**). Decision curve analysis demonstrated that the present risk score displayed a better-standardized net benefit for infection than other risk scores, indicating better clinical usefulness (**Supplementary Figure 15**).

DISCUSSION

The present study is the first to develop a readily implementable, simple, and robust risk score including seven easily acquired parameters for post-AMI infection detection among patients with STEMI in clinical routine. Importantly, this risk score was validated in an independent validation cohort, as well as in various subgroups.

In the current study, the incidence of post-AMI infection was 11.8%, slightly higher than previously reported (10 and 3.9%) (4, 17). The elevated infection rate might be related to the prolonged median intensive care unit stay (4 days vs. 1 day) (18). However, the incidence was lower than a recent study including the octogenarian cohort undergoing primary PCI (28.9%) (19). In this regard, the different infection definitions and study populations might contribute to this discrepancy.

At present, several studies have reported predictive markers or established risk scores for infection in patients with cardiac surgery or critical illnesses. Fowler et al. identified and validated a risk model of 12 variables to detect cardiac surgery patients at high risk of major infections (8). Moreover, several predictive models have been validated to assess the infection risk in critically ill patients, such as the intensive care infection score (20). Yet, little research has been published on infection prediction models for patients with STEMI. Although our previous research has validated and compared the predictive significance of several clinical risk scores for post-AMI infection (13–15), these scores had relatively poor discriminatory powers and were not established specifically for infection. The present study is the first to develop and validate a risk model to predict infection in such patients and performed well across a broad range of patient subgroups.

Notably, diabetes mellitus (DM) generally causes an increase in susceptibility to infection among diabetics compared to those without DM (21). In the current study, we also documented that DM was an important risk factor of infection for patients with STEMI. However, DM with insulin therapy displayed better predictive value for post-AMI infection than DM *per se*. This observation is consistent with the previous results that patients with insulin therapy had a greater hazard of infection (22). Therefore, insulin use was incorporated into the final risk model instead of DM. In patients with type

2 DM, metformin is routinely used as the first-line oral drug; with disease progression, the vast majority of patients eventually have to use insulin to keep blood glucose levels within the desired range (23). Insulin therapy thus might represent the increased severity of DM to some extent, which would be more prone to develop infection (24). To better understand the potential mechanisms, further research should be performed to evaluate the relationship between insulin therapy and infection in detail.

Additionally, several risk factors (age and WBC count, etc.), significantly associated with infection by the multivariable analysis, were largely similar to risk factors previously identified. Serum albumin levels, an easily available biomarker, have been proven to be related to postoperative infections (25). Besides, findings from a systemic review demonstrated that the transradial PCI approach in STEMI patients significantly reduced major and access site bleeding, as well as the length of hospital stay, that was associated with the risk of infection (26). Importantly, hemorrhage is known to cause increased susceptibility to infection. Experimental studies also demonstrated that even a simple hemorrhage produced a significant depression of cellular immunity and the immunosuppression increased the susceptibility to sepsis (27). Essebag et al. also reported that clinically significant pocket hematomas were associated with a significantly increased infection risk in patients with cardiac implantable electronic device surgery (28). Thus, it is reasonable that the parameter transfemoral approach was finally included in the present risk score.

Importantly, it is widely recognized that the Killip classification and the diuretic use reflect the status of cardiac function. An increasing number of studies have demonstrated the complicated and vicious interactions between heart failure and infection (29, 30). The decline in cardiac function induces a rise in pulmonary pressure, subsequently leading to pulmonary edema and accumulation of pneumonia-related pathogens (Chlamydophila or streptococcus pneumonia), which in turn exhibit deleterious impacts on the respiratory infection (31). In addition, a recent study suggested that incident diuretic use markedly increased the emergency room visits or hospitalization rates related to pneumonia or COPD (32). However, due to the lack of relevant studies, the effects and underlying mechanisms of diuretics on infections remain unclear and need to be evaluated in further research.

The present risk score was based on simple, dichotomized factors, and thus can be rapidly and easily calculated in clinical practice. The identification of high-risk patients has important clinical implications, as several included factors are adaptable. Serum albumin levels and transfemoral PCI approaches can be modified, and more restrictive use of diuretic medications, as well as frequent blood glucose monitoring, are warranted to minimize the risk of infection. Additionally, this risk score might be helpful to select high-risk patients in future research to test interventions that reduce infections in such patients. Furthermore, although the present risk score was developed limitedly in patients with STEMI, the predictive value was also good in patients with NSTE-ACS. Thus, the utility of this risk score might be extended to all patients with ACS.

Several limitations should be mentioned. First, the score was exclusively developed in patients with STEMI and validated in patients with NSTE-ACS, but these findings should be used with caution when applied to other patients, such as critically ill patients. Second, infections are sometimes difficult to diagnose and might be overestimated occasionally. However, infections were defined as infections requiring antibiotic administration in this study to reduce misdiagnosis and overdiagnosis. Moreover, further study should be performed to evaluate the role of antibiotic type on outcomes. Third, the candidate variables for the risk-adjustment model were restricted to those available in our patient cohort, which would make the score less predictive accuracy than those with more included variables. Lastly, new biomarkers were not included in this risk score, while incorporating novel biomarkers would likely develop a more robust and productive scoring system. Noticeably, some inflammatory indicators, such as C-reactive protein and procalcitonin, were not included in this model since they were unconventional detection indexes, especially before the PCI procedure. Nonetheless, this risk-prediction instrument was established using commonly available clinical variables and would as such be more accessible clinically.

In summary, this study represents a simple-to-use risk score combining widely available clinical variables for infection estimation in patients with STEMI after PCI and can be applied in clinical routine. This scoring model might aid in risk stratification of infection and provoke future research into the best strategies to reduce or prevent infection development.

DATA AVAILABILITY STATEMENT

The raw data supporting the conclusions of this article will be made available by the authors, without undue reservation.

AUTHOR CONTRIBUTIONS

NT, PH, and YuL designed the study and revised the manuscript. LW, PC, YD, YaL, WC, ZX, LZ, and HF participated in the collection and assembly of data. CD and YuL did the statistical analysis. LW and YuL drafted the manuscript. All authors contributed to the critical revision of the article and approved the final manuscript.

FUNDING

This work was supported by Shuangqing Talent Program Project of Guangdong Provincial People's Hospital (Grant Nos. KJ012019095 and KJ012019084), High-Level Hospital Construction Project (Grant No. DFJH2020021), Outstanding Young Medical Talents in Guangdong Province (KJ012019456), China Youth Research Funding (Grant No. 2017-CCA-VG-02), and the National Natural Science Foundation of China (Grant

No. 81803327). The funders had no role in the study design, data collection and analysis, the decision to publish, or the preparation of the manuscript.

ACKNOWLEDGMENTS

We would like to thank Wenfei He (Department of Cardiology, The Second People's Hospital of Nanhai District, Guangdong Provincial People's Hospital's Nanhai Hospital, Foshan, China) for collecting clinical data.

SUPPLEMENTARY MATERIAL

The Supplementary Material for this article can be found online at: https://www.frontiersin.org/articles/10.3389/fcvm.2022.845307/full#supplementary-material

REFERENCES

1. Santos M, Oliveira M, Vieira S, Magalhaes R, Costa R, Brochado B, et al. Predictors and mid-term outcomes of nosocomial infection in ST-elevation myocardial infarction patients treated by primary angioplasty. *Kardiol Pol.* (2021) 79:988–94. doi: 10.33963/KP.a2021.0058
2. Lian XJ, Dai YN, Xue JH, Zeng LH, Wang LT, Xue L, et al. Ticagrelor and the risk of infections during hospitalization in patients with ST-elevation myocardial infarction undergoing percutaneous coronary intervention. *Atherosclerosis.* (2021) 331:6–11. doi: 10.1016/j.atherosclerosis.2021.06.924
3. Truffa AA, Granger CB, White KR, Newby LK, Mehta RH, Hochman JS, et al. Serious infection after acute myocardial infarction: incidence, clinical features, and outcomes. *JACC Cardiovasc Interv.* (2012) 5:769–76. doi: 10.1016/j.jcin.2012.03.018
4. Putot A, Chague F, Manckoundia P, Cottin Y, Zeller M. Post-Infectious myocardial infarction: new insights for improved screening. *J Clin Med.* (2019) 8:827. doi: 10.3390/jcm8060827
5. Eagle KA, Lim MJ, Dabbous OH, Pieper KS, Goldberg RJ, Van de Werf F, et al. A validated prediction model for all forms of acute coronary syndrome: estimating the risk of 6-month postdischarge death in an international registry. *JAMA.* (2004) 291:2727–33. doi: 10.1001/jama.291.22.2727
6. Morrow DA, Antman EM, Charlesworth A, Cairns R, Murphy SA, de Lemos JA, et al. TIMI risk score for ST-elevation myocardial infarction: a convenient, bedside, clinical score for risk assessment at presentation: an intravenous nPA for treatment of infarcting myocardium early II trial substudy. *Circulation.* (2000) 102:2031–7. doi: 10.1161/01.cir.102.17.2031
7. Kansy A, Jacobs JP, Pastuszko A, Mirkowicz-Malek M, Manowska M, Jezierska E, et al. Major infection after pediatric cardiac surgery: external validation of risk estimation model. *Ann Thorac Surg.* (2012) 94:2091–5. doi: 10.1016/j.athoracsur.2012.07.079
8. Fowler VG Jr., O'Brien SM, Muhlbaier LH, Corey GR, Ferguson TB, Peterson ED. Clinical predictors of major infections after cardiac surgery. *Circulation.* (2005) 112:I358–65. doi: 10.1161/CIRCULATIONAHA.104.525790
9. Chen JY, He PC, Liu YH, Wei XB, Jiang L, Guo W, et al. Association of parenteral anticoagulation therapy with outcomes in Chinese patients undergoing percutaneous coronary intervention for Non-ST-segment elevation acute coronary syndrome. *JAMA Intern Med.* (2019) 179:186–94. doi: 10.1001/jamainternmed.2018.5953
10. Liu Y, Wang L, Lin Y, Chen W, Xu Z, Chen P, et al. Development and validation of a risk score for predicting post-acute myocardial infarction infection in patients undergoing percutaneous coronary intervention: study protocol for an observational study. *Front Cardiovasc Med.* (2021) 8:675142. doi: 10.3389/fcvm.2021.675142
11. Thiele H, Kurz T, Feistritzer HJ, Stachel G, Hartung P, Lurz P, et al. General versus local anesthesia with conscious sedation in transcatheter aortic valve implantation: the randomized SOLVE-TAVI trial. *Circulation.* (2020) 142:1437–47. doi: 10.1161/CIRCULATIONAHA.120.046451
12. Peduzzi P, Concato J, Kemper E, Holford TR, Feinstein AR. A simulation study of the number of events per variable in logistic regression analysis. *J Clin Epidemiol.* (1996) 49:1373–9. doi: 10.1016/s0895-4356(96)00236-3
13. Wang L, Huang G, Peng Q, Duan C, Dai Y, Shao S, et al. Risk predictive ability of ACEF score for infection in patients with ST-segment elevation myocardial infarction undergoing percutaneous coronary intervention. *Eur J Prev Cardiol.* (2020) 27:220–2. doi: 10.1177/2047487319873142
14. Liu Y, Dai Y, Chen J, Huang C, Duan C, Shao S, et al. Predictive value of the Canada Acute Coronary Syndrome risk score for post-acute myocardial infarction infection. *Eur J Intern Med.* (2020) 71:57–61. doi: 10.1016/j.ejim.2019.10.012
15. Liu Y, Wang L, Chen W, Zeng L, Fan H, Duan C, et al. Validation and comparison of six risk scores for infection in patients With ST-Segment elevation myocardial infarction undergoing percutaneous coronary intervention. *Front Cardiovasc Med.* (2020) 7:621002. doi: 10.3389/fcvm.2020.621002
16. Vickers AJ, Elkin EB. Decision curve analysis: a novel method for evaluating prediction models. *Med Decis Making.* (2006) 26:565–74. doi: 10.1177/0272989X06295361
17. Piccaro de Oliveira P, Gonzales V, Lopes RD, Schmidt MM, Garofallo S, Santos RP, et al. Serious infections among unselected patients with ST-elevation myocardial infarction treated with contemporary primary percutaneous coronary intervention. *Am Heart J.* (2016) 181:52–9. doi: 10.1016/j.ahj.2016.08.005
18. Shavadia JS, Chen AY, Fanaroff AC, de Lemos JA, Kontos MC, Wang TY. Intensive care utilization in stable patients with ST-Segment elevation myocardial infarction treated with rapid reperfusion. *JACC Cardiovasc Interv.* (2019) 12:709–17. doi: 10.1016/j.jcin.2019.01.230
19. Leistner DM, Munch C, Steiner J, Lauten A, Landmesser U, Stahli BE. Effect on outcomes: infections complicating percutaneous coronary interventions in patients >/=80 years of age. *Am J Cardiol.* (2019) 23:1806–11. doi: 10.1016/j.amjcard.2019.03.003
20. van der Geest PJ, Mohseni M, Linssen J, Duran S, de Jonge R, Groeneveld AB. The intensive care infection score - a novel marker for the prediction of infection and its severity. *Crit Care.* (2016) 20:180. doi: 10.1186/s13054-016-1366-6
21. Muller LM, Gorter KJ, Hak E, Goudzwaard WL, Schellevis FG, Hoepelman AI, et al. Increased risk of common infections in patients with type 1 and type 2 diabetes mellitus. *Clin Infect Dis.* (2005) 41:281–8. doi: 10.1086/431587
22. Donnelly JP, Nair S, Griffin R, Baddley JW, Safford MM, Wang HE, et al. Association of diabetes and insulin therapy with risk of hospitalization for infection and 28-day mortality risk. *Clin Infect Dis.* (2017) 64:435–42. doi: 10.1093/cid/ciw738
23. Nathan DM, Buse JB, Davidson MB, Ferrannini E, Holman RR, Sherwin R, et al. Medical management of hyperglycaemia in type 2 diabetes mellitus: a consensus algorithm for the initiation and adjustment of therapy: a consensus statement from the American Diabetes Association and the European Association for the Study of Diabetes. *Diabetologia.* (2009) 52:17–30. doi: 10.1007/s00125-008-1157-y
24. Yamashita S, Yamaguchi H, Sakaguchi M, Satsumae T, Yamamoto S, Shinya F. Longer-term diabetic patients have a more frequent incidence of nosocomial infections after elective gastrectomy. *Anesth Analg.* (2000) 91:1176–81. doi: 10.1097/00000539-200011000-00025
25. Wang Y, Li X, Ji Y, Tian H, Liang X, Li N, et al. Preoperative serum albumin level as a predictor of postoperative pneumonia after femoral neck fracture surgery in a geriatric population. *Clin Interv Aging.* (2019) 14:2007–16. doi: 10.2147/CIA.S231736
26. Singh S, Singh M, Grewal N, Khosla S. Transradial vs transfemoral percutaneous coronary intervention in ST-Segment elevation myocardial infarction: a systemic review and meta-analysis. *Can J Cardiol.* (2016) 32:777–90. doi: 10.1016/j.cjca.2015.08.019

27. Stephan RN, Kupper TS, Geha AS, Baue AE, Chaudry IH. Hemorrhage without tissue trauma produces immunosuppression and enhances susceptibility to sepsis. *Arch Surg.* (1987) 122:62–8. doi: 10.1001/archsurg.1987.01400130068010
28. Essebag V, Verma A, Healey JS, Krahn AD, Kalfon E, Coutu B, et al. Clinically significant pocket hematoma increases long-term risk of device infection: bruise control infection study. *J Am Coll Cardiol.* (2016) 67:1300–8. doi: 10.1016/j.jacc.2016.01.009
29. Eurich DT, Marrie TJ, Minhas-Sandhu JK, Majumdar SR. Risk of heart failure after community acquired pneumonia: prospective controlled study with 10 years of follow-up. *BMJ.* (2017) 356:j413. doi: 10.1136/bmj.j413
30. Remick J, Georgiopoulou V, Marti C, Ofotokun I, Kalogeropoulos A, Lewis W, et al. Heart failure in patients with human immunodeficiency virus infection: epidemiology, pathophysiology, treatment, and future research. *Circulation.* (2014) 129:1781–9. doi: 10.1161/CIRCULATIONAHA.113.004574
31. Al-Kindi SG, ElAmm C, Ginwalla M, Mehanna E, Zacharias M, Benatti R, et al. Heart failure in patients with human immunodeficiency virus infection: epidemiology and management disparities. *Int J Cardiol.* (2016) 218:43–6. doi: 10.1016/j.ijcard.2016.05.027
32. Vozoris NT, Wang X, Austin PC, O'Donnell DE, Aaron SD, To TM, et al. Incident diuretic drug use and adverse respiratory events among older adults with chronic obstructive pulmonary disease. *Br J Clin Pharmacol.* (2018) 84:579–89. doi: 10.1111/bcp.13465

Conflict of Interest: The authors declare that the research was conducted in the absence of any commercial or financial relationships that could be construed as a potential conflict of interest.

frontiers | Frontiers in Cardiovascular Medicine

ORIGINAL RESEARCH
published: 27 April 2022
doi: 10.3389/fcvm.2022.888753

Enrichment of the Postdischarge GRACE Score With Deceleration Capacity Enhances the Prediction Accuracy of the Long-Term Prognosis After Acute Coronary Syndrome

Shoupeng Duan[1,2,3,4†], *Jun Wang*[1,2,3,4†], *Fu Yu*[1,2,3,4†], *Lingpeng Song*[1,2,3,4], *Chengzhe Liu*[1,2,3,4], *Ji Sun*[1,2,3,4], *Qiang Deng*[1,2,3,4], *Yijun Wang*[1,2,3,4], *Zhen Zhou*[1,2,3,4], *Fuding Guo*[1,2,3,4], *Liping Zhou*[1,2,3,4], *Yueyi Wang*[1,2,3,4], *Wuping Tan*[1,2,3,4], *Hong Jiang*[1,2,3,4*] and *Lilei Yu*[1,2,3,4*]

[1] Department of Cardiology, Renmin Hospital of Wuhan University, Wuhan, China, [2] Cardiac Autonomic Nervous System Research Centre of Wuhan University, Wuhan, China, [3] Cardiovascular Research Institute, Wuhan University, Wuhan, China, [4] Hubei Key Laboratory of Cardiology, Wuhan, China

Background: Cardiac autonomic nerve imbalance has been well documented to provide a critical foundation for the development of acute coronary syndrome (ACS) but is not included in the postdischarge GRACE score. We investigated whether capturing cardiac autonomic nervous system (ANS)-related modulations by 24-h deceleration capacity (DC) could improve the capability of existing prognostic models, including the postdischarge Global Registry of Acute Coronary Events (GRACE) score, to predict prognosis after ACS.

Method: Patients with ACS were assessed with 24-h Holter monitoring in our department from June 2017 through June 2019. The GRACE score was calculated for postdischarge 6-month mortality. The patients were followed longitudinally for the incidence of major adverse cardiac events (MACEs), set as a composite of non-fatal myocardial infarction and death. To evaluate the improvement in its discriminative and reclassification capabilities, the GRACE score with DC model was compared with a model using the GRACE score only, using area under the receiver-operator characteristic curve (AUC), Akaike's information criteria, the likelihood ratio test, category-free integrated discrimination index (IDI) and continuous net reclassification improvement (NRI).

Results: Overall, 323 patients were enrolled consecutively. After the follow-up period (mean, 43.78 months), 41 patients were found to have developed MACEs, which were more frequent among patients with DC < 2.5 ms. DC adjusted for the GRACE score independently predicted the occurrence of MACEs with an adjusted hazard ratio (HR) of 0.885 and 95% CI of 0.831–0.943 ($p < 0.001$). Moreover, adding DC to the GRACE score only model increased the discriminatory ability for MACEs, as indicated by the likelihood ratio test ($\chi^2 = 9.277$, 1 df; $p < 0.001$). The model including the GRACE score

OPEN ACCESS

Edited by:
Jinwei Tian,
The Second Affiliated Hospital of Harbin Medical University, China

Reviewed by:
Liliane Lins-Kusterer,
Universidade Federal da Bahia, Brazil
Xiaoxiang Yan,
Shanghai Jiao Tong University, China
Yisong Cheng,
Sichuan University, China

***Correspondence:**
Lilei Yu
lileiyu@whu.edu.cn
Hong Jiang
hong-jiang@whu.edu.cn

†These authors have contributed equally to this work

Specialty section:
This article was submitted to General Cardiovascular Medicine, a section of the journal Frontiers in Cardiovascular Medicine

Received: *03 March 2022*
Accepted: *01 April 2022*
Published: *27 April 2022*

Citation:
Duan S, Wang J, Yu F, Song L, Liu C, Sun J, Deng Q, Wang Y, Zhou Z, Guo F, Zhou L, Wang Y, Tan W, Jiang H and Yu L (2022) Enrichment of the Postdischarge GRACE Score With Deceleration Capacity Enhances the Prediction Accuracy of the Long-Term Prognosis After Acute Coronary Syndrome. Front. Cardiovasc. Med. 9:888753. doi: 10.3389/fcvm.2022.888753

combined with DC yielded a lower corrected Akaike's information criterion compared to that with the GRACE score alone. Incorporation of the DC into the existing model that uses the GRACE score enriched the net reclassification indices ($NRIe^{>0}$ 7.3%, $NRIne^{>0}$ 12.8%, $NRI^{>0}$ 0.200; $p = 0.003$). Entering the DC into the GRACE score model enhanced discrimination (IDI of 1.04%, $p < 0.001$).

Conclusion: DC serves as an independent and effective predictor of long-term adverse outcomes after ACS. Integration of DC and the postdischarge GRACE score significantly enhanced the discriminatory capability and precision in the prediction of poor long-term follow-up prognosis.

Keywords: acute coronary syndrome, GRACE score, deceleration capacity, autonomic nerve, long-term prognosis

INTRODUCTION

Acute coronary syndrome (ACS) occurs in people who are prone to exacerbations and adverse outcomes, and optimizing the risk stratification of these patients is of considerable clinical interest (1, 2). Therefore, even if the optimal treatment is known, identifying which ACS patients will benefit the most from early interventional treatment can be challenging. Currently, the Global Registry of Acute Coronary Events (GRACE) score is the most well-established risk stratification tool for the prediction of in-hospital and long-term mortality and the risk of myocardial infarction after ACS (3, 4). Although it has been well established that the overall prognosis after ACS is worse among those with cardiac autonomic nerve imbalance than among those without cardiac autonomic nerve imbalance (5–8), the GRACE score does not include data from wearable devices that test cardiac autonomic function.

Notably, the value of 24-h deceleration capacity (DC), a feasible and non-invasive indicator that captures autonomic activity-related modulations of heart rate, adds valuable and repeatable information for timely identification of ACS patients at higher risk and aid in risk stratification (5–8). Accordingly, previous studies have also demonstrated that DC may serve as a predictor of mortality and outperformed a standard measure of heart rate variability (HRV) (8). Moreover, adjustment of the admission GRACE score, calculated for the prediction of in-hospital mortality, by short-term DC improves the accuracy of prediction of the composite of mortality, including in-hospital, 30 and 180-day mortality, among patients with suspected ACS (9). However, whether the readily accessible clinical 24-h DC remains a significant prognostic factor to enhance the predictability of prognostic models, including the postdischarge GRACE score, for ACS patients after long-term follow-up remains unclear.

Therefore, we investigated the value in long-term prognosis of 24-h DC added to the postdischarge GRACE score among ACS patients and the underlying incremental prognostic value of entering DC into an existing model including the postdischarge GRACE score only.

Abbreviations: GRACE, Global Registry of Acute Coronary Events; CABG, coronary artery bypass grafting; PCI, Percutaneous Transluminal Coronary Intervention; ACS, acute coronary syndromes; STEMI, ST segment Elevation Myocardial Infarction; NSTE-ACS, non-ST-elevation acute coronary syndromes; MI, myocardial infarction; SBP, Systolic blood pressure; DBP, Diastolic blood pressure; eGFR, glomerular filtration rate; NLR, neutrophil-to-lymphocyte ratio; PLT, platelet count; PLR, platelet-to-lymphocyte ratio; TG, triglycerides; TC, total cholesterol; HDL-C, high-density lipoprotein cholesterol; LDL-C, low-density lipoprotein cholesterol; Apo A1, Apolipoprotein A1; Apo B, Apolipoprotein B; Lp (a), lipoprotein a; hs-CRP, high-sensitivity C-reactive protein; CK-MB, creatine kinase-MB; SDNN, standard deviation of all normal sinus RR intervals; SDANN, standard deviation average of normal-to-normal (NN) intervals; pNN50, percentage of the number of times that the difference between adjacent normal RR intervals > 50 ms in the total number of NN intervals; rMSSD, root mean square successive difference; HF, high-frequency power; LF, low-frequency power; LF/HF, low-frequency/high-frequency ratio; DC, deceleration capacity; MACEs, major adverse cardiac events; AUC, receiver-operator characteristic curve; NRI, net reclassification index; IDI, integrated discrimination improvement; IQR, interquartile range.

METHODS

Patient Population

We retrospectively enrolled 323 consecutive patients with ACS at Renmin Hospital of Wuhan University from June 2017 through June 2019. The previously established guidelines addressed the process and criteria for acute coronary syndrome diagnosis (10). ACS included non-ST-elevation ACS (NSTE-ACS) and ST-elevation ACS (STE-ACS). Patients with NSTE-ACS included those presenting with unstable angina (UA) and non-ST-segment elevation myocardial infarction (non-STEMI), and patients with STE-ACS included those presenting with ST-elevation myocardial infarction (STEMI). The main exclusion criteria were as follows: atrial fibrillation, pacemaker implantation, use of any medications that affect heart rate, severe liver or renal insufficiency < 30 ml/(min 1.73 m^2), inflammatory or infectious disease, depressive disorder, hyperthyroidism and excessive alcohol consumption. The flowchart of participant enrollment is presented in **Figure 1**. Due to the purely retrospective observational, our study was exempt from requiring ethics approval and informed consent from eligible patients by the Renmin Hospital of Wuhan University Ethics Committee.

Laboratory Examinations

Venous blood specimens were collected when patients were initially referred to the emergency department or cardiology department. All participants were subjected to routine whole

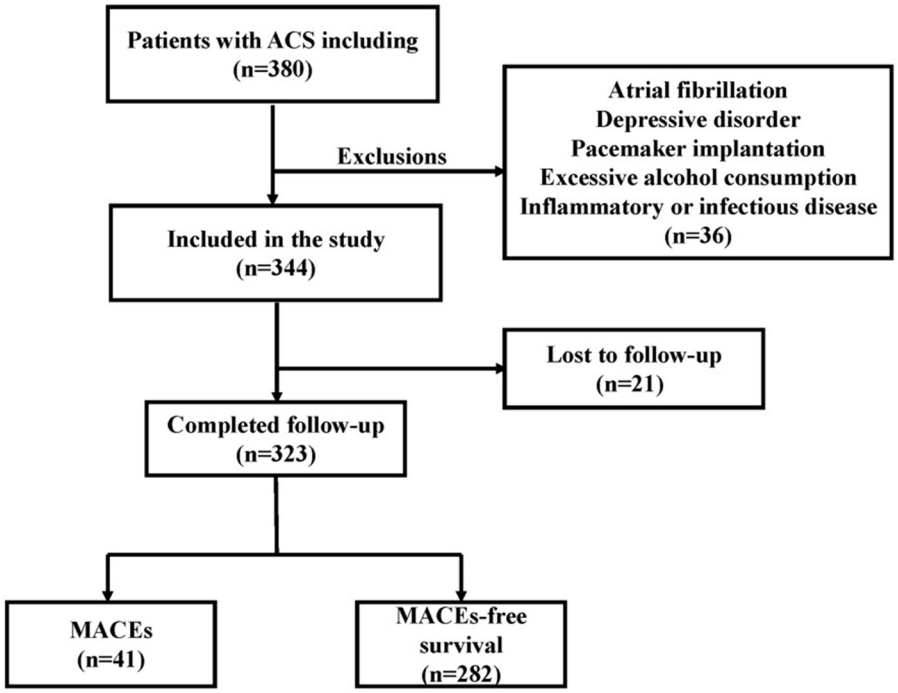

FIGURE 1 | Flowchart of patient enrollment.

blood analysis, including routine blood, blood glucose, kidney function, and plasma lipid analyses.

Holter Monitoring and DC Analysis

All participants included in this study underwent 24-h Holter monitoring (DMS300-4A, DM Software, Inc., USA) recordings after coronary angiography. The 24-h mean heart rate, time-domain parameters [i.e., standard deviation of all normal sinus RR intervals (SDNN), standard deviation average of normal-to-normal (NN) intervals (SDANN), percentage of the number of times that the difference between adjacent normal RR intervals >50 ms in the total number of NN intervals (pNN50), root mean square successive difference (rMSSD)], frequency-domain parameters [i.e., high-frequency power (HF), low-frequency power (LF), and low-frequency/high-frequency ratio (LF/HF)] and DC were automatically specifically calculated via commercial software (H-Scribe Analysis System, Mortara Instrument, Inc., Milwaukee, WI, USA) as shown in a previous reference (11, 12). Frequency domain parameters yield a more accurate and detailed quantification of heart rate than time domain parameters (13, 14). Morevore, the predictive value of LF/HF may be superior to other parameters of HRV (15–17). DC analysis is divided into three steps. First, the RR scatter plot shows the scatter of the full range of beat-to-beat RR intervals, from which the starting time for analysis is selected. The analysis length and number of cardiac cycles were then chosen, with the analysis length generally defaulting to a full 24 h. Finally, the X (0), X (1), X (- 1), and X (- 2) values reflected in the heart rate deceleration curve were substituted into the formula $DC = [x(0) + X(1) + X(-1) + X(-2)]/4$ to compute the 24 h DC, and the resulting unit was ms.

GRACE Score

The GRACE score was calculated at discharge to predict 6-month mortality (https://www.outcomes-umassmed.org/grace). The parameters of the GRACE score include age, heart rate, systolic blood pressure on arrival, creatinine level, percutaneous transluminal coronary intervention (PCI) during in-hospital period, coronary artery bypass grafting (CABG) during in-hospital period, previous myocardial infarction (MI), ST-segment depression, increased levels of cardiac enzyme/marker and congestive heart failure.

Follow-Up

The average time to follow-up was 43.78 months. Patients were discharged, and follow-up was conducted through an outpatient follow-up or telephone follow-up. At the end of the follow-up, a total of 21 cases (6.1%) were lost, and 323 patients (93.9%) were followed to the end. The clinical endpoint of our study was a composite endpoint clinical events of major adverse cardiovascular events (MACEs), including death and non-fatal myocardial infarction. Two experienced physicians adjudicated the endpoint events according to medical record reviewing.

Statistical Analysis

Continuous variables are represented by a mean plus a standard deviation (SD) or as the median with interquartile range (IQR) determined by skewness, whereas categorical variables

are summarized as frequencies and percentages. All participants were stratified into three groups based on their DC [low-risk group (DC > 4.5 ms), intermediate-risk group (DC > 2.5 ms, and DC ≤ 4.5 ms), and high-risk group (DC ≤ 2.5 ms)]. Differences between groups were analyzed with one-way analysis of variance (ANOVA), the Mann–Whitney U test or the Kruskal–Wallis test depending on the normality of the distribution. Categorical variables were analyzed with the chi square (χ^2) test. Survival free from MACEs was analyzed by the Kaplan–Meier method. Final covariates were age, sex, past history and laboratory results according to the results of the pre-survey. We used univariate Cox regression analyses first performed to determine the potential predictors of MACEs, followed by multivariate Cox analyses of significant variables with a p-value < 0.05 to improve the accuracy of the conclusions. Differences were considered statistically significant at $p < 0.05$. Statistical analysis was performed with SPSS software (version 23; SPSS).

The predictability of MACEs using DC, GRACE score and GRACE score combine with DC by receiver operator characteristic (ROC) curve analysis. We compared whether adding DC to the GRACE score would enhance the discriminative and reclassification capabilities of the models. The fit of each nested model was compared via the χ^2 likelihood ratio test to assess whether the logistic regression model that integrated DC and the postdischarge GRACE score supported a significantly better fit than the model including the GRACE score alone. Comparison of the nested and non-nested models, including the GRACE score or DC or LF/HF added to the GRACE score, was weighted by calculating the corrected Akaike's information criterion (AICc), delta-AICc (δ AICc), and Akaike weights (wi) to represent the probability that a given model was the best predictive model in the set (18).

Predicted probabilities (%) of MACEs were generated by logistic regression models using the GRACE score alone and the GRACE score combined with LF/HF or DC. The addition of DC and LF/HF to the existing models with the GRACE score was evaluated with the predicted probabilities of MACEs implementing multiple methods of improvement in discrimination: increase in the area under the receiver operating characteristic curve (AUC), category-free continuous net reclassification improvement ($cNRI^{>0}$) and integrated discrimination improvement (IDI). Given the presence of missing specific predefined clinical risk thresholds for the models containing the GRACE score, categorical NRI was not employed. The net percentage of patients with the event of interest correctly assigned a higher predicted risk was defined as the event NRI (NRIe), and the net percentage of persons without the event of interest correctly assigned a lower predicted risk was defined as the non-event NRI (NRIne). Total NRI was defined as the sum of the net percentages of persons with and without the events of interest correctly assigned a different predicted risk. The IDI was equal to the enhancement in discrimination slope defined as the mean difference in predicted risks between those with and without events. The IDI was equal to the difference in the initial and updated models in the discrimination slope formed between the mean predicted probabilities (%) of patients with and without events.

RESULTS

Clinical Baseline Characteristics

The baseline features of all of the enrolled ACS patients classified into three groups according to the DC value are presented in **Table 1**. Our results indicated that patients with lower DC (≤2.5 ms) were likely to be older ($p < 0.001$) and have non-ST-elevation ACS (NSTE-ACS) ($p = 0.004$); higher creatinine levels ($p = 0.047$), glucose levels ($p = 0.032$) and average heart rate ($p < 0.001$); lower esti mated glomerularfiltrationrate (eGFR) ($p = 0.016$), SDNN ($p < 0.001$), rMSSD ($p < 0.001$), Pnn50 ($p < 0.001$), LF ($p < 0.001$), HF ($p < 0.001$), and LF/HF ($p = 0.031$); a higher GRACE score ($p < 0.001$) and GRACE risk ($p = 0.001$); history of MI ($p = 0.021$); and increased creatine kinase-MB (CK-MB) levels ($p = 0.034$) and incidence of MACEs ($p < 0.001$).

The Relationship Between DC and MACEs

The incidence of MACEs among the patients with ACS in this study was collected over an average follow-up of 43.78 months. Forty-one patients experienced MACEs, including 10 patients in the low-risk group (5.5%, $n = 183$), 17 patients in the intermediate-risk group (18.1%, $n = 94$), and 14 patients in the high-risk group (30.4%, $n = 46$). Kaplan–Meier analysis indicated that the incidence of MACEs was significantly different among patients with ACS based on DC values ($\chi^2 = 26.089$, $p < 0.001$, **Figure 2**). Besides patients in the high-risk group had a higher incidence of MACEs than those in the intermediate-risk and low-risk groups. In addition, those with intermediate risk were more susceptible to MACEs than those with low risk ($p < 0.05$).

Predictors of MACEs

Univariate Cox analysis showed that history of MI, NSTE-ACS, neutrophil-to-lymphocyte ratio (NLR), platelet-to-lymphocyte ratio (PLR), creatinine, lipoprotein a [Lp (a)], DC, and GRACE score (all $p < 0.05$) were potential predictors of MACEs in patients with ACS (**Table 2**). Multivariate Cox analysis consistently showed that DC (HR: 0.885, 95% CI: 0.831–0.943, $p < 0.001$) and the GRACE score (HR: 1.020, 95% CI: 1.007–1.034, $p = 0.002$) were risk factors for MACEs at the final follow-up (**Table 2**).

Moreover, subgroup analysis was based on STEMI and NSTE-ACS patients. Univariate Cox analysis showed that PLR, NLR, high-sensitivity C-reactive protein (hs-CRP), DC, and GRACE score (all $p < 0.05$) were predictors of MACEs for all of the evaluated STEMI patients, as shown in **Table 3**. Furthermore, for all of the evaluated STEMI patients, independent influencing factors for the incidence of MACEs included DC (HR: 0.901, 95% CI: 0.828–0.981, $p = 0.016$) and the GRACE score (HR: 1.024, 95% CI: 1.001–1.048, $p = 0.043$) according to multivariate Cox analysis (**Table 3**).

Subsequent univariate Cox analysis further indicated that previous MI, NLR, creatinine, DC, GRACE score, and systolic blood pressure (SBP) (all $p < 0.05$) were potential predictors of MACEs among patients with NSTE-ACS, as shown in **Table 4**. For all of the evaluated NSTE-ACS patients, multivariate

TABLE 1 | Baseline characteristics of the study population categorized by deceleration capacity (DC).

	Low risk group (DC > 4.5 ms) (*n* = 183)	Intermediate risk group (DC > 2.5 ms, and DC ≤ 4.5 ms) (*n* = 94)	High risk group (DC ≤ 2.5 ms) (*n* = 46)	F/Z/χ2	*P*-value
Male, *n* (%)	114 (62.3)	57 (60.6)	35 (76.1)	3.592	0.166
Age (years)	61.43 ± 10.18	67.47 ± 9.21	65.13 ± 11.45	11.587	<0.001
Hypertension (%)	113 (61.7)	68 (72.3)	27 (58.7)	3.799	0.150
Duration of hypertension (years)	10.00 (5.00, 12.00)	10.00 (5.25, 18.75)	10.00 (3.00, 15.00)	2.596	0.273
Diabetes (%)	47 (25.7)	23 (24.5)	14 (30.4)	0.594	0.743
Duration of diabetes (years)	6.00 (2.00, 15.00)	5.00 (2.00,10.00)	10.00 (2.00, 17.00)	0.727	0.695
Current smoker (%)	65 (35.5)	30 (31.9)	17 (37.0)	0.479	0.787
Duration of smoking (years)	10.00 (0.000, 20.00)	17.50 (4.50, 20.00)	10.00 (6.00, 17.50)	0.692	0.708
Current smoking cigarettes (per day)	28.00 (20.00, 30.00)	30.00 (17.25, 40.00)	30.00 (21.50, 40.00)	1.292	0.524
History of drinking (%)	42 (23.0)	14 (14.9)	7 (15.2)	3.196	0.202
Family history (%)	17 (9.3)	3 (3.2)	3 (6.5)	3.521	0.172
Previous PCI (%)	56 (30.6)	26 (27.7)	11 (23.9)	0.885	0.642
Clinical presentation				11.272	0.004
STEMI	115 (62.8)	43 (45.7)	19 (41.3)		
NSTE-ACS	68 (37.2)	51 (54.3)	27 (58.7)		
Neutrophil ($\times 10^9$/L)	3.98 (3.01, 4.86)	3.98 (3.16, 4.97)	4.24 (3.15, 5.71)	1.756	0.416
Lymphocyte ($\times 10^9$/L)	1.67 (1.32, 2.08)	1.52 (1.14, 1.92)	1.49 (1.21, 2.02)	4.969	0.083
NLR	2.29 (1.78, 3.20)	2.46 (1.88, 3.63)	2.63 (1.94, 4.45)	4.398	0.111
PLT ($\times 10^9$/L)	203.85 ± 55.28	205.61 ± 52.73	194.83 ± 60.48	0.628	0.535
PLR	121.88 (88.24, 156.99)	133.24 (95.97, 183.55)	122.32 (92.34, 162.58)	3.512	0.173
hs-CRP (mg/L)	0.90 (0.50, 3.85)	0.65 (0.50, 5.00)	1.97 (0.32, 5.68)	1.322	0.516
eGFR ml/(min1.73 m^2)	91.13 ± 17.05	84.59 ± 17.28	88.43 ± 21.58	4.205	0.016
Creatinine (μmol/L)	69.00 (56.00, 81.00)	72.00 (57.75, 87.25)	75.00 (60.75, 91.00)	6.135	0.047
Uric acid (mmol/L)	375.26 ± 112.51	376.20 ± 114.29	402.57 ± 154.30	1.003	0.368
Glucose (mmol/L)	5.90 ± 2.21	6.46 ± 2.38	6.87 ± 3.59	3.473	0.032
TG (mmol/L)	1.48 (1.06, 1.99)	1.40 (1.08, 1.84)	1.15 (0.80, 1.73)	6.009	0.051
TC (mmol/L)	4.16 ± 1.10	4.24 ± 1.05	4.06 ± 0.94	0.440	0.644
HDL-C (mmol/L)	1.08 ± 0.29	1.06 ± 0.33	1.06 ± 0.27	0.065	0.937
LDL-C (mmol/L)	2.44 ± 1.00	2.44 ± 1.00	2.23 ± 0.84	0.873	0.419
Lp (a) (g/L)	152.00 (64.00, 298.00)	143.50 (67.00, 332.50)	134.00 (62.25, 295.25)	0.176	0.916
Average heart rate (bpm)	66.13 ± 7.41	72.89 ± 9.15	75.52 ± 12.63	30.948	<0.001
SDNN (ms)	119.00 (101.00, 137.00)	98.00 (79.00, 118.50)	97.00 (74.75, 120.00)	38.431	<0.001
SDANN (ms)	74.00 (50.00, 106.00)	77.00 (41.50, 100.00)	76.00 (53.00, 98.00)	0.837	0.658
rMSSD (ms)	31.00 (25.00, 46.00)	25.50 (19.00, 56.25)	17.00 (13.00, 27.75)	40.389	<0.001
Pnn50	6.00 (3.00, 12.00)	2.47 (0.14, 10.98)	1.00 (0.47, 1.99)	53.298	<0.001
LF (ms^2)	286.00 (215.50, 459.10)	128.50 (81.68, 198.48)	101.50 (53.50, 160.18)	115.529	<0.001
HF (ms^2)	202.00 (127.70, 294.00)	86.00 (46.75, 188.95)	71.10 (48.50, 225.00)	55.470	<0.001
LF/HF	1.50 (1.00, 2.37)	1.29 (0.80, 2.38)	1.30 (0.67, 1.81)	6.946	0.031
GRACE score	90.68 ± 23.73	105.77 ± 22.99	107.93 ± 32.06	16.121	<0.001
GRACE risk				18.142	0.001
High	52 (28.4)	9 (9.6)	5 (10.8)		
Intermediate	90 (49.2)	55 (58.5)	24 (52.2)		
Low	41 (22.4)	30 (31.9)	17 (37.0)		
SBP (mmHg)	133.65 ± 18.52	133.48 ± 21.12	131.79 ± 19.81	0.160	0.852
DBP (mmHg)	76.73 ± 11.63	76.31 ± 12.93	76.88 ± 12.39	0.048	0.953
History of MI (%)	22 (12.0)	13 (13.8)	13 (28.3)	7.773	0.021
ST-segment (%)	19 (10.4)	18 (19.1)	5 (10.9)	4.435	0.109
CK-MB increase (%)	73 (39.9)	50 (53.2)	26 (56.5)	6.752	0.034
Troponin rise (%)	0.04 (0.01, 0.25)	0.03 (0.01, 0.45)	0.05 (0.02, 0.38)	2.028	0.363

(Continued)

TABLE 1 | Continued

	Low risk group (DC > 4.5 ms) (*n* = 183)	Intermediate risk group (DC > 2.5 ms, and DC ≤ 4.5 ms) (*n* = 94)	High risk group (DC ≤ 2.5 ms) (*n* = 46)	F/Z/χ2	*P*-value
Cardiac arrest (%)	1 (0.5)	2 (2.1)	0 (0.0)	1.777	0.538
In-hospital PCI (%)	88 (48.1)	37 (39.4)	20 (43.5)	1.955	0.376
MACEs (%)	10 (5.5)	17 (18.1)	14 (30.4)	24.160	<0.001
Deaths (%)	0 (0.0)	3 (3.2)	6 (13.0)	20.000	<0.001
Non-fatal re-infarction (%)	6 (3.3)	11 (11.7)	7 (15.2)	11.135	0.004

DC, deceleration capacity; STEMI, ST segment Elevation Myocardial Infarction; NSTE-ACS, non-ST-elevation acute coronary syndromes; SBP, Systolic blood pressure; DBP, Diastolic blood pressure; eGFR, glomerular filtration rate; NLR, neutrophil-to-lymphocyte ratio; PLT, platelet count; PLR, platelet-to-lymphocyte ratio; TG, triglycerides; TC, total cholesterol; HDL-C, high-density lipoprotein cholesterol; LDL-C, low-density lipoprotein cholesterol; Apo A1, Apolipoprotein A1; Apo B, Apolipoprotein B; Lp (a), lipoprotein a; MI, myocardial infarction; hs-CRP, high-sensitivity C-reactive protein; CK-MB, creatine kinase-MB; SDNN, standard deviation of all normal sinus RR intervals; SDANN, standard deviation average of normal-to-normal (NN) intervals; pNN50, percentage of the number of times that the difference between adjacent normal RR intervals >50 ms in the total number of NN intervals; rMSSD, root mean square successive difference; HF, high-frequency power; LF, low-frequency power; LF/HF, low-frequency/high-frequency ratio; MACEs, major adverse cardiac events.

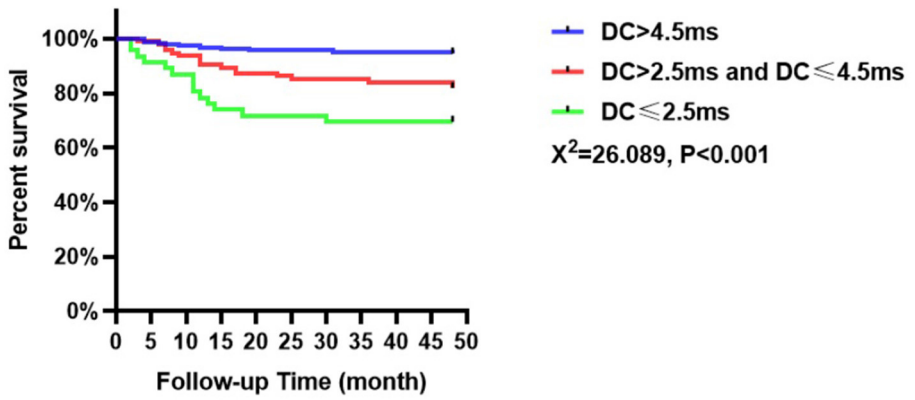

FIGURE 2 | Cumulative survival of MACEs in patients with ACS based on the DC value.

Cox analysis indicated that NLR (HR: 1.041, 95% CI: 1.000–1.084, $p = 0.048$), creatinine (HR: 1.013, 95% CI: 1.003–1.024, $p = 0.011$), DC (HR: 0.894, 95% CI: 0.811–0.986, $p = 0.025$), GRACE score (HR: 1.019, 95% CI: 1.002–1.036, $p = 0.024$), and SBP (HR: 1.034, 95% CI: 1.015–1.053, $p < 0.001$) were independent predictors for MACEs (**Table 4**).

To assess whether models that included the GRACE score combined with DC or LF/HF presented a significantly better fit than those limited to the GRACE score alone, we compared nested models using the likelihood-ratio test. Our results demonstrated that the addition of DC ($\chi^2 = 9.227$, df = 1, $p < 0.001$) significantly enriched the predictive power of the existing model including the GRACE score to predict the incidence of MACEs (**Table 5**). In addition, the inclusion of LF/HF ($\chi^2 = 0.329$, df = 1, $p = 0.416$) did not optimize the model fit.

The model including the GRACE score and DC had the lowest AICc and the highest Akaike's weight compared to the other two models, GRACE score alone and GRACE score with LF/HF (**Table 5**).

DC, but not LF/HF, combined with the GRACE score could improve the net reclassification of the updated model in predicting MACEs at the last follow-up date (**Table 6**, **Central illustration**). Employing continuous NRI ($NRI^{>0}$), DC enhanced reclassification by 7.3% for patients with MACEs and by 12.8% for patients without MACEs, demonstrating a significant overall improvement in net reclassification (NRI 0.200, $p = 0.003$). Entering DC into a logistic regression model including the GRACE score appeared to predict a lower risk of MACEs than the GRACE score alone in both the MACE and MACE-free survival groups. The addition of LF/HF did not improve reclassification (NRI 0.04, $p = 0.573$). The addition of DC, but not LF/HF to the established model including the GRACE score promoted integrated discrimination, as evident in **Table 6**, **Figure 3**. Moreover, our results generated an IDI of 1.04%, $p < 0.001$.

As presented in **Figure 3**, the c-statistic was 0.711 (95% CI 0.619–0.804, $p < 0.001$) for model 1 including the GRACE score only and 0.746 (95% CI 0.668–0.824, $p < 0.001$) for model 2 containing DC only. However, it was 0.765 (95% CI 0.686–0.844, $p < 0.001$) for the model including the GRACE score and DC (**Table 7**). For the prediction of MACEs, the positive c-statistic of the combined GRACE score was significantly improved in model 3 (AUC: 0.765; c-statistic: 0.783; 95% CI: 0.686–0.844; $p < 0.001$).

TABLE 2 | Predictors of the occurrence of major adverse cardiovascular events (MACEs) in patients with acute coronary syndrome (ACS): results of univariate and multivariate cox-regression analyses.

Indicators	Univariate				Multivariate			
	P-value	HR	95%CI		*P*-value	HR	95%CI	
Female (%)	0.547	0.817	0.423	1.577				
Age (years)	0.072	1.029	0.997	1.061				
Hypertension (%)	0.362	1.367	0.698	2.679				
Diabetes (%)	0.357	1.362	0.706	2.630				
Current smoker (%)	0.523	1.227	0.655	2.298				
History of drinking (%)	0.412	0.696	0.293	1.655				
Family history (%)	0.558	0.654	0.158	2.707				
History of MI (%)	0.001	2.922	1.513	5.643	0.172	1.672	0.800	3.496
Previous PCI (%)	0.118	1.649	0.880	3.088				
NSTE-ACS (%)	0.030	2.005	1.070	3.755	0.261	1.461	0.755	2.830
Neutrophil ($\times 10^9$/L)	0.204	1.016	0.991	1.042				
Lymphocyte ($\times 10^9$/L)	0.698	1.011	0.958	1.066				
NLR	0.001	1.053	1.021	1.087	0.191	1.052	0.975	1.135
PLT ($\times 10^9$/L)	0.753	0.999	0.994	1.005				
PLR	0.021	1.003	1.001	1.006	0.559	0.999	0.994	1.003
hs-CRP (mg/L)	0.509	1.004	0.992	1.016				
eGFR ml/(min1.73 m^2)	0.138	0.988	0.973	1.004				
Creatinine (μmol/L)	<0.001	1.011	1.006	1.015	0.160	1.005	0.998	1.011
Uric acid (μmol/L)	0.302	1.001	0.999	1.004				
Glucose (mmol/L)	0.955	1.003	0.891	1.131				
TG (mmol/L)	0.353	0.845	0.592	1.206				
TC (mmol/L)	0.710	0.945	0.703	1.271				
HDL-C (mmol/L)	0.443	0.645	0.211	1.977				
LDL-C (mmol/L)	0.457	0.880	0.630	1.231				
Lp (a) (g/L)	0.027	1.001	1.000	1.002	0.083	1.001	1.000	1.002
Average heart rate (bpm)	0.760	1.005	0.973	1.038				
SDNN (ms)	0.138	0.992	0.982	1.003				
SDANN (ms)	0.993	0.999	0.992	1.008				
rMSSD (ms)	0.566	0.997	0.985	1.008				
Pnn50	0.551	0.988	0.950	1.028				
LF (ms^2)	0.057	0.998	0.996	1.001				
HF (ms^2)	0.708	1.001	0.999	1.002				
LF/HF	0.074	0.750	0.547	1.029				
DC (ms)	<0.001	0.876	0.832	0.923	<0.001	0.885	0.831	0.943
GRACE score	<0.001	1.033	1.022	1.044	0.002	1.020	1.007	1.034
SBP (mmHg)	0.159	1.011	0.996	1.027				
DBP (mmHg)	0.566	1.007	0.982	1.033				
Aspirin (%)	0.225	0.633	0.302	1.325				
Clopidogrel (%)	0.871	1.052	0.570	1.941				
Ticagrelor (%)	0.365	0.518	0.125	2.147				
Statins (%)	0.241	0.539	0.192	1.513				
β-blocker (%)	0.169	1.563	0.828	2.950				
ACEI (%)	0.576	1.246	0.576	2.698				
ARB (%)	0.264	1.467	0.749	2.875				
CCB (%)	0.137	1.611	0.860	3.017				
In-hospital PCI (%)	0.904	0.963	0.519	1.784				
The number of stent	0.574	0.895	0.608	1.318				

NSTE-ACS, non-ST-elevation acute coronary syndromes; SBP, Systolic blood pressure; DBP, Diastolic blood pressure; eGFR, glomerular filtration rate; NLR, neutrophil-to-lymphocyte ratio; PLT, platelet count; PLR, platelet-to-lymphocyte ratio; TG, triglycerides; TC, total cholesterol; HDL-C, high-density lipoprotein cholesterol; LDL-C, low-density lipoprotein cholesterol; Apo A1, Apolipoprotein A1; Apo B, Apolipoprotein B; Lp (a), lipoprotein a; MI, myocardial infarction; hs-CRP, high-sensitivity C-reactive protein; CK-MB, creatine kinase-MB; SDNN, standard deviation of all normal sinus RR intervals; SDANN, standard deviation average of normal-to-normal (NN) intervals; pNN50, percentage of the number of times that the difference between adjacent normal RR intervals >50 ms in the total number of NN intervals; rMSSD, root mean square successive difference; HF, high-frequency power; LF, low-frequency power; LF/HF, low-frequency/high-frequency ratio; DC, deceleration capacity; ACEI, angiotensin converting enzyme inhibitor; ARB, angiotensin receptor blockers; CCB, calcium ion channel blockers; PCI, Percutaneous Transluminal Coronary Intervention.

TABLE 3 | Predictors of the occurrence of MACEs in patients with ST- segment Elevation Myocardial Infarction (STEMI): results of univariate and multivariate Cox-regression analyses.

Indicators	Univariate				Multivariate			
	P-value	HR	95% CI		*P*-value	HR	95% CI	
Female (%)	0.498	0.676	0.218	2.097				
Age (years)	0.094	1.043	0.993	1.096				
Hypertension (%)	0.463	0.691	0.257	1.855				
Diabetes (%)	0.066	2.523	0.939	6.776				
Current smoker (%)	0.233	1.824	0.679	4.899				
History of drinking (%)	0.540	0.676	0.193	2.371				
Family history (%)	0.745	0.714	0.094	5.409				
Past history of MI	0.162	2.242	0.723	6.954				
Previous PCI (%)	0.148	2.073	0.772	5.566				
Neutrophil ($\times 10^9$/L)	0.807	0.981	0.838	1.148				
Lymphocyte ($\times 10^9$/L)	0.087	0.433	0.166	1.131				
NLR	0.046	1.117	1.002	1.246	0.759	0.959	0.735	1.251
PLT ($\times$109/L)	0.795	1.001	0.993	1.010				
PLR	0.013	1.006	1.001	1.010	0.574	1.003	0.992	1.015
hs-CRP (mg/L)	0.043	1.018	1.001	1.035	0.622	1.006	0.982	1.032
eGFR ml / (min1.73 m^2)	0.728	0.995	0.966	1.024				
Creatinine (μmol/L)	0.369	1.005	0.994	1.016				
Uric acid (μmol/L)	0.324	1.002	0.998	1.006				
Glucose (mmol/L)	0.604	1.047	0.879	1.248				
TG (mmol/L)	0.156	0.569	0.261	1.240				
TC (mmol/L)	0.338	0.788	0.483	1.284				
HDL-C (mmol/L)	0.112	0.166	0.018	1.518				
LDL-C (mmol/L)	0.436	0.818	0.493	1.357				
Lp (a) (g/L)	0.145	1.001	0.999	1.003				
Average heart rate (bpm)	0.620	0.985	0.929	1.045				
SDNN (ms)	0.269	0.990	0.973	1.008				
SDANN (ms)	0.315	0.991	0.975	1.008				
rMSSD (ms)	0.426	0.992	0.972	1.012				
Pnn50	0.374	1.022	0.974	1.073				
LF (ms^2)	0.153	0.998	0.994	1.001				
HF (ms^2)	0.064	1.002	0.999	1.003				
LF/HF	0.145	0.698	0.429	1.133				
DC (ms)	0.003	0.888	0.820	0.961	0.016	0.901	0.828	0.981
GRACE score	0.002	1.031	1.011	1.052	0.043	1.024	1.001	1.048
SBP (mmHg)	0.466	0.990	0.965	1.016				
DBP (mmHg)	0.085	0.958	0.913	1.006				
Aspirin (%)	0.540	0.629	0.143	2.768				
Clopidogrel (%)	0.206	1.977	0.687	5.690				
Ticagrelor (%)	0.970	0.962	0.127	7.284				
Statins (%)	0.197	0.377	0.086	1.659				
β-blocker (%)	0.488	0.699	0.254	1.924				
ACEI (%)	0.634	1.357	0.387	4.762				
ARB (%)	0.419	1.594	0.514	4.942				
CCB (%)	0.841	1.123	0.362	3.483				
In-hospital PCI (%)	0.142	2.206	0.766	6.351				
The number of stent	0.510	1.181	0.720	1.938				

TABLE 4 | Predictors of the occurrence of MACEs in patients with Non-ST segment elevation myocardial infarction/ unstable angina (NSTEMI/UA): results of univariate and multivariate Cox-regression analyses.

Indicators	Univariate				Multivariate			
	P-value	HR	95%CI		*P*-value	HR	95%CI	
Female (%)	0.652	0.829	0.366	1.875				
Age (years)	0.528	1.013	0.973	1.055				
Hypertension (%)	0.082	2.386	0.895	6.359				
Diabetes (%)	0.687	0.828	0.331	2.073				
Current smoker (%)	0.740	1.159	0.484	2.775				
History of drinking (%)	0.940	0.955	0.286	3.190				
Family history (%)	0.719	0.692	0.094	5.117				
Past history of MI	0.005	3.243	1.432	7.344	0.159	1.937	0.772	4.858
Previous PCI (%)	0.428	1.391	0.615	3.149				
Neutrophil ($\times 10^9$/L)	0.311	1.013	0.988	1.039				
Lymphocyte ($\times 10^9$/L)	0.698	1.010	0.960	1.063				
NLR	0.024	1.042	1.005	1.079	0.048	1.041	1.000	1.084
PLT ($\times 10^9$/L)	0.648	0.998	0.991	1.006				
PLR	0.381	1.002	0.998	1.005				
hs-CRP (mg/L)	0.630	0.994	0.969	1.019				
eGFR	0.251	0.989	0.970	1.008				
Creatinine (μmol/L)	<0.001	1.021	1.013	1.030	0.011	1.013	1.003	1.024
Uric acid (μmol/L)	0.600	1.001	0.998	1.004				
Glucose (mmol/L)	0.717	0.971	0.829	1.138				
TG (mmol/L)	0.886	1.029	0.697	1.519				
TC (mmol/L)	0.493	1.156	0.764	1.751				
HDL-C (mmol/L)	0.666	1.341	0.354	5.084				
LDL-C (mmol/L)	0.926	1.024	0.625	1.677				
Lp (a) (g/L)	0.092	1.001	0.999	1.003				
Average heart rate	0.579	1.011	0.973	1.051				
SDNN (ms)	0.424	0.995	0.982	1.008				
SDANN (ms)	0.904	0.999	0.988	1.011				
rMSSD (ms)	0.628	1.004	0.988	1.020				
Pnn50	0.177	0.958	0.900	1.020				
LF (ms2)	0.241	0.999	0.997	1.001				
HF (ms2)	0.408	0.999	0.997	1.001				
LF/HF	0.715	0.926	0.612	1.400				
DC (ms)	<0.001	0.866	0.803	0.934	0.025	0.894	0.811	0.986
GRACE score	<0.001	1.031	1.017	1.045	0.024	1.019	1.002	1.036
SBP (mmHg)	0.014	1.024	1.005	1.044	<0.001	1.034	1.015	1.053
DBP (mmHg)	0.075	1.027	0.997	1.057				
Aspirin (%)	0.640	0.812	0.339	1.944				
Clopidogrel (%)	0.632	0.819	0.362	1.853				
Ticagrelor (%)	0.238	0.300	0.041	2.215				
Statins (%)	0.673	0.733	0.173	3.108				
β-blocker (%)	0.061	2.552	0.957	6.800				
ACEI (%)	0.849	1.100	0.413	2.931				
ARB (%)	0.657	1.210	0.522	2.803				
CCB (%)	0.202	1.666	0.760	3.652				
In-hospital PCI (%)	0.304	0.632	0.264	1.514				
The number of stent	0.319	0.729	0.392	1.357				

TABLE 5 | Akaike's information criteria and likelihood ratio test to determine the best fitting model for prediction MACEs.

Akaike's information criteria							Likelihood ratio test		
Model	**AICc**	**δAICc**	**Relative likelihood**	**wi**	**wj/wi**	**Model**	**χ^2**	**Df**	***P*-value**
GRACE score	781.44	5.82	0.15	0.14	4.18	GRACE score			
GRACE + LF/HF	776.35	4.29	0.21	0.20	5.35	GRACE+LF/HF	0.329	1	0.416
GRACE + DC	743.28	1.15	0.83	0.79	21.73	GRACE+DC	9.227	1	<0.001

TABLE 6 | Net reclassification improvement for model improvement with the addition of DC or LF/HF to GRACE.

	GRACE vs. GRACE + DC				GRACE vs. GRACE + LF/HF			
	NRIe	**NRIne**	**Total**	***P*-value**	**NRIe**	**NRIne**	**Total**	***P*-value**
UP	22	123	145		20	132	152	
DWN	19	159	178		21	150	171	
Total	41	282	323		41	282	323	
$NRI^{>0}$	0.073	0.128	0.200	0.003	−0.024	0.064	0.040	0.573
	IDIe	**IDIne**	**Total**	***P*-value**	**IDIe**	**IDIne**	**Total**	***P*-value**
Final	0.0089	0.0015	0.0104	<0.001	0.0003	0.0001	0.0004	0.422

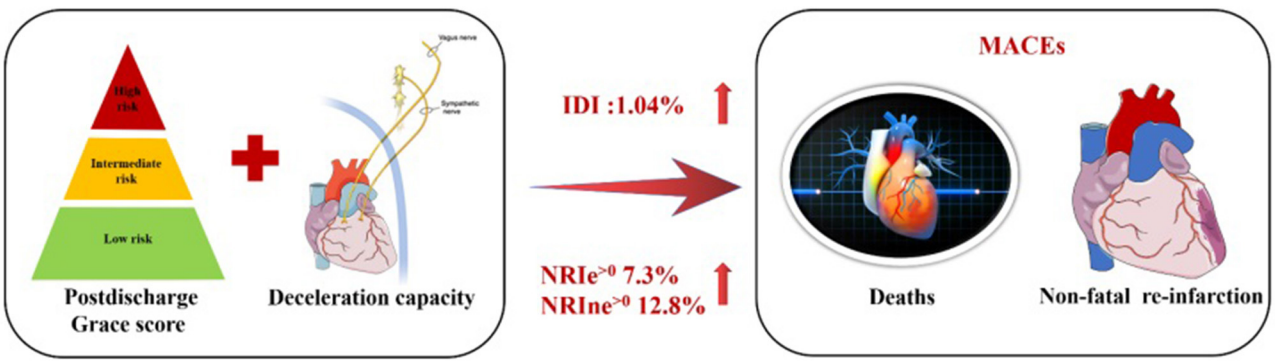

Central illlustration | Combined efficacies of DC and postdischarge GRACE score for risk stratification in patients with ACS.

DISCUSSION

Our studies now demonstrate that for ACS patients, wearable monitoring of cardiac ANS-related modulations by means of 24-h DC yields prognostic information beyond the known risk predictors. DC significantly optimizes risk stratification by the GRACE score concerning the prediction of MACEs during long-term follow-up. The prediction model including the postdischarge GRACE score and DC provided incremental prognostic information for long-term cohorts with established ACS. Furthermore, adding DC, rather than LF/HF, to the GRACE score could effectively improve the ability and accuracy of the GRACE score alone to predict MACEs after ACS.

Accumulating evidence supports the notion that the GRACE score provides valuable and independent prognostic information for ACS and enriches reliable risk stratification for identifying whether performing early PCI will benefit patients with ACS (3, 4, 19). In addition, previous study indicated that the GRACE score could predict short-term and long-term prognosis for ACS patients (20, 21). Although it is well established that the strong and effective prognostic value of the GRACE score has been confirmed by much evidence (3, 4, 19–21), early risk stratification remains urgently needed for further optimization, especially for low-risk patients with ACS. Therefore, previous studies have recently explored ways to improve the predictability of the prognostic GRACE score, including adding NT-pro-BNP (22), 2-h postload plasma glucose (23), plasma glucose blood inflammation-related indicators (24), plasma myeloperoxidase and trimethylamine N-oxide (25), serum acid uric acid (26) and nutritional risk index (27) to the GRACE score. The findings indicate that blood biochemical indexes and biomarkers provide incremental prognostic information for the predictive capacity of the GRACE score-based prognostic models. However, few studies have specifically focused on non-invasive markers and the GRACE score together to assess the joint prognostic effect.

Notably, the routine detection index of 24-h DC has also been considered to be a useful means for the screening and surveillance of high-risk post-MI patients (8). Moreover, our data are consistent with the finding that autonomic nervous system (ANS) imbalance carries a high risk for acute adverse events (28–30). The difference in risk between STEMI and NSTE-ACS may be explained by the different pathogenesis of the two diseases (31, 32). Therefore, our available data further demonstrated that DC remains an effective predictor in STEMI or NSTE-ACS.

In addition, other non-invasive indicators for the assessment of cardiac autonomic nerve function include HRV (7) and heart rate turbulence (33). However, heart rate turbulence and HRV indirectly reflect ANS modulation due to their poor stability, which limits their application in clinical practice (34–36). Nevertheless, DC is not susceptible to external interference and can reflect parasympathetic activity. Thus, in our study, DC, rather than LF/HF, could effectively increase the predictive capability of the postdischarge GRACE score-based prognostic models. A retrospective study that enrolled 1,821 patients with suspected ACS indicated a positive and independent correlation between short-term DC and short-term mortality among patients with suspected ACS (9). However, another study focused on the association between short-term DC combined with the admission GRACE score and short-term mortality, rather than the potential association between the 24-h DC combined with postdischarge GRACE score and long-term MACEs, which previously limited our understanding of the insights into the potential association between integration of the 24-h DC and postdischarge GRACE score and long-term poor outcomes. In addition, we used the 24-h Holter recordings to estimate the 24-h DC, which has been used as a daily clinical indicator in our practice. Additionally, patient's restrictively selected in the current study to minimize the impact of confounding factors on DC. Furthermore, we found that DC combined with the postdischarge GRACE score may reflect the interactions between ANS imbalance and adverse events, which may better predict poor long-term ensuing episodes of ACS. Given the recent increasing interest in individualized therapy for risk assessment, we believe that DC provides early valuable information for lifestyle modifications and monitoring of patients with ACS.

Physiologically, the ANS plays a crucial role in maintaining and promoting cardiac physiological function (37, 38). Pathologically, increasing research has confirmed that the context of acute myocardial ischemia could trigger an organismal stress response, induce cardiac sympathetic hyperactivity and suppress vagal activity, subsequently leading to coronary constriction, especially culprit vessel vasoconstriction, thus accelerating focal ischemia and hypoxia and causing the deterioration of myocardial ischemia (34, 39). In addition, previous clinical and basic research has shown that the vagus nerve of the ANS is involved in the regulation of the inflammatory response (40, 41), and the potential link among the ANS, inflammation and coronary artery physiology was confirmed by our previous studies (42, 43). Furthermore, our data confirmed that injured cardiac autonomic nerves in the setting of myocardial ischemia subsequently developed an elevated risk of MACEs after ACS. Therefore, we believe that the combination of DC and the GRACE score could enhance risk discrimination and provide important incremental prognostic information for long-term follow-up after ACS.

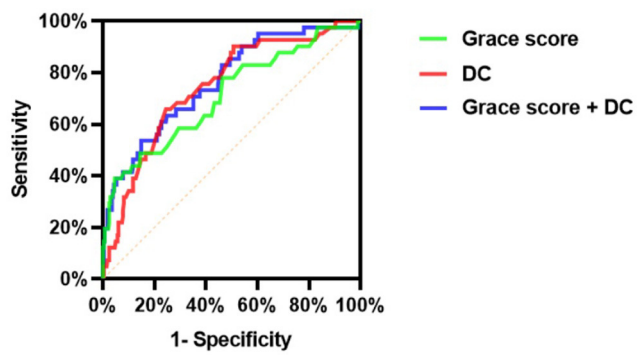

FIGURE 3 | Comparison of discrimination and reclassification abilities of predictive models for MACEs (Model 1: Grace score; Model 2: DC; Model 3: Grace score + DC).

STUDY LIMITATIONS

First, due to the purely retrospective observational design with long-term follow-up, our results were almost inevitably affected by recall bias and lost follow-up (44, 45). Second, this study has a small sample size and likely suffered from a lack of power. Our findings should be validated with larger samples and prospective studies in the future. Third, our study did not include coronary physiology, which might improve the predictive power when combined with DC and postdischarge GRACE scores. Thus, many known confounding factors were eliminated, but there was no guarantee about other unknown confounding factors. Finally, because it was a purely observational study, whether individualized and comprehensive therapy based on DC-optimized risk models translates into better outcomes remains to be established. Finally, we included only patients wih sinusrhythm, and the influence

TABLE 7 | ROC analysis comparing the predictive efficacies of related variables for the incidence of MACEs during follow up.

Model	AUC	SE	*P*-value	95%CI	Cut-off	Sensitivity	Specificity	Youden index	C-statistic
Model 1	0.711	0.047	<0.001	0.619–0.804	116.5	48.8	85.5	0.343	0.726
Model 2	0.746	0.040	<0.001	0.668–0.824	3.51	53.7	85.1	0.388	0.759
Model 3	0.765	0.040	<0.001	0.686–0.844	-	65.9	75.5	0.414	0.783

Model 1, Grace score; Model 2, DC; Model 3, Grace score + DC.

of the non-sinus rhythm in patients with ACS remains to be seen.

CONCLUSIONS

Our study indicates that wearable devices that automatically evaluate the cardiac ANS by means of the 24-h DC value tend to be a useful risk-stratified indicator for MACEs among ACS patients, regardless of the type of ACS. Moreover, DC further optimized the GRACE score, which has long been regarded as the gold standard for quantitative risk assessment after ACS, providing increased discriminatory ability and accuracy for prognostic information. Where applicable, we highlight that attention should be given to implementing DC as part of comprehensive cardiovascular evaluation and clinical decision-making to enable us to design individualized prognostic therapies.

DATA AVAILABILITY STATEMENT

The datasets used and/or analyzed during this study are available from the corresponding author on reasonable request. Requests to access these datasets should be directed to LY, lileiyu@whu.edu.cn.

ETHICS STATEMENT

Ethical approval was not provided for this study on human participants because this was a retrospective observational study, the Renmin Hospital of Wuhan University Ethics Committee granted an exemption from requiring ethics approval and informed consent from eligible patients was waived. The Ethics Committee waived the requirement of written informed consent for participation.

AUTHOR CONTRIBUTIONS

LY and HJ: substantial contributions to conception and design, data acquisition, or data analysis, and interpretation. LS, CL, JS, QD, YiW, ZZ, FG, LZ, YuW, and WT: drafting the article or critically revising it for important intellectual content. SD, JW, and FY: final approval of the version to be published and agreement to be accountable for all aspects of the work in ensuring that questions related to the accuracy or integrity of the work are appropriately investigated and resolved. All authors contributed to the article and approved the submitted version.

FUNDING

National Natural Science Foundation of China [81871486, 81970287, and 82100530].

REFERENCES

1. Khot UN, Khot MB, Bajzer CT, Sapp SK, Ohman EM, Brener SJ, et al. Prevalence of conventional risk factors in patients with coronary heart disease. *JAMA*. (2003) 290:898–904. doi: 10.1001/jama.290.7.898
2. Greenland P, Knoll MD, Stamler J, Neaton JD, Dyer AR, Garside DB, et al. Major risk factors as antecedents of fatal and nonfatal coronary heart disease events. *JAMA*. (2003) 290:891–7. doi: 10.1001/jama.290.7.891
3. Fox KA, Dabbous OH, Goldberg RJ, Pieper KS, Eagle KA, Van de Werf F, et al. Prediction of risk of death and myocardial infarction in the six months after presentation with acute coronary syndrome: prospective multinational observational study (GRACE). *BMJ*. (2006) 333:1091. doi: 10.1136/bmj.38985.646481.55
4. Eagle KA, Lim MJ, Dabbous OH, Pieper KS, Goldberg RJ, Van de Werf F, et al. A validated prediction model for all forms of acute coronary syndrome: estimating the risk of 6-month postdischarge death in an international registry. *JAMA*. (2004) 291:2727–33. doi: 10.1001/jama.291.22.2727
5. Bauer A, Barthel P, Müller A, Ulm K, Huikuri H, Malik M, et al. Risk prediction by heart rate turbulence and deceleration capacity in postinfarction patients with preserved left ventricular function retrospective analysis of 4 independent trials. *J Electrocardiol*. (2009) 42:597–601. doi: 10.1016/j.jelectrocard.2009.07.013
6. Kisohara M, Stein PK, Yoshida Y, Suzuki M, Iizuka N, Carney RM, et al. Multi-scale heart rate dynamics detected by phase-rectified signal averaging predicts mortality after acute myocardial infarction. *Europace*. (2013) 15:437–43. doi: 10.1093/europace/eus409
7. Tsuji H, Larson MG, Venditti FJ Jr, Manders ES, Evans JC, Feldman CL, et al. Impact of reduced heart rate variability on risk for cardiac events. the framingham heart study. *Circulation*. (1996) 94:2850–5. doi: 10.1161/01.CIR.94.11.2850
8. Bauer A, Kantelhardt JW, Barthel P, Schneider R, Mäkikallio T, Ulm K, et al. Deceleration capacity of heart rate as a predictor of mortality after myocardial infarction: cohort study. *Lancet*. (2006) 367:1674–81. doi: 10.1016/S0140-6736(06)68735-7
9. Eick C, Duckheim M, Groga-Bada P, Klumpp N, Mannes S, Zuern CS, et al. Point-of-care testing of cardiac autonomic function for risk assessment in patients with suspected acute coronary syndromes. *Clin Res Cardiol*. (2017) 106:686–94. doi: 10.1007/s00392-017-1104-3
10. Mendis S, Thygesen K, Kuulasmaa K, Giampaoli S, Mähönen M, Ngu Blackett K, et al. World Health Organization definition of myocardial infarction: 2008-09 revision. *Int J Epidemiol*. (2011) 40:139–46. doi: 10.1093/ije/dyq165
11. Eick C, Rizas KD, Zuern CS, Bauer A. Automated assessment of cardiac autonomic function by means of deceleration capacity from noisy, nonstationary ECG signals: validation study. *Ann Noninvasive Electrocardiol*. (2014) 19:122–8. doi: 10.1111/anec.12107
12. Catai AM, Pastre CM, Godoy MF, Silva ED, Takahashi ACM, Vanderlei LCM. Heart rate variability: are you using it properly? standardisation checklist of procedures. *Braz J Phys Ther*. (2020) 24:91–102. doi: 10.1016/j.bjpt.2019.02.006
13. Wang X, Liu B, Xie L, Yu X, Li M, Zhang J. Cerebral and neural regulation of cardiovascular activity during mental stress. *Biomed Eng Online*. (2016) 15:160. doi: 10.1186/s12938-016-0255-1
14. Heart rate variability. Standards of measurement, physiological interpretation, and clinical use. task force of the European society of cardiology and the North American society of pacing and electrophysiology. *Eur Heart J*. (1996) 17:354–81.
15. Hanss R, Bein B, Weseloh H, Bauer M, Cavus E, Steinfath M, et al. Heart rate variability predicts severe hypotension after spinal anesthesia. *Anesthesiology*. (2006) 104:537–45. doi: 10.1097/00000542-200603000-00022
16. Pan Y, Yu Z, Yuan Y, Han J, Wang Z, Chen H, et al. Alteration of autonomic nervous system is associated with severity and outcomes in patients with COVID-19. *Front Physiol*. (2021) 12:630038. doi: 10.3389/fphys.2021.630038
17. Filipovic M, Jeger R, Probst C, Girard T, Pfisterer M, Gürke L, et al. Heart rate variability and cardiac troponin I are incremental and independent predictors of one-year all-cause mortality after major noncardiac surgery in patients

at risk of coronary artery disease. *J Am Coll Cardiol.* (2003) 42:1767–76. doi: 10.1016/j.jacc.2003.05.008
18. Wagenmakers EJ, Farrell S. AIC model selection using Akaike weights. *Psychon Bull Rev.* (2004) 11:192–6. doi: 10.3758/BF03206482
19. Elbarouni B, Goodman SG, Yan RT, Welsh RC, Kornder JM, Deyoung JP, et al. Validation of the global registry of acute coronary event (GRACE) risk score for in-hospital mortality in patients with acute coronary syndrome in Canada. *Am Heart J.* (2009) 158:392–9. doi: 10.1016/j.ahj.2009.06.010
20. Raposeiras-Roubín S, Abu-Assi E, Cambeiro-González C, Álvarez-Álvarez B, Pereira-López E, Gestal-Romaní S, et al. Mortality and cardiovascular morbidity within 30 days of discharge following acute coronary syndrome in a contemporary European cohort of patients: How can early risk prediction be improved? the six-month GRACE risk score. *Rev Port Cardiol.* (2015) 34:383–91. doi: 10.1016/j.repc.2014.11.020
21. Alnasser SM, Huang W, Gore JM, Steg PG, Eagle KA, Anderson FA Jr, et al. Late consequences of acute coronary syndromes: global registry of acute coronary events (GRACE) follow-up. *Am J Med.* (2015) 128:766–75. doi: 10.1016/j.amjmed.2014.12.007
22. Onda T, Inoue K, Suwa S, Nishizaki Y, Kasai T, Kimura Y, et al. Reevaluation of cardiac risk scores and multiple biomarkers for the prediction of first major cardiovascular events and death in the drug-eluting stent era. *Int J Cardiol.* (2016) 219:180–5. doi: 10.1016/j.ijcard.2016.06.014
23. Chattopadhyay S, George A, John J, Sathyapalan T. Adjustment of the GRACE score by 2-hour post-load glucose improves prediction of long-term major adverse cardiac events in acute coronary syndrome in patients without known diabetes. *Eur Heart J.* (2018) 39:2740–5. doi: 10.1093/eurheartj/ehy233
24. Oncel RC, Ucar M, Karakas MS, Akdemir B, Yanikoglu A, Gulcan AR, et al. Relation of neutrophil-to-lymphocyte ratio with GRACE risk score to in-hospital cardiac events in patients with ST-segment elevated myocardial infarction. *Clin Appl Thromb Hemost.* (2015) 21:383–8. doi: 10.1177/1076029613505763
25. Tan Y, Zhou J, Yang S, Li J, Zhao H, Song L, et al. Addition of plasma myeloperoxidase and trimethylamine N-Oxide to the GRACE score improves prediction of near-term major adverse cardiovascular events in patients with ST-segment elevation myocardial infarction. *Front Pharmacol.* (2021) 12:632075. doi: 10.3389/fphar.2021.632075
26. Centola M, Maloberti A, Castini D, Persampieri S, Sabatelli L, Ferrante G, et al. Impact of admission serum acid uric levels on in-hospital outcomes in patients with acute coronary syndrome. *Eur J Intern Med.* (2020) 82:62–7. doi: 10.1016/j.ejim.2020.07.013
27. Ma XT, Shao QY, Li QX, Yang ZQ, Han KN, Liang J, et al. Nutritional risk index improves the grace score prediction of clinical outcomes in patients with acute coronary syndrome undergoing percutaneous coronary intervention. *Front Cardiovasc Med.* (2021) 8:773200. doi: 10.3389/fcvm.2021.773200
28. Schwartz PJ, La Rovere MT, Vanoli E. Autonomic nervous system and sudden cardiac death. experimental basis and clinical observations for post-myocardial infarction risk stratification. *Circulation.* (1992) 85:I77–91.
29. Münzel T, Schmidt FP, Steven S, Herzog J, Daiber A, Sørensen M. Environmental noise and the cardiovascular system. *J Am Coll Cardiol.* (2018) 71:688–97. doi: 10.1016/j.jacc.2017.12.015
30. Dutta P, Courties G, Wei Y, Leuschner F, Gorbatov R, Robbins CS, et al. Myocardial infarction accelerates atherosclerosis. *Nature.* (2012) 487:325–9. doi: 10.1038/nature11260
31. McManus DD, Gore J, Yarzebski J, Spencer F, Lessard D, Goldberg RJ. Recent trends in the incidence, treatment, and outcomes of patients with STEMI and NSTEMI. *Am J Med.* (2011) 124:40–7. doi: 10.1016/j.amjmed.2010.07.023
32. Park HW, Yoon CH, Kang SH, Choi DJ, Kim HS, Cho MC, et al. Early- and late-term clinical outcome and their predictors in patients with ST-segment elevation myocardial infarction and non-ST-segment elevation myocardial infarction. *Int J Cardiol.* (2013) 169:254–61. doi: 10.1016/j.ijcard.2013.08.132
33. Schmidt G, Malik M, Barthel P, Schneider R, Ulm K, Rolnitzky L, et al. Heart-rate turbulence after ventricular premature beats as a predictor of mortality after acute myocardial infarction. *Lancet.* (1999) 353:1390–6. doi: 10.1016/S0140-6736(98)08428-1
34. Huikuri HV, Stein PK. Heart rate variability in risk stratification of cardiac patients. *Prog Cardiovasc Dis.* (2013) 56:153–9. doi: 10.1016/j.pcad.2013.07.003
35. Makai A, Korsós A, Makra P, Forster T, Abrahám G, Rudas L. Spontaneous baroreflex sensitivity and heart rate turbulence parameters: parallel responses to orthostasis. *Clin Auton Res.* (2008) 18:74–9. doi: 10.1007/s10286-008-0458-z
36. Segerson NM, Wasmund SL, Abedin M, Pai RK, Daccarett M, Akoum N, et al. Heart rate turbulence parameters correlate with post-premature ventricular contraction changes in muscle sympathetic activity. *Heart Rhythm.* (2007) 4:84–9. doi: 10.1016/j.hrthm.2006.10.020
37. Horackova M, Armour JA. Role of peripheral autonomic neurones in maintaining adequate cardiac function. *Cardiovasc Res.* (1995) 30:26–35. doi: 10.1016/0008-6363(95)00105-0
38. Dyavanapalli J, Dergacheva O, Wang X, Mendelowitz D. Parasympathetic vagal control of cardiac function. *Curr Hypertens Rep.* (2016) 18:22. doi: 10.1007/s11906-016-0630-0
39. Schäfer D, Nil M, Herzig D, Eser P, Saner H, Wilhelm M. Good reproducibility of heart rate variability after orthostatic challenge in patients with a history of acute coronary syndrome. *J Electrocardiol.* (2015) 48:696–702. doi: 10.1016/j.jelectrocard.2015.04.004
40. Williams DP, Koenig J, Carnevali L, Sgoifo A, Jarczok MN, Sternberg EM, et al. Heart rate variability and inflammation: A meta-analysis of human studies. *Brain Behav Immun.* (2019) 80:219–26. doi: 10.1016/j.bbi.2019.03.009
41. Tracey KJ. The inflammatory reflex. *Nature.* (2002) 420:853–9. doi: 10.1038/nature01321
42. Wang J, Liu W, Chen H, Liu C, Wang M, Chen H, et al. Novel insights into the interaction between the autonomic nervous system and inflammation on coronary physiology: a quantitative flow ratio study. *Front Cardiovasc Med.* (2021) 8:700943. doi: 10.3389/fcvm.2021.700943
43. Liu C, Yu Z, Chen H, Wang J, Liu W, Zhou L, et al. Relationship between immunoinflammation and coronary physiology evaluated by quantitative flow ratio in patients with coronary artery disease. *Front Cardiovasc Med.* (2021) 8:714276. doi: 10.3389/fcvm.2021.714276
44. Xiaonan X, Ilir A, Kim Mimi Y, Wang T, Lin J, Ghavamian R, et al. New methods for estimating follow-up rates in cohort studies. *BMC Med Res Methodol.* (2017) 17:155. doi: 10.1186/s12874-017-0436-z
45. Vena JE, Sultz HA, Carlo GL, Fiedler RC, Barnes RE. Sources of bias in retrospective cohort mortality studies: a note on treatment of subjects lost to follow-up. *J Occup Med.* (1987) 29:256–61.

Conflict of Interest: The authors declare that the research was conducted in the absence of any commercial or financial relationships that could be construed as a potential conflict of interest.

Publisher's Note: All claims expressed in this article are solely those of the authors and do not necessarily represent those of their affiliated organizations, or those of the publisher, the editors and the reviewers. Any product that may be evaluated in this article, or claim that may be made by its manufacturer, is not guaranteed or endorsed by the publisher.

frontiers | Frontiers in Cardiovascular Medicine

ORIGINAL RESEARCH
published: 20 June 2022
doi: 10.3389/fcvm.2022.903778

Markers of Atrial Cardiopathy in Severe Embolic Strokes of Undetermined Source

Maurizio Acampa[1], Alessandra Cartocci[2], Carlo Domenichelli[1], Rossana Tassi[1], Francesca Guideri[1], Pietro Enea Lazzerini[3†] and Giuseppe Martini[1†]*

[1] Stroke Unit, Department of Emergency-Urgency and Transplants, Azienda Ospedaliera Universitaria Senese, "Santa Maria alle Scotte" General Hospital, Siena, Italy, [2] Department of Medical Biotechnology, University of Siena, Siena, Italy, [3] Department of Medical Sciences, Surgery and Neurosciences, University of Siena, Siena, Italy

OPEN ACCESS

Edited by:
Nicola Mumoli,
ASST Ovest Milanese, Italy

Reviewed by:
Ching-Hui Sia,
National University of Singapore, Singapore
Igor Giarretta,
Circolo Hospital and Macchi Foundation, Italy

***Correspondence:**
Maurizio Acampa
M.Acampa@ao-siena.toscana.it

[†] These authors have contributed equally to this work

Specialty section:
This article was submitted to General Cardiovascular Medicine, a section of the journal Frontiers in Cardiovascular Medicine

Received: 24 March 2022
Accepted: 30 May 2022
Published: 20 June 2022

Citation:
Acampa M, Cartocci A, Domenichelli C, Tassi R, Guideri F, Lazzerini PE and Martini G (2022) Markers of Atrial Cardiopathy in Severe Embolic Strokes of Undetermined Source. Front. Cardiovasc. Med. 9:903778. doi: 10.3389/fcvm.2022.903778

Background and Purpose: The current definition of embolic strokes of undetermined source (ESUS) seems to be too broad, including strokes due to heterogeneous mechanisms, such as atrial cardiopathy and other occult cardiac conditions, aortic arch plaques, and non-stenosing atherosclerosis, that can be differently associated with clinical stroke severity at the time of presentation. The aim of our study was to assess the possible association between neurological deficit severity and presence of markers of atrial cardiopathy in ESUS.

Methods: We retrospectively reviewed the medical records of a cohort of 226 ESUS patients (105 M, 121 F), that were divided into two groups according to the severity of neurological deficit (99 mild strokes with NIHSS $\leq$5 and 127 severe strokes with NIHSS >5). The following indices of atrial cardiopathy were evaluated: P wave dispersion, P wave max, P wave min, P wave mean, P wave index, P wave axis, left atrial size.

Results: Patients with severe ESUS were significantly older (74 $\pm$ 12 vs. 67 $\pm$ 14 years, $P < 0.001$) and female sex was prevalent (67 vs. 36%, $P > 0.001$); they had higher values of P-wave-dispersion (51 $\pm$ 14 vs. 46 $\pm$ 13, $P = 0.01$), P-wave-max (131 $\pm$ 20 vs. 125 $\pm$ 15 ms, $P = 0.01$), P-wave-index (16 $\pm$ 5 vs. 15 $\pm$ 5 ms, $P = 0.01$), left atrial size (20 $\pm$ 6 vs. 18 $\pm$ 4 cm^2, $P = 0.01$), left atrial volume index (31 $\pm$ 14 vs. 27 $\pm$ 11 ml/m^2, $P = 0.04$), in comparison with mild ESUS. An abnormal P wave axis was detected more frequently in severe ESUS (21 vs. 9%, $P = 0.01$). Furthermore, multivariate logistic regression showed that age (OR = 1.21 for each 5-year increase, 95% CI 1.09–1.35), sex (OR = 3.24 for female sex, 95% CI 1.82–5.76) and PWD (OR = 1.32 for each 10-ms increase, 95% CI 1.07–1.64) were the best subset of associated variables for severe ESUS.

Conclusions: Our findings shed light on specific clinical characteristics of severe ESUS including the presence of atrial cardiopathy that could play a pathogenic role in this subgroup of patients. Searching for atrial fibrillation in these patients is especially important to perform the most appropriate therapy.

Keywords: ischemic stroke, ESUS, atrial cardiopathy, atrial fibrillation, cardioembolism, ECG, P-wave-dispersion

INTRODUCTION

Embolic strokes of undetermined source (ESUS) represent 17% of ischemic strokes (1). Even if embolism is presumably the underlying mechanism of these strokes, the current definition of ESUS seems to be too broad (2), including heterogeneous causes, such as occult cardiac conditions (atrial cardiopathy, patent foramen ovale), aortic arch plaques, or non-stenosing atherosclerosis of large cervical and intracranial arteries. These different possible mechanisms have suggested a reexamination of the ESUS concept (3), with the goal of improving specificity for detecting patients with a cardioembolic cause, in order to provide a more appropriate therapy for secondary stroke prevention.

Although clinical characteristics alone cannot reliably classify the underlying cause of ischemic stroke (4), higher National Institutes of Health Stroke Scale (NIHSS) score is usually associated with cardioembolic etiology (5). Furthermore, patients with severe ESUS (NIHSS score >5) have different clinical characteristics and outcome with higher mortality rate in comparison with patients with mild ESUS (6). These findings suggest a possible role of cardioembolic mechanisms (especially due to atrial cardiopathy) in determining severe ESUS.

In this view, we assessed the possible relationships between severity of neurological deficit at the time of presentation and prevalence of markers of atrial cardiopathy in ESUS patients.

MATERIALS AND METHODS

The data that support the findings of this study are available from the corresponding author upon reasonable request. We retrospectively reviewed the medical records of a cohort of 226 patients, admitted consecutively to our Stroke Unit (Siena University Hospital) for ESUS from January 1st 2017 to 30th December 2020. The eligibility criteria were based on the definition of ESUS, proposed by the Cryptogenic Stroke/ESUS International Working Group (7). Neurological status at admission was assessed by using the NIHSS score. All patients underwent neuroimaging examination (brain CT with angio-CT scan and/or brain magnetic resonance imaging), extracranial and transcranial arterial ultrasound, transthoracic echocardiography, 12-lead electrocardiogram, 24-h electrocardiogram. The study was approved by the Ethics Committee of the University Hospital of Siena, Italy.

Markers of Atrial Cardiopathy

P Wave Duration and P Wave Dispersion

Simultaneous 12-lead ECG (25 mm/s and 10 mV/cm) was recorded by means of commercially available imaging system (Cardioline ECT WS 2000, Remco Italia, Vignate-Milano, Italy) in all subjects in supine position (during spontaneous breathing) at the time of admission. Paper-printed ECGs were scanned and digitized in order to achieve greater precision in detecting and measuring P waves (8); onscreen measurement of P wave duration was made by a single observer (M.A.), that had no knowledge about the severity of ESUS, by means of Adobe Photoshop CC 2017 software. P wave duration was measured from the beginning of the P wave deflection from the isoelectric line to the end of the deflection returning to isoelectric line in all simultaneous 12 leads. Our measurement method has been reported in our previous study (9), that demonstrated acceptable intra observer and inter observer errors in the measurement of P-wave duration in 12-lead ECGs, according to other previous papers (8, 10). The following indices were derived from measurements of each ECG: the maximum P wave duration (P max), the minimum P wave duration (P min), the P wave dispersion (PWD), defined as the difference between P maximum and P minimum, P-wave-mean and P-wave-index (the average and standard deviation of P wave duration across all 12 leads). Normal PWD values were lower than 40 ms (11–13).

P-Wave Axis

P-wave axis was determined by measuring the positive or negative P-wave deflections on all six limb leads and then calculating the net direction of electric activity using the hexaxial reference system. Automated analysis of ECG data was conducted including selective averaging to obtain representative durations and amplitudes of ECG components to calculate the frontal P-wave axis. An abnormal PWA was defined as any value outside the range between 0 and 75° (14).

Left Atrial Size and Mitral/Aortic Valve Disease

Left atrial size was evaluated by transthoracic echocardiography, measuring left atrial area in four-chamber apical view and left atrial volume index using the biplane area-length method (15). Furthermore, the presence of some minor-risk potential cardioembolic sources, such as mitral and aortic valve calcifications, was also evaluated.

Non-stenotic Carotid Plaques

According to the methods previously described (16), we evaluated the possible presence of non-stenotic (<50% diameter stenosis) atherosclerotic carotid artery plaques in all patients.

Statistical Analysis

Statistical analysis was performed using the GraphPad Instat computer software (version 3.06 for Windows, GraphPad Software Inc., La Jolla, CA, USA). All results were presented as mean ± SD values. Normal distribution of quantitative variables was preliminary tested using the Kolmogorov–Smirnov test. Patients were dichotomized into two groups according to the severity of neurological deficit evaluated by NIHSS score: mild ischemic stroke was defined as presenting NIHSS score of 0–5 and severe ischemic stroke as presenting NIHSS score of 6–41. We also performed a sample size and power analysis to define the number of subjects to include in the ESUS cohort: a sample size of 226 was estimated considering a chi-squared test, with alpha of 0.05, power of 0.95 and a medium effect size of 0.25.

Mann-Whitney test was performed to compare age, electrocardiographic and echocardiographic markers of atrial cardiopathy in patients with mild stroke and severe stroke. The two-sided Fisher's exact test was performed to evaluate statistical correlation between categorical variables in both groups of patients. To determine the factors associated with severe ESUS a multivariate logistic regression was performed (with the stepwise

TABLE 1 | Characteristics of ESUS patients with mild and severe neurological deficit.

	Mild ESUS (NIHSS ≤5) (*n* = 99)	Severe ESUS (NIHSS >5) (*n* = 127)	*P*-Value
Age (years)	67 ± 14	74 ± 12	**0.0001**
Women/men	36:63	85:42	**0.0001**
Cardiovascular risk factors			
Hypertension, *n* (%)	52 (52%)	82 (65%)	0.07
Diabetes mellitus, *n* (%)	25 (25%)	21 (17%)	0.1
Hypercholesterolemia, *n* (%)	38 (38%)	47 (37%)	0.8
Previous CAD, *n* (%)	7 (7%)	12 (9%)	0.6
Previous stroke, *n* (%)	7 (7%)	10 (8%)	1
Current smoking, *n* (%)	24 (24%)	25 (20%)	0.4
Minor-risk potential embolic sources, *n* (%)			
Mitral valve calcifications	22 (22%)	51 (40%)	**0.004**
Aortic valve calcifications	33 (33%)	54 (42%)	0.1
Non-atrial fibrillation atrial dysrhythmias	1 (1%)	1 (0.7%)	1
Hypokinetic/akinetic left ventricle	2 (2%)	5 (3%)	0.4
Moderate-to-severely dilated left atrium	1 (1%)	10 (7%)	**0.02**
Atrial septal aneurysm	15 (15%)	14 (11%)	0.4
Patent foramen ovale	16 (16%)	12 (9%)	0.1
Aortic arch atherosclerotic plaques	1 (1%)	3 (2%)	0.6
Carotid artery non-stenotic plaques	59 (59%)	76 (60%)	1
Atrial cardiopathy markers			
PWD (ms)	46 ± 13	51 ± 14	**0.01**
P wave max (ms)	125 ± 15	131 ± 20	**0.01**
P wave min (ms)	79 ± 15	81 ± 20	0.7
P wave mean (ms)	103 ± 13	107 ± 18	0.05
P wave index (ms)	15 ± 5	16 ± 5	**0.01**
PR interval (ms)	166 ± 35	171 ± 33	0.3
P wave axis (degree)	47 ± 22	50 ± 27	0.3
Left atrial area (cm^2)	18 ± 4	20 ± 6	**0.01**
High PWD (>40 ms), *n* (%)	53 (53%)	87 (68%)	**0.02**
Abnormal P wave axis, *n* (%)	9 (9%)	27 (21%)	**0.01**
LA dilation (>20 cm^2), *n* (%)	28 (28%)	54 (42%)	**0.03**
LA volume (ml)	48 ± 19	54 ± 24	0.1
LA volume index (ml/m^2)	27 ± 11	31 ± 14	**0.04**

Data are expressed as mean ± SD. CAD, coronary artery disease; PWD, P wave dispersion; LA, left atrium. Bold values are statistically significant (p < 0.05).

procedure based on Akaike's criterion) and corresponding Odds Ratio (OR) and their confidence intervals (CI) were calculated. A *P* value below 0.05 was considered statistically significant.

RESULTS

We enrolled 226 patients with ESUS (105 males, 121 females). Patients were divided into two groups according to the severity of neurological deficit: 99 patients with mild stroke (NIHSS ≤5) and 127 with severe stroke (NIHSS >5).

In severe ESUS the average age was higher (74 ± 12 vs. 67 ± 14 years, $P < 0.001$) and female sex was prevalent (66 vs. 36%, $P < 0.001$).

Both groups were similar in terms of other cardiovascular risk factors (**Table 1**).

The presence of non-stenotic (<50% diameter stenosis) atherosclerotic carotid artery plaques was also similar in both groups.

Moreover, there were no differences between patients with severe and mild ESUS regarding minor-risk potential embolic sources, except for mitral valve calcifications (40% of patients in severe ESUS vs. 22% in mild ESUS; $P = 0.004$).

Markers of Atrial Cardiopathy

Patients with severe ESUS had higher values of PWD (51 ± 14 vs. 46 ± 13, $P = 0.01$), P max (131 ± 20 vs. 125 ± 15 ms, $P = 0.01$), and P wave index (16 ± 5 vs. 15 ± 5 ms, $P = 0.01$). The number of patients with increased PWD (>40 ms) was higher in severe ESUS than in mild ESUS (87/127 vs. 53/99; $P =$

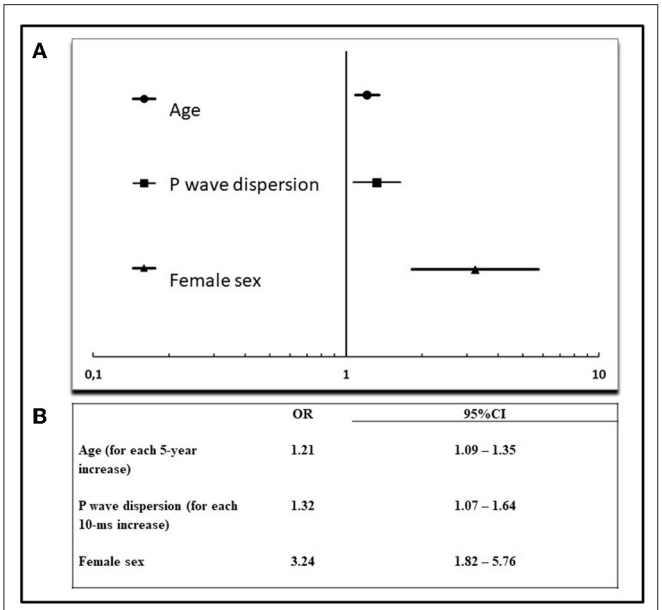

	OR	95%CI
Age (for each 5-year increase)	1.21	1.09 – 1.35
P wave dispersion (for each 10-ms increase)	1.32	1.07 – 1.64
Female sex	3.24	1.82 – 5.76

FIGURE 1 | Multivariate analysis of factors associated with severe ESUS. **(A)** Forest plot of significant factors associated with severe ESUS (according to Akaike's information criterion), **(B)** results of multivariate analysis. OR, odds ratio; CI, confidence interval.

0.02). Furthermore, an abnormal P wave axis was detected more frequently in severe stroke patients (21 vs. 9%, *P*: 0.01).

Left atrial size was significantly increased in severe ESUS in comparison with mild ESUS in terms of area (20 ± 6 vs. 18 ± 4 cm^2, $P = 0.01$) and volume (31 ± 14 vs. 27 ± 11 ml/m^2, $P = 0.04$); in particular, the percentage of patients with increased left atrial area (>20 cm^2) was higher in severe ESUS than in mild ESUS (54/127 vs. 28/99; $P = 0.03$) and, similarly, the number of patients with moderate-severe LA dilation (≥ 30 cm^2) was significantly higher in severe than in mild ESUS (10/127 vs. 1/99; $P = 0.02$) (**Table 1**).

Multivariate Analysis

Multivariate logistic regression model was constructed to determine the factors associated with severe ESUS. The following variables were initially evaluated: age, sex, PWD, P-max, P-mean, P index, PQ interval, abnormal P axis, left atrial area, left atrial volume index, atrial dilation (left atrial area >20 cm^2), moderate-severe atrial dilation (left atrial area ≥30 cm^2), MV disease. Akaike's information criterion showed that the best subset of associated variables for severe ESUS were the following: age (OR = 1.21 for each 5-year increase, 95% CI: 1.09–1.35), sex (OR = 3.24 for female sex, 95% CI: 1.82–5.76), PWD (OR = 1.32 for each 10 ms increase, 95% CI: 1.07–1.64) (**Figure 1**).

DISCUSSION

The novel findings of our study are the following: there is a significant association between markers of atrial cardiopathy and severe ESUS, and this association, specifically for PWD, is independent of other clinical characteristics such as age and sex.

Indeed, in patients with severe ESUS we found the presence of both electrocardiographic and echocardiographic markers of atrial cardiopathy, including an increased P wave dispersion, P wave index, a higher rate of abnormal P wave axis, an increased left atrial size and a higher frequency of mitral valve calcifications in comparison with mild ESUS patients. These markers besides being atrial cardiopathy markers, also represent significant predictors of AF. Indeed, previous studies demonstrated that left atrial volume index is associated with new-onset AF and stroke recurrence in ESUS patients (17), many electrocardiographic markers of atrial cardiopathy can predict AF occurrence (18) and mitral valve calcification, even when asymptomatic, is associated with increased risk for AF (19) and stroke (20).

These findings suggest that atrial cardiopathy can represent the pathogenic mechanism underlying severe ESUS, while in mild ESUS other pathogenic mechanisms need to be explored.

Moreover, patients with severe ESUS are also characterized by additional and specific clinical characteristics, such as older age and higher prevalence of female sex, according to a previous study (6), that demonstrated that women have more severe ESUS compared with men.

The identification of possible cardioembolic mechanisms underlying severe ESUS could be particularly important to perform an appropriate therapy in this clinical subtype of ESUS where atrial cardiopathy could cause cardioembolism by itself or by promoting atrial fibrillation. The hypothesis that many ESUSs were determined by cardioembolic mechanisms based on silent and paroxysmal atrial fibrillation has been the rationale of RESPECT-ESUS and NAVIGATE trials (21, 22), that, however, didn't demonstrate the superiority of anticoagulants in ESUS. Nevertheless, a subanalysis of the NAVIGATE trial suggested a beneficial effect of anticoagulant therapy in ESUS associated with increased left atrial size (atrial diameter ≥46 mm) (23), confirming a possible pathogenic role of atrial cardiopathy in these patients.

Among various electrocardiographic and echocardiographic markers of atrial cardiopathy, our multivariate analysis showed that PWD represents the most significant atrial marker associated with severe ESUS.

Previous studies demonstrated that high PWD values correlate with both atrial cardiopathy and higher risk of AF, regardless of the increased atrial size (24–27). In this view, high PWD (even in presence of a normal left atrium size) represents an index of atrial electrical heterogeneity, reflecting the presence of atrial microarchitecture change and site-dependent conduction delay, also due to inflammatory mechanisms, that can favor AF occurrence (9, 28, 29).

Our results are particularly important because they suggest that severe ESUS patients are characterized by higher risk of atrial cardiopathy. However, even if atrial cardiopathy is a condition that encompasses alterations in macrostructure and microstructure that are associated with ischemic stroke also independent of atrial fibrillation

occurrence (30), current evidence doesn't suggest the efficacy of anticoagulant therapy in ESUS only associated to atrial cardiopathy without identification of AF episodes (31). For this reason, an intensive ECG monitoring is particularly important to detect subclinical AF and to choose the most appropriate therapy in this subgroup of ESUS (32).

Furthermore, the ongoing ARCADIA trial (33), comparing apixaban and aspirin in ESUS associated with atrial cardiopathy, will provide further data about the possible beneficial effects of anticoagulants in this subgroup of ESUS, also regardless of AF occurrence.

Our study has some limitations. The recruitment was mono-centric and we have no data about the ECG monitoring in the long-term, even if previous studies confirmed PWD as a predictor of AF after ischemic stroke in short- and long-term (18, 24, 34).

Furthermore, although ESUS is usually characterized by mild symptoms, most of our patients were affected by severe ESUS, because our Stroke Unit is a Comprehensive Stroke Center, that usually admits and treats the most complex and severe strokes from the entire South-East Tuscany.

Further studies are necessary to better characterize clinical characteristics of ESUS patients, to identify different pathogenic mechanisms underlying various subtypes of ESUS.

CONCLUSIONS

Our findings shed light on specific clinical characteristics of severe ESUS including the presence of atrial cardiopathy that could play a pathogenic role in this subgroup of patients. Searching for atrial fibrillation in these patients is especially important in order to perform the most appropriate therapy.

DATA AVAILABILITY STATEMENT

The raw data supporting the conclusions of this article will be made available by the authors, without undue reservation.

ETHICS STATEMENT

The studies involving human participants were reviewed and approved by Ethics Committee of the University Hospital of Siena, Italy. The patients/participants provided their written informed consent to participate in this study.

AUTHOR CONTRIBUTIONS

MA conception and design of the work. MA, PL, CD, FG, RT, and GM substantial contributions to the acquisition of data for the work. MA, PL, and AC substantial contributions to the analysis of data for the work and drafting the work. MA, PL, GM, and AC substantial contributions to the interpretation of data for the work and revising the draft of the work critically for important intellectual content. MA, PL, FG, RT, CD, GM, and AC final approval of the version to be published and agreement to be accountable for all aspects of the work in ensuring that questions related to the accuracy or integrity of any part of the work are appropriately investigated and resolved. All authors contributed to the article and approved the submitted version.

REFERENCES

1. Ntaios G. Embolic stroke of undetermined source: JACC review topic of the week. *J Am Coll Cardiol.* (2020) 75:333–40. doi: 10.1016/j.jacc.2019.11.024
2. Paciaroni M, Kamel H. Do the results of RE-SPECT ESUS call for a revision of the embolic stroke of undetermined source definition? *Stroke*. (2019) 50:1032–3. doi: 10.1161/STROKEAHA.118.024160
3. Albers GW, Bernstein R, Brachmann J, Camm AJ, Fromm P, Goto S, et al. Reexamination of the embolic stroke of undetermined source concept. *Stroke.* (2021) 52:2715–22. doi: 10.1161/STROKEAHA.121.035208
4. Kamel H, Healey JS. Cardioembolic stroke. *Circ Res.* (2017) 120:514–26. doi: 10.1161/CIRCRESAHA.116.308407
5. Pierik R, Algra A, van Dijk E, Erasmus ME, van Gelder IC, Koudstaal PJ, et al. Distribution of cardioembolic stroke: a cohort study. *Cerebrovasc Dis.* (2020) 49:97–104. doi: 10.1159/000505616
6. Leventis I, Perlepe K, Sagris D, Sirimarco G, Strambo D, Georgiopoulos G, et al. Characteristics and outcomes of embolic stroke of undetermined source according to stroke severity. *Int J Stroke.* (2020) 15:866–71. doi: 10.1177/1747493020909546
7. Hart RG, Diener HC, Coutts SB, Easton JD, Granger CB, O'Donnell MJ, et al. Embolic strokes of undetermined source: the case for a new clinical construct. *Lancet Neurol.* (2014) 13:429–38. doi: 10.1016/S1474-4422(13)70310-7
8. Dilaveris PE, Gialafos JE. P-wave duration and dispersion analysis: methodological considerations. *Circulation.* (2001) 103:E111. doi: 10.1161/01.CIR.103.21.e111
9. Acampa M, Lazzerini PE, Guideri F, Tassi R, Lo Monaco A, Martini G. Inflammation and atrial electrical remodeling in patients with embolic strokes of undetermined source. *Heart Lung Circ.* (2019) 28:917–22. doi: 10.1016/j.hlc.2018.04.294
10. Magnani JW, Williamson M, Ellinor PT, Monahan KM, Benjamin EJ. P wave indices: current status and future directions in epidemiology, clinical and research applications. *Circ Arrhythm Electrophysio.* (2009) 2:72–9. doi: 10.1161/CIRCEP.108.806828
11. Acampa M, Lazzerini PE, Martini G. How to identify patients at risk of silent atrial fibrillation after cryptogenic stroke: potential role of P wave dispersion. *J Stroke.* (2017) 19:239–41. doi: 10.5853/jos.2016.01620
12. Acampa M, Guideri F, Tassi R, Dello Buono D, Celli L, di Toro Mammarella L, et al. P wave dispersion in cryptogenic stroke: a risk factor for cardioembolism? *Int J Cardiol.* (2015) 190:202–4. doi: 10.1016/j.ijcard.2015.04.185
13. Pérez-Riera AR, de Abreu LC, Barbosa-Barros R, Grindler J, Fernandes-Cardoso A, Baranchuk A. P-wave dispersion: an update. *Indian Pacing Electrophysiol J.* (2016) 16:126–33. doi: 10.1016/j.ipej.2016.10.002
14. Rangel MO, O'Neal WT, Soliman EZ. Usefulness of the electrocardiographic P-wave axis as a predictor of atrial fibrillation. *Am J Cardiol.* (2016) 117:100–4. doi: 10.1016/j.amjcard.2015.10.013
15. Lang RM, Badano LP, Mor-Avi V, Afilalo J, Armstrong A, Ernande L, et al. Recommendations for cardiac chamber quantification by echocardiography in adults: an update from the American society of echocardiography and the European association of cardiovascular imaging. *J Am Soc Echocardiogr.* (2015) 28:1–39. doi: 10.1016/j.echo.2014.10.003
16. Acampa M, Lazzerini PE, Manfredi C, Guideri F, Tassi R, Domenichelli C, et al. Non-stenosing carotid atherosclerosis and arterial stiffness

in embolic stroke of undetermined source. *Front Neurol.* (2020) 11:725. doi: 10.3389/fneur.2020.00725
17. Tan BYQ, Ho JSY, Sia CH, Boi Y, Foo ASM, Dalakoti M, et al. Left atrial volume index predicts new-onset atrial fibrillation and stroke recurrence in patients with embolic stroke of undetermined source. *Cerebrovasc Dis.* (2020) 49:285–91. doi: 10.1159/000508211
18. Cameron A, Cheng HK, Lee RP, Doherty D, Hall M, Khashayar P, et al. Biomarkers for atrial fibrillation detection after stroke: systematic review and meta-analysis. *Neurology.* (2021) 97:e1775–89. doi: 10.1212/WNL.0000000000012769
19. O'Neal WT, Efird JT, Nazarian S, Alonso A, Michos ED, Szklo M, et al. Mitral annular calcification progression and the risk of atrial fibrillation: results from MESA. *Eur Heart J Cardiovasc Imaging.* (2018) 19:279–84. doi: 10.1093/ehjci/jex093
20. Fashanu OE, Bizanti A, Al-Abdouh A, Zhao D, Budoff MJ, Thomas IC, et al. Progression of valvular calcification and risk of incident stroke: the multi-ethnic study of atherosclerosis (MESA). *Atherosclerosis.* (2020) 307:32–8. doi: 10.1016/j.atherosclerosis.2020.06.009
21. Diener HC, Sacco RL, Easton JD, Granger CB, Bernstein RA, Uchiyama S, et al. Dabigatran for prevention of stroke after embolic stroke of undetermined source. *N Engl J Med.* (2019) 380:1906–17. doi: 10.1056/NEJMoa1813959
22. Hart RG, Sharma M, Mundl H, Kasner SE, Bangdiwala SI, Berkowitz SD, et al. Rivaroxaban for stroke prevention after embolic stroke of undetermined source. *N Engl J Med.* (2018) 378:2191–201. doi: 10.1056/NEJMoa1802686
23. Healey JS, Gladstone DJ, Swaminathan B, Eckstein J, Mundl H, Epstein AE, et al. Recurrent stroke with rivaroxaban compared with aspirin according to predictors of atrial fibrillation: secondary analysis of the NAVIGATE ESUS randomized clinical trial. *JAMA Neurol.* (2019) 76:764–73. doi: 10.1001/jamaneurol.2019.0617
24. Acampa M, Lazzerini PE, Guideri F, Tassi R, Andreini I, Domenichelli C, et al. Electrocardiographic predictors of silent atrial fibrillation in cryptogenic stroke. *Heart Lung Circ.* (2019) 28:1664–9. doi: 10.1016/j.hlc.2018.10.020
25. Dilaveris P, Gialafos E, Sideris S, Theopistou AM, Andrikopoulos GK, Kyriakidis M, et al. Simple electrocardiographic markers for the prediction of paroxysmal idiopathic atrial fibrillation. *Am Heart J.* (1998) 135:733–8. doi: 10.1016/S0002-8703(98)70030-4
26. Tükek T, Akkaya V, Atilgan D, Demirel E, Ozcan M, Güven O, et al. Effect of left atrial size and function on P-wave dispersion: a study in patients with paroxysmal atrial fibrillation. *Clin Cardiol.* (2001) 24:676–80. doi: 10.1002/clc.4960241008
27. Turhan H, Yetkin E, Atak R, Altinok T, Senen K, Ileri M, et al. Increased P-wave duration and P-wave dispersion in patients with aortic stenosis. *Ann Noninvasive Electrocardiol.* (2003) 8:18–21. doi: 10.1046/j.1542-474X.2003.08104.x
28. Acampa M, Lazzerini PE, Guideri F, Tassi R, Cartocci A, Martini G, et al. P-wave dispersion and silent atrial fibrillation in cryptogenic stroke: the pathogenic role of inflammation. *Cardiovasc Hematol Disord Drug Targets.* (2019) 19:249–52. doi: 10.2174/1871529X19666190410145501
29. Lazzerini PE, Laghi-Pasini F, Acampa M, Srivastava U, Bertolozzi I, Giabbani B, et al. Systemic inflammation rapidly induces reversible atrial electrical remodeling: the role of interleukin-6-mediated changes in connexin expression. *J Am Heart Assoc.* (2019) 8:e011006. doi: 10.1161/JAHA.118.011006
30. Chen LY, Ribeiro ALP, Platonov PG, Cygankiewicz I, Soliman EZ, Gorenek B, et al. P wave parameters and indices: a critical appraisal of clinical utility, challenges, and future research-A consensus document endorsed by the international society of electrocardiology and the international society for holter and non-invasive electrocardiology. *Circ Arrhythm Electrophysiol.* (2022) 15:e010435. doi: 10.1161/CIRCEP.121.010435
31. Lattanzi S, Acampa M, Norata D, Broggi S, Caso V. A critical assessment of the current pharmacotherapy for the treatment of embolic strokes of undetermined source. *Expert Opin Pharmacother.* (2022) 1–11. doi: 10.1080/14656566.2022.2071125. [Epub ahead of print].
32. Bhat A, Mahajan V, Chen HHL, Gan GCH, Pontes-Neto OM, Tan TC. Embolic stroke of undetermined source: approaches in risk stratification for cardioembolism. *Stroke.* (2021) 52:e820–36. doi: 10.1161/STROKEAHA.121.034498
33. Kamel K, Longstreth WT Jr, Tirschwell DL, Kronmal RA, Broderick JP, Palesch YY, et al. The atrial cardiopathy and antithrombotic drugs in prevention after cryptogenic stroke randomized trial: rationale and methods. *Int J Stroke.* (2019) 14:207–14. doi: 10.1177/1747493018799981
34. Marks D, Ho R, Then R, Weinstock JL, Teklemariam E, Kakadia B, et al. Real-world experience with implantable loop recorder monitoring to detect subclinical atrial fibrillation in patients with cryptogenic stroke: the value of P wave dispersion in predicting arrhythmia occurrence. *Int J Cardiol.* (2021) 327:86–92. doi: 10.1016/j.ijcard.2020.11.019

Conflict of Interest: The authors declare that the research was conducted in the absence of any commercial or financial relationships that could be construed as a potential conflict of interest.

Publisher's Note: All claims expressed in this article are solely those of the authors and do not necessarily represent those of their affiliated organizations, or those of the publisher, the editors and the reviewers. Any product that may be evaluated in this article, or claim that may be made by its manufacturer, is not guaranteed or endorsed by the publisher.

frontiers | Frontiers in Cardiovascular Medicine

ORIGINAL RESEARCH
published: 01 July 2022
doi: 10.3389/fcvm.2022.900850

Left Ventricular Diastolic Dysfunction Is Not Associated With Pulmonary Edema in Septic Patients. A Prospective Observational Cohort Study

Ursula Kahl[1], Leah Schirren[1], Yuanyuan Yu[1], Susanne Lezius[2], Marlene Fischer[1,3], Maja Menke[1], Christoph Sinning[4], Axel Nierhaus[3], Maren Vens[2,5], Christian Zöllner[1], Stefan Kluge[3], Matthias S. Goepfert[1,6] and Katharina Roeher[1]*

[1] Klinik und Poliklinik für Anästhesiologie Universitätsklinikum Hamburg-Eppendorf, Hamburg, Germany, [2] Institut für Medizinische Biometrie und Epidemiologie Universitätsklinikum Hamburg-Eppendorf, Hamburg, Germany, [3] Klinik für Intensivmedizin Universitätsklinikum Hamburg-Eppendorf, Hamburg, Germany, [4] Klinik und Poliklinik für Kardiologie Universitäres Herz- und Gefäßzentrum Universitätsklinikum Hamburg-Eppendorf, Hamburg, Germany, [5] Institut für Medizinische Biometrie und Statistik Universität zu Lübeck, Universitätsklinikum Schleswig-Holstein Campus Lübeck, Lübeck, Germany, [6] Klinik für Anästhesie und Intensivmedizin Alexianer St. Hedwigkliniken Berlin, Berlin, Germany

OPEN ACCESS

Edited by:
Michael Henein,
Umeå University, Sweden

Reviewed by:
Gen-Min Lin,
Hualien Armed Forces General Hospital, Taiwan
Madhumita Premkumar,
Post Graduate Institute of Medical Education and Research (PGIMER), India

***Correspondence:**
Ursula Kahl
u.kahl@uke.de
orcid.org/0000-0003-2096-9647

Specialty section:
This article was submitted to General Cardiovascular Medicine, a section of the journal Frontiers in Cardiovascular Medicine

Received: 21 March 2022
Accepted: 06 June 2022
Published: 01 July 2022

Citation:
Kahl U, Schirren L, Yu Y, Lezius S, Fischer M, Menke M, Sinning C, Nierhaus A, Vens M, Zöllner C, Kluge S, Goepfert MS and Roeher K (2022) Left Ventricular Diastolic Dysfunction Is Not Associated With Pulmonary Edema in Septic Patients. A Prospective Observational Cohort Study. Front. Cardiovasc. Med. 9:900850. doi: 10.3389/fcvm.2022.900850

Purpose: We aimed to investigate whether left ventricular diastolic dysfunction (LVDD) is associated with pulmonary edema in septic patients.

Methods: We conducted a prospective cohort study in adult septic patients between October 2018 and May 2019. We performed repeated echocardiography and lung ultrasound examinations within the first 7 days after diagnosis of sepsis. We defined LVDD according to the 2016 recommendations of the American Society of Echocardiography and—for sensitivity analysis—according to an algorithm which has been validated in septic patients. We quantified pulmonary edema using the lung ultrasound score (LUSS), counting B-lines in four intercostal spaces.

Results: We included 54 patients. LVDD was present in 51 (42%) of 122 echocardiography examinations. The mean (±SD) LUSS was 11 ± 6. There was no clinically meaningful association of LVDD with LUSS ($B = 0.55$ [95%CI: −1.38; 2.47]; $p = 0.571$). Pneumonia was significantly associated with higher LUSS ($B = 4.42$ [95%CI: 0.38; 8.5]; $p = 0.033$).

Conclusion: The lack of a clinically meaningful association of LVDD with LUSS suggests that LVDD is not a major contributor to pulmonary edema in septic patients.

Trial Registration: NCT03768752, ClinicalTrials.gov, November 30th, 2018 - retrospectively registered.

Keywords: diastolic dysfunction, lung edema, extravascular lung water, pneumonia, ultrasound, echocardiography, sepsis

INTRODUCTION

In septic patients, left ventricular diastolic dysfunction (LVDD) is common (1, 2) and associated with weaning from mechanical ventilation (3) and with mortality (1, 2, 4). Septic patients may develop new onset transient LVDD as a sign of sepsis-induced cardiomyopathy (5–7). In septic patients with pre-existing LVDD, LV diastolic function may further aggravate during sepsis.

Endothelial dysfunction with increased vascular permeability is a hallmark of sepsis and can result in pulmonary edema (8). Pulmonary edema is associated with multi-organ dysfunction and mortality (9). LVDD increases hydrostatic pressure and thus potentially aggravates pulmonary edema. In non-septic patients, there is an association between LVDD and hydrostatic pulmonary edema (10–15). Whether there is an association between LVDD and pulmonary edema in septic patients remains uncertain.

We, therefore, aimed to investigate whether septic patients with LVDD—compared to patients with normal LV diastolic function—have more severe pulmonary edema, quantified by the lung ultrasound score (LUSS). Specifically, we tested the hypothesis that LVDD is associated with LUSS in septic patients.

PATIENTS AND METHODS

Study Registration and Ethical Information

We conducted this prospective cohort study between October 2018 and May 2019 in the Department of Intensive Care Medicine (ICU) at the University Medical Center Hamburg-Eppendorf. Ethical approval for this study was provided by the ethics committee of the Hamburg Chamber of Physicians on June 26th, 2018 (reference number PV5769). Patients or their legal representatives provided written informed consent. The study was registered at ClinicalTrials.gov on November 30th, 2018 with the Identifier: NCT03768752. The manuscript adheres to the applicable STROBE guidelines.

Study Population

Sepsis was defined according to the Sepsis-3 definition (16). Patients were excluded when they were younger than 18 years, had mitral valve disease, persistent or permanent atrial fibrillation, any form of extrinsic cardiac restraint, any implanted mechanical cardiac device, or required extracorporeal membrane oxygenation.

Ultrasound Examination to Assess LVDD and LUSS

We performed both echocardiography and lung ultrasound daily during the first 7 days after diagnosis of sepsis. Examinations were discontinued earlier, if patients no longer fulfilled sepsis criteria or received palliative care. Ultrasound examinations were conducted by a single experienced investigator (UK). Only images with clearly identifiable anatomic structures and Doppler velocity curves without an angular error above 20° were accepted for interpretation. 2D-images were measured once, in Doppler-images three signals were measured and averaged. Ultrasound images and slopes were analyzed *post hoc* by two independent examiners (UK, LS) and numeric values were averaged. For details on the ultrasound examination see **Supplement 1**.

The echocardiographic examination of LV diastolic function was in line with the recommendations of the European Society of Intensive Care Medicine (17) and the respective PRICES checklist is available as **Supplement 2**. We performed echocardiography to assess ejection fraction, stroke volume, Doppler-derived cardiac index, mitral inflow velocity (E- and A-wave), deceleration time of the E-wave, mitral annular tissue velocity (lateral and septal e'- and a'-wave), left atrial maximum volume index, tricuspid regurgitation velocity. We determined and graded LVDD according to the 2016 recommendations of the American Society of Echocardiography (ASE) (18), In patients with preserved LV ejection fraction, LVDD is diagnosed if more than two of the following parameters meet the pathologic threshold: average lateral and septal E/e'-ratio >14, septal e' <7 cm/s or lateral e' <10 cm s^{-1}, tricuspid regurgitation velocity >2.8 m s^{-1}, and left atrial maximum volume index >34 ml m^{-2}. Patients with reduced LV ejection fraction are assumed to have LVDD. In both groups, LVDD is graded in the categories 1, 2, and 3 according to the parameters E/A-ratio ($\leq$0.8, >0.8– <2; $\geq$2), E > 50 cm s^{-1}, E/e'-ratio >14, tricuspid regurgitation velocity >2.8 m s^{-1} and left atrial maximum volume index >34 ml m^{-2} (18). For sensitivity analysis, we defined LVDD based on a second algorithm which has been validated specifically for septic patients (19). This algorithm defines LVDD as a septal e' <0.08 m s^{-1}, and grades LVDD according to the septal E/e'-ratio in the categories 1 (E/e' $\leq$ 8), 2 (8> E/e' <13), and 3 (E/e'$\geq$13) (19).

We performed lung ultrasound and used the LUSS to quantify pulmonary edema on a scale of 0–32 by counting and adding B-lines in the intercostal spaces 3/4 and 6/7 on the left and right side during one full breathing cycle (20).

Statistical Analysis

Statistical calculations were performed with SPSS Version 24 (IBM SPSS Statistics for Windows Released 2016. Armonk, NY: IBM Corp.). All tests were performed on the 5% level. Sensitivity analyses were not adjusted for multiplicity.

Prior to patient enrolment, we calculated group sample sizes of 25 and 25 to detect a difference in LUSS of 5 points with an assumed standard deviation (SD) of 6 in each group at the 0.05 significance level (alpha) with 80% power using a two-sided Mann-Whitney Test. The calculation was performed with the "Inequality Test for Two Means (Simulation)" module of Pass 2008 with 10,000 simulations.

We assessed the association between LVDD and LUSS using a linear mixed model. LUSS was modeled as a metric variable and included as the dependent variable. LVDD was modeled as a binary variable (normal LV diastolic function vs. LVDD grade 1–3) and included as the independent variable of interest. We included clinically relevant potential confounders: age, sex, SOFA score, cardiac index, pneumonia, positive pressure ventilation and fluid balance. Clustering of repeated measurements was accounted for by using a random intercept for the individual patients. The model was gradually reduced following an augmented stepwise backwards approach with respect to changes

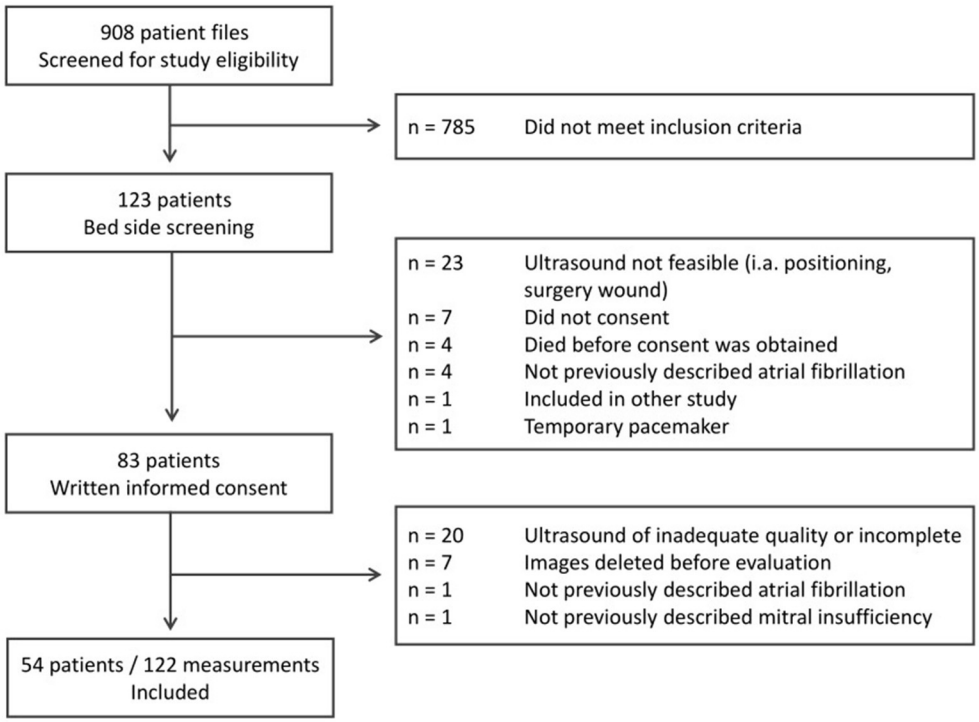

FIGURE 1 | Identification and inclusion of study participants for this prospective observational cohort study.

in parameter estimates ≥10%. Distributional assumptions of the residuals in all linear models were checked with QQ plots. We conducted a sensitivity analysis with LVDD modeled as a categorical variable with four manifestations (normal LV diastolic function, LVDD grade 1, 2, and 3).

Reliability of echocardiography examinations between the two examiners (UK, LS) for the primary endpoint (LUSS), as well for the ultrasound parameters E and septal e' was assessed using intra-class correlation coefficients (ICC).

RESULTS

We analyzed 122 echocardiography examinations in 54 patients (**Figure 1** and **Tables 1**, **2**). Details on sepsis severity and therapy are provided in **Supplements 2**, **3**.

Applying the 2016 ASE recommendations, LVDD was present in 51 (42%) of 122 echocardiography examinations (**Supplement 4**). The mean (±SD) LUSS was 10.7 ± 6.4; 11.0 ± 6.5 when LVDD was present, and 10.7 ± 6.2 when it was not (**Figure 2**). There was no clinically meaningful association of LVDD with LUSS ($B = 0.55$ [95%CI: −1.38; 2.47]; $p = 0.571$) (**Table 3**). Pneumonia was significantly associated with higher LUSS ($B = 4.42$ [95%CI: 0.38; 8.5]; $p = 0.033$; **Table 3**).

Applying the sepsis-specific LVDD algorithm, LVDD was present in 48 (39%) of 122 echocardiography examinations [LVDD grade 1: 5 (4%); grade 2: 21 (17%) and grade 3: 22 (18%)]. Prevalence of LVDD according to the two different algorithms is displayed in **Supplement 4**. The sensitivity analysis confirmed the results of the primary analysis (**Table 3**).

Inter-rater reliability quantified by the average ICC was 0.873 for the LUSS, 0.983 for the E-wave and 0.956 for the septal e'-wave.

DISCUSSION

We aimed to investigate whether septic patients with LVDD—compared to patients with normal LV diastolic function—have more severe pulmonary edema, quantified by the lung ultrasound score. Contrary to our hypothesis, there was no clinically meaningful association of LVDD with LUSS. Pneumonia was significantly associated with a higher LUSS. These findings were confirmed in the sensitivity analysis using the sepsis-specific definition of LVDD.

Two other studies have investigated the association between LVDD and pulmonary edema in septic patients (21, 22). Both studies defined LVDD based on an elevated E/e'-ratio and used LUSS to quantify pulmonary edema (21, 22). Santos et al. performed one echocardiography and lung ultrasound per patient and—contrary to our results—found an association between LVDD and pulmonary edema (22). The results may differ because only about one-third of their septic patients had a pulmonary source of infection (22). The study by Bataille et al. was restricted to septic patients with acute respiratory distress syndrome due to pneumonia (21). Comparable to our

TABLE 1 | Demographic and medical data.

	54 patients	
Sex – female	20	(37)
Age (years)	63	± 16
Body mass index	25.6	± 5.5
Infection site[a]		
Lungs	40	(74)
Abdomen	18	(33)
Blood stream	16	(30)
Urinary tract	11	(20)
Bones and soft tissue	5	(9)
Pleura	3	(6)
Mediastinum	3	(6)
Endocardium	3	(6)
Medical history		
Oncologic disease	20	(37)
Arterial hypertension	19	(35)
Liver cirrhosis	11	(20)
Chronic liver failure	9	(17)
Chronic kidney disease	9	(17)
Chronic obstructive pulmonary disease	9	(17)
Diabetes mellitus type II	9	(17)
Coronary heart disease	7	(13)
Myocardial infarction	7	(13)
Congestive heart failure	5	(9)
Stroke	5	(9)
Encephalopathy	5	(9)
Peripheral arterial disease	4	(7)
Dementia	4	(7)
Bronchial asthma	4	(7)
Diabetes mellitus type I	1	(2)
ICU mortality	22	(41)

Data are given in n (%) or mean ± SD.
SOFA, Sequential organ failure assessment; COPD, Chronic obstructive pulmonary disease; ICU, Intensive care unit.
[a]*Multiple sites possible.*

TABLE 2 | Ultrasound examination.

	122 examinations (54 patients)
Echocardiography	
LV ejection fraction (%)	49.96 ± 10.89
E wave (m s^{-1})	0.82 ± 0.22
A wave (m s^{-1})	0.82 ± 0.23
E/A	1.06 ± 0.44
e' lateral (m s^{-1})	0.12 ± 0.04
e' septal (m s^{-1})	0.09 ± 0.04
a' lateral (m s^{-1})	0.12 ± 0.04
a' septal (m s^{-1})	0.10 ± 0.04
E/e' lateral	7.39 ± 2.78
E/e' septal	10.12 ± 3.7
E/e' lateral and septal	8.41 ± 2.92
Tricuspid regurgitation vmax (m s^{-1})	2.08 ± 0.64
Left atrial maximum volume index (ml m^{-2})	30.62 ± 11.94
Cardiac index[a] (l min^{-1} m^{-2})	3.42 ± 1.36
Lung ultrasound	
Lung ultrasound score [b]	10.73 ± 6.38

Data are given in mean ± SD.
LV, left ventricular; E, Early mitral flow pattern; A, Atrial mitral flow pattern; E/A, Mitral valve E velocity divided by A-wave velocity; e, early mitral annular tissue velocity lateral or septal, E/e', Mitral valve inflow velocity E divided by mitral annular tissue velocity e'; vmax, maximum velocity.
[a]*Doppler-derived.* [b]*Enghard et al. (20).*

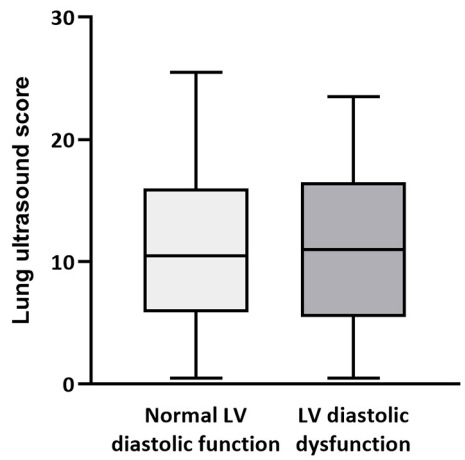

FIGURE 2 | Left ventricular diastolic dysfunction and pulmonary edema. Lung ultrasound score during examinations with normal left ventricular (LV) diastolic function (light gray box) and with LV diastolic dysfunction (dark gray box).

approach, the authors repeatedly performed echocardiography and lung ultrasound (21). In line with our results, there was no association between LVDD and pulmonary edema (21). The association of pneumonia with pulmonary edema presumably masks a clinically meaningful association between LVDD and pulmonary edema (21). Future studies on the association of LVDD with pulmonary edema should thus differentiate between patients with and without pneumonia.

The diagnosis of LVDD in septic patients is challenging. There are no clear diagnostic criteria for LVDD in septic patients (23). Importantly, different echocardiography algorithms may identify different patients as having LVDD (24). The 2016 ASE recommendations (18) are more likely to detect patients with pre-existing LVDD rather than an acute deterioration of diastolic function during sepsis, since they include parameters such as an increased left atrial maximum volume index which expresses a slow-growing adaptation and remodeling of the left atrium due to increased filling pressures (6, 25). To account for the influence of different algorithms, we performed a sensitivity analysis and defined LVDD based on a sepsis-specific algorithm (19). The results confirmed the primary analyses, thus supporting the robustness of our findings.

Our study has limitations. There is no gold standard for the ultrasonographic quantification of pulmonary edema, which

TABLE 3 | Linear mixed models.

Endpoint: lung ultrasound score	B	CI low	CI up	*p*
Main analysis				
Definition of diastolic dysfunction: ASE Algorithm[a]				
Normal LV diastolic function vs. LVDD	0.548	−1.375	2.471	0.571
Pneumonia vs. no pneumonia	4.421	0.376	8.467	0.033
No PPV vs. PPV	−1.950	−4.699	0.799	0.162
Age	−0.052	−0.161	0.056	0.340
SOFA score	−0.401	−0.823	0.021	0.062
Cardiac index	−0.320	−1.172	0.532	0.458
Sensitivity analysis				
Definition of diastolic dysfunction: Sepsis-specific Algorithm[b]				
Normal LV diastolic function vs. LVDD grade 3	2.522	−0.256	5.300	0.075
LVDD grade 1 vs. LVDD grade 3	1.371	−3.278	6.020	0.560
LVDD grade 2 vs. LVDD grade 3	−0.651	−3.664	2.363	0.669
Pneumonia vs. no pneumonia	4.076	0.321	7.831	0.034
Female vs. male sex	2.154	−1.356	5.664	0.224
No PPV vs. PPV	−1.490	−4.133	1.154	0.266
SOFA score	−0.184	−0.573	0.205	0.351
Fluid balance	0.065	−0.223	0.353	0.655

Linear mixed models: All initial models comprised the variables lung ultrasound score, left ventricular diastolic dysfunction (LVDD), age, sex, sequential organ failure assessment (SOFA) score, cardiac index, pneumonia, positive pressure ventilation (PPV) and fluid balance.

B, regression coefficient; CI, confidence interval; E/e' septal, Mitral valve inflow velocity E divided by mitral annular tissue velocity e'. [a]Nagueh et al. (18); [b]Lanspa et al. (19).

limits comparability between studies. LUSS protocols differ regarding the localization and number of examined intercostal spaces (20, 26–28). The LUSS protocol (20) used in this study has several advantages. It has been validated in septic patients (20, 29) and its LUSS values highly correlate with transpulmonary thermodilution-derived extravascular lung water (20), as well as with patient-centered outcomes such as the respiratory distress score or ICU length of stay (30).

According to the 2016 ASE recommendations the vast majority of patients with LVDD in our cohort were classified LVDD grade 1. The physiologic correlate of LVDD grade 1 are elevated filling pressures in the absence of elevated left atrial pressure (6), which may not contribute to pulmonary edema as much as LVDD grade 2 and 3. Future studies should consider comparing patients with normal diastolic function or LVDD grade 1 to patients with LVDD grade 2 or 3. Additionally, future studies should take into account parameters of right ventricular function. Unfortunately, it is not possible to consistently collect information on baseline diastolic function before the onset of sepsis. We thus cannot reliably distinguish between patients with pre-existing and new onset LVDD.

Our patient cohort was heterogeneous in regard to pre-existing conditions, infection sites, microbial spectrum and sepsis therapy. We aimed to control for this heterogeneity by adjusting the analysis for potential confounders. Most importantly, we included the SOFA score in the analysis to account for sepsis severity. Potential confounders which are part of the SOFA Score such as arterial blood pressure, vasopressor support, PaO_2/FiO_2 ratio, serum creatinine where not included as individual variables in addition to the SOFA score. Additionally, we adjusted for the cardiac index to account for systolic function and for the daily fluid balance to account for iatrogenic fluid supply or extraction in patients with and without kidney failure and renal replacement therapy. We adjusted for positive pressure ventilation to account for respiratory failure and for pneumonia to account for the pneumonia-associated risk of lung edema. As we only included 54 patients, we could not compare subgroups of patients with and without pneumonia. Future studies should differentiate between patients with and without pneumonia.

A major strength of our study is that ultrasound examinations were standardized and performed by a single examiner and two independent evaluators, showing excellent inter-rater reliability.

CONCLUSION

The lack of a clinically meaningful association of LVDD with LUSS suggests that LVDD is not a major contributor to pulmonary edema in septic patients.

DATA AVAILABILITY STATEMENT

The raw data supporting the conclusions of this article will be made available by the authors, without undue reservation.

ETHICS STATEMENT

The studies involving human participants were reviewed and approved by Ethics Comittee of the Hamburg Chamber of Physicians Ärztekammer Hamburg Weidestr. 122 b 22083 Hamburg. The patients/participants or their legal representatives provided their written informed consent to participate in this study.

AUTHOR CONTRIBUTIONS

UK: conception and design of the work, acquisition, analysis and interpretation of data, and writing of the original draft. LS: acquisition and writing of the original draft. YY: acquisition and substantial revision of the manuscript. MM: writing original draft. SL: analysis and substantial revision of the manuscript. MF: analysis and interpretation of data and substantial revision of the manuscript. CS, SK, and AN: substantial revision of the manuscript. MV and CZ: design of the work, substantial revision of the manuscript. MG: conception and design of the work and substantial revision of the manuscript. KR: conception and design of the work, interpretation of data, and writing of the original draft. All authors have approved the submitted version (and any substantially modified version that involves the author's contribution to the study), and have agreed both to be personally accountable for the author's own contributions and to ensure that questions related to the accuracy or integrity of

any part of the work, even ones in which the author was not personally involved, are appropriately investigated, resolved, and the resolution documented in the literature.

FUNDING

UK was funded by the Clinician Scientist Program of the medical faculty of the University of Hamburg, during the conduct of the study. The University of Hamburg was not involved in any of the following: study design, conduct of the research, preparation of this manuscript, analysis and interpretation of data; writing of the report; decision to submit the article for publication. MF receives financial support from the Johanna und Fritz Buch Gedächtnis-Stiftung. The Johanna und Fritz Buch Gedächtnis-Stiftung was not involved in any of the following: study design, conduct of the research, preparation of this manuscript, analysis and interpretation of data; writing of the report; decision to submit the article for publication.

SUPPLEMENTARY MATERIAL

The Supplementary Material for this article can be found online at: https://www.frontiersin.org/articles/10.3389/fcvm.2022.900850/full#supplementary-material

REFERENCES

1. Garry D, Newton J, Colebourn C. Tissue Doppler indices of diastolic function in critically ill patients and association with mortality – A systematic review. *J Intensive Care Soc.* (2016) 17:51–62. doi: 10.1177/1751143715595641
2. Sanfilippo F, Corredor C, Fletcher N, Landesberg G, Benedetto U, Foex P, et al. Diastolic dysfunction and mortality in septic patients: a systematic review and meta-analysis. *Intensive Care Med.* (2015) 41:1004–13. doi: 10.1007/s00134-015-3748-7
3. Sanfilippo F, Di Falco D, Noto A, Santonocito C, Morelli A, Bignami E, et al. Association of weaning failure from mechanical ventilation with transthoracic echocardiography parameters: a systematic review and meta-analysis. *Br J Anaesth.* (2021) 126:319–30. doi: 10.1016/j.bja.2020.07.059
4. Sanfilippo F, Corredor C, Arcadipane A, Landesberg G, Vieillard-Baron A, Cecconi M, et al. Tissue Doppler assessment of diastolic function and relationship with mortality in critically ill septic patients: a systematic review and meta-analysis. *Br J Anaesth.* (2017) 119:583–94. doi: 10.1093/bja/aex254
5. Beesley SJ, Weber G, Sarge T, Nikravan S, Grissom CK, Lanspa MJ, et al. Septic Cardiomyopathy. *Crit Care Med.* (2018). 46:625–34. doi: 10.1097/CCM.0000000000002851
6. Sanfilippo F, Scolletta S, Morelli A, Vieillard-Baron A. Practical approach to diastolic dysfunction in light of the new guidelines and clinical applications in the operating room and in the intensive care. *Ann Intensive Care.* (2018) 8:100. doi: 10.1186/s13613-018-0447-x
7. Bouhemad B, Nicolas-Robin A, Arbelot C, Arthaud M, Féger F, Rouby J-J. Isolated and reversible impairment of ventricular relaxation in patients with septic shock. *Crit Care Med.* (2008) 36:766–74. doi: 10.1097/CCM.0B013E31816596BC
8. Ince C, Mayeux PR, Nguyen T, Gomez H, Kellum JA, Ospina-Tascón GA, et al. The Endothelium in Sepsis. *Shock.* (2016). 45:259–70. doi: 10.1097/SHK.0000000000000473
9. Chung FT, Lin HC, Kuo CH, Yu CT, Chou CL, Lee KY, et al. Extravascular lung water correlates multiorgan dysfunction syndrome and mortality in sepsis. *PLoS ONE.* (2010) 5:e15265. doi: 10.1371/journal.pone.0015265
10. Cho D-H, Park S-M, Kim M-N, Kim S-A, Lim H, Shim W-J. Presence of preoperative diastolic dysfunction predicts postoperative pulmonary edema and cardiovascular complications in patients undergoing noncardiac surgery. *Echocardiography.* (2014) 31:42–9. doi: 10.1111/echo.12285
11. Frassi F, Gargani L, Gligorova S, Ciampi Q, Mottola G, Picano E. Clinical and echocardiographic determinants of ultrasound lung comets. *Eur J Echocardiogr.* (2007) 8:474–9. doi: 10.1016/j.euje.2006.09.004
12. Higashi M, Yamaura K, Ikeda M, Shimauchi T, Saiki H, Hoka S. Diastolic dysfunction of the left ventricle is associated with pulmonary edema after renal transplantation. *Acta Anaesthesiol Scand.* (2013) 57:1154–60. doi: 10.1111/aas.12168
13. Kopelnik A, Fisher L, Miss JC, Banki N, Tung P, Lawton MT, et al. Prevalence and implications of diastolic dysfunction after subarachnoid hemorrhage. *Neurocrit Care.* (2005) 3:132–8. doi: 10.1385/NCC:3:2:132
14. Li H, Li Y-D, Zhu W-W, Kong L-Y, Ye X-G, Cai Q-Z, et al. A simplified ultrasound comet tail grading scoring to assess pulmonary congestion in patients with heart failure. *Biomed Res Int.* (2018) 2018:e8474839. doi: 10.1155/2018/8474839
15. Shigematsu K, Iwashita K, Mimata R, Owaki R, Totoki T, Gohara A, et al. Preoperative left ventricular diastolic dysfunction is associated with pulmonary edema after carotid endarterectomy. *Neurol Med Chir.* (2019) 59:299–304. doi: 10.2176/nmc.oa.2019-0028
16. Singer M, Deutschman CS, Seymour CW, Shankar-Hari M, Annane D, Bauer M, et al. The third international consensus definitions for Sepsis and Septic Shock (Sepsis-3). *JAMA.* (2016) 315:801. doi: 10.1001/jama.2016.0287
17. Sanfilippo F, Huang S, Herpain A, Balik M, Chew MS, Clau-Terré F, et al. The PRICES statement: an ESICM expert consensus on methodology for conducting and reporting critical care echocardiography research studies. *Intensive Care Med.* (2020) 47:1–13. doi: 10.1007/s00134-020-06262-5
18. Nagueh SF, Smiseth OA, Appleton CP, Byrd BF, Dokainish H, Edvardsen T, et al. Recommendations for the evaluation of left ventricular diastolic function by echocardiography: an update from the American Society of Echocardiography and the European Association of Cardiovascular Imaging. *Eur Heart J Cardiovasc Imaging.* (2016) 17:1321–60. doi: 10.1093/ehjci/jew082
19. Lanspa MJ, Gutsche AR, Wilson EL, Olsen TD, Hirshberg EL, Knox DB, et al. Application of a simplified definition of diastolic function in severe sepsis and septic shock. *Crit Care.* (2016) 20:243. doi: 10.1186/s13054-016-1421-3
20. Enghard P, Rademacher S, Nee J, Hasper D, Engert U, Jorres A, et al. Simplified lung ultrasound protocol shows excellent prediction of extravascular lung water in ventilated intensive care patients. *Crit Care.* (2015) 19:36. doi: 10.1186/s13054-015-0756-5
21. Bataille B, Rao G, Cocquet P, Mora M, Masson B, Ginot J, et al. Accuracy of ultrasound B-lines score and E/Ea ratio to estimate extravascular lung water and its variations in patients with acute respiratory distress syndrome. *J Clin Monit Comput.* (2015) 29:169–76. doi: 10.1007/s10877-014-9582-6
22. Santos TM, Franci D, Gontijo-Coutinho CM, Ozahata TM, de Araújo Guerra Grangeia T, Matos-Souza JR, et al. Inflammatory lung edema correlates with echocardiographic estimation of capillary wedge pressure in newly diagnosed septic patients. *J Crit Care.* (2018) 44:392–7. doi: 10.1016/j.jcrc.2017.11.036
23. Hollenberg SM, Singer M. Pathophysiology of sepsis-induced cardiomyopathy. *Nat Rev Cardiol.* (2021) 18:424–34. doi: 10.1038/s41569-020-00492-2
24. Almeida JG, Fontes-Carvalho R, Sampaio F, Ribeiro J, Bettencourt P, Flachskampf FA, et al. Impact of the 2016 ASE/EACVI recommendations on the prevalence of diastolic dysfunction in the general population. *Eur Heart J Cardiovasc Imaging.* (2018) 19:380–6. doi: 10.1093/ehjci/jex252
25. Brown SM, Pittman JE, Hirshberg EL, Jones JP, Lanspa MJ, Kuttler KG, et al. Diastolic dysfunction and mortality in early severe sepsis and septic shock: a prospective, observational echocardiography study. *Crit Ultrasound J.* (2012) 4:8. doi: 10.1186/2036-7902-4-8
26. Bouhemad B, Brisson H, Le-Guen M, Arbelot C, Lu Q, Rouby J-J. Bedside ultrasound assessment of positive end-expiratory pressure–

induced Lung recruitment. *Am J Respir Crit Care Med.* (2011) 183:341–7. doi: 10.1164/rccm.201003-0369OC
27. Jambrik Z, Monti S, Coppola V, Agricola E, Mottola G, Miniati M, et al. Usefulness of ultrasound lung comets as a nonradiologic sign of extravascular lung water. *Am J Cardiol.* (2004) 93:1265–70. doi: 10.1016/j.amjcard.2004.02.012
28. Santos TM, Franci D, Coutinho CMG, Ribeiro DL, Schweller M, Matos-Souza JR, et al. A simplified ultrasound-based edema score to assess lung injury and clinical severity in septic patients. *Am J Emerg Med.* (2013) 31:1656–60. doi: 10.1016/j.ajem.2013.08.053
29. Long E, O'Brien A, Duke T, Oakley E, Babl FE, Pediatric Research in Emergency Departments International Collaborative. Effect of fluid bolus therapy on extravascular lung water measured by lung ultrasound in children with a presumptive clinical diagnosis of sepsis. *J Ultrasound Med.* (2019). 38:1537–44. doi: 10.1002/jum.14842
30. Gattupalli V, Jain K, Samra T. Lung ultrasound as a bedside tool for assessment of extravascular lung water in critically ill head injured patients: an observational study. *Indian J Crit Care Med.* (2019) 23:131–4. doi: 10.5005/jp-journals-10071-23135

Conflict of Interest: The authors declare that the research was conducted in the absence of any commercial or financial relationships that could be construed as a potential conflict of interest.

frontiers | Frontiers in Cardiovascular Medicine

ORIGINAL RESEARCH
published: 01 July 2022
doi: 10.3389/fcvm.2022.899290

The Systolic Pulmonary Arterial Pressure Liaises Impaired Cardiac Autonomic Control to Pro-inflammatory Status in Systemic Sclerosis Patients

Gabriel D. Rodrigues[1,2†], Marco Vicenzi[3,4†], Chiara Bellocchi[1,5], Lorenzo Beretta[5], Angelica Carandina[1,5], Eleonora Tobaldini[1,5], Stefano Carugo[1,3] and Nicola Montano[1,5]*

[1] Department of Clinical Sciences and Community Health, University of Milan, Milan, Italy, [2] Post Graduation Program in Cardiovascular Sciences, Federal Fluminense University, Niterói, Brazil, [3] Cardiovascular Disease Unit, Fondazione IRCCS Ca' Granda Ospedale Maggiore Policlinico, Milan, Italy, [4] Dyspnea Lab, Department of Clinical Sciences and Community Health, University of Milan, Milan, Italy, [5] Department of Internal Medicine, Fondazione IRCCS Ca' Granda Ospedale Maggiore Policlinico, Milan, Italy

OPEN ACCESS

Edited by:
Nicola Mumoli,
ASST Ovest Milanese, Italy

Reviewed by:
Gaetano Zizzo,
ASST Ovest Milanese, Italy
Clodoveo Ferri,
University of Modena and Reggio Emilia, Italy

***Correspondence:**
Gabriel D. Rodrigues
dias5gabriel@gmail.com

† These authors have contributed equally to this work

Specialty section:
This article was submitted to General Cardiovascular Medicine, a section of the journal Frontiers in Cardiovascular Medicine

Received: 18 March 2022
Accepted: 26 May 2022
Published: 01 July 2022

Citation:
Rodrigues GD, Vicenzi M, Bellocchi C, Beretta L, Carandina A, Tobaldini E, Carugo S and Montano N (2022) The Systolic Pulmonary Arterial Pressure Liaises Impaired Cardiac Autonomic Control to Pro-inflammatory Status in Systemic Sclerosis Patients. Front. Cardiovasc. Med. 9:899290. doi: 10.3389/fcvm.2022.899290

The current study was undertaken to test the hypothesis that systemic sclerosis (SSc) patients with higher systolic pulmonary arterial pressures (PAPs) present a blunted cardiac autonomic modulation and a pro-inflammatory profile. Thirty-nine SSc patients were enrolled (mean age 57 ± 11 years). ECG and respiration were recorded in the supine (SUP) position and during the active standing (ORT). Heart rate variability (HRV) analysis was performed on samples of 300 beats. The symbolic analysis identified three patterns, 0V%, (sympathetic) and 2UV% and 2LV%, (vagal). The %ΔORT was calculated from the differences between HRV in ORT and SUP, normalized (%) by the HRV values at rest. The PAPs was obtained non-invasively through echocardiography. For the inter-group analysis, participants were allocated in groups with higher (+PAPs ≥ median) and lower PAPs (–PAPs < median) values. At rest, the cardiac sympathetic modulation (represented by 0V%) was positively correlated with PAPs, while parasympathetic modulation (represented by 2LV%) was negatively correlated with PAPs. The dynamic response to ORT (represented by Δ0V% and Δ2LV%), sympathetic and parasympathetic were negatively and positively correlated with PAPs, respectively. The +PAPs group presented a higher inflammatory status and a blunted cardiac autonomic response to ORT (↓Δ0V% and ↑Δ2LV%) compared to the –PAPs group. These findings suggest an interplay among cardiac autonomic control, inflammatory status, and cardiopulmonary mechanics that should be considered for the assessment, monitoring, and treatment of SSc patients.

Keywords: heart rate variability, scleroderma, symbolic analysis, inflammatory reflex, autoimmune diseases

INTRODUCTION

Systemic Sclerosis (SSc) is an autoimmune disease characterized by vascular damage, autoantibodies production, and fibrosis of the skin and internal organs. SSc patients are classified into diffuse cutaneous SSc (dcSSc) or limited cutaneous SSc (lcSSc) subsets based on the extent of their skin fibrosis (1–4). The heart and lungs are frequently affected in SSc with several manifestations including conduction abnormalities, myocarditis, coronary artery disease, valvular heart disease, pericardial manifestations, associated pulmonary arterial hypertension (APAH), myocardial and pulmonary fibrosis (1–6). Due to unspecific symptoms (typically dyspnea and fatigue), cardiopulmonary impairments are often diagnosed late leading to a poor prognosis. Clinically evident cardiac involvement is associated with up to 70% mortality at 5 years (1, 7, 8). In this turn, APAH is also a relevant cause of death in SSc, despite an optimized treatment (2, 5). The non-invasive monitoring of the integrity of the pulmonary circulation through regular Doppler echocardiography and/or the functional assessment through the exercise cardiopulmonary testing should be considered in early APAH screening (9, 10).

Autonomic dysfunction was identified as an early marker of SSc progression, helping to identify cardiac involvement (11, 12). Heart rate variability (HRV) has been reported as a powerful non-invasive tool to access heart sympathetic and vagal modulation in SSc disease (11, 13). HRV predicted severe myocardial damage that is linked to ventricular arrhythmias in patients with SSc (12). Recently, HRV linear and non-linear analysis revealed that cardiac autonomic impairment follows the fibro-vascular progression in SSc. Indeed, the dcSSc subset shows a more pronounced shifted sympatho-vagal balance (i.e., sympathetic predominance and vagal withdrawal) if compared to the lcSSc in which there is a less extent of fibrosis (3). Moreover, SSc at a pre-clinical stage (14) shows an autonomic profile comparable to healthy controls (13).

In idiopathic PAH, high PAPs values were negatively correlated with vagal-mediated HRV linear indexes in time and frequency domains, and cardiac vagal modulation was lower in idiopathic PAH compared to age-matched healthy controls (15). In the same way, the augmented sympathetic discharge to the periphery was positively correlated with PAPs, highlighting that the sympathetic nervous system plays a role in the pulmonary vascular disease pathophysiology (16).

Whether sympatho-vagal balance is modulated in patients with SSc is not well described and, to our knowledge, no studies investigated the association between PAPs and cardiac autonomic modulation (i.e., HRV) in SSc patients without features of APAH. Since cardiac autonomic control is impaired in both SSc (13) and idiopathic PAH (15), we could hypothesize an association between PAPs and HRV indexes in SSc. Moreover, inflammation might be a relevant bridge between autoimmune diseases and APAH, as a possible key mechanism underlying APAH development in SSc (17, 18).

Thus, the current study was undertaken to test the hypothesis that high pulmonary arterial pressure liaises impaired cardiac autonomic function with low-grade inflammation in SSc patients, even without clinically evident APAH.

MATERIALS AND METHODS

Sample

This observational study included 39 SSc patients without a diagnosis of APAH. SSc patients were classified into dcSSc or lcSSc subsets based on the extent of their skin fibrosis (3). Patients with a definite SSc but without skin fibrosis yet with puffy fingers were categorized in the lcSSc group. The protocol was approved by the local Ethics Committee (Comitato Etico Milano Area 2), and all participants signed informed written consent before participation in the study.

Clinical Features

Clinical and laboratory parameters were extracted from medical records for the determination of total lung capacity (TLC), forced vital capacity (FVC), forced expiratory volume in 1 s (FEV_1), diffusing capacity for carbon monoxide (DLCO), left ventricular ejection fraction (LVEF) computed using the modified Simpson's formula, tricuspid annular plane systolic excursion (TAPSE, normal value when $>$ 16 mm), erythrocyte sedimentation rate (ESR, normal value from 1 to 20 mm/h), SSc-associated autoantibodies (ACA and aSCL70 positivity), C-reactive protein (CRP, normal value $<$ 0.5 mg/dL), creatinine, glucose levels, and the presence of hypergammaglobulinemia.

According to the current recommendation, right atrial pressure (RAP) was estimated from the spontaneous changes of the inferior vena cava dimension during the expiratory-inspiratory phase, and set in different levels (5, 10, or 15 mmHg) according to the current guideline for the echocardiographic assessment of the right heart in adults (19). Doppler sampling of tricuspid regurgitation velocity was used to derive the right atrial-ventricular gradient through the simplified Bernoulli's equation. Non-invasive PAPs estimate was obtained through echocardiography adding the RAP to the right atrial-ventricular gradient (19). The APAH was clinically ruled out according to the following exclusion criteria (9, 10): (1) DLCO $<$ 60%; and (2) NYHA functional class $\geq$ 2.

Cardiac Autonomic Modulation Assessment

All the participants underwent the recording of ECG and respiration (thoracic belt record) by an *ad hoc* telemetric system device (BT16 Plus, Marazza Spa, Monza, ITA). The signals were recorded at rest (supine position for 5 min) and during active standing (orthostatic position for 5 min) with spontaneous breathing. The absence of a stable sinus rhythm on ECG and ongoing therapy with beta-blocker drugs were considered exclusion criteria for this study.

The HRV was evaluated through specific software (Heart Scope II, AMPS, ITA) on short samples of 300 beats at supine (SUP) and orthostatic (ORT) positions. To assess the autonomic dynamic response to ORT, we calculated the ΔORT% (HRV in SUP position–HRV in ORT position/HRV in SUP position).

Non-linear dynamics of HRV were evaluated by symbolic analysis. The R-R dynamics were classified into three patterns families: (a) patterns with no variation (0V; all three symbols were equal); (b) patterns with one variation (1V; two consequent symbols were equal and the remaining symbol was different); and (c) patterns with two liked (2LV) and unlike (2UV) variations (e.g., all symbols were different from the previous one). The percentage of the patterns with no variation (0V) and with two variations (2UV or 2LV) were calculated as a predominance of sympathetic and parasympathetic cardiac autonomic modulation, respectively (13). However, the pattern of 1V was not associated with any autonomic tests used to validate the method (20).

Statistical Analysis

The Shapiro–Wilk test was used to evaluate the normality of the samples. The Spearman's correlation was used to test the association between PAPs and HRV indexes. Mann–Whitney *U* test was used for the inter-group analysis. The analysis of covariance (ANCOVA) was employed, using age as a co-variable to confirm the results from the inter-group analysis. For descriptive analysis, the median and the interquartile range (IQR 25–75%) were calculated for PAPs values. For the other variables, means and standard deviation were used. *P*-value < 0.05 was considered statistically significant. The software used was SPSS Statistics version 21.0 (IBM Corp., Armonk, NY, United States) and GraphPad Prism version 8.0 (GraphPad Software Inc., San Diego, CA, United States).

RESULTS

Our cohort was mainly composed of females and lcSSc subjects (77%) with a mean age of 57 ± 11 yrs. Overall clinical features are listed in **Table 1**. Mean disease duration was >than 3 years. All participants had a DLCO > 60% and belonged to the NYHA functional class I, thus excluding suspicion of APAH diagnosis. After patients' allocation into two subgroups based on PAPs values above or below the median (median 30, IQR 27–34 mmHg; the +PAPs and –PAPs groups, respectively), significantly higher CRP levels were found in the +PAPs (1.01 ± 1.04 mg/dL) compared to the –PAPs group (0.40 ± 0.25 mg/dL; $p = 0.02$). No other clinical differences were found between +PAPs and –PAPs groups, except for higher age in the +PAPs. To note, these results were confirmed also after ANCOVA, which included age and SSc subset as co-variables.

At rest, PAPs positively correlated with cardiac sympathetic modulation (represented by 0V%) and negatively correlated with vagal modulation (represented by 2LV%) (see **Figures 1A,C**).

When the autonomic dynamic response to ORT was assessed, the Δ0V% was negatively and Δ2LV% positively correlated with PAPs values (see **Figures 1B,D**). Other clinical features were not associated with HRV. As shown in **Figure 2** the +PAPs group presented a blunted autonomic response to orthostatic stress (lower Δ0V% and higher Δ2LV%) compared to the –PAPs group, while at rest HRV indexes did not show differences between –PAPs and +PAPs groups.

DISCUSSION

This study showed that in SSc patients without a diagnosis of APAH: (1) at rest, PAPs values are positively correlated with sympathetic- and negatively correlated with vagal-mediated indexes of symbolic HRV analysis; (2) higher PAPs values are correlated to a blunted cardiac autonomic responses at active standing test (i.e., reduced Δ0V% and increased Δ2LV% and 2LV; (3) the +PAPs group presented higher CRP values (attributable to a low-grade inflammation) and a

TABLE 1 | Participants' characteristics and clinical features.

	All	-PAPs	+PAPs	*p*-value
Personal characteristics				
N	39	19	20	–
Sex (M/F)	9/30	4/15	6/14	–
Age (years)	57 ± 11	56 ± 10	64 ± 11	0.03*
SSc subsets (dcSSc/lcSSc)	6/33	3/16	3/17	–
Disease duration (years)	11 ± 8	10 ± 8	13 ± 9	0.17
Controlled arterial hypertension (*n*)	4	2	2	–
Antibodies				
Anti-Scl-70+ (*n*)	11	7	4	–
ACA+ (*n*)	17	7	10	–
ANA+ (*n*)	11	7	4	–
Spirometry				
TLC (L)	5.33 ± 1.30	5.17 ± 1.44	5.43 ± 1.24	0.72
FVC (L)	3.20 ± 1.00	3.43 ± 1.03	3.03 ± 0.96	0.30
FEV_1 (L)	2.48 ± 0.92	2.72 ± 1.15	2.30 ± 0.67	0.08
DLCO SB, ml/mmHg/min	24.16 ± 35.35	16.52 ± 10.27	30.55 ± 46.92	0.58
DLCO SB, %	80 ± 17%	83 ± 12%	77 ± 20%	
DLCO SB/VA, ml/mmHg/min/L	7.65 ± 15.35	4.44 ± 1.59	9.52 ± 19.34	0.46
DLCO SB/VA, %	90 ± 18%	92 ± 10%	90 ± 22%	
Echocardiography				
LVEF (%)	61 ± 12	59 ± 16	63 ± 6	0.60
TAPSE (mm)	23 ± 5	24 ± 5	22 ± 5	0.39
PAPs (mmHg)	31 ± 8	25 ± 4	37 ± 6	<0.001*
Biochemical				
CRP (mg/dL)	0.73 ± 1.01	0.40 ± 0.25	1.01 ± 1.04	0.02*
ESR (mm/hour)	22 ± 18	20 ± 12	24 ± 12	0.84
γ-globulin (g/dL)	16.94 ± 7.07	16.70 ± 4.09	17.31 ± 10.78	0.74
Creatinine (mg/dL)	0.84 ± 0.21	0.76 ± 0.08	0.93 ± 0.30	0.26
Glucose (mg/dL)	87 ± 9	89 ± 10	84 ± 5	0.28

*SSc, systemic sclerosis; lcSSc, limited cutaneous SSc; dcSSc, diffuse cutaneous SSc; Anti-Scl-70+, anti-topoisomerase I; ACA+, anti-centromere antibodies positive; TLC, total lung capacity; FVC, forced vital capacity; FEV1, forced expiratory volume in 1 s; DLCO SB, diffusing capacity for carbon monoxide; DLCO SB/VA, diffusing capacity corrected for alveolar volume; LVEF, left ventricular ejection fraction; TAPSE, tricuspid annular plane systolic excursion; PAPs, mean pulmonary artery pressure; CRP, C reactive protein; ESR, erythrocyte sedimentation rate; PAPs-, PAPs group of PAPs < median; PAPs+, group of PAPs ≥ median; *p < 0.05 from Mann–Whitney U test (–PAPs vs. +PAPs).*

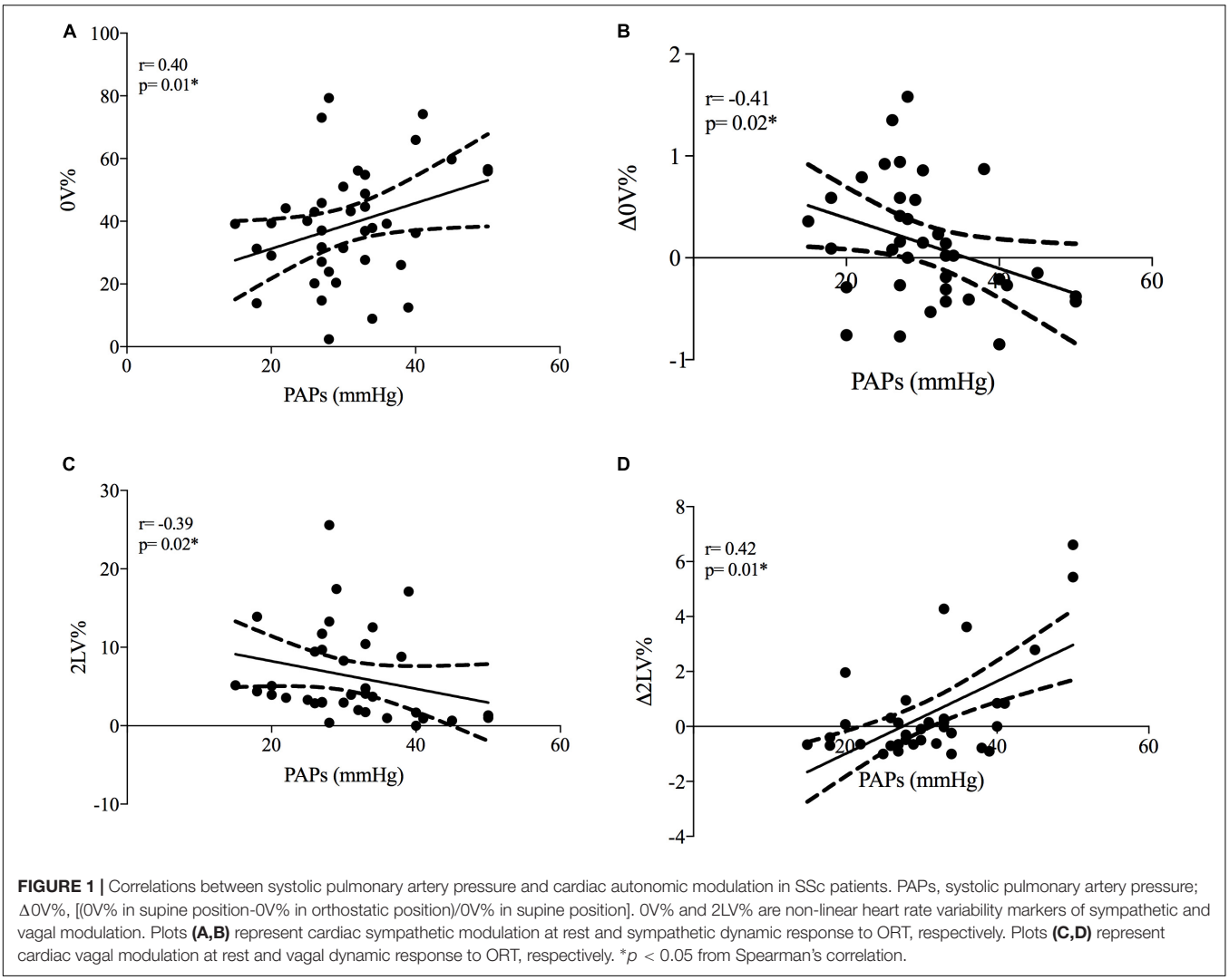

FIGURE 1 | Correlations between systolic pulmonary artery pressure and cardiac autonomic modulation in SSc patients. PAPs, systolic pulmonary artery pressure; Δ0V%, [(0V% in supine position-0V% in orthostatic position)/0V% in supine position]. 0V% and 2LV% are non-linear heart rate variability markers of sympathetic and vagal modulation. Plots **(A,B)** represent cardiac sympathetic modulation at rest and sympathetic dynamic response to ORT, respectively. Plots **(C,D)** represent cardiac vagal modulation at rest and vagal dynamic response to ORT, respectively. *$p < 0.05$ from Spearman's correlation.

blunted cardiac autonomic modulation compared to the –PAPs group. Overall, our findings suggest that a cardiac autonomic assessment through a non-invasive tool such as HRV and active standing test, may unmask a preclinical derangement of cardiopulmonary circulation.

Autonomic Nervous System and Cardiopulmonary Mechanics in Systemic Sclerosis and Associated Pulmonary Arterial Hypertension

From a previous study in idiopathic pulmonary arterial hypertension, vagal-mediated HRV was negatively associated with high values of invasively assessed PAPs (15). Indeed, a cardiac vagal withdrawal seems to be a consequence of an increased sympathetic drive, suggesting that cardiac vagal modulation is suppressed by sympathetic overactivity (13, 15). In line with these observations, our results showed that the sympathetic- and vagal-mediated indexes of HRV symbolic analysis were correlated with PAPs. Moreover, a previous study described a cardiac autonomic dysfunction in SSc patients with APAH (21). However, further studies with others HRV approaches and a more representative sample size are needed to confirm this finding.

As well known, the hemodynamic determinants of pulmonary pressure are represented by: (1) the cardiac output (CO) that determines the amount of blood flow; (2) the left ventricular end-diastolic pressure (LVEDP) that reflects the impact of the post-capillary component; and (3) the arterial pulmonary circulation, that reflects the pre-capillary component (22). In this complex hemodynamic scenario, the increased LVEDP, as well as the decreased CO, and impaired baroreflex control seem to be all factors of sympathetic overactivity in left heart disease (LHD) (23). Similarly, in severe PAH, a right ventricular (RV) failure, due to the pulmonary vascular remodeling, can reduce the systemic CO, provoking a compensatory sympathetic response (24). Moreover, an impaired baroreflex (16) and chemoreflex (25) sensitivities are associated with disease severity in PAH. Otherwise, it was suggested that the peripheral chemoreflex was not a direct mediator of cardiac baroreflex dysfunction in PAH (26). Thus, the sympathetic overactivity in LHD and PAH could be explained, in part, because of a compensatory response from

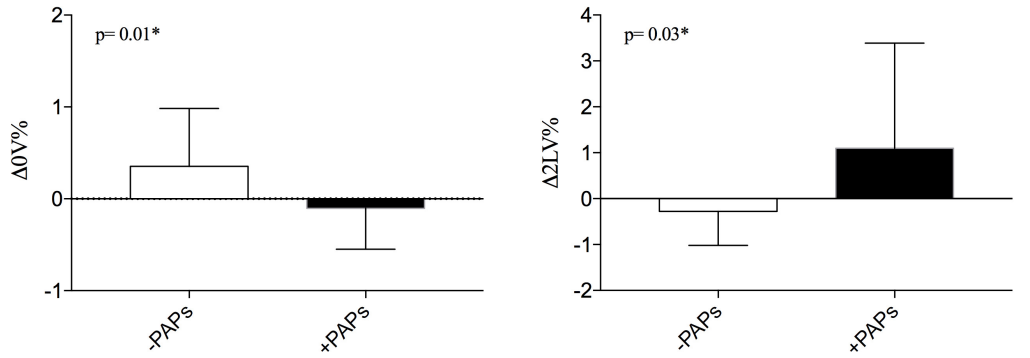

FIGURE 2 | Comparisons of dynamic cardiac response to active standing test between –PAPs and +PAPs groups between. PAPs, mean pulmonary artery pressure; PAPs-, PAPs group of PAPs < median; PAPs+, group of PAPs ≥ median; Δ0V%, [(0V% in supine position-0V% in orthostatic position)/0V% in supine position]. 0V% and 2LV% are non-linear heart rate variability markers of sympathetic and vagal modulation. *$p < 0.05$ from Mann–Whitney *U* test.

an augmented neurohumoral activation to compensate harmed cardiac output mechanics (27).

From our data, an augmented sympathetic heart modulation was positively correlated with pulmonary arterial pressure values irrespective of the cause of PAPs increasing, suggesting that cardiac sympathetic activity could be a reactivity to the blunted response of the right heart and the pulmonary circulation (28, 29). The initially altered RV after-load induces a compensatory reaction of RV itself in order to reduce hemodynamic stress and preserve contractility (e.g., normal values of TAPSE). These compensatory adaptations were linked with enhanced sympathetic activity, which in PAH is actively involved in the pulmonary vascular disease progression (28, 29). Thus, the interplay between sympathetic overactivity and augmented PAPs might be an early marker of RV dysfunction in SSc patients, which deserves further studies.

The Interplay Among Cardiopulmonary Hemodynamic, Autonomic Control, and Inflammation

Our findings are consistent with the concept of the physiological "reserve" of the autonomic nervous system (30, 31), highlighting that the high variation (Δ) is related to better cardiovascular adjustments during autonomic stress tests and orthostatic tolerance (30). From our results, while the +PAPs group seems to present a lower autonomic reserve, the –PAPs group is closer to a normal physiological response to active standing (e.g., increased sympathetic response with a vagal withdrawal).

From the inter-group analysis, the +PAPs group shows higher CRP values compared to the –PAPs group (**Table 1**), with a biological meaning of low-grade inflammation (defined as CRP < 1.0 mg/dL) (32, 33). The low-grade chronic inflammation plays an essential role in the extracellular matrix deposition process leading to cardiopulmonary fibrosis, which represents a major cause of mortality in SSc (34–36). Moreover, in chronic cardiovascular diseases, low-grade inflammation is a marker of vascular disease leading to progression of atherosclerosis and driving ischemic events (32, 33, 37). It is conceivable that a slightly altered inflammatory status induces systemic and pulmonary vascular dysfunction and remodeling with consequent impaired cardiac autonomic modulation. These hypotheses are worthy to be further investigated in SSc.

Clinical Applications and Future Directions

Our data showed that inflammation is related to HRV and high PAPs. Besides the standard treatment of SSc, which aims to control the inflammatory status and disease progression, other type of treatment should be considered. For future directions pharmacological and non-pharmacological approaches that stimulate the vagus nerve activity could be employed to reduce inflammation *via* the anti-inflammatory cholinergic reflex (38, 39).

Limitations

Our study has some limitations. We estimated PAPs by echocardiogram but an invasive measurement of PAPs may assist a better recognition of physiological mechanisms. Moreover, the absence of other parameters of RV structure and function is limiting a comprehensive description of right heart remodeling/overload. The small number of dcSSc enrolled precluded further analyses across different SSc subsets. However, the prevalence of cardiovascular disorders (e.g., arterial hypertension, diastolic dysfunction, altered PAPs values) is not different between lcSSc and dcSSc sub-types (40). Thus, once APAH was excluded, we can suppose that the inter-group analysis is not affected by other bias of selection. Also, we did not evaluate additional markers of inflammation alternative to CRP (such as IL-6, TNF). Further studies with a larger sample size are needed to confirm our observations.

CONCLUSION

Augmented PAPs plays a role in cardiac autonomic control in a cohort of SSc without APAH. High PAPs values were associated with a cardiac sympathetic predominance and a pro-inflammatory status in SSc. These findings encourage the inclusion of HRV analysis (linear and non-linear methods) and active standing test in the screening of PAH in SSc.

Further studies might be conducted to investigate the putative mechanisms underlying the interplay of cardiopulmonary, inflammatory, and autonomic impairments in SSc, such as inflammatory reflex, baroreflex, and chemoreflex control.

DATA AVAILABILITY STATEMENT

The raw data supporting the conclusions of this article will be made available by the authors, without undue reservation.

ETHICS STATEMENT

The studies involving human participants were reviewed and approved by Comitato Etico Milano Area 2. The patients/participants provided their written informed consent to participate in this study.

AUTHOR CONTRIBUTIONS

GR, MV, and CB: substantial contributions to the conception or design of the work and drafting the work. GR, MV, AC, and CB: acquisition and analysis. GR, MV, LB, ET, and CB: interpretation of data for the work. GR, MV, CB, LB, AC, ET, SC, and NM: revising it critically for important intellectual content. GR, MV, CB, LB, AC, ET, SC, and NM: final approval of the version to be published, agreement to be accountable for all aspects of the work in ensuring that questions related to the accuracy, and integrity of any part of the work are appropriately investigated and resolved. SC, ET, and NM: supervision. SC and NM: funding. All authors have read and agreed to the published version of the manuscript.

FUNDING

This research was funded by the Italian Ministry of Health, Ricerca Corrente RC_2021 to NM.

ACKNOWLEDGMENTS

We acknowledge the GILS (Gruppo Italiano per la Lotta alla Sclerodermia) for all support.

REFERENCES

1. Ferri C, Emdin M, Giuggioli D, Carpeggiani C, Maielli M, Varga A, et al. Autonomic dysfunction in systemic sclerosis: time and frequency domain 24-hour heart rate variability analysis. *Br J Rheumatol.* (1997) 36:669–76. doi: 10.1093/rheumatology/36.6.669
2. Komócsi A, Vorobcsuk A, Faludi R, Pintér T, Lenkey Z, Költo G, et al. The impact of cardiopulmonary manifestations on the mortality of SSc: a systematic review and meta-analysis of observational studies. *Rheumatology (Oxford).* (2012) 51:1027–36. doi: 10.1093/rheumatology/ker357
3. Van Den Hoogen F, Khanna D, Fransen J, Johnson SR, Baron M, Tyndall A, et al. Classification criteria for systemic sclerosis: an American college of rheumatology/ European league against rheumatism collaborative initiative. *Arthritis Rheum.* (2013) 65:2737–47.
4. Papo M, Cohen-Aubart F, Trefond L, Bauvois A, Amoura Z, Emile J, et al. Systemic histiocytosis (Langerhans cell histiocytosis, Erdheim Chester disease, Destombes Rosai Dorfman disease): from oncogenic mutations to inflammatory disorders. *Curr Oncol Rep.* (2019) 2:62. doi: 10.1007/s11912-019-0810-6
5. Tyndall AJ, Bannert B, Vonk M, Airo P, Cozzi F, Carreira PE, et al. Causes and risk factors for death in systemic sclerosis: a study from the EULAR Scleroderma Trials and Research (EUSTAR) database. *Ann Rheum Dis.* (2010) 69:1809–15. doi: 10.1136/ard.2009.114264
6. Butt SA, Jeppesen JL, Torp-Pedersen C, Sam F, Gislason GH, Jacobsen S, et al. Cardiovascular manifestations of systemic sclerosis: a Danish nationwide cohort study. *J Am Heart Assoc.* (2019) 8:e013405. doi: 10.1161/JAHA.119.013405
7. Ferri C, Valentini G, Cozzi F, Sebastiani M, Michelassi C, La Montagna G, et al. Systemic sclerosis: demographic, clinical, and serologic features and survival in 1,012 Italian patients. *Medicine (Baltimore).* (2002) 81:139–53. doi: 10.1097/00005792-200203000-00004
8. Hachulla E, Carpentier P, Gressin V, Diot E, Allanore Y, Sibilia J, et al. Risk factors for death and the 3-year survival of patients with systemic sclerosis: the French ItinerAIR-Sclerodermie study. *Rheumatology.* (2009) 48:304–8. doi: 10.1093/rheumatology/ken488
9. Weatherald J, Montani D, Jevnikar M, Jaïs X, Savale L, Humbert M. Screening for pulmonary arterial hypertension in systemic sclerosis. *Eur Respir Rev.* (2019) 28:190023.
10. Santaniello A, Casella R, Vicenzi M, Rota I, Montanelli G, De Santis M, et al. Cardiopulmonary exercise testing in a combined screening approach to individuate pulmonary arterial hypertension in systemic sclerosis. *Rheumatology.* (2020) 59:1581–6. doi: 10.1093/rheumatology/kez473
11. Bienias P, Ciurzyński M, Korczak D, Jankowski K, Glińska-Wielochowska M, Liszewska-Pfejfer D, et al. Pulmonary hypertension in systemic sclerosis determines cardiac autonomic dysfunction assessed by heart rate turbulence. *Int J Cardiol.* (2010) 141:322–5. doi: 10.1016/j.ijcard.2008.11.093
12. Sebestyén V, Szucs G, Páll D, Ujvárosy D, Ötvös T, Csige I, et al. Electrocardiographic markers for the prediction of ventricular arrhythmias in patients with systemic sclerosis. *Rheumatology.* (2020) 59:478–86. doi: 10.1093/rheumatology/kez644
13. Rodrigues GD, Tobaldini E, Bellocchi C, Santaniello A, Caronni M, Severino A, et al. Cardiac autonomic modulation at rest and during orthostatic stress among different systemic sclerosis subsets. *Eur J Intern Med.* (2019) 6:75–80. doi: 10.1016/j.ejim.2019.06.003
14. Leroy EC, Medsger TA. Criteria for the classification of early systemic sclerosis. *J Rheumatol J.* (2001) 28:1573–6.
15. Yi HT, Hsieh YC, Wu TJ, Huang JL, Lin WW, Liang KW, et al. Heart rate variability parameters and ventricular arrhythmia correlate with pulmonary arterial pressure in adult patients with idiopathic pulmonary arterial hypertension. *Heart Lung.* (2014) 43:534–40. doi: 10.1016/j.hrtlng.2014.05.010
16. Velez-Roa S, Ciarka A, Najem B, Vachiery JL, Naeije R, Van de Borne P. Increased sympathetic nerve activity in pulmonary artery hypertension. *Circulation.* (2004) 110:1308–12. doi: 10.1161/01.CIR.0000140724.90898.D3
17. Rabinovitch M, Guignabert C, Humbert M, Nicolls MR. Inflammation and immunity in the pathogenesis of pulmonary arterial hypertension. *Circ Res.* (2014) 115:165–75. doi: 10.1161/CIRCRESAHA.113.301141
18. Wang RR, Yuan TY, Wang JM, Chen YC, Zhao JL, Li MT, et al. Immunity and inflammation in pulmonary arterial hypertension: from pathophysiology mechanisms to treatment perspective. *Pharmacol Res.* (2022) 180:106238. doi: 10.1016/j.phrs.2022.106238
19. Rudski LG, Lai WW, Afilalo J, Hua L, Handschumacher MD, Chandrasekaran K, et al. Guidelines for the echocardiographic assess- ment of the right heart in adults: a report from the American Society of Echocar- diography endorsed by the European Association of Echocardiography, a registered branch of the European Society of Cardiology, and the Canadian Society of

Echocardiography. *J Am Soc Echocardiogr.* (2010) 23:685–713. doi: 10.1016/j.echo.2010.05.010
20. Guzzetti S, Borroni E, Garbelli PE, Ceriani E, Della Bella P, Montano N, et al. Symbolic dynamics of heart rate variability: a probe to investigate cardiac autonomic modulation. *Circulation.* (2005) 112:465–70. doi: 10.1161/CIRCULATIONAHA.104.518449
21. Bienias P, Ciurzyński M, Glińska-Wielochowska M, Szewczyk A, Korczak D, Kalińska-Bienias A, et al. Heart rate turbulence assessment in systemic sclerosis: the role for the detection of cardiac autonomic nervous system dysfunction. *Rheumatology.* (2010) 49:355–60. doi: 10.1093/rheumatology/kep394
22. Vonk Noordegraaf A, Chin KM, Haddad F, Hassoun PM, Hemnes AR, Hopkins SR, et al. Pathophysiology of the right ventricle and of the pulmonary circulation in pulmonary hypertension: an update. *Eur Respir J.* (2019) 53:1801–900. doi: 10.1183/13993003.01900-2018
23. Wensel R, Jilek C, Dorr M, Francis DP, Stadler H, Lange T, et al. Impaired cardiac autonomic control relates to disease severity in pulmonary hypertension. *Eur Respir J.* (2009) 34:895–901. doi: 10.1183/09031936.00145708
24. Leimbach WN Jr., Wallin BG, Victor RG, Aylward PE, Sundlöf G, Mark AL. Direct evidence from intraneural recordings for increased central sympathetic outflow in patients with heart failure. *Circulation.* (1986) 73:913–9. doi: 10.1161/01.cir.73.5.913
25. Vicenzi M, Deboeck G, Faoro V, Loison J, Vachiéry J-L, Naeije R. Exercise oscillatory ventilation in heart failure and in pulmonary arterial hypertension. *Int J Cardiol.* (2016) 202:736–40. doi: 10.1016/j.ijcard.2015.09.087
26. Paula-Ribeiro M, Ribeiro IC, Aranda LC, Silva TM, Costa CM, Ramos R, et al. Cardiac baroreflex dysfunction in patients with pulmonary arterial hypertension at rest and during orthostatic stress: role of the peripheral chemoreflex. *J Appl Physiol (1985).* (2021) 131:794–807. doi: 10.1152/japplphysiol.00152.2021
27. Fauchier L, Babuty D, Melin A, Bonnet P, Cosnay P, Fauchieret JP. Heart rate variability in severe right or left heart failure: the role of pulmonary hypertension and resistances. *Eur J Heart Fail.* (2004) 6:181–5. doi: 10.1016/j.ejheart.2003.09.007
28. Vonk Noordegraaf A, Westerhof BE, Westerhof N. The relationship between the right ventricle and its load in pulmonary hypertension. *J Am Coll Cardiol.* (2017) 69:236–43. doi: 10.1016/j.jacc.2016.10.047
29. Vaillancourt M, Chia P, Sarji S, Nguyen J, Hoftman N, Ruffenach G, et al. Autonomic nervous system involvement in pulmonary arterial hypertension. *Respir Res.* (2017) 18:201. doi: 10.1186/s12931-017-0679-6
30. Convertino VA, Rickards CA, Ryan KL. Autonomic mechanisms associated with heart rate and vasoconstrictor reserves. *Clin Auton Res.* (2012) 22:123–30. doi: 10.1007/s10286-011-0151-5
31. Rodrigues GD, Gurgel JL, Gonçalves TR, Soares PP. The physical capacity of rowing athletes cannot reverse the influence of age on heart rate variability during orthostatic stress. *An Acad Bras Cienc.* (2021) 29:e20201677. doi: 10.1590/0001-3765202120201677
32. Ridker PM, Lüscher TF. Anti-inflammatory therapies for cardiovascular disease. *Eur Heart J.* (2014) 35:1782–91.
33. Lüscher TF. Cardio-oncology: low-grade inflammation as a common pathway of cancer and cardiovascular disease. *Eur Heart J.* (2019) 40:3871–4. doi: 10.1093/eurheartj/ehz928
34. O'Reilly S. Innate immunity in systemic sclerosis pathogenesis. *Clin Sci.* (2014) 126:329–37.
35. Mahoney JM, Taroni J, Martyanov V, Wood TA, Greene CS, Pioli PA. Systems level analysis of systemic sclerosis shows a network of immune and profibrotic pathways connected with genetic polymorphisms. *PLoS Comput Biol.* (2015) 11:e1004005. doi: 10.1371/journal.pcbi.1004005
36. Żoiłkiewicz J, Stochmal A, Rudnicka L. The role of adipokines in systemic sclerosis: a missing link? *Arch Dermatol Res.* (2019) 311:251–63. doi: 10.1007/s00403-019-01893-1
37. Arnold N, Lechner K, Waldeyer C, Shapiro MD, Koenig W. Inflammation and cardiovascular disease: the future. *Eur Cardiol.* (2021) 17:16–e20.
38. Tracey KJ. The inflammatory reflex. *Nature.* (2002) 420:853–9.
39. Bellocchi C, Carandina A, Montinaro B, Targetti E, Furlan L, Rodrigues G, et al. The interplay between autonomic nervous system and inflammation across systemic autoimmune diseases. *Int J Mol Sci.* (2022) 23:2449. doi: 10.3390/ijms23052449
40. Meier FM, Frommer KW, Dinser R, Walker UA, Czirjak L, Denton CP, et al. Update on the profile of the EUSTAR cohort: an analysis of the EULAR Scleroderma Trials and Research group database. *Ann Rheum Dis.* (2012) 71:1355–60. doi: 10.1136/annrheumdis-2011-200742

Conflict of Interest: The authors declare that the research was conducted in the absence of any commercial or financial relationships that could be construed as a potential conflict of interest.

Publisher's Note: All claims expressed in this article are solely those of the authors and do not necessarily represent those of their affiliated organizations, or those of the publisher, the editors and the reviewers. Any product that may be evaluated in this article, or claim that may be made by its manufacturer, is not guaranteed or endorsed by the publisher.

frontiers | Frontiers in Cardiovascular Medicine

BRIEF RESEARCH REPORT
published: 11 July 2022
doi: 10.3389/fcvm.2022.887248

The Potential Anti-remodeling Effect of Paroxetine After Myocardial Infarction May Be Blunted by Beta-Blockers

Oriol Iborra-Egea[1,2†], Alberto Aimo[3,4†], Nicola Martini[4], Carolina Galvez-Monton[1,2], Silvia Burchielli[4], Giorgia Panichella[3], Claudio Passino[3,4], Michele Emdin[3,4] and Antoni Bayes-Genis[1,2,5]*

[1] ICREC (Heart Failure and Cardiac Regeneration) Research Programme, Health Sciences Research Institute Germans Trias i Pujol (IGTP), Barcelona, Spain, [2] Hospital Universitari Germans Trias i Pujol, Badalona, Spain, [3] Institute of Life Sciences, Scuola Superiore Sant'Anna, Pisa, Italy, [4] Cardiology Division, Fondazione Toscana Gabriele Monasterio, Pisa, Italy, [5] CIBER Cardiovascular, Instituto de Salud Carlos III, Madrid, Spain

OPEN ACCESS

Edited by:
Gian Marco Rosa,
San Martino Hospital (IRCCS), Italy

Reviewed by:
Stefano Benenati,
San Martino Hospital (IRCCS), Italy
Edoardo Elia,
University of Genoa, Italy

***Correspondence:**
Antoni Bayes-Genis
abayesgenis@gmail.com

[†] These authors have contributed equally to this work

Specialty section:
This article was submitted to General Cardiovascular Medicine, a section of the journal Frontiers in Cardiovascular Medicine

Received: 01 March 2022
Accepted: 24 June 2022
Published: 11 July 2022

Citation:
Iborra-Egea O, Aimo A, Martini N, Galvez-Monton C, Burchielli S, Panichella G, Passino C, Emdin M and Bayes-Genis A (2022) The Potential Anti-remodeling Effect of Paroxetine After Myocardial Infarction May Be Blunted by Beta-Blockers. Front. Cardiovasc. Med. 9:887248. doi: 10.3389/fcvm.2022.887248

Background: Left ventricular (LV) remodeling consists in maladaptive changes in cardiac geometry and function following an insult such as ST-segment elevation myocardial infarction (STEMI). Interventions able to prevent LV remodeling after a STEMI are expected to improve the outcome of this condition. Paroxetine has inhibitory effects on GRK2, also known as beta-adrenergic receptor kinase 1 (ADRBK1). This drug does not yield beneficial effects on LV remodeling in patients with STEMI and LV ejection fraction $\leq$ 45%.

Methods: We compared the molecular effects of paroxetine and drugs for neurohormonal antagonism (beta-blockers, angiotensin converting enzyme inhibitors/angiotensin receptor blockers, mineralocorticoid receptor antagonists), using a bioinformatic approach integrating transcriptomic data in a swine model of post-MI and available evidence from the literature and massive public databases.

Results: Among standard therapies for MI, beta-blockers are the only ones acting directly upon GKR2, but the mechanism of action overlaps with angiotensin-converting enzyme inhibitors/angiotensin receptor blockers with respect to the AT2R-mediated anti-hypertensive response. Moreover, beta-blockers could have anti-fibrotic and anti-inflammatory effects through the regulation of myocyte-specific enhancer factors, endothelins and chemokines.

Conclusion: The additive benefit of paroxetine on the background of the standard therapy for STEMI, which includes beta-blockers, is expected to be limited. Nonetheless, paroxetine becomes particularly interesting when a beta-blocker is contraindicated (for example, in hypotensive individuals) or poorly tolerated.

Keywords: cardiac remodeling, myocardial infarction, paroxetine, artificial intelligence (AI), beta-blockers (BB)

INTRODUCTION

In-hospital and 30-day mortality associated with ST-segment elevation myocardial infarction (STEMI) has steadily declined over the last decades given the implementation of percutaneous coronary intervention and medical therapy for neurohormonal antagonism (1). This has been accompanied by a striking raise of patients who survive the acute event, but have an increased risk of heart failure (HF) and sudden chronic death (1). The rate of HF hospitalization rate is 4.4% in the first year after STEMI, and around 1.0% per year thereafter (2). In turn, patients who are hospitalized for HF during the first year have a risk of dying or being re-hospitalized for HF increased by 2-and 6-fold, respectively (2).

Left ventricular (LV) remodeling consists in maladaptive changes in cardiac geometry and function developing as a result to the loss of viable myocardium and an increased wall stress. This process involves multiple mechanisms such as tissue resorption, extracellular matrix (ECM) degradation, deposition of granulation tissue and vessel formation, followed by scar maturation, fibrosis and hypertrophy in the remote myocardium. LV remodeling eventually leads to impaired ventricular function and HF (3). Interventions able to prevent LV remodeling after STEMI are expected to improve the outcome of this condition.

A recent study found that paroxetine has no beneficial effects on LV remodeling in patients with STEMI and LV ejection fraction $\leq$ 45%. Specifically, paroxetine treatment was not associated with a recovery in LV ejection fraction compared to placebo (4). The rationale behind this trial was that paroxetine relieves LV remodeling when administered as a stand-alone medication to mice with MI (5). This effect was explained by an inhibitory effect of paroxetine on GRK2, also known as beta-adrenergic receptor kinase 1 (ADRBK1). GRK2 levels and activity have been reported to be enhanced in patients or in preclinical models of several disorders, including cardiac hypertrophy and HF, and to contribute to disease progression by a variety of mechanisms related to its multifunctional roles (6).

In this study, we aimed to elucidate whether the beneficial effects of pirfenidone observed in pre-clinical models do not translate into a clinical benefit because of overlapping mechanisms of action with other therapeutic approaches. Thus, we analyzed the molecular effects of drugs for neurohormonal antagonism (beta-blockers, angiotensin converting enzyme inhibitors/angiotensin receptor blockers, and mineralocorticoid receptor antagonists), which are recommended for patients with MI and systolic dysfunction.

METHODS

Proteins Involved in Post-MI Remodeling or Modulated by Pirfenidone

Articles published over the last 10 years on the molecular pathophysiology of post-MI remodeling were searched in PubMed on October 7, 2020 with the following keywords: post(title) and [infarct*(title) or stroke (title)] and [myocardial (title) or cardiovascular (title) or cardiac (title)] AND [pathophysiology (Title/Abstract) OR pathogenesis (Title/Abstract) OR molecular (Title/Abstract)]. If the involvement of a protein candidate in post-MI remodeling was not well established, an additional PubMed search was performed, including all protein names according to UniProtKB.

Post-MI Gene Expression Data in Swine

The Gene Expression Omnibus (7) and Array Express (8) public repositories were searched for gene expression data on post-MI remodeling with the following query (on December 9, 2020). No gene expression datasets from human myocardial tissue biopsies could be found. Our group previously employed microarray gene expression profiling of porcine cDNA to compare myocardial gene expression at baseline, 1, 4, and 6 weeks after surgically induced MI and in sham-operated controls (9). The swine transcriptomics were translated to their human equivalents *via* Reciprocal Best Hits (RBH) with BLAST and Gene Name Correspondence and the InParanoid database (10). Microarray data was processed using the GEO2R tool (7), and processed using the neqc method (11) and Linear Models for Microarray Analysis (12). We only considered genes with an adjusted p-value of < 0.01 (Benjamini-Hochberg false discovery rate), and log(fold-change) > 0.25. For introduction into the protein network, gene information was mapped one-to-one with proteins. In the end, 4,737 proteins were included. This information was used as experimental reference to model the algorithms and contrast the *in silico* findings to ensure their adhere to experimental evidence.

Molecular Mechanisms of Action of Drugs

Artificial neural network (ANN) strategy can identify relationships among network regions (generalization) (13), allowing to infer the likelihood of a relationship between ≥ 2 sets of proteins. In this case, we tested each protein against the post-MI remodeling signature. Next, the model is validated using different data sets from the literature and databases. This system attempts to find the shortest distance between the 2 protein sets, generating a list of proteins ranked by their association with disease pathophysiology. ANN scores were calculated for angiotensin converting enzyme inhibitors (ACEi; target gene ACE, Uniprot P12821), angiotensin receptor blockers (ARB; target gene AGTR1, Uniprot P30556), beta-blockers (target gene ADRB1, Uniprot P08588), and mineralocorticoid receptor antagonists (MRA; target gene NR3C2, Uniprot P08235).

We then constructed a protein-protein interaction (PPI) network that contains all post-MI effectors to investigate the biological interactions of ACEi, ARB, beta-blockers, and MRA targets using the String platform (14). All scores rank from 0 to 1, with 1 being the highest possible confidence in judging the interaction as true. Here we used a minimum score of 0.9 to investigate how ACEi/ARB, beta-blockers, and MRA targets interact with our molecular characterization of post-MI remodeling, which includes 222 proteins. Unsupervised clustering was performed using a K-Means approach,

with the number of clusters (K = 10) determined through the elbow method.

RESULTS

Beta-Blockers Selectively Target GRK2 Signaling Pathway

The constructed ANN network identified GRK2 signaling pathway as one of the main targeted mechanisms by gold-standard drugs during the pathology characterization. Through a PPI analysis, we found that beta-blockers strongly modulate GRK2 activity (blue dots in **Figure 1**), as well as venous smooth muscle contraction, which in turn is related to the renin-angiotensin-aldosterone (RAA) pathway, and includes several family-members of GRK2.

Moreover, this targeted mechanism of action seems to be specific of beta-blockers, as only beta-blockers appear to act directly upon GRK2.

ACEi Reinforce Beta-Blockers Mechanism of Action Upon GRK2 by AT2R-Mediated Vasodilation

By inhibiting AGTR1, ACEi disrupt the ACE/Angiotensin II/AT1R molecular cascade and allows AT2R to exert vasodilation functions. GRK2 is described to desensitize beta-adrenergic receptors to G-protein coupled receptors (GPCRs), such as AT2R. Here we identified that this binding blocks G-protein coupling and leads to internalization of AT2R *via* the b-arrestin Arrb1. AT2R then cannot compete with AT1R, which results in vasoconstriction and thus increases arterial blood pressure.

By decreasing the levels of Angiotensin II/AT1R complex, ACEi balances AT2R expression, induce vasodilation through a nitric oxide/bradykinin-dependent pathway and exert a synergistic effect upon GRK2 direct inhibition by beta-blockers.

ARBs work very similarly to ACEi, but act by blocking AT1R directly (which also increases AT2R effect), inciting vasodilation, but do not compete directly with the same proteins as beta-blockers.

MRAs have not been found to act upon any common signaling pathway with GRK2 or beta-blockers.

Regulation of Myocyte-Specific Enhancers, Endothelins and Chemokines Drive Anti-fibrotic and Anti-inflammatory Properties

Our analysis also shows that beta-blockers could also have anti-fibrotic and anti-inflammatory effects in post-MI LV remodeling with myocyte-specific enhancer factors (MEF2A, MEF2C, MEF2D), endothelins (EDN and EDNRA) and a series of chemokines, such as CXCL1, CXCL2, and IL-8, as mediators.

Upon the MI insult, MEFs transmits a stress response in cell growth, survival and apoptosis *via* CAMKII and the MAPK pathways. At the same time, our analysis uncovers the important role of RELA (P65) as a mediator of this pro-inflammatory cascade by directly regulating endothelial cells and T-cells expression of EDN and EDNRA or CXCL1 and CXCL2, respectively.

DISCUSSION

In this manuscript, we wanted to investigate why paroxetine could have failed to improve LV remodeling in STEMI patients with LVEF < 45% in a recent trial (4), despite the very interesting pre-clinical findings studies (5), attributed to the inhibition of GRK2.

We hypothesized that this beneficial effect seen in mice could be lost when translated to the clinical setting because STEMI patients already receive other pharmacological treatments that could be masking this effect. For this reason, we wanted to investigate if these other treatments could already be acting upon GRK2 or similar processes.

Among standard therapies for MI, beta blockers are the only ones acting directly upon GKR2, but the mechanism of action overlaps with angiotensin-converting enzyme inhibitors/angiotensin receptor blockers with respect to the AT2R-mediated anti-hypertensive response.

AT2R is a G-protein-coupled receptor and the physiological function of GPCRs is regulated by G protein–coupled receptor kinases (GRKs). The blockade of beta-adrenergic receptors significantly increases the affinity of GPCR for b-arrestin in the cytoplasm, leading to the formation of a complex and thereby terminating signal transduction (15).

We were able to incorporate hundreds of thousands of protein interactions into our models, making them the most robust possible and the most trustworthy considering the current state of scientific knowledge. We report that the inhibitory effects of paroxetine and beta-blockers are overlapping, and the additive benefit of paroxetine on the background of the standard therapy for STEMI, which includes beta-blockers (1), is expected to be limited. This conclusion is in agreement with the proposed limited efficacy of paroxetine modulation in the post-MI setting. Then, therapy with paroxetine may become particularly interesting when a beta-blocker is contraindicated (for example, in hypotensive individuals) or when is poorly tolerated.

Future studies should investigate the possibility to replace beta-blockade with selective modulation of GRK2 to reverse LV remodeling after a STEMI.

LIMITATIONS

Our approach has some limitations. The AI-based models used in this study only incorporate information that has already been described and demonstrated experimentally. As knowledge on paroxetine and post-MI omics information is rapidly evolving, it is likely that the mechanism of action is more multifactorial than currently presented. Any future discovery of protein function or new information that changes what we know about the disease or the drugs under study cannot be captured and may change the results presented here. Finally, the pharmacological effect of these drugs upon STEMI could encompass, and be

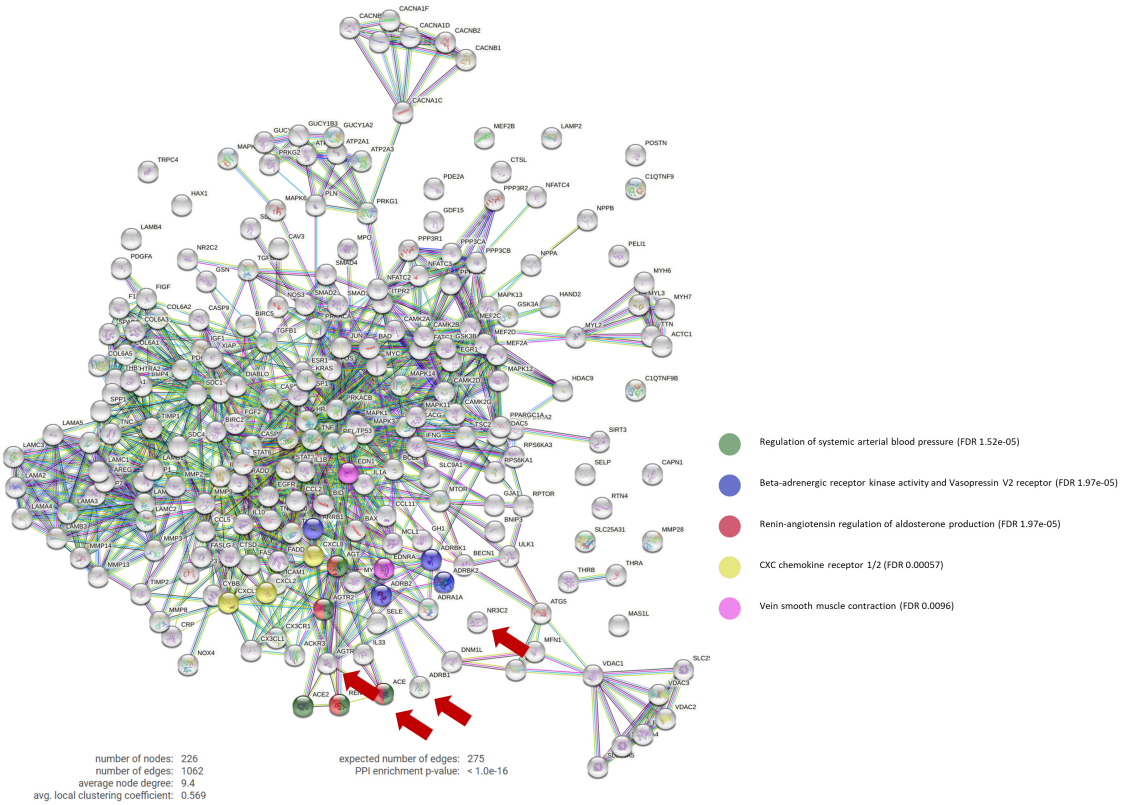

FIGURE 1 | Protein-Protein interaction network. PPi network that contains the interactions between the main targets of ACEi, BB, MRA, and ARB treatments (ACE1, ADRB1, NR3C2, and AGTR1, respectively) and our curated molecular characterization of post-MI remodeling (which includes 222 proteins). BB main effect involve the Beta-adrenergic receptor kinase activity and vasopressin V2 receptor biological pathways (in blue), which include GPRK2 modulation. Number of nodes: 226; Number of connections: 1,062; Expected number of random connections: 275; PPi Enrichment *p*-value: < 1.0e-16; PPi, Protein-protein interaction; ACEi, angiotensin converting enzyme inhibitors; BB, beta-blockers; MRA, mineralocorticoid receptor antagonists; ARB, angiotensin receptor blockers.

affected by, other molecular signaling cascades, as well as by a wide variety of physiological affected pathways. Although our models show that GRK2 signaling is the most robust pathway affected, it is likely that other pathways may be involved as well.

DATA AVAILABILITY STATEMENT

The datasets presented in this study can be found in online repositories. The names of the repository/repositories and accession number(s) can be found below: https://www.ncbi.nlm.nih.gov/geo/, GSE34569.

ETHICS STATEMENT

The animal study was reviewed and approved by the Animal Experimentation Unit Ethical Committee of the Catalan Institute of Cardiovascular Sciences (ICCC) [Permit No. 4563; Departament de Medi ambient i Habitatge (DMAH), Generalitat de Catalunya]. The protocol complied with all guidelines concerning the use of animals in research and teaching, as defined by The Guide for the Care and Use of Laboratory Animals (NIH Publication No. 80–23, revised 1996).

AUTHOR CONTRIBUTIONS

OI-E and AA contributed to conception and design of the study. OI-E performed all bioinformatic analyses. AA wrote the first draft of the manuscript. OI-E, AA, AB-G, and ME wrote sections of the manuscript. AB-G and ME supervised the study. All authors contributed to manuscript revision, read, and approved the submitted version.

FUNDING

This work was supported in part by the grants from MICINN (PID2019-110137RB-I00, PLEC2021-008194), Instituto de Salud Carlos III (PIC18/00014, ICI19/00039, ICI20/00135, PI21/01700, PI21/01703), Red RICORS (PI21/01703), CIBERCV (CB16/11/00403) as a part of the Plan Nacional de I+D+I, and it was co-funded by the ISCIII-Subdirección General de Evaluación y el Fondo Europeo de Desarrollo Regional (FEDER) and AGAUR (2017-SGR-483, 2019PROD00122).

REFERENCES

1. Ibanez B, James S, Agewall S, Antunes MJ, Bucciarelli-Ducci C, Bueno H, et al. 2017 ESC guidelines for the management of acute myocardial infarction in patients presenting with ST-segment elevation: the task force for the management of acute myocardial infarction in patients presenting with ST-segment elevation of the European society of cardiology (ESC). *Eur Heart J.* (2018) 39:119–77.
2. Taniguchi T, Shiomi H, Morimoto T, Watanabe H, Ono K, Shizuta S, et al. Incidence and prognostic impact of heart failure hospitalization during follow-up after primary percutaneous coronary intervention in ST-segment elevation myocardial infarction. *Am J Cardiol.* (2017) 119:1729–39.
3. Gombozhapova A, Rogovskaya Y, Shurupov V, Rebenkova M, Kzhyshkowska J, Popov SV, et al. Macrophage activation and polarization in post-infarction cardiac remodeling. *J Biomed Sci.* (2017) 24:13.
4. Pilgrim T, Vollenbroich R, Deckarm S, Gräni C, Dobner S, Stark AW, et al. Effect of paroxetine-mediated G-protein receptor kinase 2 inhibition vs placebo in patients with anterior myocardial infarction: a randomized clinical trial. *JAMA Cardiol.* (2021) 6:1171–6. doi: 10.1001/jamacardio.2021.2247
5. Schumacher SM, Gao E, Zhu W, Chen X, Chuprun JK, Feldman AM, et al. Paroxetine-mediated GRK2 inhibition reverses cardiac dysfunction and remodeling after myocardial infarction. *Sci Transl Med.* (2015) 7:277ra31.
6. Murga C, Arcones AC, Cruces-Sande M, Briones AM, Salaices M, Mayor F Jr. G Protein-coupled receptor kinase 2 (GRK2) as a potential therapeutic target in cardiovascular and metabolic diseases. *Front Pharmacol.* (2019) 10:112.
7. Barrett T, Wilhite SE, Ledoux P, Evangelista C, Kim IF, Tomashevsky M, et al. NCBI GEO: archive for functional genomics data sets–update. *Nucleic Acids Res.* (2013) 41:D991–5. doi: 10.1093/nar/gks1193
8. Athar A, Füllgrabe A, George N, Iqbal H, Huerta L, Ali A, et al. ArrayExpress update - from bulk to single-cell expression data. *Nucleic Acids Res.* (2019) 47:D711–5. doi: 10.1093/nar/gky964
9. Prat-Vidal C, Gálvez-Montón C, Nonell L, Puigdecanet E, Astier L, Solé F, et al. Identification of temporal and region-specific myocardial gene expression patterns in response to infarction in swine. *PLoS One.* (2013) 8:e54785. doi: 10.1371/journal.pone.0054785
10. Sonnhammer EL, Östlund G. InParanoid 8: orthology analysis between 273 proteomes mostly eukaryotic. *Nucleic Acids Res.* (2015) 43:D234–9. doi: 10.1093/nar/gku1203
11. Shi W, Oshlack A, Smyth GK. Optimizing the noise versus bias trade-off for illumina whole genome expression beadchips. *Nucleic Acids Res.* (2010) 38:e204. doi: 10.1093/nar/gkq871
12. Smyth GK. Linear models and empirical bayes methods for assessing differential expression in microarray experiments. *Stat Appl Gene Mol Biol.* (2004) 3:1–25.
13. Pujol A, Mosca R, Farrés J, Aloy P. Unveiling the role of network and systems biology in drug discovery. *Trends Pharm Sci.* (2010) 31:115–23.
14. Gomez de Agüero M, Ganal-Vonarburg SC, Fuhrer T, Rupp S, Uchimura Y, Li H, et al. The maternal microbiota drives early postnatal innate immune development. *Science.* (2016) 351:1296–302. doi: 10.1126/science.aad2571
15. Gurevich VV, Gurevich EV. GPCR signaling regulation: the role of GRKs and arrestins. *Front Pharmacol.* (2019) 10:125. doi: 10.3389/fphar.2019.00125

Conflict of Interest: The authors declare that the research was conducted in the absence of any commercial or financial relationships that could be construed as a potential conflict of interest.

frontiers | Frontiers in Cardiovascular Medicine

TYPE Original Research
PUBLISHED 14 October 2022
DOI 10.3389/fcvm.2022.1030618

OPEN ACCESS

EDITED BY
Jinwei Tian,
The Second Affiliated Hospital of Harbin Medical University, China

REVIEWED BY
Shuo Wang,
Department of Neonatology, Xiangya Hospital, Central South University, China
Cheng-Chao Ruan,
Fudan University, China
Yusheng Pang,
Guangxi Medical University, China
Cheng Wang,
Department of Pediatrics, The Second Xiangya Hospital, Central South University, China
Zhi Xin Shan,
Guangdong Provincial People's Hospital, China
Jie Tian,
Children's Hospital of Chongqing Medical University, China

*CORRESPONDENCE
Junbao Du
junbaodu1@126.com
Hongfang Jin
jinhongfang51@126.com

†These authors have contributed equally to this work

SPECIALTY SECTION
This article was submitted to General Cardiovascular Medicine, a section of the journal Frontiers in Cardiovascular Medicine

RECEIVED 29 August 2022
ACCEPTED 27 September 2022
PUBLISHED 14 October 2022

CITATION
Wang Y, Wang Y, He B, Tao C, Han Z, Liu P, Wang Y, Tang C, Liu X, Du J and Jin H (2022) Plasma human growth cytokines in children with vasovagal syncope.
Front. Cardiovasc. Med. 9:1030618.
doi: 10.3389/fcvm.2022.1030618

Plasma human growth cytokines in children with vasovagal syncope

Yuanyuan Wang[1†], Yaru Wang[1†], Bing He[2†], Chunyan Tao[1], Zhenhui Han[3], Ping Liu[1], Yuli Wang[1], Chaoshu Tang[4,5], Xueqin Liu[1], Junbao Du[1,4*] and Hongfang Jin[1*]

[1]Department of Pediatrics, Peking University First Hospital, Beijing, China, [2]Department of Pediatrics, People's Hospital of Wuhan University, Hubei, China, [3]Department of Cardiology, Children's Hospital of Kaifeng, Kaifeng, China, [4]Key Laboratory of Molecular Cardiovascular Sciences, Ministry of Education, Beijing, China, [5]Department of Physiology and Pathophysiology, Health Science Centre, Peking University, Beijing, China

Purpose: The study was designed to investigate the profile of plasma human growth cytokines in pediatric vasovagal syncope (VVS).

Materials and methods: In the discovery set of the study, plasma human growth cytokines were measured using a Quantiboby Human Growth Factor Array in 24 VVS children and 12 healthy controls. Scatter and principal component analysis (PCA) diagrams were used to describe the samples, an unsupervised hierarchical clustering analysis was used to categorize the samples. Subsequently, the cytokines obtained from the screening assays were verified with a suspension cytokine array in the validation set of the study including 53 VVS children and 24 controls. Finally, the factors associated with pediatric VVS and the predictive value for the diagnosis of VVS were determined.

Results: In the discovery study, the differential protein screening revealed that the plasma hepatocyte growth factor (HGF), transforming growth factor b1 (TGF-b1), insulin-like growth factor binding protein (IGFBP)-4, and IGFBP-1 in children suffering from VVS were higher than those of the controls (all adjust P- value < 0.05). However, the plasma IGFBP-6, epidermal growth factor (EGF), and IGFBP-3 in pediatric VVS were lower than those of the controls (all adjust P- value < 0.01). Meanwhile, the changes of 7 differential proteins were analyzed by volcano plot. Unsupervised hierarchical cluster analysis demonstrated that patients in the VVS group could be successfully distinguished from controls based on the plasma level of seven differential proteins. Further validation experiments showed that VVS patients had significantly higher plasma concentrations of HGF, IGFBP-1, and IGFBP-6, but lower plasma concentrations of EGF and IGFBP-3 than controls. The logistics regression model showed that increased plasma concentration of HGF and IGFBP-1 and decreased plasma concentration of EGF were correlated with the development of pediatric VVS. ROC curve analysis showed that the abovementioned 3 proteins were useful for assisting the diagnosis of VVS.

Conclusion: Plasma human growth cytokine profiling changed in pediatric VVS. Elevated plasma concentrations of HGF and IGFBP-1, and decreased EGF were associated factors in the development of pediatric VVS. The abovementioned three proteins are helpful for the diagnosis of pediatric VVS.

KEYWORDS

vasovagal syncope, human growth cytokine, plasma sample, children, validation

Introduction

Syncope is common in children and is thought to be a transient loss of consciousness due to transient cerebral hypoperfusion with the loss of muscle tone and a failure to maintain posture. Vasovagal syncope (VVS) accounts for 60–70% of pediatric syncope (1–3). Syncopal recurrent episodes can severely affect physical and psychological health and even result in unpredictable injuries to children due to falls (4).

A previous study demonstrated that the flow-mediated vasodilation was enhanced in children with VVS at the supine position (5), suggesting that children and adolescents with VVS had excessive vasodilation (6, 7). Similarly, levels of hydrogen sulfide in plasma and erythrocytes were also remarkably increased in supine VVS children (8, 9). Furthermore, serum endothelin 1 (ET-1) was significantly increased in pediatric VVS at supine and initial tilt positions (10), whereas another study suggested that plasma ET-1 was not increased during tilt and before syncope (11). The imbalance between vasoconstriction and vasodilation may be associated with neurohumoral dysregulation, but the regulatory mechanisms for vascular dysfunction in children with VVS remain unclear. It is reported that vascular growth cytokines play an essential role in regulating vasomotor function directly or indirectly. For instance, epidermal growth factor (EGF) (12), platelet-derived growth factor (PDGF) (13), and fibroblast growth factor (FGF) (14) were associated with vasoconstriction. On the contrary, insulin-like growth factor binding protein (IGFBP)-1 (15) and hepatocyte growth factor (HGF) (16) were related to vasodilation.

However, the expression profile of growth cytokines in the plasma and the possible pathophysiologic and clinical significance in the development of pediatric VVS remain unclear. In recent years, cytokine antibody arrays enable us to precisely identify the expression of multiple cytokines simultaneously. At present, it has been extensively applied in the research field because of its advantages of high detection sensitivity and specificity, and the high throughput of arrays (17, 18). The suspension cytokine array can also be used to verify the selected biomarkers with very low protein concentrations by low-dose plasma samples. Therefore, in this study, the cytokine antibody arrays were used to determine the expression profile of cytokines, and the suspension cytokine arrays were used to validate the changes in growth cytokine expression to clarify whether plasma growth cytokines were involved in the development of pediatric VVS and its possible clinical implication.

Materials and methods

Study participants

As shown in **Figure 1**, the VVS group consisted of pediatric patients with VVS admitted to the Peking University First Hospital from April 2016 to January 2019 and the control group included healthy children identified as healthy based on their medical history, physical examination, and laboratory inspection from a middle school. In the discovery set of the study, there were 24 children in the VVS group and another 12 children in the control group. While, in the validation set of the study, 53 children were included in the VVS group and another 24 children served as controls.

Inclusion criteria of the study patients: (1) children aged 5–18 years; (2) patients diagnosed with VVS; (3) with adequate plasma samples. The following patients were excluded: (1) with incomplete clinical data; (2) hemolysis of plasma specimens; (3) patients with neurological, metabolic, cardiovascular, or mental disease.

The diagnostic criteria of pediatric VVS are as follows (19, 20): (1) with predisposing factors such as persistent standing, or a sultry environment; (2) with syncope or presyncope clinically; (3) with a positive response appearance in baseline head-up tilt test (BHUTT): significant blood pressure (BP) drop [systolic BP (SBP) $\leq$ 80 mmHg or diastolic BP (DBP) $\leq$ 50 mmHg or mean BP drop by $\geq$ 25%]; and (or) heart rate (HR) decline (HR $<$ 75 bpm for those at 4–6 years old, HR $<$ 65 bpm for those at ~8 years old or HR $<$ 60 bpm for those over 8 years old; and (4) excluding other possible causes of syncope, such as cardiac syncope and cerebrovascular diseases. The children in the control group met the following conditions: (1) no syncope or presyncope occurred clinically; and (2) no positive findings on physical and laboratory examinations. The research was

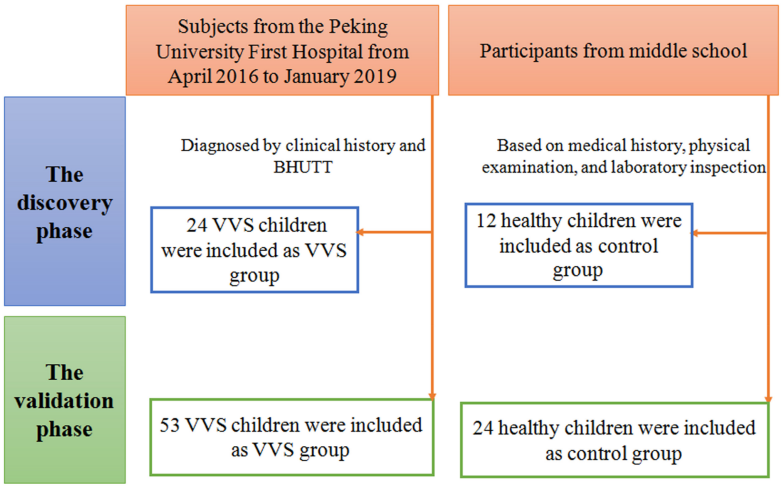

FIGURE 1
Flow-chart of patient inclusion. In the discovery phase, a total of 36 subjects were included, including 24 cases in the VVS group and 12 cases in the control group. In the validation phase, a total of 77 cases were included, including 53 cases in the VVS group and 24 cases in the control group. BHUTT, baseline head-up tilt test; VVS, vasovagal syncope.

permitted by the Biomedical Research Ethics Committee of Peking University First Hospital (2018 [112]) and followed the Declaration of Helsinki. The informed consent was approved by the Committee of Peking University First Hospital and was acquired from the subjects' guardians.

BHUTT

Subjects fasted for more than 4 h and were asked to avoid taking any drugs that affected autonomic nervous function before the test. Firstly, the patient lay on his back on a tilt bed (SHUT-100A, Standard, Jiangsu and ST-711, Juchi, Beijing, China) for at least 10 min. The multi-lead electrocardiogram (ECG) monitor (General Electric, New York, NY, USA) was used to continuously measure HR and ECG, and a Finapres Medical System-FMS (FinometerPRO, FMS Company, Netherlands) was applied to dynamically monitor BP in a warm and quiet condition. Subsequently, the tilt bed was tilted at 60°, and the ECG, HR, and BP were measured until the appearance of a positive response, or otherwise, the child finished the whole test duration of 45 min if no positive response was observed (21, 22).

Plasma specimen collection

Blood samples of the participants were collected before the patients with BHUTT. Totally 2 ml of venous blood was obtained from subjects in the VVS and control groups under fasting, quiet and supine states. The blood was anticoagulated with ethylene diamine tetraacetic acid and centrifuged at 4°C at 2,000 r/min for 20 min. Subsequently, the supernatant was acquired and added with aprotinin in a ratio of 1:100. The plasma was then immediately frozen at −80°C until further detection.

Cytokine antibody arrays

Plasma levels of human growth cytokines in 24 VVS patients and 12 healthy children were detected by cytokine antibody arrays. The Human Growth Factor Array 1 (QAH-GF-1, Quantiboby; RayBiotech; Norcross, GA, USA) was used to detect 40 selected cytokines simultaneously. The assay was carried out in strict accordance with the instructions and sandwich immunoassay principle. Eighty microliters (μl) of detection antibody cocktail were applied to each well to immobilize the antibody targeting the selected cytokine at a

TABLE 1 Clinical characteristics of the study population in the discovery study.

Groups	VVS (n = 24)	Control (n = 12)	χ^2/t	P-value
Sex (M/F) (n)	10/14	7/5	0.348	0.555
Age (years old)	11.2 ± 2.5	10.5 ± 0.8	1.250	0.221
Height (cm)	153.1 ± 16.2	149.3 ± 3.2	1.105	0.279
Weight (kg)	44.2 ± 13.1	43.5 ± 5.6	0.210	0.835
Supine HR (bpm)	83.8 ± 17.3	82.1 ± 8.1	0.315	0.755
Supine SBP (mmHg)	110.0 ± 11.0	112.0 ± 7.0	−0.449	0.657
Supine DBP (mmHg)	67.0 ± 7.0	63.0 ± 9.0	1.706	0.097

VVS, vasovagal syncope; HR, heart rate; SBP, systolic blood pressure; DBP, diastolic blood pressure.
Normally distributed data are displayed with mean ± standard deviation; Categorical variables are presented by numbers.

TABLE 2 Clinical characteristics of the study population in the validation study.

Groups	VVS ($n = 53$)	Control ($n = 24$)	$\chi^2/Z/t$	*P*-value
Sex (M/F) (*n*)	21/32	14/10	2.333	0.127
Age (years old)	10.0 (8.0, 13.0)	10.0 (10.0, 11.0)	−0.190	0.849
Height (cm)	152.0 (132.5, 161.0)	146.0 (139.3, 150.8)	−0.991	0.322
Weight (kg)	40.6 ± 12.5	39.4 ± 9.2	0.438	0.663
Supine HR (bpm)	81.8 ± 14.2	82.5 ± 8.4	−0.228	0.820
Supine SBP (mmHg)	107.0 (100.5, 116.5)	110.5 (106.0, 115.0)	−0.886	0.376
Supine DBP (mmHg)	66.4 ± 7.6	64.8 ± 9.1	0.806	0.423

VVS, vasovagal syncope; HR, heart rate; SBP, systolic blood pressure; DBP, diastolic blood pressure.
Normally distributed data are displayed with mean ± standard deviation and non-normally distributed data are presented by median (P_{25}, P_{75}); Categorical variables are displayed with numbers.

specific location on the surface of the array glass. Cytokines present in the plasma were recognized by the corresponding antibodies and conjugated with Cy3 equivalent dye-conjugated streptavidin to detect the binding cytokines. The signals can be visualized using fluorescent dye by InnoScan 300 Microarray Scanner (Innopsys, Carbonne, France), and were detected with a Cy3 (532 nm) wavelength (green channel). The catalog number of the Q-Analyzer Tool specific for this array is QAH-GF-1-SW.

Suspension cytokine arrays

The concentrations of cytokines identified in the cytokine antibody array were further validated in plasma samples from 53 VVS patients and 24 control children using the Human Premixed Multi-Analyte Kit (Luminex 200 system; Cat: LXSAHM-01 [L130457] and LXSAHM-07 [L130460]; Luminex Corporation, Austin, TX, USA) according to the manual. The selected cytokines included IGFBP-6, EGF, HGF, IGFBP-1, IGFBP-4, and IGFBP-3. An amount of 50 μl sample was added to each well and incubated with RD2-1 diluted magnetic beads for 2 h in the dark. After three washes using a Magnetic Plate Washer (Tecan), the samples were incubated with the diluted biotin-antibody cocktail for 1 h in a dark environment. After discarding the biotin-antibody cocktail, it was rewashed with a Magnetic Plate Washer (Tecan) three times. And the streptavidin-conjugated phycoerythrin was used to visualize the captured cytokines and the specific concentration of each cytokine was calculated automatically using a Luminex 200 array reader (Luminex Corporation, Austin, TX, USA).

Statistical analysis

As the analysis software, language R (version number 4.1.2) was used in the screening of the differentially expressed proteins. The analysis method is moderated *t*-statistics, and

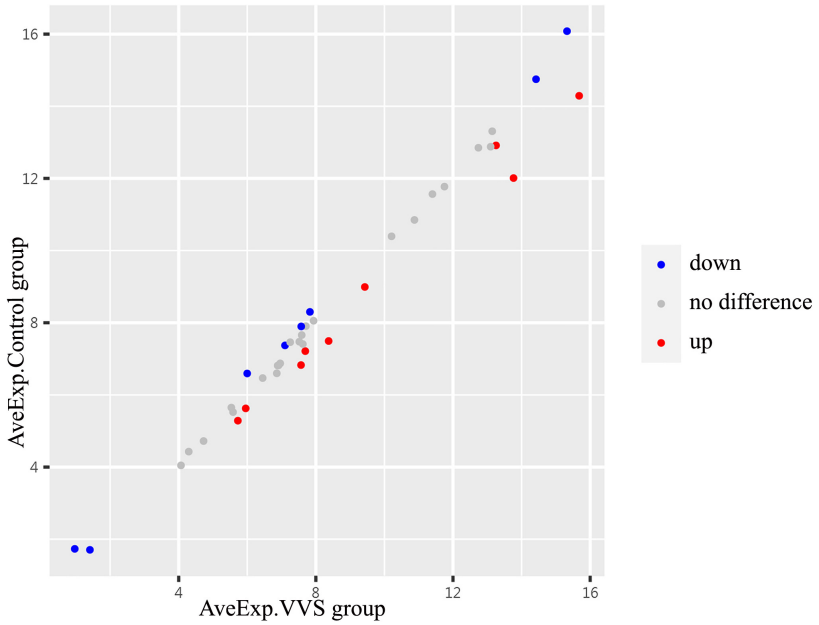

FIGURE 2
The centralized tendency of two sets of chip data was evaluated by scatter plot. Red presents up-regulation, blue presents down-regulation, and gray presents no difference. The X- and Y-axis show the average plasma protein concentrations of VVS group and of the control group, respectively. AveExp.VVS group, the average plasma protein concentration of the VVS group; AveExp.Control group, the average plasma protein concentration of the control group.

the data package is limma. Adjust *P*- value (Adj. *P*. Val, BH method corrected *P*- value) < 0.05 and fold change > 1.2 or < 0.83 [absolute logFC (expression difference multiple in 2 is the bottom) > 0.263] were used to select the differential proteins. After the screening of the differential proteins, it was visualized by volcano plot, with the drawing function being ggplot2, and the data packet ggfortify. The principal component analysis (PCA) plot adopts the prcomp function, the drawing function is autoplot, and the data packet is ggfortify. The cluster heatmap analysis method is the heatmap.2 function and the data packet is gplots.

In the analysis of the clinical characteristics of the study population and biomarkers verification, the software of SPSS 23.0 (IBM, Armonk, NY, USA) was carried out. Data normality was verified by the Kolmogorov-Smirnov test. The measurement variables with a normal distribution were displayed with mean ± standard deviation (SD). Otherwise, the data were displayed with median (P_{25}, P_{75}), respectively. When the two sets of measurement data met the normal distribution, the independent sample *t*- test was applied to compare the difference between the groups, or otherwise, the Mann-Whitney U test was adopted. The categorical variables were displayed with the number of cases. Categorical variables were compared with the χ^2 test between groups. The multivariate analysis was achieved by a logistic regression model (conditional forward method). *P*- values of <0.05 were thought to be remarkably different.

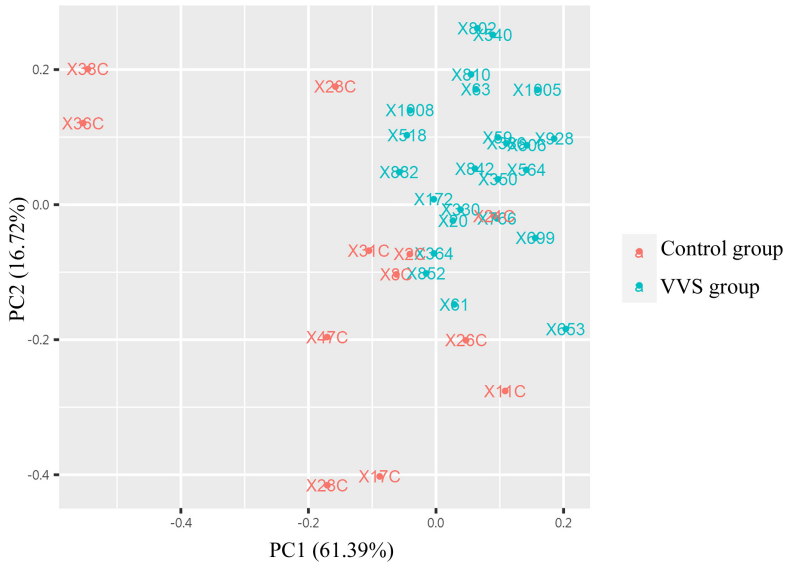

FIGURE 3
The analysis of principal component analysis (PCA) between the two groups. PCA analysis showed that the data tended to clustered distribution and were distributed in two-dimensional space, suggesting that samples have good representativeness and biological repeatability, and are suitable for further analysis. The red color presents the control group, and the green color presents the VVS group. VVS, vasovagal syncope.

TABLE 3 Plasma protein profile between VVS and control groups in the discovery study.

Biomarkers	VVS group	Control group	Log FC	*P*-value	Adj. *P*. Val	Log_2 (FC)
Log_2 IGFBP-4 (pg/ml)	15.7 ± 0.6	14.3 ± 1.1	1.389	<0.001	<0.001	2.619
Log_2 HGF (pg/ml)	7.6 ± 0.5	6.8 ± 0.5	0.741	<0.001	<0.001	1.671
Log_2 IGFBP-6 (pg/ml)	14.4 ± 0.2	14.8 ± 0.1	−0.328	<0.001	<0.001	0.797
[&]Log_2 (EGF + 1) (pg/ml)	0.9 (0.5, 1.3)	1.6 (1.3, 2.1)	−0.764	<0.001	0.001	0.589
Log_2 IGFBP-3 (pg/ml)	15.4 (15.2, 15.6)	16.2 (16.0, 16.3)	−0.757	<0.001	0.002	0.592
Log_2 TGF-b1 (pg/ml)	13.7 (13.3, 14.4)	12.7 (11.2, 13.9)	1.755	<0.001	0.004	3.376
Log_2 IGFBP-1 (pg/ml)	8.4 ± 1.0	7.5 ± 0.8	0.879	0.007	0.030	1.839

IGFBP, insulin-like growth factor binding protein; HGF, hepatocyte growth factor; EGF, epidermal growth factor; TGF-b1, transforming growth factor beta-1; Adj. *P*. Val, BH method adjusted *p*-value; Normally distributed data are displayed with mean ± standard deviation and non-normally distributed data are presented by median (P_{25}, P_{75}); Log_2(FC), Log_2 (fold change).

[&]To prevent the calculation site from being negative, the EGF is expressed on a log2-scale by adding 1 to the original plasma concentration.

And other biomarkers plasma concentrations of the assessed proteins are expressed on a log2-scale.

Differentially expressed proteins (DEPs) are defined as those with Adj. *P*. Val < 0.05, and fold change > 1.2 or <0.83 (absolute logFC > 0.263).

Results

Participants information

In the discovery set of the study, there were 24 patients in the VVS group and 12 healthy children in the control group, and the mean age was 11.2 ± 2.5 and 10.5 ± 0.8 years, respectively. The validation study was conducted among 53 children in the VVS group and 24 children in the control group, and their median age was 10.0 (8.0, 13.0) years and 10.0 (10.0, 11.0) years, respectively. There was no statistical significance in gender, age, height, weight, supine HR, SBP, and DBP between the two groups in the discovery set of the study or the validation set of the study (**Tables 1**, **2**).

Discovery of plasma protein profile between two groups

In the discovery test, a cytokine antibody array was used for comparing the profile of human growth factors between the two groups. To show the distribution of test values after the normalized quantile and guarantee the accuracy and reliability of data, the scatter plot (**Figure 2**) and PCA plot (**Figure 3**) were employed to assess the distribution of the data, and this evaluation showed relatively good representativeness of the applied samples in the study. Seven differential proteins were identified between the VVS group and control group by volcano plot analysis (differentially altered proteins were identified as those with Adj. *P*. Val. < 0.05, and fold change > 1.2 or <0.83 (absolute logFC > 0.263) (**Table 3** and **Figure 4**). Specifically, the VVS patients had higher plasma protein concentrations of IGFBP-4, transforming growth factor b1 (TGF-b1), HGF, and IGFBP-1, but lower levels of IGFBP-6, EGF, and IGFBP-3 than the controls. Unsupervised hierarchical cluster analysis demonstrated that children with VVS can be distinguished from healthy children based on the plasma concentration of seven differential proteins (**Figure 5**). The plasma concentration profile of the seven different proteins between the control group and the VVS group was shown in **Figure 6**. The compared results of the other 33 proteins between the two groups were detailed in **Supplementary Table 1**.

Validation of plasma protein profile between two groups

To validate the data screened by cytokine antibody array, the human suspension cytokine array was used for measuring the levels of growth cytokines. As shown in **Table 4**, the data of plasma protein concentrations or fluorescence suggested that

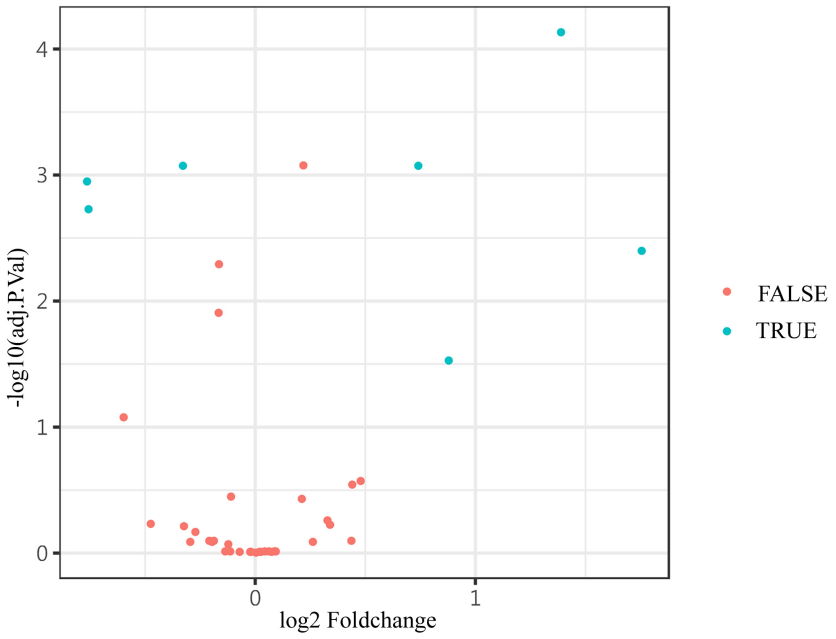

FIGURE 4
The volcano plot showed the expression of differential proteins. The differential levels of proteins (blue) and non-differential substances (red) were identified by Adj. *P*. values < 0.05, and fold change > 1.2 or <0.83 (absolute logFC > 0.263) in the volcano plot. The Adj. *P*. values were converted to -log10 (Adj. *P*. value) so that the higher the values on the y-axis, the more remarkably the difference in protein level changes with smaller Adj. *P*. values. The fold change is log-converted, so negative values and positive values indicated a decrease and an increase in protein levels, respectively. Blue (true) and red (false) represent significant and non-significant expression proteins, respectively.

plasma levels of HGF, IGFBP-6, and IGFBP-1 were higher in the VVS patients than in the controls. However, the result of plasma EGF and IGFBP-3 were lower in the VVS patients than in the controls. The following cytokines, IGFBP-4, and TGF-b1 could not be detected because the concentrations were too low or below the detection range of the standard curve.

Plasma growth cytokines were associated factors for the development of pediatric vasovagal syncope

Demographic characteristics and the cytokines with a *P*- value < 0.1 in univariate analysis were introduced into multivariate logistic analysis, including gender, age, BMI, HGF, EGF, IGFBP-6, IGFBP-1, and IGFBP-3. According to the results of multivariate logistics regression analysis, increased HGF and IGFBP-1 and decreased EGF were associated factors in the development of pediatric VVS (**Table 5**).

Diagnostic value of plasma insulin-like growth factor binding protein-1, epidermal growth factor, and hepatocyte growth factor

Based on the above results, the abilities of plasma IGFBP-1, EGF, and HGF to predict the diagnosis of pediatric VVS were further examined. As shown in **Figure 7**, the areas under the receiver operator characteristic curve of the logarithm of

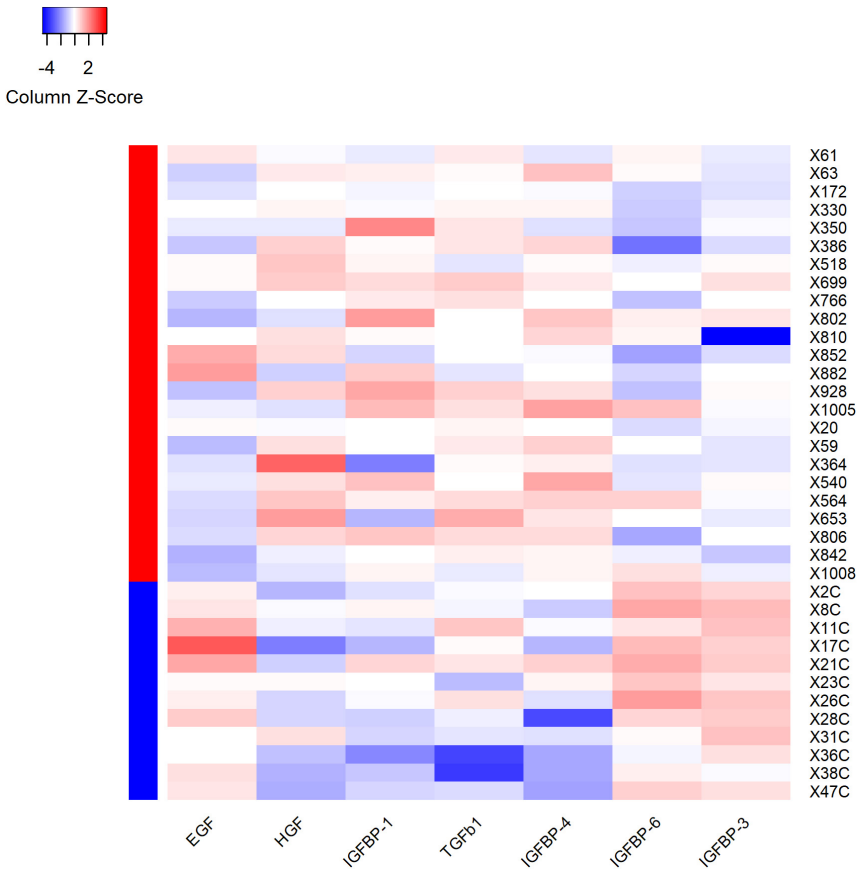

FIGURE 5
Heatmap showed the outcomes of hierarchical cluster analysis (HCA) independently performed on both samples' and variables' dimensions, for the seven differential expression proteins. Each row in the figure represents a subject, and each column represents a protein. The average protein expression level of the same patient was used as the benchmark. If the expression level of protein is higher than the average level, it is considered positive and marked as red; on the contrary, the expression level of protein is considered negative and marked as blue. The red and blue colors in the left column stand for the VVS group and control group, respectively. For plasma HGF, IGFBP-1, TGF-b1 and IGFBP-4, the proportion of red color in the VVS group was significantly higher than that in the control group, which means that the above four proteins in the VVS group were significantly higher than those in the control group. However, the proportion of blue color of plasma EGF, IGFBP-3, and IGFBP-6 proteins in the control group was remarkably higher than that in the VVS group, which means that the above three plasma protein concentrations were remarkably higher in the control group than those in the VVS group. IGFBP, insulin-like growth factor binding protein; HGF, hepatocyte growth factor; EGF, epidermal growth factor; TGF-b1, transforming growth factor b1.

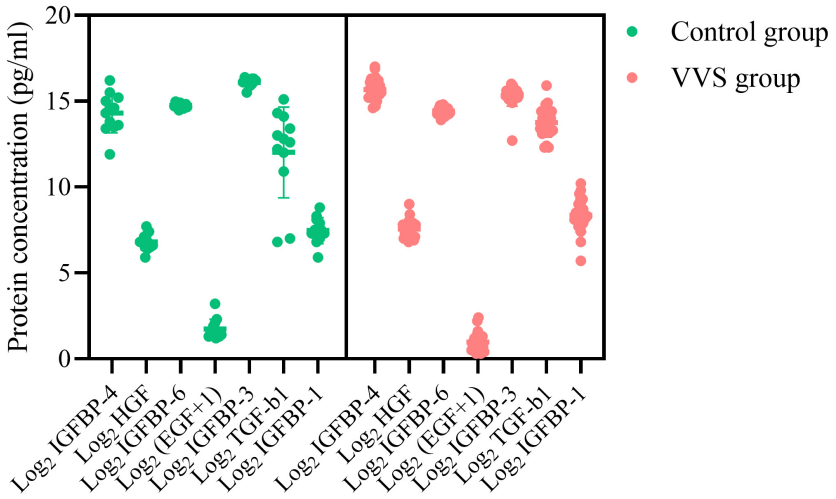

FIGURE 6
Plasma concentration profiles of seven differential proteins in the control group and the VVS group. The longitudinal axis represents the seven proteins, and the transversal axis represents the protein concentration. The EGF is expressed on a log2-scale by adding 1 to the original plasma concentration; and other biomarker plasma concentrations of the assessed proteins are expressed on a log2-scale. The green color and red color of the graph stand for the subjects in the control group and the VVS group, respectively. VVS, vasovagal syncope; IGFBP, insulin-like growth factor binding protein; HGF, hepatocyte growth factor; EGF, epidermal growth factor; TGF-b1, transforming growth factor b1.

plasma IGFBP-1, EGF + 1, and HGF to base 2 were 0.674, 0.880, and 0.822, respectively. When the cut-off values of the logarithm of plasma IGFBP-1, EGF + 1, and HGF to base 2 were over 13.5 pg/ml, less than 3.4 pg/ml, or over 6.1 pg/ml, the sensitivities of predicting pediatric VVS were 52.8, 77.4, and 83.0%, respectively, and the specificities of predicting pediatric VVS were 83.3, 100, and 79.2%, respectively.

Discussion

This study, for the first time, showed a characteristic plasma growth cytokine variation profile of a significantly increased plasma HGF, IGFBP-6, and IGFBP-1 and decreased plasma EGF and IGFBP-3. Plasma HGF, IGFBP-1, and EGF were associated factors for the development of pediatric VVS. The above findings would be extremely helpful in understanding the pathogenesis of VVS in children. In addition, plasma HGF, IGFBP-1, and EGF would be useful for assisting in the diagnosis of pediatric VVS.

Vasovagal syncope is a common entity of pediatric syncope and its recurrence can seriously affect patients' physical and mental health. Therefore, it is crucial to elucidate the pathogenesis of pediatric VVS and further develop effective preventive strategies. However, till now, the pathogenesis of pediatric VVS has not been clear.

It is well known that excessive vasodilation is one of the pathogenesis of pediatric VVS (23), but the exact mechanism remains unclear. This study indicated that the plasma IGFBP-1 in pediatric patients with VVS was higher than that in controls, but how the IGFBP-1 was involved in pathogenesis

TABLE 4 Plasma proteins validation in VVS and control groups.

Biomarkers	VVS group (*n*)	Control group (*n*)	*t*/*Z*	*P*-value
Log_2 HGF (pg/ml)	6.5 ± 0.5	5.8 ± 0.6	5.001	<0.001
Log_2 IGFBP-6 (pg/ml)	16.8 (16.6, 17.0)	16.6 (16.3, 16.8)	−2.364	0.018
[&]Log_2 (EGF + 1) (pg/ml)	2.5 (1.7, 3.2)	4.4 (3.9, 5.0)	−5.318	<0.001
Log_2 IGFBP-1 (pg/ml)	13.6 ± 1.1	13.0 ± 0.7	2.649	0.010
[#]Log_2 IGFBP-3 (pg/ml)	11.6 ± 0.5	11.8 ± 0.5	−2.013	0.048

[#]The biomarkers expressed by fluorescence signal-BKG.
[&]The EGF is expressed on a log2-scale by adding 1 to the original plasma concentration; and other biomarker plasma concentrations of the assessed proteins are expressed on a log2-scale.
Normally distributed data are displayed with mean ± standard deviation and non-normally distributed data are presented by median (P_{25}, P_{75}).
HGF, hepatocyte growth factor; IGFBP, insulin-like growth factor binding protein; EGF, epidermal growth factor.

TABLE 5 Logistic multivariate regression analysis of variables.

Characteristics	B	SE	Wald	*P*-value	OR (95% CI)
Log_2 (EGF + 1)	−0.995	0.332	8.994	0.003	0.370 (0.193–0.709)
Log_2 HGF	2.051	0.701	8.572	0.003	7.778 (1.970–30.708)
Log_2 IGFBP-1	1.227	0.528	5.395	0.020	3.412 (1.211–9.611)
Constant	−24.471	9.092	7.244	0.007	–

Characteristics enrolled in the logistic multivariate regression analysis: gender, age, BMI, log_2 (EGF + 1), log_2 IGFBP-6, log_2 HGF, log_2 IGFBP-1, and log_2 IGFBP-3.
HGF, hepatocyte growth factor; IGFBP, insulin-like growth factor binding protein; EGF, epidermal growth factor.

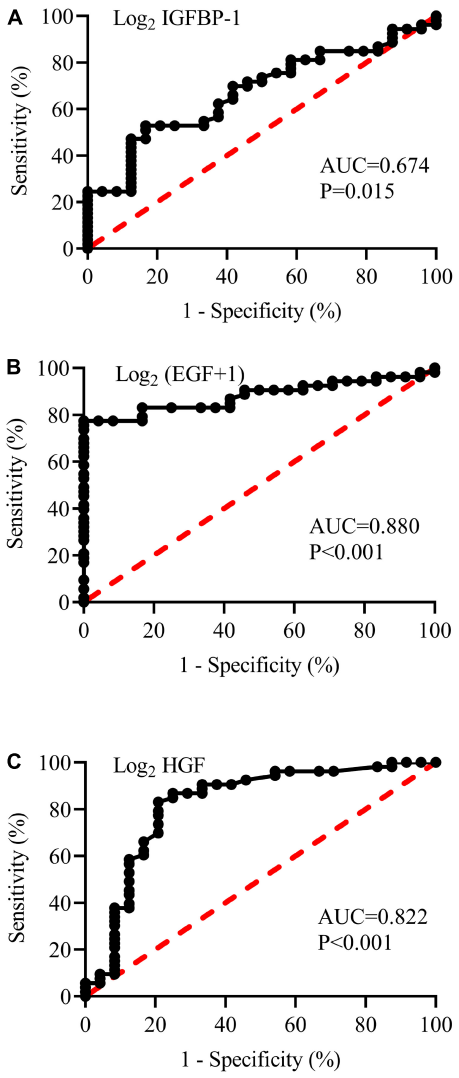

FIGURE 7
Receiver operating characteristic (ROC) curves of plasma concentrations of log_2 IGFBP-1 **(A)**, log_2 (EGF + 1) **(B)**, and log_2 HGF **(C)** to analyze the prediction of the diagnosis of VVS in children. The longitudinal axis represents sensitivity to predict the diagnosis of pediatric VVS. The transversal axis represents the false positive rate (1-specificity) of the prediction. The 45° red dotted line is the reference line, indicating that the sensitivity is equal to the false positive rate, with no predictive value at all. The black curve is farther from the reference line and closer to the upper left corner of the graph, indicating higher diagnostic efficiency. The areas under the ROC curve of log_2 IGFBP-1 **(A)**, log_2 (EGF + 1) **(B)**, and log_2 HGF **(C)** were 0.674, 0.880, and 0.822, respectively (all $P < 0.05$). The EGF is expressed on a log2-scale by adding 1 to the original plasma concentration; and other biomarker plasma concentrations of the assessed proteins are expressed on a log2-scale. AUC, area under the curve; IGFBP-1, insulin-like growth factor binding protein-1; HGF, hepatocyte growth factor; EGF, epidermal growth factor.

in children with VVS remains unclear. Based on the previous studies, IGFBP-1 is a 30 kDa protein that can dilate blood vessels, reduce vascular resistance and increase cardiac blood flow (24, 25). It was reported that the production of basal NO was increased in transgenic IGFBP-1 overexpressed mice (26). IGFBP-1 can upregulate eNOS mRNA expression by stimulating the phosphorylation of endothelial nitric oxide synthase (eNOS) in the PI3K/AKT pathway. In the VVS cases, the high plasma concentration of IGFBP-1 would likely stimulate the upregulation of eNOS mRNA expression, which increased the release of NO from the vascular endothelium, resulting in excessive vasodilation (27, 28). However, whether and how IGFBP-1 is involved in the development of pediatric VVS merit further studies.

In addition to IGFBP-1, another cytokine, HGF, was also found to be significantly higher in the plasma of children with VVS than that of the controls. HGF is a multifunctional factor involved in the proliferation, differentiation, and regeneration of different cells *via* binding with its specific receptor c-met (29). In addition, HGF plays a part in the expression of eNOS in endothelial cells (30). This was also confirmed by western blot analysis in human saphenous vein endothelial cells (HGSVEC), suggesting that the upregulation of eNOS expression could be detected after 2 h by HGSVEC treated with HGF, reached its peak at 6–8 h, and remained at a high level 16 h later (31). In human coronary artery endothelial cells, the secretion of endothelin-1 was significantly reduced in a concentration-dependent manner in the presence of HGF (32). Similarly, HGF has been shown to induce rapid microvasodilation, which can be inhibited by NO blockers, suggesting that the short-term effect is the result of HGF-induced upregulation of eNOS expression (33). Therefore, we suspected that plasma HGF was likely involved in the pathogenesis of VVS and it might increase NO secretion by stimulating endothelial cells *via* eNOS phosphorylation, leading to excessive vasodilation and then facilitating the development of VVS. Whereas, further explorations are still needed to reveal the significance of disturbed growth cytokine HGF secretion in the pathogenesis of pediatric VVS.

Epidermal growth factor, a vasoconstrictor, was significantly decreased in the children with VVS in this study. EGF, a globular protein of approximately 6 kDa, composes of 53-amino acids (34) and promotes cell proliferation and differentiation to replace senescence and death cells with new cells (35). Also, it was found that EGF could induce the contraction of isolated rat pulmonary arteries in a dose-dependent manner; when low concentrations of EGF are insufficient to induce vasoconstriction, EGF can enhance the effect of angiotensin II and participate in the pathophysiological processes of pulmonary circulation (12). A study on chronic hypoxia (CH) disease showed that EGF receptors were necessary to enhance the depolarization-mediated vasoconstriction following CH, and EGF-induced pulmonary arteries contraction of CH by ROK-associated Ca^{2+} sensitization (36, 37). As a consequence, EGF is thought to play a part in vasoconstriction. In this study,

the decreased plasma concentration of EGF in pediatric VVS suggested that the reduced vasoconstriction was likely to induce VVS under the circumstance of postural changes.

The data of multivariate logistic regression analysis showed that increased plasma concentrations of HGF and IGFBP-1 and decreased plasma concentrations of EGF were involved in the pathogenesis of pediatric VVS. In a word, the increased plasma HGF and IGFBP-1 with the vasodilating features might facilitate the syncopal episode, while increased plasma EGF might cause vasoconstriction in children and further reduce the possibility of VVS episodes to a certain degree.

However, there were still some limitations in this research, such as single-center and limited sample size. Moreover, we did not conduct studies on animal models to further investigate the possible mechanisms behind it. In the future, multicenter-based and large sample-sized studies should be performed to further elucidate the involvement of these cytokines in the pathogenesis of VVS. The exact role of cytokines discovered in the development of VVS needs to be illustrated *via* animal studies.

Data availability statement

The original contributions presented in this study are included in the article/**Supplementary material**, further inquiries can be directed to the corresponding authors.

Ethics statement

The studies involving human participants were reviewed and approved by Committee of Peking University First Hospital. Written informed consent to participate in this study was provided by the participants' legal guardian/next of kin.

Author contributions

YYW, CYT, HJ, XL, CST, and JD: conception and design of the study. YYW, BH, YRW, ZH, PL, XL, YLW, and CYT: collection of data. YYW, YRW, ZH, XL, HJ, and JD: data checking. YYW, BH, ZH, YRW, CST, HJ, and JD: analysis and interpretation of data. YYW, BH, and JD: drafting the manuscript. YRW, PL, BH, YLW, HJ, and JD: revising the manuscript. YYW, BH, YRW, HJ, and JD: final approval of the version to be submitted. All authors contributed to the article and approved the submitted version.

Funding

This study was supported by the National High-Level Hospital Clinical Research Funding (Multi-center Clinical Research Project of Peking University First Hospital) (2022CR59).

Acknowledgments

Thanks to all the researchers who worked on the study and the children and guardians who participated in the study.

Conflict of interest

The authors declare that the research was conducted in the absence of any commercial or financial relationships that could be construed as a potential conflict of interest.

Publisher's note

Supplementary material

The Supplementary Material for this article can be found online at: https://www.frontiersin.org/articles/10.3389/fcvm.2022.1030618/full#supplementary-material

References

1. Mathias CJ, Deguchi K, Schatz I. Observations on recurrent syncope and presyncope in 641 patients. *Lancet.* (2001) 357:348–53. doi: 10.1016/S0140-6736(00)03642-4

2. Alexis MF, Stephen CH, Robert FR, Phillip AL, Win-Kuang S. Vasovagal syncope. *Ann Intern Med.* (2000) 133:714–25. doi: 10.7326/0003-4819-133-9-200011070-00014

3. Chen L, Wang C, Wang H, Tian H, Tang C, Jin H, et al. Underlying diseases in syncope of children in China. *Med Sci Monit.* (2011) 17:H49–53. doi: 10.12659/msm.881795

4. Varga E, Worum F, Szabo Z, Varga M, Lorincz I. Motor vehicle accident with complete loss of consciousness due to vasovagal syncope. *Forensic Sci Int.* (2002) 130:156–9. doi: 10.1016/s0379-0738(02)00377-8

5. Zhang Q, Du J, Li Y, Ai Y. Endothelial function in children with vasovagal syncope *via* color Doppler flow imaging. *Chin J Pract Pediatr.* (2005) 20:482–4. doi: 10.1016/j.scib.2018.09.019

6. Marquez MF, Allende R, Marquez-Velasco R, Hermosillo AG. Role of nitric oxide in vasovagal syncope. A puzzle solved but there could be another piece. *Heart.* (2018) 104:786. doi: 10.1136/heartjnl-2017-312820

7. Stewart JM, Suggs M, Merchant S, Sutton R, Terilli C, Visintainer P, et al. Postsynaptic α1-adrenergic vasoconstriction is impaired in young patients with vasovagal syncope and is corrected by nitric oxide synthase inhibition. *Circ Arrhythm Electrophysiol.* (2016) 9:1–10. doi: 10.1161/CIRCEP.115.003828

8. Zhang F, Li X, Stella C, Chen L, Liao Y, Tang C, et al. Plasma hydrogen sulfide in differential diagnosis between vasovagal syncope and postural orthostatic tachycardia syndrome in children. *J Pediatr.* (2012) 160:227–31. doi: 10.1016/j.jpeds.2011.08.008

9. Yang J, Li H, Ochs T, Zhao J, Zhang Q, Du S, et al. Erythrocytic hydrogen sulfide production is increased in children with vasovagal syncope. *J Pediatr.* (2015) 166:965–9. doi: 10.1016/j.jpeds.2014.12.021

10. Magerkurth C, Riedel A, Braune S. Permanent increase in endothelin serum levels in vasovagal syncope. *Clin Auton Res.* (2005) 15:299–301. doi: 10.1007/s10286-005-0291-6

11. White M, Cernacek P, Courtemanche M, Stewart D, Talajic M, Mikes E, et al. Impaired endothelin-1 release in tilt-induced syncope. *Am J Cardiol.* (1998) 81:460–4. doi: 10.1016/s0002-9149(97)00938-7

12. Rippetoe PE, Olson JW, Altiere RJ, Pauly TH, Gillespie MN. Epidermal growth factor augments reactivity to angiotensin II in the rat pulmonary circulation. *Am Rev Respir Dis.* (1989) 140:821–4. doi: 10.1164/ajrccm/140.3.821

13. Zhang ZW, Yanamoto H, Nagata I, Miyamoto S, Nakajo Y, Xue JH, et al. Platelet-derived growth factor-induced severe and chronic vasoconstriction of cerebral arteries: proposed growth factor explanation of cerebral vasospasm. *Neurosurgery.* (2010) 66:728–35. doi: 10.1227/01.NEU.0000366111.08024.26

14. Tassi E, Lai EY, Li L, Solis G, Chen Y, Kietzman WE, et al. Blood pressure control by a secreted FGFBP1 (Fibroblast growth factor-binding protein). *Hypertension.* (2018) 71:160–7. doi: 10.1161/HYPERTENSIONAHA.117.10268

15. Rajwani A, Ezzat V, Smith J, Yuldasheva NY, Duncan ER, Gage M, et al. Increasing circulating IGFBP1 levels improves insulin sensitivity, promotes nitric oxide production, lowers blood pressure, and protects against atherosclerosis. *Diabetes.* (2012) 61:915–24. doi: 10.2337/db11-0963

16. Makondo K, Kimura K, Kitamura N, Kitamura T, Yamaji D, Jung BD, et al. Hepatocyte growth factor activates endothelial nitric oxide synthase by Ca(2+)- and phosphoinositide 3-kinase/Akt-dependent phosphorylation in aortic endothelial cells. *Biochem J.* (2003) 374(Pt. 1):63–9. doi: 10.1042/BJ20030326

17. Zhu X, Zhang K, He W, Yang J, Sun X, Jiang C, et al. Proinflammatory status in the aqueous humor of high myopic cataract eyes. *Exp Eye Res.* (2016) 142:13–8. doi: 10.1016/j.exer.2015.03.017

18. Wei Y, Liu B, Sun J, Lv Y, Luo Q, Liu F, et al. Regulation of Th17/Treg function contributes to the attenuation of chronic airway inflammation by icariin in ovalbumin-induced murine asthma model. *Immunobiology.* (2015) 220:789–97. doi: 10.1016/j.imbio.2014.12.015

19. Wang C, Li Y, Liao Y, Tian H, Huang M, Dong X, et al. 2018 Chinese Pediatric Cardiology Society (CPCS) guideline for diagnosis and treatment of syncope in children and adolescents. *Sci Bull.* (2018) 63:1558–64.

20. Sheldon RS, Grubb BP, Olshansky B, Shen W-K, Calkins H, Brignole M, et al. 2015 heart rhythm society expert consensus statement on the diagnosis and treatment of postural tachycardia syndrome, inappropriate sinus tachycardia, and vasovagal syncope. *Heart Rhythm.* (2015) 12:e41–63. doi: 10.1016/j.hrthm.2015.03.029

21. Wang Y, Zhang C, Chen S, Liu P, Wang Y, Tang C, et al. Heart rate variability predicts therapeutic response to metoprolol in children with postural tachycardia syndrome. *Front Neurosci.* (2019) 13:1214. doi: 10.3389/fnins.2019.01214

22. Li H, Wang Y, Liu P, Chen Y, Feng X, Tang C, et al. Body mass index (BMI) is associated with the therapeutic response to oral rehydration solution in children with postural tachycardia syndrome. *Pediatr Cardiol.* (2016) 37:1313–8. doi: 10.1007/s00246-016-1436-1

23. Liao Y, Du J. Pathophysiology and individualized management of vasovagal syncope and postural tachycardia syndrome in children and adolescents: an update. *Neurosci Bull.* (2020) 36:667–81. doi: 10.1007/s12264-020-00497-4

24. Conti E, Carrozza C, Capoluongo E, Volpe M, Crea F, Zuppi C, et al. Insulin-like growth factor-1 as a vascular protective factor. *Circulation.* (2004) 110:2260–5. doi: 10.1161/01.CIR.0000144309.87183.FB

25. Katz LE, Gralewski KA, Abrams P, Brar PC, Gallagher PR, Lipman TH, et al. Insulin-like growth factor-I and insulin-like growth factor binding protein-1 are related to cardiovascular disease biomarkers in obese adolescents. *Pediatr Diabetes.* (2016) 17:77–86. doi: 10.1111/pedi.12242

26. Aziz A, Haywood NJ, Cordell PA, Smith J, Yuldasheva NY, Sengupta A, et al. Insulinlike growth factor-binding protein-1 improves vascular endothelial repair in male mice in the setting of insulin resistance. *Endocrinology.* (2018) 159:696–709. doi: 10.1210/en.2017-00572

27. Slater T, Haywood NJ, Matthews C, Cheema H, Wheatcroft SB. Insulin-like growth factor binding proteins and angiogenesis: from cancer to cardiovascular disease. *Cytokine Growth Factor Rev.* (2019) 46:28–35. doi: 10.1016/j.cytogfr.2019.03.005

28. Sugawara J, Suh DS, Faessen GH, Suen LF, Shibata T, Kaper F, et al. Regulation of insulin-like growth factor-binding protein-1 by nitric oxide under hypoxic conditions. *J Clin Endocrinol Metab.* (2000) 85:2714–21. doi: 10.1210/jcem.85.8.6709

29. Wang LS, Wang H, Zhang QL, Yang ZJ, Kong FX, Wu CT. Hepatocyte growth factor gene therapy for ischemic diseases. *Hum Gene Ther.* (2018) 29:413–23. doi: 10.1089/hum.2017.217

30. Akira UA, Hiroshi K, Shuji A, Yoshihiro T, Masataka K, Kazuhisa T, et al. Hepatocyte growth factor stimulates nitric oxide production through endothelial nitric oxide synthase activation by the phosphoinositide 3-Kinase/Akt pathway and possibly by mitogen-activated protein kinase in vascular endothelial cells. *Hypertens Res.* (2004) 27:887–95. doi: 10.1291/hypres.27.887

31. Purdie KJ, Whitley GS, Johnstone AP, Cartwright JE. Hepatocyte growth factor-induced endothelial cell motility is mediated by the upregulation of inducible nitric oxide synthase expression. *Cardiovasc Res.* (2002) 54:659–68. doi: 10.1016/s0008-6363(02)00255-9

32. Haug C, Schmid-Kotsas A, Zorn U, Bachem MG, Schuett S, Gruenert A, et al. Hepatocyte growth factor is upregulated by low-density lipoproteins and inhibits endothelin-1 release. *Am J Physiol Heart Circ Physiol.* (2000) 279:H2865–71. doi: 10.1152/ajpheart.2000.279.6.H2865

33. Cartwright JE, Tse WK, Whitley GS. Hepatocyte growth factor induced human trophoblast motility involves phosphatidylinositol-3-kinase, mitogen-activated protein kinase, and inducible nitric oxide synthase. *Exp Cell Res.* (2002) 279:219–26. doi: 10.1006/excr.2002.5616

34. Aybay C, Karakus R, Yucel A. Characterization of human epidermal growth factor in human serum and urine under native conditions. *Cytokine.* (2006) 35:36–43. doi: 10.1016/j.cyto.2006.07.005

35. Abud HE, Watson N, Heath JK. Growth of intestinal epithelium in organ culture is dependent on EGF signalling. *Exp Cell Res.* (2005) 303:252–62. doi: 10.1016/j.yexcr.2004.10.006

36. Norton CE, Sheak JR, Yan S, Weise-Cross L, Jernigan NL, Walker BR, et al. Augmented pulmonary vasoconstrictor reactivity following chronic hypoxia requires Src kinase and EGFR signaling. *Am J Respir Cell Mol Biol.* (2020) 62:61–73. doi: 10.1165/rcmb.2018-0106OC

37. Norton CE, Weise-Cross L, Ahmadian R, Yan S, Jernigan NL, Paffett ML, et al. Altered lipid domains facilitate enhanced pulmonary vasoconstriction following chronic hypoxia. *Am J Respir Cell Mol Biol.* (2020) 62:709–18. doi: 10.1165/rcmb.2018-0318OC

frontiers | Frontiers in Cardiovascular Medicine

TYPE Original Research
PUBLISHED 18 October 2022
DOI 10.3389/fcvm.2022.998079

OPEN ACCESS

EDITED BY
Lan Huang,
Xinqiao Hospital, China

REVIEWED BY
Tobias Reichlin,
Bern University Hospital, Switzerland
Martín R. Arceluz,
Hospital of the University
of Pennsylvania, United States

*CORRESPONDENCE
Eyal Nof
Eyal.nof@sheba.health.gov.il

SPECIALTY SECTION
This article was submitted to
General Cardiovascular Medicine,
a section of the journal
Frontiers in Cardiovascular Medicine

RECEIVED 19 July 2022
ACCEPTED 23 September 2022
PUBLISHED 18 October 2022

CITATION
Sabbag A, Nissan J, Beinart R, Sternik L, Kassif I, Kogan A, Ram E and Nof E (2022) Early de-cannulation from extracorporeal membrane oxygenation following ventricular tachycardia radiofrequency ablation. *Front. Cardiovasc. Med.* 9:998079. doi: 10.3389/fcvm.2022.998079

Early de-cannulation from extracorporeal membrane oxygenation following ventricular tachycardia radiofrequency ablation

Avi Sabbag[1,2], Johnatan Nissan[1,2], Roy Beinart[1,2], Leonid Sternik[2,3], Igal Kassif[2,3], Alexander Kogan[2,3], Eilon Ram[2,3] and Eyal Nof[1,2]*

[1]Davidai Arrhythmia Center, Sheba Medical Center, Ramat Gan, Israel, [2]Sackler Faculty of Medicine, Tel Aviv University, Tel Aviv-Yafo, Israel, [3]Department of Cardiac Surgery, Sheba Medical Center, Ramat Gan, Israel

Objectives: Ventricular tachycardia ablation (VTA) with hemodynamic compromise presents a challenge. Veno-arterial extracorporeal membrane oxygenation (VA-ECMO) support allows the safe completion of the procedure. There are limited data regarding the safety of weaning off VA-ECMO at the end of the procedure. We report our experience with early VA-ECMO de-cannulation after VTA.

Materials and methods: All patients undergoing VA-ECMO-assisted VTA, between January 2013 and December 2020 at a large tertiary center were included. Clinical characteristics, history of arrhythmia, procedural details, and outcomes were collected. Patients weaned from VA-ECMO immediately at the end of the procedure were compared to those that were de-cannulated at a later time.

Results: A total of 46 patients (93.5% male, age 62 ± 10 years) were ablated with VA-ECMO support. Most had ischemic cardiomyopathy (65%) and (70%) presented with VT storm. The clinical VT was induced in the majority of patients (76%). A total of 99 VTs were induced of which 76 (77%) were targeted and successfully ablated. Non-inducibility was achieved in 74% of cases and most patients (83%) were de-cannulated at the end of the procedure on the procedure table. Survival at 1 year was higher among early de-cannulated patients (86 vs. 38% [log-rank p-value < 0.001]). At 1-year follow-up, 91.3% of surviving patients were free of appropriate ICD shocks.

Conclusion: De-cannulation from VA-ECMO may be done immediately at the conclusion of VTA in most cases. Failure to timely wean off VA-ECMO is a strong predictor of mortality.

KEYWORDS

vetricular tachycardia, extracorporeal membrane oxygenation, ablation, circulatory support, early de-cannulation

Introduction

Ventricular tachycardia ablation (VTA) has been well established as an important and effective therapy for drug refractory arrhythmia in the context of structurally abnormal hearts (1). Yet, the procedure is challenging since 70% of VTs are not tolerated by the patients limiting the ability to carry out extensive activation or entrainment mapping (2). Furthermore, even when adopting a substrate-based approach one must nevertheless strive to achieve complete non-inducibility at the end of the ablation. This may result in the repeated induction of VTs until the desired endpoint is met. The combined effect of anesthesia, positive pressure ventilation, fluid overload, and reduced cardiac output during VTs may lead to acute decompensations requiring rescue circulatory support accompanied by high mortality risk (3).

The preemptive use of circulatory support in selected high-risk patients has been demonstrated to be both safe and effective (4). It allowed prolonged mapping during VT thus increasing the likelihood of achieving complete and successful ablation as well as preventing hemodynamic collapse (4). While several circulatory support systems have been explored with similar rates of success (5, 6), veno-arterial extracorporeal membrane oxygenation (VA-VA-ECMO) may offer hemodynamic support without limiting access to the LV and without inducing electromagnetic interference (7). The safety of using VA-ECMO to support VT in high-risk patients has been reported (7) but, to the extent of our knowledge, the feasibility of immediate de-cannulation at the end of the ablation has not been specifically evaluated. Therefore, we sought to determine the safety and feasibility of immediate de-cannulation, preemptive deployment of VA-ECMO support, at the end of the ablation procedure, a preemptive deployment of VA-ECMO support.

Materials and methods

Study design

All cases of structurally abnormal heart that underwent VTA supported with a VA-ECMO at the Sheba Medical Center from January 2013 to December 2020 were reviewed and retrospectively analyzed. A structurally abnormal heart was defined as any cardiomyopathy, valvulopathy, or congenital heart disease impairing the ventricular function. Patient data, including demographics, and clinical and procedural features were obtained from our VTA registry. Only cases with a preemptive deployment of the system, done specifically to support the VTA procedure, were included. Preemptive VA-ECMO use was defined as the pre-planned deployment of the system in hemodynamically stable patients prior to the initiation of the VTA. Patients supported by VA-ECMO due to cardiogenic shock prior to the VTA or cases of unplanned and urgent introduction of VA-ECMO during VTA due to acute decompensation were excluded from the current analysis (**Figure 1**). The main study endpoints were a composite of VT, VF, or appropriate ICD shock as well as in-hospital all-cause mortality, defined as death occurring before discharge from the index hospitalization including transfer to other acute care facilities (8) and all-cause mortality. The study was approved by the local ethical board. Due to the retrospective nature of the analysis, no individual consent was required.

Study population

Patients were referred for VTA in accordance with current guideline indications (1). Prior to the procedure, all patients underwent a clinical evaluation including the assessment of their functional status, an echocardiographic exam, and a review of arrhythmia history. The preemptive VA-ECMO support was planned when one or more of the following criteria were met: (1) severe aortic stenosis; (2) severe pulmonary hypertension; (3) severe (NYHA functional class III–IV) or decompensated heart failure; (4) documentation of hemodynamically unstable VT; and (5) previously failed VTA when the reason for failure was the instability of VT or patient during the procedure; and (6) Idiopathic dilated cardiomyopathy.

Patients were considered in VT storm if presented with three sustained ventricular arrhythmia requiring defibrillation. Decompensated heart failure was defined as acute worsening signs and symptoms of HF resulting in hospitalization. The diagnosis of severe AS required a mean trans-valvular gradient of $\geq$40 mmHg, a maximal velocity $\geq$ m/s, a calculated aortic valve area of $\leq$1 cm^2, or a calcium score $\geq$ 2,000 in men and $\geq$1,500 in women (9). Pulmonary hypertension was defined as severe when systolic pulmonary artery pressure (sPAP) estimated by echocardiography was $\geq$60 mmHg or when right heart catheterization measured a mean pulmonary artery pressure (mPAP) $\geq$ 35 mmHg or mPAP $\geq$ 25 mmHg with low cardiac index (<2 L/min/m^2) (10). Each patient's eligibility criteria for ECMO-supported VTA are shown in a **Supplementary Table**.

Extracorporeal membrane oxygenation

The VA-ECMO circuit setup included a centrifugal pump and a coated polymethylpentene oxygenator (Revolution [Sorin, Italy], Centrimag [Levitronix, Waltham, MA], and Rotaflow

Abbreviations: CL, cycle length; LVAD, left ventricular assist device; LVEF, left ventricular ejection fraction; SMVT, sustained monomorphic ventricular tachycardia; VA-ECMO, veno-arterial extracorporeal membrane oxygenation; VT, ventricular tachycardia; VTA, ventricular tachycardia ablation.

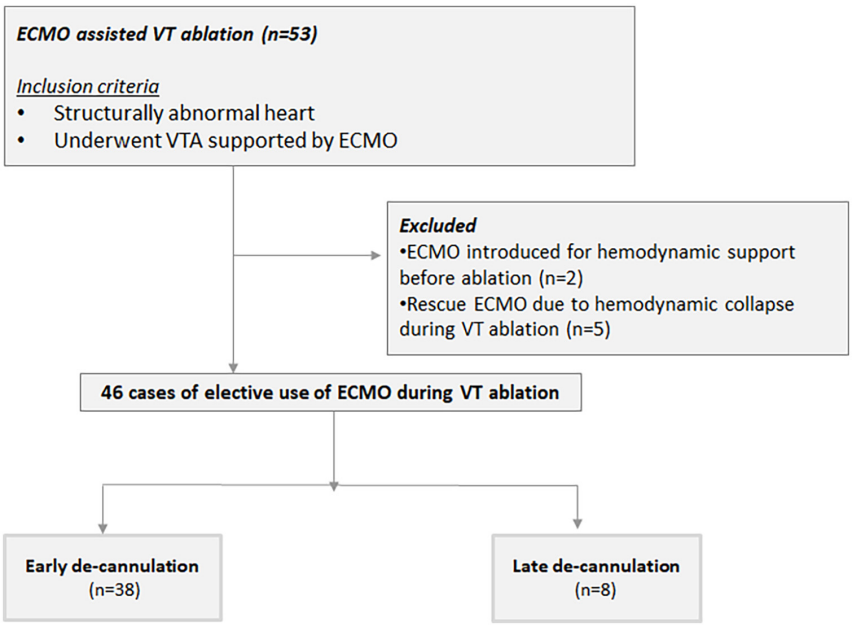

FIGURE 1
Flowchart summary from consent and eligibility for the study 1-year follow-up.

[Maquet, Germany]). The left femoral artery and vein were percutaneously cannulated in all patients. An outlet (23/25F) and inlet (15/17F) cannula were advanced to the right atrium and external iliac artery, respectively. The pump was set to a minimal baseline flow of 1.7–2 L/min. During VT or programmed stimulation, the flow was increased up to 3.5–4 L/min as needed to maintain hemodynamic stability and adequate systemic organ perfusion. A target ACT of 300 s was mandatory throughout the procedure.

Ablation procedure

Electro-anatomical mapping was performed (CARTO 3 or XP, Biosense Webster, Diamond Bar, CA, USA) using a 3.5-mm tip open irrigated catheter (NaviStar ThermoCool, Biosense Webster, Diamond Bar Ca). Voltage maps were created during sinus rhythm. Peak-to-peak bipolar electrogram amplitude < 0.5 mV was defined as dense scar, voltage ≥ 0.5 and <1.5 mV as scar border zone (11). Epicardial mapping and ablation were carried out when deemed necessary.

All inducible sustained monomorphic ventricular tachycardia (SMVT) were targeted for ablation. Sites were targeted for ablation if pacing entrained the SMVT with concealed fusion and a post-pacing interval (PPI) within 30 ms of the VT cycle length (CL) or by activation mapping. In any case, scar substrate modification ("scar de-channeling") was performed. Sites with low amplitude fractionated electrograms with stimulation to QRS, late potentials, or the best pace map sites were targeted. Pace mapping and entrainment mapping utilized unipolar stimuli with a strength of 10 mA and a pulse width of 2 ms. Radiofrequency (RF) energy was delivered at a power of 25–50 Watts targeting an impedance drop of at least 10 ohms. The endpoint of all procedures was non-inducibility of any VT with programmed stimulation (PS) at a basic drive train of 600 and 400 ms with up to three extrastimuli. A procedure was defined as successful if the patient was non-inducible for any VT following PS. Partial success was declared when only the clinical VT was no longer inducible and acute procedural failure was declared if the clinical VT was still inducible.

At the end of the ablation, the feasibility of immediate de-cannulation from ECMO in the electrophysiology lab was assessed based on the following criteria: (1) a mean atrial pressure $\geq$ 60 mmHg for at least 5 mins with minimal ECMO flow (<1 L/min) and minimal ionotropic support (<0.02 mcg/Kg/min of noradrenaline); (2) oxygen saturation $>$ 92% on $FiO_2 \leq 40\%$; (3) post-ablation lactate level $<$ 30 mmg/dl; and (4) no severe acute complication, such as tamponade. Patients meeting all of these criteria were gradually weaned of circulatory support. Patients successfully weaned from ECMO before leaving the EP lab were defined as early de-cannulation (group A) and those that required additional prolonged support were considered late de-cannulation (group B).

Blood pressure was measured continuously and lactate levels were monitored carefully to identify any sign of decompensation and need for the reinstitution of circulatory support. If mean blood pressure $>$ 60 was maintained on minimal ECMO flow

(<1 L/min), we proceeded with de-cannulation. If the above-mentioned blood pressure could not be maintained in a patient, ECMO flow was increased and he was transferred to the intensive care unit (ICU) for another attempt. The decision to wean off ECMO in ICU was made at the discretion of the attending physician). Prior to VA-ECMO removal, protamine was administered with a target ACT of <180 s. After the removal of ECMO cannulas, manual pressure was applied to the groin. Immediate de-cannulation was defined as completing the entire weaning process before leaving the procedure room.

Follow-up

Following the ablation, all patients were admitted to a monitored bed until discharged. Procedural and post-procedural complications were noted. All patients were seen at the device clinic 1 and 3 months after the procedure as well as continued biannual device examinations. The occurrence of VT and appropriate device therapies were collected. Mortality data were extracted from the Israeli National Population Register and were available for all cases. The date on heart transplantation or the implantation of a left ventricular assist device was collected from the national heart transplant register and was also available for all cases. The Institutional Review Board of Sheba Medical Center approved this registry on the basis of strict maintenance of participants' anonymity during database analyses. No individual consent was obtained.

Statistical analysis

Data are presented as mean ± standard deviation if normally distributed or as median (interquartile range) if non-normally distributed. Continuous variables were tested with the Kolmogorov–Smirnov test for normal distribution. Categorical variables were given as frequencies and percentages. A chi-squared test or Fisher's exact test was used for the comparison of categorical variables between groups, and Student's *t*-test or the Mann–Whitney *U* test was performed for the comparison of continuous variables between the groups. All-cause mortality and freedom from appropriate ICD therapy were calculated using Kaplan–Meier analysis with the procedure serving as the index event. All *p*-values were two-tailed and were considered statistically significant if their value was <0.05. Statistical analyses were performed using SPSS Statistics (IBM, Chicago, IL, USA).

Results

A total of 53 patients underwent VTA supported by VA-ECMO between January 2014 and December 2020 (**Figure 1**). Of these, two required VA-ECMO for hemodynamic support regardless of the ablation. Due to hemodynamic collapse during VTA, VA-ECMO was urgently introduced as a bailout strategy in five patients. These patients were excluded from the current analysis. In the remaining 46 consecutive cases (93.5% male, age 62 ± 10 years), VA-ECMO was placed preemptively, specifically to support the ablation procedure, forming the study population. Patients' clinical characteristics at baseline are shown in **Table 1**. The majority of patients had ischemic cardiomyopathy were being chronically treated with class III antiarrhythmic drugs on a long-term basis and had VT storm. Half had an NYHA functional class III or IV.

Forty patients underwent early de-cannulation in the electrophysiology lab immediately following ablation. Thirty-eight of these remained free of circulatory support for the remainder of the hospital stay and formed group A – successful early de-cannulation. Group B comprised patients for whom early de-cannulation was deemed impossible (n = 6) and two patients who required reestablishment of VA-ECMO support due to progressive hemodynamic compromise within 24 h of the procedure. Group A tended to be younger and showed a trend toward lower left ventricular ejection fraction (LVEF) when compared to patients in group B (**Table 1**). We found no other statistically significant differences between the groups. Of note, five patients from group B were successfully de-cannulated within 24 h of the ablation. None of those required further circulatory support.

Details for the ablation procedures are shown in **Table 2**. The left ventricle was accessed *via* retrograde approach in the majority of cases (N = 38, 83%) followed by substrate mapping in sinus rhythm in 43 (93%). Epicardial access was performed in 12 (26%) cases. VTs were successfully induced in the vast majority of cases (89%) with a median of two (IQR 1–3) distinct circuits in each case. The induction of multiple VTs (≥3) was not common and observed in almost a third of cases. Entrainment and full activation mapping were performed in six (13%) and 31 (67%) cases, respectively, targeting a median of two (IQR 1–3) circuits. Complete non-inducibility was achieved in 34 (74%) cases, and clinical VT alone was eliminated in 39 (93%). When comparing groups A and B, we found a higher rate of activation mapping in latter (67 vs. 100%, p = 0.03), a greater proportion of inducing multiple VTs (24 vs. 64%, p = 0.04), and a higher rate of achieving non-inducibility in the former (82 vs. 38%, p = 0.02).

Less inducible VTs and non-inducibility at the end of the procedure were the only predictors of successful early de-cannulation (1.45 [1.02–2.06], p = 0.037 and 0.13 [0.03–0.70], p = 0.018, respectively). Failure of immediate de-cannulation was predicted by the induction of multiple distinct VTs with a 45% increased risk of failure for each additional circuit (OR = 1.45 95% CI = 1.02–2.06; p = 0.037). Additionally, a high lactic acid level (≥20 mg/dl) close to the end of the procedure showed a trend toward higher risk of early weaning failure (**Table 3**).

10.3389/fcvm.2022.998079

TABLE 1 Patient baseline characteristics.

	All ($N = 46$)	Early de-cannulation ($N = 38$)	No early de-cannulation ($N = 8$)	p-value
Male	43 (93.5)	35 (92.1)	8 (100)	1
Age	62 ± 10	61.5 ± 10.6	67.6 ± 3	0.005
Hypertension	23 (50)	19 (50)	4 (50)	1
Diabetes mellitus	14 (30.4)	12 (31.6)	2 (25)	1
Chronic kidney disease	9 (19.6)	7 (18.4)	2 (25)	0.645
Atrial fibrillation	17 (37)	12 (31.6)	5 (62.5)	0.125
Ischemic cardiomyopathy	30 (65.2)	25 (65.8)	5 (62.5)	1
Non- Ischemic cardiomyopathy	12 (26.1)	10 (26.3)	2 (25)	1
Chronic obstructive lung diseases	4 (8.7)	4 (10.5)	0	1
Past VT ablation	23 (50)	19 (50)	4 (50)	1
NYHA FC III-IV	23 (50)	18 (47.4)	5 (62.5)	0.699
Decompensated HF	10 (21.7)	7 (18.4)	3 (37.5)	0.344
VT storm	32 (69.6)	25 (65.8)	7 (87.5)	0.403
Presenting arrhythmia				
Monomorphic VT	44 (95.6)	36 (94.7)	8 (100)	1
Polymorphic VT	1 (2.2)	1 (2.6)	0	1
Ventricular fibrillation	1 (2.2)	1 (2.6)	0	1
Hemodynamically unstable VT/VF	24 (52.2)	20 (52.6)	4 (50)	1
Antiarrhythmic drugs				
Amiodarone	32 (65.3)	25 (65.8)	7 (87.5)	0.403
Sotalol	10 (21.7)	10	0	0.171
Baseline vitals				
Heart rate		70.9 ± 18	74 ± 18	0.641
Systolic BP		117 ± 25	108 ± 19	0.358
Diastolic BP		67 ± 15	67 ± 10	0.992
Chronic medical treatment				
Beta blockers	46 (100)	38 (100)	8 (100)	-
ACE/ARB	39 (84.8)	32 (84.2)	7 (87.5)	1
MRA	38 (82.6)	31 (81.6)	7 (82.6)	1
LVEF,%	19.5 ± 8.5	20.3 ± 9	15.6 ± 5	0.053
LVEF < 20%		26 (68.4)	8 (100)	0.09
SPAP		43 ± 17	48 ± 18	0.479
Severe PHTN	6 (15.8)	4 (12.1)	2 (40)	0.169
≥Moderate RV dysfunction,%	13 (28)	9 (24.3)	4 (50)	0.202
PAAINESD score	19.4 ± 7.01	18.8 ± 7.2	22 ± 5.7	0.247

ACE, angiotensin-converting enzyme; ARB, angiotensin II receptor blockers; BP, blood pressure; LVEF, left ventricle ejection fraction; NYHA, New York Heart Association; PHTN, pulmonary hypertension; RV, right ventricle; SPAP, systolic pulmonary arterial pressure; VT, ventricular tachycardia; VF, ventricular fibrillation.

Short-term outcomes

A total of nine (19.6%) had major adverse outcomes (Table 4). A single patient sustained a stroke and two developed vascular complications requiring surgical intervention (pseudo-aneurysm and thrombotic occlusion of a femoral artery). In addition, one patient developed intractable cardiogenic shock and died despite continued VA-ECMO support. Another was initially weaned from VA-ECMO but deteriorated within 24 h and was urgently reconnected to VA-ECMO. He underwent implantation of a left ventricular assist device (LVAD, HeartMate 3^{TM}, Abbott Laboratories, Chicago, IL, USA) within 6 days. He developed acute right ventricular failure soon thereafter and a right ventricular assist device was implanted (Levitronix) but he died within a few days. A sixth patient was weaned off the VA-ECMO but died from septic shock due to hospital-acquired pneumonia. A seventh patient was kept off VA-ECMO support until he was implanted with LVAD (HeartMate 3^{TM}) but died within 24 h of the procedure, 26 days after the ablation. Finally, two patients developed cardiogenic shock that was successfully managed and they recovered. Overall, in-hospital mortality was higher among patients that were not successfully weened of ECMO in the EP lab (5 vs. 50%, $p = 0.005$).

Post-discharge outcomes

Over a median follow-up of 15.9 (6.9–31.3) months, a total of 15 (32.6%) patients died. All-cause mortality at 1 year was higher among patients that failed immediate de-cannulation 86 vs. 38% at 1 year (log-rank $p < 0.001$, Figure 2). At 1 year of

10.3389/fcvm.2022.998079

TABLE 2 Procedural data.

	All (*N* = 46)	Early de-cannulation (*N* = 38)	No early de-cannulation (*N* = 8)	*p*-value
General anesthesia	41 (89.1)	33 (87)	8 (100)	0.569
Access				
Trans septal	4 (8.7)	3 (7.9)	1 (12.5)	
Retrograde	38 (82.6)	32 (69.6)	6 (13)	
Combined access	4 (8.7)	3 (7.9)	1 (12.5)	
Mapping technique				
VT induction (Any)	41 (89.1)	34 (89.5)	8 (100%)	1
VT induction (clinical)	35 (76.1)	28 (73.7)	7 (87.5)	0.658
Pace-mapping	37 (80.4)	29 (76.3)	8 (100)	0.324
Activation mapping	31 (67.4)	23 (60.5)	8 (100)	0.03
Entrainment	6 (13)	4 (10.5)	2 (25)	0.277
Substrate mapping	43 (93.5)	35 (92.1)	8 (100)	1
Ablation strategy				
Endocardial	33 (71.7)	28 (60.9)	5 (62.5)	
Epicardial	2 (4.3)	2 (5.3)	0	
Endocardial + epicardial	10 (21.7)	7 (18.4)	3 (37.5)	
Trans-coronary	1 (2.2)	1 (2.6)	0	
Lactic acid	14.7 ± 11.7	11.9 ± 4	23 ± 24	0.182
Number of VTs induced	2 (1–3)	2 (1–2)	3 (1–7)	0.079
Induction of ≥ 3 VTs	9 (23.7)	5 (62.5)	14 (30.4)	0.044
Number of VTs targeted	2 (1–3)	2 (1–2)	2 (1–3)	0.416
Procedure duration, min	280 (227–335)	385 (236–405)	255 (221–283)	0.147
Acute outcomes				
Elimination of clinical VT	39 (92.8)	33 (86.8)	6 (75)	0.587
Non-inducibility	34 (74)	31 (81.6)	3 (37.5)	0.02
Inducibility not tested	6 (13)	4 (10.5)	2 (25)	1
Failure	1 (2.2)	1 (2.6)	0	1

VT, ventricular tachycardia.

follow-up, 91.3% of surviving patients were free of appropriate ICD shocks and VT.

Discussion

This study adds to the accumulating experience of preemptive use of VA-ECMO to support VT ablation in high-risk patients and presents, for the first time, the clinical impact of routine early de-cannulation at the end of the procedure. Early de-cannulation was performed successfully in the majority (82.6%) of cases despite the relatively high-risk profile of our cohort. This was predicted by a lower number of inducible VTs and by achieving non-inducibility at the end of the ablation. Failure to wean off VA-ECMO support was associated with multiple distinct VTs circuits induced and by high lactic acid levels, measured close to the end of the procedure. Furthermore, failure to wean off VA-ECMO, prolonged VA-ECMO support, or urgent re-cannulation following an apparently successful weaning process was all associated with excess mortality. This highlights the critical importance of the early post-procedural course as a powerful predictor of poor outcomes and a possible trigger for urgent intervention.

Drug refractory VTs in the presence of structurally abnormal hearts pose a high stake therapeutic challenge. Often, VTA

TABLE 3 Predictors of failed early de-cannulations.

	OR (95% CI)	*p*-value
LVEF,%	0.913 (0.81–1.03)	0.155
Non-inducibility	**0.135 (0.03–0.70)**	**0.018**
Age	1.08 (0.98–1.19)	0.127
PAAINESD	1.07 (0.95–1.21)	0.246
Number of VT induced	**1.45 (1.02–2.06)**	**0.037**
Induction of ≥ 3 VTs	**5.4 (1.07–27)**	**0.041**
Lactic acid ≥ 20 mg/dl	6.6 (0.86–50.541)	0.069

LVEF, left ventricle ejection fraction; VT, ventricular tachycardia. Bold indicates statistically segnificnt findings.

TABLE 4 Complications.

	Early de-cannulation ($N = 38$)	No early de-cannulation ($N = 8$)	*p*-value
Vascular complication	2 (5.3)	0	1
CVA	1 (2.6)	0	1
Cardiogenic shock	**3 (7.9)**	**4 (50)**	**0.012**
Tamponade	0	0	NA
In-hospital mortality	**2 (5.2)**	**4 (50%)**	**0.005**
Any major complication[#]	**5 (13.2)**	**4 (50)**	**0.017**

CVA, cerebrovascular accident. [#]Major complication includes CVA, vascular complication requiring intervention or new cardiogenic shock, cardiac tamponade, and in-hospital death. Bold indicates statistically significnt findings.

is the only strategy that may offer long-term freedom for arrhythmia. In recent years, it became clear that the safe and effective execution of these procedures requires careful risk stratification and preparation. Acute hemodynamic collapse during the ablation has been associated with extremely high mortality despite rescue attempts with circulatory support. Importantly, this was frequently observed during sinus rhythm or pace mapping. Therefore, hemodynamic collapse may not be avoided by limiting the procedure to a substrate base approach. As a result, the preemptive use of circulatory support systems during VTA emerges as an important approach for selected high-risk patients. The PAINESD score has gained acceptance as a useful risk stratification scheme (12) developed to predict hemodynamic collapse during VTA and the need for the preemptive use of circulatory support. As described above, we have used a different set of criteria for patient selection, but the PAINESD score of our patients is comparable to previous publications, allowing for comparisons with previous cohorts.

Veno-arterial extracorporeal membrane oxygenation is used, typically, in acute settings of typical providing support for a few days to a few weeks, depending on the clinical scenario and patient condition. It is used both as a bridge for recovery and a bridge for a different definitive treatment or until the patient dies. Increased experience and the growing number of specialist centers registered with ELSO have led to increased use of VA-VA-ECMO in more elective cases, such as in high-risk percutaneous coronary intervention, high-risk percutaneous structural heart procedures, and is being used as a "stand-by" for different high-risk procedures.

Published reports of VTA with hemodynamic support also describe the use of Impella ventricular support device and/or TandemHeart. Nevertheless, VA-ECMO has the potential for more complete hemodynamic support (up to 5 l/min) as well as respiratory support. Furthermore, the system does not affect the access to the LV as the Impella and may be used in the presence of the mechanical aortic valve.

Importantly, in previous reports, patients were kept on circulatory support for at least 24 h after the procedure (7). The utilization of VA-ECMO is associated with a risk of significant complications. While those have been shown to be well balanced by the benefit of intra-procedural support and the prevention of hemodynamic collapse, more prolonged use

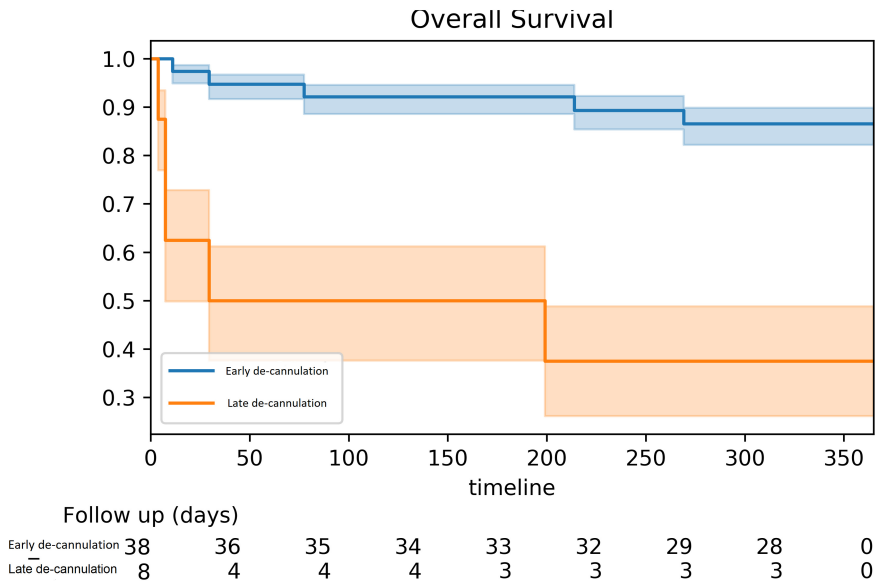

FIGURE 2
Kaplan–Meier survival analysis in early vs. late de-cannulation.

must be further justified. The use of VA-ECMO mandates continued anticoagulation resulting in an ongoing risk of major bleeding, particularly at the cannula insertion site. Similarly, the risk of nosocomial infection (13) and limb ischemia increases dramatically as a function of the duration of therapy. Lastly, maintaining VA-ECMO support takes a significant toll on hospital's limited resources. Therefore, minimizing the exposure to VA-ECMO is a priority when possible. Our results show that immediate de-cannulation is feasible and safe in the majority of cases. Therefore, we propose that a careful weaning process at the end of VTA, particularly when successful, should be attempted in most cases. Our results are consistent with a recent study by Muser et al. reporting a similar rate of 96% immediate removal of circulatory support at the end of the procedure (4). Notably, in that cohort, the Impella 2.5 or Impella CP pLVAD devices (Abiomed, Inc., Danvers, MA, USA) were used, not the VA-ECMO (4).

Despite our previous statement, premature weaning may be detrimental. Two cases in which immediate cannulation was performed, followed by the reinstitution of VA-ECMO support soon thereafter, resulted in death within 30 days. This happened despite the implantation of an LVAD system in one of the patients. It is possible that uninterrupted VA-ECMO support as a bridge to LVAD would have resulted in a better outcome. In our cohort, the indication of multiple VTs, probably as a maker of advanced cardiomyopathy with the extensive electrical substrate, emerged as a sign of poor outcome and should merit caution. Additional risk factors that approached statistical significance were advanced age and very low LVEF (<20%).

It is probable that the cumulative time a patient spent in VT may have a substantial impact on his hemodynamic stability even with ECMO support. While the rate of activation mapping was higher in the late cannulation group, it did not result in a longer overall procedural duration and it was not a predictor of failed early de-cannulation. We were unable to report the total time spent in VT during the procedure or the longest VT episode and therefore could not draw specific conclusions on the importance of limiting the duration of activation mapping. Nevertheless, based on our early clinical experience, our current practice is to limit the duration of mapping for a single VT circuit to a maximum of 30 mins.

Lastly, while ECMO may allow comprehensive activation mapping and safer execution of post-ablation programmed stimulation protocols, circulatory support should not be regarded as a means to improve acute success (non-inducibility) in most VTAs. Rather, it should be regarded as a tool that enables the safe completion of VTAs in very high-risk patients. The rates of non-inducibility achieved in our cohort are comparable to several recent VTA studies but are by no means superior to them. Yet the patients comprising our cohort were substantially sicker, with lower LVEFs, more advanced HF, a higher proportion of VT storm, and previous failed ablations and we perfumed aggressive program stimulation protocols (up to 3 and even 4 extra-stimuli) as a routine. Therefore, the use of ECMO support may enable a high-risk patient to complete a comprehensive and rigorous VTA that would otherwise be impossible.

Limitations

We acknowledge several limitations. Mainly the retrospective nature of this analysis of a single-center experience. Furthermore, the study's sample size precluded extensive statistical analysis. Yet, our cohort is very similar to previously published reports allowing generalization of our results to other high-risk patients with structurally abnormal hearts intended for ECMO-supported VTA. Moreover, the question of immediate early de-cannulation is unlikely to be tested in a randomized prospective fashion emphasizing the importance of reports like this one. Our pre-procedural evaluation protocol did not include advanced imaging aimed at identifying the arrhythmogenic substrate. The use of multimodality computed tomography and particularly cardiac magnetic resonance, when clinically feasible, may have reduced mapping and ablation time, thus contributing to the safety of the procedures (14, 15). Lastly, the study was not designed to assess the benefit of ECMO support for VT ablation in high-risk patients.

Conclusion

Immediate de-cannulation from VA-ECMO support at the end of VT ablation is feasible in the majority of cases. Close hemodynamic monitoring and a careful weaning process are warranted. The likelihood of success is high when complete non-inducibility was achieved and lower when multiple VT circuits were induced. Further study is needed to better define the predictors of successful immediate de-cannulation.

Data availability statement

The raw data supporting the conclusions of this article will be made available by the authors, without undue reservation.

Ethics statement

The studies involving human participants were reviewed and approved by Sheba Medical Center's Ethical Board. Due to the retrospective nature of the analysis, no individual consent was required. Written informed consent for participation was not required for this study in accordance with the national legislation and the institutional requirements.

Author contributions

AS, RB, and EN contributed to conception and design of the study. JN and EN organized the database. AS and JN performed the statistical analysis. AS and EN wrote the first draft of the manuscript. RB, LS, IK, AK, and ER wrote sections of the manuscript. All authors contributed to manuscript revision, read, and approved the submitted version.

Conflict of interest

The authors declare that the research was conducted in the absence of any commercial or financial relationships that could be construed as a potential conflict of interest.

Publisher's note

Supplementary material

The Supplementary Material for this article can be found online at: https://www.frontiersin.org/articles/10.3389/fcvm.2022.998079/full#supplementary-material

References

1. Priori SG, Blomström-Lundqvist C, Mazzanti A, Blom N, Borggrefe M, Camm J, et al. 2015 ESC Guidelines for the management of patients with ventricular arrhythmias and the prevention of sudden cardiac death: the task force for the management of patients with ventricular arrhythmias and the prevention of sudden cardiac death of the European Society of Cardiology (ESC). endorsed by: Association for European Paediatric and Congenital Cardiology (AEPC). *Eur Heart J.* (2015) 36:2793–867. doi: 10.1093/eurheartj/ehv316

2. Zeppenfeld K, Stevenson WG. Ablation of ventricular tachycardia in patients with structural heart disease. *Pac Clin Electrophysiol.* (2008) 31:358–74. doi: 10.1111/j.1540-8159.2008.00999.x

3. Enriquez A, Liang J, Gentile J, Schaller RD, Supple GE, Frankel DS, et al. Outcomes of rescue cardiopulmonary support for periprocedural acute hemodynamic decompensation in patients undergoing catheter ablation of electrical storm. *Heart Rhythm.* (2018) 15:75–80. doi: 10.1016/j.hrthm.2017.09.005

4. Muser D, Liang JJ, Castro SA, Hayashi T, Enriquez A, Troutman GS, et al. Outcomes with prophylactic use of percutaneous left ventricular assist devices in high-risk patients undergoing catheter ablation of scar-related ventricular tachycardia: a propensity-score matched analysis. *Heart Rhythm.* (2018) 15:1500–6. doi: 10.1016/j.hrthm.2018.04.028

5. Aryana A, Gearoid O'Neill P, Gregory D, Scotti D, Bailey S, Brunton S. Procedural and clinical outcomes after catheter ablation of unstable ventricular tachycardia supported by a percutaneous left ventricular assist device. *Heart Rhythm.* (2014) 11:1122–30. doi: 10.1016/j.hrthm.2014.04.018

6. Bunch TJ, Darby A, May HT, Ragosta M, Lim DS, Taylor AM, et al. Efficacy and safety of ventricular tachycardia ablation with mechanical circulatory support compared with substrate-based ablation techniques. *Europace.* (2012) 14:709–14. doi: 10.1093/europace/eur347

7. Baratto F, Pappalardo F, Oloriz T, Bisceglia C, Vergara P, Silberbauer J, et al. Extracorporeal membrane oxygenation for hemodynamic support of ventricular tachycardia ablation. *Circ Arrhythm Electrophysiol.* (2016) 9:e004492. doi: 10.1161/CIRCEP.116.004492

8. Krumholz HM, Brindis RG, Brush JE, Cohen DJ, Epstein AJ, Furie K, et al. Standards for statistical models used for public reporting of health outcomes: an American Heart Association scientific statement from the quality of care and outcomes research interdisciplinary writing group: cosponsored by the council on epidemiology and prevention and the stroke council. endorsed by the American College of Cardiology Foundation. *Circulation.* (2006) 113:456–62. doi: 10.1161/CIRCULATIONAHA.105.170769

9. Baumgartner H, Falk V, Bax JJ, De Bonis M, Hamm C, Holm PJ, et al. 2017 ESC/EACTS Guidelines for the management of valvular heart disease. *Eur Heart J.* (2017) 38:2739–91. doi: 10.1016/j.rec.2017.12.013

10. Nathan SD, Barbera JA, Gaine SP, Harari S, Martinez FJ, Olschewski H, et al. Pulmonary hypertension in chronic lung disease and hypoxia. *Eur Respir J.* (2019) 53:1801914. doi: 10.1183/13993003.01914-2018

11. Marchlinski FE, Callans DJ, Gottlieb CD, Zado E. Linear ablation lesions for control of unmappable ventricular tachycardia in patients with ischemic and nonischemic cardiomyopathy. *Circulation.* (2000) 101:1288–96. doi: 10.1161/01.cir.101.11.1288

12. Santangeli P, Muser D, Zado ES, Magnani S, Khetpal S, Hutchinson MD, et al. Acute hemodynamic decompensation during catheter ablation of scar-related ventricular tachycardia: incidence, predictors, and impact on mortality. *Circ Arrhythm Electrophysiol.* (2015) 8:68–75. doi: 10.1161/CIRCEP.114.002155

13. Sun HY, Ko WJ, Tsai PR, Sun CC, Chang YY, Lee CW, et al. Infections occurring during extracorporeal membrane oxygenation use in adult patients. *J Thorac Cardiovasc Surg.* (2010) 140:1125–32.e2. doi: 10.1016/j.jtcvs.2010.07.017

14. Soto-Iglesias D, Penela D, Jáuregui B, Acosta J, Fernández-Armenta J, Linhart M, et al. Cardiac magnetic resonance-guided ventricular tachycardia substrate ablation. *JACC Clin Electrophysiol.* (2020) 6:436–47. doi: 10.1016/j.jacep.2019.11.004

15. Andreu D, Penela D, Acosta J, Fernández-Armenta J, Perea RJ, Soto-Iglesias D, et al. Cardiac magnetic resonance-aided scar dechanneling: influence on acute and long-term outcomes. *Heart Rhythm.* (2017) 14:1121–8. doi: 10.1016/j.hrthm.2017.05.018

frontiers | Frontiers in Cardiovascular Medicine

TYPE Original Research
PUBLISHED 28 October 2022
DOI 10.3389/fcvm.2022.990188

OPEN ACCESS

EDITED BY
Massimiliano Ruscica,
University of Milan, Italy

REVIEWED BY
Jahan Marcu,
University of the Sciences,
United States
Nathalia Barreto,
DOC24, Brazil

*CORRESPONDENCE
Lucio Marinelli
lucio.marinelli@unige.it

SPECIALTY SECTION
This article was submitted to General Cardiovascular Medicine, a section of the journal Frontiers in Cardiovascular Medicine

RECEIVED 09 July 2022
ACCEPTED 11 October 2022
PUBLISHED 28 October 2022

CITATION
Rosa GM, Puce L, Mori L, Currà A, Fattapposta F, Porto I, Bragazzi NL, Trompetto C and Marinelli L (2022) Nabiximols effect on blood pressure and heart rate in post-stroke patients of a randomized controlled study. *Front. Cardiovasc. Med.* 9:990188. doi: 10.3389/fcvm.2022.990188

Nabiximols effect on blood pressure and heart rate in post-stroke patients of a randomized controlled study

Gian Marco Rosa[1,2], Luca Puce[3], Laura Mori[2,3], Antonio Currà[4], Francesco Fattapposta[5], Italo Porto[1,2], Nicola Luigi Bragazzi[6], Carlo Trompetto[2,3] and Lucio Marinelli[2,3]*

[1]Cardiology Clinic, Department of Internal Medicine and Medical Specialties, University of Genoa, Genova, Italy, [2]IRCCS Ospedale Policlinico San Martino, Genova, Italy, [3]Department of Neuroscience, Rehabilitation, Ophthalmology, Genetics, Maternal and Child Health, University of Genoa, Genova, Italy, [4]Department of Medical-Surgical Sciences and Biotechnologies, A. Fiorini Hospital, Sapienza University of Rome, Latina, Italy, [5]Department of Human Neurosciences, Sapienza University of Rome, Rome, Italy, [6]Laboratory for Industrial and Applied Mathematics (LIAM), Department of Mathematics and Statistics, York University, Toronto, ON, Canada

Background: Cannabinoids may be useful to treat pain, epilepsy and spasticity, although they may bear an increased risk of cardiovascular events. This study aims to evaluate the cardiovascular safety of nabiximols, a cannabis-based drug, in patients with spasticity following stroke, thus presenting an increased cardiovascular risk.

Methods: This is an ancillary study stemming from the SativexStroke trial: a randomized double-blind, placebo-controlled, crossover study aimed at assessing the effect of nabiximols on post-stroke spasticity. Patients were treated with nabiximols oromucosal spray or placebo and assessed before and after two phases of 1-month duration each. Only the phase with the active treatment was considered for each patient who completed the study. The average values of blood pressure (diastolic, systolic, differential) and heart rate from the first 5 days of the phase (lowest nabiximols dosage) were compared to the average values recorded during the last 5 days at the end of the phase (highest nabiximols dosage). Baseline comparisons between gender, stroke type and affected side and correlation between age and blood pressure and heart rate were performed. The study was registered with the EudraCT number 2016-001034-10.

Results: Thirty-four patients completed the study and were included in the analysis. Thirty-one were taking antihypertensive drugs and, among these, 12 were taking beta-blockers. During the study, no arrhythmic events were recorded, blood pressure and heart rate did not show pathological fluctuations, and no cardiovascular or cerebrovascular events occurred. At baseline blood pressure and heart rate were comparable concerning

gender, stroke type and affected side. A significant direct correlation emerged between differential blood pressure and age and an inverse correlation between diastolic blood pressure and age. No correlation emerged between systolic blood pressure or heart rate and age. Blood pressure and heart rate did not change during nabiximols treatment compared to the baseline condition.

Conclusion: This ancillary study adds evidence that, in patients who already underwent a cerebrovascular accident, nabiximols does not determine significant blood pressure and heart rate variation or cardiovascular complications. These data support the cardiovascular safety of nabiximols, encouraging more extensive studies involving cannabinoids characterized by slow absorption rates.

KEYWORDS

stroke, THC, CBD, cannabinoid, cerebrovascular disorders, blood pressure, heart rate, Sativex

Introduction

The word "cannabis" refers to all products derived from the plant *Cannabis sativa*. Cannabinoids are a group of substances found in the cannabis plant. The main cannabinoids are delta-9-tetrahydrocannabinol (THC) and cannabidiol (CBD). THC is the substance that is primarily responsible for the effects of marijuana on a person's mental state (1).

It has been demonstrated that cannabinoids, which were previously used only for recreational purposes, can also be utilized in clinical practice to treat various pathologies, especially pain and chemotherapy-induced nausea, epilepsy and spasticity (2, 3).

The effects of all these substances are mediated through the endocannabinoid system via the interaction with the CB receptors, particularly the CB_1 receptors, which are located in the myocardium, aorta, vascular endothelium, in platelets, and in the central and peripheral nervous system. Conversely, CB_2 receptors are found in immune cells (4). Since cannabinoids interact with CB_1 receptors, they exert many cardiovascular effects, as has been shown by various studies conducted both on animal models (5, 6) and on humans (7).

The main cardiovascular effects of cannabinoids can be summarized as: enhanced sympathetic tone, increased catecholamine levels and increased heart rate at lower doses, and bradycardia/hypotension at higher doses, owing to parasympathetic stimulation occurring at these latter doses (8–10). Other cardiovascular effects which may be identified are platelet activation, endothelial dysfunction and oxidative stress (11, 12).

All these effects can be ascribed to THC; by contrast, CBD has been shown to reduce heart rate and blood pressure, improve vasodilation in models of endothelial dysfunction, and reduce inflammation and vascular hyper-permeability in diabetic models (13). Furthermore, in an interesting study, Mathew found that healthy volunteers who experienced orthostatic hypotension after smoking marijuana presented reduced cerebral blood velocity on transcranial Doppler (14). This reduction in cerebral blood flow can increase the risk of ischemic stroke and the likelihood of falls. This effect raises an important concern regarding the effects of marijuana in older subjects. A further effect of smoking marijuana is an increase in the amount of carboxyhemoglobin due to combustion, thereby causing an additional decrease in oxygen supply (15). Furthermore, many case reports have linked marijuana use to procoagulant effects, thus causing thrombus formation and leading to acute myocardial infarction in young adults (16–18). On the other hand, in many reported cases of cannabis-induced acute myocardial infarction, coronary angiography has documented coronary spasm in the absence of major atherosclerotic lesions (19).

In an interesting study, Mittleman et al. showed that marijuana smoking was associated with a 4.8-fold increased risk of myocardial infarction within 1 h of use, though this higher risk appeared to decrease rapidly thereafter (20). Finally, the pharmacokinetics of cannabinoids varies according to the route of administration, the most common route being inhalation via smoking or vaporization (21). As inhalation (*via* smoking or vaporization) is the fastest method of intoxication, the availability of THC is predictable (22). Indeed, plasma THC levels are detectable within a short time (seconds or minutes) after inhalation and reach a maximum after 15–20 min (22). Furthermore, edible forms of marijuana are now gaining popularity among users (23). Edible forms of marijuana often contain very high amounts of THC and, owing to the erratic absorption of oral marijuana, its effects are delayed (23). Oral consumption is slower to take effect, inducing peak levels at 2–3 h, and its effects are less predictable in most cases,

TABLE 1 Nabiximols titration scheme.

Day	Number of sprays		
	Morning	Afternoon/Evening	Total per day
1	0	1	1
2	0	1	1
3	0	2	2
4	0	2	2
5	1	2	3
6	1	3	4
7	1	4	5
8	2	4	6
9	2	5	7
10	3	5	8
11	3	6	9
12	4	6	10
13	4	7	11
14	5	7	12

leading to higher levels of complications. In a study on health volunteers, inhalation and IV injection elicited similar plasma THC concentrations and clinical effects, and both caused major acute cardiovascular effects, while oral ingestion induced less predictable and delayed peak plasma THC concentrations (23). THC metabolism includes Phase I reactions, mainly consisting of hydroxylation by the hepatic CYP P450, 2C9, 2C19 and 3A4 enzyme system, and Phase II reactions, which involve the oxidation of alcohols and conjugation with glucoronic acid. THC main metabolites are active 11-OH-THC and inactive THC, which are produced by oxidation (23). THC is excreted mostly as hydroxylated and carboxylated metabolites via feces or urine (24, 25). Both slow release from lipid-storage compartments and significant enterohepatic circulation contribute to the long half-life of THC (> 4 days) (25). CBD metabolism is similar to that of THC, but is subject to a significant first-pass effect; unlike THC, a large proportion of the dose is excreted unchanged in the feces (23). When THC and CBD are simultaneously administered, pharmacokinetic interference may arise; CBD partially inhibits the hydroxylation of THC to 11-OH-THC at CYP P450 and slightly slows the metabolism of 11-OH-THC to THC-COOH (23).

Among the currently used synthetic cannabinoids, a combination of THC and CBD has recently been introduced in order to improve pharmacokinetics and pharmacodynamics. Nabiximols, which is a combination of delta-9-tetrahydrocannabinol THC and cannabidiol CBD in a 1:1 ratio, has recently been introduced into the market. This drug is administered via the oromucosal route to treat spasticity, and various studies conducted in animal models have recently analyzed its pharmacokinetics and pharmacodynamics (26, 27). With regard to pharmacokinetics, THC and CBD might (23, 28, 29) reciprocally interact by interfering with their pharmacokinetics. This interaction depends largely on the ratio of the two drugs and their time of administration. Dose-ratio studies in animals have shown that the simultaneous administration of the two drugs produces a response pattern similar to that observed with a lower dose of THC, suggesting that CBD blocks the effects of THC (30). Studies conducted in humans have shown no significant differences from the effects observed in animal studies (31, 32). Recently, a double-blind randomized placebo-controlled crossover pilot study (SativexStroke Trial) was conducted in the Neurorehabilitation Unit of our Polyclinic to assess the efficacy and safety profile of nabiximols in post-stroke spasticity (33). This pilot study demonstrated the lack of efficacy of nabiximols to treat post-stroke spasticity (34). The aim of the current sub-study was to analyze the cardiovascular safety of nabiximols in a cohort of patients affected by post-stroke spasticity.

TABLE 2 Baseline patient characteristics.

Gender	
Male	24 (71%)
Female	10 (29%)
Age (y)	68 (59–72)
Stroke type	
Hemorrhagic	13 (38%)
Ischemic	21 (62%)
Affected hemisphere	
Left	13 (38%)
Right	21 (62%)
Time after stroke (y)	4.2 (1.7–5.6)
ECG findings	
Slight changes in the recovery phase	1 (3%)
Previous acute myocardial infarction	1 (3%)
Supraventricular ectopic beats	4 (12%)
Ventricular ectopic beats	2 (6%)
Right branch block	2 (6%)
Atrial fibrillation	4 (12%)

Values are reported as number (%) or median (Q1–Q3).

Materials and methods

Study design

This is an ancillary study stemming from the SativexStroke trial: a randomized double-blind, placebo controlled, crossover study aimed at assessing the effect of nabiximols on post-stroke spasticity. It has been performed at the

TABLE 3 Cardiovascular parameters at baseline.

	Gender		Stroke type		Affected hemisphere	
	Male (n = 24)	Female (n = 10)	Ischemic (n = 21)	Hemorrhagic (n = 13)	Right (n = 21)	Left (n = 13)
Diastolic BP	78 ± 6	74 ± 9	78 ± 8	75 ± 6	76 ± 6	77 ± 8
Systolic BP	127 ± 14	126 ± 13	126 ± 14	127 ± 13	128 ± 12	123 ± 15
Differential BP	49 ± 13	52 ± 11	48 ± 13	52 ± 12	52 ± 13	46 ± 9
Pulse frequency	69 ± 8	76 ± 9	71 ± 9	72 ± 8	72 ± 9	70 ± 8

Values are reported as mean ± standard deviation.

outpatient service for the treatment of spasticity of the Neurorehabilitation Unit, IRCCS Ospedale Policlinico San Martino (Genova, Italy) in accordance with the Declaration of Helsinki and Good Clinical Practice guidelines. The trial has been registered on the EudraCT platform with number 2016-001034-10.

This study lasted 10 weeks and consisted into two phases: phase 1 and 2, both of them lasting 4 weeks. Phase 1 and 2 were separated by a 2-weeks wash-out interval. During each phase, patients had been taking nabiximols and then placebo or vice-versa in a crossover design following 1:1 randomization.

Each patient was examined 4 times during 10 weeks: before (T0) and after (T1) phase 1, as well as before (T2) and after (T3) phase 2.

Participants

Adult stroke survivors were recruited according to the following inclusion criteria: (1) male or female patients of at least 18 years of age; (2) spasticity secondary to stroke that occurred at least 3 months earlier; (3) CHA2DS2VASc score < 7 assessed by the cardiologist and reflecting acceptable cardiovascular risk; (4) spasticity rated between 1 and 3 on the Modified Ashworth Scale at the level of at least one of the following muscle groups: wrist flexors, elbow flexors, knee extensors, foot plantar flexors; (5) ability (physical ability or supportive person) to comply with the study requirements correctly and to follow the study procedure and restrictions.

Exclusion criteria were: (1) presence of concomitant parkinsonism; (2) significant peripheral nervous system pathology detectable on clinical basis; (3) current smokers; (4) contraindication to treatment with nabiximols; (5) alcohol or drug abuse, including current consumption of cannabis herb or other cannabinoid-based drugs within 30 days prior to study entry; (6) treatment with botulinum toxin injection in the last 4 months; (7) clinically significant impaired renal function or impaired hepatic function at baseline, (8) females of child bearing potential, pregnant or lactating and male patients whose partner is of child bearing potential who are not willing to use effective contraception.

Procedures

Patients who gave informed consent to participate underwent a preliminary screening visit to ensure that they fulfilled the study selection criteria, followed by a cardiological evaluation (including ECG and echocardiogram) to assess cardiovascular risk.

At the beginning of each phase (T0 and T2), patients were provided with a form to daily record heart rate, blood pressure (systolic/diastolic) and adverse events. Outcome measures were collected and instructions on how to take the oromucosal spray were provided, along with a schedule to gradual increase daily sprays to reach the highest tolerable dose up to a maximum of 12 sprays/day in a 14-days period and then maintain such daily dose until the end of each phase (T1 and T3) (**Table 1**).

Patients were required to continue all concomitant medications throughout the study.

Outcomes

The main and secondary outcomes have been reported in the first report (34).

To the aim of this ancillary study, we considered the daily measurement of blood pressure and heart rate as reported by the patients in the provided form. For each patient who completed the study, we considered only the phase with the active treatment. The average values of blood pressure and heart rate from the first 5 days of the phase (while taking the smallest number of nabiximols sprays) were considered baseline T0 values. The average values recorded during the last 5 days at the end of the phase (while taking the highest number of sprays) were considered T1 values. Regarding heart rate, we consider the self-reported average number of beats per minute, regardless of the presence of an arrhythmia.

Statistical analysis

Cardiovascular parameters (systolic, diastolic and differential blood pressure; heart rate) are reported as

mean ± standard deviation. Sprays number is reported as median (range).

Baseline comparisons where performed using Mann-Whitney U test. Baseline correlations between age and cardiovascular parameters and between the number of sprays taken at T1 and T0-T1 difference of blood pressure and heart rate were performed using Spearman rank test. Cardiovascular parameter comparisons between baseline condition and during nabiximols treatment were performed using Wilcoxon signed rank test. This is a pilot study and no preliminary data about cardiovascular parameter variation during nabiximols treatment were available, so power analysis was not performed. For all tests significance level was set at $p < 0.05$.

Results

Only the 34 subjects who completed nabiximols cycles where included in the study (**Table 2**).

Patients taking anti-hypertensive drugs were 31, among these those taking beta-blockers were 12.

Baseline analysis

Comparing the 24 male and 10 female patients, no difference emerged for baseline diastolic ($U = 77, p = 0.1$), systolic ($U = 113$, $p = 0.8$), differential ($U = 86$, $p = 0.2$) and heart rate ($U = 74$, $p = 0.08$).

Comparing the 21 patients who had an ischemic stroke and the 13 who had a hemorrhagic stroke, no difference emerged for baseline diastolic ($U = 111$, $p = 0.4$), systolic ($U = 131$, $p = 0.8$), differential ($U = 120$, $p = 0.5$) and heart rate ($U = 119$, $p = 0.5$).

Comparing the 21 patients with a right and the 13 with a left hemispheric stroke, no difference emerged for baseline diastolic ($U = 129, p = 0.8$), systolic ($U = 102, p = 0.2$), differential ($U = 97$, $p = 0.2$) and heart rate ($U = 116$, $p = 0.5$) (**Table 3**).

Diastolic blood pressure inversely correlated with age (Rho = −0.4, $p = 0.014$), while systolic pressure did not (Rho = 0.1, $p = 0.4$). A significant direct correlation emerged between age and differential blood pressure (Rho = 0.5, $p = 0.008$) (**Figure 1**). Age and heart rate did not correlate (Rho = −0.07, $p = 0.7$).

Nabiximols effect

On average, at T1 patients were taking 9 nabiximols sprays (range 1–12), corresponding to 24.3mg of THC and 22.5mg of CBD.

No significant changes of diastolic ($Z = -1.2$, $p = 0.2$), systolic ($Z = -1.2$, $p = 0.2$) and differential ($Z = -0.1$, $p = 0.9$) blood pressure as well as heart rate ($Z = -0.06$, $p = 1.0$) before and during nabiximols treatment (**Figure 2**). The number of sprays taken at T1 did not correlate with T0-T1 variation of diastolic (Rho = −0.10, $p = 0.4$), systolic (Rho = −0.13, $p = 0.3$) and differential (Rho = −0.23, $p = 0.2$) blood pressure, nor variation of heart rate (Rho = 0.07, $p = 0.8$).

Discussion

Excluding nicotine, cannabis is the drug of abuse most commonly used by adolescents worldwide (35). Recently, however, the widespread consumption of cannabinoids has not been limited to recreational use nor to young adults. Indeed, cannabinoids are also gaining popularity among the elderly as a method of treating chronic illnesses (36).

The present study is the first to evaluate the effects of a cannabinoid drug (nabiximols) in patients with post-stroke spasticity. This drug has been widely studied in patients with multiple sclerosis (2, 3) and also in patients with amyotrophic lateral sclerosis (37), but not in stroke survivors, who are much more numerous, given the high prevalence of stroke (38). These latter patients have a worse cardiovascular risk profile, and this drug offers various advantages: it can be administered by the oromucosal route, presents a balanced THC:CBD ratio, and is probably safe from the cardiovascular point of view, since, to our knowledge, nabiximols-related stroke events have not been reported in the literature so far (39). By contrast, stroke events have been described in the case of cannabinoid intake via the inhalatory route (9). In our study, all patients underwent a preliminary cardiological evaluation and their blood pressure and heart rate were monitored daily.

Only one patient complained of tachycardia during phase 2, when on active treatment, and decided to exit the study (although tachycardia had already been recorded in phase 1, while the patient was taking placebo). As regards the differential pressure, our population behaves like the general population since we have observed that the differential blood pressure increases with age.

No cardiovascular treatment-emergent adverse drug effects emerged during nabiximols treatment, namely no significant fluctuation of blood pressure and heart rate, nor ischemic or hemorrhagic events occurred. During nabiximols treatment (T1), self-assessed blood pressure and heart rate did not change compared to the baseline condition. No patients showed significant acceleration or decrease in heart rate or change in rhythm and none required an additional ECG or cardiological evaluation during the study.

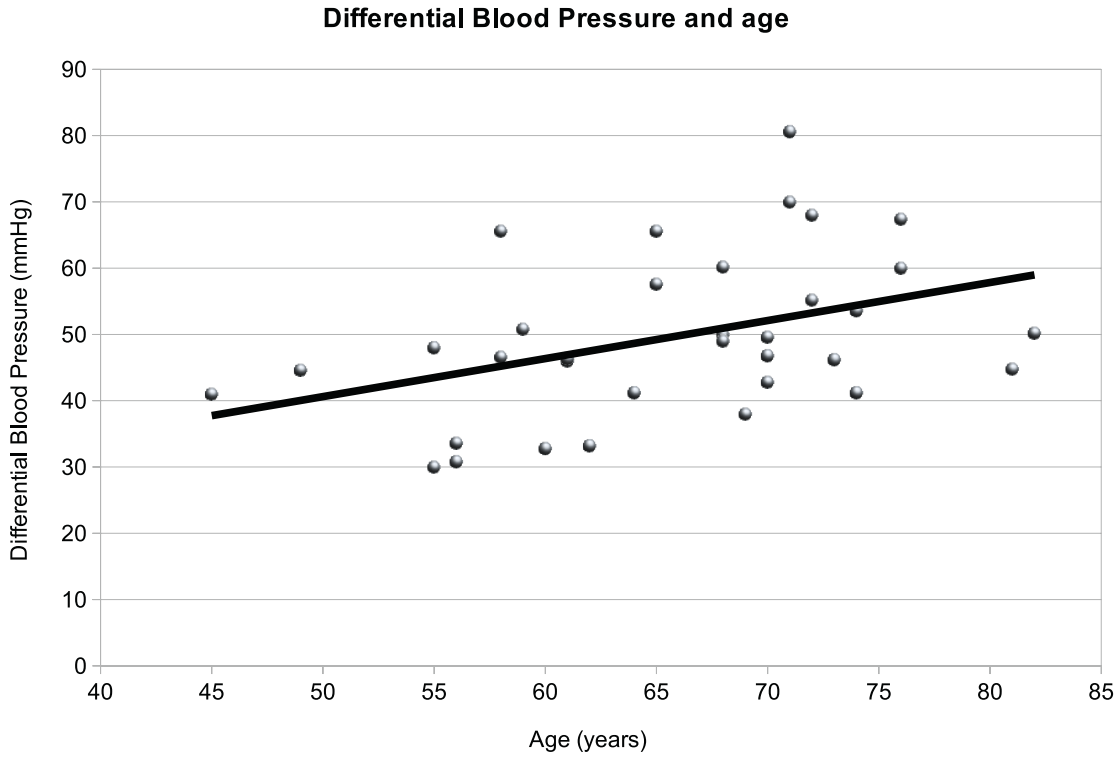

FIGURE 1
Graphical representation of the relationship between differential arterial pressure and age. With increasing age also differential arterial pressure increases.

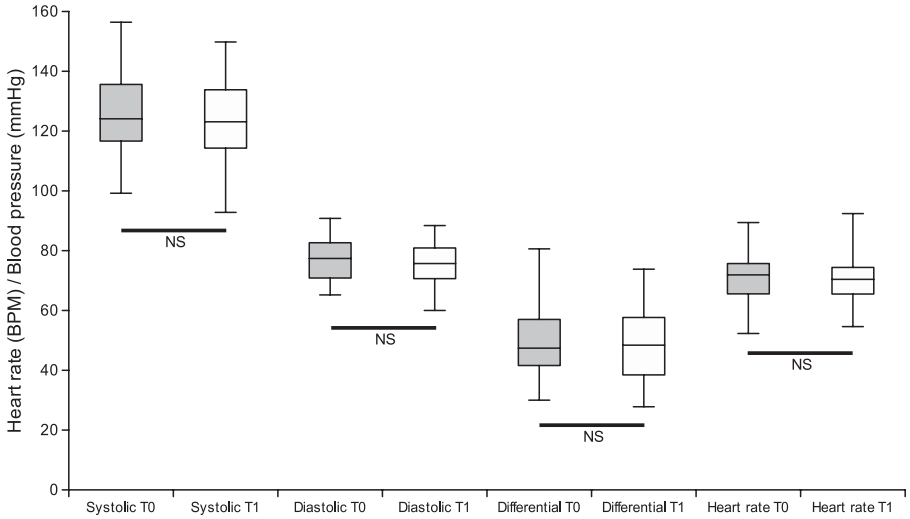

FIGURE 2
Graphical representation of comparison between cardiovascular parameters: systolic arterial pressure, diastolic arterial pressure, differential arterial pressure and heart rate measured at T0 vs. T1.

The patients reached a very variable number of sprays at T1, depending on the individual highest tolerated dose. To further investigate a possible dose-related effect of nabiximols on blood pressure and heart rate we sought a correlation between the number of sprays at T1 and cardiovascular parameter variation between T0 and T1, however, the lack of correlation confirms that, nabiximols did not affect blood pressure and heart rate in our population over 4 weeks. This may be also ascribed

to the fact that oromuscosal administration allows different pharmacokinetics with fewer fluctuations in blood pressure and heart rate. Unfortunately, however, the expected improvement in spasticity in stroke patients was not found, as previously published (34). This additional result of the SativexStroke trial was that nabiximols displayed a good safety profile and was well tolerated, particularly from the cardiovascular point of view.

The main limitation of the present study is the low number of participants since it was single-center. Another limitation of the study is the fact that, as regards the cardiovascular effects of nabiximols, we considered baseline (T0) values those obtained at the beginning of the active phase, while patients had already started nabiximols, although at a very low dosage. If nabiximols effect on cardiovascular parameters was not dose-dependent and effective even while taking a small number of sprays and consequently before nabiximols could reach plasma steady state, such effect cannot be appreciated by our protocol. Further studies are needed to clarify this aspect. Blood pressure and heart rate were self-assessed by patients. This might have introduced inaccuracies related to a systematic or occasional error in parameter sampling. We tried to mitigate possible measurement errors by analyzing the average values across 5 consecutive days, although this approach, along with the requirement to measure parameters only once per day, greatly reduced the temporal resolution of outcome assessments. It is therefore obvious that short-term (minutes and hours) fluctuations of blood pressure and heart rate could not have been appreciated in this study.

Conclusion

In conclusion, an interesting result of this pilot study is the good cardiovascular safety profile of nabiximols in patients with stroke. In these patients, the possible beneficial effect of cannabinoids, such as delaying atherosclerotic progression and inflammation, may deserve further investigation. Furthermore, because of the rapidly changing landscape of cannabis laws and marijuana use in western countries, there is a pressing need for refined policy, education of both clinicians and the public, and new research. Carefully designed, prospective, short- and long-term studies are needed to obtain conclusive data on the safety and efficacy of cannabinoid drugs.

Data availability statement

The raw data supporting the conclusions of this article will be made available by the authors, without undue reservation.

Ethics statement

The studies involving human participants were reviewed and approved by the Comitato Etico Regionale della Liguria. The patients/participants provided their written informed consent to participate in this study.

Author contributions

LMa conceived and designed the study, collected data as principal investigator, performed statistical analyses, and drafted the manuscript. LP and LMo performed patients evaluation and collected data. GR performed the cardiological evaluation and revised the manuscript. AC, FF, IP, NB, and CT critically revised the work for important intellectual content. All authors approved the final version.

Funding

This was an investigator-initiated study, the insurance policy covering the study was provided by Almirall Group, the drug samples (nabiximols and placebo) packaged for the double-blind condition were provided free of charge by GW Pharma. Almirall Group also contributed partially to the total costs of the research, providing the devices for blood pressure and heart rate measurements, covering the costs of consumable materials and partially compensating for research time (40% of total costs). The funder was not involved in the study design, collection, analysis, interpretation of data, the writing of this article, or the decision to submit it for publication.

Conflict of interest

CT received partial funding for other research projects from Almirall Group.

The remaining authors declare that the research was conducted in the absence of any commercial or financial relationships that could be construed as a potential conflict of interest.

Publisher's note

References

1. D'Souza DC, Perry E, MacDougall L, Ammerman Y, Cooper T, Wu Y-T, et al. The psychotomimetic effects of intravenous delta-9-tetrahydrocannabinol in healthy individuals: implications for psychosis. *Neuropsychopharmacology.* (2004) 29:1558–72. doi: 10.1038/sj.npp.1300496

2. Watson SJ. Marijuana and medicine: assessing the science base: a summary of the 1999 institute of medicine report. *Arch Gen Psychiatry.* (2000) 57:547–52. doi: 10.1001/archpsyc.57.6.547

3. Novotna A, Mares J, Ratcliffe S, Novakova I, Vachova M, Zapletalova O, et al. A randomized, double-blind, placebo-controlled, parallel-group, enriched-design study of nabiximols* (Sativex®), as add-on therapy, in subjects with refractory spasticity caused by multiple sclerosis: Sativex for refractory spasticity in MS. *Eur J Neurol.* (2011) 18:1122–31. doi: 10.1111/j.1468-1331.2010.03328.x

4. Alfulaij N, Meiners F, Michalek J, Small-Howard AL, Turner HC, Stokes AJ. Cannabinoids, the heart of the matter. *J Am Heart Assoc.* (2018) 7:e009099. doi: 10.1161/JAHA.118.009099

5. Lépicier P, Bouchard J-F, Lagneux C, Lamontagne D. Endocannabinoids protect the rat isolated heart against ischaemia. *Br J Pharmacol.* (2003) 139:805–15. doi: 10.1038/sj.bjp.0705313

6. Lake KD, Compton DR, Varga K, Martin BR, Kunos G. Cannabinoid-induced hypotension and bradycardia in rats mediated by CB1-like cannabinoid receptors. *J Pharmacol Exp Ther.* (1997) 281:1030–7.

7. Liu J, Gao B, Mirshahi F, Sanyal AJ, Khanolkar AD, Makriyannis A, et al. Functional CB1 cannabinoid receptors in human vascular endothelial cells. *Biochem J.* (2000) 346:835–40.

8. Iannaccone G, Porto I. Marijuana influence on cardiac modulation and heart rate: novel hypotheses and gaps in evidence. *Minerva Cardiol Angiol.* (2021) 69:466–8. doi: 10.23736/S2724-5683.20.05497-3

9. Thomas G, Kloner RA, Rezkalla S. Adverse cardiovascular, cerebrovascular, and peripheral vascular effects of marijuana inhalation: what cardiologists need to know. *Am J Cardiol.* (2014) 113:187–90. doi: 10.1016/j.amjcard.2013.09.042

10. Fisher BAC, Ghuran A, Vadamalai V, Antonios TF. Cardiovascular complications induced by cannabis smoking: a case report and review of the literature. *Emerg Med J.* (2005) 22:679–80. doi: 10.1136/emj.2004.014969

11. Deusch E, Kress HG, Kraft B, Kozek-Langenecker SA. The procoagulatory effects of delta-9-tetrahydrocannabinol in human platelets. *Anesth Analg.* (2004) 99:1127–30. doi: 10.1213/01.ANE.0000131505.03006.74

12. Han KH, Lim S, Ryu J, Lee C-W, Kim Y, Kang J-H, et al. CB1 and CB2 cannabinoid receptors differentially regulate the production of reactive oxygen species by macrophages. *Cardiovasc Res.* (2009) 84:378–86. doi: 10.1093/cvr/cvp240

13. Stanley CP, Hind WH, O'Sullivan SE. Is the cardiovascular system a therapeutic target for cannabidiol? *Br J Clin Pharmacol.* (2013) 75:313–22. doi: 10.1111/j.1365-2125.2012.04351.x

14. Mathew RJ, Wilson WH, Humphreys D, Lowe JV, Wiethe KE. Middle cerebral artery velocity during upright posture after marijuana smoking. *Acta Psychiatr Scand.* (1992) 86:173–8. doi: 10.1111/j.1600-0447.1992.tb03247.x

15. Jones RT. Cardiovascular system effects of marijuana. *J Clin Pharmacol.* (2002) 42:58S–63S. doi: 10.1002/j.1552-4604.2002.tb06004.x

16. Pacher P, Steffens S, Haskó G, Schindler TH, Kunos G. Cardiovascular effects of marijuana and synthetic cannabinoids: the good, the bad, and the ugly. *Nat Rev Cardiol.* (2018) 15:151–66. doi: 10.1038/nrcardio.2017.130

17. Marchetti D, Spagnolo A, De Matteis V, Filograna L, De Giovanni N. Coronary thrombosis and marijuana smoking: a case report and narrative review of the literature. *Drug Test Anal.* (2016) 8:56–62. doi: 10.1002/dta.1898

18. Patel RS, Kamil SH, Bachu R, Adikey A, Ravat V, Kaur M, et al. Marijuana use and acute myocardial infarction: a systematic review of published cases in the literature. *Trends Cardiovasc Med.* (2020) 30:298–307. doi: 10.1016/j.tcm.2019.08.003

19. Richards JR, Bing ML, Moulin AK, Elder JW, Rominski RT, Summers PJ, et al. Cannabis use and acute coronary syndrome. *Clin Toxicol.* (2019) 57:831–41. doi: 10.1080/15563650.2019.1601735

20. Mittleman MA, Lewis RA, Maclure M, Sherwood JB, Muller JE. Triggering myocardial infarction by marijuana. *Circulation.* (2001) 103:2805–9. doi: 10.1161/01.cir.103.23.2805

21. Latif Z, Garg N. The impact of marijuana on the cardiovascular system: a review of the most common cardiovascular events associated with marijuana use. *JCM.* (2020) 9:1925. doi: 10.3390/jcm9061925

22. Singh A, Saluja S, Kumar A, Agrawal S, Thind M, Nanda S, et al. Cardiovascular complications of marijuana and related substances: a review. *Cardiol Ther.* (2018) 7:45–59. doi: 10.1007/s40119-017-0102-x

23. Huestis MA. Human cannabinoid pharmacokinetics. *Chem Biodivers.* (2007) 4:1770–804. doi: 10.1002/cbdv.200790152

24. Williams PL, Moffat AC. Identification in human urine of delta 9-tetrahydrocannabinol-11-oic acid glucuronide: a tetrahydrocannabinol metabolite. *J Pharm Pharmacol.* (1980) 32:445–8. doi: 10.1111/j.2042-7158.1980.tb12966.x

25. Johansson E, Agurell S, Hollister LE, Halldin MM. Prolonged apparent half-life of delta 1-tetrahydrocannabinol in plasma of chronic marijuana users. *J Pharm Pharmacol.* (1988) 40:374–5. doi: 10.1111/j.2042-7158.1988.tb05272.x

26. Long LE, Chesworth R, Huang X-F, McGregor IS, Arnold JC, Karl T. A behavioural comparison of acute and chronic Delta9-tetrahydrocannabinol and cannabidiol in C57BL/6JArc mice. *Int J Neuropsychopharmacol.* (2010) 13:861–76. doi: 10.1017/S1461145709990605

27. Malone DT, Jongejan D, Taylor DA. Cannabidiol reverses the reduction in social interaction produced by low dose Delta (9)-tetrahydrocannabinol in rats. *Pharmacol Biochem Behav.* (2009) 93:91–6. doi: 10.1016/j.pbb.2009.04.010

28. Benowitz NL, Nguyen TL, Jones RT, Herning RI, Bachman J. Metabolic and psychophysiologic studies of cannabidiol-hexobarbital interaction. *Clin Pharmacol Ther.* (1980) 28:115–20. doi: 10.1038/clpt.1980.139

29. Hunt CA, Jones RT, Herning RI, Bachman J. Evidence that cannabidiol does not significantly alter the pharmacokinetics of tetrahydrocannabinol in man. *J Pharmacokinet Biopharm.* (1981) 9:245–60. doi: 10.1007/BF01059266

30. Zuardi AW, Hallak JEC, Crippa JAS. Interaction between cannabidiol (CBD) and Δ(9)-tetrahydrocannabinol (THC): influence of administration interval and dose ratio between the cannabinoids. *Psychopharmacology.* (2012) 219:247–9. doi: 10.1007/s00213-011-2495-x

31. Karschner EL, Darwin WD, McMahon RP, Liu F, Wright S, Goodwin RS, et al. Subjective and physiological effects after controlled Sativex and oral THC administration. *Clin Pharmacol Ther.* (2011) 89:400–7. doi: 10.1038/clpt.2010.318

32. Karschner EL, Darwin WD, Goodwin RS, Wright S, Huestis MA. Plasma cannabinoid pharmacokinetics following controlled oral delta9-tetrahydrocannabinol and oromucosal cannabis extract administration. *Clin Chem.* (2011) 57:66–75. doi: 10.1373/clinchem.2010.152439

33. Marinelli L, Balestrino M, Mori L, Puce L, Rosa GM, Giorello L, et al. A randomised controlled cross-over double-blind pilot study protocol on THC:CBD oromucosal spray efficacy as an add-on therapy for post-stroke spasticity. *BMJ Open.* (2017) 7:e016843. doi: 10.1136/bmjopen-2017-016843

34. Marinelli L, Puce L, Mori L, Leandri M, Rosa GM, Currà A, et al. Cannabinoid effect and safety in spasticity following stroke: a double-blind randomized placebo-controlled study. *Front Neurol.* (2022) 13:892165. doi: 10.3389/fneur.2022.892165

35. Ramo DE, Liu H, Prochaska JJ. Tobacco and marijuana use among adolescents and young adults: a systematic review of their co-use. *Clin Psychol Rev.* (2012) 32:105–21. doi: 10.1016/j.cpr.2011.12.002

36. Mahvan TD, Hilaire ML, Mann A, Brown A, Linn B, Gardner T, et al. Marijuana use in the elderly: implications and considerations. *Consult Pharm.* (2017) 32:341–51. doi: 10.4140/TCP.n.2017.341

37. Riva N, Mora G, Sorarù G, Lunetta C, Ferraro OE, Falzone Y, et al. Safety and efficacy of nabiximols on spasticity symptoms in patients with motor neuron disease (CANALS): a multicentre, double-blind, randomised, placebo-controlled, phase 2 trial. *Lancet Neurol.* (2019) 18:155–64. doi: 10.1016/S1474-4422(18)30406-X

38. Wissel J, Manack A, Brainin M. Toward an epidemiology of poststroke spasticity. *Neurology.* (2013) 80:S13–9. doi: 10.1212/WNL.0b013e3182762448

39. Prieto González JM, Vila Silván C. Safety and tolerability of nabiximols oromucosal spray: a review of more than 15 years" accumulated evidence from clinical trials. *Expert Rev Neurother.* (2021) 21:755–78. doi: 10.1080/14737175.2021.1935879

frontiers | Frontiers in Cardiovascular Medicine

TYPE Original Research
PUBLISHED 10 November 2022
DOI 10.3389/fcvm.2022.900353

OPEN ACCESS

EDITED BY
Pietro Enea Lazzerini,
University of Siena, Italy

REVIEWED BY
Yunxia Zhang,
China-Japan Friendship Hospital, China
Thomas M. Hofbauer,
Medical University of Vienna, Austria

*CORRESPONDENCE
Yuanhua Yang
yyh1031@sina.com
Jiuchang Zhong
jczhong@sina.com

SPECIALTY SECTION
This article was submitted to General Cardiovascular Medicine, a section of the journal Frontiers in Cardiovascular Medicine

RECEIVED 20 March 2022
ACCEPTED 21 October 2022
PUBLISHED 10 November 2022

CITATION
Miao R, Dong X, Gong J, Li Y, Guo X, Wang J, Huang Q, Wang Y, Li J, Yang S, Kuang T, Liu M, Wan J, Zhai Z, Zhong J and Yang Y (2022) Single-cell RNA-sequencing and microarray analyses to explore the pathological mechanisms of chronic thromboembolic pulmonary hypertension.
Front. Cardiovasc. Med. 9:900353.
doi: 10.3389/fcvm.2022.900353

Single-cell RNA-sequencing and microarray analyses to explore the pathological mechanisms of chronic thromboembolic pulmonary hypertension

Ran Miao[1,2], Xingbei Dong[3], Juanni Gong[2], Yidan Li[4], Xiaojuan Guo[5], Jianfeng Wang[6], Qiang Huang[6], Ying Wang[7], Jifeng Li[2], Suqiao Yang[2], Tuguang Kuang[2], Min Liu[8], Jun Wan[9], Zhenguo Zhai[10], Jiuchang Zhong[11]* and Yuanhua Yang[2]*

[1]Medical Research Center, Beijing Institute of Respiratory Medicine, Beijing Chao-Yang Hospital, Capital Medical University, Beijing, China, [2]Department of Respiratory and Critical Care Medicine, Beijing Institute of Respiratory Medicine, Beijing Chao-Yang Hospital, Capital Medical University, Beijing, China, [3]Chinese Academy of Medical Sciences and Peking Union Medical College, Beijing, China, [4]Department of Echocardiography, Beijing Chao-Yang Hospital, Capital Medical University, Beijing, China, [5]Department of Radiology, Beijing Chao-Yang Hospital, Capital Medical University, Beijing, China, [6]Department of Interventional Radiology, Beijing Chao-Yang Hospital, Capital Medical University, Beijing, China, [7]Department of Pathology, Beijing Chao-Yang Hospital, Capital Medical University, Beijing, China, [8]Department of Radiology, China-Japan Friendship Hospital, Beijing, China, [9]Department of Respiration, Beijing Anzhen Hospital, Capital Medical University, Beijing, China, [10]Department of Pulmonary and Critical Care Medicine, Center of Respiratory Medicine, China-Japan Friendship Hospital, National Clinical Research Center for Respiratory Diseases, Beijing, China, [11]Heart Center and Beijing Key Laboratory of Hypertension, Beijing Chao-Yang Hospital, Capital Medical University, Beijing, China

Objective: The present study aimed to explore the pathological mechanisms of chronic thromboembolic pulmonary hypertension (CTEPH) using a gene chip array and single-cell RNA-sequencing (scRNA-seq).

Materials and methods: The mRNA expression profile GSE130391 was downloaded from the Gene Expression Omnibus database. The peripheral blood samples of five CTEPH patients and five healthy controls were used to prepare the Affymetrix microRNA (miRNA) chip and the Agilent circular RNA (circRNA) chip. The pulmonary endarterectomized tissues from five CTEPH patients were analyzed by scRNA-seq. Cells were clustered and annotated, followed by the identification of highly expressed genes. The gene chip data were used to identify disease-related mRNAs and differentially expressed miRNAs and circRNAs. The protein–protein interaction (PPI) network and the circRNA–miRNA–mRNA network were constructed for each cell type.

Results: A total of 11 cell types were identified. Intersection analysis of highly expressed genes in each cell type and differentially expressed mRNAs were performed to obtain disease-related genes in each cell type. TP53, ICAM1, APP, ITGB2, MYC, and ZYX showed the highest degree of connectivity in the PPI network of different types of cells. In addition, the circRNA–miRNA–mRNA network for each cell type was constructed.

Conclusion: For the first time, the key mRNAs, miRNAs, and circRNAs, as well as their possible regulatory relationships, during the progression of CTEPH were analyzed using both gene chip and scRNA-seq data. These findings may contribute to a better understanding of the pathological mechanisms of CTEPH.

KEYWORDS

chronic thromboembolic pulmonary hypertension, single-cell RNA-sequencing, microarray, circRNA, miRNA, mRNA

Introduction

Chronic thromboembolic pulmonary hypertension (CTEPH) is a rare small-vessel arteriopathy characterized by persistent pulmonary arterial obstruction that is caused by organized fibrotic thrombi with secondary microvascular remodeling, which may lead to increased vascular resistance, pulmonary hypertension, and heart failure (1). Pulmonary endarterectomy is currently the standard therapy and the only curative treatment for CTEPH, which is associated with a 5-year survival rate of 83% for operable patients (2). However, not all patients with CTEPH are eligible for surgery. Moreover, CTEPH is often diagnosed at an advanced stage due to misdiagnosis or delayed symptoms, resulting in a poor prognosis; the 5-year survival rate of CTEPH patients is less than 40% (3). Therefore, it is of great clinical significance to further explore the pathophysiological mechanisms of CTEPH.

Various genes, cell types, and signal transduction systems are involved in the occurrence and development of CTEPH (4). Gene microarray and sequencing technology have been widely used to analyze intracellular transcription and signaling pathways (5). In addition, several dysregulated mRNAs, microRNAs (miRNAs), and circular RNAs (circRNAs) in CTEPH have been identified by bulk RNA sequencing (RNA-seq) and chip array analyses (6, 7). For example, Gu et al. (6) analyzed pulmonary artery endothelial cells from five CTEPH patients and five donors for lung transplantation (controls) using Affymetrix gene chip analysis and identified 1,614 differentially expressed (DE) genes in CTEPH. Meanwhile, Halliday et al. (8) characterized the molecular and functional features associated with CTEPH using multiple methods, including bulk RNA-seq. Furthermore, Wang et al. (9) performed miRNA microarray analysis and found that the miRNA let-7d plays a crucial role in CTEPH progression. Additionally, our previous analysis using an Agilent circRNA chip showed that hsa_circ_0046159 was significantly upregulated in CTEPH compared with that in normal blood samples (10). Importantly, single-cell RNA-seq (scRNA-seq) is an emerging technique that can reveal the expression profile of individual cells, making it possible to provide an atlas of the single-cell landscape of pulmonary endarterectomized tissues in CTEPH (11, 12). Taken together, bulk RNA-seq and chip array analyses are mainly used to detect the overall gene expression changes in CTEPH, while scRNA-seq can identify different cell clusters and provide the expression profiles of individual cells.

The present study aimed to obtain a more comprehensive understanding of the pathological mechanisms of CTEPH using gene chip array and scRNA-seq analyses. The mRNA expression profile GSE130391 was downloaded from the Gene Expression Omnibus (GEO) database, and the Affymetrix miRNA chip and the Agilent circRNA chip were prepared using the peripheral blood samples from CTEPH patients and healthy controls. In addition, the pulmonary endarterectomized tissues of CTEPH patients were analyzed by scRNA-seq. Then, the circRNA–miRNA–mRNA network was constructed for each cell type. Our data may provide some insights for the development of CTEPH treatment.

Abbreviations: CTEPH, chronic thromboembolic pulmonary hypertension; scRNA-seq, single-cell RNA-sequencing; miRNAs, microRNAs; circRNAs, circular RNAs; PPI, protein–protein interaction; RNA-seq, RNA sequencing; DE, differentially expressed; GEO, gene expression omnibus; GO, gene ontology; BP, biological process; KEGG, Kyoto Encyclopedia of genes and genomes; NK, natural killer; ICAM1, intercellular adhesion molecule-1; APP, amyloid beta precursor protein; ITGB2, integrin subunit beta 2; MYC, MYC proto-oncogene, bHLH transcription factor; ZYX, Zyxin; PTGS2, prostaglandin-endoperoxide synthase 2; TGFB1, transforming growth factor beta 1; PASMCs, pulmonary artery smooth muscle cells.

Materials and methods

Tissue collection and scRNA-seq

Pulmonary endarterectomized tissues were collected from five patients who were diagnosed with CTEPH (13) and underwent a pulmonary endarterectomy between October 2019 and June 2020 at the Beijing Chao-Yang Hospital, Capital Medical University. The baseline characteristics of these patients are shown in **Table 1**. The patients were treated with one of the following anticoagulants for at least 3 months: warfarin, rivaroxaban, and low-molecular-weight heparin. All treatments were carried out in accordance with the guidelines.

TABLE 1 Baseline characteristics of patients with CTEPH.

Characteristic	Value (number of patients)
Female:Male	1:4
Age (years, mean ± SD)	45.00 ± 13.34
BMI (kg/m^2, mean ± SD)	25.18 ± 1.18
mPAP (mmHg, mean ± SD)	54.40 ± 3.21
PAWP (mmHg, mean ± SD)	9.60 ± 2.51
PVR (dyn.sec/cm^5, mean ± SD)	1098.60 ± 103.70
WHO FC I–II:WHO FC III–IV	1:4
CI [L/(min·m^2), mean ± SD]	1.78 ± 0.13
Family history of venous thromboembolism	0
Smoking	2
Bed rest over 24 h	0
Other CTEPH risk factors	
Pulmonary embolism	3
Venous thromboembolism	2
Inflammatory bowel disease	0
Splenectomy	0

CTEPH, chronic thromboembolic pulmonary hypertension; BMI, body mass index; mPAP, mean pulmonary arterial pressure; PAWP, pulmonary artery wedge pressure; PVR, pulmonary vascular resistance; WHO FC, World Health Organization function classification; CI, cardiac index; SD, standard deviation.

Tissues samples were then stored in MACS Tissue Storage Solution (Miltenyi Biotec, Bergisch Gladbach, Germany). This study was approved by the Ethics Committee of Beijing Chao-Yang Hospital, Capital Medical University (Approval number: 2019-K-28) and conformed to the principles outlined in the Declaration of Helsinki. The requirement for written informed consent was waived because discarded pulmonary endarterectomized tissues were used in this study. The tissue samples were dissociated to a single-cell suspension and subjected to 10 × Genomics scRNA-seq using the Illumina NovaSeq platform (Illumina Inc., USA).

Cell clustering

The scRNA-seq data of five pulmonary endarterectomized tissue samples were integrated by Cell Ranger and then filtered by the R package Seurat (14) with the following filtering conditions: gene number > 200; at least one gene expressed in three cells, and mitochondrial gene expression ratio ≤ 20%. Then, all cells were clustered by the Seurat package, and a two-dimensional scatter diagram was displayed using the UMAP method. Marker genes corresponding to each cell cluster were identified using the FindMarkers function in the Seurat package based on differential analysis. The clusters were then annotated with the marker genes to identify the cell type.

Identification of highly expressed genes

Significantly highly expressed genes in each cell type were identified using the Seurat package (14). The default threshold parameters were set as follows: min.pct = 0.1; only.pos = TRUE; and logfc.threshold = 0.25. Each time, one cell type was assigned

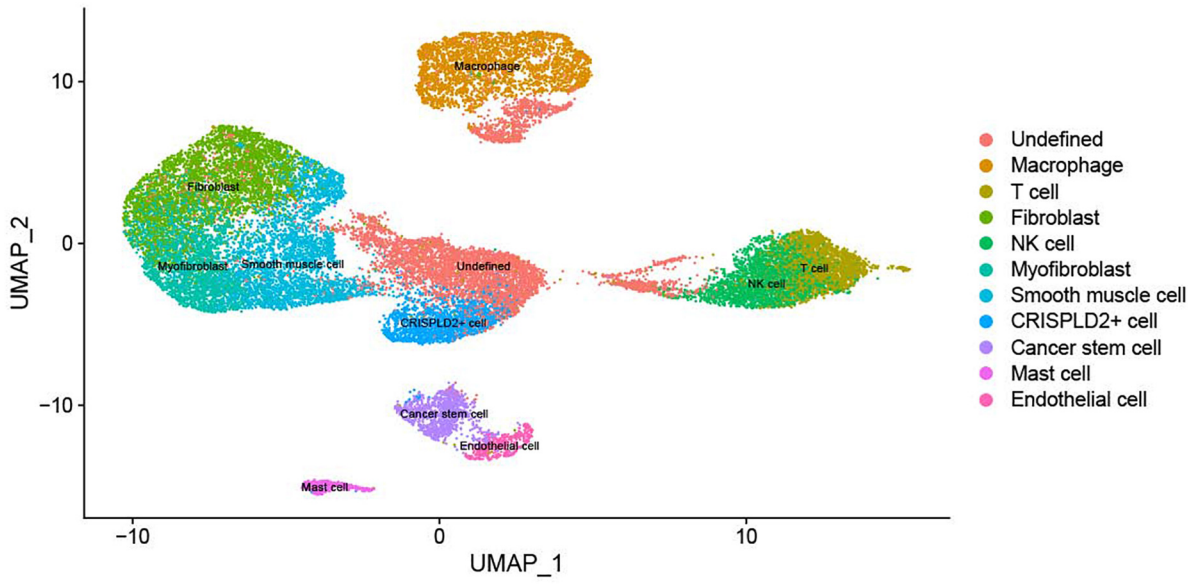

FIGURE 1
The UMAP plot of 11 cell subtypes in all samples. Different colors indicate different cell types.

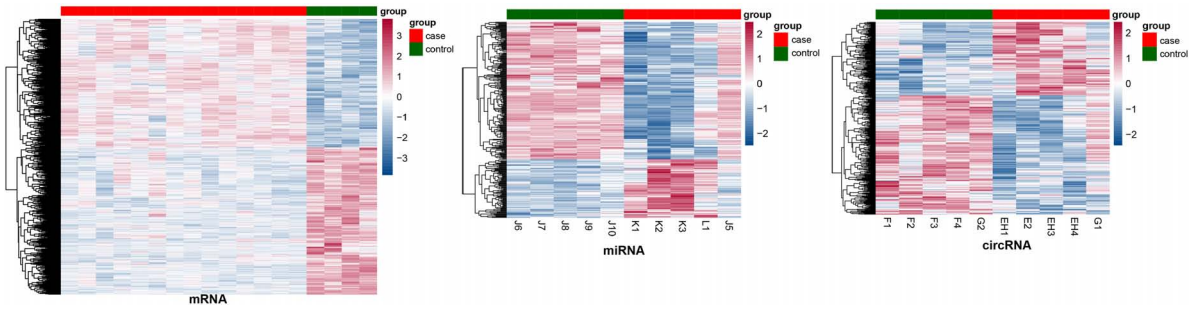

FIGURE 2
The heatmaps of differentially expressed mRNAs, miRNAs, and circRNAs.

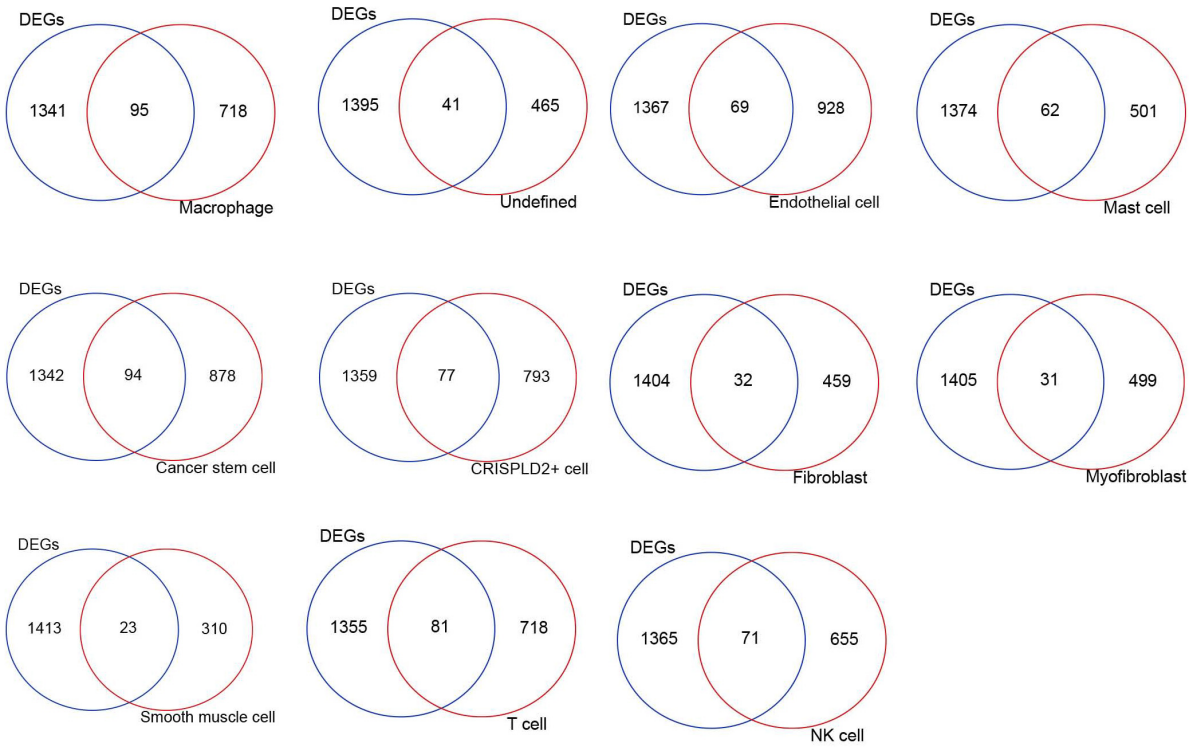

FIGURE 3
The intersection Venn diagram of differentially expressed mRNAs and highly expressed genes in each cell type.

as the comparison group to the other cell types. Genes that met all of the following criteria were screened: (1) expressed in 10% of cells in at least one of the two groups; (2) highly expressed in the comparison group; (3) logFC was greater than 0.25.

Preparation and preprocessing of miRNA and circRNA expression data

Peripheral blood samples were collected from five CTEPH patients who were admitted to the Beijing Chao-Yang Hospital, Capital Medical University, and from five healthy subjects who underwent a routine physical examination at the same hospital between March 2016 and April 2016. This study was approved by the Ethics Committee of Beijing Chao-Yang Hospital, Capital Medical University (Approval number: 2015-7-24-8) and performed in accordance with the principles outlined in the Declaration of Helsinki. The requirement for written informed consent was waived because discarded blood samples were used in this study, while the research involved no risk to the subjects and the waiver did not adversely affect the rights and welfare of the subjects. The total RNA was extracted from the

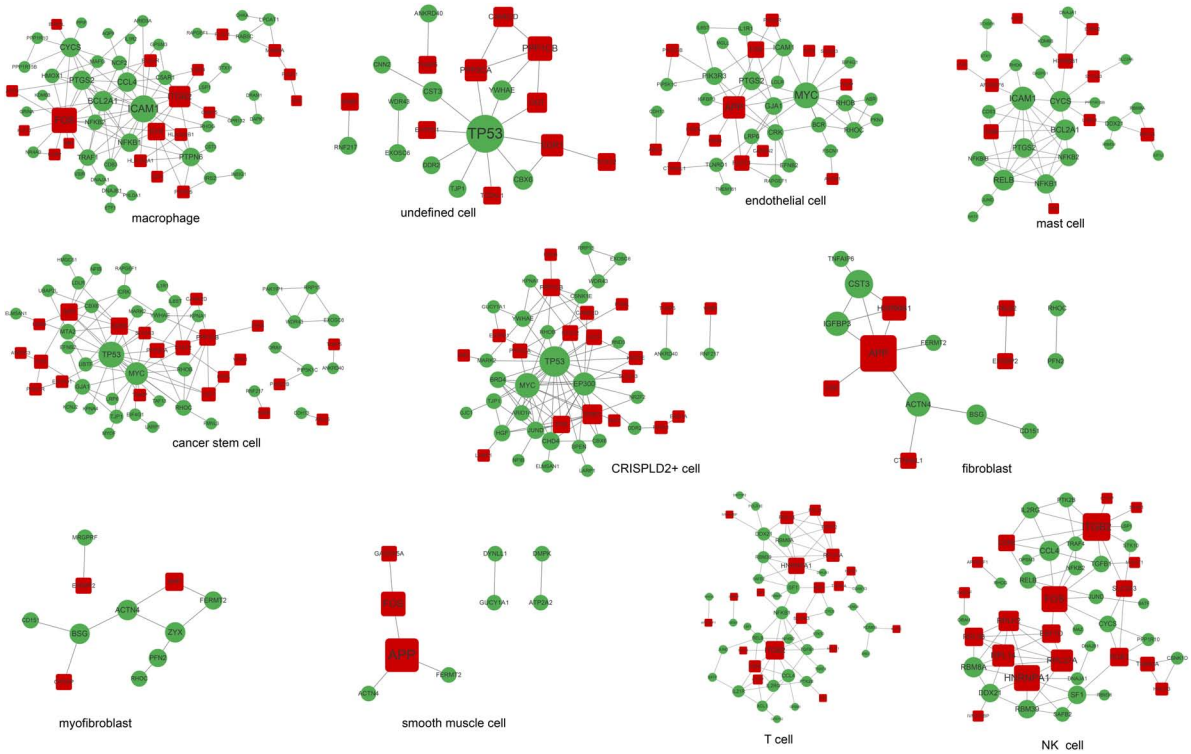

FIGURE 4
The PPI networks are associated with disease-related genes in each cell type. Red squares represent upregulated mRNAs; green circles represent downregulated mRNAs; gray lines represent protein interactions.

TABLE 2 The numbers of nodes and relation pairs (edges) in the PPI network of each cell type.

Cell type	Nodes	Edges
Macrophages	61	112
Undefined cells	21	21
Endothelial cells	39	62
Mast cells	33	53
Cancer stem cells	60	91
CRISPLD2^{+} cells	48	96
Fibroblasts	15	15
Myofibroblasts	11	10
Smooth muscle cells	9	6
T cells	52	82
NK cells	45	78

peripheral blood samples using an RNAprep Pure Blood Kit (Tiangen Biotech Co., Ltd., Beijing, China) and prepared for the Affymetrix miRNA chip and Agilent circRNA chip analyses (10).

The miRNA expression profile in the CEL format was preprocessed by Expression Console (version 1.4), including RMA normalization, distinguishing probe signals from background signals, and integrating probe signals into probe set signals. The circRNA expression profile was preprocessed using the Feature Extraction package, and the chip data were normalized by GeneSpring GX. Two probes (CBC1 and CBC2) with different lengths were used to detect one circRNA; therefore, the detection data of the two probes were mutually verified, and the accuracy of the results was improved.

Identification and preprocessing of the gene expression profile

The gene expression profiles of both patients and healthy controls were searched in the GEO database, with 'chronic thromboembolic pulmonary hypertension' as the keyword. The GSE130391 dataset (8), consisting of 14 CTEPH pulmonary artery samples and 4 control pulmonary artery samples, was finally included in this study. The GPL10558 Illumina HumanHT-12 V4.0 Expression Beadchip platform was used.

The Series Matrix File was downloaded from the GEO database, and the corresponding expression data of CTEPH and control samples were extracted. After processing of the log(2) signal intensity with the Affymetrix Microarray Suite (version MAS 5.0) (15), the probe ID

10.3389/fcvm.2022.900353

TABLE 3 The top 10 gene nodes in the PPI network of each cell type.

Cell type	Gene node													
Macrophages	ICAM1	FOS	ITGB2	BCL2A1	CYCS	CCL4	PTGS2	PTPN6	NFKB1	SYK				
Undefined cells	TP53	PPP1CB	EGR1	PPP3CA	YWHAE	OGT	CST3	CBX6	CAMK2D					
Endothelial cells	MYC	APP	PTGS2	ICAM1	GJA1	PIK3R3	F2R	CRK	RHOC	RHOB				
Mast cells	ICAM1	CYCS	RELB	BCL2A1	PTGS2	NFKB1	NFKB2	NFKBIB	DDX21	HSP90B1	CD69			
Cancer stem cells	TP53	MYC	EGR1	APP	PPP1CB	RHOC	GJA1	MTA2	STAT2	YWHAE	PPP3CA			
CRISPLD2^{+} cells	TP53	MYC	EP300	EGR1	CHD4	JUND	PPP1CB	FOS	HGF	YWHAE	BRD4			
Fibroblasts	APP	CST3	HSP90B1	IGFBP3	ACTN4	BSG								
Myofibroblasts	ZYX	BSG	ACTN4	PFN2	FERMT2	APP								
Smooth muscle cells	APP	FOS												
T cells	ITGB2	HNRNPA1	NFKB1	SF1	RPL27A	RBM8A	RPL14	DDX21	CCL4	RPLP2	RBM39	IL2RG	CD69	IL21R
NK cells	ITGB2	HNRNPA1	FOS	RPL27A	RPL14	RPLP2	RBM8A	CCL4	SF1	RPL38	EEF1D	RBM39	DDX21	PGK1

was converted into the gene symbol. Probes that did not correspond to the gene symbol were removed. For different probes mapped to the same gene, the mean value of the probes was taken as the final gene expression value.

Identification of differentially expressed mRNAs, miRNAs, and circRNAs

Differentially expressed mRNAs, miRNAs, and circRNAs between the CTEPH and control groups were identified using the empirical Bayes t-test provided by the R package limma (version 3.40.6) (16). The thresholds were set at $p < 0.05$ and $|\log \text{fold change (FC)}| > 0.5$. CircRNAs that were identified as DE circRNAs by both probes were used for further analysis.

Identification of disease-related genes

A Venn diagram of gene intersection was developed using significantly highly expressed genes in each cell type and DE mRNAs to obtain disease-related mRNAs in single cells.

Construction of the protein–protein interaction network

The STRING database (17) was used to predict the interactions between DE genes. The input gene sets were disease-related genes in each cell type, and the species was *Homo sapiens*. The PPI score was set to 0.4 (medium confidence). After obtaining the PPI pairs, Cytoscape software (version 3.4.0) (18) was used to construct the network. The CytoNCA plug-in (version 2.1.6) (19) was used to analyze the degree of connectivity of the node, and the parameter was set without weight. The proteins with a higher degree of connectivity were obtained and named hub proteins.

Prediction of drugs for disease-related mRNAs in single cells

Based on the disease-related mRNAs in each cell type, drug-gene interactions were predicted using the online drug-gene interaction database (20). The default parameters were set as follows: Source Databases, 22; Gene Categories, 43; and Interaction Types, 31. Meanwhile, approved antineoplastic or immunotherapeutic drugs were screened. We mainly focused on the relation pairs with reference support. The drug–gene network was then constructed by Cytoscape software.

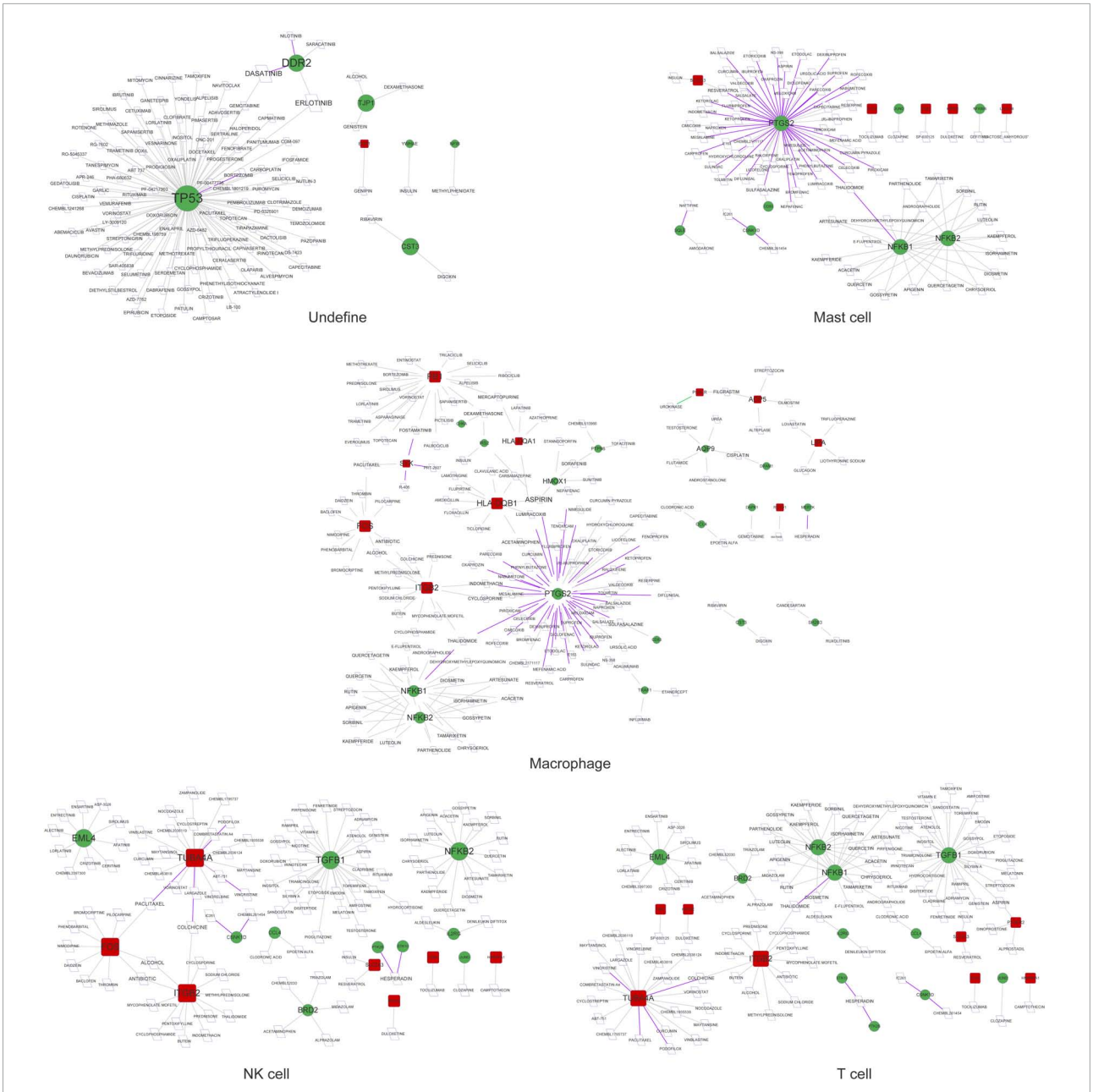

FIGURE 5
The drug–gene network in undefined cells, mast cells, macrophages, NK cells, and T cells. Red squares represent upregulated mRNAs; green circles represent downregulated mRNAs; purple lines represent the drug as an antagonist or inhibitor; green lines represent the drug as a promoter or adjuvant; gray lines represent an unknown effect.

Construction of the single-cell, disease-related circRNA–miRNA–mRNA network

Based on the disease-related mRNAs in each cell type, miRNAs were predicted using the online database mirwalk3.0 (21). The thresholds were set as follows: binding probability, 0.95; and binding site position, 3′-UTR. The miRNAs should appear in either the miRDB or the TargetScan database. After the miRNA–mRNA relation pairs were obtained, intersection analysis with DE miRNAs identified by a previous analysis was performed. Then, the DE miRNA–DE mRNA relation pairs were obtained.

Based on the disease-related miRNAs and circRNAs identified by a previous analysis, the miRNA–circRNA relation pairs were predicted using miranda software (22). A score

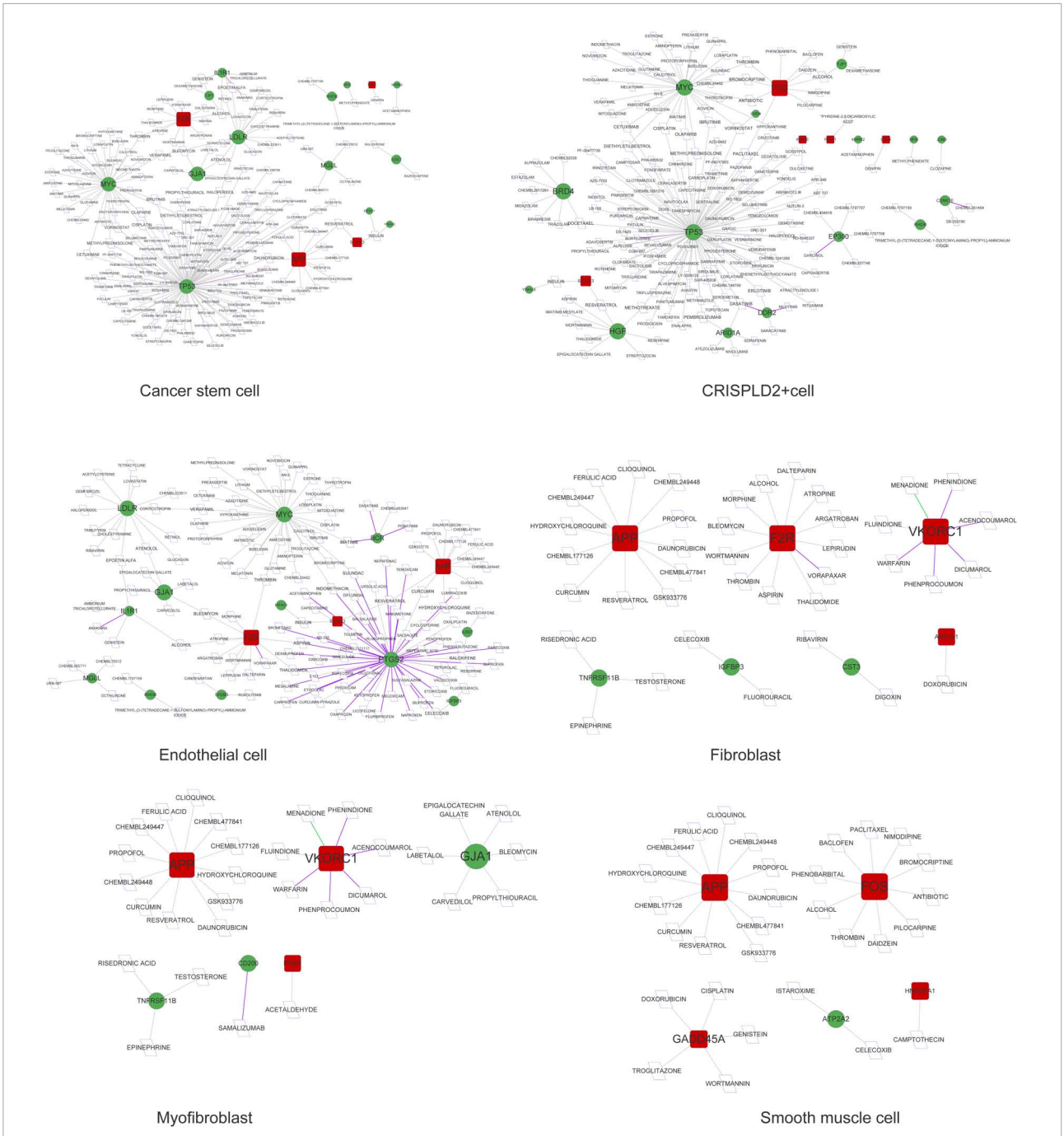

FIGURE 6
The drug–gene network in cancer stem cells, CRISPLD2^{+} cells, endothelial cells, fibroblasts, myofibroblasts, and smooth muscle cells. Red squares represent upregulated mRNAs; green circles represent downregulated mRNAs; purple lines represent the drug as an antagonist or inhibitor; green lines represent the drug as a promoter or adjuvant; gray lines represent an unknown effect.

of > 140 was used as the threshold. The relation pairs with an opposite expression direction of miRNAs and circRNAs were screened as the final circRNA–miRNA relation pairs.

The circRNA–miRNA–mRNA relation regulated by the same miRNA was screened using the miRNA–mRNA relation pairs and the circRNA–miRNA relation pairs. As circRNAs competitively bind to miRNAs to regulate mRNAs, the circRNA–miRNA–mRNA relation with a consistent expression direction of the circRNAs and mRNAs was screened. Finally, the network was constructed, and the degree of connectivity of each node in the network was analyzed.

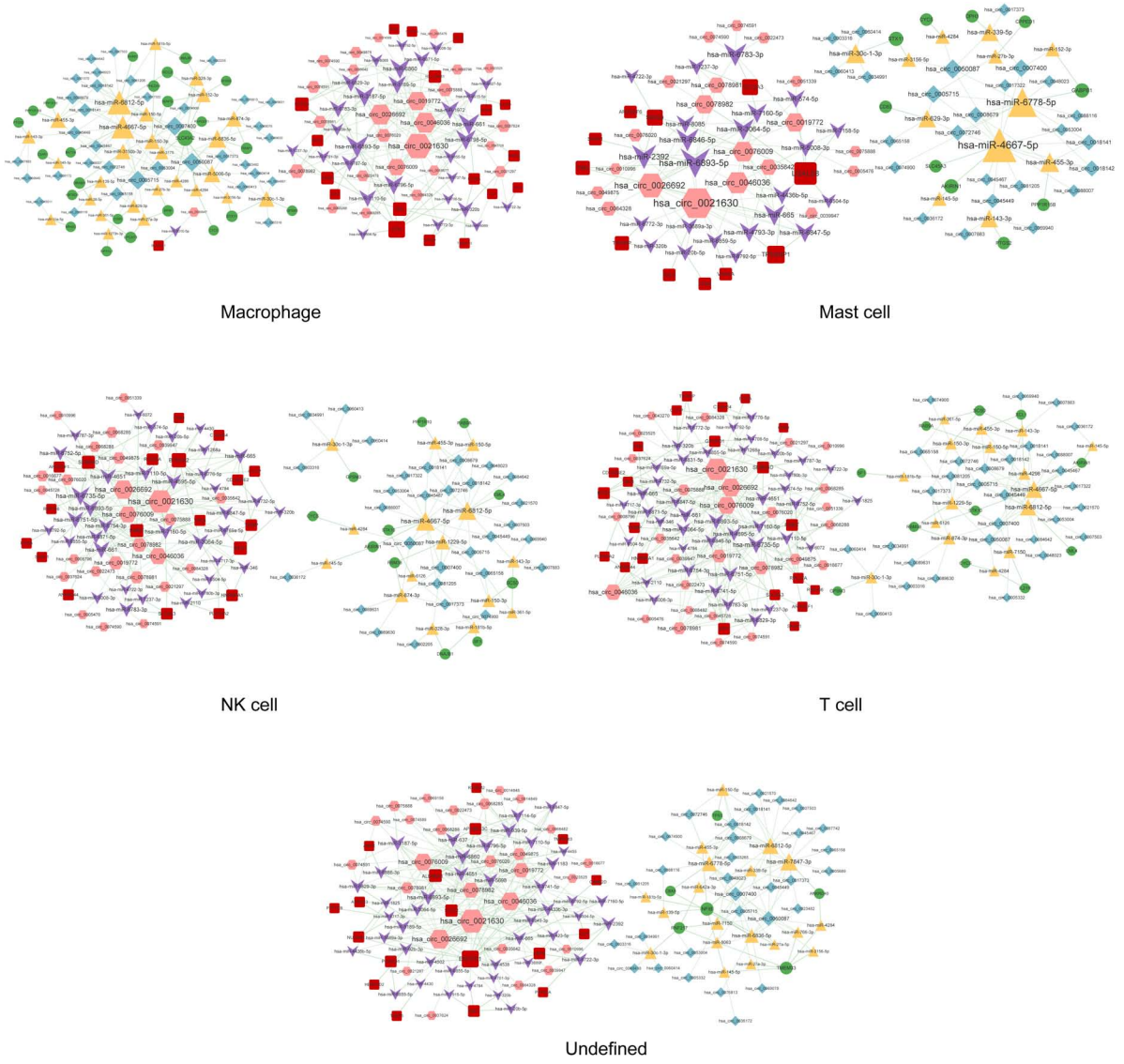

FIGURE 7
The circRNA–miRNA–mRNA regulatory network in macrophages, mast cells, NK cells, T cells, and undefined cells. Red squares represent upregulated mRNAs; green circles represent downregulated mRNAs; yellow triangles represent upregulated miRNAs; purple arrows represent downregulated miRNAs; pink hexagons represent upregulated circRNAs; blue rhombuses represent downregulated circRNAs; dotted lines indicate competitive binding of circRNAs to miRNA; solid lines indicate regulation of mRNAs by miRNAs. The node size represents the degree of connectivity.

Function analysis of the circRNA–miRNA–mRNA network in each cell type

In the circRNA–miRNA–mRNA network of each cell type, the mRNAs were analyzed by Gene Ontology (GO) (23) biological process (BP) and Kyoto Encyclopedia of Genes and Genomes (KEGG) (24) pathway enrichment analyses using the R package clusterProfiler (version 3.8.1) (25). The BP or pathway with an adjusted p-value of less than 0.05 was considered statistically significant.

Results

Eleven cell types were identified

The expression matrix of 22,333 genes in 27,140 cells was obtained after scRNA-seq analysis. The cells were then clustered

into 17 clusters, with 11 cell types: macrophages, undefined cells, endothelial cells, mast cells, cancer stem cells, CRISPLD2$^+$ cells, fibroblasts, myofibroblasts, smooth muscle cells, T cells, and natural killer (NK) cells. The two-dimensional distribution scatter plot of the 11 cell types in all samples is shown in **Figure 1**.

Significantly highly expressed genes in each cell type

The genes highly expressed in the 11 cell types were identified using the FindMarkers function in the Seurat package. There were 813, 506, 997, 563, 972, 870, 491, 530, 333, 799, and 726 highly expressed genes in the macrophages, undefined cells, endothelial cells, mast cells, cancer stem cells, CRISPLD2$^+$ cells, fibroblasts, myofibroblasts, smooth muscle cells, T cells, and NK cells, respectively.

Identification of differentially expressed mRNAs, miRNAs, and circRNAs

After preprocessing, the expression matrixes of 20,169 mRNAs, 2,578 miRNAs, and 87,935 circRNAs were obtained. Differential expression analysis identified 1,436 DE (670 upregulated and 766 downregulated) mRNAs, 294 DE (88 upregulated and 206 downregulated) miRNAs, and 233 DE (89 upregulated and 144 downregulated) circRNAs. The heatmaps of these DE RNAs are shown in **Figure 2**.

Identification of disease-related genes in single cells

The intersection analysis of the highly expressed genes in the 11 cell types and DE mRNAs showed that there were 95, 41, 69, 62, 94, 77, 32, 31, 23, 81, and 71 disease-related genes in the macrophages, undefined cells, endothelial cells, mast cells, cancer stem cells, CRISPLD2$^+$ cells, fibroblasts, myofibroblasts, smooth muscle cells, T cells, and NK cells, respectively (**Figure 3**).

Construction of protein–protein interaction networks based on disease-related genes in single cells

A total of 11 networks were constructed based on the disease-related mRNAs in single cells (**Figure 4**). The numbers of nodes and relation pairs in each cell type are shown in **Table 2**. The top 10 genes with a high degree of connectivity are shown in **Table 3**. TP53 had the highest degree of connectivity in the PPI networks of the cancer stem cells, CRISPLD2$^+$ cells, and undefined cells. Intercellular adhesion molecule-1 (ICAM1) had the highest degree in the PPI networks of the macrophages and mast cells. Amyloid beta precursor protein (APP) had the highest degree in the PPI networks of the fibroblasts and smooth muscle cells. Integrin subunit beta 2 (ITGB2) had the highest degree in the PPI networks of the T cells and NK cells. MYC proto-oncogene and bHLH transcription factor (MYC) had the highest degrees in the PPI network of the endothelial cells. Zyxin (ZYX) had the highest degree in the PPI network of the myofibroblasts.

Prediction of drugs for disease-related genes in single cells

As shown in **Figures 5**, **6**, prostaglandin-endoperoxide synthase 2 (*PTGS2*), *TP53*, *APP*, transforming growth factor beta 1 (*TGFB1*), and *MYC* were regulated by multiple drugs, suggesting that they may serve as potential drug targets.

Construction of the disease-related circRNA–miRNA–mRNA network in single cells

A total of 291, 318, 262, 145, 530, 563, 21, 52, 59, 313, and 276 circRNA–miRNA–mRNA relations were identified in the macrophages, undefined cells, endothelial cells, mast cells, cancer stem cells, CRISPLD2$^+$ cells, fibroblasts, myofibroblasts, smooth muscle cells, T cells, and NK cells, respectively. The constructed networks are shown in **Figures 7**, **8**. The numbers of circRNA–miRNA–mRNA network nodes and relation pairs in each cell type are shown in **Table 4**.

Function analysis of circRNA–miRNA–mRNA networks

The function of the circRNA–miRNA–mRNA network in each cell type was analyzed based on the mRNAs in the network. As shown in **Figure 9**, the endothelial cells, fibroblasts, macrophages, smooth muscle cells, and undefined cells were significantly enriched in 11, 21, 5, 20, and 53 GO BP pathways, respectively. Meanwhile, the CRISPLD2$^+$ cells, endothelial cells, macrophages, myofibroblasts, and undefined cells were significantly enriched in 2, 3, 9, 2, and 12 KEGG pathways, respectively.

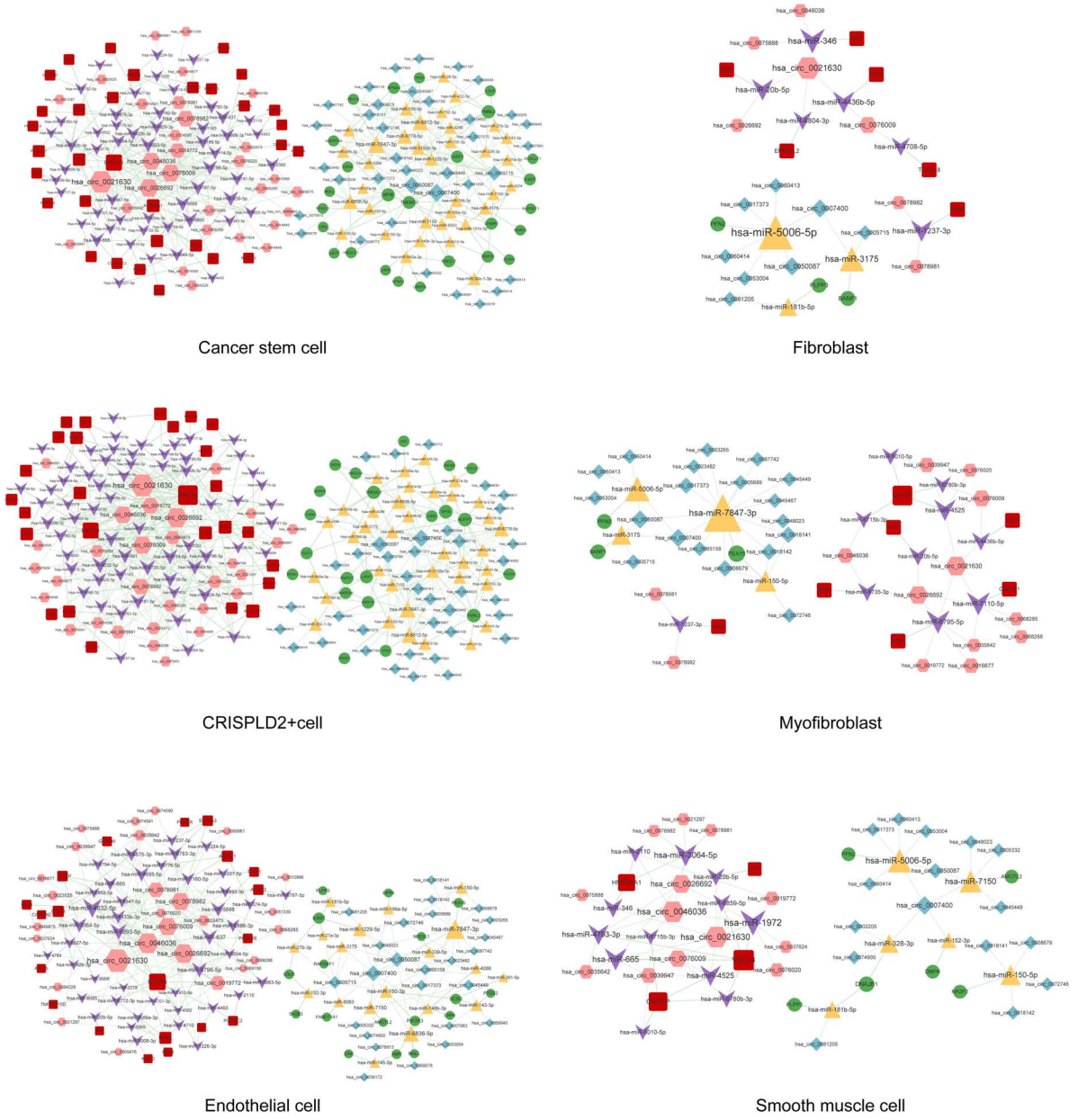

FIGURE 8
The circRNA–miRNA–mRNA regulatory network in cancer stem cells, fibroblasts, CRISPLD2^{+} cells, myofibroblasts, endothelial cells, and smooth muscle cells. Red squares represent upregulated mRNAs; green circles represent downregulated mRNAs; yellow triangles represent upregulated miRNAs; purple arrows represent downregulated miRNAs; pink hexagons represent upregulated circRNAs; blue rhombuses represent downregulated circRNAs; dotted lines indicate competitive binding of circRNAs to miRNA; solid lines indicate regulation of mRNAs by miRNAs. The node size represents the degree of connectivity.

Discussion

Chronic thromboembolic pulmonary hypertension is a major cause of severe pulmonary hypertension (1), but the underlying molecular mechanisms remain incompletely understood. In this study, we performed both gene chip array and scRNA-seq analyses to explore the pathogenic mechanisms of CTEPH. We identified highly expressed genes in 11 cell types, and then intersection analysis with DE mRNAs was performed to obtain disease-related genes in each cell type. TP53, ICAM1, APP, ITGB2, MYC, and ZYX had the highest degrees of connectivity in the PPI networks of different cell types, suggesting that they may play important roles in the progression of CTEPH. The circRNA–miRNA–mRNA regulatory network

TABLE 4 The numbers of nodes and relation pairs (edges) in the circRNA–miRNA–mRNA network of each cell type.

Cell type	Node				Edge		
	circRNA	miRNA	mRNA	Total	circRNA–miRNA	miRNA–mRNA	Total
Macrophages	61	57	43	161	213	78	291
Undefined cells	59	62	24	145	258	79	337
Endothelial cells	52	62	37	151	216	78	294
Mast cells	45	35	21	101	120	39	159
Cancer stem cells	66	88	58	212	322	151	473
CRISPLD2$^+$ cells	68	99	48	215	375	161	536
Fibroblasts	15	9	9	33	21	9	30
Myofibroblasts	32	14	10	56	52	14	66
Smooth muscle cells	29	18	10	57	57	20	77
T cells	59	58	33	150	236	76	312
NK cells	56	51	30	137	201	69	270

in each cell type was then constructed to further elucidate the molecular mechanisms underlying the progression of CTEPH.

Chronic thromboembolic pulmonary hypertension is characterized by pulmonary vascular remodeling resulting from increased pulmonary arterial pressures. Fibroblasts, smooth muscle cells, endothelial cells, and myofibroblasts all play important roles in vascular remodeling (26, 27). In addition, hypertrophy caused by the increased proliferation or reduced apoptosis of vascular smooth muscle cells as well as the excessive proliferation of endothelial cells eventually results in lumen obliteration (27). APP is a type I single-pass transmembrane glycoprotein with receptor-like structural characteristics; however, its cellular function remains unclear (28, 29). A previous study has shown that the serum levels of amyloid-beta, which is produced by proteolysis of APP, are significantly increased in patients with chronic obstructive pulmonary disease with poor pulmonary function (30). Here, we found that APP was a hub node in the PPI networks of fibroblasts, smooth muscle cells, endothelial cells, and myofibroblasts. As APP can be regulated by a variety of drugs, it may serve as a potential drug target for CTEPH. *APP* was also involved in the circ_0026692-miR-20b-5p-*APP* and circ_0021630-miR-20b-5p-*APP* regulatory axes in all four cell types. Moreover, recent evidence has revealed that chronic obstructive pulmonary disease increases the risk of complications and mortality in patients with CTEPH during the early postoperative period after a pulmonary endarterectomy (31). Taken together, the above data imply that fibroblasts, smooth muscle cells, endothelial cells, and myofibroblasts may be involved in the development of CTEPH *via* the circ_0026692/circ_0021630–miR-20b-5p–*APP* regulatory axis.

Accumulating evidence has suggested that the immune system plays a key role in the pathogenesis of CTEPH (32). Moreover, increased systemic inflammation is related to local inflammatory cell infiltration in major pulmonary arteries at the advanced stage of CTEPH (7). In this study, four types of immune cells were identified. ICAM1 had the highest degree of connectivity in macrophages and mast cells, while ITGB2 had the highest degree of connectivity in T cells and NK cells. Soluble ICAM1 is present in the normal circulation, and its level is elevated in patients with endothelial activation-related disorders. Furthermore, the upregulation of ICAM1 affects the adhesion of circulating immune cells to the pulmonary endothelium, thereby promoting immune cell migration and perivascular infiltration (33). Blair et al. (34) also have reported that ICAM1 is essential for inflammatory cell recruitment in pulmonary vascular lesions in pulmonary arterial hypertension. *ITGB2* encodes an integrin beta chain involved in cell adhesion. A recent study has reported that inhibition of broad-spectrum integrin improves distal pulmonary artery remodeling, suggesting that integrin may contribute to the pathogenesis of pulmonary arterial hypertension (35). Collectively, we speculated that these immune cells might be associated with inflammatory cell recruitment in CTEPH by regulating the expression of *ICAM1* and *ITGB2*. In addition, circ_0021630 had the highest degree of connectivity in the circRNA–miRNA–mRNA regulatory networks of the four types of immune cells, indicating the regulatory potential of circ_0021630 in CTEPH-related immune responses.

TP53 had the highest degree of connectivity in the PPI networks of cancer stem cells, CRISPLD2$^+$ cells, and undefined cells. *CRISPLD2* is an endogenous anti-inflammatory gene in lung fibroblasts, which can inhibit proinflammatory signaling in pulmonary epithelial cells (36). GO analysis showed that undefined cells were associated with the positive regulation of striated muscle cell apoptosis. Striated muscles, which are affected in pulmonary arterial hypertension, are associated with exercise intolerance in these patients (37). The TP53 encoding protein (p53) is a transcription factor involved in DNA repair, cell cycle arrest, and apoptosis (38). Dysregulation

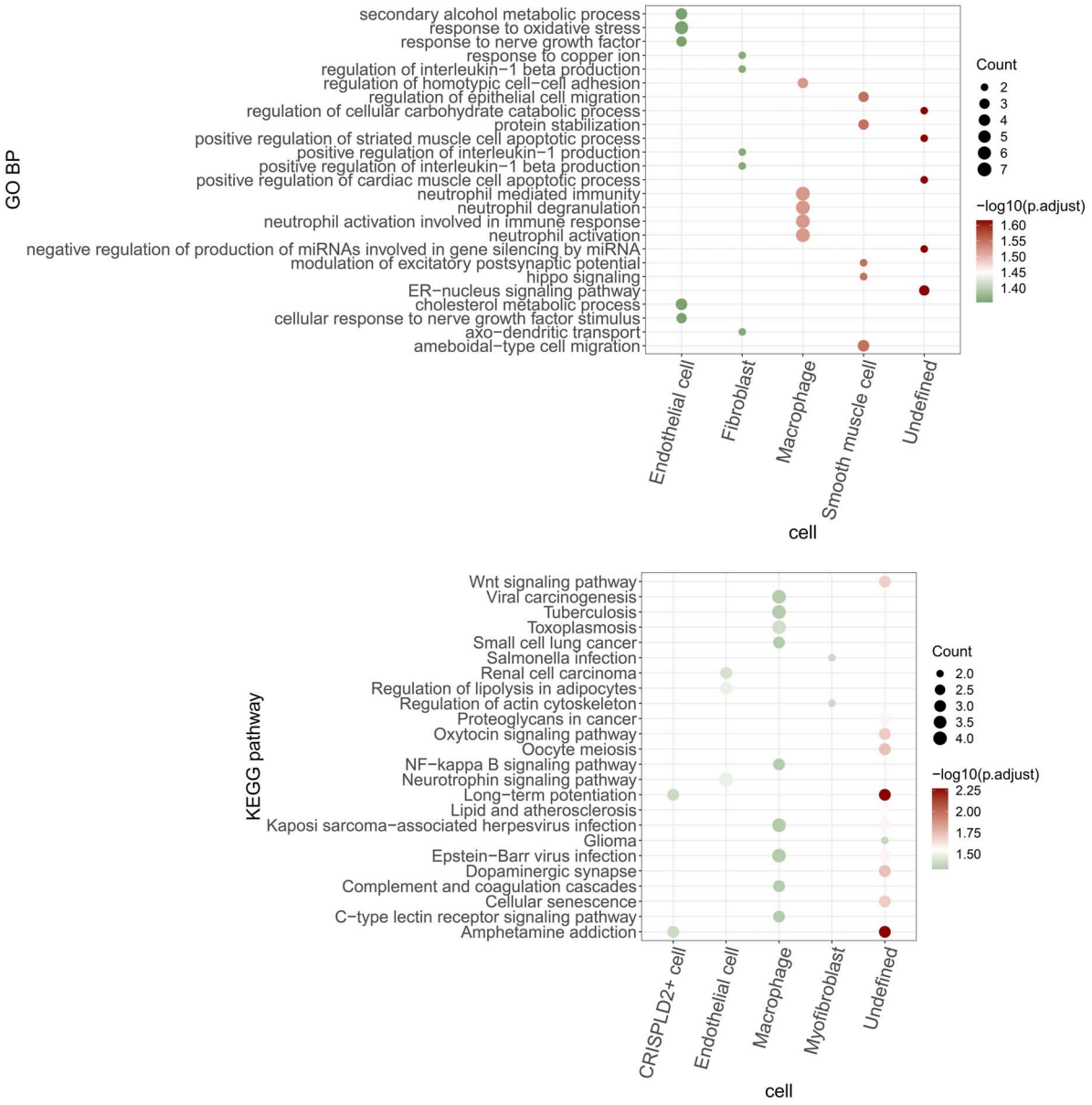

FIGURE 9
GO BP and KEGG pathways are enriched by mRNAs in the circRNA–miRNA–mRNA regulatory network of each cell type. The bubble size indicates the number of enriched genes. The color shows the enrichment significance and red is the most significant.

of p53 in pulmonary artery smooth muscle cells (PASMCs) plays an important role in vascular remodeling, a key process contributing to the progression of CTEPH (39, 40). Meanwhile, inhibition of TP53 suppresses mitochondrial respiration and induces glycolysis in PASMCs, which show a proliferative phenotype similar to that of cancer cells. Hence, CTEPH is considered a cancer-like disease in terms of PASMC remodeling (41). *TP53* is also involved in a circRNA–miRNA–mRNA regulatory network (e.g., circ_0007400–miR-6812-5p–*TP53*) in cancer stem cells and CRISPLD2^{+} cells. These data suggest that circ_0007400 may act as a competing endogenous RNA in cancer stem cells and CRISPLD2^{+} cells to promote the progression of CTEPH by regulating *TP53*.

There are some limitations in this study that must be addressed. First, we only performed bioinformatics analysis without verification experiments. Second, the sample size was relatively small. The measurement of the key circRNA and miRNA expression in tissues and studies with a large sample size are needed to validate the current findings. Thirdly, tissue samples were collected from patients undergoing pulmonary endarterectomy because it is currently the only curative treatment for CTEPH. However, it should be noted

that pulmonary endarterectomy samples were derived from large vessels, while CTEPH is also related to a small vessel arteriopathy.

In conclusion, fibroblasts, smooth muscle cells, endothelial cells, and myofibroblasts may be involved in the development of CTEPH *via* the circ_0026692/circ_0021630–miR-20b-5p–*APP* regulatory axis. Additionally, macrophages, mast cells, T cells, and NK cells may be associated with inflammatory cell recruitment in CTEPH by regulating the expression of *ICAM1* and *ITGB2*. Moreover, circ_0007400 may contribute to the progression of CTEPH by acting as a competing endogenous RNA to regulate *TP53* in cancer stem cells and CRISPLD2^{+} cells. Our study, for the first time, identified the key mRNAs, miRNAs, and circRNAs, as well as their possible regulatory relations, in CTEPH using both gene chip array and scRNA-seq analyses. These data may contribute to a better understanding of the pathological mechanisms of CTEPH.

Data availability statement

The datasets generated and analyzed during the current study are available from the corresponding authors on reasonable request.

Ethics statement

This study was approved by the Ethics Committee of Beijing Chao-Yang Hospital, Capital Medical University (Approval numbers: 2019-K-28 and 2015-7-24-8) and performed in accordance with the principles outlined in the Declaration of Helsinki. The requirement for written informed consent was waived because discarded pulmonary endarterectomized tissues and blood samples were used in this study, while the research involved no risk to the subjects and the waiver did not adversely affect the rights and welfare of the subjects.

Author contributions

RM, ZZ, JZ, and YY: conception and design of the research. RM, XD, JG, YL, XG, JFW, QH, and YW: acquisition of data. RM, XD, JG, YL, XG, JFW, QH, YW, JL, SY, TK, ML, and JW: analysis and interpretation of data. RM, XD, JG, YL, XG, JFW, and QH: statistical analysis. RM, YL, SY, ML, ZZ, JZ, and YY: funding acquisition. RM, XD, and JG: drafting the manuscript. RM, JW, ZZ, JZ, and YY: revision of manuscript for important intellectual content. All authors read and approved the final manuscript.

Funding

This study was supported by National Natural Science Foundation of China (Project numbers: 81300044, 31670928, 81871356, 92168117, 81770253, 81871328, and 81900047), Beijing Natural Science Foundation (Project numbers: 7162069 and 7182149), Beijing Municipal Administration of Hospitals' Youth Programme (Project number: QML20160301), the Reform and Development Program of Beijing Institute of Respiratory Medicine (ysrh2022007), the National Key Research and Development Program of China (Project number: 2016YFC0905600), the National Major Research Plan Training Program of China (91849111), and Chinese Academy of Medical Sciences Central Public-interest Scientific Institution Basal Research Fund Young Medical Talents Award Project (Project number: 2018RC320013).

Conflict of interest

The authors declare that the research was conducted in the absence of any commercial or financial relationships that could be construed as a potential conflict of interest.

Publisher's note

All claims expressed in this article are solely those of the authors and do not necessarily represent those of their affiliated organizations, or those of the publisher, the editors and the reviewers. Any product that may be evaluated in this article, or claim that may be made by its manufacturer, is not guaranteed or endorsed by the publisher.

References

1. Mahmud E, Madani MM, Kim NH, Poch D, Ang L, Behnamfar O, et al. Chronic thromboembolic pulmonary hypertension: evolving therapeutic approaches for operable and inoperable disease. *J Am Coll Cardiol.* (2018) 71:2468–86. doi: 10.1016/j.jacc.2018.04.009

2. Quadery SR, Swift AJ, Billings CG, Thompson AAR, Elliot CA, Hurdman J, et al. The impact of patient choice on survival in chronic thromboembolic pulmonary hypertension. *Eur Respir J.* (2018) 52:1800589. doi: 10.1183/13993003.00589-2018

3. Scudeller PG, Terra-Filho M, Freitas Filho O, Galas F, Andrade TD, Nicotari DO, et al. Chronic thromboembolic pulmonary hypertension: the impact of advances in perioperative techniques in patient outcomes. *J Bras Pneumol.* (2021) 47:e20200435. doi: 10.36416/1806-3756/e20200435

4. Opitz I, Kirschner MB. Molecular research in chronic thromboembolic pulmonary hypertension. *Int J Mol Sci.* (2019) 20:784. doi: 10.3390/ijms20030784

5. Li X, Liao Z, Deng Z, Chen N, Zhao L. Combining bulk and single-cell RNA-sequencing data to reveal gene expression pattern of chondrocytes in the osteoarthritic knee. *Bioengineered.* (2021) 12:997–1007. doi: 10.1080/21655979.2021.1903207

6. Gu S, Su P, Yan J, Zhang X, An X, Gao J, et al. Comparison of gene expression profiles and related pathways in chronic thromboembolic pulmonary hypertension. *Int J Mol Med.* (2014) 33:277–300. doi: 10.3892/ijmm.2013.1582

7. Miao R, Dong X, Gong J, Wang Y, Guo X, Li Y, et al. Possible immune regulation mechanisms for the progression of chronic thromboembolic pulmonary hypertension. *Thromb Res.* (2021) 198:122–31. doi: 10.1016/j.thromres.2020.11.032

8. Halliday SJ, Matthews DT, Talati MH, Austin ED, Su YR, Absi TS, et al. A multifaceted investigation into molecular associations of chronic thromboembolic pulmonary hypertension pathogenesis. *JRSM Cardiovasc Dis.* (2020) 9:2048004020906994. doi: 10.1177/2048004020906994

9. Wang L, Guo LJ, Liu J, Wang W, Yuan JX, Zhao L, et al. MicroRNA expression profile of pulmonary artery smooth muscle cells and the effect of let-7d in chronic thromboembolic pulmonary hypertension. *Pulm Circ.* (2013) 3:654–64. doi: 10.1086/674310

10. Miao R, Gong J, Zhang C, Wang Y, Guo X, Li J, et al. Hsa_circ_0046159 is involved in the development of chronic thromboembolic pulmonary hypertension. *J Thromb Thrombolysis.* (2020) 49:386–94. doi: 10.1007/s11239-019-01998-4

11. Miao R, Dong X, Gong J, Li Y, Guo X, Wang J, et al. Cell landscape atlas for patients with chronic thromboembolic pulmonary hypertension after pulmonary endarterectomy constructed using single-cell RNA sequencing. *Aging.* (2021) 13:16485–99. doi: 10.18632/aging.203168

12. Miao R, Dong X, Gong J, Li Y, Guo X, Wang J, et al. Examining the development of chronic thromboembolic pulmonary hypertension at the single-cell level. *Hypertension.* (2022) 79:562–74. doi: 10.1161/hypertensionaha.121.18105

13. Humbert M, Kovacs G, Hoeper MM, Badagliacca R, Berger RMF, Brida M, et al. 2022 ESC/ERS Guidelines for the diagnosis and treatment of pulmonary hypertension. *Eur Heart J.* (2022) 43:3618–731. doi: 10.1093/eurheartj/ehac237

14. Stuart T, Butler A, Hoffman P, Hafemeister C, Papalexi E, Mauck WM III, et al. Comprehensive integration of single-cell data. *Cell.* (2019) 177:1888–902.e21. doi: 10.1016/j.cell.2019.05.031

15. Gautier L, Cope L, Bolstad BM, Irizarry RA. Affy–analysis of affymetrix genechip data at the probe level. *Bioinformatics.* (2004) 20:307–15. doi: 10.1093/bioinformatics/btg405

16. Smyth GK. LIMMA: Linear models for microarray data. In: Gentleman R, Carey VJ, Huber W, Irizarry RA, Dudoit S editors. *Bioinformatics and Computational Biology Solutions Using R and Bioconductor. Statistics for Biology and Health*. New York, NY: Springer (2005). p. 397–420.

17. Szklarczyk D, Franceschini A, Wyder S, Forslund K, Heller D, Huerta-Cepas J, et al. STRING v10: protein-protein interaction networks, integrated over the tree of life. *Nucleic Acids Res.* (2015) 43:D447–52. doi: 10.1093/nar/gku1003

18. Shannon P, Markiel A, Ozier O, Baliga NS, Wang JT, Ramage D, et al. Cytoscape: a software environment for integrated models of biomolecular interaction networks. *Genome Res.* (2003) 13:2498–504. doi: 10.1101/gr.1239303

19. Tang Y, Li M, Wang J, Pan Y, Wu FX. CytoNCA: a cytoscape plugin for centrality analysis and evaluation of protein interaction networks. *Biosystems.* (2015) 127:67–72. doi: 10.1016/j.biosystems.2014.11.005

20. Griffith M, Griffith OL, Coffman AC, Weible JV, McMichael JF, Spies NC, et al. DGIdb: mining the druggable genome. Nat Methods. (2013) 10:1209–10. doi: 10.1038/nmeth.2689

21. Sticht C, De La Torre C, Parveen A, Gretz N. MiRWalk: an online resource for prediction of microRNA binding sites. *PLoS One.* (2018) 13:e0206239. doi: 10.1371/journal.pone.0206239

22. Enright AJ, John B, Gaul U, Tuschl T, Sander C, Marks DS. MicroRNA targets in *Drosophila*. *Genome Biol.* (2003) 5:R1. doi: 10.1186/gb-2003-5-1-r1

23. Ashburner M, Ball CA, Blake JA, Botstein D, Butler H, Cherry JM, et al. Gene ontology: tool for the unification of biology. The gene ontology consortium. *Nat Genet.* (2000) 25:25–9. doi: 10.1038/75556

24. Kanehisa M, Goto S. KEGG: kyoto encyclopedia of genes and genomes. *Nucleic Acids Res.* (2000) 28:27–30. doi: 10.1093/nar/28.1.27

25. Yu G, Wang LG, Han Y, He QY. Clusterprofiler: an R package for comparing biological themes among gene clusters. *Omics.* (2012) 16:284–7. doi: 10.1089/omi.2011.0118

26. Zhang J, Tang L, Dai F, Qi Y, Yang L, Liu Z, et al. ROCK inhibitors alleviate myofibroblast transdifferentiation and vascular remodeling via decreasing TGFβ1-mediated RhoGDI expression. *Gen Physiol Biophys.* (2019) 38:271–80. doi: 10.4149/gpb_2019017

27. Mandegar M, Fung YC, Huang W, Remillard CV, Rubin LJ, Yuan JX. Cellular and molecular mechanisms of pulmonary vascular remodeling: role in the development of pulmonary hypertension. *Microvasc Res.* (2004) 68:75–103. doi: 10.1016/j.mvr.2004.06.001

28. Wasco W, Gurubhagavatula S, Paradis MD, Romano DM, Sisodia SS, Hyman BT, et al. Isolation and characterization of APLP2 encoding a homologue of the Alzheimer's associated amyloid beta protein precursor. *Nat Genet.* (1993) 5:95–100. doi: 10.1038/ng0993-95

29. Wasco W, Bupp K, Magendantz M, Gusella JF, Tanzi RE, Solomon F. Identification of a mouse brain cDNA that encodes a protein related to the Alzheimer disease-associated amyloid beta protein precursor. *Proc Natl Acad Sci U.S.A.* (1992) 89:10758–62. doi: 10.1073/pnas.89.22.10758

30. Bu XL, Cao GQ, Shen LL, Xiang Y, Jiao SS, Liu YH, et al. Serum amyloid-beta levels are increased in patients with chronic obstructive pulmonary disease. *Neurotox Res.* (2015) 28:346–51. doi: 10.1007/s12640-015-9552-x

31. Kamenskaya O, Loginova I, Chernyavskiy A, Edemskiy A, Lomivorotov VV, Karaskov A. Chronic obstructive pulmonary disease in patients with chronic thromboembolic pulmonary hypertension: prevalence and implications for surgical treatment outcome. *Clin Respir J.* (2018) 12:2242–8. doi: 10.1111/crj.12898

32. Koudstaal T, Boomars KA, Kool M. Pulmonary arterial hypertension and chronic thromboembolic pulmonary hypertension: an immunological perspective. *J Clin Med.* (2020) 9:561. doi: 10.3390/jcm9020561

33. Karavolias GK, Georgiadou P, Gkouziouta A, Kariofillis P, Karabela G, Tsiapras D, et al. Short and long term anti-inflammatory effects of bosentan therapy in patients with pulmonary arterial hypertension: relation to clinical and hemodynamic responses. *Expert Opin Ther Targets.* (2010) 14:1283–9. doi: 10.1517/14728222.2010.523421

34. Blair LA, Haven AK, Bauer NN. Circulating microparticles in severe pulmonary arterial hypertension increase intercellular adhesion molecule-1 expression selectively in pulmonary artery endothelium. *Respir Res.* (2016) 17:133. doi: 10.1186/s12931-016-0445-1

35. Lemay S-E, Montesinos MS, Grobs Y, Shimauchi T, Breuils Bonnet S, Martineau S, et al. Role of Integrin Signaling in Pulmonary Arterial Hypertension. *Circulation.* (2021) 144:A10717.

36. Zhang H, Kho AT, Wu Q, Halayko AJ, Limbert Rempel K, Chase RP, et al. CRISPLD2 (LGL1) inhibits proinflammatory mediators in human fetal, adult, and COPD lung fibroblasts and epithelial cells. *Physiol Rep.* (2016) 4:e12942. doi: 10.14814/phy2.12942

37. Manders E, Rain S, Bogaard HJ, Handoko ML, Stienen GJ, Vonk-Noordegraaf A, et al. The striated muscles in pulmonary arterial hypertension: adaptations beyond the right ventricle. *Eur Respir J.* (2015) 46:832–42. doi: 10.1183/13993003.02052-2014

38. Meireles Da Costa N, Palumbo A Jr, De Martino M, Fusco A, Ribeiro Pinto LF, Nasciutti LE. Interplay between HMGA and TP53 in cell cycle control along tumor progression. *Cell Mol Life Sci.* (2021) 78:817–31. doi: 10.1007/s00018-020-03634-4

39. Wang Y, Huang X, Leng D, Li J, Wang L, Liang Y, et al. DNA methylation signatures of pulmonary arterial smooth muscle cells in chronic thromboembolic pulmonary hypertension. *Physiol Genomics.* (2018) 50:313–22. doi: 10.1152/physiolgenomics.00069.2017

40. Wang Z, Yang K, Zheng Q, Zhang C, Tang H, Babicheva A, et al. Divergent changes of p53 in pulmonary arterial endothelial and smooth muscle cells involved in the development of pulmonary hypertension. *Am J Physiol Lung Cell Mol Physiol.* (2019) 316:L216–28. doi: 10.1152/ajplung.00538.2017

41. Wakasugi T, Shimizu I, Yoshida Y, Hayashi Y, Ikegami R, Suda M, et al. Role of smooth muscle cell p53 in pulmonary arterial hypertension. *PLoS One.* (2019) 14:e0212889. doi: 10.1371/journal.pone.0212889

frontiers | Frontiers in Cardiovascular Medicine

TYPE Original Research
PUBLISHED 30 November 2022
DOI 10.3389/fcvm.2022.1042139

OPEN ACCESS

EDITED BY
Junjie Xiao,
Shanghai University, China

REVIEWED BY
Rajiv Sankaranarayanan,
Liverpool University Hospitals NHS Foundation Trust, United Kingdom
Ythan H. Goldberg,
Albert Einstein College of Medicine, United States
Jian Wu,
Fudan University, China
Zhi Xin Shan,
Guangdong Provincial People's Hospital, China
Dachun Xu,
Tongji University, China

*CORRESPONDENCE
Qingchun Zeng
qingchunzeng@smu.edu.cn
Dingli Xu
dlxugz@163.com
Yunshan Ning
nys@smu.edu.cn

†These authors have contributed equally to this work

SPECIALTY SECTION
This article was submitted to General Cardiovascular Medicine, a section of the journal Frontiers in Cardiovascular Medicine

RECEIVED 12 September 2022
ACCEPTED 14 November 2022
PUBLISHED 30 November 2022

CITATION
Zhao H, Li P, Zhong G, Xie K, Zhou H, Ning Y, Xu D and Zeng Q (2022) Machine learning models in heart failure with mildly reduced ejection fraction patients.
Front. Cardiovasc. Med. 9:1042139.
doi: 10.3389/fcvm.2022.1042139

Machine learning models in heart failure with mildly reduced ejection fraction patients

Hengli Zhao[1,2,3,4†], Peixin Li[1,2,3†], Guoheng Zhong[1,2,3†], Kaiji Xie[1,2,3], Haobin Zhou[1,2,3], Yunshan Ning[4*], Dingli Xu[1,2,3*] and Qingchun Zeng[1,2,3*]

[1]State Key Laboratory of Organ Failure Research, Department of Cardiology, Nanfang Hospital, Southern Medical University, Guangzhou, China, [2]Guangdong Provincial Key Laboratory of Shock and Microcirculation, Southern Medical University, Guangzhou, China, [3]Bioland Laboratory (Guangzhou Regenerative Medicine and Health Guangdong Laboratory), Guangzhou, China, [4]School of Laboratory Medicine and Biotechnology, Southern Medical University, Guangzhou, China

Objective: Heart failure with mildly reduced ejection fraction (HFmrEF) has been recently recognized as a unique phenotype of heart failure (HF) in current practical guideline. However, risk stratification models for mortality and HF re-hospitalization are still lacking. This study aimed to develop and validate a novel machine learning (ML)-derived model to predict the risk of mortality and re-hospitalization for HFmrEF patients.

Methods: We assessed the risks of mortality and HF re-hospitalization in HFmrEF (45–49%) patients enrolled in the TOPCAT trial. Eight ML-based models were constructed, including 72 candidate variables. The Harrell concordance index (C-index) and DeLong test were used to assess discrimination and the improvement in discrimination between models, respectively. Calibration of the HF risk prediction model was plotted to obtain bias-corrected estimates of predicted versus observed values.

Results: Least absolute shrinkage and selection operator (LASSO) Cox regression was the best-performing model for 1- and 6-year mortality, with a highest C-indices at 0.83 (95% CI: 0.68–0.94) over a maximum of 6 years of follow-up and 0.77 (95% CI: 0.64–0.89) for the 1-year follow-up. The random forest (RF) showed the best discrimination for HF re-hospitalization, scoring 0.80 (95% CI: 0.66–0.94) and 0.85 (95% CI: 0.71–0.99) at the 6- and 1-year follow-ups, respectively. For risk assessment analysis, Kansas City Cardiomyopathy Questionnaire (KCCQ) subscale scores were the most important predictor of readmission outcome in the HFmrEF patients.

Conclusion: ML-based models outperformed traditional models at predicting mortality and re-hospitalization in patients with HFmrEF. The results of the risk assessment showed that KCCQ score should be paid increasing attention to in the management of HFmrEF patients.

KEYWORDS

heart failure, machine learning (ML), heart failure with mildly reduced ejection fraction, random forest (RF), LASSO Cox regression analysis

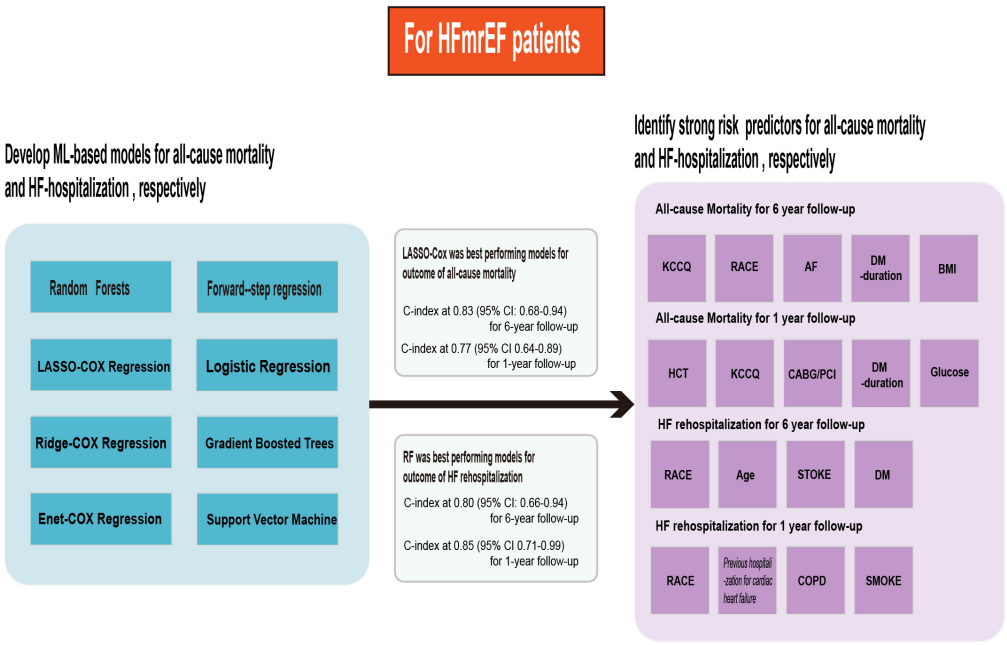

GRAPHICAL ABSTRACT

In this study, we first selected heart failure patients whose LVEF was 45–49%. We then developed eight machine learning-based prediction models for the outcomes of all-cause mortality and HF rehospitalization. We selected the best-performing prediction model for different outcomes and then further demonstrated the risk factors involved.

Introduction

Heart failure (HF), a major public health concern, has affected an estimated 20 million patients globally and has become one of the leading causes of hospitalization in adults >65 years, making it a substantial threat to human health. The 2021 ESC guidelines for chronic HF categorize patients into three subgroups based on whether their left ventricular ejection fraction (LVEF) is reduced (HFrEF, EF ≤40%), mildly reduced (HFmrEF; EF 41–49%), or preserved (HFpEF; EF ≥50%). Among these subgroups, HFmrEF has recently attracted increasing attention (1). Data from the ESC Heart Failure Long-Term Registry showed that in the outcome of all-cause mortality, there was no significant difference in all-cause mortality between HFmrEF and HFrEF or HFpEF, while the mortality rate was markedly higher among HFrEF patients than among HFpEF patients (2). Regarding outcomes of 1-year death and hospitalization incidences, HFmrEF and HFpEF patients showed lower rates than HFrEF patients. Indeed, the clinical characteristics, risk prediction and therapeutic strategy of HFmrEF are still obscure. Accurately predicting outcomes such as mortality and rehospitalization in HF is critically important to patients, their clinicians and healthcare systems, but it has proven to be a difficult task because the outcomes are affected by many risk factors.

Machine learning (ML) is a scientific discipline that focuses on how computers learn from data to improve predictive performance and generalization of models by considering higher-dimensional and possibly non-linear effects of variables, incorporating more variables (3). It has been extensively utilized in the cardiovascular field of diagnosis, image analysis and risk assessment (4). Compared with conventional statistical models, it has the ability to automatically learn from large datasets with a labeled output or outcome to conduct predictive analytics, allowing the user to glean knowledge from past data and apply it to future predictions. Recent evidence indicates that ML-based HF risk models that include clinical, laboratory, and biomarker data have demonstrated superior performance over traditional HF risk models but have been verified only in HFrEF and HFpEF populations. Therefore, predictive models for HF with

Abbreviations: HF, heart failure; ML, machine learning; LVEF, left ventricular ejection fraction; HFrEF, heart failure with reduced ejection fraction; HFmrEF, heart failure with mildly reduced ejection fraction; HFpEF, heart failure with preserved ejection fraction; KCCQ, Kansas City Cardiomyopathy Questionnaire; RF, random forest; LASSO, least absolute shrinkage and selection operator; C-index, Harrell concordance index; ROC, receiver operating characteristic; AUC, area under the receiver operating characteristic curve; BMI, body mass index; ALP, alkaline phosphatase; CHF-HOSP, hospitalization for cardiac heart failure; COPD, chronic obstructive pulmonary disease; VIMP, variable importance; eGFR, estimated glomerular filtration rate; CR, creatinine; CABG, coronary artery bypass graft; PCI, percutaneous coronary intervention; ACE, angiotensin-converting enzyme; ARBs, angiotensin receptor blockers; NT-proBNP, N-terminal pro-brain natriuretic peptide; WHtR, waist-to-height ratio; HCT, hematocrit; ePVS, estimated plasma volume status.

HFrEF or HFpEF are available, but risk assessments of death and hospitalization in patients with HFmrEF are still limited.

Materials and methods

Study population

The design, enrollment criteria, and participant characteristics of the TOPCAT trial have been described previously. Briefly, it is a multicenter, randomized, double-blind, placebo-controlled trial of aldosterone antagonist therapy (NCT00094302), which includes 3,445 adult patients with symptoms of HF and documented LVEF ≥45%, aged 50 years or older (5). In the present analysis, we selected 519 patients whose LVEF was 45–49%, the data collected included all baseline demographics, clinical data, laboratory results, electrocardiography and Kansas City Cardiomyopathy Questionnaire (KCCQ) scores. A detailed description is provided in the supplement and a list of markers is shown in **Supplementary Table 1**.

Outcomes of interest

The outcomes of interest in this study were all-cause mortality and HF hospitalization through 1 year and the entire follow-up (up to 6 years per subject). All-cause mortality was defined as death from any cause, and hospitalization for HF was defined as sudden presentation to an acute care facility with aggravated HF requiring overnight hospitalization.

Candidate variables

In the present analysis, 87 candidate variables were considered, including all baseline demographics, clinical data, laboratory results, electrocardiography, and KCCQ scores. Some categorical candidate variables were harmonized and merged to facilitate analysis. A total of 72 predictor variables were included after excluding 6 covariates for a >20% missing rate and 8 for merged values, and another EF value was used as a screening condition and was not considered a variable (**Supplementary Table 1**).

Model development and evaluation

The study population was randomly split into training (70%) and validation datasets (30%). Data imputation was performed on each dataset separately by using the missForest approach, which can cope with different types of variables, especially for multivariate data consisting of continuous and categorical variables (6). Different methods were used to model and optimize the training datasets to reduce the prediction error. These models were then checked on validation subsets to test the models' performance and determine the best predictors. All of the steps were repeated 50 times. The analytical procedures followed in this study are shown in **Figure 1**.

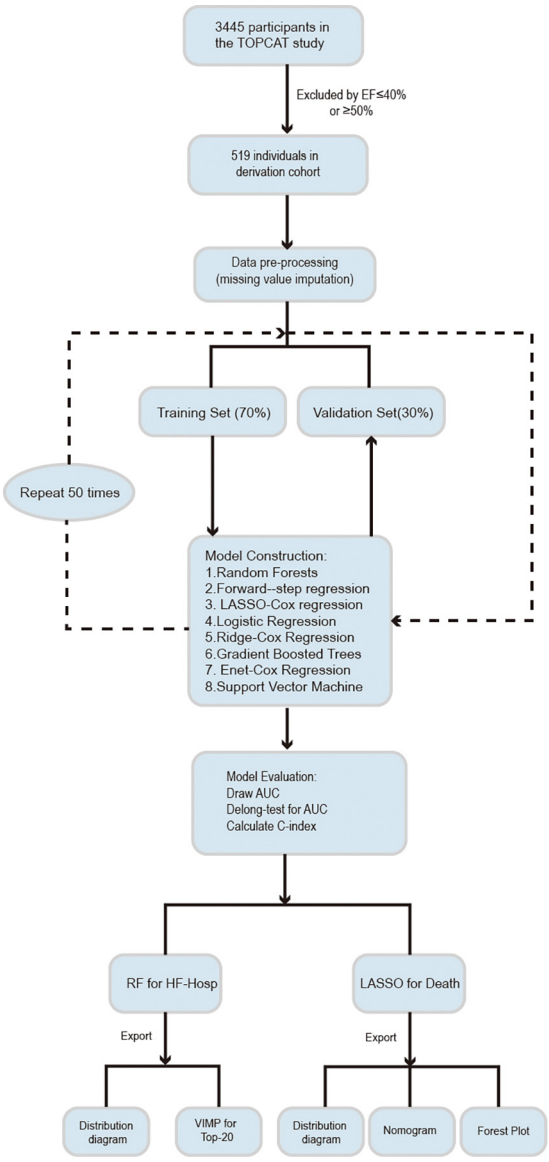

FIGURE 1
Analysis overview for identifying best performing risk prediction model.

Machine learning-based methods

Heart failure prediction models were developed by incorporating the 72 variables identified previously, yielding

the following eight candidate ML-based and conventional Cox regression algorithms for assessing the risk of mortality and HF hospitalization through 1 and 6 years of follow-up:

Random forest (RF);
Forward stepwise Cox regression;
Least absolute shrinkage and selection operator (LASSO) Cox regression;
Logistic regression;
Ridge Cox regression;
Gradient boosted trees;
Elastic net Cox regression;
Support vector machine (SVM).

Analyses were performed using R version 4.0.4 (R Foundation for Statistical Computing, Vienna, Austria). Various R packages were used to conduct this analysis. The package missForest (6) was used for imputation, randomForest (7) was used for RF, glmnet (8) was used for LASSO, ridge and elastic-net Cox regression, and the package gbm (9) was used for gradient boosted trees. e1071 (10) software was used for the SVM.

Model evaluation

The discriminatory performance of each model against the validation dataset was calculated using the Harrell concordance index (C-index) (11) or the area under the receiver operating characteristic (ROC) curve (AUC). The DeLong test was used to assess discrimination between models (12). Calibration of the HF risk prediction model was plotted to obtain bias-corrected (overfitting-corrected) estimates of predicted versus observed values based on subsetting the predictions into intervals. The prediction distribution of the models was plotted based on the order of the predicted risk for each patient.

Sensitivity analyses

Sensitivity analysis was computed for all patients from the TOPCAT study whose LVEF was 45–49%. These different models were developed for this population to predict all-cause mortality and HF hospitalization and were followed throughout the study period (13). The importance of each variable was calculated, and the incremental improvement in each variable was assessed over 50 cycles of simulation. In addition, 1-year all-cause mortality and HF hospitalization predictions were evaluated to see how the model's performance changed over a relatively short follow-up period.

Results

Study cohort and participant baseline characteristics

A total of 519 patients with LVEF values ranging from 45 to 49% were included (**Table 1**), of whom 63.5% were male and 91.3% were white, with a mean age of 66.1 years and a median body mass index (BMI) of 31.4 kg/m^2. Over a 6-year follow-up, a total of 97 patients died, accounting for 18.6% of the total number of participants, and 59 patients (11.3%) were hospitalized for worsening HF. During the first year of follow-up, the incidence of all-cause mortality and HF hospitalization was 5.1% (31) and 4.6% (24), respectively. Among the imputation cohort, some candidate variables, for example, glucose, alkaline phosphatase (ALP), hematocrit, waist circumference, and physical limitation, had missing values. After processing them, they exhibited close agreement with the original data, which showed that the method we chose was reliable.

Machine learning for prediction of heart failure mortality outcome

The 72 predictor covariates incorporated into the risk prediction models included demographics, clinical history, vital signs, social history, laboratory, and electrocardiographic parameters (**Supplementary Table 1**).

The C-indices and C-statistic for ML-based HFmrEF risk prediction models are displayed in **Table 2**. The results of eight prediction models for all-cause mortality showed that LASSO Cox regression performed the best at both the 1- and 6-year follow-ups. Compared with the other seven models, LASSO Cox regression had the highest overall C-statistic, at 0.78 over 6 years and 0.75 for 1 year. The C-indices for LASSO regression were also the highest, at 0.83 [95% confidence interval (CI): 0.68–0.94] and 0.77 (95% CI: 0.64–0.89) at the 6- and 1-year follow-ups, respectively. This was in contrast to the ridge regression model; across both short and long follow-ups, the ridge Cox regression model had the lowest C-index [1 year: 0.52 (95% CI: 0.38–0.65); 6 years: 0.51 (95% CI: 0.38–0.63)]. **Figure 2A** shows the ability of the models to discriminate groups by mortality using ROC curves.

Machine learning for prediction of heart failure hospitalization outcome

Table 3 shows the results of the C-indices and C-statistic for eight prediction models of HF hospitalization. Of the eight models, RF showed the best discrimination, with the highest

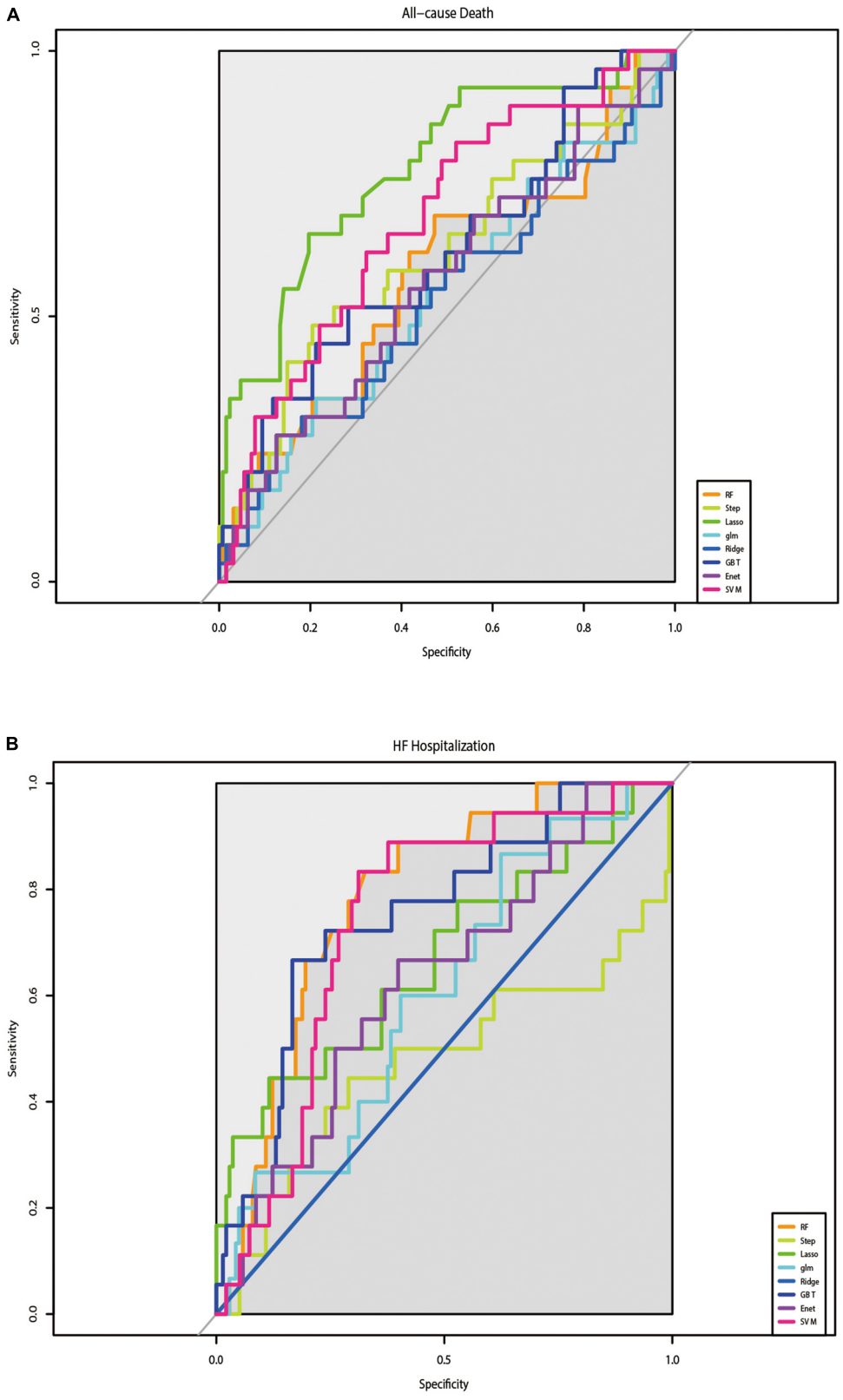

FIGURE 2
Results of the discrimination for all-cause mortality and HF-Hospitalization in ROC curves. **(A)** The performance of eight prediction models for all-cause mortality was assessed by ROC curves. **(B)** The performance of eight prediction models for re-hospitalize was assessed by ROC curves.

overall C-statistic of 0.80 over a maximum of 6 years of follow-up and 0.85 for 1 year. The C-indices for RF were also the highest, at 0.80 (95% CI: 0.66–0.94) and 0.85 (95% CI: 0.71–0.99) at the 6- and 1-year follow-ups, respectively. The DeLong test showed that the RF model was different from the step-forward and ridge regression models, especially the latter (p-value = 0.0017, <0.0001, respectively). The performance of the models in discriminating HF hospitalization was assessed by ROC curves (Figure 2B).

TABLE 1 Baseline characteristics of patients (N = 519).

	Original cohort	Imputation cohort
Male	330 (63.5%)	330 (63.5%)
Age	66.1 (9.23)	66.1 (9.23)
White patients	474 (91.3%)	474 (91.3%)
Heart rate, bpm	69.7 (13.39)	69.7 (13.39)
SBP	127.9 (13.80)	127.9 (13.80)
DBP	77.5 (9.72)	77.5 (9.72)
BMI	31.4 (7.01)	31.4 (7.01)
Serum potassium	4.26 (0.47)	4.26 (0.47)
Serum calcium	102.74 (6.32)	102.77 (6.19)*
Serum sodium	141.40 (4.32)	141.40 (4.32)
Creatinine	1.11 (0.30)	1.10 (0.30)*
HCT	40.85 (5.54)	40.85 (5.52)*
WBC	7.05 (2.05)	7.05 (2.05)
Waist Circumference	104.84 (16.67)	104.88 (16.66)*
GFR	69.67 (19.91)	69.67 (19.91)
NYHA_CLASS		
I and II	335 (64.5%)	335 (64.5%)
III and IV	184 (35.4%)	184 (35.5%)
Current smoker	81 (15.6%)	81 (15.6%)
Ever-smoker	206 (39.7%)	206 (39.7%)
Hemoglobin, g/dl	13.58 (1.74)	13.58 (1.74)
Glucose	112.74 (41.37)	112.83 (41.30)*
ALP	105.24 (60.71)	105.42 (59.83)*
QRS duration, ms	102.13 (31.14)	102.13 (31.14)
Cooking salt score	4.75 (3.62)	4.75 (3.62)
KCCQ scores		
Physical limitation	56.38 (22.77)	56.39 (22.68)*
Symptom stability score	51.78 (24.13)	51.78 (24.13)
Symptom frequency score	57.95 (24.30)	57.95 (24.30)
Symptom burden score	59.59 (23.78)	59.59 (23.78)
Total symptom score	58.77 (23.06)	58.77 (23.06)
Self-efficacy score	65.99 (24.72)	65.99 (24.72)
Quality of life score	49.78 (22.86)	49.78 (22.86)
Overall summary score	54.68 (21.13)	54.68 (21.13)
Clinical summary score	57.60 (21.02)	57.60 (21.02)

ALP, alkaline phosphatase; BMI, body mass index; DBP, diastolic blood pressure; GFR, glomerular filtration rate; HCT, hematocrit; KCCQ, Kansas City Cardiomyopathy Questionnaire; NYHA, new york heart association; SBP, systolic blood pressure; WBC, white blood count.
*Indicates imputation cohort is different from the original cohort.

Characteristic variables of mortality

For the outcome of mortality, LASSO regression showed the best performance. To improve clinical usability, we further constructed a model made of the variables filtered by LASSO regression. The forest plot of the variables found by multivariate Cox regression is shown in Figures 3A,B. During the 6-year follow-up, 16 covariates were selected by LASSO, and only four variables (age, race, stroke, and DM) played significant roles in the prediction models (p-values = 0.01, 0.03, 0.01, and 0.00, respectively) (Figure 3A). Figure 3B shows the nine independent variables selected by LASSO over 1 year of follow-up. Among the nine variables, race, previous hospitalization for cardiac heart failure (CHF-HOSP), chronic obstructive pulmonary disease (COPD), smoking, and blood glucose showed a significant influence on the short-term mortality of HFmrEF patients.

A risk score for 1- and 6-year mortality was created using a nomogram (Figures 3C,D). Scores for the 6-year follow-up, ranging from 0 to 300, were assigned points as follows: for age, the points went from 0 to 100, with higher scores for older age. For race, white had a score of 0, black 35 and other races 70 points. Patients with HFmrEF without diabetes, with diabetes, and with diabetes-related microvascular complications showed increasing risk scores of 0, 35, and 70 points, respectively. Figure 3D shows the risk scores at the 1-year follow-up. Among the nine variables, the race score ranged from 0 to 89, CHF-HOSP ranged from 0 to 31 points, COPD added a risk score of 34 points and its absence 0, and the glucose score was positively correlated with risk points at the 6-year follow-up. The calibration of the LASSO-based model is plotted in Supplementary Figure 1.

Characteristic variables of heart failure hospitalization

The RF model showed the best performance at predicting the outcome of HF hospitalization. RF addressed each feature in the order of mean decrease accuracy to rank the importance of its variables. To further clarify the important variables, we graphed the top 20 covariates identified by the variable importance (VIMP) metric (Figure 4). Values of mean decrease accuracy are shown in Supplementary Tables 2, 3.

Figure 4A shows that KCCQ scores, including symptom frequency, clinical summary, overall summary, social limitation, physical limitation, and total symptoms, all exhibited a major influence on long-term HF hospitalization. Asthma, race, and BMI also played important roles in the prediction model. Compared with the long-term follow-up characteristics, which were closely related to quality of life, variables that predicted short-term HF hospitalization were more correlated with previous clinical history and clinical laboratory results, such

TABLE 2 Discrimination of the models for mortality.

	Death-6 year			Death-1 year		
	C-index	AUC	DeLong test	C-index	AUC	DeLong test
RF	0.56 (0.42–0.69)	0.58	0.0297*	0.67 (0.54–0.80)	0.68	0.6682
Step-forward	0.68 (0.59–0.82)	0.62	0.0126*	0.50 (0.36–0.64)	0.49	0.0011*
Lasso	0.83 (0.66–0.94)	0.78	1	0.77 (0.64–0.89)	0.75	1
Logistic	0.55 (0.41–0.69)	0.54	0.0051*	0.53 (0.40–0.66)	0.46	0.0095*
Ridge	0.52 (0.38–0.65)	0.53	0.0057*	0.51 (0.38–0.63)	0.52	0.0900
GBT	0.61 (0.45–0.73)	0.62	0.0530	0.76 (0.62–0.89)	0.77	0.9209
Elastic-net	0.54 (0.44–0.71)	0.55	0.0160*	0.54 (0.41–0.67)	0.54	0.2378
SVM	0.58 (0.47–0.69)	0.58	0.0036*	0.64 (0.54–0.75)	0.62	0.4207

GBT, gradient boosted trees; RF, random forest; SVM, support vector machine; AUC, area under the curve.
*Indicates $p < 0.05$.

as hematocrit, estimated glomerular filtration rate (eGFR), creatinine (CR), coronary artery bypass graft (CABG) surgery, and percutaneous coronary intervention (PCI). The candidate variables are ranked by importance in **Figure 4B**. The calibration of the RF-based model is plotted in **Supplementary Figure 2**.

Distribution of outcomes

Figure 5 shows the predicted distribution of the best performance models, which were sorted by risk. These models were LASSO Cox regression for the outcome of all-cause death and RF for hospitalization with HF exacerbation. The prediction models with positive clustering of patients who died or were hospitalized with HF aggravation (**Figure 5**) indicated that the models accurately stratified patients at risk of death and hospitalization. **Figures 5A,B** show the distribution of all-cause mortality at the 1- and 6-year follow-ups, respectively. **Figure 5C** shows the distribution of HF hospitalizations at the 1-year follow-up, and **Figure 5D** shows the distribution at the 6-year follow-up.

Discussion

Heart failure with an LVEF of 40–49% was first established as a category in 2013. Later, in 2016, the ESC defined HF with an LVEF range of 40–49% as a new subtype of HF: heart failure with mildly reduced ejection fraction (HFmrEF), which was redefined to HF with a mildly reduced (41–49%) ejection fraction in the 2021 ESC guidelines (1, 14). Compared with HFpEF and HFrEF, HFmrEF is less well studied. The pharmacological treatment for HFmrEF has been updated in the 2021 ESC guidelines, which propose that diuretics, angiotensin-converting enzyme (ACE) inhibitors, angiotensin receptor blockers (ARBs), and beta blockers may be considered for this category to reduce the risks of HF hospitalization and death. But the issue of whether these patients represent a distinct HF subtype that may benefit from therapies salutary for patients with HFrEF requires further study.

Accurately predicting prognosis plays an important role in choosing a therapeutic regimen and improving the outcome of HF. In this cohort of 519 individuals in the TOPCAT trial with LVEF ranging from 41 to 49%, we developed and validated eight alternative risk models for the prediction of HF hospitalization and all-cause mortality. Our model includes abundant suits of clinical risk factors that are measurable and accessible in history taking. The RF model performed the best, with good validation and excellent accuracy and calibration for rehospitalization, and a LASSO regression model was the best model for mortality prediction.

In both prediction models, patients' physical conditions, as evaluated and quantified by the KCCQ scores, were the strongest predictors of both death toll and HF readmission over a 6-year follow-up. When combined with NT-proBNP, KCCQ could serve as an optional tool for quick and convenient risk fractionation (15–17). In our models, KCCQ accounted for a large amount of mortality and HF readmission prediction because it represents a status health quality of life and could be influenced by many factors, such as gender, race, non-cardiovascular and cardiovascular comorbidities. In recent years, with the rapid development of the internet, smartphones, and wearable health devices, KCCQ can be obtained instantaneously for physicians working in telehealth (18). Therefore, the KCCQ has the advantage of a quick overview of patients' HF risk for physicians in remote areas or clinics. The KCCQ also record clinically meaningful changes over time, making it promising to support joint decision-making and more efficient medical interventions to quickly identify patients at higher risk stratification of mortality and readmission.

Based on our results, AF seems to confer both short- and long-term risk of all-cause death and cardiovascular rehospitalization. In research carried out by David M. Kaye, both

HFmrEF and HFpEF patients with AF had remarkably increased pulmonary capillary wedge pressure, decreased cardiac index and reduced left ventricular work index. At similar levels of systemic circulation workload, AF patients fail to adapt their oxygen consumption to the increase in workload, which is accompanied by an irreversibly impaired cardiac index and ventricular working index (19). A cohort study in the ESC Heart Failure Long-Term Registry found that AF increased with increasing LVEF, accounting for poor cardiovascular outcomes only in HFpEF and HFmrEF patients and not in HFrEF patients (20). In our ML-based modeling results, AF is also one of the top predictors of all-cause mortality. However, the current guidelines suggest that patients with HFmrEF are less likely to suffer from AF and non-cardiac comorbidities. Therefore, the relationship between the occurrence of AF and the prognosis of HFmrEF warrants further study and exploration.

TABLE 3 Discrimination of the models for HF hospitalization.

	HF-hospitalization-6 year			HF-hospitalization-1 year		
	C-index	AUC	DeLong test	C-index	AUC	DeLong test
RF	0.80 (0.66–0.94)	0.78	1	0.85 (0.71–0.99)	0.84	1
Step-forward	0.56 (0.43–0.70)	0.48	0.0017*	0.67 (0.53–0.81)	0.67	0.0503
Lasso	0.72 (0.59–0.86)	0.67	0.2429	0.49 (0.36–0.62)	0.47	0.0016
Logistic	0.62 (0.48–0.76)	0.60	0.0437*	0.43 (0.33–0.54)	0.58	0.1632
Ridge	0.50 (0.34–0.66)	0.50	<0.0001*	0.63 (0.51–0.75)	0.39	0.0037
GBT	0.77 (0.63–0.91)	0.75	0.3605	0.81 (0.67–0.94)	0.81	0.6428
Elastic-net	0.65 (0.51–0.78)	0.63	0.0048*	0.61 (0.50–0.73)	0.60	0.0130
SVM	0.78 (0.64–0.93)	0.74	0.3488	0.70 (0.59–0.82)	0.40	0.3292

GBT, gradient boosted trees; RF, random forest; SVM, support vector machine; AUC, area under the curve.
*Indicates $p < 0.05$.

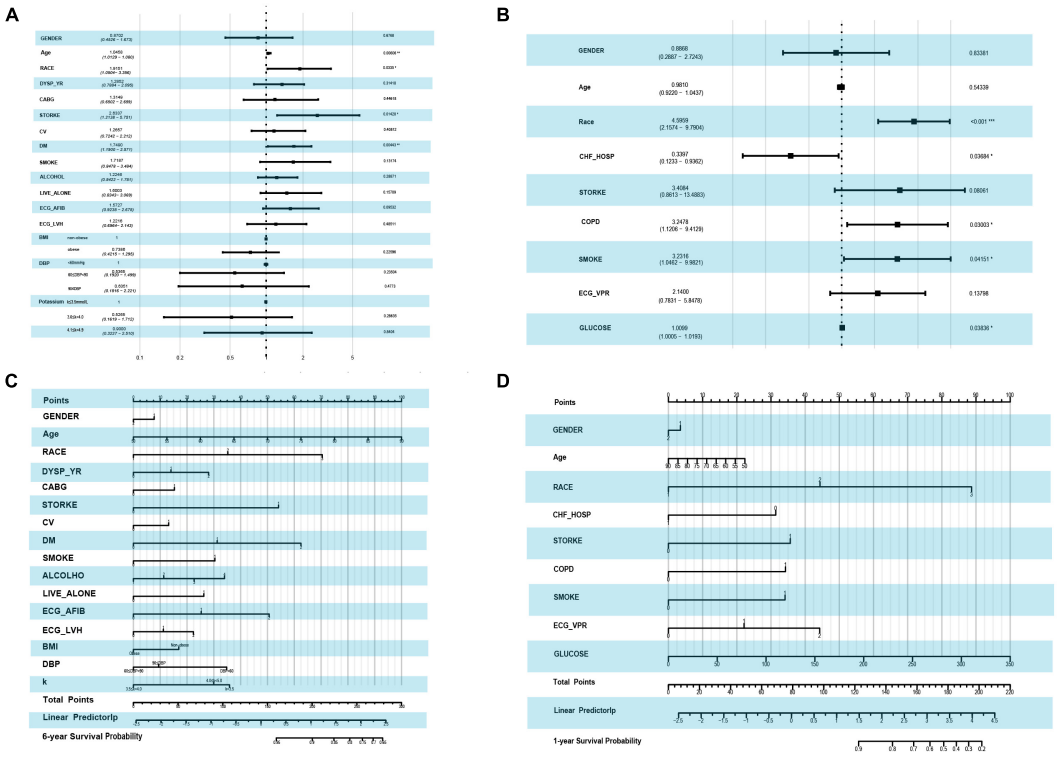

FIGURE 3
Forest plot by using the multi-variable COX regression and the risk score nomogram. **(A)** Forest plot of variables selected by LASSO COX regression in the end point event of all-cause mortality at 6-year follow-up. **(B)** Forest plot of variables selected by LASSO in the end point event of all-cause mortality at 1-year follow-up. **(C)** Nomogram for predicting 6-year all-cause mortality based on variables selected by LASSO COX regression. **(D)** Nomogram for predicting 1-year all-cause mortality based on variables selected by LASSO COX regression.

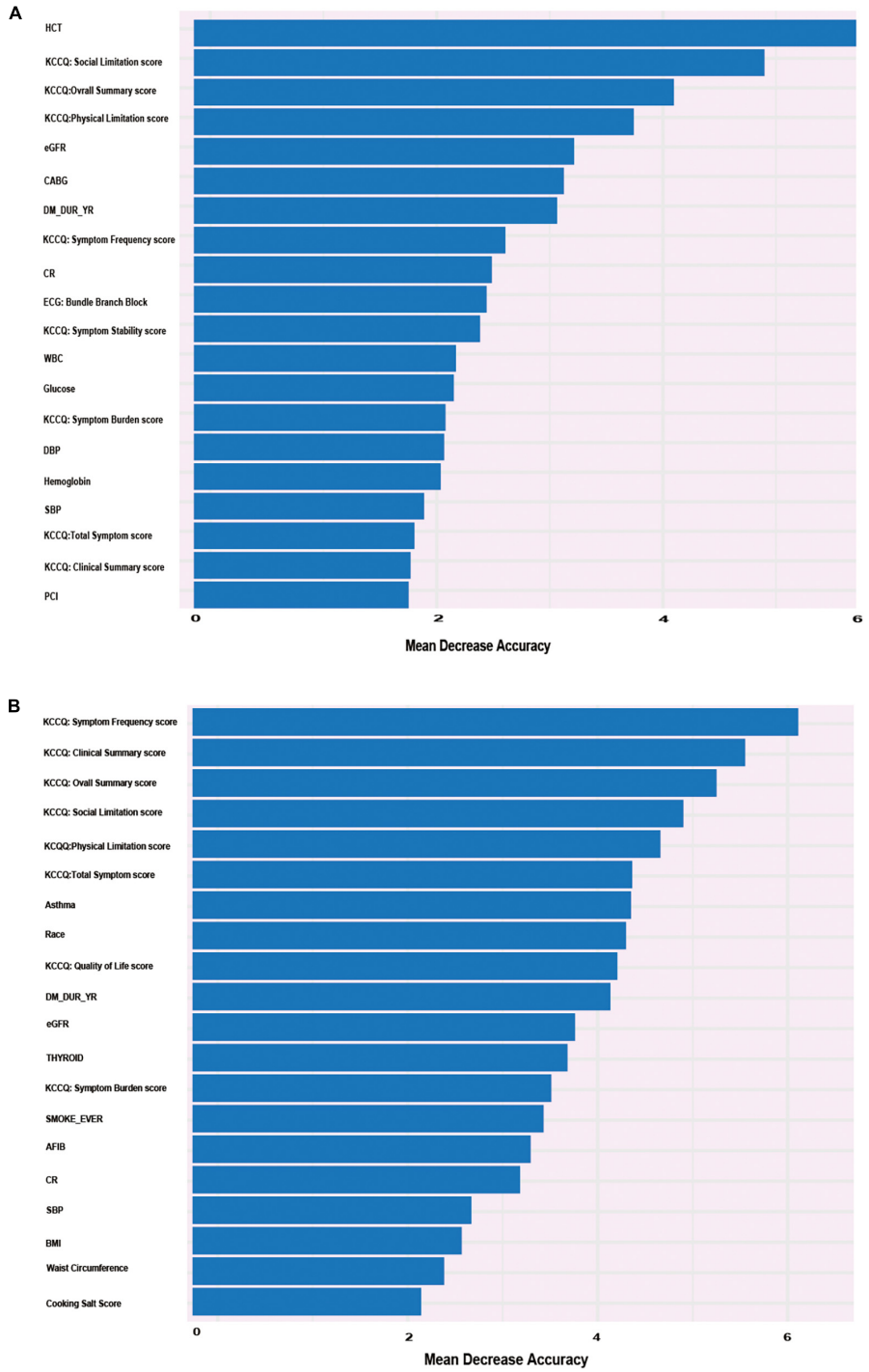

FIGURE 4
Alluvial plot of the 20 most important parameters for HF re-hospitalization risk prediction identified by the VIMP metric in the RF model in the derivation cohort. **(A)** Twenty most important parameters for predicting the risk of re-hospitalization for heart failure at 6-year follow-up identified by VIMP method. **(B)** Twenty most important parameters for predicting the risk of re-hospitalization for heart failure at 1-year follow-up identified by VIMP method.

High BMI is proven a risk factor for HF, patients with a normal or low BMI have a higher mortality and readmission rate than those with a relatively high BMI. The phenomenon is termed the "obesity paradox" (21–25). This also existed according to an investigation of HFmrEF patients (26). In our ML-based models, patients with high BMI had lower scores

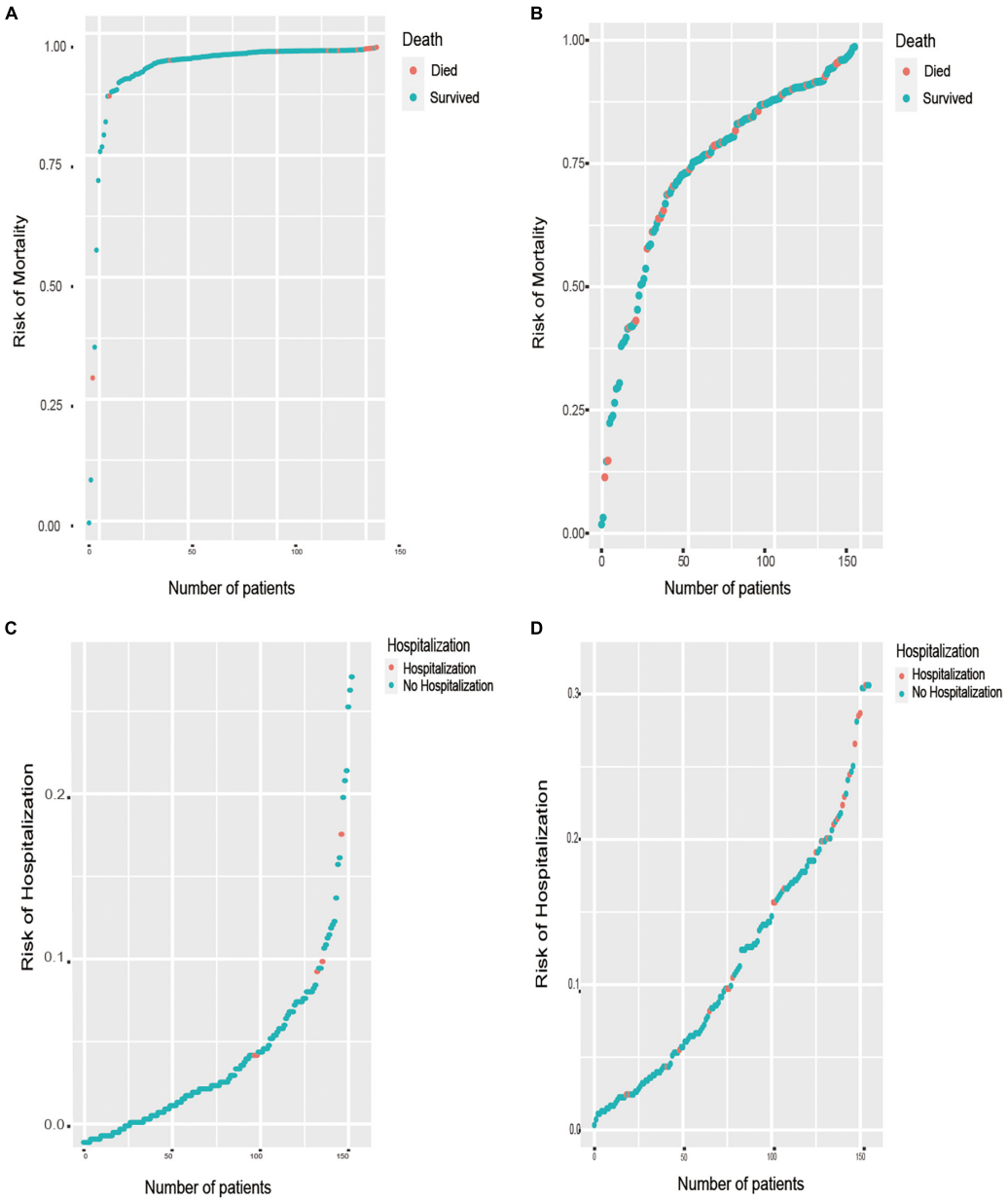

FIGURE 5
Prediction distributions of patients with HFmrEF in the outcomes of all-cause mortality and HF hospitalization. **(A)** The distribution of all-cause mortality at the 1-year follow-ups, which there is a positive correlation between the number of patient deaths and the risk of mortality. **(B)** The distribution of all-cause mortality at the 6-year follow-ups. **(C)** The distribution of re-hospitalization at the 1-year follow-ups, which there is a positive correlation between the number of patients' hospitalization and the risk of hospitalization. **(D)** The distribution of re-hospitalization at the 6-year follow-ups.

than those with low BMI. To the best of our knowledge, a high percentage of body fat mass indicates good nutrition situations, and this is probably relevant to a lower risk of short-term relapse of cardiac events in HFmrEF patients. Moreover, it is also considered that the obesity paradox may be attributed to the intrinsic limitations of BMI as an index of obesity. Other body mass measures, such as body fat distribution, body fat rate and fat-free mass, are probably more accurate for examining the relationship of body composition with health outcomes. For instance, Chandramouli et al. recently reported that the obesity paradox is manifested only when BMI is used as a weight parameter. When the waist-to-height ratio (WHtR) is used, the opposite association emerges (26). Therefore, further studies are needed to develop metrics for better analysis of body composition, better estimation of various obesity phenotypes and better prediction of mortality and rehospitalization in HF.

Another risk factor, eGFR was significant in our predicting model for mortality and readmission in cohort of HFmrEF. Patients with chronic HF are vulnerable to renal impairment (RI), and conversely, impaired renal function is associated with a higher mortality risk in HF patients. Research examining the relationship between all subtypes of HF and the prognostic impact of chronic kidney disease shows that in HFpEF patients, although the incident rate of CKD is higher, CKD is less important with a weaker correlation with all-cause death, have a less risk score compared with conventional risk markers, and exerts insufficient differentiation for prediction of mortality (27). These findings are in line with our results. In the cohort of HFmrEF in the TOPCAT trial, eGFR was a more powerful predictor of mortality in patients with HFmrEF than in those with HFpEF. We speculate that morbidity of CKD may give rise to sympathetic and neurohormonal activation and cause further deterioration of HF. This was also believed to be associated with other underlying diseases that impair renal function such as hypertension and diabetes which are prevalent among HFmrEF patients. This link was further evidenced by the Meta-Analysis Global Group in Chronic Heart Failure (MAGGIC) meta-analysis, which showed a lower mortality rate and lower association between CKD and death in patients with HFpEF than in HFmrEF (28).

Consistent with the 6-year findings, LASSO regression and the RF method showed the best predictive performance for 1-year mortality and readmission, respectively. Interestingly, unlike the top 20 risk factors screened by the RF model in the 6-year rehospitalization prediction, hematocrit (HCT) was proposed as one of the most important risk factors. Although association between HCT and incident HF has not been well established, several follow-up studies have elucidated that higher levels of HCT were associated with an increased risk of developing HF and coronary events (29–32). Additionally, Gagnon et al. proposed that both low and high HCT levels were positively associated with the occurrence of cardiovascular events (33). All of the above-mentioned findings suggest that the usage of hemoglobin and HCT for the estimation of plasma volume may represent a useful tool in the field of HF. Recently, estimated plasma volume status (ePVS), a relatively simple and non-invasive plasma volume estimation based on hemoglobin and hematocrit, was prompted to be a better predictor of both post-discharge and bedside clinical assessments (34). Kobayashi et al. and Grodin proposed that ePVS was associated with systemic congestion and deterioration of HF, regardless of other influencing factors (32, 35). Consequently, it could be a useful congestion index in patients with HF, in line with our findings in HFmrEF patients. Hemodynamic congestion develops and progresses slowly but eventually gives rise to symptomatic congestion and consequently urgent hospitalization. Accordingly, HCT may represent a convenient clinical indicator in patients with HFmrEF. This also suggests that ePVS might be an additional phenotypic characteristic considered for clinical study and for tailoring personalized therapies for HF patients.

DM has been recognized as an independent risk factor for the development of HF. Previous study conducted by Bhambhani et al. have reported that diabetes mellitus could predict the incident of HFmrEF, and this finding could be further confirmed in our study (36). In this study, we found DM was one of the strongest predictors of both the primary and mortality endpoints in the HFmrEF patients. And DM patients with HF treated with sodium–glucose co-transporter 2 inhibitors (SGLT2i) have shown impressive protective effects (37). In addition, the importance of other predictors in the prediction of readmission and mortality of HFmrEF differed greatly, including BP, smoking, age and stroke for predicting death, and WBC, CR and Salt intake for predicting HF re-hospitalization. In this regard, ML improved the prediction accuracy, letting us find novel relationships that were not hypothesis driven and shed light on some ignored risk factors.

Our study also has certain limitations. First, the TOPCAT trial was conducted between 2006 and 2012. Missing values of biomarkers such as circulating natriuretic peptides and high-sensitivity troponin affected our analysis and were not available to assess dynamic risk prediction scores. And due to the time period of the TOPCAT study, patients with HFmEF were not treated with SGLT-2 antagonists, which could alter the risk profile of these patients and potentially affected the model outputs. Second, we enrolled 519 patients with LVEF ranged from 41 to 49%. Unfortunately, the TOPCAT trial excluded the population with an LVEF greater than 45%. Therefore, we did not include adult patients with symptoms of HF and documented LVEF <45%. Third, given that our research is a *post hoc* analysis of the TOPCAT trial, and the TOPCAT study population was predominantly white males, therefore, our predicting models may not perform as well to the general population. Therefore, further validation of the role of ML in phenomenological mapping and sex-specific classification criteria is needed in a wide range of HFmrEF clinical data.

Conclusion

Machine learning-based models outperformed traditional models at predicting mortality and re-hospitalization in patients with HFmrEF. The results of the risk assessment showed that KCCQ score should be paid increasing attention to in the management of HFmrEF patients.

Data availability statement

The original contributions presented in this study are included in the article/**Supplementary material**, further inquiries can be directed to the corresponding authors.

Author contributions

HeZ, PL, YN, DX, and QZ contributed to the design of the work. HeZ, PL, and GZ contributed to the analysis of the work. HeZ, PL, GZ, KX, and HaZ contributed to the interpretation of data. HeZ, PL, KX, YN, DX, and QZ wrote the original manuscript. HeZ, GZ, KX, HaZ, YN, DX, and QZ revised the manuscript for important intellectual content. HeZ, GZ, HaZ, YN, and QZ wrote the revised manuscript. KX, HaZ, YN, DX, and QZ approved the revised version to be published. HeZ, PL, GZ, KX, HaZ, YN, DX, and QZ agreed to be accountable for all aspects of the work. All authors contributed to the article and approved the submitted version.

Funding

This work was supported by the National Natural Science Foundation of China (82070403 and 82270374 to QZ), the Science and Technology Program of Guangdong Province (2021A0505030031 to QZ), the Frontier Research Program of Guangzhou Regenerative Medicine and Health Guangdong Laboratory (2018GZR110105001 to QZ), and the Youth Science and Technology Innovation Talent Program of Guangdong TeZhi plan (2019TQ05Y136 to QZ).

Acknowledgments

We thank TOPCAT trial investigators for conducting this trial and making these data available and National Institutes of Heart, Lung, and Blood Institute's Biologic Specimen and Data Repository Information Coordinating Center for approving our permissions.

Conflict of interest

The authors declare that the research was conducted in the absence of any commercial or financial relationships that could be construed as a potential conflict of interest.

Publisher's note

All claims expressed in this article are solely those of the authors and do not necessarily represent those of their affiliated organizations, or those of the publisher, the editors and the reviewers. Any product that may be evaluated in this article, or claim that may be made by its manufacturer, is not guaranteed or endorsed by the publisher.

Supplementary material

The Supplementary Material for this article can be found online at: https://www.frontiersin.org/articles/10.3389/fcvm.2022.1042139/full#supplementary-material

References

1. McDonagh TA, Metra M, Adamo M, Gardner RS, Baumbach A, Böhm M, et al. 2021 ESC Guidelines for the diagnosis and treatment of acute and chronic heart failure. *Eur Heart J.* (2021) 42:3599–726.

2. Chioncel O, Lainscak M, Seferovic PM, Anker SD, Crespo-Leiro MG, Harjola VP, et al. Epidemiology and one-year outcomes in patients with chronic heart failure and preserved, mid-range and reduced ejection fraction: an analysis of the ESC Heart Failure Long-Term Registry. *Eur J Heart Fail.* (2017) 19:1574–85. doi: 10.1002/ejhf.813

3. Fralick M, Colak E, Mamdani M. Machine learning in medicine. *N Engl J Med.* (2019) 380:2588–9. doi: 10.1056/NEJMc1906060

4. Deo RC. Machine learning in medicine. *Circulation.* (2015) 132:1920–30. doi: 10.1161/CIRCULATIONAHA.115.001593

5. Pitt B, Pfeffer MA, Assmann SF, Boineau R, Anand IS, Claggett B, et al. Spironolactone for heart failure with preserved ejection fraction. *N Engl J Med.* (2014) 370:1383–92. doi: 10.1056/NEJMoa1313731

6. Stekhoven DJ, Buhlmann P. MissForest–non-parametric missing value imputation for mixed-type data. *Bioinformatics.* (2012) 28:112–8. doi: 10.1093/bioinformatics/btr597

7. Liaw A, Wiener M. *Classification and regression by RandomForest*. Berlin: ResearchGate (2001).

8. Simon N, Friedman J, Hastie T, Tibshirani R. Regularization paths for cox's proportional hazards model via coordinate descent. *J Stat Softw.* (2011) 39:1–13. doi: 10.18637/jss.v039.i05

9. Freund Y, Schapire RE. A decision-theoretic generalization of on-line learning and an application to boosting. *J Comput Syst Sci.* (1997) 55:119–39.

10. Bennett KP, Campbell C. Support vector machines: hype or hallelujah? *ACM SIGKDD Explor Newslett.* (2000) 2:1–13. doi: 10.1145/380995.380999

11. Harrell FJ Jr, Califf RM, Pryor DB, Lee KL, Rosati RA. Evaluating the yield of medical tests. *JAMA.* (1982) 247:2543–6. doi: 10.1001/jama.247.18.2543

12. DeLong ER, DeLong DM, Clarke-Pearson DL. Comparing the areas under two or more correlated receiver operating characteristic curves: a nonparametric approach. *Biometrics.* (1988) 44:837–45. doi: 10.2307/2531595

13. Angraal S, Mortazavi BJ, Gupta A, Khera R, Ahmad T, Desai NR, et al. Machine learning prediction of mortality and hospitalization in heart failure with preserved ejection fraction. *JACC Heart Fail.* (2020) 8:12–21. doi: 10.1016/j.jchf.2019.06.013

14. Ponikowski P, Voors AA, Anker SD, Bueno H, Cleland JGF, Coats AJS, et al. 2016 ESC Guidelines for the diagnosis and treatment of acute and chronic heart failure: the task force for the diagnosis and treatment of acute and chronic heart failure of the European Society of Cardiology (ESC) developed with the special contribution of the Heart Failure Association (HFA) of the ESC. *Eur Heart J.* (2016) 37:2129–200. doi: 10.1093/eurheartj/ehw128

15. Luo N, O'Connor CM, Cooper LB, Sun JL, Coles A, Reed SD, et al. Relationship between changing patient-reported outcomes and subsequent clinical events in patients with chronic heart failure: insights from HF-ACTION. *Eur J Heart Fail.* (2019) 21:63–70. doi: 10.1002/ejhf.1299

16. Nichols GA, Pesa J, Sapp DS, Patel A. The association between heart failure hospitalization and self-reported domains of health. *Qual Life Res.* (2020) 29:953–8. doi: 10.1007/s11136-019-02373-9

17. Pokharel Y, Khariton Y, Tang Y, Nassif ME, Chan PS, Arnold SV, et al. Association of serial kansas city cardiomyopathy questionnaire assessments with death and hospitalization in patients with heart failure with preserved and reduced ejection fraction: a secondary analysis of 2 randomized clinical trials. *JAMA Cardiol.* (2017) 2:1315–21. doi: 10.1001/jamacardio.2017.3983

18. Hu D, Liu J, Zhang L, Bai X, Tian A, Huang X, et al. Health status predicts short- and long-term risk of composite clinical outcomes in acute heart failure. *JACC Heart Fail.* (2021) 9:861–73. doi: 10.1016/j.jchf.2021.06.015

19. Kaye DM, Silvestry FE, Gustafsson F, Cleland JG, van Veldhuisen DJ, Ponikowski P, et al. Impact of atrial fibrillation on rest and exercise haemodynamics in heart failure with mid-range and preserved ejection fraction. *Eur J Heart Fail.* (2017) 19:1690–7. doi: 10.1002/ejhf.930

20. Zafrir B, Lund LH, Laroche C, Ruschitzka F, Crespo-Leiro MG, Coats AJS, et al. Prognostic implications of atrial fibrillation in heart failure with reduced, mid-range, and preserved ejection fraction: a report from 14 964 patients in the European Society of Cardiology Heart Failure Long-Term Registry. *Eur Heart J.* (2018) 48:4277–84. doi: 10.1093/eurheartj/ehy626

21. Lavie CJ, Alpert MA, Arena R, Mehra MR, Milani RV, Ventura HO. Impact of obesity and the obesity paradox on prevalence and prognosis in heart failure. *JACC Heart Fail.* (2013) 1:93–102. doi: 10.1016/j.jchf.2013.01.006

22. Cheng RK, DePasquale EC, Deng MC, Nsair A, Horwich TB. Obesity in heart failure: impact on survival and treatment modalities. *Expert Rev Cardiovasc Ther.* (2013) 11:1141–53. doi: 10.1586/14779072.2013.824691

23. Carbone S, Lavie CJ, Elagizi A, Arena R, Ventura HO. The impact of obesity in heart failure. *Heart Fail Clin.* (2020) 16:71–80. doi: 10.1016/j.hfc.2019.08.008

24. Matsuhiro Y, Nishino M, Ukita K, Kawamura A, Nakamura H, Yasumoto K, et al. Underweight is associated with poor prognosis in heart failure with preserved ejection fraction. *Int Heart J* (2021) 62:1042–51. doi: 10.1536/ihj.21-195

25. Gentile F, Sciarrone P, Zamora E, De Antonio M, Santiago E, Domingo M, et al. Body mass index and outcomes in ischaemic versus non-ischaemic heart failure across the spectrum of ejection fraction. *Eur J Prev Cardiol* (2021) 28:948–55. doi: 10.1177/2047487320927610

26. Chandramouli C, Tay WT, Bamadhaj NS, Tromp J, Teng TK, Yap JJL, et al. Association of obesity with heart failure outcomes in 11 Asian regions: a cohort study. *PLoS Med* (2019) 16:e1002916. doi: 10.1371/journal.pmed.1002916

27. Löfman I, Szummer K, Dahlström U, Jernberg T, Lund LH. Associations with and prognostic impact of chronic kidney disease in heart failure with preserved, mid-range, and reduced ejection fraction. *Eur J Heart Fail.* (2017) 19:1606–14. doi: 10.1002/ejhf.821

28. Meta-analysis Global Group in Chronic Heart Failure [MAGGIC]. The survival of patients with heart failure with preserved or reduced left ventricular ejection fraction: an individual patient data meta-analysis. *Eur Heart J.* (2012) 33:1750–7. doi: 10.1093/eurheartj/ehr254

29. Huang CY, Lin TT, Wu YF, Chiang FT, Wu CK. Long-term prognostic value of estimated plasma volume in heart failure with preserved ejection fraction. *Sci Rep.* (2019) 9:14369. doi: 10.1038/s41598-019-50427-2

30. Coglianese EE, Qureshi MM, Vasan RS, Wang TJ, Moore LL. Usefulness of the blood hematocrit level to predict development of heart failure in a community. *Am J Cardiol.* (2012) 109:241–5. doi: 10.1016/j.amjcard.2011.08.037

31. Sorlie PD, Garcia-Palmieri MR, Costas RJ, Havlik RJ. Hematocrit and risk of coronary heart disease: the puerto rico health program. *Am Heart J.* (1981) 101:456–61. doi: 10.1016/0002-8703(81)90136-8

32. Grodin JL, Philips S, Mullens W, Nijst P, Martens P, Fang JC, et al. Prognostic implications of plasma volume status estimates in heart failure with preserved ejection fraction: insights from TOPCAT. *Eur J Heart Fail.* (2019) 21:634–42. doi: 10.1002/ejhf.1407

33. Gagnon DR, Zhang TJ, Brand FN, Kannel WB. Hematocrit and the risk of cardiovascular disease–the Framingham study: a 34-year follow-up. *Am Heart J.* (1994) 127:674–82. doi: 10.1016/0002-8703(94)90679-3

34. Ling HZ, Flint J, Damgaard M, Bonfils PK, Cheng AS, Aggarwal S, et al. Calculated plasma volume status and prognosis in chronic heart failure. *Eur J Heart Fail.* (2015) 17:35–43. doi: 10.1002/ejhf.193

35. Kobayashi M, Girerd N, Duarte K, Preud'homme G, Pitt B, Rossignol P. Prognostic impact of plasma volume estimated from hemoglobin and hematocrit in heart failure with preserved ejection fraction. *Clin Res Cardiol.* (2020) 109:1392–401. doi: 10.1007/s00392-020-01639-4

36. Bhambhani V, Kizer JR, Lima JAC, van der Harst P, Bahrami H, Nayor M, et al. Predictors and outcomes of heart failure with mid-range ejection fraction. *Eur J Heart Fail.* (2018) 20:651–9. doi: 10.1002/ejhf.1091

37. Becher PM, Schrage B, Ferrannini G, Benson L, Butler J, Carrero JJ, et al. Use of sodium-glucose co-transporter 2 inhibitors in patients with heart failure and type 2 diabetes mellitus: data from the Swedish Heart Failure Registry. *Eur J Heart Fail.* (2021) 23:1012–22. doi: 10.1002/ejhf.2131

frontiers | Frontiers in Cardiovascular Medicine

TYPE Review
PUBLISHED 23 January 2023
DOI 10.3389/fcvm.2023.1093053

OPEN ACCESS

EDITED BY
Nikolaos Fragakis,
Aristotle University Medical School, Greece

REVIEWED BY
Conrado Roberto Hoffmann Filho,
Hospital Regional Hans Dieter Schmidt, Brazil
Prem P. Kushwaha,
Case Western Reserve University, United States

*CORRESPONDENCE
Maria Donniacuo
✉ maria.donniacuo@unicampania.it

†These authors have contributed equally to this work

SPECIALTY SECTION
This article was submitted to General Cardiovascular Medicine, a section of the journal Frontiers in Cardiovascular Medicine

RECEIVED 08 November 2022
ACCEPTED 09 January 2023
PUBLISHED 23 January 2023

CITATION
Donniacuo M, De Angelis A, Rafaniello C, Cianflone E, Paolisso P, Torella D, Sibilio G, Paolisso G, Castaldo G, Urbanek K, Rossi F, Berrino L and Cappetta D (2023) COVID-19 and atrial fibrillation: Intercepting lines. *Front. Cardiovasc. Med.* 10:1093053. doi: 10.3389/fcvm.2023.1093053

COVID-19 and atrial fibrillation: Intercepting lines

Maria Donniacuo[1*†], Antonella De Angelis[1†], Concetta Rafaniello[1], Eleonora Cianflone[2], Pasquale Paolisso[3,4], Daniele Torella[5], Gerolamo Sibilio[6], Giuseppe Paolisso[7], Giuseppe Castaldo[8,9], Konrad Urbanek[8,9], Francesco Rossi[1], Liberato Berrino[1†] and Donato Cappetta[1,10†]

[1]Department of Experimental Medicine, University of Campania "Luigi Vanvitelli", Naples, Italy, [2]Department of Medical and Surgical Sciences, Magna Græcia University, Catanzaro, Italy, [3]Cardiovascular Center Aalst, OLV Hospital, Aalst, Belgium, [4]Department of Advanced Biomedical Sciences, University of Naples "Federico II", Naples, Italy, [5]Department of Experimental and Clinical Medicine, Magna Græcia University, Catanzaro, Italy, [6]Santa Maria delle Grazie Hospital, Pozzuoli, Italy, [7]Department of Advanced Medical and Surgical Sciences, University of Campania "Luigi Vanvitelli", Naples, Italy, [8]Department of Molecular Medicine and Medical Biotechnology, University of Naples "Federico II", Naples, Italy, [9]CEINGE Advanced Biotechnologies, Naples, Italy, [10]Department of Biological and Environmental Sciences and Technologies, University of Salento, Lecce, Italy

Almost 20% of COVID-19 patients have a history of atrial fibrillation (AF), but also a new-onset AF represents a frequent complication in COVID-19. Clinical evidence demonstrates that COVID-19, by promoting the evolution of a prothrombotic state, increases the susceptibility to arrhythmic events during the infective stages and presumably during post-recovery. AF itself is the most frequent form of arrhythmia and is associated with substantial morbidity and mortality. One of the molecular factors involved in COVID-19-related AF episodes is the angiotensin-converting enzyme (ACE) 2 availability. Severe acute respiratory syndrome coronavirus 2 (SARS-CoV-2) uses ACE2 to enter and infect multiple cells. Atrial ACE2 internalization after binding to SARS-CoV-2 results in a raise of angiotensin (Ang) II, and in a suppression of cardioprotective Ang(1–7) formation, and thereby promoting cardiac hypertrophy, fibrosis and oxidative stress. Furthermore, several pharmacological agents used in COVID-19 patients may have a higher risk of inducing electrophysiological changes and cardiac dysfunction. Azithromycin, lopinavir/ritonavir, ibrutinib, and remdesivir, used in the treatment of COVID-19, may predispose to an increased risk of cardiac arrhythmia. In this review, putative mechanisms involved in COVID-19-related AF episodes and the cardiovascular safety profile of drugs used for the treatment of COVID-19 are summarized.

KEYWORDS

COVID-19, inflammation, atrial fibrillation, COVID-19 drugs, atrial remodeling

1. Introduction

An outburst of pneumonia caused by severe acute respiratory syndrome coronavirus 2 (SARS-CoV-2) was reported in December 2019, prompting Health Agencies to issue a public health emergency (1). Since then, the viral infection has reached epidemic proportions, affecting nearly 300 million people in 2 years (2). Most cases are asymptomatic or associated with mild symptoms, but a significant minority of patients develops severe symptoms that can result in multiple organ failure and death (3). Mortality rate is increased by age, pre-existing cardiovascular diseases and metabolic disorders conditions such as hypertension, heart failure,

type 2 diabetes and obesity (4–6). The main extra-pulmonary site involved in COVID-19 is the cardiovascular system. Early cardiac injury, evidenced by elevated cardiac biomarkers, is associated to mortality, and has been reported in hospitalized COVID-19 patients (7).

Due to the initial lack of knowledge of COVID-19 pathophysiology and thus, effective treatments, compassionate and emergency use of drugs including numerous antibodies have been approved. During the pandemic phase, several drug classes have been used either as monotherapy or in combination to minimize disease severity (8–10; **Figure 1**).

Cardiac manifestations related to COVID-19 infection include arrhythmias, acute myocardial infarction and myocarditis (11). While the etiology of cardiac manifestations is multifactorial, it is possible that also genetic background, such as clinically silent and previously unrecognized channelopathies, can make these patients susceptible to cardiac arrhythmias. Interestingly, atrial fibrillation (AF) and COVID-19 infection appear to share some pathophysiological features, both being driven by an immune response, with inflammatory markers, such as C-reactive protein and cytokine interleukin (IL)-6, correlating with disease severity and mortality (12–14). Therefore, it is understandable that a high incidence of AF with COVID-19 has been reported (15–17).

Although a common immunoinflammatory substrate between COVID-19 and AF has emerged, a few studies have evaluate whether the COVID-19 inflammatory mediators are uniquely responsible for AF or whether this arrhythmia is related to a non-specific product of severe viral respiratory illness.

2. The outline of AF pathophysiology

Atrial fibrillation (AF), the most common type of cardiac arrhythmia, is an evolving age-related disease where co-morbidities or lifestyle conditions, such as hypertension, diabetes mellitus, obesity, chronic kidney disease and inflammatory diseases, play a pivotal role (18, 19). In 30% of cases, however, the arrhythmia manifests in asymptomatic subjects not affected by any of the previous pathologies, significantly reducing the quality of life (20).

Atrial fibrillation (AF) pathogenesis is associated with atrial electrical and structural remodeling (21, 22). Short and long-term electrical remodeling present different substrates: the former is related to an altered intracellular Ca^{2+} level *via* ryanodine receptors (RyRs) and voltage-dependent L-type Ca^{2+} current inactivation, the latter is related to reduce levels of mRNA transcript encoding ion channels or to post-transcriptional mechanisms (23). From the structural viewpoint, pro-fibrotic atrial remodeling has been shown to increase the AF susceptibility, contributing to the transition from paroxysmal to persistent or permanent AF (24). Myocardial fibrosis and the activation of its molecular and cellular drivers have been observed in atrial tissue of AF patients, demonstrating also a positive correlation between the degree of atrial fibrosis and the persistence of AF (25). Of note, pharmacotherapy with anti-fibrotic potential (i.e., statins and renin-angiotensin-aldosterone system (RAAS) inhibitors) effectively limits the formation of this structural substrate of AF (26).

Further, inflammation and reactive oxygen species also contribute to unbalanced homeostasis of atrial myocardium, promoting not only the onset but also the AF duration. Inflammatory cell infiltration and increased serum levels of inflammatory mediators, such as tumor necrosis factor-α (TNF-α), interleukin (IL)-1β, IL-6, IL-8, and IL-10, have been found in AF patients, correlating with AF duration and severity (27). Accordingly, treatments pointing at decreasing inflammatory response and oxidative stress have shown promising results by alleviating atrial structural and electrical remodeling (28).

Undoubtedly, a deeper understanding of the underlying AF pathophysiology as well as the individual patient characteristics are still needed to expand the effective and safe therapeutic armamentarium, and optimize a personalized pharmacotherapy.

2.1. AF in COVID-19 patients

Atrial fibrillation (AF) is the most common form of arrhythmia in COVID-19 patients, and can be the first sign even prior to evident respiratory distress (29). Almost 20% of COVID-19 patients have a history of AF, but also a new-onset AF represents a frequent complication in COVID-19 with a risk ranging between 10 and 18% (30–32). In a multicenter retrospective cohort study, the incidence of AF during hospitalization is 10% and the incidence of new-onset AF in patients without a pre-existing history of atrial arrhythmias is 4% (33).

Clinical evidence from hospitalized patients has demonstrated that COVID-19, by promoting the evolution toward a prothrombotic state, increases the susceptibility to AF during the infective stages and presumably during post-recovery (34). Meta-analysis studies revealed that pre-existing AF in patients with COVID-19 is associated with increased in-hospital mortality, post-discharge mortality and mechanical ventilation use (35). New-onset AF in the context of COVID-19-related pneumonia is linked to adverse prognosis, suggesting a correlation with the degree of inflammatory and hypoxemic viral insult that increase the hypercoagulable state, endothelial dysfunction, and oxidative stress (36). In general, as for all critically ill patients in which AF independently increases the risk of stroke, length of hospitalization, and death (37), this arrhythmia complicates the clinical course also in COVID-19 patients.

2.2. AF and COVID-19: Mechanistic insights

In attempt to outline a pathophysiology of COVID-19-related AF, several putative mechanisms have been proposed. They include a reduced availability of angiotensin-converting enzyme (ACE) 2, binding of viral spike protein to CD147 or sialic acid, enhancement of inflammatory signaling culminating in cytokine storm, endothelial damage and increased adrenergic drive (38; **Figure 2**).

Angiotensin-converting enzyme 2 (ACE2) converts angiotensin (Ang) I and Ang II into active peptides Ang(1–9) and Ang(1–7), respectively, which provide counter-regulatory effects for the classical RAAS axis (39, 40). After the cleavage of the viral spike protein, SARS-CoV-2 uses ACE2 to enter and infect host cells such as cardiomyocytes, pericytes, pneumocytes, endothelial cells, and macrophages (41–43). This interaction results in a reduction of ACE2 on the cell surface, suppressing a key pathway for the degradation of Ang II to form cardioprotective Ang(1–7). The consequent increase in Ang II/Ang(1–7) ratio shifts the balance to Ang II thereby promoting cardiac hypertrophy, vasoconstriction, tissue fibrosis, and oxidative stress (9). Moreover, atrial ACE2 catabolizes transforming growth factor-β1 (TGF-β1), the principal pro-fibrotic cytokine (44).

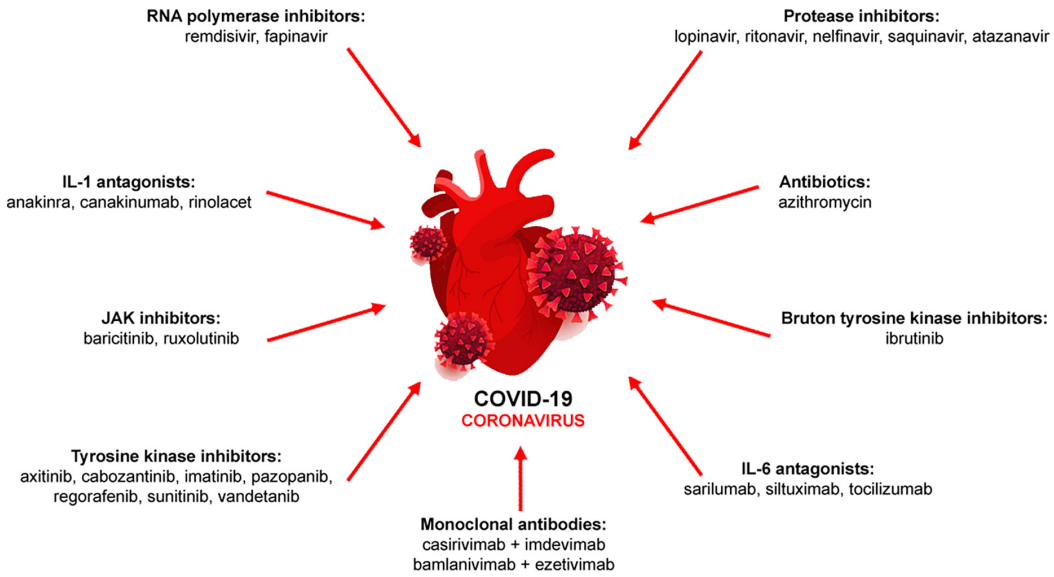

FIGURE 1
Pharmacological therapy of COVID-19. Antiviral (RNA polymerase and protease inhibitors, monoclonal antibodies), immunomodulatory (IL-1 and IL-6 antagonists, JAK inhibitors) or other drugs (antibiotics, tyrosine kinase inhibitors) are used either alone or in combination.

This may underlie atrial arrhythmogenesis and potentially increase the susceptibility to AF in COVID-19 patients (45). ACE2 is also involved in the regulation of the cardiac action potential. Ang(1–7) modulates Ca^{2+} homeostasis and cellular electrophysiology in atrial tissue and pulmonary veins (46, 47). Experimental animal studies have demonstrated an increased expression of ACE2 receptor following treatment with ACE inhibitors and angiotensin receptor blockers (48). Studies on ACE2 expression conducted in experimental models and human transcriptome to identify the organs more susceptible to this infection have revealed a low level in the lung, mainly limited to a small fraction of type II alveolar epithelial cells (49). It has been hypothesized that the massive release of inflammatory cytokines is responsible of an increase in ACE2 expression, thus potentiating the infection (50–52).

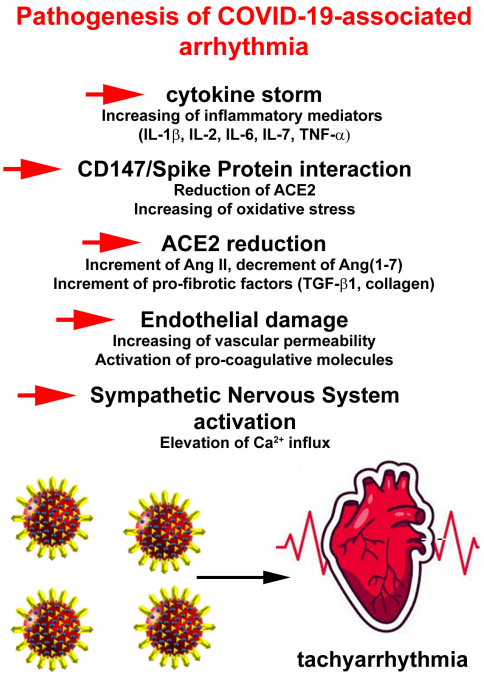

FIGURE 2
Pathophysiology of COVID-19-related atrial fibrillation (AF) events. Putative mechanisms include a reduced availability of angiotensin-converting enzyme 2, binding of viral spike protein to CD147 or sialic acid, enhancement of inflammatory signaling culminating in cytokine storm, endothelial damage, and increased adrenergic drive.

CD147 is an adjunctive player that facilitates SARS-CoV-2 invasion into host cells, including cardiomyocytes, by interacting with viral spike protein (53, 54). Although the involvement of CD147 in SARS-CoV-2 infection is still debated, it may represent a possible therapeutic target to challenge COVID-19 (55, 56). Furthermore, CD147 upregulates cytokine expression, stimulates oxidative stress in cardiomyocytes and promotes negative ionotropic effects (57). In cardiomyocytes, CD147 is a strong inducer of IL-18 that activates matrix metalloproteinases (MMPs) and circulating IL-18 levels positively correlates with AF development (58). MMP-9 increases extracellular matrix components degradation but can also activate TGF-β1, favoring myocardial adverse remodeling. Higher plasma levels of MMP-9 found in AF patients suggest that MMP-9 can be a marker of atrial remodeling (59). Interestingly, also in COVID-19 patients increased circulating MMP-9 is found (60). Although the role of this protease in tissue damage and repair at the pulmonary level remains to be clarified, the emerging picture is that the levels of MMP-9 increases during the course of the disease and correlates with the number of circulating inflammatory cells (61, 62).

The spike proteins of several coronaviruses bind to sialic acid on the cell surface (63). N-acetylneuraminic acid, the predominant sialic acid in human glycoproteins and gangliosides. By activating RhoA signaling, N-acetylneuraminic acid may trigger cardiac fibrosis and atrial enlargement, contributing to AF pathophysiology (64, 65).

Another promising marker involved in extracellular matrix formation is galectin-3 that plays a role in the progression of atrial fibrosis. It is expressed in fibroblasts, activated macrophages,

neutrophils and mast cells and participates in several processes involved in fibrogenesis. In AF, elevated levels of galectin-3 correlate with advanced disease and worse outcomes (66). Notably, galectin-3 levels are increased in serum of COVID-19 patients and correlates with COVID-19 severity (67, 68). Increased levels of aldosterone, another key player in adverse myocardial remodeling, are also found (67). A distinctive hallmark of SARS-CoV-2 infection is systemic immune cell over-activation, with an imbalance between T–helper–1 (Th1) and Th2 cells, elevated levels of IL-1β, IL-2, IL-6, IL-7, interferons, TNF-α, monocyte chemoattractant protein-1 and macrophage inflammatory protein-1A among others (69–72). At the cardiac level, pro-inflammatory cytokines, in particular IL-6, stimulates vascular smooth muscle proliferation, endothelial cell and platelets activation, and leads to apoptosis or necrosis of myocardial cells, which may mediate intra-atrial repolarization and conduction disturbances (73). Raised levels of IL-6 in COVID-19 deaths suggest that virus-driven hyper-inflammation is strictly correlated to and increased susceptibility to lethal arrhythmia (74). SARS-CoV-2, through its binding to ACE2, purinergic receptors and components of the complement-mediated pathway, also stimulates the formation of the Nod-like receptor pyrin domains-containing 3 (NLRP3) inflammasome (75, 76). The NLRP3 inflammasome, in turn, triggers an immune response that leads to a further release of pro-inflammatory cytokines, inflammatory cell death, and Ang II-mediated tissue remodeling (77). There is a causal link between activation of the NLRP3 inflammasome in atrial cardiomyocytes and AF development. The mechanisms underlying the pro-arrhythmic effects of NLRP3 inflammasome take account of abnormal diastolic RyR2-mediated sarcoplasmic reticulum Ca^{2+} release with generation of pro-arrhythmic delayed afterdepolarizations (DADs), continued activation of ultra-rapid delayed rectifier K^{+} current with action potential abbreviation, and atrial hypertrophy and fibrosis (27, 38, 78).

Another relevant pathophysiological component in patients with severe COVID-19 is endothelial dysfunction that may be related, in addition and in combination to cytokine network, to progression and worsening of AF episodes (79–81). The mechanisms are various and not completely understood. It has been hypothesized that a downregulation of ACE2 activates the kallikrein-bradykinin system, increasing vascular permeability to immune cells, which upon activated, produce reactive oxygen species, cytokine and vasoactive molecules release, which lead to endothelial cell dysfunction and loss (82, 83). Impairment of endothelium compartment by SARS-CoV-2, by amplifying the expression of pro-coagulative molecules (i.e., tissue factor) and reducing the level of endothelial antithrombotic molecules, may be responsible for an enhancement of the coagulation cascade (84).

Lastly, in COVID-19 as well as in other viral infection, the activation of sympathetic nervous system takes place (85, 86). The mechanisms linking the increase in the sympathetic tone to AF episodes can involve increase in Ca^{2+} influx and overload in cardiomyocytes. This elevates the frequency of spontaneous diastolic Ca^{2+} release *via* RyR with subsequent generation of DADs and action potentials, which increase the probability of AF events (87).

Overall, there are several common pathophysiological points between COVID-19 and AF, and a potential mechanistic link emerges as a valid working hypothesis. Additionally, pre-existing genetic background consisting of ion-channel and gap junctional protein abnormalities may form the molecular substrate that favors the abnormal conduction properties and electrical activity in the atrial myocardium.

2.3. AF management in COVID-19 patients

Deregulation of the coagulation system and the risk of thromboembolism are highly relevant for both AF and COVID-19. Pre-existing antithrombotic therapy may be associated with lower odds of COVID-19 death (88, 89). Although no specific therapy has been recommended, anticoagulant therapy is required. Systemic anticoagulants have been reported to reduce mortality in hospitalized patients with COVID-19 and symptoms of coagulation disorders (90). The use of non-vitamin K antagonist oral anticoagulants (NOACs) in hospitalized COVID-19 patients with AF is a therapeutic alternative (91).

However, clinical findings have demonstrated relevant interactions between COVID-19 drugs and anticoagulants. In particular, lopinavir/ritonavir, *via* cytochrome P450 CYP3A4, may increase the bleeding risk, and NOACs should be avoided (92). As heparins are not expected to interact, they may be considered a safe option. In addition to the antithrombotic effect, heparin anti-inflammatory actions are relevant in this setting (93).

There are few data on the efficacy of rhythm and rate control in patients with AF and COVID-19, and combination therapy with antiarrhythmics and anticoagulants is associated with substantial side effects (94). Cardioversion should be considered in patients with hemodynamic instability, and intravenous amiodarone is the antiarrhythmic drug of choice for rhythm control (95). Rate control may be achieved by intravenous diltiazem (96). In stable patients on antiviral treatment, the interruption of antiarrhythmic drugs is preferable while the initiation of rate control therapy with β-blockers or non-dihydropyridine calcium channel blockers allows the use of antiviral drugs without risk of prolongation of the QT interval (97). Generally, drug-drug interactions should be considered before starting therapy.

To date, it is not clear if AF events experienced by COVID-19 patients are transitory phenomena or they progress into permanent AF. Nonetheless, it remains critical to direct a strict focus to adverse effects of COVID-19 and plan specific screening for irregular heartbeats. To avoid complications, an accurate diagnosis of AF is crucial and remains a major challenge.

A randomized trial recruiting more than 1,000 patients with confirmed COVID-19 has demonstrated that therapeutic-dose anticoagulation does not affect the probability of survival to hospital discharge (98). Therefore, assessing the risk for anticoagulation measures by lowering therapeutic-dose anticoagulation in COVID-19 patients at high risk of AF is a strategy that is worth investigating, although it must be taken into account that AF, without adequate treatment, leads to serious complications.

2.4. Risk of drug-related cardiac arrhythmias during COVID-19 therapy

Pharmacological agents commonly used in COVID-19 patients may have a risk of inducing electrophysiological changes and severe and potentially fatal cardiac dysfunction, such as torsades de pointes, ventricular tachycardia and fibrillation (99).

Furthermore, patients with underlying heart disease such as inherited arrhythmia syndromes (long QT or Brugada syndromes) are predisposed to an increased risk of cardiac arrhythmias (100). The sum of pharmacotherapy and hereditary factors represents a hazardous combination of pro-arrhythmogenic effects. The use of lopinavir/ritonavir combination has been associated with and increased QT prolongation through a multichannel blocking properties (101). Ibrutinib, the first human Bruton's tyrosine kinase inhibitor (TKI), has been largely studied in hospitalized COVID-19 patients due to its potential to lessen lung inflammation and injury (102, 103). However, clinical data have revealed an increased risk of atrial and ventricular arrhythmias, sinoatrial arrest, and heart failure; therefore, patients on ibrutinib therapy must be carefully monitored (104). The postulated mechanism seems to be a disrupted Ca^{2+} handling in the myocardium, favoring DADs. Other TKIs exert *in vitro* inhibitory activity against SARS-CoV-2 (105), although patients treated with TKIs have experienced cardiac toxicity (106). This pro-arrhytmogenic effect may be related to a modulation of ionic channels (decreasing K^+ current amplitude, and interfering with Na^+ and Ca^{2+} currents).

Remdesivir is an antiviral drugs initially used in patients infected by Ebola virus, and authorized for treatment of COVID-19 disease in hospitalized patients (107). Few studies on remdesivir have pointed out its adverse effects on the cardiovascular system. COVID-19 patients with an oxygen saturation of less than 94% receiving intravenous remdesivir have experienced AF and adverse events are more prevalent in patients undergoing invasive ventilation. However, the interpretation is inconclusive due to small sample size, short follow-up and absence of a control group (108). In another study, elevated plasma concentration of remdesivir following intravenous administration significantly increased the risk of QT prolongation and torsades de pointes (109). The analysis of EudraVigilance database has revealed a two-fold increased risk of an adverse cardiac event associated with remdesivir in comparison with hydroxychloroquine and azithromycin. Cardiac arrhythmias are the most reported events (110). Additional evidence has shown that remdesivir, for its chemical structure of adenosine nucleotide analog and pharmacological profile, may act as a blocker of the atrioventricular node and be pro-arrhythmic especially in patients with structural heart disease (111). Thus, the use of other drugs and a pre-existing risk have to be considered to establish cardiovascular risk for patients with COVID-19 qualified for remdesivir treatment.

3. Conclusion

Although most of the symptoms in COVID-19 patients involve the respiratory system, a significant fraction of patients presents serious cardiovascular complications. Arrhythmias are one of the main cardiac manifestations of COVID-19 with AF being the most common form of arrhythmia in these patients. While the pathophysiology underlying AF onset in COVID-19 patients are incompletely understood, from the clinical and basic research emerges an array of common mechanisms in the onset of AF and COVID-19 development. A direct viral invasion of myocardial cells, systemic inflammation with the release of inflammatory cytokines and pro-fibrotic mediators, along with changes in ion channel physiology and local RAAS, have been noted.

Pharmacological agents commonly used in COVID-19 patients may carry a risk of inducing electrophysiological changes and the management of arrhythmias should be based on evidence-based guidelines, with consideration of severity of COVID-19, the nature of AF and the concomitant use of antimicrobial and anti-inflammatory drugs. Finally, "off label" or "new" drugs used in acute COVID-19, vaccines with favorable efficacy and safety profile, and residual risk related to the "long COVID syndrome," need attention also in the context of arrhythmic manifestations.

Author contributions

MD, KU, FR, and DC: conceptualization and writing. MD, CR, EC, and DC: literature collection and visualization. AD, PP, DT, GS, GP, GC, KU, LB, and DC: review and editing. All authors contributed to the article and approved the submitted version.

Funding

This review was supported by the Italian Ministry of Education, the University and Research grants [PRIN-2017XZMBYX (AD) and PRIN-2017NKB2N4 (LB)].

Conflict of interest

The authors declare that the research was conducted in the absence of any commercial or financial relationships that could be construed as a potential conflict of interest.

Publisher's note

References

1. Jee Y. WHO international health regulations emergency committee for the COVID-19 outbreak. *Epidemiol Health.* (2020) 42:E2020013. doi: 10.4178/epih.e2020013

2. WHO. *The World Health Organization COVID-19 Dashboard Provides Up-to-Date Epidemiological Data About the COVID-19 Pandemic*. Geneva: WHO (2020).

3. Mohanty S, Satapathy A, Naidu M, Mukhopadhyay S, Sharma S, Barton L, et al. Severe acute respiratory syndrome coronavirus-2 (SARS-CoV-2) and coronavirus disease 19 (COVID-19)–anatomic pathology perspective on current knowledge. *Diagn Pathol.* (2020) 15:103. doi: 10.1186/s13000-020-01017-8

4. Wu Z, McGoogan J. Characteristics of and important lessons from the coronavirus disease 2019 (COVID-19) outbreak in china: summary of a report of 72314 cases from the Chinese center for disease control and prevention. *JAMA.* (2020) 323:1239–42. doi: 10.1001/jama.2020.2648

5. Zhou F, Yu T, Du R, Fan G, Liu Y, Liu Z, et al. Clinical course and risk factors for mortality of adult inpatients with COVID-19 in Wuhan, China: a retrospective cohort study. *Lancet.* (2020) 395:1054–62. doi: 10.1016/S0140-6736(20)30566-3

6. Martínez-Rubio A, Ascoeta S, Taibi F, Soldevila J. Coronavirus disease 2019 and cardiac arrhythmias. *Eur Cardiol.* (2020) 15:e66. doi: 10.15420/ecr.2020.23

7. Shi S, Qin M, Shen B, Cai Y, Liu T, Yang F, et al. Association of cardiac injury with mortality in hospitalized patients with COVID-19 in Wuhan, China. *JAMA Cardiol.* (2020) 5:802–10. doi: 10.1001/jamacardio.2020.0950

8. Scavone C, Brusco S, Bertini M, Sportiello L, Rafaniello C, Zoccoli A, et al. Current pharmacological treatments for COVID-19: what's next? *Br J Pharmacol.* (2020) 177:4813–24. doi: 10.1111/bph.15072

9. Mascolo A, Scavone C, Rafaniello C, De Angelis A, Urbanek K, di Mauro G, et al. The role of renin-angiotensin-aldosterone system in the heart and lung: focus on COVID-19. *Front Pharmacol.* (2021) 12:667254. doi: 10.3389/fphar.2021.667254

10. Scavone C, Mascolo A, Rafaniello C, Sportiello L, Trama U, Zoccoli A, et al. Therapeutic strategies to fight COVID-19: which is the status artis? *Br J Pharmacol.* (2022) 179:2128–48. doi: 10.1111/bph.15452

11. Gopinathannair R, Merchant F, Lakkireddy D, Etheridge S, Feigofsky S, Han J, et al. COVID-19 and cardiac arrhythmias: a global perspective on arrhythmia characteristics and management strategies. *J Interv Card Electrophysiol.* (2020) 59:329–36. doi: 10.1007/s10840-020-00789-9

12. Liu F, Li L, Xu M, Wu J, Luo D, Zhu Y, et al. Prognostic value of interleukin-6, C-reactive protein, and procalcitonin in patients with COVID-19. *J Clin Virol.* (2020) 127:104370. doi: 10.1016/j.jcv.2020.104370

13. Tian W, Jiang W, Yao J, Nicholson C, Li R, Sigurslid H, et al. Predictors of mortality in hospitalized COVID-19 patients: a systematic review and meta-analysis. *J Med Virol.* (2020) 92:1875–83. doi: 10.1002/jmv.26050

14. Chung M, Martin D, Sprecher D, Wazni O, Kanderian A, Carnes C, et al. C-reactive protein elevation in patients with atrial arrhythmias: inflammatory mechanisms and persistence of atrial fibrillation. *Circulation.* (2001) 104:2886–91. doi: 10.1161/hc4901.101760

15. Hu L, Chen S, Fu Y, Gao Z, Long H, Ren H, et al. Risk factors associated with clinical outcomes in 323 coronavirus disease 2019 (COVID-19) hospitalized patients in Wuhan, China. *Clin Infect Dis.* (2020) 71:2089–98. doi: 10.1093/cid/ciaa539

16. Wang D, Hu B, Hu C, Zhu F, Liu X, Zhang J, et al. Clinical characteristics of 138 hospitalized patients with 2019 novel coronavirus-infected pneumonia in Wuhan, China. *JAMA.* (2020) 323:1061–9. doi: 10.1001/jama.2020.1585

17. Bhatla A, Mayer M, Adusumalli S, Hyman M, Oh E, Tierney A, et al. COVID-19 and cardiac arrhythmias. *Heart Rhythm.* (2020) 17:1439–44. doi: 10.1016/j.hrthm.2020.06.016

18. Benjamin E, Levy D, Vaziri S, D'Agostino R, Belanger A, Wolf P. Independent risk factors for atrial fibrillation in a population-based cohort. The Framingham heart study. *JAMA.* (1994) 271:840–4.

19. Roselli C, Rienstra M, Ellinor P. Genetics of atrial fibrillation in 2020: GWAS, genome sequencing, polygenic risk, and beyond. *Circ Res.* (2020) 127:21–33.

20. Miyasaka Y, Barnes M, Gersh B, Cha S, Bailey K, Abhayaratna W, et al. Secular trends in incidence of atrial fibrillation in Olmsted County, Minnesota, 1980 to 2000, and implications on the projections for future prevalence. *Circulation.* (2006) 114:119–25.

21. Molina C, Abu-Taha I, Wang Q, Roselló-Díez E, Kamler M, Nattel S, et al. Profibrotic, electrical, and calcium-handling remodeling of the atria in heart failure patients with and without atrial fibrillation. *Front Physiol.* (2018) 9:1383. doi: 10.3389/fphys.2018.01383

22. Pluteanu F, Nikonova Y, Holzapfel A, Herzog B, Scherer A, Preisenberger J, et al. Progressive impairment of atrial myocyte function during left ventricular hypertrophy and heart failure. *J Mol Cell Cardiol.* (2018) 114:253–63. doi: 10.1016/j.yjmcc.2017.11.020

23. Aistrup G, Arora R, Grubb S, Yoo S, Toren B, Kumar M, et al. Triggered intracellular calcium waves in dog and human left atrial myocytes from normal and failing hearts. *Cardiovasc Res.* (2017) 113:1688–99.

24. Xu J, Cui G, Esmailian F, Plunkett M, Marelli D, Ardehali A, et al. Atrial extracellular matrix remodeling and the maintenance of atrial fibrillation. *Circulation.* (2004) 109:363–8.

25. Ma J, Chen Q, Ma S. Left atrial fibrosis in atrial fibrillation: mechanisms, clinical evaluation and management. *J Cell Mol Med.* (2021) 25:2764–75.

26. Hindricks G, Potpara T, Dagres N, Arbelo E, Bax J, Blomström-Lundqvist C, et al. 2020 ESC Guidelines for the diagnosis and management of atrial fibrillation developed in collaboration with the European association for cardio-thoracic surgery (EACTS): the task force for the diagnosis and management of atrial fibrillation of the European society of cardiology (ESC) developed with the special contribution of the European heart rhythm association (EHRA) of the ESC. *Eur Heart J.* (2021) 42:373–498.

27. Yao C, Veleva T, Scott L Jr., Cao S, Li L, Chen G, et al. Enhanced cardiomyocyte NLRP3 inflammasome signaling promotes atrial fibrillation. *Circulation.* (2018) 138:2227–42.

28. Sirish P, Li N, Timofeyev V, Zhang X, Wang L, Yang J, et al. Molecular mechanisms and new treatment paradigm for atrial fibrillation. *Circ Arrhythm Electrophysiol.* (2016) 9:e003721. doi: 10.1161/CIRCEP.115.003721

29. Harhay J, Khan M, Shah S, Malhotra A. SARS-COV-2 presenting as new onset atrial fibrillation: a case report. *Cureus.* (2020) 12:e8054.

30. Inciardi R, Adamo M, Lupi L, Cani D, Di Pasquale M, Tomasoni D, et al. Characteristics and outcomes of patients hospitalized for COVID-19 and cardiac disease in Northern Italy. *Eur Heart J.* (2020) 41:1821–9. doi: 10.1093/eurheartj/ehaa388

31. Spinoni E, Mennuni M, Rognoni A, Grisafi L, Colombo C, Lio V, et al. Contribution of atrial fibrillation to in-hospital mortality in patients with COVID-19. *Circ Arrhythm Electrophysiol.* (2021) 14:e009375. doi: 10.1161/CIRCEP.120.009375

32. Colon C, Barrios J. Atrial arrhythmias in COVID-19 patients. *JACC Clin Electrophysiol.* (2021) 6:1189–90. doi: 10.1016/j.jacep.2020.05.015

33. Musikantow D. Atrial fibrillation in patients hospitalized with COVID-19: incidence, predictors, outcomes, and comparison to influenza. *JACC Clin Electrophysiol.* (2021) 7:1120–30. doi: 10.1016/j.jacep.2021.02.009

34. Tirandi A, Ramoni D, Montecucco F, Liberale L. Predicting mortality in hospitalized COVID-19 patients. *Intern Emerg Med.* (2022) 17:1571–4. doi: 10.1007/s11739-022-03017-6

35. Niedziela J, Jaroszewicz J, Wita K, Cieśla D, Gąsior M. High in-hospital and post-discharge mortality in patients with a pre-existing diagnosis of heart failure hospitalized due to COVID-19. *Kardiol Pol.* (2022) 80:90–2. doi: 10.33963/KP.a2021.0163

36. Maisano A, Vitolo M, Imberti J, Bonini N, Albini A, Valenti A, et al. Atrial fibrillation in the setting of acute pneumonia: not a secondary arrhythmia. *Rev Cardiovasc Med.* (2022) 23:176. doi: 10.31083/j.rcm2305176

37. Wang R, Macha K, Haupenthal D, Gaßmann L, Siedler G, Stoll S, et al. Acute care and secondary prevention of stroke with newly detected versus known atrial fibrillation. *Eur J Neurol.* (2022) 29:1963–71. doi: 10.1111/ene.15338

38. Young L, Antwi-Boasiako S, Ferrall J, Wold L, Mohler P, El Refaey M. Genetic and non-genetic risk factors associated with atrial fibrillation. *Life Sci.* (2022) 299:120529. doi: 10.1016/j.lfs.2022.120529

39. El-Arif G, Khazaal S, Farhat A, Harb J, Annweiler C, Wu Y, et al. Angiotensin II type I receptor (AT1R): the gate towards COVID-19-associated diseases. *Molecules.* (2022) 27:2048. doi: 10.3390/molecules27072048

40. García-Escobar A, Vera-Vera S, Jurado-Román A, Jiménez-Valero S, Galeote G, Moreno R. Calcium signaling pathway is involved in the shedding of ACE2 catalytic ectodomain: new insights for clinical and therapeutic applications of ACE2 for COVID-19. *Biomolecules.* (2022) 12:76. doi: 10.3390/biom12010076

41. Samavati L, Uhal B. ACE2, much more than just a receptor for SARS-COV-2. *Front Cell Infect Microbiol.* (2020) 10:317. doi: 10.3389/fcimb.2020.00317

42. Avolio E, Carrabba M, Milligan R, Kavanagh Williamson M, Beltrami A, Gupta K, et al. The SARS-CoV-2 Spike protein disrupts human cardiac pericytes function through CD147 receptor-mediated signalling: a potential non-infective mechanism of COVID-19 microvascular disease. *Clin Sci (Lond).* (2021) 135:2667–89. doi: 10.1042/CS20210735

43. Hoffmann M, Kleine-Weber H, Schroeder S, Krüger N, Herrler T, Erichsen S, et al. SARS-CoV-2 cell entry depends on ACE2 and TMPRSS2 and is blocked by a clinically proven protease inhibitor. *Cell.* (2020) 181:271–80.e8. doi: 10.1016/j.cell.2020.02.052

44. Goudis C, Kallergis E, Vardas P. Extracellular matrix alterations in the atria: insights into the mechanisms and perpetuation of atrial fibrillation. *Europace.* (2012) 14:623–30. doi: 10.1093/europace/eur398

45. Rodrigues R, Costa de Oliveira S. The impact of angiotensin-converting enzyme 2 (ACE2) expression levels in patients with comorbidities on COVID-19 severity: a comprehensive review. *Microorganisms.* (2021) 9:1692. doi: 10.3390/microorganisms9081692

46. Lu Y, Chen Y, Kao Y, Wu T, Chen S, Chen Y. Extracellular matrix of collagen modulates intracellular calcium handling and electrophysiological characteristics of HL-1 cardiomyocytes with activation of angiotensin II type 1 receptor. *J Card Fail.* (2011) 17:82–90. doi: 10.1016/j.cardfail.2010.10.002

47. Fong S, Agrawal S, Gong M, Zhao J. Modulated calcium homeostasis and release events under atrial fibrillation and its risk factors: a meta-analysis. *Front Cardiovasc Med.* (2021) 8:662914. doi: 10.3389/fcvm.2021.662914

48. Ferrario C, Ahmad S, Groban L. Mechanisms by which angiotensin-receptor blockers increase ACE2 levels. *Nat Rev Cardiol.* (2020) 17:378. doi: 10.1038/s41569-020-0387-7

49. Blume C, Jackson C, Spalluto C, Legebeke J, Nazlamova L, Conforti F, et al. A novel ACE2 isoform is expressed in human respiratory epithelia and is upregulated in response to interferons and RNA respiratory virus infection. *Nat Genet.* (2021) 53:205–14. doi: 10.1038/s41588-020-00759-x

50. Gheware A, Ray A, Rana D, Bajpai P, Nambirajan A, Arulselvi S, et al. ACE2 protein expression in lung tissues of severe COVID-19 infection. *Sci Rep.* (2022) 12:4058. doi: 10.1038/s41598-022-07918-6

51. Iwasaki M, Saito J, Zhao H, Sakamoto A, Hirota K, Ma D. Inflammation triggered by SARS-CoV-2 and ACE2 augment drives multiple organ failure of severe COVID-19: molecular mechanisms and implications. *Inflammation.* (2021) 44:13–34. doi: 10.1007/s10753-020-01337-3

52. Zou X, Chen K, Zou J, Han P, Hao J, Han Z. Single-cell RNA-seq data analysis on the receptor ACE2 expression reveals the potential risk of different human organs vulnerable to 2019-nCoV infection. *Front Med.* (2020) 14:185–92. doi: 10.1007/s11684-020-0754-0

53. Behl T, Kaur I, Aleya L, Sehgal A, Singh S, Sharma N, et al. CD147-spike protein interaction in COVID-19: get the ball rolling with a novel receptor and therapeutic target. *Sci Total Environ.* (2021) 808:152072. doi: 10.1016/j.scitotenv.2021.152072

54. Wang K, Chen W, Zhang Z, Deng Y, Lian J, Du P, et al. CD147-spike protein is a novel route for SARS-CoV-2 infection to host cells. *Signal Transduct Target Ther.* (2020) 5:283. doi: 10.1038/s41392-020-00426-x

55. Fenizia C, Galbiati S, Vanetti C, Vago R, Clerici M, Tacchetti C, et al. SARS-CoV-2 entry: at the crossroads of CD147 and ACE2. *Cells.* (2021) 10:1434. doi: 10.3390/cells10061434

56. Mahdian S, Zarrabi M, Panahi Y, Dabbagh S. Repurposing FDA-approved drugs to fight COVID-19 using in silico methods: targeting SARS-CoV-2 RdRp enzyme and host cell receptors (ACE2, CD147) through virtual screening and molecular dynamic simulations. *Inform Med Unlocked.* (2021) 23:100541. doi: 10.1016/j.imu.2021.100541

57. Peng X, Wang Y, Xi X, Jia Y, Tian J, Yu B, et al. Promising therapy for heart failure in patients with severe COVID-19: calming the cytokine storm. *Cardiovasc Drugs Ther.* (2021) 35:231–47. doi: 10.1007/s10557-020-07120-8

58. Pituch-Noworolska A. NK cells in SARS-CoV-2 infection. *Cent Eur J Immunol.* (2022) 47:95–101. doi: 10.5114/ceji.2022.113078

59. Li X, Guo X, Chang Y, Zhang N, Sun Y. Analysis of alterations of serum inflammatory cytokines and fibrosis makers in patients with essential hypertension and left ventricular hypertrophy and the risk factors. *Am J Transl Res.* (2022) 14:4097–103.

60. Ueland T, Holter J, Holten A, Müller K, Lind A, Bekken G, et al. Distinct and early increase in circulating MMP-9 in COVID-19 patients with respiratory failure. *J Infect.* (2020) 81:e41–3. doi: 10.1016/j.jinf.2020.06.061

61. Gelzo M, Cacciapuoti S, Pinchera B, Rosa AD, Cernera G, Scialò F, et al. Matrix metalloproteinases (MMP) 3 and 9 as biomarkers of severity in COVID-19 patients. *Sci Rep.* (2022) 12:1212. doi: 10.1038/s41598-021-04677-8

62. Savic G, Stevanovic I, Mihajlovic D, Jurisevic M, Gajovic N, Jovanovic I, et al. MMP-9/BDNF ratio predicts more severe COVID-19 outcomes. *Int J Med Sci.* (2022) 19:1903–11. doi: 10.7150/ijms.75337

63. Matrosovich M, Herrler G, Klenk H. Sialic acid receptors of viruses. *Top Curr Chem.* (2015) 367:1–28. doi: 10.1007/128_2013_466

64. Hu W, Xie J, Zhu T, Meng G, Wang M, Zhou Z, et al. Serum N-acetylneuraminic acid is associated with atrial fibrillation and left atrial enlargement. *Cardiol Res Pract.* (2020) 2020:1358098. doi: 10.1155/2020/1358098

65. Kochi A, Tagliari A, Forleo G, Fassini G, Tondo C. Cardiac and arrhythmic complications in patients with COVID-19. *J Cardiovasc Electrophysiol.* (2020) 31:1003–8. doi: 10.1111/jce.14479

66. Clementy N, Piver E, Bisson A, Andre C, Bernard A, Pierre B, et al. Galectin-3 in atrial fibrillation: mechanisms and therapeutic implications. *Int J Mol Sci.* (2018) 19:976. doi: 10.3390/ijms19040976

67. Cannavo A, Liccardo D, Gelzo M, Amato F, Gentile I, Pinchera B, et al. Serum galectin-3 and aldosterone: potential biomarkers of cardiac complications in patients with COVID-19. *Minerva Endocrinol.* (2022) 47:270–8. doi: 10.23736/S2724-6507.22.03789-7

68. Cervantes-Alvarez E, la Rosa N, la Mora M, Valdez-Sandoval P, Palacios-Jimenez M, Rodriguez-Alvarez F, et al. Galectin-3 as a potential prognostic biomarker of severe COVID-19 in SARS-CoV-2 infected patients. *Sci Rep.* (2022) 12:1856. doi: 10.1038/s41598-022-05968-4

69. Tang D, Comish P, Kang R. The hallmarks of COVID-19 disease. *PLoS Pathog.* (2020) 16:e1008536. doi: 10.1371/journal.ppat.1008536

70. Farahani M, Niknam Z, Mohammadi Amirabad L, Amiri-Dashatan N, Koushki M, Nemati M, et al. Molecular pathways involved in COVID-19 and potential pathway-based therapeutic targets. *Biomed Pharmacother.* (2022) 145:112420. doi: 10.1016/j.biopha.2021.112420

71. Aleebrahim-Dehkordi E, Molavi B, Mokhtari M, Deravi N, Fathi M, Fazel T, et al. T helper type (Th1/Th2) responses to SARS-CoV-2 and influenza A (H1N1) virus: from cytokines produced to immune responses. *Transpl Immunol.* (2022) 70:101495. doi: 10.1016/j.trim.2021.101495

72. Mazzoni A, Salvati L, Maggi L, Annunziato F, Cosmi L. Hallmarks of immune response in COVID-19: exploring dysregulation and exhaustion. *Semin Immunol.* (2021) 55:101508. doi: 10.1016/j.smim.2021.101508

73. Li S, Wang J, Yan Y, Zhang Z, Gong W, Nie S. Clinical characterization and possible pathological mechanism of acute myocardial injury in COVID-19. *Front Cardiovasc Med.* (2022) 9:862571. doi: 10.3389/fcvm.2022.862571

74. Shukla, A, Misra S. Antimicrobials in COVID-19: strategies for treating a COVID-19 pandemic. *J Basic Clin Physiol Pharmacol.* (2022). doi: 10.1515/jbcpp-2022-0061

75. Che Mohd Nassir C, Zolkefley M, Ramli M, Norman H, Abdul Hamid H, Mustapha M. Neuroinflammation and COVID-19 ischemic stroke recovery-evolving evidence for the mediating roles of the ACE2/angiotensin-(1-7)/Mas receptor axis and NLRP3 inflammasome. *Int J Mol Sci.* (2022) 23:3085. doi: 10.3390/ijms23063085

76. Rodrigues T, de Sá K, Ishimoto A, Becerra A, Oliveira S, Almeida L, et al. Inflammasomes are activated in response to SARS-CoV-2 infection and are associated with COVID-19 severity in patients. *J Exp Med.* (2021) 218:e20201707. doi: 10.1084/jem.20201707

77. Caporali S, De Stefano A, Calabrese C, Giovannelli A, Pieri M, Savini I, et al. Anti-inflammatory and active biological properties of the plant-derived bioactive compounds luteolin and luteolin 7-glucoside. *Nutrients.* (2022) 14:1155. doi: 10.3390/nu14061155

78. Saljic A, Heijman J, Dobrev D. Emerging antiarrhythmic drugs for atrial fibrillation. *Int J Mol Sci.* (2022) 23:4096. doi: 10.3390/ijms23084096

79. Ruhl L, Pink I, Kühne J, Beushausen K, Keil J, Christoph S, et al. Endothelial dysfunction contributes to severe COVID-19 in combination with dysregulated lymphocyte responses and cytokine networks. *Signal Transduct Target Ther.* (2021) 6:418. doi: 10.1038/s41392-021-00819-6

80. Nägele M, Haubner B, Tanner F, Ruschitzka F, Flammer A. Endothelial dysfunction in COVID-19: current findings and therapeutic implications. *Atherosclerosis.* (2020) 314:58–62. doi: 10.1016/j.atherosclerosis.2020.10.014

81. Otifi H, Adiga B. Endothelial dysfunction in covid-19 infection. *Am J Med Sci.* (2022) 363:281–7. doi: 10.1016/j.amjms.2021.12.010

82. Cooper S, Boyle E, Jefferson S, Heslop C, Mohan P, Mohanraj G, et al. Role of the renin-angiotensin-aldosterone and Kinin-Kallikrein systems in the cardiovascular complications of COVID-19 and long COVID. *Int J Mol Sci.* (2021) 22:8255. doi: 10.3390/ijms22158255

83. Bittner Z, Schrader M, George S, Amann R. Pyroptosis and its role in SARS-CoV-2 infection. *Cells.* (2022) 11:1717. doi: 10.3390/cells11101717

84. Chen A, Wang C, Zhu W, Chen W. Coagulation disorders and thrombosis in COVID-19 patients and a possible mechanism involving endothelial cells: a review. *Aging Dis.* (2022) 13:144–56. doi: 10.14336/AD.2021.0704

85. Fischer L, Barop H, Ludin S, Schaible H. Regulation of acute reflectory hyperinflammation in viral and other diseases by means of stellate ganglion block. A conceptual view with a focus on covid-19. *Auton Neurosci.* (2022) 237:102903. doi: 10.1016/j.autneu.2021.102903

86. Stute N, Stickford J, Province V, Augenreich M, Ratchford S, Stickford A. COVID-19 is getting on our nerves: sympathetic neural activity and haemodynamics in young adults recovering from SARS-CoV-2. *J Physiol.* (2021) 599:4269–85. doi: 10.1113/JP281888

87. Bers D. Cardiac excitation-contraction coupling. *Nature.* (2022) 415:198–205. doi: 10.1038/415198a

88. Raatikainen P, Lassila R. COVID-19: another reason for anticoagulation in patients with atrial fibrillation. *Heart.* (2022) 108:902–4. doi: 10.1136/heartjnl-2022-320845

89. Gawałko M, Kapłon-Cieślicka A, Hohl M, Dobrev D, Linz D. COVID-19 associated atrial fibrillation: incidence, putative mechanisms and potential clinical implications. *Int J Cardiol Heart Vasc.* (2020) 30:100631. doi: 10.1016/j.ijcha.2020.100631

90. Qin W, Dong F, Zhang Z, Hu B, Chen S, Zhu Z, et al. Low molecular weight heparin and 28-day mortality among patients with coronavirus disease 2019: a cohort study in the early epidemic era. *Thromb Res.* (2021) 198:19–22. doi: 10.1016/j.thromres.2020.11.020

91. Russo V, Rago A, Carbone A, Bottino R, Ammendola E, Della Cioppa N, et al. Atrial fibrillation in COVID-19: from epidemiological association to pharmacological implications. *J Cardiovasc Pharmacol.* (2020) 76:138–45. doi: 10.1097/FJC.0000000000000854

92. Gronich N, Stein N, Muszkat M. Association between use of pharmacokinetic-interacting drugs and effectiveness and safety of direct acting oral anticoagulants: nested case-control study. *Clin Pharmacol Ther.* (2021) 110:1526–36. doi: 10.1002/cpt.2369

93. Lindahl U, Li J. Heparin–an old drug with multiple potential targets in covid-19 therapy. *J Thromb Haemost.* (2020) 18:2422–4. doi: 10.1111/jth.14898

94. Harrison S, Fazio-Eynullayeva E, Lane D, Underhill P, Lip G. Atrial fibrillation and the risk of 30-day incident thromboembolic events, and mortality in adults $\geq$ 50 years with COVID-19. *J Arrhythm.* (2020) 37:231–7. doi: 10.1002/joa3.12458

95. Shah D, Umar Z, Ilyas U, Nso N, Zirkiyeva M, Rizzo V. New-onset atrial fibrillation in COVID-19 infection: a case report and review of literature. *Cureus.* (2022) 14:e23912. doi: 10.7759/cureus.23912

96. Marcianò G, Roberti R, Palleria C, Mirra D, Rania V, Casarella A, et al. SARS-CoV-2 treatment: current therapeutic options and the pursuit of tailored therapy. *Appl Sci.* (2021) 11:7457. doi: 10.3390/app11167457

97. Karamchandani K, Quintili A, Landis T, Bose S. Cardiac arrhythmias in critically Ill patients with COVID-19: a brief review. *J Cardiothorac Vasc Anesth.* (2021) 35:3789–96. doi: 10.1053/j.jvca.2020.08.013

98. REMAP-CAP Investigators, ACTIV-4a Investigators, ATTACC Investigators, Goligher E, Bradbury C, McVerry B, et al. Therapeutic anticoagulation with heparin in critically ill patients with covid-19. *N Engl J Med.* (2021) 385:777–89. doi: 10.1056/NEJMoa2103417

99. Gasperetti A, Schiavone M, Tondo C, Mitacchione G, Viecca M, Galli M, et al. QT interval monitoring and drugs management during COVID-19 pandemic. *Curr Rev Clin Exp Pharmacol.* (2021) 16:306–17. doi: 10.2174/1574884715666201224155042

100. Wu C, Postema P, Arbelo E, Behr E, Bezzina C, Napolitano C, et al. SARS-CoV-2, COVID-19, and inherited arrhythmia syndromes. *Heart Rhythm.* (2020) 17:1456–62. doi: 10.1016/j.hrthm.2020.03.024

101. Fresse A, Viard D, Romani S, Gérard A, Lepelley M, Rocher F, et al. Spontaneous reported cardiotoxicity induced by lopinavir/ritonavir in COVID-19. An alleged past-resolved problem. *Int J Cardiol.* (2021) 324:255–60. doi: 10.1016/j.ijcard.2020.10.028

102. Thibaud S, Tremblay D, Bhalla S, Zimmerman B, Sigel K, Gabrilove J. Protective role of Bruton tyrosine kinase inhibitors in patients with chronic lymphocytic leukaemia and COVID-19. *Br J Haematol.* (2020) 190:e73–6. doi: 10.1111/bjh.16863

103. Treon S, Castillo J, Skarbnik A, Soumerai J, Ghobrial I, Guerrera M. The BTK inhibitor ibrutinib may protect against pulmonary injury in COVID-19-infected patients. *Blood.* (2020) 135:1912–5. doi: 10.1182/blood.2020006288

104. Salem J, Manouchehri A, Bretagne M, Lebrun-Vignes B, Groarke J, Johnson D, et al. Cardiovascular toxicities associated with ibrutinib. *J Am Coll Cardiol.* (2019) 74:1667–78. doi: 10.1016/j.jacc.2019.07.056

105. Coleman C, Sisk J, Mingo R, Nelson E, White J, Frieman M. Abelson kinase inhibitors are potent inhibitors of severe acute respiratory syndrome coronavirus and Middle East respiratory syndrome coronavirus fusion. *J Virol.* (2016) 90:8924–33. doi: 10.1128/jvi.01429-16

106. Hartmann J, Haap M, Kopp H, Lipp H. Tyrosine kinase inhibitors–a review on pharmacology, metabolism and side effects. *Curr Drug Metab.* (2009) 10:470–81. doi: 10.2174/138920009788897975

107. Malin J, Suárez I, Priesner V, Fätkenheuer G, Rybniker J. Remdesivir against COVID-19 and other viral diseases. *Clin Microbiol Rev.* (2020) 34:e162–120. doi: 10.1128/CMR.00162-20

108. Grein J, Ohmagari N, Shin D, Diaz G, Asperges E, Castagna A, et al. Compassionate use of Remdesivir for patients with severe covid-19. *N Engl J Med.* (2020) 382:2327–36. doi: 10.1056/NEJMoa2007016

109. Michaud V, Dow P, Al Rihani S, Deodhar M, Arwood M, Cicali B, et al. Risk assessment of drug-induced long QT syndrome for some COVID-19 repurposed drugs. *Clin Transl Sci.* (2021) 14:20–8. doi: 10.1111/cts.12882

110. Rafaniello C, Ferrajolo C, Sullo M, Gaio M, Zinzi A, Scavone C, et al. Cardiac events potentially associated to Remdesivir: an analysis from the European spontaneous adverse event reporting system. *Pharmaceuticals (Basel).* (2021) 14:611. doi: 10.3390/ph14070611

111. Bistrovic P, Lucijanic M. Remdesivir might induce changes in electrocardiogram beyond bradycardia in patients with coronavirus disease 2019-the pilot study. *J Med Virol.* (2021) 93:5724–5. doi: 10.1002/jmv.27177

frontiers | Frontiers in Cardiovascular Medicine

TYPE Original Research
PUBLISHED 16 June 2023
DOI 10.3389/fcvm.2023.1156353

OPEN ACCESS

EDITED BY
Pietro Enea Lazzerini,
University of Siena, Italy

REVIEWED BY
Pengchao Tian,
Chinese Academy of Medical Sciences and Peking Union Medical College, China
Paolo Sciarrone,
Gabriele Monasterio Tuscany Foundation (CNR), Italy

*CORRESPONDENCE
Takatoshi Kasai
kasai-t@mx6.nisiq.net

RECEIVED 01 February 2023
ACCEPTED 08 June 2023
PUBLISHED 16 June 2023

CITATION
Naito R, Kasai T, Tomita Y, Kasagi S, Narui K and Momomura S-I (2023) Clinical outcomes of chronic heart failure patients with unsuppressed sleep apnea by positive airway pressure therapy.
Front. Cardiovasc. Med. 10:1156353.
doi: 10.3389/fcvm.2023.1156353

Clinical outcomes of chronic heart failure patients with unsuppressed sleep apnea by positive airway pressure therapy

Ryo Naito[1,2], Takatoshi Kasai[1,2,3]*, Yasuhiro Tomita[3], Satoshi Kasagi[3], Koji Narui[3] and Shin-Ichi Momomura[4]

[1]Department of Cardiovascular Biology and Medicine, Juntendo University Graduate School of Medicine, Tokyo, Japan, [2]Cardiovascular Respiratory Sleep Medicine, Juntendo University Graduate School of Medicine, Tokyo, Japan, [3]Sleep Center, Toranomon Hospital, Tokyo, Japan, [4]Department of Medicine, Saitama Citizens Medical Center, Saitama, Japan

Introduction: Heart failure (HF) is an advanced stage of cardiac disease and is associated with a high rate of mortality. Previous studies have shown that sleep apnea (SA) is associated with a poor prognosis in HF patients. Beneficial effects of PAP therapy that is effective on reducing SA on cardiovascular events, were not yet established. However, a large-scale clinical trial reported that patients with central SA (CSA) which was not effectively suppressed by continuous positive airway pressure (CPAP) revealed poor prognosis. We hypothesize that unsuppressed SA by CPAP is associated with negative consequences in patients with HF and SA, including either obstructive SA (OSA) or CSA.

Methods: This was a retrospective observational study. Patients with stable HF, defined as left ventricular ejection fraction of ≤50%; New York Heart Association class ≥ II; and SA [apnea–hypopnea index (AHI) of ≥15/h on overnight polysomnography], treated with CPAP therapy for 1 month and performed sleep study with CPAP were enrolled. The patients were classified into two groups according to AHI on CPAP (suppressed group: residual AHI ≥ 15/h; and unsuppressed group: residual AHI < 15/h). The primary endpoint was a composite of all-cause death and hospitalization for HF.

Results: Overall, data of 111 patients including 27 patients with unsuppressed SA, were analyzed. The cumulative event-free survival rates were lower in the unsuppressed group during a period of 36.6 months. A multivariate Cox proportional hazard model showed that the unsuppressed group was associated with an increased risk for clinical outcomes (hazard ratio 2.30, 95% confidence interval 1.21–4.38, $p = 0.011$).

Conclusion: Our study suggested that in patients with HF and SA including either OSA or CSA, presence of unsuppressed SA even on CPAP was associated with worse prognosis as compared to those with suppressed SA by CPAP.

KEYWORDS

heart failure, unsuppressed sleep apnea, continuous positive airway pressure therapy, death, clinical outcome

Introduction

Heart failure (HF) is an advanced stage of cardiac disease and is associated with a high rate of mortality (1, 2). Detection of patients' backgrounds that contribute to an increased risk of mortality could aid in improving survival rates in HF patients. Several studies have reported that the presence of sleep apnea (SA) is associated with a poor prognosis in patients with HF

(3). Continuous positive airway pressure (CPAP) therapy for SA, either obstructive or central SA (OSA and CSA, respectively) can improve cardiac function and probably clinical outcomes in those patients (4–7). However, a large-scale clinical trial reported patients with CSA which was not effectively suppressed by CPAP revealed poor prognosis (8). Only one study suggested such relationship between unsuppressed CSA and poor prognosis and there are no studies showing unsuppressed OSA by CPAP in patients with HF. We hypothesize that unsuppressed SA including either OSA or CSA by CPAP, is associated with negative consequences in patients with HF and SA. Therefore, we investigated that the prognosis of patients with unsuppressed SA by CPAP therapy in HD patients with SA including either OSA and CSA.

Materials and methods

Study population

Consecutive patients with HF and moderate to severe SA who were followed up at the cardiovascular center of Toranomon Hospital (Tokyo, Japan) between January 1, 2001, and March 1, 2005, were enrolled in the study.

The inclusion criteria were as follows: (1) HF with mildly reduced ejection fraction (HFmrEF) or those with reduced ejection fraction (HFrEF) on echocardiography within 1 month before the diagnostic sleep study and New York Heart Association (NYHA) class II or above; (2) stable clinical status, defined as no hospital admissions within 1 month before study enrollment and receiving optimal medical therapy for at least 1 month before study enrollment; (3) having undergone a diagnostic sleep study and received a diagnosis of moderate-to-severe SA, which was defined as an AHI ≥15; (4) receiving CPAP therapy and another sleep study with CPAP on 1 month after initiation. The exclusion criteria were as follows: (1) age below 20 or above 80 years, (2) presence of known untreated neoplasms, (3) history of stroke with neurologic deficits, and (4) history of severe chronic pulmonary diseases.

They were classified into two groups according to the AHI on CPAP (unsuppressed group, residual AHI ≥ 15/h; and suppressed group, residual AHI < 15/h). Informed consent was obtained from all the patients who participated in the study. The study was conducted in compliance with the Declaration of Helsinki and in accordance with the ethics policies of the institutions involved.

Sleep study and CPAP

As sleep studies, overnight polysomnography was performed according to standard protocol and criteria (9). Electrocardiograms, electroencephalograms, electrooculograms, and electromyograms were performed, and thoracoabdominal motion was monitored using respiratory inductance plethysmography. Air flow was measured using an oronasal thermal airflow sensor and nasal pressure cannula or through nasal mask when sleep studies were done with CPAP, and oxyhemoglobin saturation (SO_2) was monitored using oximetry. Respiratory events (i.e., apneas or hypopneas) were scored according to the American Academy of Sleep Medicine (AASM) scoring manual 2020 updates (10). Apnea with and without ribcage and/or abdominal movement was defined as obstructive and central apnea, respectively. Hypopnea was classified as obstructive if any of the following conditions existed: (1) paradoxical chest and abdominal movement during hypopnea events, (2) snoring during hypopnea events, or (3) flow limitation. Otherwise, the hypopneas were classified as central. We defined patients with predominantly CSA as having an AHI of ≥15/h, of which >50% were central events (5). All patients were offered CPAP therapy after the diagnosis of moderate to severe SA. The CPAP was titrated to determine the appropriate pressure level for each patient. In patients whose apnea or hypopnea could not effectively suppressed, the best pressure level which can well control obstructive respiratory events was determined. Patients were instructed to use the device with that pressure level while sleeping at home. One month after initiation of CPAP, patients underwent another polysomnography with CPAP and data from the polysomnography was used as baseline data on CPAP in the present study. Patients who stopped using CPAP after polysomnography with CPAP was determined as CPAP dropout cases.

Other data

The following variables were obtained from the clinical chart at the time of polysomnography with CPAP: body mass index (BMI); blood pressure (BP); heart rate; LVEF on echocardiograms; plasma norepinephrine (PNE) and brain natriuretic peptide (BNP) levels; NYHA class; etiology of HF; the presence of atrial fibrillation (AF); and administered drugs. The frequency of death and hospitalization was also assessed. The end point was a composite of death and hospitalization. Follow-up ended on March, 2006, and the prognosis was assessed by analyzing the medical records of patients who died and of those who continued to be followed up at our hospital. Information about the circumstances and the date of death was obtained from the families of patients who died at home. The reasons for hospitalization or the causes of death were determined from the institutions to which the patients had been admitted.

Statistical analysis

The data of all variables were presented as mean ± standard deviation or median and interquartile range. The baseline characteristics were compared using Student's *t*-test or the Mann–Whitney *U*-test for continuous variables, while the χ^2 test or Fisher's exact test was used for categorical variables. Event-free survival between the groups was compared using the Kaplan–Meier estimate with the log-rank test, and hazard ratios (HRs) were calculated using the Cox proportional hazards model. Median follow-up time was calculated from the Kaplan-Meier product-limit estimates of the survival function. Univariate analysis was based on the proportional hazards model to determine the associations between prognosis and the following variables obtained at the time of polysomnography with CPAP:

age, sex, BMI, AF etiology of HF, NYHA class, systolic or diastolic BP, heart rate, LVEF, BNP and PNE levels, sleep study data on CPAP such as total sleep time (TST), percentage of slow wave sleep and rapid eye movement (REM) sleep per TST, arousal index, percentage of time spent $SO_2 < 90\%$ (%TST $SO_2 < 90\%$), lowest SO_2, percentages of central AHI over total AHI (% central/total AHI), unsuppressed SA, and CPAP dropout cases. Variables with a p value below 0.1 in univariate analysis were included in multivariate analysis. Statistical significance was set at $p < 0.05$. All statistical analyses were performed using a statistical software package (SPSS, version 11.0 for Windows; SPSS Inc., Chicago, IL).

Results

A total of 111 patients were enrolled in this study. Fifty patients had the primary outcomes (18 and 32 in the unsuppressed and the suppressed groups, respectively with the median follow-up period of 36.6 months. Characteristics of the patients are shown in Table 1. The unsuppressed group tended to be older and have lower diastolic BP, and have significantly higher PNE level than the suppressed group. A prevalence of atrial fibrillation was significantly higher in the unsuppressed group. However, there were no difference in other baseline characteristics between two groups. Polysomnographic data for diagnostic and on CPAP studies were shown in Table 2. On the diagnostic study, in unsuppressed group, total AHI was significantly greater with a higher %central/total AHI. Indeed, percentage of predominant CSA on diagnostic study was significantly high in unsuppressed group (77.8% in unsuppressed group vs. 29.8% in suppressed group, $p < 0.001$). In addition, percentage of slow wave sleep per TST was significantly lower in the unsuppressed group. In both groups, all parameters were significantly improved by CPAP except for the increased %central/total AHI and no changes in TST. Comparing on CPAP study data (i.e., baseline data for the survival analyses), AHI on CPAP was significantly higher with higher %central/toral AHI on CPAP and with more hypoxic burden. Following on CPAP study, 13 patients (15.5%) in the suppressed group and 7 patients (25.9%) in the unsuppressed group dropped out from their CPAP therapy ($p = 0.345$).

Kaplan-Meier estimation of cumulative event-free survival for all-cause mortality and hospitalization for HF revealed a significantly worse clinical outcome in the unsuppressed group compared to the suppressed group (log-rank test $p < 0.001$) (Figure 1). A multivariate Cox proportional hazard model showed that unsuppressed SA in addition to AF and CPAP dropout were associated with an increased risk for clinical outcomes (Table 3).

TABLE 1 Baseline characteristics of patients in the two groups.

	Suppressed ($n = 84$)	Unsuppressed ($n = 27$)	p
Age, years	60.9 ± 13.2	66.4 ± 11.6	0.054
Male sex, n (%)	80 (95.2)	24 (88.8)	0.358
BMI, kg/m^2	26.4 ± 6.0	27.6 ± 6.1	0.397
Ischemic etiology, n (%)	24 (28.6)	8 (30.0)	0.916
AF, n (%)	28 (33.3)	17 (63.0)	0.012
NYHA class, n (%)			0.628
II	44 (52.4)	12 (44.4)	
III + IV	40 (47.6)	15 (55.6)	
Systolic BP, mmHg	127.5 ± 11.3	123.5 ± 11.3	0.160
Diastolic BP, mmHg	78.7 ± 8.3	74.3 ± 10.3	0.064
HR, /min	75.8 ± 10.2	73.8 ± 9.3	0.417
LVEF, %	41.8 ± 12.7	42.9 ± 11.3	0.724
BNP, pg/ml	134.0 (287.8)	153.0 (283.5)	0.477
PNE, pg/ml	528.0 ± 241.4	569.5 ± 171.1	0.040
Medications			
Beta-blockers, n (%)	48 (57.1)	18 (66.7)	0.381
ACE inhibitors/ARBs, n (%)	68 (81.0)	23 (85.2)	0.619
Aldosterone-blockers, n (%)	20 (23.8)	6 (22.2)	0.865
Diuretics, n (%)	68 (81.0)	20 (74.1)	0.443
Implantable cardiac device, n (%)			
Cardiac pacemaker, n (%)	9 (10.7)	2 (7.4)	0.248
Implantable cardioverter defibrillator, n (%)	4 (4.8)	0 (0)	0.617

Continuous data were shown as mean ± standard deviation or median (interquartile range).

ACE, angiotensin-converting enzyme; AF, atrial fibrillation; ARB, angiotensin II receptor blocker; BMI, body mass index; BNP, brain natriuretic peptide; BP, blood pressure; HR, heart rate; LVEF, left ventricular ejection fraction; NYHA, New York Heart Association; PNE, plasma norepinephrine.

Discussion

In this study, we demonstrated that the unsuppressed SA, residual AHI ≥ 15 on CPAP, was associated with increased clinical outcomes in patients HF with SA including either OSA or CSA accompanied by the presence of AF and the dropout from the CPAP therapy.

Previous studies reported that SA is associated with negative health consequences in patients with HF (11–13). Recurrent episodes of apneas during sleep followed by arousals generate repetitive hypoxia-reoxygenation, increased intrathoracic negative pressure, and exaggerated sympathetic nervous activity (6), all of which contribute to an increased ventricular afterload. CPAP is effective to suppress apneas and hypopneas in HF patients with OSA and in a half of patients with CSA (6), improving cardiac function, and potentially leading to improvements in the prognosis in patients with HF. However, previous clinical trial examining the efficacy of CPAP therapy in patients with HF and CSA, revealed that CPAP therapy did not significantly reduce incident clinical outcomes including mortality, heart transplantation or hospitalization for cardiovascular events (6, 8, 12, 13). Interestingly, a *post hoc* analysis of that trial reported that the study population whose AHI was reduced below 15/h on CPAP had better prognoses with regard to heart transplantation-free survival rates compared to those whom AHI on CPAP therapy was 15 or greater (14). Similar to this result, our study demonstrated that residual AHI ≥ 15 on CPAP therapy was associated with worse clinical outcomes in patients HF with SA, compared to those with residual AHI < 15. However, our study provides novel findings that such unsuppressed SA can be one of the important prognostic factor even in patients with HF and

TABLE 2 Polysomnographic findings.

	Suppressed ($N = 84$)			Unsuppressed ($N = 27$)		
	Diagnostic study	On CPAP study	$p^{\dagger}$	Diagnostic study	On CPAP study	$p^{\dagger}$
TST (min)	322.8 ± 79.1	336.8 ± 79.6	0.137	309.6 ± 94.4	341.6 ± 95.6	0.369
Total AHI no./h	44.2 ± 17.6	5.1 ± 3.6	<0.001	51.6 ± 14.2*	21.3 ± 7.5*	<0.001
%central/total AHI	21.6 (57.1)	31.9 (62.5)	0.001	81.6 (28.7)*	86.0 (38.6)*	0.023
%TST SO_2 < 90% (%)	17.6 (46.4)	0.2 (1.2)	<0.001	19.1 (45.7)	2.1 (7.7)**	0.002
Lowest SO_2%	75.3 ± 13.8	96.3 ± 1.6	<0.001	75.6 ± 13.0	84.9 ± 4.5*	0.002
Arousal index no./h	41.1 ± 19.6	15.8 ± 10.1	<0.001	43.6 ± 20.0	17.6 ± 8.4	<0.001
Sleep stage % of TST						
Slow wave sleep (%)	6.0 (12.5)	15.5 (13.1)	<0.001	0 (2.6)**	12.0 (21.5)	0.022
REM sleep (%)	9.9 ± 6.4	17.1 ± 7.1	<0.001	9.6 ± 5.8	18.3 ± 7.0	0.005

AHI, apnea–hypopnea index; CPAP, continuous positive airway pressure; REM, rapid eye movement; SO_2, oxyhemoglobin saturation; TST, total sleep time.
Data were shown as mean ± standard deviation or median (interquartile range).
*$p < 0.05$ comparing with suppressed group.
**$p < 0.01$ comparing with suppressed group.
$^{\dagger}p$ for comparing between diagnostic and on CPAP studies.

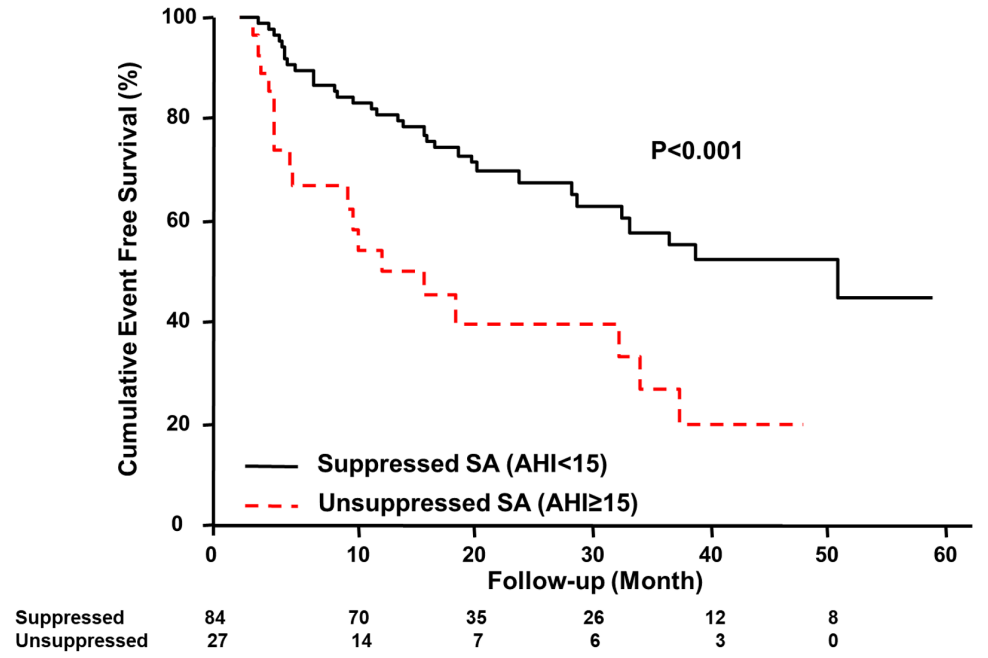

FIGURE 1
Kaplan–Meier estimation of event-free survival. Kaplan–Meier estimation of cumulative event-free survival for all-cause mortality and hospitalization for HF showing a significantly worse clinical outcome in the unsuppressed group. AHI, apnea-hypopnea index; SA, sleep apnea; HF, heart failure.

SA. Our subgroup analyses for type of SA (obstructive- or central-dominant SA) showed that unsuppressed SA had worse prognoses than suppressed SA in the obstructive-dominant SA while no statistical difference was observed between the two groups in the central-dominant SA. Type of SA had statistically significant interaction between clinical events and residual SA (p for interaction = 0.018). The finding is consistent with previous studies showing evidence on the detrimental effect of central apneas in patients with HF regardless of LVEF (15, 16).

Backdrop of the worse clinical outcomes in the unsuppressed- compared to the suppressed group, is partly explained by patients' characteristics in terms of relatively higher age, lower diastolic BP, significantly higher PNE level, and prevalence of AF in the unsuppressed group than those in the suppressed group. Indeed, the multivariate Cox regression analyses demonstrated that unsuppressed SA and presence of AF were associated with worse clinical outcomes. Considering the severer SA with more CSA on the diagnostic sleep study, which are generally associated with pulmonary congestion (17), in the unsuppressed group, we speculated that unsuppressed SA is indicatives of unfavorable patients' backgrounds such as more volume overloaded and pulmonary congestion in association with more impaired cardiac function, all of which are associated with poor prognoses in patients with HF.

TABLE 3 Results of univariate and multivariate analysis assessing prognostic factors for clinical outcomes.

	Univariable			Multivariable		
	HR	95%CI	*P*	HR	95%CI	*P*
Age (1 y.o. increase)	1.03	1.01–1.06	0.014	1.01	0.98–1.04	0.483
Log-transformed BNP (1 increase)	1.49	1.13–1.96	0.005	1.40	1.04–1.89	0.026
AF – yes	2.13	1.22–3.73	0.008	1.94	1.04–3.62	0.037
CPAP dropout – yes	4.67	2.50–8.73	<0.001	3.43	1.52–7.74	0.003
Unsuppressed SA – yes	2.64	1.48–4.74	0.001	2.30	1.21–4.38	0.011

AF, atrial fibrillation; BP, blood pressure; BNP, brain natriuretic peptide; CI, confidence interval; HR, hazard ratio; REM, rapid eye movement.

Patients with unsuppressed SA have greater total AHI with more hypoxic burden compared with those with suppressed SA. Recently, hypoxic burden rather than frequency of respiratory events (i.e., AHI) is regarded as having more impact of clinical outcome in patients with HF and SA (18). In the present study however, neither %TST $SO_2 < 90\%$ nor lowest SO_2 were not associated with increased risk of clinical events even in the univariate analyses. Relationships between hypoxic burden in patients with unsuppressed SA should be elucidated in the further study.

Clinical implications and future perspectives

Our findings imply the needs of assessment for unsuppressed SA in patients with HF and SA treated with CPAP therapy. To stratify patients at risk of mortality and hospitalization, it should be enhanced to evaluate residual AHI especially in HF patients who have already been initiated into CPAP therapy. In such cases, because undergoing polysomnography may not be feasible, residual AHI which was provided by CPAP device will also be applicable because the AHI provided by CPAP or other positive airway pressure device is accurate and acceptable (19–21). We previously reported that in patients with unsuppressed SA, replacement of CPAP by bi-level positive airway pressure or adaptive-servo ventilation (ASV) led improvements of cardiac function with sufficient suppression of their SA (22, 23). However, there are no data suggesting the long-term prognostic impact of such sufficient suppression of SA in patients with HF and unsuppressed SA. ASV which is reported as providing short-term improvement of cardiac function in patients with HF and SA especially in cases with predominant CSA, failed to show long-term mortality benefit rather showed potentials to be harmful in patients with HF and predominant CSA in a large-scale clinical trial, the SERVE-HF trial (24). Another large-scale randomized controlled trial (25) examined the efficacy of ASV in patients with HF and SA including either OSA or CSA. In the trial, although ASV markedly reduced AHI, again ASV failed to show the benefit in the primary endpoint, which was the combination of cardiovascular hospitalizations, death from any cause, new-onset atrial fibrillation, and delivery of an appropriate discharge from an implantable cardioverter-defibrillator (26) in either overall, OSA subgroup or CSA subgroup. However, in CSA subgroup which did not include planned number of subjects because of the SERVE-HF trial leading to underpower to show the statistical significance, sufficient suppression of SA by ASV tended to have mortality benefit. In addition, although ASV is acceptable for HF patients with OSA with some CSA component, whether ASV provide beneficial effects on clinical outcomes in patients with almost pure OSA and no/limited CSA component remains controversial. Further studies are needed to examine how we treat residual AHI in those patients to improve their prognoses.

Limitations

This was retrospective analyses of the single-center observational study with a relatively small sample size. Moreover, since the present study was observational in nature, other unknown confounders might have affected the prognosis even after the multivariate analysis. Therefore, our data should be interpreted carefully, and further studies with larger sample size and intervention to improve unsuppressed SA are required to confirm our data. A recent study suggested that variability of the residual AHI may alter particularly in patients with HF (27). Thus, status regarding unsuppressed SA may also alter. Since our data were collected between 2001 and 2005, during which contemporary clinical practice of HF were not yet established, pharmacological therapy for HF were not fully optimized, which might have affected the observed outcomes in the study population.

Conclusions

Our study demonstrated that patients with HF and SA were associated with worse prognosis in patients with residual AHI ≥ 15 compared to those with residual AHI < 15.

Data availability statement

The raw data supporting the conclusions of this article will be made available by the authors, without undue reservation.

Ethics statement

The studies involving human participants were reviewed and approved by the ethics committee of the institutions involved. The patients/participants provided their written informed consent to participate in this study.

Author contributions

TK: methodology, investigation, review and editing, and supervision; RN: original draft preparation; YT, SK, KN and S-IM: supervision. All authors contributed to the article and approved the submitted version.

Funding

Grant to The Intractable Respiratory Diseases and Pulmonary Hypertension Research Group, from the Ministry of Health, Labor and Welfare, Japan, Grant/Award Number: 20FC1027; JSPS KAKENHI, Grant/Award Number: JP17K09527, 21K08116, 21K16034; a research grant from the Japanese Center for Research on Women in Sport, Juntendo University.

Conflict of interest

RN and TK are affiliated with a department endowed by Philips Respironics, ResMed, and Fukuda Denshi.

The remaining authors declare that the research was conducted in the absence of any commercial or financial relationships that could be construed as a potential conflict of interest

Publisher's note

References

1. Savarese G, Lund LH. Global public health burden of heart failure. *Card Fail Rev*. (2017) 3(1):7–11. doi: 10.15420/cfr.2016:25:2

2. Benjamin EJ, Virani SS, Callaway CW, Chamberlain AM, Chang AR, Cheng S, et al. Heart disease and stroke statistics-2018 update: a report from the American heart association. *Circulation*. (2018) 137(12):e67–492. doi: 10.1161/CIR.0000000000000558

3. Naito R, Kasai T, Narui K, Momomura SI. Association between frequency of central respiratory events and clinical outcomes in heart failure patients with sleep apnea. *J Clin Med*. (2022) 11(9):2403. doi: 10.3390/jcm11092403

4. Naito R, Kasai T, Dohi T, Takaya H, Narui K, Momomura SI. Factors associated with the improvement of left ventricular systolic function by continuous positive airway pressure therapy in patients with heart failure with reduced ejection fraction and obstructive sleep apnea. *Front Neurol*. (2022) 13:781054. doi: 10.3389/fneur.2022.781054

5. Kasai T, Narui K, Dohi T, Yanagisawa N, Ishiwata S, Ohno M, et al. Prognosis of patients with heart failure and obstructive sleep apnea treated with continuous positive airway pressure. *Chest*. (2008) 133(3):690–6. doi: 10.1378/chest.07-1901

6. Kasai T. Sleep apnea and heart failure. *J Cardiol*. (2012) 60(2):78–85. doi: 10.1016/j.jjcc.2012.05.013

7. Kasai T, Bradley TD. Obstructive sleep apnea and heart failure. *J Am Coll Cardiol*. (2011) 57(2):119–27. doi: 10.1016/j.jacc.2010.08.627

8. Bradley TD, Logan AG, Kimoff RJ, Sériès F, Morrison D, Ferguson K, et al. Continuous positive airway pressure for central sleep apnea and heart failure. *N Engl J Med*. (2005) 353(19):2025–33. doi: 10.1056/NEJMoa051001

9. American Academy of Sleep Medicine, editors. *Sleep technicians and technologists*. Darien, IL: AASM Facility Standards for Accreditation (2020).

10. American Academy of Sleep Medicine. *The AASM manual for the scoring of sleep and associated events: Rules, terminology and technical specifications*. Version 2.6. Westchester, IL: American Academy of Sleep Medicine (2020).

11. Yumino D, Wang H, Floras JS, Newton GE, Mak S, Ruttanaumpawan P, et al. Prevalence and physiological predictors of sleep apnea in patients with heart failure and systolic dysfunction. *J Card Fail*. (2009) 15(4):279–85. doi: 10.1016/j.cardfail.2008.11.015

12. Oates CP, Ananthram M, Gottlieb SS. Management of sleep disordered breathing in patients with heart failure. *Curr Heart Fail Rep*. (2018) 15(3):123–30. doi: 10.1007/s11897-018-0387-7

13. Drager LF, McEvoy RD, Barbe F, Lorenzi-Filho G, Redline S. INCOSACT Initiative (international collaboration of sleep apnea cardiovascular trialists). Sleep apnea and cardiovascular disease: lessons from recent trials and need for team science. *Circulation*. (2017) 136(19):1840–50. doi: 10.1161/CIRCULATIONAHA.117.029400

14. Arzt M, Floras JS, Logan AG, Kimoff RJ, Series F, Morrison D, et al. Suppression of central sleep apnea by continuous positive airway pressure and transplant-free survival in heart failure: a post hoc analysis of the Canadian continuous positive airway pressure for patients with central sleep apnea and heart failure trial (CANPAP). *Circulation*. (2007) 115(25):3173–80. doi: 10.1161/CIRCULATIONAHA.106.683482

15. Emdin M, Mirizzi G, Giannoni A, Poletti R, Iudice G, Bramanti F, et al. Prognostic significance of central apneas throughout a 24-hour period in patients with heart failure. *J Am Coll Cardiol*. (2017) 70(11):1351–64. doi: 10.1016/j.jacc.2017.07.740

16. Borrelli C, Gentile F, Sciarrone P, Mirizzi G, Vergaro G, Ghionzoli N, et al. Central and obstructive apneas in heart failure with reduced, mid-range and preserved ejection fraction. *Front Cardiovasc Med*. (2019) 6:125. doi: 10.3389/fcvm.2019.00125

17. Solin P, Bergin P, Richardson M, Kaye DM, Walters EH, Naughton MT. Influence of pulmonary capillary wedge pressure on central apnea in heart failure. *Circulation*. (1999) 99(12):1574–9. doi: 10.1161/01.CIR.99.12.1574

18. Oldenburg O, Wellmann B, Buchholz A, Bitter T, Fox H, Thiem U, et al. Nocturnal hypoxaemia is associated with increased mortality in stable heart failure patients. *Eur Heart J*. (2016) 37(21):1695–703. doi: 10.1093/eurheartj/ehv624

19. Ueno K, Kasai T, Brewer G, Takaya H, Maeno Ki, Kasagi S, et al. Evaluation of the apnea-hypopnea index determined by the S8 auto-CPAP, a continuous positive airway pressure device, in patients with obstructive sleep apnea-hypopnea syndrome. *J Clin Sleep Med JCSM Off Publ Am Acad Sleep Med*. (2010) 6(2):146–51. PMID: 20411691.

20. Ikeda Y, Kasai T, Kawana F, Kasagi S, Takaya H, Ishiwata S, et al. Comparison between the apnea-hypopnea indices determined by the REMstar auto M series and those determined by standard in-laboratory polysomnography in patients with obstructive sleep apnea. *Intern Med Tokyo Jpn*. (2012) 51(20):2877–85. doi: 10.2169/internalmedicine.51.8249

21. Imanari S, Tomita Y, Kasagi S, Kawana F, Kimura Y, Ishiwata S, et al. Evaluation of the apnea-hypopnea Index determined by adaptive servo-ventilation devices in patients with heart failure and sleep-disordered breathing. *Front Cardiovasc Med*. (2021) 8:680053. doi: 10.3389/fcvm.2021.680053

22. Dohi T, Kasai T, Narui K, Ishiwata S, Ohno M, Yamaguchi T, et al. Bi-Level positive airway pressure ventilation for treating heart failure with central sleep apnea that is unresponsive to continuous positive airway pressure. *Circ J*. (2008) 72(7):1100–5. doi: 10.1253/circj.72.1100

23. Kasai T, Kasagi S, Maeno Ki, Dohi T, Kawana F, Kato M, et al. Adaptive servo-ventilation in cardiac function and neurohormonal Status in patients with heart failure and central sleep apnea nonresponsive to continuous positive airway pressure. *JACC Heart Fail*. (2013) 1(1):58–63. doi: 10.1016/j.jchf.2012.11.002

24. Cowie MR, Woehrle H, Wegscheider K, Angermann C, d'Ortho MP, Erdmann E, et al. Adaptive servo-ventilation for central sleep apnea in systolic heart failure. *N Engl J Med*. (2015) 373(12):1095–105. doi: 10.1056/NEJMoa1506459

25. Lyons OD, Floras JS, Logan AG, Beanlands R, Cantolla JD, Fitzpatrick M, et al. Design of the effect of adaptive servo-ventilation on survival and cardiovascular hospital admissions in patients with heart failure and sleep apnoea: the ADVENT-HF trial. *Eur J Heart Fail*. (2017) 19(4):579–87. doi: 10.1002/ejhf.790

26. Bradley TD. The ADVENT-HF trial. *Eur Soc Cardiol*. (2022). 26–29 August, Barcelona, Spain.

27. Rossetto A, Midelet A, Baillieul S, Tamisier R, Borel JC, Prigent A, et al. Factors associated with residual apnea-hypopnea index variability during continuous positive airway pressure treatment. *Chest*. (2023) 163:S0012369223000405. doi: 10.1016/j.chest.2022.12.048

Frontiers in
Cardiovascular Medicine

Innovations and improvements in cardiovascular treatment and practice

Focuses on research that challenges the status quo of cardiovascular care, or facilitates the translation of advances into new therapies and diagnostic tools.

Discover the latest Research Topics

See more →

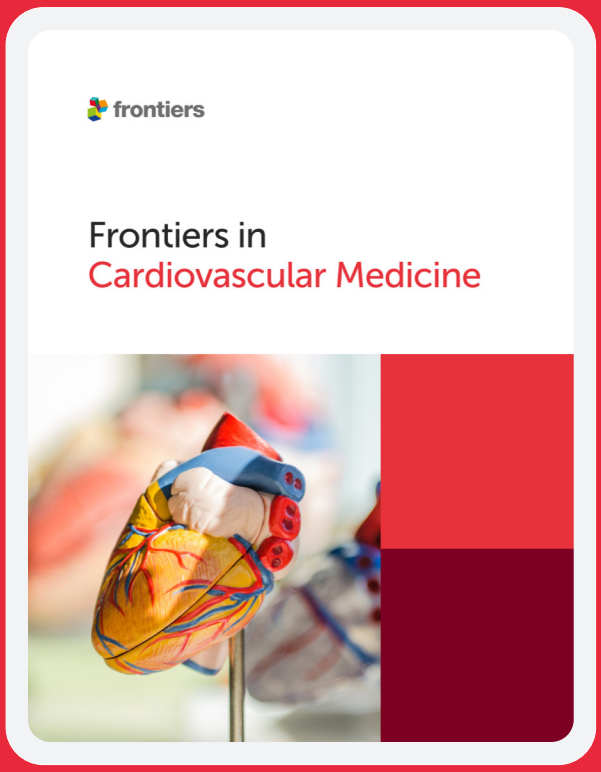

Frontiers

Avenue du Tribunal-Fédéral 34
1005 Lausanne, Switzerland
frontiersin.org

Contact us

+41 (0)21 510 17 00
frontiersin.org/about/contact